
Identification of Lung Carcinoma Biomarkers Associated with Tumour Development and Drug Resistance

**Thesis Submitted to Maynooth University for the degree
of Doctor of Philosophy**



Abduladim Hmmer BSc., MSc.

April 2018

Supervisor

Dr. Paul Dowling
Department of Biology
Maynooth University
Callan Building
Maynooth
Co. Kildare

Co- Supervisor

Prof. Kay Ohlendieck
Department of Biology
Maynooth University
Callan Building
Maynooth
Co. Kildare

Head of Department

Prof. Paul Moynagh
Department of Biology
Maynooth University
Callan Building
Maynooth
Co. Kildare

Co- Supervisor

Dr. Kathy Gately
Department of Clinical Medicine
Trinity Translational Medicine Institute
St. James's Hospital
Trinity College Dublin
Dublin 8
Co. Dublin

Table of content

List of tables.....	xix
Publications	xxiii
Declaration	xxv
Acknowledgement	xxvi
Dedication	xxviii
List of abbreviations.....	xxix
Abstract	xxxix
1. Introduction	1
1.1. Lung cancer	1
1.2. Prevalence of lung cancer.....	1
1.3. Risk factors	3
1.4. Classification of lung cancer	5
1.4.1. Neuroendocrine lung tumours (NETs)	7
1.4.2. Non-neuroendocrine non-small cell lung tumours	10
1.5. Lung cancer metastasis.....	13
1.6. TNM staging	15
1.7. Lung cancer grading.....	19
1.8. Lung cancer screening of high risk groups.....	20
1.8.1. Low-dose computed tomography	20
1.8.2. Sputum cytology.....	21
1.8.3. Bronchoscopy.....	21

1.8.4. Chest x-ray	21
1.8.5. Thoracoscopy or Thoracotomy	22
1.9. Tumour protein markers.....	22
1.9.1. History of clinically used tumour markers.....	24
1.9.2. Biomarkers for discriminating between SqCC and AD.....	28
1.10. Biofluids, breath and tissues as sources of biomarkers	29
1.10.1. Blood.....	29
1.10.2. Exhaled breath condensate.....	30
1.10.3. BALF	32
1.10.4. FFPE tissue.....	34
1.11. Non-malignant lung diseases	35
1.11.1. Sarcoidosis	36
1.11.2. Asthma	37
1.11.3. Chronic bronchitis	38
1.11.4. Acute bronchitis.....	39
1.11.5. Pneumonia.....	39
1.26.6. Tuberculosis	39
1.26.7. Cystic fibrosis.....	40
1.26.8. Pulmonary oedema	41
1.26.9. Acute respiratory distress syndrome (ARDS).....	41
1.11.10. Benign lung nodules	41
1.12. Lung cancer treatment	43
1.13. Label-free proteomics.....	46
1.14. Validation approaches (ELISA, IHC, MRM).....	47

1.15. Cell culture models of drug resistance	48
1.16. Metabolomics.....	50
1.17. Aim of the project.....	52
Materials and methods.....	54
2.1. BALF samples.....	54
2.1.1. BALF protein content	54
2.1.2. Sample preparation for label-free mass spectroscopy	55
2.1.3. Sample desalting using C18 spin column at 1500 x g for 1 min.....	56
2.1.4. Label-free MS/MS protocol	56
2.1.5. Label-free MS/MS data processing	57
2.1.6. ELISA biomarkers validation.....	58
2.2. Metabolomics analysis.....	61
2.2.1. Serum samples preparation	61
2.2.2. UHPLC/MS protocol	62
2.2.3. GC/MS protocol	62
2.2.4. Data processing	62
2.2.5. Metabolomics' biomarkers validation	62
2.3. Formaldehyde-fixed paraffin-embedded tissue (FFPE) samples.....	66
2.3.1. Tissue sample collection	66
2.3.2. Protein extraction and digestion for LC-MS/MS	67
2.3.3. Protein digestion.....	67
2.3.4. LC-MS/MS protocol.....	68
2.3.5. Processing mass spectroscopy raw files	68
2.3.6. Tissue microarrays validation of heterogeneity	70

2.4. Drug resistance- based biomarkers heterogeneity	72
2.4.1. Cell culture	72
2.4.2. Cell lysis.....	72
2.4.3. Mitochondrial enrichment.....	73
2.4.4. Samples protein quantification.....	73
2.4.5. Label-free mass spectroscopy	74
2.4.6. Western blot	75
2.4.6. TMRE mitochondrial membrane potential assay kit (cat. #ab113852).....	80
2.4.7. Basic metabolic phenotyping	80
2.4.8. H1975 mitochondrial distribution pattern (Lackner, 2013).....	84
2.4.9. Cell cycle of GDC-0980 parent and resistant H1975 and A549 cells.....	85
2.4.10. Western blot validation of cell cycle	85
2.4.11. Histone acetylation of GDC-0980 parent and resistant H1975 and A549 cells	86
2.4.12. Histone co-localization in H1975	87
2.4.13. Western blot validation of lysine acetyl-transferases and histone deacetylases	88
2.4.14. Functional validation of HDAC role in GDC-0980 resistance	89
2.4.15. Western blot validation of cell survival, apoptosis and evasion biomarkers .	92
3. Bronchoalveolar lavage discovery work.....	95
3.1. Introduction.....	95
3.2. Experimental design	96
3.3. Results	97

3.3.1. The cut-off value for lung adeno and squamous carcinomas proteome signature.....	97
3.3.2. Comparison of lung adenocarcinoma lavage proteome to the control lavage .	98
3.3.3. Comparison of lung squamous carcinoma lavage proteome to the control lavage.....	100
3.3.4. Classification of proteins found changed in AD and SqCC compared to control.	104
3.3.5. Proteome signature differentiating between lung AD and SqCC.....	105
3.3.6. Classification of proteins that could differentiate between lung AD and lung SqCC.....	108
3.3.7. ELISA verification	109
3.3.8. Metabolism in non-small cell lung cancer	112
3.4. Discussion.....	114
4. Metabolic biomarkers discovery work.....	126
4.1. Introduction.....	126
4.2. Experimental design	127
4.3. Results.....	128
4.3.1. Elevated serum metabolites levels detected by LC/MS and GC/MS analysis in NSCLC compared to control	128
4.3.2. Lowered serum metabolites levels detected by LC/MS and GC/MS analysis in NSCLC compared to control	129
4.3.3. Serum levels of some acetyl co-A precursors	130
4.3.4. Serum glutamate levels.....	131
4.4. Discussion.....	132

5. Tumour heterogeneity	139
5.1. Introduction	139
5.2. Experimental design	140
5.3. Results	141
5.3.1. Principal component analysis.....	141
5.3.2. Heat map analysis.....	143
5.3.3. Analysis of shared elevated protein levels in all tumour tissue parts per patient	144
5.3.4. Analysis of proteins diminished in all tumour tissue samples per patient.....	149
5.3.5. Formaldehyde-fixed paraffin-embedded tumour tissue versus lavage fluid analysis	153
5.3.6. Tissue microarray validation.....	162
5.4. Discussion	166
6. Cell cycle biomarkers in cancer	177
6.1. Introduction	177
6.2. Experimental design	179
6.3. Results	181
6.3.1. H1975 growth curve	181
6.3.2. Mass spectrometry analysis of cell cycle control proteins.....	182
6.3.3. Cell cycle profile	185
6.3.3. Proteins that affecting cell cycle progression.....	198
6.4. Discussion	233

7. GDC-0980 resistant H1975 lung adenocarcinoma cells energy phenotyping	253
7.1. Introduction	253
7.2. Experimental design	254
7.3. Results	255
7.3.1. Glycolysis in the GDC-0980 resistant H1975 cells (GDC-0980 non-treated).	255
7.3.2. Glycolysis in the GDC-0980 resistant H1975 cells (GDC-0980 treated).	256
7.3.3. Mitochondrial cytoplasmic distribution	257
7.3.4. Cell cycle-based mitochondrial activity	258
7.3.5. Pyruvate dehydrogenase	259
7.3.6. Superoxide dismutase	260
7.3.7. Succinate dehydrogenase complex flavoprotein subunit A	261
7.3.8. Prohibitin B	262
7.3.9. Voltage-dependent anionic channels	263
7.3.10. Heat shock protein 60	264
7.3.11. Cytochrome C Oxidase IV	265
7.3.12. Cytochrome c	266
7.3.13. Acetyl co-A precursors	267
7.3.14. Seahorse cell energy phenotyping	269
7.3.15. Mitochondrial respiration- oxygen consumption rate (OCR).	270
7.3.16. Extracellular acidification rate (ECAR)	271
7.4. Discussion	273
8.1. Discussion	281
8.2. Conclusion	295

8.3. Future Plans.....	297
References.....	298
Appendicies.....	372

List of figures

Figure 1: The major environmental causes of lung cancer (Cuadras et al., 2016).....	3
Figure 2: The main histological types of lung cancer.....	9
Figure 3: A systematic reference of the thoracic lymph nodes used in Olympus CT scan lymph node mapping for TNM staging.....	18
Figure 4: Olympus CT scan lymph node mapping for TNM staging (Abramyuk et al., 2012).....	19
Figure 5: Integration of tumour markers with other diagnostic modalities. Modified from (Holdenrieder et al., 2016).....	27
Figure 6: Color-coded pre-stained protein marker.....	76
Figure 7: western blot loading control for treated (R+) and non-treated GDC-0980 resistant cells compared to their matching parent cells (P).	79
Figure 8: The number of proteins excluded per fold change cut-off value.	97
Figure 9: PANTHER GO-Slim Biological Process Analysis of proteins found lowered or elevated in adenocarcinoma (AD) and squamous cell carcinoma (SqCC) lavages compared to the control (C): healthy individuals and sarcoid patients lavages.....	104
Figure 10: PANTHER GO-Slim Biological Process of unique proteins that were found elevated/lowered in adenocarcinoma (AD) and have opposite profile in squamous cell carcinoma (SqCC) lavages compared to the control: healthy individuals and sarcoid patients lavages.	108
Figure 11: ELISA verification.....	111
Figure 12: Extracellular lipocalin receptor-mediated intracellular signalling.....	121
Figure 13: Serum levels of various metabolites in the patients with NSCLC and controls.	130

Figure 14: Glutamate levels in non-small cell lung cancer compared to control group	131
Figure 15: Acetyl Co-A as a central metabolite intermediate for amino acids and fatty acids.....	133
Figure 16: Principal component analysis (PCA).....	142
Figure 17: Heat map comparison of total proteomes.	143
Figure 18: Venn diagrams showing shared up-regulated proteins compared to normal control tissue from the same patient in the three different parts (Q1, Q2, Q3) of the same tumour specimen per patient.....	144
Figure 19: Venn diagrams showing the shared proteins diminished in the three parts (Q1, Q2, Q3) of the same tumour specimen in each patient.....	149
Figure 20: String analysis (GO:0070062 extracellular exosomes) of heterogeneously overexpressed proteins found shared in at least all parts of one FFPE tissue sample and low in the lung lavage from adenocarcinoma.....	155
Figure 21: String analysis (GO:0070062 extracellular exosomes) of heterogeneously down regulated proteins found shared in all parts of at least one tissue sample and elevated in the lung lavage from adenocarcinoma.....	157
Figure 22: String analysis (GO:0070062 extracellular exosomes) of proteins heterogeneously overexpressed in both FFPE and lung lavage from adenocarcinoma compared to normal controls.	159
Figure 23: String analysis (GO:0070062 extracellular exosomes) of heterogeneously down regulated proteins that were shared in all parts of at least one tissue sample and in the lung lavage from adenocarcinoma.....	161

Figure 24: Immunohistochemical staining of FFPE-based TMA for lactate dehydrogenase A (brown) in normal lung tissues (A), lung adenocarcinoma (B) and lung squamous cell carcinoma (C).....	163
Figure 25: Immunohistochemical staining of FFPE-based TMA for pyruvate dehydrogenase (brown) in lung adenocarcinoma (A) and lung squamous cell carcinoma (B). 0, 1, 2, 3 represent reactivity scoring (colour intensity).....	164
Figure 26: Immunohistochemical staining of FFPE-based TMA for Talin-1 (brown) in normal lung tissues (A), lung adenocarcinoma (B) and lung squamous cell carcinoma (C).....	165
Figure 27: Growth curves of GDC-0980 sensitive P (A), resistant non-treated (B) and resistant treated R+ cells (C).....	181
Figure 28: Cell cycle profile of GDC-0980 sensitive parent (P) and resistant (R) H1975 cells and A549 adenocarcinoma cells.....	185
Figure 29: Comparison of cell cycle phases of GDC-0980 sensitive parent (P) and resistant (R) H1975 and A549 adenocarcinoma cells..	186
Figure 30: Immunoblotting comparison of histone 3 (H3) levels in GDC-0980 sensitive parent (P) and resistant (R) A549 lung adenocarcinoma cells. P1, P2, P3 and R1, R2, R3 represent triplicates of 20 µg of total cell protein..	187
Figure 31: western blot comparison of histone 3 (H3) protein abundance levels in GDC-0980 sensitive parent (P) and resistant (R) H1975 adenocarcinoma cells. P1, P2, P3 and R1, R2, R3 represent triplicates of 20 µg of cells lysate total protein..	188
Figure 32: Nuclear histone 3 localisation. (P): GDC-0980 parent sensitive cells..	189
Figure 33: Nuclear histone 3 localisation.....	190
Figure 34: Nuclear histone 3 localisation. (R+): GDC-0980 resistant H1975 cells grown in media containing 1 µM GDC-0980.	191

Figure 35: Comparison of cyclin D1 abundance in GDC-0980 sensitive parent (P) cells and resistant (R) H1975 adenocarcinoma cells.....	192
Figure 36: Comparison of cyclin D3 abundance in GDC-0980 sensitive parent (P) and resistant (R) H1975 adenocarcinoma cells..	193
Figure 37: Western blotting comparison of cyclin A2 protein abundance in GDC-0980 sensitive parent (P) and resistant (R) H1975 adenocarcinoma cells.....	194
Figure 38: Comparison of cyclin B1 abundance in GDC-0980 sensitive parent (P) and resistant (R) H1975 adenocarcinoma cells..	195
Figure 39: Comparison of cyclin H abundance in GDC-0980 sensitive parent (P) and resistant (R) H1975 adenocarcinoma cells..	196
Figure 40: Comparison of cyclin dependent kinase 6 protein (CDK6) abundance in GDC-0980 sensitive parent (P) and resistant (R) H1975 adenocarcinoma cells.....	197
Figure 41: Comparison of P53 levels in GDC-0980 sensitive parent (P) and resistant H1975 lung adenocarcinoma cells. (A): no drug treatment and (R-)(B) when cells were incubated in medium containing 1 μ M GDC-0980 (R+).....	198
Figure 42: Comparison of 14.3.3 zeta/delta (ζ/δ) protein abundance in GDC-0980 sensitive parent (P) and resistant (R) H1975 adenocarcinoma cells.....	199
Figure 43: Comparison of 14.3.3 epsilon (ϵ) protein abundance in GDC-0980 sensitive parent (P) and resistant (R) H1975 adenocarcinoma cells.....	200
Figure 44: Comparison of 14.3.3 gamma [8] protein abundance in GDC-0980 sensitive parent (P) and resistant (R) H1975 adenocarcinoma cells.....	201
Figure 45: Comparison of 14.3.3 alpha/beta protein abundance levels in GDC-0980 sensitive parent (P) and resistant (R) H1975 adenocarcinoma cells.....	202
Figure 46: Comparison of p21 protein abundance in GDC-0980 sensitive parent (P) and resistant (R) H1975 adenocarcinoma cells..	203

Figure 47: Comparison of Proliferating cells nuclear antigen (PCNA) abundance in GDC-0980 sensitive parent (P) and resistant (R) H1975 adenocarcinoma cells.....	204
Figure 48: Comparison of the ubiquitination level of PCNA (Ub-PCNA) protein abundance levels in GDC-0980 sensitive parent (P) and resistant (R) H1975 adenocarcinoma cells.....	205
Figure 49: Comparison of Bcl-associated X large protein (BAX) abundance in GDC-0980 sensitive parent (P) and resistant (R) H1975 adenocarcinoma cells..	206
Figure 50: Comparison of the levels of BCL-XL abundance in GDC-0980 sensitive parent (P) and resistant (R) H1975 adenocarcinoma cells.....	207
Figure 51: Comparison of the levels of Nuclear factor kappa B1 (P105/P50) abundance and its degradation in GDC-0980 sensitive parent (P) and resistant (R) H1975 adenocarcinoma cells.....	208
Figure 52: comparison of the Rel- associated protein [Rel-A] abundance levels in GDC-0980 sensitive parent (P) and resistant (R) H1975 adenocarcinoma cells..	209
Figure 53: Comparison of Rel-B protein abundance levels in GDC-0980 sensitive parent (P) and resistant (R) H1975 adenocarcinoma cells.....	210
Figure 54: Comparison of c-Rel protein abundance levels in GDC-0980 sensitive parent (P) and resistant (R) H1975 adenocarcinoma cells.....	211
Figure 55: Comparison of general control of amino acid synthesis (GCN5L2) protein abundance levels in GDC-0980 sensitive parent (P) and resistant (R) H1975 adenocarcinoma cells.....	212
Figure 56: Comparison of p300/CBP-associated protein (PCAF) abundance levels in GDC-0980 sensitive parent (P) and resistant (R) H1975 adenocarcinoma cells.....	213
Figure 57: comparison of histone deacetylase I (HDAC I) protein abundance levels in GDC-0980 sensitive parent (P) and resistant (R) H1975 adenocarcinoma cells.....	214

Figure 58: Comparison of histone deacetylase II (HDAC II) protein abundance levels in GDC-0980 sensitive parent (P) and resistant (R) H1975 adenocarcinoma cells.....	215
Figure 59: Comparison of histone deacetylase III (HDAC III) protein abundance levels in GDC-0980 sensitive parent (P) and resistant (R) H1975 adenocarcinoma cells...	216
Figure 60: Comparison of histone deacetylase IV (HDAC IV) protein abundance levels in GDC-0980 sensitive parent (P) and resistant (R) H1975 adenocarcinoma cells...	217
Figure 61: Comparison of histone deacetylase VI (HDAC VI) protein abundance levels in GDC-0980 sensitive parent (P) and resistant (R) H1975 adenocarcinoma cells...	218
Figure 62: Comparison of phosphorylated HDACs IV and V (P- HDAC IV & V) protein abundance in GDC-0980 sensitive parent (P) and resistant (R) H1975 adenocarcinoma cells.....	219
Figure 63: Comparison of acetylated levels of lysine 9 of histone 3 (H3) protein in GDC-0980 sensitive parent (P) and resistant (R) H1975 adenocarcinoma cells..	220
Figure 64: Comparison of acetylated lysine 9 of histone 3 (H3K9) protein abundance levels in GDC-0980 sensitive parent (P) and resistant (R) A549 adenocarcinoma cells..	221
Figure 65: Comparison of acetylated lysine 18 of histone 3 (H3K18) protein abundance levels in GDC-0980 sensitive parent (P) and resistant (R) H1975 adenocarcinoma cells.	222
Figure 66: Comparison of acetylated lysine 18 of histone 3 (H3K18) protein abundance levels in GDC-0980 sensitive parent (P) and resistant (R) A549 adenocarcinoma cells..	223
Figure 67: Comparison of acetylated lysine 27 of histone 3 (H3K27) protein abundance levels in GDC-0980 sensitive parent (P) and resistant (R) H1975 adenocarcinoma cells..	224

Figure 68: Comparison of histone 4 protein abundance in GDC-0980 sensitive parent (P) and resistant (R) H1975 adenocarcinoma cells.....	225
Figure 69: Comparison of acetylated lysine 5 of histone 4 (H4K5) protein abundance levels in GDC-0980 sensitive parent (P) and resistant (R) H1975 adenocarcinoma cells..	226
Figure 70: Dose-response curve of GDC-0980 for GDC-0980 resistant [R-] and parent [P] H1975 lung adenocarcinoma cells.....	227
Figure 71: SAHA dose response curve.	228
Figure 72: KEGG pathway analysis of the proteins found upregulated in the GDC-0980 resistant cells compared to the parent cells in both treated (R+) and non-treated (R-) cells.....	231
Figure 73: KEGG pathway analysis of cell cycle proteins.....	232
Figure 74: Summary of experimental findings of cell cycle control proteins in H1975 cells.....	237
Figure 75: Seahorse basic principle.....	254
Figure 76: KEGG pathway analysis of up-regulated glycolysis enzymes in GDC-0980 non-treated resistant cells H1975 (R-).....	255
Figure 77: KEGG pathway analysis of up-regulated glycolysis enzymes in GDC-0980 non-treated resistant cells H1975 (R+).....	256
Figure 78: Mito-Tracker®-red mitochondrial labelling-based confocal imaging of GDC-0980 parent (P) and resistant (R) H1975 lung adenocarcinoma cells.....	257
Figure 79: TMRE labelling of mitochondrial activity of GDC-0980 sensitive (P) and resistant (R) H1975 lung adenocarcinoma cells in the presence [+] or absence of the drug incubation [-].....	258

Figure 80: Comparison of pyruvate dehydrogenase abundance in GDC-0980 sensitive parent (P) and resistant (R) H1975 adenocarcinoma cells.....	259
Figure 81: Comparison of superoxide dismutase (SOD1) abundance between GDC-0980 sensitive parent (P) and resistant (R) H1975 adenocarcinoma cells..	260
Figure 82: Comparison of succinate dehydrogenase complex flavoprotein subunit A (SDHA) abundance between GDC-0980 sensitive parent (P) and resistant (R) H1975 adenocarcinoma cells.....	261
Figure 83: Comparison of prohibitin B abundance between GDC-0980 sensitive parent (P) and resistant (R) H1975 adenocarcinoma cells.....	262
Figure 84: Comparison of the abundance of voltage-dependent anionic channels (VDAC) between GDC-0980 sensitive parent (P) and resistant (R) H1975 adenocarcinoma cells.....	263
Figure 85: Comparison of heat shock protein 60 (HSP60) abundance between GDC-0980 sensitive parent (P) and resistant (R) H1975 adenocarcinoma cells..	264
Figure 86: Comparison of cytochrome oxidase (COX IV) protein abundance levels in GDC-0980 sensitive parent (P) and resistant (R) H1975 adenocarcinoma cells.....	265
Figure 87: Comparison of cytochrome c protein abundance in GDC-0980 sensitive parent (P) and resistant (R) H1975 adenocarcinoma cells.....	266
Figure 88: Comparison of acetyl Co-A and its main precursors, pyruvate, free fatty acids, acetoacetic acid and β -hydroxy butyrate, in GDC-0980 sensitive parent (P) and resistant (R) H1975 adenocarcinoma cells.....	268
Figure 89: Seahorse energy phenotyping of GDC-0980 resistant H1975 cells in the presence of 1 μ M final concentration GDC-0980 or absence of the drug compared to GDC-0980 native H1975 lung adenocarcinoma cells.....	269

Figure 90: Mitochondrial respiration activity (aerobic respiration) of GDC-0980 resistant H1975 cells compared to GDC-0980 sensitive H1975 lung adenocarcinoma cells (P).....	270
Figure 91: Extracellular acidification rates (Glycolysis) of GDC-0980 resistant H1975 cells compared to GDC-0980 sensitive (P) H1975 lung adenocarcinoma cells.....	271
Figure 92: Summary of chapter findings.....	277

List of tables

Table 1: The 7th edition of IASLC TNM staging system (Chassagnon et al., 2017)..	17
Table 2: Biomarkers commonly used in diagnosis of lung cancers.....	26
Table 3: Benign lower respiratory tract nodules (Borczuk, 2008).....	45
Table 4: FDA-approved targeted therapy for NSCLC	46
Table 5: Patient lavage samples biodata.....	55
Table 6: Plasma samples biodata	58
Table 7: ELISA kits used for BALF validation.	60
Table 8: ELISA antibodies working concentrations and standard serial concentrations.	61
Table 9: FFPE tissue samples biodata.....	66
Table 10: FFPE tissue sample preparation for mass spectroscopy	69
Table 11: Composition of 4x Laemmli sample loading buffer.....	76
Table 12: Composition of SDS-PAGE running buffer	76
Table 13: Mitochondrial membrane marker antibody sampler kit (Cat.# 8674T).....	79
Table 14: Cyclin Antibody Sampler Kit (cat. #9869)	86
Table 15: Acetyl-Histone Antibody Sampler Kit (cat. #9927).....	89
Table 16: Lysine Acetyl Transferase, deacetylase Antibody Sampler Kits	90
Table 17: NF-Kb family member antibody sampler kit (cat. #4766).....	92
Table 18: 14-3-3 Family Antibody Sampler Kit (cat. #9769).	93
Table 19: Miscellaneous antibodies.	93
Table 20: Top 30 significantly elevated proteins in AD compared to normal controls	98
Table 21: Top 30 significantly lowered proteins in AD compared to normal controls	99
Table 22: Top 30 significantly elevated proteins in SqCC compared to the controls	100

Table 23: Top 30 significantly lowered proteins in SqCC compared to normal controls	101
Table 24: Top 30 significantly elevated proteins in both AD and SqCC compared to controls	102
Table 25: Top 30 significantly lowered proteins in both AD and SqCC compared to control.....	103
Table 26: Proteins significantly elevated in SqCC but lowered in AD compared to the control.....	105
Table 27: Proteins significantly elevated in AD but lowered in SqCC compared to the control.....	106
Table 28: Protein families detected elevated by mass spectrometry in lavage from AD and SqCC patients compared to normal control individuals and selected for verification by ELISA	110
Table 29: Enzymes found by LC-MS/MS to be decreased in both lung AD and SqCC	112
Table 30: Enzymes found by LC-MS/MS to be elevated in both AD and SqCC of lungs	113
Table 31: Metabolites significantly up-regulated in sera of lung cancer patients and controls	128
Table 32: Metabolites found downregulated in sera of lung cancer patients compared to the control normal individuals	129
Table 33: Top 30 proteins of 488 proteins found significantly elevated in all parts of the tumour tissue of patient #1	145
Table 34: Top 30 proteins of 352 proteins found significantly elevated in all parts of the tumour of patient #2	146

Table 35: Top 30 proteins of 396 proteins found significantly elevated in all parts of the tumour specimen from patient #3	147
Table 36: Top 5 proteins of 99 proteins found significantly elevated in all parts of the tumour tissue of patient #4.....	148
Table 37: Proteins significantly lowered in all parts of the tumour tissue of patient #1	150
Table 38: Proteins significantly lower in all parts of the tumour tissue of patient #2	151
Table 39: Proteins significantly low in all parts of the tumour specimen from patient #3	152
Table 40: proteins significantly low in all parts of the tumour tissue of patient 4	153
Table 41: Summary of FFPE specimens heterogeneity and availability in BALF	153
Table 42: Proteins elevated in tumour tissues but lowerd in lavage.	154
Table 43: down-regulated proteins in tumour tissues found elevated in lavage.....	156
Table 44: Top 30 proteins found elevated in one or more tumour quadrants and in the lavage.....	158
Table 45: Top 30 proteins found down regulated in one or more quadrants and in the lavage.....	160
Table 46: Tissue microarray (TMAs) scoring	162
Table 47: Cell cycle regulatory proteins found by mass spectrometry significantly elevated in resistant cells (R+) compared with parent cells	182
Table 48: Cell cycle regulating proteins found significantly elevated in the resistant cells (R-) compared with parent cells by mass spectrometry.	183
Table 49: Cell cycle regulatory proteins found by mass spectrometry significantly down regulated in resistant cells (R+) compared with parent cells by mass spectrometry .	183

Table 50: Cell cycle regulatory proteins found by mass spectrometry significantly down regulated in the resistant cells (R-) compared with parent cells	184
Table 51: Western blot assessment of proteins affecting the cell cycle.....	229
Table 52: Western blot analysis of HAT/HDAC and histone acetylation of GDC-0980 resistant H1975 (treated and non-treated) cells compared to the sensitive parent cells.	230
Table 53: Summary of western blot and biochemical assays findings	272

Publications

Hmmier, A., O'Brien, M.E., Lynch, V., Clynes, M., Morgan, R. & Dowling, P. 2017, "Proteomic analysis of bronchoalveolar lavage fluid (BALF) from lung cancer patients using label-free mass spectrometry", *BBA Clinical*, vol. 7, pp. 97-104.

Hmmier, A., Dowling P. 2018, "DIGE Analysis Software and Protein Identification Approaches". *Methods Mol Biol.* 1664:41-50. doi: 10.1007/978-1-4939-7268-5_4.

Conferences

Hmmier, A., Dowling P. 2015, "Label-free LC-MS analysis of bronchoalveolar lavage fluid identifies TIMP-1, Cystatin C and MIF as potential lung cancer biomarkers". *BSPR 2015 annual meeting* at University of Reading (20-22 July 2015), UK. Poster presentation

Hmmier, A., Gately, K. & Dowling, P. 2017, "HDACs Play a Role in Development of GDC-0980 Resistance in H1975 Lung Adenocarcinoma", *Oncology annual meetings*, Zurich, Switzerland. Abstract published in OXFORD UNIV PRESS, OXFORD, pp. 28. Poster presentation.

Maynooth University biology research day

Hmmier, A., Dowling P. 2015, "Label-free LC-MS analysis of bronchoalveolar lavage fluid identifies TIMP-1, Cystatin C and MIF as potential lung cancer biomarkers" *biology research day, Maynooth University*, Poster presentation.

Hmmier, A., Dowling P. 2016, "Metabolomic profiling of human serum from lung cancer patients" *biology research day, Maynooth University*, Poster presentation.

Hmmier A., Gately K., Dowling P., 2017 "Cell cycle of GDC-0980 resistant A549 and H1975 adenocarcinoma cell lines". *Biology research day, Maynooth University*, Poster presentation.

Hmmier A., Gately K., Dowling, P. 2017 “Examining the Role of Histone Deacetylases Play in The Development of Resistance to GDC-0980 in Lung Adenocarcinoma”
biology research day, Maynooth University, Poster presentation.

Declaration

This thesis has not been submitted in whole or part to this or any other university for any degree, and is the original work of the author.

Abduladim Himmier

Signed: _____

Date: _____ 06/06/2018

Acknowledgement

I would like to acknowledge my country, The State of Libya, for granting me a full package scholarship sum of €300,000 covering all living expenses and comprehensive medical insurance for my family, one-year language preparation, four years university tuition fees and all costs of my Ph.D. project and publications.

I would like to acknowledge people who were behind the successful completion of my Ph.D. training: Prof. Martin Clynes (National Institute for Cellular Biotechnology, NICB-DCU) for his remote advices, consultation and support (Thank you very much, Prof. Martin Clynes). Dr. Anne Marie Larkin from NICB-DCU for her great consultation and assistance with the IHC (Thank you very much, Dr. Anne Marie Larkin). Dr. Lynch V from NICB-DCU for collaboration during lung lavage research work (Thank you very much, Dr. Lynch V). Dr. Kathy Gately from Trinity Translational Medicine Institute, Saint-Jamse's Hospital, Trinity College Dublin (TTMI-TCD) for her great collaboration and excellent co-supervision on the tumour heterogeneity and drug resistance (Thank you very much, Dr. Kathy Gately). Prof. Jacintha O'Sullivan (TTMI) for her invaluable consultation on metabolic profiling of drug resistant cell lines using Seahorse (Thank you very much, Prof. Jacintha O'Sullivan). Dr. Mary O'Sullivan (TTMI) for using the Cytell® machine for cell cycle profiling (Thank you very much, Dr. Mary O'Sullivan). Consultant Dr. Ross Morgan and O'Brien ME at Beaumont hospital-department of respiratory medicine for their collaboration on the lung lavage research work and providing clinical samples for biomarkers validation (Thank you very much, Dr. Ross Morgan and O'Brien ME). Dr. Ilona Dix- Maynooth university for her assistance with the Confocal microscopy (Thank you very much, Dr. Ilona Dix).

I would like to pass my special thanks to Professor Kevin Kavanagh for his advice, consultation and welcoming me in his laboratory during my work on cell lines (Thank

you very much, Prof. Kevin Kavanagh). Also not to forget Prof. Paul Moynagh and the departmental administrative staff for their great communication to facilitate the research work within the department (Thank you very much, Prof. Paul Moynagh, Thank you for all).

Finally, I would like to express my sincere gratitude to my supervisor Dr. Paul Dowling for his outstanding and excellent management of my Ph.D. project including the broad range of collaborations, consultation, advice and operating my Ph.D. grant (thank you very much, Dr. Paul Dowling). I also would like to thank my co-supervisor Prof. Kay Ohlendieck for his remote consultation (Thank you very much, Prof. Kay Ohlendieck). Thank you very much to all post-graduate students whom somehow were part of my Ph.D. training success at Maynooth University.

Abduladim Abobaker Mohamed Hम्मier
Maynooth, Co. Kildare
30th of May 2018

Dedication

"To my parents"

"May Allah have mercy on them and keep them in paradise"

-Amin-

also to

My children, my wife, my sisters, my brothers,

and my friends for their patience and support

during my work on this project.

List of abbreviations

Abbreviation	Full name
A549	Lung Adenocarcinoma Cell Line
Ab	Antibody
AC	A Typical Carcinoid
AcAcA	Acetoacetic Acid
ACN	Acetonitrile
AD	Adenocarcinoma
AGP	A1-Acid Glycoprotein
ALK	Anaplastic Lymphoma Kinase
ANOVA	Analysis Of Variance
APC	Antigen Presenting Cells
ApoD	Apolipoprotein D
ApoM	Apolipoprotein M
ARDS	Acute Respiratory Distress Syndrome
ASC	Adenosquamous Lung Carcinoma
ATM	Ataxia-Telangiectasia Mutated Kinase
ATP	Adenosine Triphosphate
BALF	Bronchoalveolar Lavage Fluid
BAX	B-Cell Lymphoma 2-Associated X Protein
BCL-XL	B-Cell Lymphoma-Extra Large
BOH	3-Hydroxy Butyric Acid
BrdU	Bromodeoxyuridine
BSA	Bovine Serum Albumin

CA-19-9	Cancer Antigen
Ca-PCNA	Cancer-Specific-PCNA
CAK	Cyclin-Dependent Kinase-Activating Kinases
Cat. No	Catalogue Number
CDK	Cyclin-Dependent Kinase
CE-MS	Capillary Electrophoresis Coupled To Mass Spectrometry
CEA	Carcinoembryonic Antigen
CFTR	Cystic Fibrosis Transmembrane Conductance Regulator
CK-AE1	Acidic Cytokeratins
CK-AE3	Basic Cytokeratins
CKs	Cytokeratins
CO ₂	Carbon Dioxide
Co-A	Coenzyme A
COPD	Chronic Obstructive Disease
COX IV	Cytochrome C Oxidase IV
COX-II	Cyclooxygenase II
CT-SCAN	Computed Tomography
CYFRA 19	Cytokeratin Fragment 19
Cyt. C	Cytochrome C
DAPI	Diamidino-2-Phenylindole
DD	Differential Diagnosis
DMEM	Dulbecco's Modified Eagle Medium
DNA	Deoxyribonucleic Acid
DSQ	Dual Stage Quadrupole
DTT	Dithiothreitol

EBC	Exhaled Breath Condensate
ECAR	Extracellular Acidification Rate
ECL	Enhanced Luminol-Based Chemiluminescent
EDTA	Ethylenediaminetetraacetic Acid
EF2	Elongation Factor 2
EGF	Epidermal Growth Factor
EGFR	Epidermal Growth Factor Receptor
ELISA	Enzyme-Linked Immunosorbent Assay
EMA	Epithelial Membrane Antigen
EMT	Endothelial-Mesenchymal Transition
ERV	Expiratory Reserve Volume
ESMO	European Society For Medical Oncology
F	Female
F(ab) ₂	Fragment Antibodies
FA	Formaldehyde
FABP	Fatty Acid-Binding Protein
FASN	Fatty Acid Synthase
FASP	Filter Aided Sample Preparation
FCCP	Carbonyl Cyanide 4-(Trifluoromethoxy)Phenylhydrazone
FDA	Food And Drug Administration
FFAs	Free Fatty Acids
FFPE	Formaldehyde-Fixed Paraffin-Embedded
FGF	Fibroblast Growth Factor
FRA	Folate Receptor Alpha
g	Gram

GC	Gas Chromatography
GCN5L2	General Control Of Amino Acid Synthesis Protein 5-Like 2
GDH	Glutamate Dehydrogenase
GLP	Good Laboratory Practice
GLUT	Glucose Transporter
GS	Glutamine Synthetase
H	Histone
H ₂ SO ₄	Sulfuric Acid
HATs	Histone Acetyl Transferases
HBDH	3-Hydroxybutyrate Dehydrogenase Enzyme
HCl	Hydrochloric Acid
HDACs	Histone Deacetylases
HER2	Herciptin 2
HRP	Horse Radish Peroxidase
<i>hrs</i>	Hours
HSP	Heat Shock Protein
IAA	Iodoacetamide
IASLC	International Association For The Study Of Lung Cancer
IC	Inhibitory Concentration
IgG	Immunoglobulin G
IgG (H+L)	Immunoglobulin (Heavy-Light)
IHC	Immunohistochemistry
ISF	Interstitial Fluid
ISH	In Situ Hybridization
iTRAQ	Isobaric Tag For Relative And Absolute Quantitation

K	Lysine
k-Ras	Kirsten Rat Sarcoma
KCl	Potassium Chloride
KH ₂ PO ₄	Potassium Biphosphate
LC-MS/MS	Liquid Chromatography-Mass Spectrometry
LCNEC	Large Cell Neurpendocrine Carcinoma
LD-CT	Low Dose CT
LDH	Lactate Dehydrogenase
LDHA	Lactate Dehydrogenase A
LDHB	Lactate Dehydrogenase B
LN	Lymph Nodes
Ln	Natural Logarythme
LT	Lung Tissue
LTQ	Linear Ion Trap
M	Male
M	Molar
m-TOR	Mammalian Target Of Rapamycin
mAb	Monoclonal Antibody
MALDI	Matrix-Assisted Laser Desorption/Ionization
MCT	Monocarboxylate Transporters
MDC1	Mediator Of DNA Damage Check Point 1
MDM2	Mouse Double Minute 2 Homolog
MHC	Major Histocpmpatibility Cells
MIF	Microphage Migration Inhibition Factor
ml	Milliliter

mM	Millimolar
MMP	Matrix Metallo-Proteinases
MPC	Mitochondrial Pyruvate Carriers
MRI	Magnetic Resonance Intensity
MRM	Multiple Reaction Monitoring
mRNA	Massenger RNA
N/C	Nucleuos/Cytoplasm
Na ₂ HPO ₄	Sodium Biphosphate
NaCl	Sodium Chloride
NAD	Nicotinamide Adenine Dinucleotide (Oxidized)
NADH	Nicotinamide Adenine Dinucleotide(Reduced)
NCAM	Neural Cell Adhesion Molecule
NE	Neuroendocrine
NETs	Neuroendocrine Tumours
NFKB	Nuclear Factor Kappa B
ng	Nanogram
NGAL	Neutrophil Lipocalin-2
NH ₄ HCO	Ammonium Bicarbonate
NK	Natural Killers
nl	Nanolitre
nM	Nanomolar
NS	Never Smoke
NSCLC	Non-Small Cell Lung Cancer
NSCLC-NOS	NSCLC- Not Otherwise Specified
NSE	Neuron-Specific Enolase

OBP2A/2B	Odorant-Binding Protein 2A And 2B
OCR	Oxygen Consumption Rate
OD	Optic Density
OP	Oxidative Phosphorylation
γ	Gamma
P	Parent
Pab	Polyclonal Antibody
PBS	Phosphate Buffered Saline
PCA	Principal Component Analysis
PCAF	P300/CBP-Associated Factor
PCNA	Proliferating Cell Nuclear Antigen
PCR	Polymerase Chain Reaction
PDAC	Pancreatic Ductal Adenocarcinoma
PDH	Pyruvate Dehydrogenase
PDHC	Pyruvate Dehydrogenase Complex
PDK	Pyruvate Dehydrogenase Kinase
PDT	Photodynamic Therapy
PEP	Phosphoenolpyruvate
PET-scan	Positron Emission Tomography
pg	Picogram
PGDS	Prostaglandin D Synthase
PGRP	Progastrin-Releasing Peptide
PHB1	Prohibitin B1
PI3K	Phosphatidyl Inositol Tri-Phosphate Kinase
PKB	Protein Kinase B

PKM	Pyruvate Kinase Muscular
PPAR	Peroxisome Proliferator-Activated Receptor
pRB	Retinoplastoma Protein
ProGRP	Progastrin-Releasing Peptide
PS	Passive Smoking
PS-F	PS-Fpassive Smokers Free
PSA	Prostate Surface Antigen
PTM	Post-Translation Modification
Q	Quadrant
QC	Quality Control
QSP	Quiescence-Specific Protein
R	Resistant Cells
R-	Resistant Un-Treated
R+	Resistant Treated
RAR	Retinoic Acid Receptor
RBP	Retinol-Binding Protein
RET	Receptor Tyrosine-Protein Kinase
RIA	Radioimmunoassay
RNA	Ribonucleic Acid
ROS	Reactive Oxygen Species
rpm	Round Per Minute
RPMI	Roswell Park Memorial Institute Medium
RT	Retention Time
RT	Room Temperature
RT-PCR	Real Time Polymerase Chain Reaction

RUNX3	Runt-Related Transcription Factor 3
RXR	Retinoid X Nuclear Receptor
SAHA	Suberanimohydroxamic Acid
SCC	Small Cell Carcinoma
SCCA	Squamous Cell Carcinoma Antigen
SCLC	Small Cell Lung Cancer
SDHA	Succinate Dehydrogenase A
SDS	Sodium Dodecylsulphate
SELDI	Surface-Enhanced Laser Desorption/Ionization
SGS	Second Generation Sequencing
SILAC	Stable Isotope Labelling With Amino Acids In Cell Culture
SOD1	Superoxide Dismutase
SQ	Squamous Carcinoma
SqCC	Squamous Cell Carcinoma
STDV	Standard Deviation
TB	Tuberculosis
TC	Typical Carcinoid
TCA	Tricarboxylic Acid Cycle
TFA	Trifluoro Acetic Acid
TGF- β	Transforming Growth Factor Beta
TIMP	Tissue Inhibitor Of Metalloproteinase
TKI	Tyrosin Kinase Inhibitor
TM	Tumour Markers
TMA _s	Tissue Microarrays
TMB	Tetramethylbenzidine

TMRE	Tetramethylrhodamine, Ethyl Ester
TNF	Tumour Necrosis Factor
TNF- α	Tumour Necrosis Factor Alpha
TNM	Tumour/Lymph Node/Metastasis
TPA	Tissue Polypeptide Antigen
TTF1	Thyroid Transcription Factor 1
TTF1	Thyroid Transcription Factor 1
Ub-PCNA	Ubiquitinated-PCNA
UHPLC	Ultra High Pressure Liquid Chromatography
V	Voltage
VDAC	Voltage Dependent Anionic Channel
VEGF	Vascular Endothelial Growth Factor
VEGP	Von Ebner's-Gland Protein
WBCs	White Blood Cells
WHO	World Health Organization
α/β	Alpha/Beta
μg	Microgram
μl	Microlitre
μM	Micro Molar
μm	Micrometer

Abstract

Lung cancer is the most common cause of death from cancer worldwide, estimated to be responsible for nearly one in five (1.59 million deaths, 19.4% of the total). Lung cancer is acknowledged as a complex and heterogeneous disease, not only at the biochemical level (genes, proteins, metabolites) but also at the tissue, organism, and population level. In the past decade, with the advancements in high-throughput profiling technologies, a huge amount of work has been done to derive biomarkers to supplement clinical diagnosis. The levels of a variety of different biomarkers, such as proteins and metabolites, in biological fluid or tissue/cells could potentially detect cancer at an early stage, determine cancer subtype, or monitor the sensitivity/resistance to cancer treatment.

The research in this thesis aims to discover new biomarkers, using proteomic techniques, with the potential to supplement current clinical criteria for the management of lung cancer patients. Label-free mass spectrometry of bronchoalveolar lavage fluid (BALF), blood (serum), tissue and cell lines was performed to identify candidate biomarkers and perturbed cellular pathways. Validation of significant results was performed using immunological methods and biochemical assays.

These studies have yielded valuable information that has unravelled several key molecular events of lung cancer tumorigenesis, including proteomic signature of lung cancer in BALF, tissue and blood. BALF analysis identified a promising signature distinguish between adenocarcinoma of the lung and squamous cell carcinoma of the lung. Many proteins found to be significant changed in abundance in BALF also displayed similar trends in tissue specimens. Tumour heterogeneity was also evident when examining tumour specimens, reinforcing the need for panels of biomarkers and multiple sampling. A strong metabolic pattern was also evident during proteomics

based investigations of clinical material, a result that was confirmed using metabolomics platforms to screen patient samples. Drug resistant protein patterns were also identified using label-free mass spectrometry on cell lines models demonstrating resistance to Apatolisib (GDC-0980), a dual phosphatidylinositol-3-kinase and mammalian target of rapamycin kinase inhibitor. Early in vitro data on resistant mechanisms associated with new lung cancer treatments is crucial to allow resistance to be detected in patients and to understand and potentially target resistant pathways. The molecular analysis of a variety of biospecimens has allowed the discovery of relevant candidate biomarkers and consequently the identification of novel proteins that may have a role in the development of lung cancer and establishment of drug resistance. There is a need for incorporating findings from multiple discovery platforms and multiple sample types into a lung cancer specific data framework that can improve our level of understanding of the disease process.

Chapter 1

Introduction

1. Introduction

1.1. Lung cancer

Cancer is one of the feared life-threatening diseases, and its global incidence has increased concomitantly with the increase in population size (Chen et al., 2016, Saika and Sobue, 2013, Vollmer et al., 1985). Cancer does not discriminate poor from rich people, and the disease prevalence is directly proportional to the mean age of the population. Lung cancers are solid tumours that are difficult to cure. Nearly 50% of people with lung cancer die within the first 12 months after diagnosis, and only 15-18% of them survive for 5 years if they receive proper treatment (Zappa and Mousa, 2016).

1.2. Prevalence of lung cancer

The cancer statistics centre of the American Cancer Society reported that lung cancer came in the second place after breast cancer in the estimated future prevalence of the disease in women (Siegel et al., 2017). In 2017, the estimated new cases of lung cancer in both sexes was 222,500 and of breast cancer 255,180. The presence of breast cancer at the top of the list likely reflects the efforts of the health authorities and civil societies to familiarize women with the disease at schools, colleges and other locations and to the availability of free mammogram examinations. From another perspective, lung cancer is at the top of the list of estimated deaths, causing 155,870 deaths compared to 41,070 deaths from breast cancer, which came in fourth place (Siegel et al., 2017). This too reflects the importance of early diagnosis in the outcome of cancer treatment. In Ireland, only 20% of lung cancers are diagnosed at stage I, while 35-40% are diagnosed at the metastatic stage (stage IV). Interestingly, between 1994 and 2014, the incidence of lung cancer among women in Ireland increased from 28 to 42 per 100,000

per year, with an annual increase in the rate of 2.3%. In contrast, in men it decreased from 70 to 52 per 100,000 per year, which represents a decline rate of 0.8% annually. Concomitantly, the number of deaths has also increased in women by 0.4% but in men it declined by 1.8%. This discrepancy might reflect the increase among Irish women (compared to men) in the number of smokers and exposure to other predisposing factors such as alcohol consumption and passive smoking. The survival rate among lung cancer patients in general has improved in Ireland, where it doubled from 9% (1994-1998) to 17.9% (2009-2013). In Ireland, during 2012-2014 about 85% of lung cancer cases were diagnosed by histopathology; treatment involved surgery in 20% of cases, chemotherapy in 33%, and radiotherapy in 36% (Irish Cancer Registry). In China, analysis of data taken from 72 national cancer registries in 2015 showed an estimate of 4,292,000 new cancer cases and 2,814,000 deaths from lung cancer, which was the leading cause of death among cancer patients (Chen et al., 2016).

In Libya, among 3307 cancer cases recorded in the eastern region cancer registry between 2003 and the end of 2005, lung carcinoma accounted for 18.9% of the cases in men but none among women (Bodalal et al., 2014, El Mistiri et al., 2007, El Mistiri et al., 2015). The survival rate among all the registered cancer cases was 19.8% in men and 28.2% in women (El Mistiri et al., 2007). According to the Western Libya cancer registry, lung cancer accounts for 15.6% of cancers, while no case among women was documented (Alhdiri et al., 2017, Taha Beyased1, 2017, TAHA BEYASED1 and NUREDDIN ASHAMMAKHI, 2017, TAHA BEYASED, 2017). In Libya, smoking is uncommon and socially unacceptable among women, this might interpret the low rate of lung cancer incidence among women compared to men and other types of cancer.

1.3. Risk factors

The best-known illness related to the modern lifestyle is depression resulting from increased daily exposure to noise from our industrial environment. Depression contributes partially to the incidence of cancer. The results of 25 independent studies including a total of 1,469,179 participants and 89,716 cancer cases showed a significant association of depression with lung and liver cancer incidence but no significant correlation with breast, prostate, colorectal or colon cancers (Jia et al., 2017). Depression is associated with reduced natural killer cells activity (Irwin and Miller, 2007), possibly due to increased cortisol levels among depressed people (Katuri et al., 2016). In industrial countries, the environment is a major contributor to the incidence of lung cancer (Cuadras et al., 2016) (Figure 1).

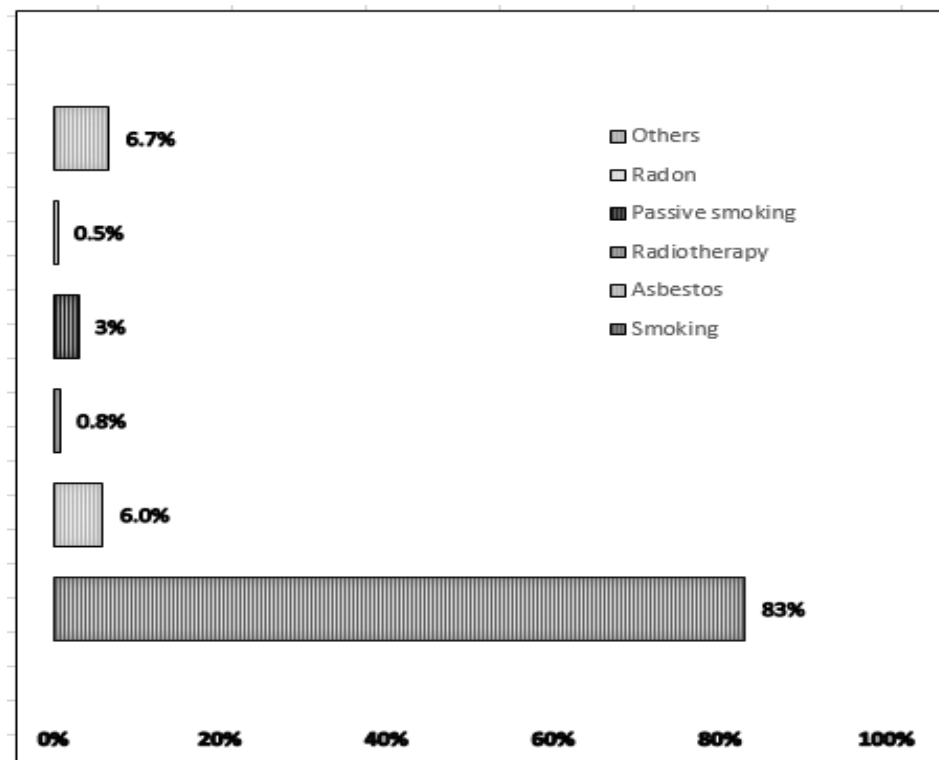


Figure 1: The major environmental causes of lung cancer (Cuadras et al., 2016)

Cigarettes smoking is a major cause of lung cancer, with 10-15% of smokers developing the disease at a late stage of life, and it accounts for almost 86% of all lung cancer cases, including passive smoking (Mattson et al., 1987). The effect of cigarette smoking as a factor predisposing to lung cancer is higher among individuals who started smoking as teenagers. Among never smokers (NS), passive smoking is less dangerous than active smoking, but it can still increase the susceptibility to lung cancer by 25% in comparison to NS who are not exposed to passive smoking. On the other hand, regular consumption of cigarettes and heavy exposure of NS to tobacco smoke contribute towards increasing the risk of lung cancer by almost 50% (Wang et al., 2015).

Smoking is responsible for almost 50% of squamous cell carcinomas (SqCC) and 20% of adenocarcinoma among smokers; the opposite percentages were seen in lung cancer patients who never smoked. Kirsten rat sarcoma 2 viral oncogen (K-Ras) gene mutation is rarely seen in patients who never smoked, but it is very common among smokers; the opposite is true for epidermal growth factor receptor (EGFR) gene amplification, which is common in patients who never smoked (Helland and Brustugun, 2009). Exposure to asbestos cement materials also contributes to the increased susceptibility to lung cancer in individuals with past lung-related diseases or genetic susceptibility to pleural mesothelioma and lung cancer (Oddone et al., 2014). Exposure to radiation is also a risk factor for lung cancer; radiation increases the rate of gene mutations in normal tissues and facilitates transition of pre-cancer tissues to malignancy (Li et al., 2017).

Genetic susceptibility to lung cancer differs from one individual to another. Oncogenes are involved in the activation of cell growth and division, whereas tumour suppressor genes suppress these processes (Bello and Rey, 1995). The correct

balance between oncogenes and tumour suppressor genes as well as the existence of a healthy DNA repair system are the most important cornerstones in protection against cancer. The gene repair machinery's ability to repair acquired mutations also plays an important role in susceptibility (Spitz et al., 2003) and/or protection against the disease (Valdiglesias et al., 2011). Genetic polymorphism, *e.g.* in epidermal growth factor receptors (EGFRs) can contribute to increased susceptibility to lung cancer and failure of treatment using tyrosine kinase inhibitors (TKI), such genetic polymorphism can be utilized in the prediction of tumour resistance to TKI (Wang et al., 2017b). DNA-repair gene polymorphism (Yu et al., 2008) can enhance and facilitate the production of bulky DNA adducts (conjugates between large reactive electrophiles and DNA) by environmental agents and is associated with increased risk of lung cancer (Munnia et al., 2017). Inheritance of the susceptibility to cancer differs between people. Death of one family member from lung cancer or current hospitalisation for treatment of lung cancer also represents a risk factor contributing to increased susceptibility of other family members to developing lung cancer; the risk is increased by daily exposure to different predisposing agents (Mattson et al., 1987).

1.4. Classification of lung cancer

Most lung cancers are incidentally detected in x-rays or CT-scans done for other reasons such as trauma or lung tuberculosis (TB) screening of some job seekers (Lana et al., 2014). Two main cornerstones in diagnosis of lung cancer are important for proper selection of treatment and precise prediction of treatment outcome. The first cornerstone is to correctly determine the histological type of the tumour (Gibbs and Thunnissen, 2001, Shimosato, 2002). The second is to stage it correctly (Heelan, 2004).

Histopathological diagnosis of lung cancer relies on cell morphology and the nucleus-to-cytoplasm size ratio (N/C ratio) (Su Lim et al., 2015) to distinguish small cell lung cancer (SCLC) from non-small lung cancer (NSCLC) by light microscopy of tissue biopsy (Gibbs and Thunnissen, 2001). Reactivity (level of expression) to at least one neuroendocrine immune-histochemical (IHC) marker helps to differentiate SCLC from NSCLC and also neuroendocrine from non-neuroendocrine non-small cell carcinomas (Feng et al., 2016). Information on the patient's lifestyle and smoking habits might aid in distinguishing between SqCC and adenocarcinoma (Okamoto et al., 2014). The concern was always about the lack of microscopic characterization reproducibility between the different sections of same biopsies as only 30% of lung carcinomas originate from a single cell and the rest are histologically heterogeneous (Junker, 2000). Incorrect histological typing or staging, late diagnosis, and complex heterogeneity of the intra-tumour microenvironment are the top factors responsible for treatment failure (Hirsch et al., 2002). Better molecular characterisation of lung carcinomas would considerably improve patient outcome by enhancing diagnosis precision and treatment selection. This is part of the scope of this study. Histologically, lung cancer is classified into two main categories: SCLC and NSCLC (Neal et al., 2014). Based on their cell type origin, primary lung tumours (Figure 2) are classified into two types: (1) neuroendocrine (NETs) carcinoma, which includes SCLC, large cell neuroendocrine carcinoma (LCNEC) and both typical and atypical forms of lung carcinoids; (2) non-neuroendocrine lung carcinomas, including SqCC and adenocarcinomas (Rekhtman, 2010).

1.4.1. Neuroendocrine lung tumours (NETs)

Neuroendocrine lung tumours account for 25% of lung cancers and are graded as low grade typical carcinoid (TC), intermediate grade atypical carcinoid (AC), or high grade carcinomas, including LCNEC and SCLC (Travis et al., 2010).

1.4.1.1. Small cell lung cancer (SCLC)

This type of lung cancer is usually seen near the bronchi and is mostly caused by chronic tobacco smoking (Figure 2). SCLC is the most commonly diagnosed lung neuroendocrine tumour, representing 20% of lung cancers and 95% of lung NETs. Only 5% of all small-cell tumours are diagnosed outside the lungs (bladder, uterus, cervix and oesophagus). Therefore, most metastatic small-cell cancers of the bones originate from primary tumours in the lung (Powell, 1988). Most patients diagnosed with SCLC have nodal metastasis in the lung hilar region. Late stages of lung SCLC commonly metastasise to the bone marrow, bones or liver (Bos et al., 2009), and in 50-80% of patients with SCLC spread to the brain (Samson et al., 2007).

SCLC tumour biopsies, based on their levels of neuroendocrine markers expression, react strongly to neural cell adhesion molecule (NCAM/CD5/6) mAbs (highly expressed) (Hiroshima et al., 2006), weakly reactive to synaptophysin and chromogranin (Hiroshima et al., 2006), very weakly reactive to cytokeratins (CKs) such as CK-AE1 and AE3 mAbs (expressed at very low amounts) (Cerilli et al., 2001). SCLC is also strongly reactive (highly expressed) (90% of SCLC) to thyroid transcription factor 1 (TTF1), which is expressed in the brain and lungs in addition to the thyroid glands, and is considered as a very specific marker for primary lung small cell carcinoma (SCLC) but not extra-pulmonary metastasis (Ordóñez, 2000).

In general, SCLC is a very aggressive cancer that spreads rapidly and has a bad prognosis. Only 5% of SCLC patients survive for 5 years from the date of diagnosis

(Rekhtman, 2010). SCLC is sensitive to radiotherapy, cisplatin, etoposide, and combination regimens (Samson et al., 2007). SCLC can be pure (70%) or mixed (30%) with NSCLC (adenocarcinoma, SqCC, large cell carcinoma or carcinoids) (Vollmer et al., 1985). Limited SCLC is treated with cisplatin + etoposide + radiotherapy, whereas extensive SCLC is treated only with chemotherapy (Byers and Rudin, 2015).

1.4.1.2. Large-cell neuroendocrine lung cancer (LCNEC)

Large-cell neuroendocrine lung cancer (LCNEC) is very rare (Figure 2). This carcinoma grows rapidly, has a poor prognosis (Filosso et al., 2017) and accounts for 3% of all lung neuroendocrine tumours (Rekhtman, 2010). LCNEC is considered to be less progressive than SCLCs, with a 5-year survival rate of 50% (Iyoda et al., 2007).

LCNEC is staged according to the staging guidelines of the American Joint Committee on Cancer (tumour, node, and metastasis; TNM) (Battafarano et al., 2005). The same criteria are applied to NSCLC, but LCNEC can be distinguished from NSCLC by its reactivity (high expression) to at least one neuroendocrine marker (*e.g.*, Synaptophysin, CD56 or chromogranin A) and thyroid transcription factor (TTF1) (Wiatrowska et al., 2001, Travis et al., 2010, Travis et al., 2015b). It is also distinguished from SCLC by the large nucleus, abundant cytoplasm, and high nucleus-to-cytoplasm ratio (Hiroshima et al., 2006). TTF1 is also expressed

Figure 2 shows the main histological types of lung cancer, how they look like under the light microscope (top panel), the rate of their incidence among lung cancer (LC) (second panel) and male and female incidence ratio (third panel). The figure also shows the correlation between smoking and the incidence of each type of lung cancer (4th and 5th panels) and the overall level of each lung cancer type aggression (6th

panel), their early metastability (7th panel) and the outcome of surgical resection (8th panel).

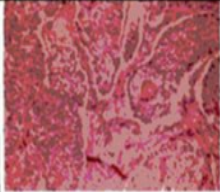
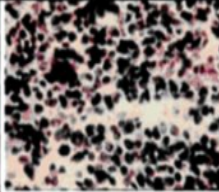
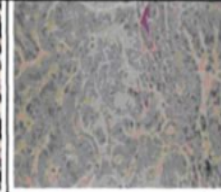
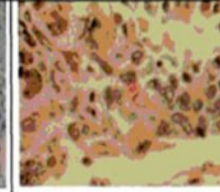
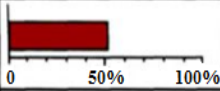
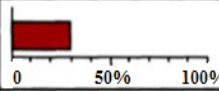
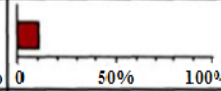
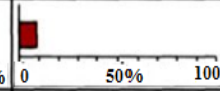




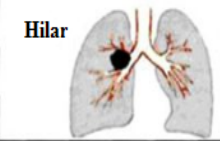
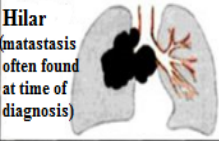
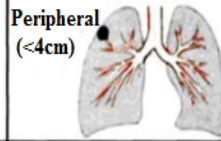
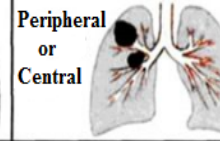
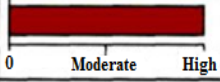
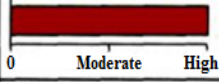
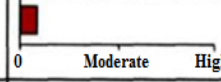

Classification of Primary Lung Carcinomas				
Type	Epidermoid (Squamous)	Small cell anaplastic (Oat)	Adenocarcinoma	Large cell anaplastic
Histology				
Incidence among LC				
Sex				
Lung position	Hilar 	Hilar (metastasis often found at time of diagnosis) 	Peripheral (<4cm) 	Peripheral or Central 
Smoking				
Growth rate	Relatively slow	Very rapid	Intermediate	Rapid
Spread	Late to hilar nodes	Very early (distally /MS)	Intermediate	Early
SR	Fair	0	Poor	Poor

Figure 2: The main histological types of lung cancer. LC: lung cancer, SR: surgical resectability (Modified from respiratory system diseases, lung cancer, PPT by Ya. Bodnar and Frank H. Netter's illustrations).

in neuroendocrine tumours outside the lungs, as in the male genitourinary tract, so it cannot be used to assess secondary tumours (Alijo Serrano et al., 2007). LCNEC is a good candidate for surgical treatment with adjuvant cisplatin-etoposide chemotherapy combined with radiotherapy (Prelaj et al., 2017).

1.4.1.3. Lung carcinoid tumours

Carcinoid tumours account for 20% of all well-differentiated neuroendocrine tumours in humans. Lung carcinoid tumours account for only 2.2% of all neuroendocrine lung tumours and are of two types: typical carcinoids (TC), which

account for 2% of lung NETs, and atypical carcinoids (ACs), the rarest lung carcinoid tumour, which accounts for only 0.2% of lung NETs (Rekhtman, 2010). Starting from the 7th edition of the International Association for the study of lung cancer (IASLC) staging committee, lung carcinoid tumours are to be staged according to the criteria used for staging NSCLC (Travis et al., 2008). In histopathological examination, carcinoids are distinguished from SCLC by their strong reactivity (high expression) to synaptophysin & chromogranin and weak reactivity to CD5/6 markers (expressed at low levels). About $50 \pm 25\%$ (Mean/STDV) of SCLCs exhibit negative or very weak reactivity to synaptophysin and chromogranin (expressed at very low levels) but strong reactivity to CD5/6 (highly expressed) (Hiroshima et al., 2006, Marchevsky and Wick, 2015). The opposite is true for reactivity to TTF1 (highly expressed), with 90% of SCLCs strongly reacting to the marker made it specific for SCLC (Ordóñez, 2000). Non-metastasized carcinoids are cured by surgery whereas metastatic carcinoids require post-surgical chemotherapy and radiotherapy (Hilal, 2017).

1.4.2. Non-neuroendocrine non-small cell lung tumours

1.4.2.1. Lung adenocarcinoma

Lung adenocarcinoma, the most common lung cancer in individuals who have never smoked, accounts for 40% of lung cancers and usually arises from the alveoli (Figure 2). The well-differentiated adenocarcinomas have papillary and acinar growth patterns, whereas the poorly differentiated ones might exist as solid cribriform clusters that can be distinguished from LCNEC only by their reactivity to neuroendocrine markers (Jiang et al., 1998, Rekhtman, 2010). Besides positive mucin staining, adenocarcinoma reacts positively in IHC with TTF-1, Napsin A, and CK7 markers (Kerr et al., 2014). Up to 20% of NSCLC have reactivity to one or

more neuroendocrine IHC markers, which is common for adenocarcinoma but not for SqCC (Rekhtman et al., 2011), though SqCC has NSCLC morphology (*i.e.*, no neuroendocrine morphological changes) (Berendsen et al., 1989, Iyoda et al., 2001). In contrast, some NSCLC resemble LCNEC morphologically but their reactivity to neuroendocrine markers is very difficult to confirm by IHC (González-Aragoneses et al., 2007).

1.4.2.2. Lung squamous cell carcinoma (SqCC)

Lung SqCC tumours (Figure 2) grow slowly, arise mainly in the large airways, and are strongly associated with chronic tobacco smoking (Kenfield et al., 2008). Lung SqCC is characterised, like any other NSCLC, by its high nucleus to cytoplasm ratio (N/C ratio) (Su Lim et al., 2015) and is diagnosed immunohistochemically by its expression of P63, P40, 4A4 and high molecular weight cytokeratins (CK5/6) or 34βE12, but not TTF1 (Rekhtman, 2010, Bini et al., 2008, Kerr et al., 2014).

In 2011, Rekhtman *et al.* tested 315 resected tumours, including adenocarcinomas (n=200) and SqCC (n=115), for their reactivity to the IHC markers commonly used to differentiate adeno from SqCC: TTF-1, P63, cytokeratin 5/6 and 34βE12. The only specific marker clustering lung adenocarcinoma from SqCC was TTF-1, and none of the SqCC specimens showed reactivity to it even in diffuse tumours. Adenocarcinomas were widely heterogeneous in responding to SqCC-specific markers. 38 Out of the 315 NSCLC tissue samples were morphologically unclassifiable small biopsies/cytology specimens. Analysis of the whole tissue sections showed that squamous cell carcinomas had a highly consistent IHC profile (negativity to TTF-1 and p63/CK5/6 AND 34βE12 with small variation). In contrast, adenocarcinoma specimens showed significant IHC heterogeneity for squamous carcinoma markers where; 32% of them showed reactivity to P63, 18% to CK-5/6,

82% to 34βE12, and 89% to TTF-1 (Rekhtman et al., 2011). A panel of TTF-1/P63 and CK5/6 markers eliminates any overlap between AD and SqCC.

Before deciding on the treatment of a patient with SqCC, samples should be analysed immunohistochemically for DNA mutations by *in situ* hybridization (ISH) or DNA-based technologies. Treatment-naive adenocarcinomas with activating EGRF mutations respond effectively to the first generation tyrosine kinase inhibitors (Gefitinib, erlotinib, afatinib) rather than to chemotherapy (Kerr et al., 2014). ALK rearrangement is very common in lung adenocarcinomas, very rare in SqCC and also seen in adenosquamous mixed lung carcinomas. Adenocarcinomas with ALK rearrangement respond well to crizotinib (Chaft et al., 2012). The second European Society for Medical Oncology (ESMO) consensus conference on lung cancer recommends that before starting treatment, the tumour should be screened for human epidermal growth factor receptor 2 (HER2) amplification, BRAF mutations, and rearrangement of serine/threonine kinases ROS1 and RET (Cardarella and Johnson, 2013, Marchetti et al., 2013).

Good laboratory practice for diagnosis of lung cancer relies on the examination of the entire tumour mass (Teng, 2005). Not all of lung tumours are intended for surgical resection, therefore, obtaining the right histopathological diagnosis using small tissue biopsies remains a high bar. However, ESMO recommends classification of specimens with no definitive morphological evidence of squamous or glandular differentiation as well as heterogeneous adenocarcinomas as NSCLC-non otherwise specified (NSCLC-NOS) (Thomas et al., 1993, Chuang et al., 1984, Edwards et al., 2000).

1.5. Lung cancer metastasis

The exchange of gases and nutrients at the cellular level between arterioles and venules occurs *via* the interstitial fluid, which is formed by secretion of plasma from the fine arterioles into the extracellular space, followed by its reabsorption through capillary venules. The plasma secreted into the interstitial space carries waste products coming from vital organs such as the lungs, liver, colon, and kidneys (Liao and von der Weid, 2015), and possibly infectious materials, including bacteria and viruses. About 90% of the interstitial fluid is reabsorbed and the rest enters the lymphatic vessels, where it is called the lymph. The lymph also helps in restoration of proteins and absorption of fats from the interstitial space back into the blood circulation.

The lymph also serves as a continuous sample of the interstitial space that is reported to the immune system. It contains micro-organisms (MOs), antigen presenting cells and B-cells (Jewell et al., 2014) that are moved towards local lymph nodes through the afferent lymphatic vessels drainage (Blum and Pabst, 2006), to the sub-capsular sinus, towards the cortical sinus, and then further to the medullary sinuses. The immunological response in the lymph nodes is initiated by antigen presenting cells (dendritic cells) capturing the microbial antigens or cancer-specific antigens (recognised by altered post-translational modification signatures, *e.g.*, an altered human glycan signature) (Summerfield and McCullough, 2009). Dendritic cells present captured antigen(s) in association with MHC-II complex to naive T- cells to start adaptive immunological responses. Dendritic cells also present the antigen in the context of MHC-II to B-lymphocytes, triggering their differentiation into antibody-producing plasma cells (Wykes and MacPherson, 2000). The antibodies facilitate micro-organisms (MOs) opsonization and clearance through the

reticuloendothelial system (bone marrow, spleen and liver) (Randolph et al., 2005). Activation of B-lymphocytes is also involved in the maturation of T-lymphocytes to generate natural killers (NK) and the memory cells (Waithman and Mintern, 2012). The lymph leaves the medullary sinuses of the lymph nodes in one direction through the efferent lymphatic vessels, which form larger lymphatic vessels as they proceed away from the lymph nodes towards the subclavian veins on the sides of the neck (Liao and von der Weid, 2015).

Metastasis of cancer cells involves morphological changes. Endothelial-mesenchymal transition (EMT) facilitates their penetration into and out of blood vessels (Castañón et al., 2017), enabling tumour cells to leave the primary tumour, enter the blood stream, or invade local lymph nodes. Cells that migrate through the blood circulation attach to the blood vessels and infiltrate into new organs by virtue of organ-specific genes (Bos et al., 2009). Cancer cells extravasate into the bone marrow relatively easily through the fenestrated endothelium lining the sinusoid capillaries. Extravasation into the pulmonary parenchyma requires the expression of certain genes that mediate vasodilatation and increase blood vessel permeability, *e.g.*, Cyclooxygenase-2 (Bos et al., 2009). Lung cancer cells grow at the primary tumour, spread into the mediastinal lymph nodes, and migrate *via* the blood to other organs, such as the liver (Wakabayashi et al., 2017). Detection of lymphatic metastasis is important for treatment decisions, prognosis and outcome. Several methods are available for mapping the thoracic lymphatic node drainage of the tumour and for sampling the sentinel node from the regional lymph nodes drainage (Karaman and Detmar, 2014).

1.6. TNM staging

Cancer staging facilitates the exchange of information between clinicians about their cancer patients in order to choose the optimal treatment protocol for each patient. The staging and grading of cancer is also helpful in prognosis and prediction of treatment outcome (Telloni, 2017). The TNM staging system provides a descriptive clinical assessment of the tumour. Staging of SCLC is different from that of NSCLC (Kodama, 1997). SCLC is staged by the American Veterans Administration System (AVAS) as limited when the tumour nodules remain in one lung lobe and extensive when they spread to the other lung and other parts of the body. The TNM staging system still needs to be adopted towards using for staging of SCLC, as well as towards decision of surgical candidates of SCLC (Chen, 2016). In the TNM staging system of NSCLC, tumour nodules that are still growing locally are referred to as (T) and the size of each nodule is recorded. Involvement of lymph nodes is symbolized as (N), and the number and sizes of lymph nodes involved is recorded. Due to the continuously increasing knowledge of cancer brought about by the use of genomic and proteomic profiling of tumours by second generation sequencing (SGS) and mass spectrometry, this staging protocol is updated annually (Telloni, 2017). TNM staging describes the size and location of the tumours and the existence of metastasis (Donnem et al., 2015). Two methods are used for TNM staging of lung cancer. Clinical staging, which is less accurate, is based on physical examination, imaging (chest x-ray, ultra-sound, CT-scan, MRI or PET-scan) and laboratory tests. Histopathologic or pathological staging is more accurate but is very invasive and not tolerated by patients because of the need for surgery.

In TNM staging of lung cancer, patients undergo a series of investigations that can include ultrasonography, computed axial tomography (CT) and magnetic resonance

imaging (MRI). Ultrasound is considered the best method for detecting lymph nodes and metastasis. It is low cost, non-invasive, reproducible, and suitable for follow-up. However, CT-scan is considered superior by almost all clinicians dealing with head and neck lymph node pathology. The addition of contrast media, digital reconstruction, temporal and spatial high resolution images and fine-cut images has made CT-scan effective and efficient for lung cancer staging (Table 1).

Magnetic resonance imaging (MRI) is convenient and effective for assessing the anatomical structure of soft tissues in head and neck cancer (Gujam et al., 2014). The International Association for the Study of Lung Cancer (IASLC) has proposed revisions based on the evaluation of outcomes in an extensive worldwide database (Tanoue and Detterbeck, 2009). The seventh TNM staging edition (Table 1) issued by the IASLC remained in use in the CT-scan Olympic software until January 2017. The only change made on the TNM staging system in the seventh edition is that the N category depends on the number of zones involved (Figures 3 & 4), and the M extends to distinguish oligo metastatic from extra thoracic spread (Edge and Compton, 2010, Chassagnon et al., 2017).

Table 1: The 7th edition of IASLC TNM staging system (Chassagnon et al., 2017)

		PRIMARY TUMOR (T)					
		T1	T2	T3	T4		
LYMPHNODES (N)	N3	Stage III B				M1	METASTASIS (M)
	N2	Stage II A		Stage III A			
	N1	Stage I A	Stage I B	Stage II A	Stage II B		
	N0	Stage I A	Stage I B	Stage II A	Stage II B		

Stage -- (--, --, --)

reset i demo

Where; *N*: number of lymph node involved, *M*: number of metastatic lesions outside lung, *T*: number of tumour nodules. Stage IA: one primary tumour nodule and no lymph node involved. Stage IB: no lymph node involved and another lung nodule might exist. Stage IIA: one or two primary tumour nodules and one lymph node is involved. Stage IIB: three lung primary nodules or two nodules and one lymph node is involved. Stage IIIA: upto four primary nodules plus one or two lymph nodes are involved. Stage IIIB: upto four primary tumour nodules and three lymph nodes are involved. Stages from IA to IIIB: no outside lung spread of the tumour (M0). Stage IV: indicates outside lung spread of the tumour (minimum of M1) regardless of the number of the primary tumour nodules and the lymph nodes involved (usually >3).

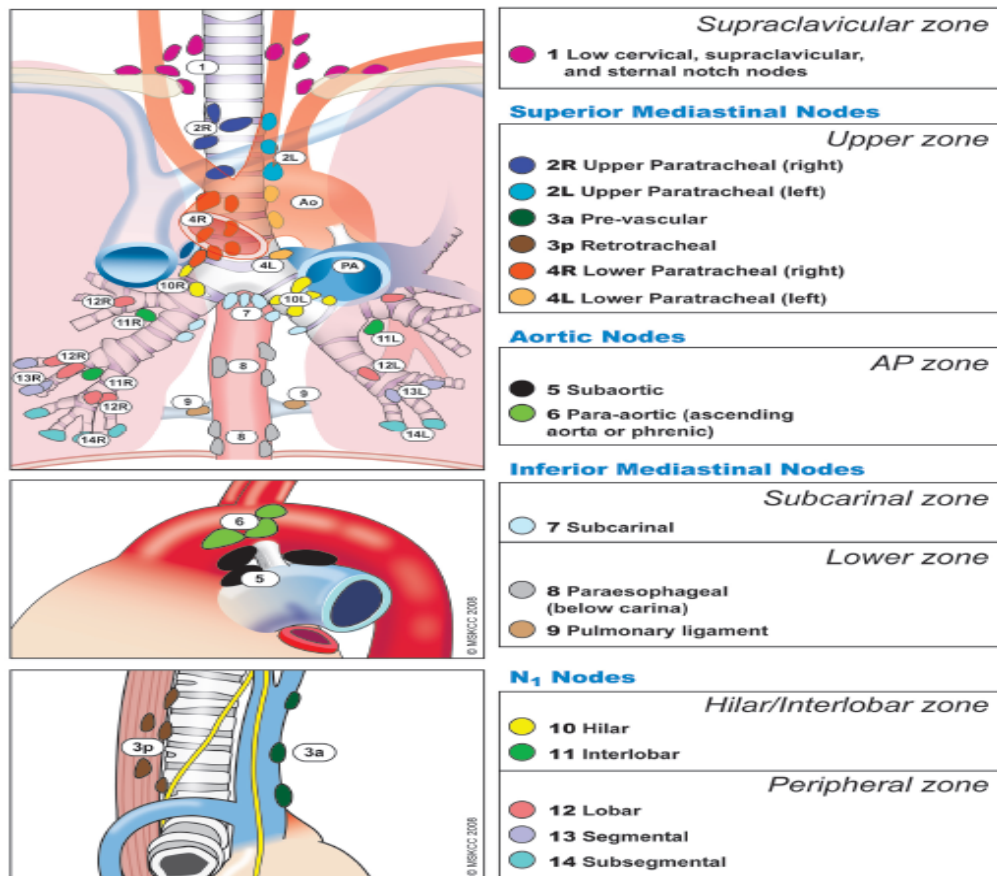


Figure 3: A systematic reference of the thoracic lymph nodes used in Olympus CT scan lymph node mapping for TNM staging. Modified from the American Joint Committee on Cancer (AJCC) 7th Edition TNM staging posters provided by the American Cancer Society (Edge and Compton, 2010).

The purpose of improving the TNM staging system is to help select the right candidates for radiotherapy or surgery. A combination of positron emission tomography (PET-scan) using 18F-FDG as a tumour tracer and computed tomography scan helps to reduce the number of CT-scan based TNM-staging candidates who queue for radiotherapy (RT) by approximately 34% (Abramyuk et al., 2012).

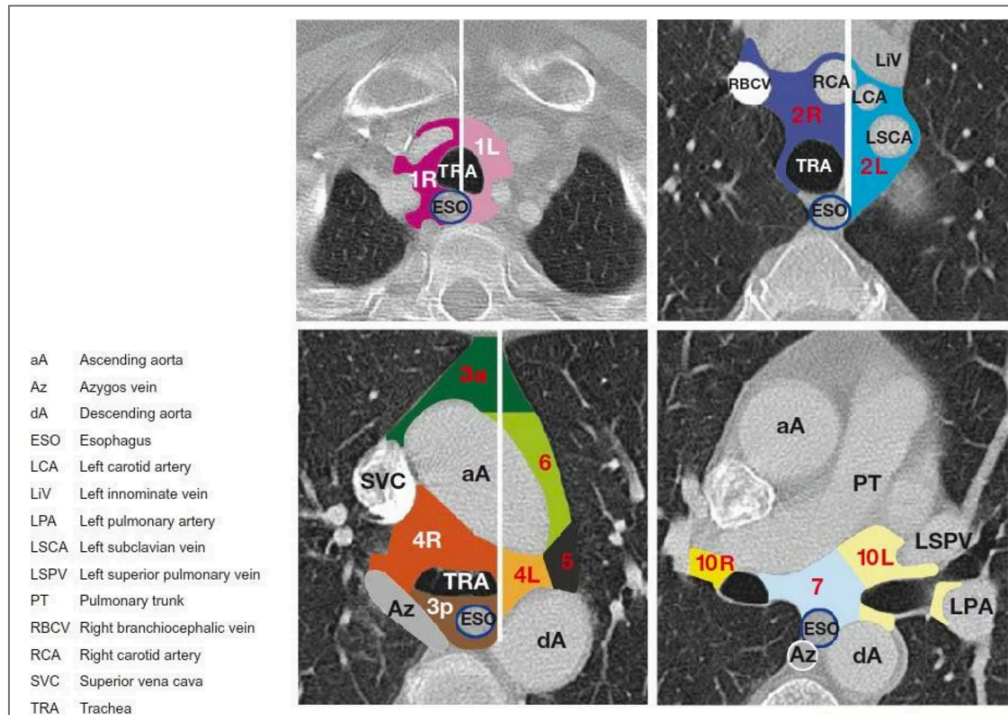


Figure 4: Olympus CT scan lymph node mapping for TNM staging (Abramyuk et al., 2012). aA: Ascending aorta, Az: Azygos vein, dA: descending aorta, ESO: esophagus, LCA: left carotid artery, LiV: left innominate vein, left pulmonary artery, LSCA: left subclavian vein, LSPV: left superior pulmonary vein, PT: pulmonary trunk, RBCV: right bronchocephalic vein, RCA: right carotid artery, superior vena cava, TRA: trachea.

1.7. Lung cancer grading

Grading of cancer is a descriptive microscopic examination of cancer biopsies reflecting how likely the lung cancer would spread rapidly, and it has important prognostic value (Carriaga and Henson, 1995). A successful histopathology report relies on collection of a representative tumour tissue biopsy that will not compromise the treatment decision. In 1988, Ehrhart described the basic techniques of biopsy acquisition and handling as well as surgical margin resection (Ehrhart, 1998). Basically, cancer is graded as well-differentiated (cells are organised as in normal tissue) or poorly differentiated (cells are not organised as in normal tissue). Depending on the percentage of abnormal cells, cancer grading is usually rated as follows:

Gx (undetermined grade): cells are very difficult to distinguish from normal tissues;

G1 (low grade): well-differentiated;

G2: (intermediate grade) moderately differentiated;

G3: (high grade) cells appear different from normal tissue control or poorly differentiated;

G4: (high grade): undifferentiated tumour cells, in which the cells of the tumour tissue biopsies appear totally different.

In Gx and G1, tumour growth is very slow. In grades 3 and 4, the organisation of the cells is heterogeneous and not unique. The tumour's ability to grow and metastasise aggressively is maximal in grade 4 (Powers et al., 1995, Carriaga and Henson, 1995).

1.8. Lung cancer screening of high risk groups

1.8.1. Low-dose computed tomography

The screening examination that is most recommended for lung cancer is low-dose computed tomography (often called low-dose CT scan or LDCT). During this test, an X-ray machine scans the body with low doses of x-ray radiation to make exceptionally detailed images of the lungs. As a benefit, low-dose computed tomography uses less ionising radiation than a standard CT scan. The benefit of screening is that it can detect disease early before the first symptoms appear, when it is most treatable. A screening test is not considered completely effective until it manages to reduce the number of deaths caused by the given disease. Screening by low-dose CT-scan was found to reduce lung cancer-specific mortality by 20% in high risk groups (Chiles, 2014). Detailed protocols demonstrating practical and technical issues to be considered have been reviewed in (Marshall et al., 2013).

1.8.2. Sputum cytology

Microscopic examination of sputum (mucus) can detect the presence of abnormal cells such as cancerous cells (Thunnissen, 2003, Ammanagi et al., 2012). Sputum may be collected by asking the patient to cough up mucus or breath in saltwater mist and then cough; it can also be collected during bronchoscopy (Su et al., 2015). However, sputum cytology is not currently used to screen people who are particularly at risk of lung cancer, such as heavy smokers.

1.8.3. Bronchoscopy

There is standard white light video bronchoscopy (WLB) and auto-fluorescence bronchoscopy. A thin tube, named a bronchoscope, is used to thoroughly examine the lungs and to take a sample of lung tissue to test for the presence of abnormal cells. The bronchoscope is inserted into the mouth or nose and passed down the trachea and into the lungs (Van't Westeinde and van Klaveren, 2011). Bronchoscopy could be indicated when a chest X-ray shows evidence of an infection, a collapsed lung, or a potentially cancerous tumour. Bronchoscopy is very effective for detecting lung cancer before it reaches an advanced stage, which reduces the risk of mortality. Also, bronchoscopy is generally safe and has minimal risk. However, in very rare cases, some patients may experience bleeding, infection, or trouble breathing after the procedure (Stahl et al., 2015, Chhajed et al., 2003).

1.8.4. Chest x-ray

Chest X-rays can also detect lung cancer, but by then the tumour is often too far advanced for treatment to be effective. Chest X-rays usually cannot detect small, potentially curable lung tumours. Also, many things seen on a chest X-ray turn out to be harmless or benign problems (van Beek et al., 2015). Lung cancer appears as a white-grey mass on a chest X-ray, but a lung mass cannot give a definitive diagnosis

because on X-rays it is often impossible to differentiate between lung cancer and other pulmonary diseases such as lung abscesses.

1.8.5. Thoracoscopy or Thoracotomy

Thoracoscopy/thoracotomy is also currently used to diagnose lung cancer. Usually under anaesthesia, a small incision is made in the chest and a tube resembling a bronchoscope is passed through it. The physician can examine the lining of the lungs, the chest wall, the mediastinum and the pericardium, and collect samples. Like bronchoscopy, this procedure is relatively risk free (Petersen et al., 2012, Onaitis et al., 2006). However, some people experience a sore throat, bleeding, infection, pneumonia or a partial or complete collapse of the lung (Kaiser and Bavaria, 1993). Thoracoscopy is very effective for diagnosing lung cancer at a much earlier stage than a chest X-ray.

1.9. Tumour protein markers

After proteins are translated, they frequently undergo various modifications, such as acetylation, methylation and phosphorylation. These post-translational modifications regulate the production, function, and half-life of proteins, as well as their immunological makeup. The regulation of protein production and function inside cells is governed by their response to extracellular stimuli, such as growth hormones and inflammatory mediators. Proteins are produced in amounts that are suitable for coping with the routine cellular processes, but they are upregulated or downregulated in certain normal and abnormal conditions. In some circumstances, the changes in protein expression and modifications are controllable and reversible. For example, in inflammation, cells return to their normal state when the causative stimulus disappears. But in cancer, the changes are beyond the control capability of the cells. In principle, any detectable increase in a protein's abundance or in its

posttranslational modifications in cancer might serve as a biomarker of the disease. But in practice, after more than 50 years of research on cancer biomarkers, early correct diagnosis and correct choice of treatment sometimes seem very difficult to achieve, despite the advances in imaging technologies, biomarker discovery, and instrumentation. These difficulties are rooted in the complexity of cancer, the dynamic changes in tumour cell populations within the tumour environment, and the existence of heterogeneity. Treatment failure, development of drug resistance, and relapse of the disease remain major challenges. Moreover, detection of cancer before it can be visualised by imaging systems has to rely on molecular biomarkers used for screening for lung cancer in people who are at risk, such as chronic smokers or in occupational medicine services.

Cancer biomarkers, also called tumour markers, can be general or specific. If the affected organ produces a specific protein, the tumour marker will be unique and specific, *e.g.* prostate specific antigen (PSA) in prostate cancer. Other tumour markers are associated with several malignancies, such as CA-19-9 glycoprotein antigen in carcinoma of lung, stomach and pancreas (Steinberg, 1990). The disadvantage of using tumour markers in diagnosis is that they are not consistently elevated in all patients (Hara et al., 2008). The clinical utility of these markers is restricted to monitoring patients with lung cancer (Figure 5) in order to minimise exposure to the low dose x-rays and radionuclides used for monitoring treatment outcome. Table 2 lists some protein biomarkers used for diagnosis, prognosis and staging of lung cancer.

1.9.1. History of clinically used tumour markers

The first cancer biomarker, carcinoembryonic antigen (CEA), was reported in 1965 (GOLD and FREEDMAN, 1965). After further research, the same group argued in 1967 that CEA is specific to cancers of the gastrointestinal tract (Thomson et al., 1969), but later, CEA was demonstrated to be elevated in different cancers, including lung, breast, and genitourinary tract tumours (Reynoso G, 1972).

The clinical utility of biomarkers relies on the use of cut-off values that distinguish benign from cancerous or diseased tissues. The initial established cut-off value of CEA was 2.5 ng/ml (Reynoso G, 1972), but later it was found that 10-17% of normal people have plasma values > 2.5 ng/ml (Vincent and Chu, 1973, Concannon et al., 1973). From the beginning of the 1970s, stress was placed on the need for distinguishing early from late stages of cancer in terms of their complexity. CEA was reported to be > 2.5 ng/ml in patients with bronchial carcinomas (Reynoso G, 1972). But this finding was not consistent because about 22% of patients with advanced metastatic lung cancer were reported to have CEA levels within normal values (< 2 ng/ml) (Meeker et al., 1973). In 1974, Joseph *et al.* reported that the CEA cut-off value for bronchogenic carcinoma was < 5 ng/ml, and consequently concluded that CEA is not a good diagnostic or prognostic biomarker for bronchogenic cancers (Concannon et al., 1974). CEA failed to discriminate between bronchial carcinoma and chronic bronchitis (Pauwels and Van der Straeten, 1975).

Progastrin-releasing peptide (ProGRP) can diagnose SCLC with a sensitivity of 76% (Korse et al., 2015). Combining Pro-GRP with CEA increases the sensitivity to 91%. Squamous cell carcinoma antigen (SCCA) is used to differentiate between adenocarcinoma and SqCC. SCCA combined with CEA can differentiate between

adenocarcinoma and the very rare adenosquamous lung carcinoma (ASC) (Jin et al., 2017b). The value of combining biomarkers was also shown by combining CYFRA 19 with neuron-specific antigen (NSE) and CEA (Lequaglie et al., 1995) in diagnosis of lung adenocarcinoma. Another example of using biomarkers panels is the combination of CEA as a general tumour marker, SCCA as a marker specific for SqCC, NSE as a marker for AD tumour in addition to the small cell lung carcinoma specific biomarker Progastrin-releasing peptide (ProGRP). This panel was accurate in predicting the presence of lung cancer and distinguishing small from non-small lung cancers (Molina et al., 2016). When this panel was evaluated in the diagnosis of lung nodules, it identified eight out of twelve lung cancers among patients negatively diagnosed by CT-scanning (Yang et al., 2015).

Tissue polypeptide antigen (TPA) is not sensitive for diagnosis of SCLC, but its sensitivity increases when it is combined with lactate dehydrogenase. One advantage of integrating lung tumour markers with other diagnostic tools for monitoring treatment (Table 2, Figure 5) is to reduce exposure to radiation and stressful diagnostic procedures (Holdenrieder et al., 2016).

Table 2: Biomarkers commonly used in diagnosis of lung cancers

Biomarker	Lung cancer type	DD	P/S	T (M/S)
CEA	NSCLC, AD			+
HE4	NSCLC	+		+
CA-15-3	NSCLC, AD		+	+
CYFRA 21-1	NSCLC	+		+
NSE	SCLC, NET	+		+
ProGRP	SCLC	+	+	+
Chromogranin A	SCLC, NET	+		+
SCCA	NSCLC, SCLC	+		

DD: Differential diagnosis. P/S: Prognosis/Staging. T(M/S): Treatment (Monitoring/ Surveillance). AD: Adenocarcinoma. NSCLC: Non-small cell lung cancer. SCLC: small cell lung cancer. NET: neuroendocrine tumour. CEA: carcinoembryonic antigen. HE4: Human epididymis protein 4. CA-#: Cancer carbohydrate antigen. CYFRA 21-1: Cytokeratin 19 fragment. NSE: Neuron-specific enolase. ProGRP: Progastrin-releasing peptide. SCCA: Squamous cell carcinoma antigen. Modified from (Holdenrieder et al., 2016).

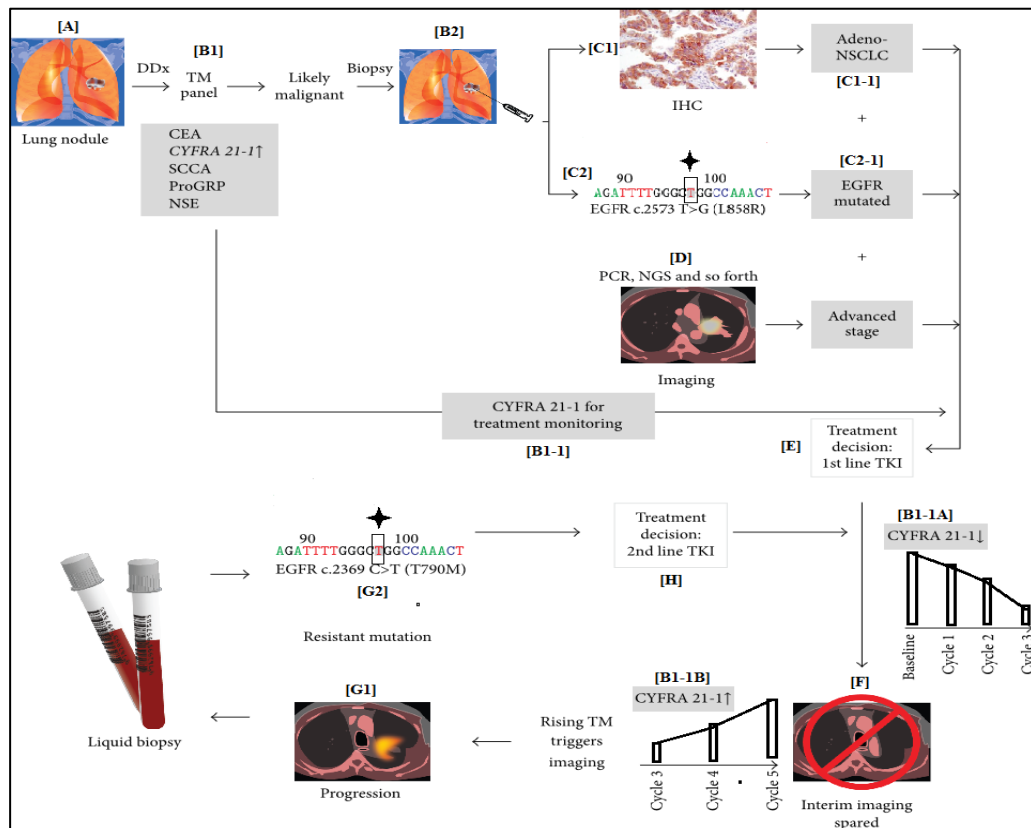


Figure 5: Integration of tumour markers with other diagnostic modalities. Modified from (Holdenrieder et al., 2016). DDX: Differential diagnosis. TM: Tumour marker. IHC: Immunohistochemistry. NSCLC: Non-small cell lung cancer. EGFR: Epidermal growth factor receptor. PCR: Polymerase chain reaction. NGS: Next generation sequencing. TKI: Tyrosine kinase inhibitor. CYFRA 21-1: Soluble fragment of cytokeratine 19 (fragment 21-1) detected in serum. CEA: carcinoembryonic antigen. SCCA: Squamous cell carcinoma antigen. ProGRP: Progastrin-releasing peptide. NSE: Neuron-specific enolase. TM: Tumour marker. C2369T: Cytosine at nucleotide number 2369 in EGFR gene changed to thymine (point mutation) and the encoded amino acid changed to methionine instead of threonine (T790M) in the EGFR peptide. T2573G: In EGFR gene, nucleotide thymine changed to guanine (the number denotes its location in the EGFR gene. The encoded amino acid changed from leucine to arginine. A: nodule discovery, B1: biomarker panel assessed in blood (serum/plasma), B2: taking biopsy from the nodule using fine needle aspiration (FNA) for IHC typing (C1) and mutational analysis using microchips and hybridization to known mutations (C2), E: treatment decision based on the type of cancer (C1-1) and the mutated gene involved (C2-1). In advanced cases, further investigation might include global mutational screening using NGS and further mutation confirmation by PCR and direct sequencing. Before start of treatment, elevated biomarker(s) (B1-1) used to monitor the treatment efficiency [tumour is good responding to the treatment (B1-1A) and treatment failure after some time due to tumour heterogeneity or development of resistance to treatment (B1-1B)]. In treatment failure, again CT-scan (G1) is required and liquid biopsies are collected for further mutational analysis (G2) to decide another treatment combination (H).

1.9.2. Biomarkers for discriminating between SqCC and AD

The previous differential diagnosis of NSCLC *vs.* SCLC for treatment decisions has been superseded by a need for a more precise classification. SqCC is a malignant epithelial tumour showing keratinisation and/or intercellular bridges. Keratinisation can be in the form of pearl formation or single cell. In poorly differentiated tumours, these features can be difficult to define. AD is diagnosed histologically by the formation of glandular spaces, papillary structures, surface alveolar growth, and/or intracytoplasmic mucin in the tumour. While biomarkers that differentiate SqCC from AD have been reported, additional markers would help enhance diagnostic accuracy (Agackiran et al., 2012, Li et al., 2014, Patnaik et al., 2015, Zhan et al., 2015). In 2015, the World Health Organisation (WHO) published its classification of lung tumours (Scagliotti et al., 2009). IHC markers such as p40 and TTF-1 are recommended for definitive histological diagnosis of SCC and AD when diagnosis based solely on morphological features is inconclusive. Recent developments in targeted therapies, such as pemetrexed and bevacizumab, require precise typing of NSCLCs, since these drugs are inappropriate for SqCC due to the increased risk of hemoptysis (Reck et al., 2009, Sandler et al., 2006, Travis et al., 2015a, Hellmann et al., 2013). Most candidate biomarkers discussed in the literature in terms of their sensitivity in discriminating between SqCC and AD are tissue-based proteins, but a biofluid-based biomarker would be a major advantage because only a small amount of tissue is available for testing, and rebiopsying is difficult and sometimes impossible.

1.10. Biofluids, breath and tissues as sources of biomarkers

1.10.1. Blood

Blood is a biological fluid that supplies the tissues with nutrients and oxygen, and this delivery is controlled by the blood circulation and blood pressure (Klabunde, 2012). Erythrocytes are responsible for gas exchange between the pulmonary alveoli and the circulation collateral capillaries, and also between the capillaries and body tissues. The circulation also plays a major role in defending the body against invasion by pathogenic micro-organisms, supplying the affected organ with white blood cells, the major immune cells defending against pathogens.

All cellular biological waste is pooled in the blood, so blood is used in routine laboratory investigations and in measurement of tumour markers. Waste products are transported by the blood to the liver to increase their water solubility before they are eliminated through the kidneys, so urine is also used for routine laboratory investigations. Carbon dioxide is either delivered into the lung (so exhaled breath is used for diagnosis of some pulmonary as well as systemic diseases) or converted into bicarbonate to neutralize acids formed from cellular metabolism.

From the diagnostic point of view, blood is a liquid tissue consisting of a complex and dynamic mixture of biomolecules reflecting the overall normal or pathophysiological state of the body. The levels of these molecules, especially those used in diagnosis of diseases other than kidney diseases, depend mainly on the performance of two organs, the kidneys (Bellomo and Ronco, 2005, Karim et al., 2002, LAVENDER, 1946, MILNE, 1955) and lungs (Brambilla et al., 2003, McFadden, 1970, Nattie, 1990). In renal failure, the clinical utility of tumour biomarkers is completely lost (Nomura et al., 1998, Trojan et al., 2013) mainly because dehydration leads to haemoconcentration (Aranda et al., 2017). Insufficient

fluid intake is also responsible for the variability of biomarkers' levels in blood. Dilution due to overhydration or dialysis might also affect the clinical utility of biomarkers in terms of multiple reaction monitoring (MRM). Heart diseases also affect the consistency of biomarkers due to the effect of oedema. The choice of candidate volunteers for discovery and validation of biomarkers, especially in cancers, should fulfil certain criteria to minimize the presence of outliers and the loss of statistical significance. This also should be considered in the assessment of their clinical utility in terms of excluding false positive results arising from food, disease (Cioppa, 2017) and drug interaction (Forman and Young, 1976).

1.10.2. Exhaled breath condensate

Exhaled breath is a good source of biomarkers that can reflect various pathophysiological conditions of the respiratory system, including asthma, lung carcinoma and chronic obstructive airway disease (Montuschi and Barnes, 2002). The exhaled breath can be investigated as a vapour (Dallinga et al., 2014) or as a liquid condensate (Konstantinidi et al., 2015). The latter is optimal for proteomic analysis, which requires liquid samples, but though using exhaled breath condensate (EBC) is not invasive, many challenging issues limit its routine (Md, 2017). The major issues include its limited protein content ($< 1\mu\text{g/ml}$), its limited content of biomarkers, and the lack of reference values (Montuschi, 2007, Hayes et al., 2016). EBC should be obtained without exhausting the patient, and the patient should be asked to breathe normally. Following good standard protocols for EBC collection increases its clinical utility as a monitoring biomarker, also called multiple reaction monitoring (MRM). In 2005, the first guidelines for the collection and preservation of breath condensate were published jointly by the American Thoracic Society and the European Respiratory Society. The guidelines suggest collection of breath

condensate for no longer than 10 minutes to avoid patient exhaustion (Horváth et al., 2005). The guidelines also detail other considerations for collecting breath condensate, especially for MRM. These considerations include consumed food, smoking before collection, and room temperature. Body temperature also plays a role in the consistency of breath condensate samples because hyperthermia leads to hyperventilation as a consequence of the decrease in alveolar carbon dioxide pressure (hypocapnia) (Tsuji et al., 2016). This lowers the water content of exhaled breath and thus its ability to carry relatively large molecules and even intact cells. Label-free mass spectroscopy has maximised the number of detected volatile and non-volatile biomarkers in the breath condensate (Hayes et al., 2016).

The first relatively quantitative proteomic profiling of breath condensate of healthy people was done by Muccilli *et al.* in 2015, who successfully identified 165 proteins using label-free mass spectroscopy, 113 of which had not been identified in breath condensate previously (Muccilli et al., 2015). Most breath condensate proteins were cytokeratins, up to 20% were the inflammatory cytokines, interleukines, TNF- α , and angiogenic factors such as vascular endothelial growth factor (VEGF). In NSCLC, Cystatin-A, which is responsible for the induction of TNF- α and interleukins (Magister and Kos, 2013, Kopitar-Jerala, 2006), accounted for up to 2% of the breath condensate proteome (Muccilli et al., 2015, Magister and Kos, 2013). Other proteins identified by mass spectroscopy in breath condensate from NSCLC patients included actin, desmoplakin and other mediators of pre-inflammation and pre-fibrosis. The vasoconstrictor endothelin-1 was one of the active peptides found to be increased in non-small cell carcinoma (Carpagnano et al., 2004). Survivin, cyclooxygenase II [COX II], and matrix metallo-proteinase 9 (MMP-9) were also elevated in the breath condensate from a patient with NSCLC (Carpagnano et al., 2010). The clinical utility

of breath condensate in diagnosis and monitoring of lung cancer would be conditioned with the development of an economical analytical method that can detect biomarkers at the concentrations present in breath condensate.

1.10.3. BALF

Bronchoalveolar lavage (BALF) is collected routinely from both paediatric and elderly patients (Brajer-Luftmann et al., 2016, Ramsey et al., 2017) for diagnosis of different lung diseases (Meyer et al., 2012), especially infiltrative lung diseases to detect opportunistic infections in immunocompromised patients (Brownback and Simpson, 2013). BALF is collected in the surgical theatre by bronchoscopy. Bronchoscopes are either rigid metal or flexible fibre-optic. Bronchoscopy is performed for investigation and surgical purposes and requires anaesthesia. The use of conscious sedation with fast, short acting anaesthetics such as ketamines is the standard technique for simple bronchoscopic procedures, but general anaesthesia is mandatory for long bronchoscopic surgery (Chadha et al., 2015).

The similarity between the inflammatory cells profile (associated with lung diseases including carcinomas) harvested in the lavage (eg: decreased T lymphocytes in lung carcinomas, increased polymorphonuclear leucocytes in asbestosis and cystic fibrosis or degraded alveolar macrophages in proteinosis) and their clinical laboratory manifestation in these diseases gave rise to the assumption that BALF can reflect the overall status of the lungs (Gee and Fick, 1980). BALF has been used for decades in clinical proteomics research, and with the emergence of non-invasive label-free mass spectrometry and polymerase chain reaction (PCR)-based techniques, the composition of lung lavage has become better characterized and the proteomic signatures of various lung diseases has become superior to single or combinations of diagnostic protein biomarkers (Plymoth et al., 2003).

In healthy people, proteins such as albumin, transferrin and α 1- antitrypsin are seen in BALF, but inflammatory mediators and increased cell count are absent (Obertacke et al., 1987). The earliest study on normal references for cytological and proteomic values for BAL fluid was conducted in 1974 (Reynolds and Newball, 1974). The clearance capacity of the lung is increased in the presence of lower respiratory tract infection (Ramsey et al., 2017).

BAL fluid can be helpful in isolating resistant microbial pathogens infecting the lungs for selection of the right antimicrobial agent (Dancewicz et al., 2009). Detection of inflammatory mediators in BAL fluid has great value in the assessment of lung allograft rejection in children (Wong et al., 2015, Benden et al., 2007). BAL fluid is also used in monitoring the progression of diseases like in paediatric pulmonary alveolar proteinosis, which is characterised by reduction in alveolar gas exchange due to accumulation of excess surfactants in the alveoli (Badiozaman et al., 2013).

Because BALF is close to tumour tissues, it has an advantage over blood because of the simplicity of its constitution and the absence of the “background” from 97% of the blood proteome. In 2015, the simplicity of the BALF proteome led to successful differentiation of lung adenocarcinoma from other lung carcinomas and non-malignant diseases (Almatroodi et al., 2015). BAL fluid has also been used for metabolic profiling of lung cancer, which showed that glutamate and glycerol metabolic pathways are altered in BALF from lung cancer patients compared to normal controls (Callejón-Leblic et al., 2016). Incorporation of gene microarrays chip discs might give more diagnostic details of lung diseases using bronchoalveolar lavage (Meyer, 2007).

However, BALF remains unsuitable for routine clinical and research use due to the collection technique and other factors (Singletary et al., 2008). Therefore, efforts continue to establish a standard protocol for BALF collection to enhance its diagnostic value (Singletary et al., 2008). The European Respiratory Society has established general guidelines for measurements and standardisation of normal human BALF (Crystal et al., 1986).

1.10.4. FFPE tissue

The standard protocol for tissue sample processing in hospitals worldwide includes fixation by formalin and moulding in paraffin. The tissues become highly stable and can be stored for a long time even at room temperature without deterioration. Proteomic analysis of formalin-fixed paraffin-embedded (FFPE) tissue would enable retrospective discovery of biomarkers in a huge archive of well-characterised clinical tissue samples. However, the proteins in FFPE tissues cannot be used in proteomic investigations with many state of the art methods because the proteins are cross-linked by formaldehyde (Dowling, 2018).

Nevertheless, the advantage of proteomic biomarkers discovery in FFPE tissue over fresh or frozen tissues is the availability of a good source of samples and the ease of handling and storage. Fresh or frozen tissues are often difficult to obtain in large numbers and relatively difficult to store in a stable form. Hence, FFPE tissues represent a potentially attractive sample pool for retrospective discovery of protein biomarkers. Immunohistochemistry (IHC) is the golden method for obtaining detailed proteomic information in hospitals. Unfortunately, IHC has low sensitivity and is not quantifiable (Hood et al., 2005).

The advantages of the mechanistic information on disease progression and manifestation offered by proximal biofluid-derived biomarkers is much appreciated.

Unfortunately, because tissue sample collection is invasive, pathologic diagnosis relies on a small amount of tissue. For decades, FFPE tissue remained the basic foundation for pathological diagnosis of diseases, mainly by IHC and *in situ* hybridization (ISH) to examine the expression of specific proteins or transcripts (Henke et al., 2006). Until recently, the ability to analyse FFPE tissues by mass spectrometry (MS) has been essentially non-existent (Hood et al., 2006, Zordan, 2011).

FFPE-based tissue samples have been thought unsuitable for proteomic analysis other than by IHC because of the extensive covalent cross-linking between the protein peptides and formaldehyde. The improved methods for extracting proteins from FFPE tissues enables their identification and quantification by tandem mass spectrometry (Scicchitano et al., 2009). Targeted proteomics based on enrichment of disease-specific proteins from high-quality tissue specimens provides great opportunities for discovery and validation of new diagnostic and prognostic biological markers in all phases of clinical trials. FFPE tissue collections, along with their relevant clinical information, are invaluable for retrospective discovery of protein biomarkers and performing various translational studies on malignant diseases (Guo et al., 2007, Kokkat et al., 2013).

1.11. Non-malignant lung diseases

Lung mucosal cells, due to their high surface area in contact with the surrounding environment, are exposed to all types of allergens, micro-organisms (eg. viruses and bacteria) and to the weather stress (cold and heat). The differences in response to allergens between individuals leads to a broad range of lung diseases (such as bronchitis, asthma, ...etc). The presence of auto-immune diseases such as sarcoidosis or genetic diseases such as cystic fibrosis would affect the overall content of lung

lavage. Therefore, when screening for lung cancer biomarkers using bronchoalveolar lavage, such conditions should be considered in the control samples and results should be interpreted along with the patients' clinical information.

1.11.1. Sarcoidosis

Sarcoidosis is an autoimmune, granulomatous, inflammatory lung disease of unknown aetiology. The disease is characterised by increased production of inflammatory cytokines due to accumulation of CD4+ T-lymphocytes in the affected lung tissues (Dubrey et al., 2016). The successful use of Rituximab targeting B-lymphocytes cells-surfaces CD20 receptors in treatment of sarcoidosis might demonstrate their role in the pathogenesis of the disease (Dubrey et al., 2016, Cinetto et al., 2015). Sarcoidosis can affect any organ, but the lungs and thoracic lymph nodes account for 90-95% of the cases (Baughman et al., 2001). Like any other autoimmune disease, treatment of sarcoidosis relies on stabilizing the condition and preventing progression. Stabilizing inflammatory cells and preventing them from further production of inflammatory mediators involves the use of corticosteroids, which can be used locally (inhaled) or systemically in the exacerbated forms of the disease (Schutt et al., 2010). The disease is usually asymptomatic, and the main complaint of patients with symptomatic disease is repetitive coughing due the dryness caused by lung tissue necrosis in the main airways as a consequence of increased inflammatory mediators, of which tumour necrosis factor (TNF- α) is the most important. Therefore, interfering with the effect of TNF- α would help in preventing further deterioration of lung tissues. Golimumab, Ustekinumab and Rituximab are monoclonal antibodies used as cytokine modulators to interfere with the effect of TNF- α and stabilizing the disease (Bargagli et al., 2011, Judson et al., 2014, Cinetto et al., 2015, Sweiss et al., 2014).

1.11.2. Asthma

Asthma is an inflammatory disease manifested in reversible obstruction of pulmonary airways. The disease affects 300,000,000 individuals worldwide with an approximate mortality of 250,000 patients annually (Bousquet et al., 2007). Studies on BALF and tissue specimens from asthma patients revealed that Th2 CD+4 T lymphocytes play a master role in predisposing to asthma (Robinson et al., 1992). Th2 lymphocytes are responsible for the release of cytokines and interleukins and activation of mast cells. This is associated with massive release of histamine, the main broncho-constrictive autacoid, and subsequent recruitment of other leucocytes, e.g. eosinophils, neutrophils and monocytes, the latter of which differentiate into macrophages (Xie and He, 2005, Khan et al., 1985, Holgate, 2008). Local inflammation in asthma leads to activation of repair mechanisms and remodelling of airway walls involving vascular, epithelial and mesenchymal morphological changes (Holgate, 2008). Eosinophils release a specific transforming growth factor (eosinophils-derived TGF- β), cytokines, and cationic proteins (Kariyawasam and Robinson, 2007). Besides interacting with mast cells, these factors contribute to increased angiogenesis and activation of epithelial-to-mesenchymal transition and the overall pathological modelling of airway walls, including fibrosis (Aceves and Broide, 2008, Wilson and Wynn, 2009). Inflammation-induced injury of the lung epithelium leads to a local increase in epidermal growth factor (EGFR) receptors that favours the epithelial cells repair process (Puddicombe et al., 2000). When epithelial cells enter the repair phase, they produce profibrotic mediators, including TGF- β , endothelin and fibroblast growth factor (FGF). These mediators modulate the release of glycoproteins, proteoglycan, collagen (types I, II, V), tenascin, and fibronectin from myofibroblasts, leading to airway thickening (Holgate et al., 2000, Brewster et

al., 1990). Such biomolecules might be confusing when found elevated in lung cancer. Therefore, these biomarkers and of course others should be excluded when seeking biomarkers for diagnosis of cancer.

1.11.3. Chronic bronchitis

Chronic obstructive pulmonary disease (COPD) is one of the leading causes of chronic bronchitis. COPD is an obstructive lung disease caused by chronic heavy smoking or chronic exposure to silica dust (silicosis). The disease is associated with goblet cell hyperplasia and overproduction of mucins, leading to small airways obstruction, epithelium remodelling, and a large decrease in alveolar compliance. The overall clinical manifestation of COPD is a large decline in pulmonary function and increased susceptibility to infection leading to chronic bronchitis. The latter is characterized by shortness of breath, wheezing, mild fever and central cyanosis due to inadequate alveolar CO_2/O_2 exchange (Kim and Criner, 2013).

Emphysema is another cause of chronic bronchitis similar to COPD, characterised by increased residual volume, the volume remaining in the lung after complete exhalation at rest). Emphysema is different from COPD in that the predisposing factor is alteration of the balance between pleural and alveolar pressure, which coordinates and facilitates smooth dynamic compression of pulmonary airways and maintenance of PaO_2 and PaCO_2 close to normal values (Robins, 1983).

Pneumoconiosis, also known as black lungs, is an occupational diseases caused by inhalation of inert inorganic dust, which can be seen in x-rays but causes no damage to the lungs, or by inhalation of coal dust and fibrogenic materials such as asbestos and crystalline silica dusts (Cullinan and Reid, 2013). Lung cancer and pulmonary hypertension are associated with pneumoconiosis (Rosenman and Zhu, 1995). Intoxication with silica and coal dust results in secretion of lipases and proteases and

consequently activation of oxygen radical production by phagocytes in the lung epithelial and alveolar cells. Consequently, monocytes are recruited and differentiate into macrophages, leading to release of proinflammatory cytokines and reactive oxygen species (ROS), which cause lung scarring (Castranova and Vallyathan, 2000).

1.11.4. Acute bronchitis

Acute bronchitis is an inflammation of the trachea and main bronchi without evidence of pneumonia caused by viral infection or other predisposing factors (Kinkade and Long, 2016). Strong coughing (with mucus) is the main symptom, but shortness of breath, wheezing, mild fever and chest tightness might occur (Wark, 2015, Knutson and Braun, 2002).

1.11.5. Pneumonia

Pneumonia is infection of one or both lungs caused by bacteria, fungi, viruses or mycoplasma (Kashyap and Sarkar, 2010). The air sacs and alveoli become full of pus and inflammatory exudates, leading to fever due to pyrogens from the microorganism, night sweating, confusion, cough with slimy products, breathing troubles, and pain (Hoare and Lim, 2006). Pneumonia can be serious in people over the age of 65 years (Wawruch et al., 2004) if not treated properly and can be very dangerous if the patient is affected by diabetes (Kornum et al., 2007), COPD (Festic and Scanlon, 2015), congestive heart failure (Nimdet and Techakehakij, 2017), or is immunocompromised (*e.g.* organ transplant) (Sanders et al., 2006) or taking chemotherapy (De Weerd et al., 2017).

1.11.6. Tuberculosis

Tuberculosis a disease caused by *Mycobacterium tuberculosis* and affects the lungs because they are the first gate of infection. Only 5-10% of people infected with *M.*

tuberculosis develop symptoms at any stage of their life, and the condition resolves spontaneously in most cases (LoBue et al., 2010). Symptoms include haemoptysis, weight loss, anorexia, fever, malaise, terminal cachexia and breathlessness (Campbell and Bah-Sow, 2006). The risk of developing serious clinical systemic manifestations is expected only in children and immunocompromised or HIV patients (Harries and Dye, 2006). The diagnosis of latent tuberculosis is made either by the tuberculin skin test or by the interferon gamma release assay, whereas pulmonary tuberculosis is diagnosed by sputum smear microscopy for acid fast bacilli (Pai, 2013), chest radiography, sputum culture, and PCR confirmation of the presence of the bacterium DNA (LoBue et al., 2010).

1.11.7. Cystic fibrosis

Cystic fibrosis is a life-limiting autosomal recessive disorder affecting mainly people of European descent and others to a minor extent (Cutting, 2015). The main two organs affected are the lungs and the pancreas; other organs include intestines, sweat glands, biliary duct, and male reproductive tract (Cutting, 2015). Genetically, cystic fibrosis is attributed to F508del in the cystic fibrosis transmembrane conductance regulator (CFTR) gene (Rommens et al., 1989). CFTR functions as a cyclic AMP-dependent chloride ion channel (Moskowitz et al., 2008, Kartner et al., 1991). The disease is characterised by viscous secretions of the pulmonary airway and pancreatic duct leading to obstruction, inflammation and damage to both organs. Loss of pancreatic exocrine would lead to poor growth and malnutrition in children if not therapeutically replaced. Therefore, screening of neonates for immunoreactive trypsinogen and CFTR alleles has become the gold standard for early detection of and intervention in cystic fibrosis (Moskowitz et al., 2008).

1.11.8. Pulmonary oedema

The filtered plasma fluid and solutes that cross the endothelium of the lung capillaries gathers in the interstitial spaces and then moved to the lymphatic vessels by means of pressure gradient. The amount of filtered plasma depends on the capillaries' vascular pressure (hydrostatic pressure) and the protein colloid pressure (Staub, 1974). Accumulation of fluid in the interstitial spaces (oedema) occurs when the filtration rate exceeds the lymphatic drainage clearance. Lung oedema might be cardiogenic (secondary oedema), in which the pulmonary capillary pressure is elevated due to left-side congestive heart failure (LCHF), or non-cardiogenic (primary) oedema resulting from increased endothelial permeability caused by inflammation (Murray, 2011, Guntupalli, 1984). The symptoms include paroxysmal *nocturnal dyspnea*, anxiety and diaphoresis. Cardiogenic oedema can be treated by diuretics, vasodilators and cardiotonic drugs such as digoxin. Pulmonary oedema is treated by treating the underlying condition (Guntupalli, 1984).

1.11.9. Acute respiratory distress syndrome (ARDS)

ARDS is a pathophysiological condition of alveolar accumulation of fluids due to increased protein content in the pulmonary oedema. ARDS causes severe symptoms, including severe hypoxemia and central cyanosis due to impaired CO₂ elimination (Matthay and Zemans, 2011). Pneumonia and gastro-oesophageal reflux diseases are the main disorders involved in the development of ARDS (Matthay et al., 2012).

1.11.10. Benign lung nodules

Among the rare benign lung nodules are papilloma nodules (squamous, glandular or mixed), which are single or multi-focal tumours found more commonly in the lower than in the upper respiratory tract (Popper et al., 1992). These benign tumours might

lead to complete airway obstruction and consequently to pneumonia (Soldatski et al., 2005).

Sclerosing haemangioma (pneumocytoma) is another benign lung neoplasm 3-5 cm in size originating from an epithelial type II pneumocyte. Haemangiomas are of two morphological types: cuboidal epithelial cells positive for thyroid transcription factor (TTF-1), epithelial membrane antigen (EMA) and cytokeratin, and round stromal cells characterised by a weakly acidic cytoplasm, and Round stromal cells of haemangioma type are positive for TTF-1 and epithelial membrane antigen (EMA), and negative for cytokeratin (Devouassoux-Shisheboran et al., 2000).

Alveolar adenoma is a rare, multi-cystic, peripheral lung neoplasm that is immunohistochemically positive for cytokeratin, TTF-1, and surfactant protein B&C (Burke et al., 1999). Type II pneumocyte papilloma is also a small (1.5 cm) peripheral neoplasm of type II pneumocyte that is positive for TTF-1 (Noguchi et al., 1986). Salivary gland type tumours are very rare benign tumours developing in the central lung and are of two types: mucous gland adenoma and pleomorphic adenomas (Moran et al., 1994). Mucinous cystadenoma is a rare cystic epithelial lung neoplasm that proliferates slowly and is positive for TTF-1 and cytokeratin 7 (Rossi et al., 2004). Pulmonary hamartoma is also a peripheral, non-neoplastic, mesenchymal, lung tissue growth; < 10% of pulmonary hamartomas are endotracheal (Gjevre et al., 1996, Hansen et al., 1992). A detailed descriptive review of the rare lung tumours and benign nodules has been published by Borczuk, *et al.* in 2008 (Table 3).

1.12. Lung cancer treatment

Limited-stage, small-cell lung cancer is treated with chemotherapy and radiation therapy or a combination of more than cytotoxic drugs for those who cannot receive radiation therapy. These approaches might be preceded by surgical resection of the tumour (Brock et al., 2005, Takenaka et al., 2015). Radiation to the brain is done for successfully treated patients (Marr and Ganti, 2016). In the treatment of extensive metastatic stage SCLC, radiation therapy might be extended to involve the common sites of metastasis, such as bones and the spine (Davies et al., 2004, Jeremic et al., 2017). Treatment of NSCLC relies on the stage at which the tumour is discovered. If the tumour is localised to the lung and is discovered at a very early stage (called occult tumour), surgical resection remains the gold standard treatment (Weigel and Martini, 2000).

Treatment of NSCLC tumours at stage 0 (carcinoma *in situ*) might involve wedge or segmental surgical resection, near-bronchus photodynamic radiotherapy, cryosurgery, and laser surgery (Griffin et al., 2006, Corti et al., 2007). Selection of the treatment protocol relies on the patient's overall general health. In stage I NSCLC, surgical resection might include wedge, segmental, sleeve or lobectomy. Stereotactic body radiation (STBR) therapy is recommended for patients who cannot undergo surgery. Still in clinical trial is a combination therapy after surgery consisting of chemotherapy and radiotherapy or chemoprevention and photodynamic therapy (PDT) (Zaric et al., 2013, Corti et al., 2007).

In addition to the previously mentioned surgical resection types intended for stage I NSCLC, surgical resection for stage II lung cancer might involve the whole lung or one or more lobes (pneumonectomy). Sometimes, surgical resection is either preceded or followed by chemotherapy and radiation, and *vice versa* (Zaric et al.,

2013). External radiation is still recommended for those who cannot tolerate surgery (Low et al., 2007).

Surgical treatment of stage IIIA NSCLC is preceded or followed by chemotherapy and/or radiotherapy (Logan et al., 1997, Cicens et al., 2009). Recommended for non-surgical treatment of stage IIIA NSCLC is a combination of chemotherapy and radiotherapy sequentially or in parallel in addition to external radiation therapy, internal radiation therapy or laser surgery as a palliative treatment (Zhu and Tsao, 2014).

Stage IIIB is usually associated with pain and cardiopulmonary complications. At this stage, chemotherapy is mandatory, and followed by radiation therapy. Laser therapy, external or internal radiation therapy is usually done as a palliative therapy to relieve symptoms.

Surgery is not used to treat stage IV NSCLC (Sculier, 2013). At this stage, treatment is limited to chemotherapy to prevent cancer progression. Targeted therapy, including monoclonal antibodies (suffixed mab) or small molecules (suffixed tinib) is highly recommended by the World Health Organisation. Table 4 summarizes some of the targeted mAbs and small molecules approved by the US Food and Drug Administration (FDA) and recommended for treatment of NSCLC in combination with chemotherapy. For example, the FDA has granted approval for Necitumumab as a first line treatment of SqCC. This mAb, in combination with the pyrimidine analogue gemcitabine, binds and antagonises the EGFR receptor. Similar approval has been given for the chemotherapeutic agent cisplatin, which binds DNA and interferes with DNA repair (Fala, 2016, Fuertes et al., 2003). To improve the quality of life, palliative therapy (such as external and/or internal radiation) and laser therapy is also used routinely.

The WHO has provided recommendations for the treatment of lung cancer detailing standard operating procedures for all oncology hospitals worldwide. The expected treatment outcome depends on the stage at which the cancer is detected, the histopathological state, the age of the patient, the presence of other diseases, and the overall health of the patient.

Table 3: Benign lower respiratory tract nodules (Borczuk, 2008)

Liebow, 1952	WHO classification, 1999 & 2004
Papilloma	<i>Epithelial</i>
Hemangioma	Papilloma
Fibroma	Squamous
Chondroma	Glandular
Lipoma	Mixed
Granular cell myoblastoma	Sclerosing hemangioma
Localized tumour of pleura	Alveolar adenoma
	Papillary adenoma
	Mucous gland adenoma
	Pleomorphic adenoma
	Mucinous cystadenoma
Miller, 1969	<i>Mesenchymal</i>
<i>Tracheal/major bronchi</i>	Hamartoma
Papilloma	Localised fibrous tumour
Polyp	Chondroma
Granular cell myoblastoma	Other soft tissue tumors
Lipoma	Clear cell tumour
Fibroma	<i>Miscellaneous</i>
Hemangioma	Thymoma
Lymphangioma	Mature teratoma
Trachopathica osteoplastica	<i>Tumourlike conditions</i>
<i>Tracheal/major bronchi or lung parenchymal</i>	Minute meningotheial nodules
Leiomyoma	Nodular lymphoid hyperplasia
Neurogenic tumors	Inflammatory pseudotumor
<i>Distal bronchial tree and lung parenchymal</i>	Localised organizing pneumonia
Hamartoma	Nodular amyloid
Arteriovenous fistula	Hyalinising granuloma
Sclerosing hemangioma	Bronchial inflammatory polyp
Plasma cell tumor	Micronodular pneumocyte hyperplasia
Xanthoma	Endometriosis
Thymoma	Others- rounded atelectasis and congenital lesions
Teratoma	

Table 4: FDA-approved targeted therapy for NSCLC

Drug	M.T.	M.O.A.	Effect	Reference
Erlotinib ^S	EGFR			(Perez-Soler, 2004)
Gefitinib ^S	EGFR		Anti-proliferation	(Tamura and Fukuoka, 2005)
Afatinib ^S	EGFR	TKI		(Giordano et al., 2016)
Ceritinib ^S	ALK			(Shaw et al., 2014)
Crizotinib ^S	ALK/ROS1		Anti-angiogenesis	(Forde and Rudin, 2012)
Bevacizumab ^M	VEGF	Antagonist	Anti-angiogenesis	(McCormack and Keam, 2008)
Cetuximab ^M	EGFR		Anti-proliferation	(Blick and Scott, 2007)
Nivolumab ^M	PD-1	Bind & Inhibit	Mediated T-killer cell activation	(Fulchiero and Jimeno, 2014)
Pembrolizumab ^M	PD-1		Mediated T-killer cell activation	(Khoja et al., 2015)
Atezolizumab ^M	PD-L1		Cell death promotion	(Fehrenbacher et al., 2016)

M.T.: molecular target, *TKI:* tyrosine kinase inhibitor, *M.O.A:* Mechanism of action, *VEGF:* vascular endothelial growth factor, *EGFR:* epidermal growth factor receptor, *VGFR:* vascular growth factor receptor, *ALK:* anaplastic lymphoma kinase, *ROS1:* receptor kinase similar to ALK, *PD:* programmed death ligand-1, ^S small molecule inhibitor, ^M monoclonal antibody.

1.13. Label-free proteomics

The principal enabling technology of proteomic discovery is mass spectrometry, which accurately identifies and quantifies proteins and provides information on their structures and modification sites. In parallel, liquid chromatography (LC) has become very efficient and reproducible in separating proteins and peptides in complex samples. Technology platforms incorporating mass spectrometry for proteomic biomarker discovery include the following: (i) pattern-based methods that produce mass spectrometry-derived protein patterns by surface-enhanced laser desorption-ionization (SELDI), (ii) matrix-assisted laser desorption-ionization (MALDI), and (iii) electrospray and identity-based methods that yield lists of sequence-identified peptides from LC-MS/MS analysis of proteolytically digested proteins (Rifai et al., 2006). Accurate protein quantitation using differential labelling

technologies, such as iTRAQ (isobaric tag for relative and absolute quantitation) and SILAC (stable isotope labelling with amino acids in cell culture) are ideal for determining relative changes in protein expression in sets of samples and can lead to the discovery of potential biomarkers (Bouchal et al., 2009, Sun et al., 2008).

Label-free quantitative mass spectrometry overcomes some of the limitations of label-based proteomics. Interest has increased in label-free strategies that can be applied to a wide variety of biological samples for biomarker discovery. Label-free quantitation has the advantage of being independent of the experimental design and allowing comparison of many samples under different conditions. Typically, hundreds of proteins can be simultaneously identified and their expression levels quantified in each sample. Thus, the effects of treatment or manipulation can be analysed across time series and underlying mechanistic pathways identified. It is also possible to dig deeper in the proteome by applying a variety of separation strategies, such as immunodepletion and nanoparticle enrichment (Morrissey et al., 2013, Yokomizo et al., 2011).

1.14. Validation approaches (ELISA, IHC, MRM)

There is general agreement that panels of biomarkers or biosignatures are more sensitive and specific than single markers. The use of large panels of biomarkers overcomes the problems caused by the substantial heterogeneity among cancers and is less likely to yield unreliable results. But developing assays for validation of biomarkers associated with disease or treatment response is difficult. The assays can be in the form of enzyme-linked immunosorbent assays (ELISA), immunohistochemistry (IHC), or mass spectrometry, each of which has its advantages and disadvantages.

Typically, studies include hundreds of patient specimens that are screened using sensitive immunotechniques such as radioimmunoassay (RIA) or ELISA for biofluids, and IHC for tumour biopsies (Zingone et al., 2014, Santra et al., 2011). Quantitative MS analysis using multiple reaction monitoring (MRM) is a convincing alternative to ELISA and IHC (Kitteringham et al., 2009). MRM uses multiple stages of mass spectrometry to quantitate proteins in a complex mixture with high sensitivity and specificity. Precise selection of a targeted chromatographically separated peptide in the first quadrupole and a specific fragment ion mass in the third quadrupole results in a high degree of specificity. Absolute quantitation is achieved by adding isotopically-labelled internal standards. Specific antibodies with the required affinity and specificity for the targets may not be available to screen for the proteins of interest using ELISA and IHC, so MRM has become increasingly attractive for detecting proteomic components in a complex mixture.

1.15. Cell culture models of drug resistance

In 1951, the HeLa (Henrietta Lacks) cell line became the first cancer cell line to be successfully propagated in cell culture. The original cells were taken from a cervical cancer. Nowadays, more than 400 lung cancer cell lines (small and non-small cell) are well-characterised and in use (Gazdar et al., 2010b). The main reason for using lung cancer cell lines to study the molecular basis of lung cancer is that they resemble the tumour tissue from which they were isolated and contain all the driving mutations, including deletions, insertions and translocations, and the associated changes in post-translation modifications found in the tumour tissues (Gazdar et al., 2010a). However, the optimal benefit from using such lung cancer cell lines as a lung malignant tumour representative cells is shortened due to their genomic vulnerability (instability), lack

of differentiation, and absence of vascular stroma responsible for formation of neovascularisation and microvascular extravasation in cancer (Bremnes et al., 2011). In drug resistance studies, proteomic-based comparative analysis of proteins from cell line lysates provides information on the proteins expressed differently in the original cell line. More specifically, certain protein subsets, such as mitochondrial, exosomal, membrane or nuclear proteins, can be enriched and studied. Moreover, proteins secreted in the culture media can be quantified and compared. The establishment of chemotherapy-resistant cancer cell lines is widely used for investigating the mechanisms of cytotoxicity and resistance to chemotherapeutic agents. Biedler and Riehm were among the earliest researchers (1970) to describe the development of drug resistance in cancer at the cell culture level. Their *in vitro* studies demonstrated cellular resistance to Actinomycin D in Chinese hamster cells (Gazdar et al., 2010b).

Drug-resistant cell lines are often established by training the cells at low concentrations of the drug. The cells are given time to recover from the drug and then the training continues at a higher dose (called pulsed treatment strategy) to mimic the chemotherapy cycles often used for cancer patients. When the cells become resistant to the drug, they are maintained constantly in its presence. The mimicking of drug-resistance, the main cancer patients' suffering issues during chemotherapy, in cell lines display up to ten-fold dose tolerance "resistance" compared to their parental cell line has a great clinical significance (McDermott et al., 2014).

Despite the large number of anti-neoplastic drugs, including the new targeted therapies, treatment failure due to acquired or intrinsic drug resistance remains problematic. Avoiding or overcoming drug resistance requires elucidation of its

mechanisms. Therapeutic targets to overcome cancer drug resistance may also serve as biomarkers (theragnostics) (Reungwetwattana and Dy, 2013, Lee et al., 2016). GDC-0980 is a class I PI3K/m-TOR dual inhibitor shown to have a promising therapeutic advantages in treatment of advanced solid tumours. The only disadvantage of using GDC-0980 in treatment of cancer is that it still can be tolerated by tumour tissue (resistance) (Dolly et al., 2016). H1975 lung adenocarcinoma cell line is a good example for the acquired form of resistance to GDC-0980 small molecule targetting PI3K/m-TOR pathways (Moore et al., 2017). A549 lung adenocarcinoma cells has an intrinsic ability to tolerate doses higher than other cell lines which is most likely attributed to the inactive mTOR pathway (Heavey et al., 2016).

1.16. Metabolomics

Metabolomics is the study of chemical processes involving metabolites, the small-molecule intermediates and products of metabolism. Living systems endeavour to maintain metabolic homeostasis and biological balance, and when an organism's systems are perturbed by disease, metabolic profiles often change. This makes metabolites exceptional candidates as cancer biomarkers and particularly useful for understanding pathophysiology. Metabolomics specifically addresses the activities of small molecules (< 10 kDa) produced by active cells during their life cycles. The most frequently used technologies in metabolomics are nuclear magnetic resonance (NMR) spectroscopy and MS. The most popular analytical methods in MS are gas chromatography-mass spectrometry (GC-MS), LC-MS, and capillary electrophoresis coupled to mass spectrometry (CE-MS). These methods make it possible to comprehensively perform high throughput discovery metabolomics. The complementarity of these techniques enables in-depth metabolome analysis.

Discovery metabolomics studies the increase and/or decrease of abundant metabolites and the effect of their fluctuations on metabolic pathways. Typically, discovery-phase metabolomics is performed to identify biomarkers to improve early diagnosis, identify resistance signatures, and assist in monitoring the disease during treatment. Recent improvements in metabolomics technologies have increased their power in biomarker discovery and validation, as demonstrated by the mounting number of metabolomics-based publications (Deidda M, 2015). Metabolites represent the downstream expression of the genome, transcriptome, and proteome in normal physiology and in pathophysiology. Indeed, by their complementarity, proteomics and metabolomics enable a more detailed overview of an organism's phenotype.

Cancer metabolism differs from normal metabolism. In the 1950s, Otto Warburg showed that cancer cells rely on anaerobic metabolism for energy, even under normal homeostatic oxygen levels. Features of cancer metabolism such as in central carbon metabolism, glycolysis, the tricarboxylic acid cycle, and oxidative phosphorylation are core considerations in the quest for accurate biomarkers, and one of the main reasons why metabolomics is one of the most rapidly developing disciplines in research, including on lung cancer (Guo et al., 2012).

1.17. Aim of the project

- 1- To identify candidate biomarkers using proteomic analysis of BALF from lung cancer patients and subsequent validation/verification of selected proteins in blood specimens and to identify candidate protein biomarkers that distinguish between adenocarcinoma (AD) and squamous cell carcinoma (Sq) of the lung when investigating bronchoalveolar lavage fluid (BALF) from lung cancer patients using label-free mass spectrometry.
- 2- To evaluate tumour specimens from lung cancer patients compared to matched control tissue and identify heterogeneity associated with abnormal protein expression associated with different areas of the tumour tissue.
- 3- Analyse a number of selected proteins from the tumour tissue work by using immunohistochemistry of tissue microarrays from lung cancer patients and identification of protein expression patterns between different types of lung cancer and associated stage/grade.
- 4- To use Metabolon diagnostics discovery platform to evaluate metabolites that may function as lung cancer biomarkers and subsequently validate the most interesting metabolites in a larger cohort of serum samples using ELISAs and biochemical assays.
- 5- To investigate the development of resistance to Apitolisib (GDC-0980), a dual phosphatidylinositol-3-kinase and mammalian target of rapamycin kinase inhibitor, in A549 and H1975 lung adenocarcinoma cell line models using mass spectrometry, and how the abundance levels of cell cycle specific proteins are perturbed in the resistant phenotype.
- 6- Label-free mass spectrometry and western blot analysis of mitochondrial associated proteins using cell line models of Apitolisib (GDC-0980) resistance.

Chapter 2

Materials and methods

2. Materials and methods

2.1. BALF samples

Bronchoalveolar lavage fluid (BALF) specimens (Table 5) were obtained from the Department of Respiratory Medicine, Beaumont hospital, Dublin 9, Ireland. Specimens containing haemolytic and/or fresh blood were excluded. Cells and cell debris was removed by centrifugation at 4000 x g for 15 min at 4°C. The supernatants were concentrated using 5-kDa Ampicon filters (Sigma; cat. #Z648019) by centrifugation at 30 g for 45 min at 4°C. ReadyPrep™ 2-D clean-up kit (Bio-Rad; cat. #163-2130) was then used to clean up the concentrated BALF: 200 µl of the BALF was combined with 300 µl of precipitating agent 1 in a 1.5-ml micro-centrifuge tube, vortexed, and incubated on ice for 15 min. 300 µl of precipitating agent 2 was then added, vortexed and centrifuged at 20,800 g for 30 min. The BALF protein pellets was suspended in 8 M urea buffer containing 0.1% ProteaseMax™ from (Promega; cat. #TB373) in 50-mM NH₄HCO₃. Total protein amount was estimated using the protein assay reagent from Bio-Rad (Bradford, 1976).

2.1.1. BALF protein content

In the Bradford reagent (Bradford, 1976) microassay protocol (Sigma-Life Science, lot #SLBH7472V), bovine serum albumin (BSA) was used as standard. Five µl of sample was combined with 295 µl of Bradford reagent in a Nunc microplate, mixed thoroughly, and incubated for 5 min in the dark. The plate was read at 595 nm in a Synergy HT BioTEK reader using KC4 kineticcalc software version #3.3/Re #10. Samples concentration was calculated using the linear equation obtained from plotting BSA serial concentrations versus corresponding optical density (OD).

Table 5: Patient lavage samples biodata

Sample	Control BALF				Cancer BALF			
Origin	healthy people		Sarcoid		AD		SqCC	
n (Male and Female)	7M	5F	4M	0F	10M	3F	8M	5F
Age (mean±STD)	68.5±7.6	70±16.6	57±16.9	0	75.7±10	82.3±11.9	70.1±9	68±8.4
				n (stage)	M/F		M/F	
				Stage I/II	3M	3F	4M	4F
				Stage III/IV	7M	0F	4M	1F

BALF: bronchoalveolar lavage, AD, adenocarcinoma, SqCC, squamous cell carcinoma, M, male, F, female, STD: standard deviation.

2.1.2. Sample preparation for label-free mass spectroscopy

BALF protein samples equivalent to 20 µg were reduced with 0.1 M dithiothreitol (DTT) (Sigma; CAS No. 3483-12-3) in 50 mM ammonium bicarbonate (Sigma-CAS No. 213-911-5) for 30 min at 37°C. Samples were then alkylated with 0.2 M iodoacetamide (IAA) (CAS No. 144-48-9) in 50 mM NH₄HCO₃ for 20 min at room temperature in the dark. Samples were then mixed with 50 mM NH₄HCO₃ in a 4:1 ratio (v/v) and subjected to two digestion steps. The first digestion was performed using Lys-C for 4 h at 37°C. The second was done using 1 µl of 1 U/µl trypsin (Sequencing grade modified trypsin; Promega ref. V5111) per 20 µg sample protein overnight for 15 h at 37°C with shaking at 6 g (Thermomixer Confort; Eppendorf AG, Hamburg, No. 5355 39149). The digestion was stopped using sample buffer (20% acetonitrile (ACN) (Fluka; CAS No. 75-05-8) containing 2% trifluoroacetic acid (TFA) (Sigma-Aldrich; Product code 101398066) and 78% double distilled water) in a 3:1 sample to buffer ratio. Samples were then vortexed, incubated for 30 min on ice, and de-salted using C18 spin columns (Thermo-Scientific, UK) according to the manufacturer's protocol.

2.1.3. Sample desalting using C18 spin column at 1500 x g for 1 min

The desalting resin was activated in C18 spin columns by centrifuging through it 200 μL of 50% methanol and equilibrated twice with 200 μL of equilibration solution (0.5% TFA in 5% ACN) followed by centrifugation. Samples were then loaded and centrifuged and the flow-through was loaded and centrifuged again. Samples after then washed three times with 400 μL of the equilibration solution by centrifugation. All centrifugations were at 1500 x g for 1 min. Sample proteins were eluted using 40 μL of 70% ACN containing 0.1 TFA, dried in the vacuum evaporator, dissolved in 25 μL of buffer A containing 0.1% TFA, and centrifuged at 20,800 g for 20 min. The top 20 μL was transferred into MS vials.

2.1.4. Label-free MS/MS protocol

Digested protein samples were analysed using a Q-Exactive mass spectrometer coupled to a Dionex RSLCnano (Thermo Scientific, Waltham, MA, USA). Peptide separation was performed using a Biobasic C18 Picofrit column (ThermoFisher Scientific, Hemel Hempstead, UK) of 100 mm length and 75 mm ID. Solvent A consisted of 2% (v/v) ACN and 0.1 % (v/v) formic acid (FA) in LC–MS grade water. Solvent B consisted of 80% (v/v) ACN and 0.08% (v/v) FA in LC–MS grade water. The solvents were used in a 2–40% gradient for 65 min at a flow rate of 250 $\mu\text{l}/\text{min}$. A full MS scan at 140,000 resolution and a range of 300–1700 m/z was followed by an MS/MS scan at 17,500 resolution and a range of 200–2000 m/z, selecting the 15 most intense ions prior to MS/MS (Top15 method) (Manzanares-Miralles et al., 2016).

2.1.5. Label-free MS/MS data processing

Raw data generated from LC-MS/MS analysis was processed using Progenesis label-free LC-MS software version 3.1 (Newcastle upon Tyne, UK). The retention times of all runs were aligned to a reference sample run yielded most peptide ions, and peak intensities were then normalized accordingly (Dowling et al., 2014). Three filter parameters were applied on the MS/MS data files before they were exported to Proteome Discoverer 1.4 software (Thermo-Scientific) for protein identification, including peptides ANOVA between the compared groups ($p < 0.05$), peaks charge ranges from +1 to +5, and > 1 isotope per peptide. The PepXML generic file generated from all exported MS/MS spectra was used for peptide identification using Proteome Discoverer 1.4 against Sequest HT (SEQUEST HT algorithm, licence Thermo Scientific, registered trademark University of Washington, USA). UniProtKB-SwissProt database (taxonomy: *Homo sapiens*) was used to search the exported data. The following search parameters were set for protein identification: (i) peptide and MS/MS masses were set to 10 ppm and 0.02 Da, respectively; (ii) not more than two missed cleavages permitted; (iii) carbamidomethylation and methionine oxidation were set as fixed and variable modifications, respectively. Data were then imported back into Progenesis software for further analysis and only peptides with XCorr. Scores > 1.9 (+1), > 2.2 (+2) > 3.75 (+3) and of high confidence were selected. To ensure proper identification of cellular proteins, the criteria applied included $p < 0.05$ between tested groups, fold change ≥ 2 and proteins with ≥ 2 peptides matched (Murphy et al., 2015).

2.1.6. ELISA biomarkers validation

2.1.6.1. Plasma samples

A total of 72 plasma samples from lung cancer patients, patients with benign lung disease (Sarcoidosis) and healthy individuals were used for initial validation of the candidate biomarkers (Table 6). Fasting blood samples were collected in EDTA-containing tubes, mixed by inversion, centrifuged at 1800 g for 20 min. The separated plasma was stored in Eppendorf tubes at -80°C (Chariot et al., 1994).

Table 6: Plasma samples biodata

	Control		NSCLC	
	Benign & Sarcoid		AD	SqCC
n (type)	26		46	
n (sex)	18M	8F	23M	23F
Average age	46±11		67±23	
n (Type)			28	18
			n (stage)	
	Stage I/II		14	7
	Stage III/IV		14	11

NSCLC: non-small cell lung cancer, AD: adenocarcinoma, SqCC: squamous cell carcinoma, M: male, F: female.

2.1.6.2. BALF candidate biomarkers

Table 7 provides information about the R&D DuoSet®Sandwich ELISA kits used in the BALF candidate biomarkers validation in plasma.

2.1.6.3. ELISA assay procedure

Two 96-well plates (R&D Systems, Catalog #DY990) were coated overnight with 100 µl of the capture antibody at room temperature (Tables 7, 8). The plates were then washed 3 times with wash buffer containing 0.05% Tween-20® in PBS, pH 7.2-

7.4 (R&D Systems, Catalog #WA126). Plates were blocked for 2 h with PBS pH 7.2-7.4 containing 1% BSA and filtered (0.2 μm ; R&D System Catalog #DY995).

This step was followed by washing three times and the residual liquid after the last wash was removed by flicking the plates against a clean paper towel. plasma samples or standards in reagent diluent were added (100 μL per well), and the plates were covered with an adhesive strip and incubated for 2 h at room temperature. The plates were washed 3 times and the remaining liquid was removed as mentioned above. 100 μL of biotinylated detection antibody diluted in reagent diluent was added to each well, and the plate was covered and incubated for 2 h at room temperature. 100 μL of the working dilution of Streptavidin-HRP was then added to each well and incubated for 20 min at room temperature in the dark, followed by 3 washes. 100 μL of substrate solution was added to each well and incubated for 20 min at room temperature. The reaction was stopped by adding 50 μL of stop solution containing 2 N H_2SO_4 (R&D Systems, Catalog #DY994). The well contents were mixed thoroughly by gently moving the plates in circles. OD was measured at 570 nm and corrected for 450 nm. For the antibodies dilutions used in the assays, refer to table 8.

2.1.6.4. Calculations of samples concentrations

The natural logarithms (Ln) of the corrected OD values was plotted against the corresponding concentrations, and the derived linear equation was used to calculate the Ln (s) of sample concentrations. The sample concentrations were calculated from their Ln values.

2.1.6.5. Statistical analysis

Wilcoxon-Mann-Whitney test (Marx, 2016) was used for calculation of the significance between the compared groups. In biomedical sciences, this test is preferred over the parametric and non-parametric methods to calculate more accurate p values between two populations using permutation (Ludbrook J., 1998).

Table 7: ELISA kits used for BALF validation.

Protein	Cat. #	Source of C. Abs	Part#	Source of D. Abs	Part#	St. Part#	
PGRP	DY7847-05	Sheep	843865	Sheep	843866	843867	
HSP70	DY1663-05	Mouse	844051	Rabbit	844052	844053	
VEGF	DY293B-05		841495	Goat	840163	840164	
MIF	DY289		840489		840490	840491	
TIMP-1	DY970		840294	Mouse	840295	840296	
Periostin	DY3548		843258		843259	843260	
Cystatin C	DY1196		842942		842943	842944	
Cathepsin V	DY1080		843097		843098	843098	
Clusterin	DY5874		843449	843450	843451		
Lipocalin-2	DY1757		Rat	842271		842272	842273

All antibodies were reconstituted in 0.5 ml reagent diluent (137 mM NaCl, 2.7 mM KCl, 8.1 mM Na₂HPO₄, 1.5 mM KH₂PO₄, PH 7.2-7.4, 0.2 µm filtered)(R&D System cat. #DY995).

Table 8: ELISA antibodies working concentrations and standard concentrations

Protein	Capture Ab		Detection Ab		Standard	
	Stock ($\mu\text{g/ml}$)	Working ($\mu\text{g/ml}$)	Stock ($\mu\text{g/ml}$)	Working (ng/ml)	Stock (ng/ml)	Standard Range* (pg/ml)
MIF	360	2	18	100	30	0-2000
Lipocalin-2	360	2	18	100	90	0-5000
TIMP-1	360	2	9	50	80	0-2000
Periostin	360	2	0.2	12	200	0-12000
Cathepsin V	720	4	360	2	140	0-4000
PGRP	100	0.8	6	100	130	0-600
VEGF	120	1	6	100	100	0-2000
HSP70	480	4	9	150	180	0-8000
Clusterin	360	2	180	1	380	0-4000
Cystatin C	360	2	18	100	80	0-2000

* Eight two-fold serial dilutions starting from the recommended highest standard concentration, Ab: antibody.

2.2. Metabolomics analysis

2.2.1. Serum samples preparation

Fasting blood samples were collected from lung cancer patients and normal controls in anticoagulant-free sterile tubes and left to coagulate for 30 min at room temperature. The serum was collected after centrifuged at 1800 g for 20 min (Kocijancic et al., 2014) and transferred into clean sterile Eppendorf tubes and frozen at -80°C . 250 μl of serum samples were shipped on dry ice (Chariot et al., 1994) to Metabolon Inc., NC, USA.

At Metabolon Inc., the serum samples were centrifuged at 20,800 g, the obtained supernatants were divided into four equal aliquots and dried overnight in nitrogen vacuum drier at medium speed without heat. Dried samples were subjected to three independent analyses, two of which were for acidic and basic amino acids using UHPLC/MS optimized and the third for GC/MS.

2.2.2. UHPLC/MS protocol

One dried specimen was reconstituted in 50 µl of 0.1% formic acid (acidic injection) and another in 50 µl of 6.5 mM NH₄HCO₃ pH 8.0 (basic injection). Samples were run on Waters Acquity UHPLC coupled to an LTQ mass spectrometer equipped with an electrospray ionization source. Two independent UHPLC/MS injections were performed: acidic and basic for monitoring positive and negative ions, respectively.

2.2.3. GC/MS protocol

The third dried specimen was reconstituted in a mixture (1:1 v/v) of N,O-bis-trimethyl-silyl-trifluoroacetamide (TFA) and a solvent containing [1(acetonitrile): 1(dichloromethane): 1(cyclohexane)] and [5% trimethylamine] at a ratio of 4:1 and heated at 60°C for 1 h. All solvents used in sample reconstitution were also used as an internal control to monitor instrument performance. The GC/MS data were analysed using Thermo-Finnigan Trace DSQ fast-scanning single-quadrupole MS.

2.2.4. Data processing

The MS/MS² data were analysed against the Metabolon's reference standard library. The library contains information about the retention time/index, mass to charge ratio (m/z), and the MS/MS spectra of 1500 standards used in making the library. The library also contains the associated adducts, multi-mers and in-source fragments of the standards. These multi-parameters were used to identify the detected metabolites. All quantifications and identifications were subjected to quality control (QC) to verify the quality of peak integration and identification.

2.2.5. Metabolomics' biomarkers validation

2.2.5.1. Serum sample handling

Fasting blood samples were collected in anticoagulant-free vacutainer tubes and allowed to clot for 30 min and centrifuged at 1800 g for 15 min. The serum was

collected (Kocijancic et al., 2014), aliquoted, and frozen in cryovials at -80°C until use (Chariot et al., 1994).

2.2.5.2. Pyruvate

The colorimetric method described in the Enzychrom™ pyruvate assay kit (Cat #EPYR-100) was used (Hansen JL and EF, 1978). 10 µl of sample or standard per well was mixed with 90 µl of enzyme mix working cocktail [94 µl enzyme mix (pyruvate oxidase and hydrogen peroxide) and 1µl of dye reagent] in a 96-well plate and incubated at room temperature for 30 min. OD was read at 570 nm (550-585 nm). A standard serial dilution ranging from zero (water as a blank) to 500 µM was used to construct the standard curve. Sample concentration was calculated using the following equation:

$$\text{Pyruvate concentration } (\mu\text{M}) = \frac{\text{Sample OD} - \text{blank OD}}{\text{Slop}}$$

Samples with OD higher than the OD of 500 µM were diluted in assay buffer, measured again and the calculated values were multiplied by the dilution factor.

2.2.5.3. Free fatty acids (FFAs)

The colorimetric method described in the Enzychrom™ free fatty acid assay kit (Cat #EFFA-100) was used (Seo et al., 2011, Lu et al., 2013). 10 µl of sample or standard was mixed with 90 µl working reagent containing (1 µl Enzyme A, 1 µl Enzyme B, 1 µl co-substrate, 1 µl dye reagent and 90 µl assay buffer) in a 96-well plate, incubated at room temperature for 30 min, and OD was read at 570 nm (550-585 nm). Free fatty acid concentrations were calculated from the following equation:

$$\text{Sample FFAs concentration } (\mu\text{M}) = \frac{\text{Sample OD} - \text{blank OD}}{\text{Slop}}$$

Samples with OD higher than the OD of 1000 µM were diluted in assay buffer, measured again and the calculated values were multiplied by the dilution factor.

2.2.5.4. Ketone bodies

The colorimetric method described by Siegel, et al. (1977) for the EnzyChrom™ ketone assay kit (EKBD-100) was used for quantitative assay of ketone bodies.

2.2.5.4.1. Acetoacetic acid (AcAc)

195 µl of assay reagent containing (195 µl AcAc buffer, 8 µl reconstituted AcAc reagent and 0.5 µl 3-hydroxybutyrate dehydrogenase enzyme) was added per well and combined with 5 µl of serum sample, water or standard. Sample blank assay reagent contained no enzyme. Samples were run in duplicates, one using the assay reagent and the other with blank reagent. The reaction mixture was incubated at room temperature for 5 min and the OD of NADH was measured at 340 nm (Hansen and Freier, 1978). The AcAc concentration was calculated from the following formula:

$$\text{AcAc concentration (mM)} = \frac{\text{OD sample} - \text{OD blank}}{\text{OD standard} - \text{OD water}} \times 8$$

8: samples dilution factor.

2.2.5.4.2. 3 β-hydroxybutyric acid (BOHB)

In each well, 195 µl of assay reagent containing (195 µl of AcAc buffer, 8 µl of reconstituted BOHB reagent and 0.5 µl of 3-hydroxybutyrate dehydrogenase enzyme) was added to 5 µl serum sample, water or standard. Sample blank assay reagent contained no enzyme. Samples were run in duplicates, one using the assay reagent and the other with the blank reagent. The reaction mixture was incubated at room temperature for 15 min and the OD of NADH was measured at 340 nm (Hansen and Freier, 1978). The BOHB concentration was calculated from the following formula:

$$\text{BOH concentration (mM)} = \frac{\text{OD sample} - \text{OD blank}}{\text{OD standard} - \text{OD water}} \times 8$$

8: samples dilution factor.

2.2.5.5. Glutamate

Glutamate Colorimetric Assay Kit (Bio vision® Catalogue #K629-100) was used according to the manufacturer's recommendations (Koçdor et al., 2003). 100 µl of reaction mixture containing [90 µl of glutamate assay buffer (part No. K629-100-1), 2 µl glutamate enzyme mix (part No. K629-100-2) and 8 µl glutamate developer (part No. K629-100-3)] was added to each well containing 50 µl of standard or serum sample (diluted 5 times in assay buffer). Sample background was performed by adding 100 µl of reaction mixture containing 2 µl of water instead of glutamate enzyme mix. The plate was mixed well, incubated at 37°C for 30 min, and the OD was measured at 450 nm in a microplate reader. Samples OD values were corrected by subtracting the blank values, and the linear equation obtained from the standard curve was used to calculate glutamate concentrations in the samples. The obtained values were multiplied by the dilution factor as following:

$$\text{Glutamate (mM)} = \frac{Sa}{Sv}$$

Sa: sample amount calculated from the standard curve $Y = a \times (-/+)b$ ($Y = \text{sample OD}$, $x = \text{sample concentration}$, a : slope (given), b : intercept (given) and Sr : sample volume added to the well. The obtained values were multiplied by sample dilution factor.

2.2.5.6. Acetyl co-A

Human acetyl co-A sandwich ELISA kit (Wuhan Fine Biological Technology Co. Ltd.; cat. #EH0606) was used to estimate the levels of acetyl Co-A in serum control and lung cancer patients' samples. The kit uses 96-well plates pre-coated with anti acetyl co-A capture antibodies, biotinylated anti acetyl co-A detection antibody, HRP-streptavidin and TMB as substrate for the peroxidase, which turns blue corresponding to the amount of glutamate in the sample. The reaction was terminated

by adding 1M H₂SO₄ and the resultant yellow colour was measured at OD 340 nm. The acetyl co-A levels were then calculated from the standard curve equation.

2.2.5.7. Statistical analysis

Wilcoxon-Mann-Whitney test (Marx et al., 2016) was used to calculate the significance of change among the compared samples. In biomedical sciences, it is preferred over the parametric and non-parametric methods to calculate more accurate p values for comparison of two populations using permutation (Ludbrook J., 1998).

2.3. Formaldehyde-fixed paraffin-embedded tissue (FFPE) samples

2.3.1. Tissue sample collection

Four formaldehyde-fixed, paraffin-embedded tumour tissue samples (Table 9) were obtained from Saint James' Hospital, Department of Thoracic Oncology, Dublin. The tumour mass together with normal surrounding lung tissue was harvested, immediately cut into four quadrant pieces, fixed in formaldehyde, and sent to the pathology laboratory for typing and grading. Three of the quadrants were moulded in a paraffin cube, cut with a microtome into 2-mm sections, and kept at 4°C.

Table 9: FFPE tissue samples biodata

	Patient 1	Patient 2	Patient 3	Patient 4
Normal tissue	13020/14	14399/14	14096/14	16693/14
Quadrant 1	13020/15	14399/15	14096/15	16693/15
Quadrant 2	13020/16	14399/16	14096/16	16693/16
Quadrant 3	13020/17	14399/17	14096/17	16693/17
Stage	pT2a N0 Stage IB	pT3 N1 Stage IIIA	pT2a N0 Stage IB	pT2b N0 Stage IIA
Histology	Invasive Adeno Lipidic(90%) Papillary (10%)	Invasive Adeno Colloid	Invasive mucinous Adeno	Mod. Differentiated Adeno Acinar (80%) Micropapillary (20%)
Sex	Male	Female	Female	Male
D.O.B	01/01/1950	10/07/1954	19/11/1941	23/07/1942
Tumour size	35 mm	80 mm	40 mm	58 mm

D.O.B: date of birth, TNM: tumour, lymph nodes. x/y: denote patient codes.

2.3.2. Protein extraction and digestion for LC-MS/MS

Protein extraction from samples for mass spectroscopy was performed using FASP™-Protein Digestion Kit (Expendeon part #: 44255) (Ostasiewicz et al., 2010, Wiśniewski et al., 2009). The procedure involves removal of the paraffin wax using two xylene–ethanol steps. Samples were first treated with 0.5 ml of xylene regardless of their weights, incubated at room temperature for 5 min with periodic gentle vortexing. This step was done twice and the solvent at the end of each step was discarded. The samples were then treated twice with 0.5 ml of absolute ethanol and the solvent was removed after each treatment. The tissue samples were then nitrogen vacuum-dried and the weight of each dried tissue sample was recorded (Table 10). Samples were then homogenized in 300 µl of UPX universal protein extraction buffer for 5 min using a dounce homogenizer, and then incubated in a thermomixer at 105°C for 30 min with agitation at 6 g. After cooling to room temperature, they were centrifuged for 15 min at 20,800 g to remove cell debris. The tissue lysates were mixed with urea buffer (prepared in Tris-hydrochloride) and the lysate volume was normalised for tissue weight used (Table 10). The lysate was applied onto a spin filter (provided), centrifuged at 20,800 g for 20 min, and washed twice with 200 µl of urea. Centrifugation was under the same conditions, and all flow-through was discarded.

2.3.3. Protein digestion

Heat-denatured samples were alkylated by adding 100 µl of 1X iodoacetamide in urea buffer (IAA) to the spin columns and incubating them for 20 min in the dark at room temperature. Afterwards, the spin filters were centrifuged at 20,800 g for 10 min and washed with 100 µl of urea sample solution. To prepare protein samples for

trypsin digestion, the spin filters were treated twice with 50 mM NH_4HCO_3 and centrifuged at 20,800 g for 10 min.

Finally, the protein was digested with 75 μl of trypsin in 50 mM NH_4HCO_3 (1 U trypsin/20 μg protein). Spin filters were mixed for 1 min, wrapped with paraffin film, and incubated overnight at 37°C. They were then transferred to new collection tubes, centrifuged at 20,800 g for 10 min and centrifuged using 50 μl of 0.5 M NaCl to release the bound peptides from the spin filter. The digestion was stopped with 50 mM NH_4HCO_3 (3:1 v/v sample to buffer ratio). Finally, the spin filters were centrifuged at 20,800 g for 5 min and the top 50 μl was transferred into MS vials.

2.3.4. LC-MS/MS protocol

Samples were run in triplicates. The Q-EXACTIVE settings were set as mentioned in section (2.1.5). Twelve raw data files were obtained per patient. Nine files represent the proteome of three different areas within the tumour, and the other three file represent the proteome of the surrounding normal tissue (table 10).

2.3.5. Processing mass spectroscopy raw files

In a separate experiment, Mass spectroscopy raw files uploaded individually into MaxQuant software. The protein-group text file was then uploaded into the Perseus software then the principal component analysis (PCA) and heat-map clustering of the proteomic signature of the tumour parts and the normal tissues were generated. The results were exported to an Excel file and the \log_2x values were converted back into numbers using the online calculator at <http://www.endmemo.com/algebra/log2.php>.

Protein abundance fold-change was then calculated using the following equations:

$$\text{Up-regulated proteins} = \frac{\text{Number corresponding to } Qx}{\text{Number correspondent to } Nc}$$

Q: quadrant, x: (1, 2, 3), Nc: normal control

$$\text{Down-regulated proteins} = \frac{\text{Number correspondent to the } Nc}{\text{Number correspondent to the } Qx}$$

Q: quadrant, x: (1, 2, 3), Nc: normal control

Where; Qx: any quadrant, Nc: normal tissue control.

Table 10: FFPE tissue sample preparation for mass spectroscopy

Sample ID	Weight (mg)	Extraction buffer (μl)	Tissue lysate (μl)	Urea (μl)/ sample
13020/14*	3	300	200	800
13020/15	5	300	120	480
13020/16	3	300	200	800
13020/17	4	300	150	600
14399/14*	3	300	200	800
14399/15	6	300	100	400
14399/16	3	300	200	800
14399/17	3	300	200	800
14096/14*	3	300	200	800
14096/15	8	300	75	300
14096/16	3	300	200	800
14096/17	9	300	66.7	266.8
16993/14*	4	300	150	600
16993/15	8	300	75	300
16693/16	3	300	200	800
16693/17	6	300	100	400

Sample ID (x/y): x denote patient code and y denote microtome cut number code,
*: normal lung tissues.

The lists of significantly upregulated and downregulated proteins per tumour quadrant were further analysed using the online Venn diagram bioinformatics and systems biology tool available at <http://bioinformatics.psb.ugent.be/webtools/Venn/>.

The upregulated and downregulated proteins shared in all three quadrants were listed. The shared upregulated and downregulated proteins in all quadrants and in all patients were filtered and listed. Further bioinformatics analysis was performed to find a common area for proper biomarkers discovery and validation.

2.3.6. Tissue microarrays validation of heterogeneity

Four candidate protein biomarkers (Talin-1, lactate dehydrogenase-A, pyruvate dehydrogenase and fatty acid synthase) were selected based on their high abundance among all tumour tissues and based on their known role in cancer. Antibodies dilutions were: Talin-1(C45F1) rabbit mAb #4021 diluted 1:50, lactate dehydrogenase-A (C4B5) rabbit mAb #3582 diluted 1:400, pyruvate dehydrogenase (C54G1) rabbit mAb #3205 diluted 1:100 and fatty acid synthase (C20G5) rabbit mAb #3180 diluted 1:50 as recommended. Two NSCLC Tissue micro arrays (TMAs) slides (serial numbers LC10013at and LC819t) were used for experimental optimization. Two LC10011a NSCLC (TMAs) containing lung adenocarcinoma (AD), lung squamous cell carcinoma (SqCC), as well as normal lung tissues (appendices 43 & 44) were used to validate Talin-1 and lactate dehydrogenase-A (LDHA) expression heterogeneity. Two LC819 TMAs containing lung adenocarcinoma and squamous cell carcinoma but not normal tissue cores were used for detection of pyruvate dehydrogenase (PDH) and fatty acid synthase (FASN) expression heterogeneity.

2.3.6.1. Immunohistochemistry protocol

The TMAs tissue sections were processed in a Dako autostainer at the National Institute of Cellular Biotechnology (NICB) in Dublin City University, Dublin.

Antigen was retrieved using Dako citrate buffer (pH 6) (Agilent Dako products code #S2031, part #S203130-2) for 20 min. The incubation time was 30 min for the primary antibodies. Counterstaining was done with haematoxylin. Dehydration of tissue sections was performed by reversing the rehydration steps, starting with 95% ethanol, then 100% ethanol, and finally xylene. All incubations were done twice for 10 min each. The tissue sections were then covered with a coverslip using mounting medium.

2.3.6.2. Intensity scoring of tissue cores

Colour intensity was assessed under a 20x optical lens for adenocarcinoma (AD), squamous carcinoma (SqCC) and normal tissue (N) cores. Staining intensity was scaled as 0 (negative), 1 (weak), 2 (good) or 3 (very strong). The number of cores per score per tissue type (AD, SqCC, N) per antibody was tabulated and a representative core per score per antibody per core tissue type is represented in the results chapter. The score of TMA cores per candidate protein is tabulated as appendices 43, 44 and 45.

2.4. Drug resistance- based biomarkers heterogeneity

2.4.1. Cell culture

GDC-0980 sensitive parent (P) and resistant H1975 (R) lung adenocarcinoma cells (NCI-H1975, ATCC[®] CRL-5908[™]) were cultured in T75 cell culture flasks with tilted neck and vented caps in Roswell Park Memorial Institute medium (RPMI-1640 medium, Sigma R5886 Lot: RNBF1079) supplemented with 10% foetal bovine serum (FBS Sigma, F7524, Lot: BCBR 1178V) and 1% penicillin-streptomycin-glutamine (Gibco[™] Cat No: 10378-016).

The media for the resistant cells was conditioned with 1 μ M GDC-0980 (R+) or GDC-0980 free media (R-). Cells were harvested at 80% confluence, washed twice with 5 ml sterile 1x PBS, detached by adding 2 ml of trypsin (1X trypsin/EDTA, product No. 59430C, Sigma Aldrich) per T75 flask for 3-5 min at 37°C. For every ml trypsin added, 3 ml of RPMI was added to deactivate the enzyme. The cell suspensions were then collected in 15-ml falcon tubes, labelled, and centrifuged for 3 min at 10 g at 15°C. The supernatants were discarded and the cell pellets were re-suspended in lysis buffer for mass spectrometry and western blot validation, frozen at -20°C for mitochondrial enrichment, or re-suspended in sterile RPMI for further cells passaging or seeding for confocal microscopy, cell cycle profiling by Cytell®, Seahorse basic metabolic measurement; or cytotoxicity study.

2.4.2. Cell lysis

Harvested cell pellets were re-suspended in 8 M urea PTMscan lysis buffer (PTMscan[®] lysis buffer, Cell Signalling Technology, Inc.), sonicated using Bandelin Sonopuls sonicator for three cycles each of 30 seconds at power setting of 50%, centrifuged at 20,800 g for 20 min at 4°C, and protein content in the supernatant

was measured using Bradford assay reagent (Pierce Detergent Compatible Bradford Assay Kit cat. #23246S) (Bradford, 1976).

2.4.3. Mitochondrial enrichment

GDC-0980 sensitive parent (P) and resistant (R) H1975 cells were cultured as mentioned in section 2.4.1. The mitochondrial isolation kit (cat. #ab110171) was purchased from Cell Signalling Technology. To enhance the mechanical disruption of the cell membrane, the cell pellets were frozen at -20°C overnight and thawed at room temperature. Cells were then suspended in 1 ml of cell lysis buffer (Buffer A, provided) and incubated for 30 min on ice. The cell suspension was then vortexed and transferred into a 2-ml Dounce homogenizer precooled at -20°C, and the cells were lysed by mechanical rupture through 30 strokes using pestle B (provided). To remove the relatively large debris, the cell lysate was centrifuged at 5400 g for 10 min at 4°C. The supernatant was then transferred into a new 2-ml centrifuge tube and the pellet was re-suspended in 1 ml of buffer A and given 30 more strokes in the pre-cooled Dounce homogenizer. The two supernatants were combined and centrifuged at 20,800 g at 4°C for 20 min. The pellet (orange) was re-suspended in 500 µl of buffer C containing protease inhibitor (provided) and kept at -80°C until protein quantitation.

2.4.4. Samples protein quantification

The Bradford Reagent Micro assay protocol (Sigma-Life Science, Lot #SLBH7472V) and micro plate reader (Synergy HT BioTEK and KC4 kineticalc software version #3.3/Re #10) at 595 nm were used to measure the protein content of supernatants. The lysate was divided into aliquots equivalent to 20 µg total protein and kept at -20°C until used for mass spectrometry analysis, western blot validation or other assays.

2.4.5. Label-free mass spectroscopy

2.4.5.1. Protein sample preparation for label-free LC-MS/MS

Samples equivalent to 20 µg of total protein (GDC-0980 parent vs. resistant (R+, R-) H1975 cells) in triplicates were reduced with 1 µl of 10 mM dithiothreitol (DTT; CAS No. 3483-12-3) in water for 30 min at 37°C and then alkylated with 1 µl of 50 mM iodoacetamide (IAA; CAS No. 144-48-9) prepared in 50 mM ammonium bicarbonate in the dark at room temperature. Next, samples were mixed with 50 mM ammonium bicarbonate (CAS No. 213-911-5) buffer in a 3:1 buffer to sample ratio. Then, protein samples were digested with 1.5 µl of trypsin (sequencing grade modified trypsin; Promega ref. V5111) at a concentration of 1 µg/µl at 37°C with shaking at 6 g overnight (minimum of 15 hours). The reaction was stopped using sample buffer containing a combination of 2 ml acetonitrile (Fluka, CAS No. 75-05-8) supplemented with 200 µl of trifluoroacetic acid (Sigma-Aldrich, prod. code 101398066) and 7.8 ml of double distilled H₂O), in a 3:1 sample to buffer ratio. The samples were vortexed, put on ice for 30 min, and de-salted using C18 spin columns (Thermo Pierce C18 spin columns) according to the manufacturer's protocol. The desalted samples were dried in nitrogen vacuum drier at a low drying rate without heat. Finally, the precipitate was dissolved in 25 µl of buffer A containing 0.1% TFA and centrifuged at 20,800 g for 20 min, and the top 20 µl of supernatant was transferred into a MS vial.

2.4.5.2. LC-MS/MS

Samples in triplicates were introduced in Q-EXACTIVE with the same settings described in section 2.1.4. The raw files were processed as mentioned in section 2.1.5. The significant (p-value ≤ 0.05) proteins found up or downregulated in GDC-

0980 resistant H1975 lung adenocarcinoma cells either cultured in (R+) or without (R-) the drug compared to the parent cells were listed in tables for further validation.

2.4.6. Western blot

Samples equivalent to 20 µg protein were used in triplicate to compare GDC-0980 sensitive parent and resistant H1975 cells cultured in RPMI medium conditioned as described in section 2.4.1. Low protein content samples were treated with 5 volumes of acetone chilled at -80°C, vortexed, and incubated overnight at -20°C. The acetone-treated samples were centrifuged at 20,800 g at 4°C for 30 min and the pellet was suspended in a volume of water equivalent to 25% of the original sample volume (4x concentrate). The protein content was measured again to calculate the volume equivalent to 20 µg protein.

2.4.6.1. SDS gel separation of cells lysate-proteome

Samples in triplicate were reduced with 5 µl of 4x sample loading buffer (Table 11) for 5 min on a thermo-mixer (Thermo-Fisher Scientific) at 1.5 g. Next, samples were cooled on ice for 2 min before being loaded on a SDS polyacrylamide gel. Proteins were resolved in 12% pre-casted SDS gels (GE healthcare Amersham™ ECL gels 12%, Lot No. 28-9898-05) at 140 V for 65 min in a horizontal electrophoresis unit (Amersham™ ECL Gel Box horizontal electrophoresis unit) using 1x electrophoresis running buffer containing 25 mM Tris-base, 192 mM glycine and 0.1% SDS (Table 12). Color-coded pre-stained protein marker (Cell-Signalling Technology, cat. #14208) (Figure 6) was used to confirm the protein molecular sizes.

Table 11: Composition of 4x Laemmli sample loading buffer

Chemical name	Quantity
1M Tris-HCl pH 6.8	2 ml
Sodium dodecyl sulphate (SDS)	0.8 g
β -mercaptoethanol	4 ml
10% Bromophenol blue	10 μ l
Glycerol	4 ml

Table 12: Composition of SDS-PAGE running buffer

10X running buffer recipe	Quantity
Glycine	144 g
Tris base	30.2 g
SDS	10 g
Double distilled H ₂ O	Up to 1 L

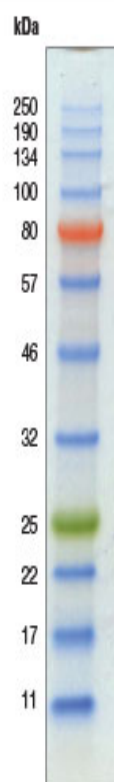


Figure 6: Color-coded pre-stained protein marker.

2. 4.6.2. Nitrocellulose membrane protein electro-transfer and antibody

incubation

The resolved proteins were electro-transferred onto nitrocellulose membrane (0.22 µm pore diameter) using One-Step transfer buffer (Thermo Scientific, product No. 84731) and Pierce G2 fast blotter (Thermo-Fisher Scientific) at 25 V for 5 to 10 min, depending on the molecular weight of the protein. The transfer cassette consists of (bottom to top) seven layers of absorbent papers soaked in transfer buffer, followed by a nitrocellulose membrane, then by the SDS gel containing the resolved proteins (with the marker to the left), then on top seven more layers of soaked absorbent paper.

The membrane was then blocked in 5% non-fat skimmed milk (Marvel skimmed milk powder, Premier Food Group Ltd., UK) prepared in 1x PBS containing 0.01% Tween-20[®] for 2 h with medium shaking. The membrane was then washed twice with 1xX PBS/0.1 Tween-20 and incubated with the primary antibody (monoclonal) overnight at 4°C on a medium speed shaker (Table 13). Then, the nitrocellulose membrane was washed twice with 1x PBS/0.1 Tween-20 and incubated with the secondary antibody, anti-mouse IgG HRP-linked antibody (Cell Signalling cat. No. 7076) or anti-rabbit IgG HRP-linked antibody (Cell Signalling cat. No. 7074) for 2 h. The membrane was again washed twice and kept in 1x PBS/0.1 Tween-20 washing buffer until developed.

2.4.6.3. Incubation of nitrocellulose membrane with HRP

The nitrocellulose membrane was incubated with 5 ml of 1:1 volume ratio of reagents A and B (ECL western blotting substrate, Pierce Thermo-Scientific, prod. #32106) for 2-3 min, and the chemiluminescent signal corresponding to the amount of the protein in the sample was captured using G-Box (G:Box Chemi-XT4 GENESys).

Images were obtained and saved as tiff files with a black background and white signal (the default G-Box settings) for further Image-J software quantitative analysis.

2.4.6.4. ECL signal measurement

Image-J software (version K 1.45) was used to measure the chemiluminescent signal in the tiff images taken by G-Box. Rectangles of the same size were drawn around the captured ECL signals and the image J corresponding numbers were compared using Prism software.

2.4.6.5. Chemiluminescent signal analysis

Image J measured values correspondent to the intensities of the bands obtained by western blot (in triplicates), the values were then divided by their correspondent loading control values and expressed as ratio, and the p values from comparing the protein abundance of the resistant cells (treated, R+ or non-treated, R-) to the parent cells were calculated using non-parametric two-way ANOVA with GraphPad Prism7.

2.4.6.6. Western blot loading control

Beta actin, alpha tubulin and glyceride-3-phosphate dehydrogenase enzyme (GAPDH) which used routinely as a loading control were all elevated in the resistant cells compared to the parent cells, so the first step was to find a loading control for the comparison of GDC-0980 treated (R+) and non-treated (R-) with the parent (P) H1975 cells. HDAC I was the best (reproducible) for comparing R- and P and PCNA was reproducible for comparing R+ and P (figure 7). These two loading controls were then used for all western blots to confirm equal amount of samples (20µg protein) and to exclude any samples loss during samples loading into the gel wells.

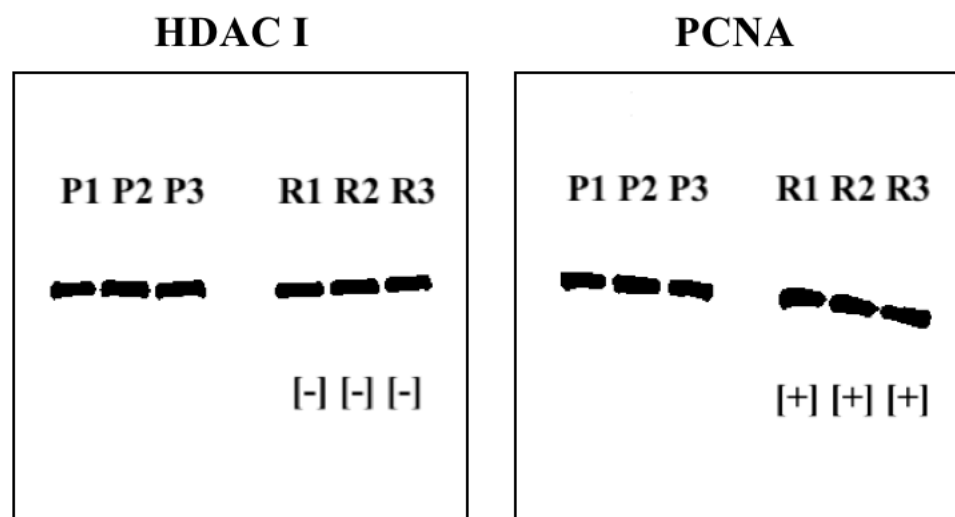


Figure 7: western blot loading control for treated (R+) and non-treated GDC-0980 resistant cells compared to their matching parent cells (P).

Table 13: Mitochondrial membrane marker antibody sampler kit (Cat.# 8674T)

Antibody	Cat. #	Blocking agent
** HSP60 (D6F1) m	12165T	5% BSA
** SDHA (D6J9M) m	11998T	
** VDAC (D73D12) m	4661T	
** PDH (C54G1) m	3205T	
** Cytochrome C (136F3) m	4280T	
** PHB1 m	2426T	
** COX IV (3E11) m	4850T	
Anti-rabbit Ig G ^Ω p	7074	
*** SOD1 (71G8) m	4266T	5% Non-fat skimmed
Anti-mouse IgG HRP-linked Ab ^Ω p	7076	milk*

HSP: heat shock protein, SDHA: P succinate dehydrogenase A, VDAC: voltage-dependent anionic channel, PDH: pyruvate dehydrogenase, PHB1: prohibitin B1 isoform, COX IV: cytochrome c oxidase 6, SOD: superoxide dismutase. IgG: immunoglobulin G, HRP: horseradish peroxidase, Ab: antibody. mAb: mono-clonal antibody, pAb: polyclonal antibodies, BSA: bovine serum albumin. Antibodies were diluted at 1:1000 in 5% w/v BSA containing 0.1% Tween-20 in 1xPBS. Incubation time was overnight in all primary antibodies and two hours for the secondary antibodies. **Rabbit mAb, ***Mouse mAb, ^Ω Secondary antibody, m: mAb, p: pAb. *Marvel skimmed milk powder (Premier Food Group Ltd., UK).

2.4.7. TMRE mitochondrial membrane potential assay kit (cat. #ab113852).

Cells were cultured as in section 2.4.1 and harvested in 1 ml PBS. To distinguish live from dead cells, the cells in 0.4% trypan blue sterile-filtered solution (cat. #T8154, CAS #72-57-1, Sigma-Aldrich® -now Merck) were counted under light microscopy using a X20 lens and hemocytometer slide. Cell suspension volumes equivalent to approximately 150,000 cells were transferred into five 1.5-ml Eppendorf tubes and the volume was made up to 200 μ l sterile media conditioned as mentioned above. Cells were then treated as follows:

Tube 1: Only cells;

Tube 2: Negative control containing 50 μ M carbonyl cyanide p- trifluoromethoxy phenylhydrazone (FCCP);

Tube 3: Containing 200 nM TMRE (tetramethylrhodamine, ethyl ester);

Tube 4: TMRE pre-treated with FCCP;

Tube 5: Stained with Mito tracker as described in its protocol).

In tube 4, cells were pre-treated with FCCP for 20 min at 37°C, and all treatments were incubated for 30 min at 37°C. Cells were then washed twice with 1x PBS and analysed in BD Accuri™ C6 Plus flow cytometer using side scatter content (SSC) at FL2 channel. The population obtained was gated into four quadrants to correlate cell cycle phase with mitochondrial membrane activity (Hikita et al., 2015, Fujiwara et al., 2015).

2.4.8. Basic metabolic phenotyping

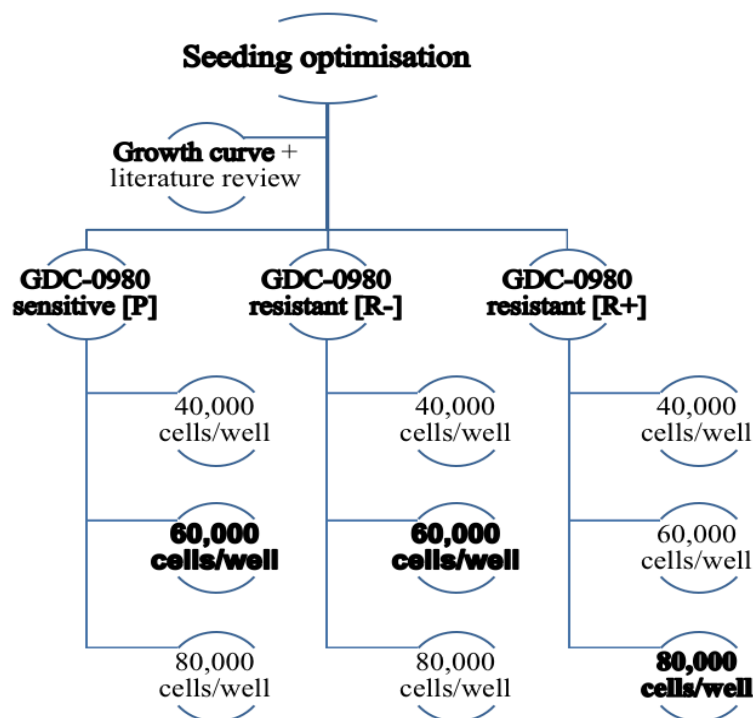
This experiment was conducted in Saint James' Hospital, Department of Surgery at the Institute of Molecular Medicine. Seahorse XF24 extracellular Flux AnalyZER and Seahorse XF24 FluxPak mini kit (Part #100867-100) were used in this experiment.

2.4.8.1. Optimisation of seeding density for seahorse analysis

Based on the growth curve, three seeding densities were used to select the optimal seeding density for producing a good Seahorse XF24 Analyzer signal (Diagrams 1 & 3). The average of six measurements of the oxygen consumption rate (**OCR**) and the extracellular acidification rate (**ECAR**) per treatment were taken.

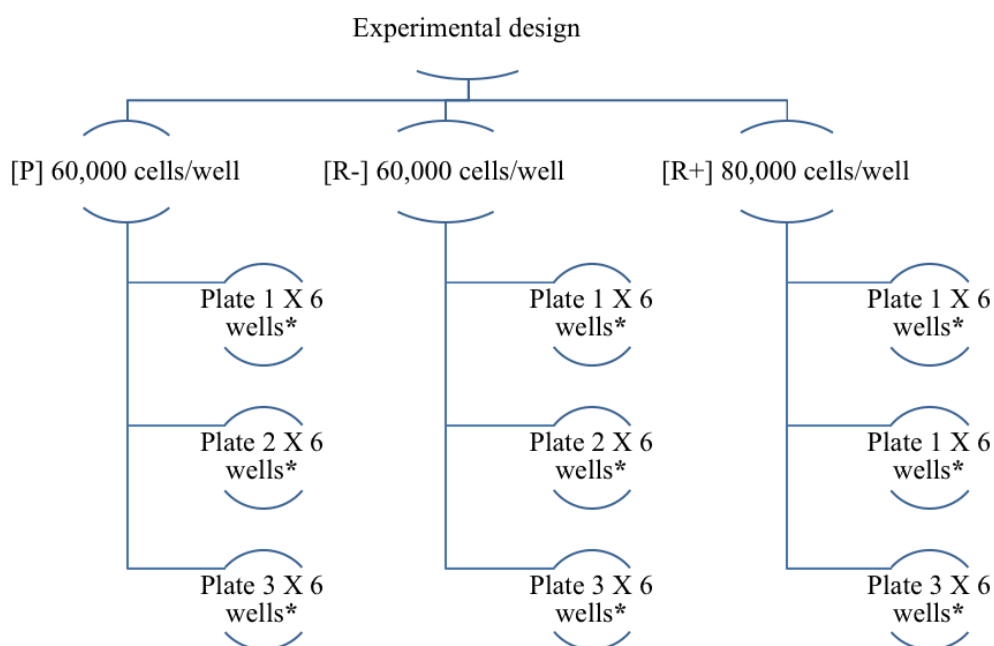
Diagrams 2 & 3 depict the experimental setup. The experiment was performed once a week for three consecutive weeks, and the average measurements of three plates per tested cells was taken: parent sensitive, resistant (drug free, R-) and resistant (plus drug, R+).

Diagram 1: Optimisation of H1975 cells seeding density for seahorse analysis



*P (Parent: GDC-0980 sensitive cells), R- (GDC-0980-resistant cells grown and assayed in GDC-0980 free RPMI/assay medium), R+ (GDC-0980-resistant cells grown and assayed in RPMI/assay medium containing 1 μ M DC-0980), numbers in **bold** are the used cells density.*

Diagram2: Seahorse experiment design



P (Parent: GDC-0980 sensitive cells), *R-* (GDC-0980-resistant cells grown and assayed in GDC-0980 free RPMI/assay medium), *R+* (GDC-0980-resistant cells grown and assayed in RPMI/assay medium containing 1 μ M DC-0980), * see plate map (diagram 3).

Diagram 3: Plate mapping for seahorse OCR and ECAR measurement

	1	2	3	4	5	6	
A	M+	P	P	R+	R-	M-	A
B	R+	R-	M+	M-	P	R+	B
C	P	R+	M+	R+	R-	R-	C
D	R-	P	R+	P	R-	M-	D
	1	2	3	4	5	6	

Where: *M-* (GDC-0980-free assay medium), *M+* (Assay medium + 1 μ M GDC-0980 final concentration), *P* (Parent: GDC-0980 sensitive cells), *R-* (GDC-0980-resistant cells grown and assayed in GDC-0980 free RPMI/assay medium), *R+* (GDC-0980-resistant cells grown and assayed in RPMI/assay medium containing 1 μ M DC-0980), OCR: oxygen consumption rate, ECAR: extracellular acidification rate.

2.4.8.2. Basic metabolism measurement protocol

GDC-0980 sensitive (P) and resistant H1975 (R) lung adenocarcinoma cells were cultured in RPMI medium containing 10% BSA and 1% streptomycin in T75 flasks. The medium for growing the resistant cells was conditioned by supplementation with a final concentration of 1 μ M GDC-0980 (R+) or GDC-0980 free media (R-). To select the optimal seeding density for H1975 cells, a growth curve was constructed using five T25 flasks for each of the three conditions. OD at 600 nm was read on five consecutive days and plotted against time. Sensitive (P), resistant treated (R+) or resistant non-treated (R-) cells were seeded at densities of 40,000, 60,000 and 80,000 cells/well, respectively, in 24-well cell culture plates (Seahorse Bioscience V7-PS, TC-treated, Part #100777-004, Lot: 26516) in 250 μ l per well and allowed to adhere overnight.

The XF24 sensor cartridge was hydrated in 1 ml of Seahorse XF Calibrant per well (Seahorse bioscience, Lot No. 089, Part No. 100840-000) overnight at 37°C in a CO₂-free incubator.

The next day, wells were washed three times with the assay medium (XF assay medium, modified DMEM, CAT No. 102352-000, part No.102365-100, Lot 08816010) supplemented with 10 mM glucose (G8270 Sigma, CAS No. 50-99-7) and 10 mM sodium pyruvate (P2256 Sigma-Aldrich, CAS No. 113-24-6) final concentration. 150 μ l of the RPMI medium was removed and 1 ml of assay medium was added, then 900 μ l was removed and 300 μ l of assay medium was added to get a final volume of 500 μ l. Cells were incubated for 40 min at 37°C in a CO₂-free incubator. In the last 20 min of incubation, the XF24 sensor cartridge was introduced into the Seahorse XF24 Analyzer after removing the lid and the utility plate. After calibration, the cartridges were placed on the tested plate and introduced into the

Seahorse XF24 Analyzer. Cells were stained with 0.5% crystal violet solution at room temperature for 20 min, washed three times with water, and incubated with 50 μ l of 0.1% Triton-X100 with shaking at 37°C for 2 h. OD was read at 595 nm, and the results from the Seahorse XF24 Analyzer were normalized by dividing their values by the corresponding crystal violet measurement. The normalized OCR and ECAR values were compared using GraphPrism® 7.0. The XF24 report generator template from Agilent was used to explain the metabolic phenotyping differences.

2.4.9. H1975 mitochondrial distribution pattern (Lackner, 2013)

MitoTracker® Red CMXRos (Cell Signalling®, Cat #9082s) was used to examine the pattern of mitochondrial distribution in the cytoplasm. Cells were seeded in a Lab-Tek II® chamber slide with cover (RS glass slide sterile/8 well, cat. #154534, lot #081315-8-1). The MitoTracker® Red CMXRos vial contains 50 μ g of lyophilized stain reconstituted in 94.1 μ l high quality DMSO to make 1 mM MitoTracker® stock solution. Each experiment condition (H1975 GDC-0980 parent cells, H1975 GDC-0980 resistant cells without drug (R-) and H1975 GDC-0980 resistant cells with drug (R+) were seeded on separate slides, and the stain was diluted directly into the medium at four different final concentrations: 100, 200, 350, and 400 nM, and then incubated for 45 min at 37°C under 5% CO₂.

The cells were then fixed using ice-cold methanol for 15 min at -20°C and then rinsed with PBS for 5 min three times. Finally, the slide chamber was removed, the slide cover was carefully placed on top of the slide aided by mounting medium (Sigma-Aldrich® -now Merck -cat. #M1289-10ML). The slide cover edges were sealed with nail polish, and the slides were examined by confocal microscopy.

2.4.10. Cell cycle of GDC-0980 parent and resistant H1975 and A549 cells

GDC-0980 sensitive parent and resistant H1975 and A549 lung adenocarcinoma cells were cultured in RPMI and F12 medium, respectively as detailed in section 2.4.1. Cells were seeded in Nunc™ MicroWell™ 96-well microplates in six replicates per treatment condition (parent P, resistant with drug R+ and resistant without drug R-) and each cell line was tested in separate plate on the same day. Cells were allowed to adhere for 24 h in medium conditioned as described in section 2.4.1 and then washed with 300 µl 1x PBS twice and fixed in pre-warmed (37°C) 4% formaldehyde (Image-iT™ Fixative Solution; 4% formaldehyde, methanol free, Cat #FB002) containing 0.3% Triton-X100 (ThermoFisher Scientific, Triton™ X-100 Surfact-Amp™ Detergent Solution, cat. #28313) (pre-warmed at 37°C) for 15 min at 37°C. Next, cells were washed twice with 1x PBS, incubated with DAPI (Invitrogen™-DAPI, cat. #D3571) (5µg/ ml final concentration) for 15 min at room temperature (Kapuscinski, 1995), and then kept in 1x PBS after two washes. Cell cycle was read in a Cytell® Cell Imaging System (GE Healthcare Life Sciences) at the Institute of Molecular Medicine, Saint James' Hospital, Trinity College Dublin.

2.4.11. Western blot validation of cell cycle

GDC-0980 sensitive parent and resistant H1975 lung adenocarcinoma treated (R+) or untreated (R-) as described in section 2.4.1 were harvested at 85% confluence and lysed in 8 M urea buffer as described in section 2.4.2. Protein content was measured using Bradford protein quantitation reagent (Pierce Detergent Compatible Bradford Assay Kit Cat#. 23246S) (Bradford, 1976) (section 2.4.4.). Sample volumes equivalent to 20 µg of total protein were used to compare GDC-0980 sensitive parent and resistant cells grown with or without the drug. The protocol detailed in section 2.4.6 was used to assess cell cycle cyclins (Table 14).

Table 14: Cyclin Antibody Sampler Kit (cat. #9869)

Antibody	Type	Cat. #	Blocking agent
** Histone H3 (D1H2) XP®	mAb	4499	5% BSA
** Cyclin B1		4138	
**Cyclin D1 (92G2)		2978	
** Histone H4 (D2X4V)		13919	
** Cyclin H		2927	
***Cyclin A2 (BF683)		4656	
***Cyclin D3 (DCS22)		2936	
Anti-rabbit IgG Ω	HRP-linked Ab	7074	5% Non-fat skimmed milk*
Anti-mouse IgG Ω		7076	

*BSA: bovine serum albumin, antibodies were diluted at 1:1000 in 5% w/v BSA (rabbit-Abs) or 1:200 in 5% w/v skimmed milk (mouse-Abs) containing 0.1% Tween-20/PBS. *Marvel skimmed milk powder (Manufacturer: Premier Food Group Ltd, UK), **Rabbit IgG mAb, Ω secondary antibody, IgG mAb, ***Mouse IgG mAb, Ω secondary antibodies, HRP: horseradish peroxidase, IgG: immunoglobulin G. mAb: monoclonal antibody, pAb: polyclonal antibodies. Incubation time was overnight in all primary antibodies and two hours for the secondary antibodies.*

2.4.12. Histone acetylation of GDC-0980 parent and resistant H1975 and A549 cells

GDC-0980 sensitive parent and resistant H1975 lung adenocarcinoma, treated (R+) and untreated (R-) (section 2.4.1) were harvested at 85% confluence and lysed in 8 M urea buffer as mentioned in section 2.4.2. Protein content was measured using Bradford protein quantitation reagent (Pierce Detergent Compatible Bradford Assay Kit cat. #23246S) (Bradford, 1976). Sample volumes equivalent to 20 µg of total protein were used to compare GDC-0980 sensitive parent and resistant cells grown with or without the drug. The protocol described in section 2.4.6 was used to assess differences in acetylation level among the cell populations. Table 15 shows the list

of the primary antibodies used. Anti-rabbit IgG, HRP-linked antibody (CellSignalling[®], cat. #7074) and HRP-linked anti-mouse IgG (CellSignalling[®], cat. #7076) were used as secondary antibodies when applicable (1:1000 and 1:2000 dilutions, respectively).

2.4.13. Histone co-localization in H1975

GDC-0980 sensitive parent and resistant H1975 lung adenocarcinoma, treated (R+) and untreated (R-) (section 2.4.1) were seeded in a Lab-Tek II[®] chamber slide with cover (RS Glass slide sterile/8 well cat. #154534, lot #081315-8-1) and allowed to adhere overnight. Then, they were washed twice with 1x PBS, fixed in 4% formaldehyde (Image-iT[™] Fixative Solution (4% formaldehyde, methanol free), cat. #FB002) containing 0.3% Triton-X100 (pre-warmed at 37°C), for 15 min at 37°C. The fixed cells were permeabilised by adding 100 µl of 0.3% Triton X-100 (Thermo-Fisher Scientific, Triton[™] X-100 Surface-Amp[™] Detergent Solution, cat. #28313) prepared in 1x PBS and washed once with 1x PBS for 5 min. The slides were blocked with 100 µl of 5% goat serum (Normal goat serum, cat. #5425, Cell Signalling Technology[®]) prepared in 1x PBS containing 0.3% Triton[™] X-100 per well for 60 min at room temperature. The blocking buffer was aspirated, the cells were washed twice with 1x PBS for 5 min, and incubated overnight at 4°C with 100 µl anti histone H3 primary antibody (Histone H3 (D1H2) XP[®] Rabbit mAb cat. #4499) diluted 1:500 in antibody dilution buffer containing 1% BSA (Cell Signalling Technology[®], cat. #9998) in 1x PBS containing 0.3% Triton[™] X-100.

Next, the cells were washed twice with 1x PBS for 5 min and incubated in the dark for 2 h with the secondary antibody (anti-rabbit IgG (H+L), F(ab)2 fragment (Alexa Fluor 488 conjugate), cat. #4412) diluted 1:400 in antibody dilution buffer at room temperature. The cells were washed with 1x PBS and stained with DAPI at a

concentration of 5µg/ml. Finally, the slide chamber was removed, the slide cover was carefully placed on top of the slide using one drop of mounting medium (Sigma-Aldrich®, now Merck, cat. #M1289-10ML), sealed with nail polish, and examined by confocal microscopy.

2.4.14. Western blot validation of lysine acetyl-transferases and histone deacetylases

GDC-0980 sensitive parent and resistant H1975 lung adenocarcinoma treated (R+) and untreated (R-) cells (section 2.4.1) were harvested at 85% confluence and lysed in 8 M urea buffer as mentioned in section 2.4.2. Protein content was measured using Bradford protein quantitation reagent (Pierce Detergent Compatible Bradford Assay Kit Cat#. 23246S) (Bradford, 1976). Samples volumes equivalent to 20 µg of total protein were used to compare GDC-0980 sensitive parent and resistant cells grown with or without the drug. The western blot protocol described in section 2.4.6 was used to assess differences in the levels of lysine acetyl-transferases (Cell Signalling®, cat. #9928) and histone deacetylases (Cell Signalling®, cat. #8686) among the cell populations. Table 16 lists the primary antibodies used. HRP-linked anti-rabbit IgG (Cell Signalling®, cat. #7074) and HRP-linked anti-mouse IgG (Cell Signalling®, cat. #7076) were used as secondary antibodies when applicable in 1:1000 and 1:2000 dilution, respectively.

Table 15: Acetyl-Histone Antibody Sampler Kit (cat. #9927)

Antibody	Type	Cat. #	Blocking agent
**Histone H3(D1H2) XP®	mAb	4499	5% BSA
**Acetyl-histone H3 (Lys 9)		9649	
**Acetyl-histone H3 (Lys 18)		13998	
**Acetyl-histone H3 (Lys 27)		8173	
**Histone H4 Antibody (L64C1)		2592	
**Acetyl-histone H4 (Lys5)		8647	
Anti-rabbit IgG ^Ω	HRP-linked Ab	7074	

BSA: bovine serum albumin, Lys: lysine, mAb: monoclonal antibody, pAb: polyclonal antibodies. Antibodies were diluted at 1:1000 in 5% w/v BSA containing 0.1% Tween-20 in 1xPBS. Incubation was overnight in all primary antibodies and two hours for the secondary antibodies. **Rabbit, ^Ω Secondary antibody.

2.4.15. Functional validation of HDAC role in GDC-0980 resistance

SAHA (Vorinostat) (Sigma-Aldrich, CAS. #149647-78-9) was used as a broadly acting HDAC inhibitor (Robey et al., 2011). A BrdU cell proliferation colorimetric ELISA kit (Cell-Signalling Technology[®], cat. #6813) was used to construct the dose-response curve for SAHA. GDC-0980 sensitive parent and resistant H1975 lung adenocarcinoma cells were cultured in RPMI medium conditioned as detailed in section 2.4.1. Cells were harvested at 70% confluence and seeded in Nunc[™] MicroWell[™] 96-well microplates in six replicates. The cells for each treatment (parent P, resistant with drug R+ and resistant without drug R-) were seeded in separate plates and allowed to adhere overnight.

A GDC-0980 dose-response curve was constructed by treating the cells with a gradient concentration starting from 10 nM to 35 μM and the percentage inhibition of growth was plotted against the log of GDC-0980 concentration.

A dose-response curve was also constructed for SAHA using a concentration gradient range from 1-20 μ M in H1975 lung adenocarcinoma cells with or without incubation with GDC-0980 to show the effect of HDAC phosphorylation on the activity of SAHA.

Table 16: Lysine Acetyl Transferase, deacetylase Antibody Sampler Kits

Antibody	Type	Cat. #	Blocking agent
*** HDAC1 (10E2)	mAb	5356	5% Non-fat skimmed milk*
*** HDAC2 (3F3)		5113	
*** HDAC3 (7G6C5)		3949	
** HDAC4 (D15C3)		7628	5% BSA
** HDAC6 (D2E5)		7558	
** Phospho-HDAC4/5 π		3443	
** PCAF (C14G9)		3378	
** GCN5L2 (C26A10)		3305	
Anti-rabbit IgG Ω	HRP-linked Ab	7074	
Anti-mouse IgG Ω	HRP-linked Ab	7076	

*HDAC: histone deacetylase, numbers denote enzyme isoforms, PCAF: P300/CBP associated factor, CBP: CREB binding protein, CREB: cAMP response element binding protein, GCN5L2: general control of amino acid synthesis, IgG: immunoglobulin G, mAb: monoclonal antibody, pAb: polyclonal antibodies, BSA: bovine serum albumin. Antibodies were diluted at 1:1000 in 5% w/v BSA (rabbit-Abs) or skimmed milk (mouse-Abs) containing 0.1% Tween-20/1xPBS. Incubation was overnight in all cases. *Marvel skimmed milk powder (Manufacturer: Premier Food Group Ltd, UK), **Rabbit, ***Mouse, Ω secondary antibodies, and π (phosphorylation site: Ser246 and Ser259 in HDAC 4, 5, respectively).*

2.4.15.1. BrdU Cell Proliferation ELISA Assay protocol

BrdU Cell Proliferation colorimetric ELISA Kit (Cell-Signalling Technology[®], cat. #6813) was used to study the cytotoxicity of vorinostat (SAHA) to GDC-0980 sensitive and resistant H1975 adenocarcinoma cells cultured either with or without GDC-0980 incubation. After incubating the cells overnight with SAHA in six replicates per concentration, they were labelled with 1x BrdU labelling reagent (final concentration) for 4 h. They were next washed 3x with 300 µl of 1x washing buffer and fixed/denatured in 200 µl 1x ready to use fixation buffer for 30 min at room temperature. The cells were washed 3x with 300 µl of 1x wash buffer and incubated for 2 h with 100 µl of 1x anti-BrdU detection mouse monoclonal antibody at room temperature. 100 µl of 1x HRP-conjugated anti-mouse secondary antibody was added per well followed by incubation at room temperature for 30 min. After 3 washes, they were left to dry at room temperature. The cells were then incubated with 100 µl of TMB substrate (part #7004) for 30 min at room temperature. Once the blue colour developed, the reaction was stopped by adding 100 µl stop solution (1 N HCl, part #7002) and the absorbance was read at 450 nm within 10 min. All measurements were uploaded into Prism 7.0 software and the log-dose response as percentage inhibition of growth was obtained.

2.4.16. Western blot validation of cell survival, apoptosis and evasion biomarkers

GDC-0980 sensitive parent and resistant H1975 lung adenocarcinoma cells, treated or untreated as mentioned in section 2.4.1, were harvested at 85% confluence and lysed in 8 M urea buffer as mentioned in section 2.4.2. Protein content was measured using Bradford protein quantitation reagent (Pierce Detergent Compatible Bradford Assay Kit Cat#. 23246S) (Bradford, 1976). Sample volumes equivalent to 20 µg of total protein were used to compare GDC-0980 sensitive parent and resistant cells grown with or without the drug. The western blot protocol mentioned in section 2.4.6 was used to evaluate the expression of the proteins involved in cell survival and evasion of apoptosis in the different cells under the specified conditions. Tables 17, 18 and 19 list all the antibodies used.

Table 17: NF-Kb family member antibody sampler kit (cat. #4766)

Antibody	Type	Cat. #	Blocking agent
** Rel-A (L8F6) p65	mAb	8242	
** Rel -B (C1E4) p70	mAb	4922	
** c- Rel p78	mAb	4727	5% BSA
**NF-KB1 (B7H5M) p105/P50 π	mAb	12540	
Anti-rabbit IgG	pAb	7074	

*Antibodies were diluted at 1:1000 in 5% w/v BSA containing 0.1% Tween-20 in 1xPBS. Incubation was overnight in all cases. **Rabbit mAb, ^Ω Secondary antibody, π P50 active, Ω P52 active.*

Table 18: 14-3-3 Family Antibody Sampler Kit (cat. #9769).

Antibody	Type	Cat. #	Blocking agent
** 14-3-3 α/β	mAb	9636	
** 14-3-3 γ	mAb	5522	
** 14-3-3 ζ/δ	mAb	7413	5% bovine serum albumin
** 14-3-3 ϵ	mAb	9635	
** 14-3-3 η	mAb	5521	
Anti-rabbit IgG ^{Ω}	pAb	7074	

*Antibodies were diluted at 1:1000 in 5% w/v BSA containing 0.1% Tween-20 in 1xPBS. Incubation was overnight in all cases. **Rabbit mAb, ^{Ω} Secondary antibody.*

Table 19: Miscellaneous antibodies.

Antibody	Type	Cat. #	Blocking agent
**P53 (7F5)	mAb	2527	
**Bax (D2E11)	mAb	5023	
**Bcl-xL (54H6)	mAb	2764	
**P21 waf1/Cip1 (12D1)	mAb	2947	5% bovine serum albumin
**PCNA (D3H8P) XP [®]	mAb	13110	
**Ubiquityl-PCNA (Lys164)	mAb	13439	
Anti-rabbit IgG ^{Ω}	pAb	7074	

*Antibodies were diluted at 1:1000 in 5% w/v BSA containing 0.1% Tween-20 in 1xPBS. Incubation was overnight in all cases. **Rabbit mAb, ^{Ω} Secondary antibody.*

Chapter 3

Bronchoalveolar lavage discovery work

3. Bronchoalveolar lavage discovery work

3.1. Introduction

Bronchoalveolar lavage collection is collected in the surgical theatre by bronchoscopy. Bronchoscopes are either rigid or fibre-optic flexible bronchoscopes. Bronchoscopy is used for investigation and surgery and requires anaesthesia.

For simple bronchoscopic procedures, conscious sedation using fast, short acting anaesthetics such as ketamines is the standard, but general anaesthesia is mandatory for long surgical procedures (Chadha et al., 2015). The similarity between lung cells obtained by biopsies and those harvested in BALF gave rise to the assumption that BALF can reflect the overall lungs status (Gee and Fick, 1980). However, collection of BALF is unsuitable as a routine clinical or research sampling procedure (Singletary et al., 2008). Therefore, efforts continue to establish a protocol for BALF collection to enhance its diagnostic value (Singletary et al., 2008). The European Respiratory Society has tried to establish general guidelines for the measurement and standardization for human normal BALF (Crystal et al., 1986). Like blood, BALF is near the tumour tissue, but it is superior in that it does not contain an abundance of proteins, for example albumin, that can mask others, especially when using mass spectrometry for comparing clinical lavage samples for biomarkers discovery.

3.2. Experimental design

The study aimed to find biomarkers for diagnosis and differentiation of lung adenocarcinoma and squamous cell carcinoma. Institutional ethical approval was granted from the Beaumont Hospital, Ethics Committee (REC reference: 10/61). BALF and blood samples were collected from patients whom were undergoing diagnostic bronchoscopy in Beaumont Hospital, Dublin, Ireland.

NSCLC samples represented all stages of the disease. BALF control samples collected from healthy individuals (7 male and 5 female) and sarcoid patients (4 male, 0 female) were compared with BALF samples from patients with NSCLC lung carcinomas (AD: 10 male, 3 female and SqCC: 8 male, 5 female) using label-free mass spectrometry. All TNM stages were included; [AD: 3 male, 3 female (stage I/II) and 7 male, 0 female (stage III/IV)] and [SqCC 4 male, 4 female (stage I/II) and 4 male, 1 female (stage III/IV)]. Age matching samples was also applied in this experiment (table 5). Candidate biomarkers were selected based on their high abundance and knowledge of their involvement in the pathogenicity of lung cancer, and validated in small number of samples using Enzyme-Linked immunosorbent assay (ELISA). The promising candidate biomarkers (Cystatine C, Lipocalin II, Heat shock protein 70 and Tissue Inhibitor of Metallo-Proteinases (TIMP-1) were then validated in a large size of NSCLC plasma samples (figure 11).

3.3. Results

3.3.1. The cut-off value for lung adeno and squamous carcinomas proteome signature.

Figure 8 shows the selection of the fold change cut-off value for the LC-MS/MS analysis comparing lung adenocarcinoma and squamous cell carcinoma lung lavages with the control lavages (healthy individuals and sarcoid) for determining which signature that can help differentiate between the two types of lung carcinoma studied in this discovery experiment. A 1.2-fold up or down change was set as the acceptable lowest fold change to differentiate between the two lung carcinomas. The columns represent the number of proteins additionally excluded after applying 1.2 fold change as a cut-off value. This figure helps to decide which method is appropriate for validating such changes in expression.

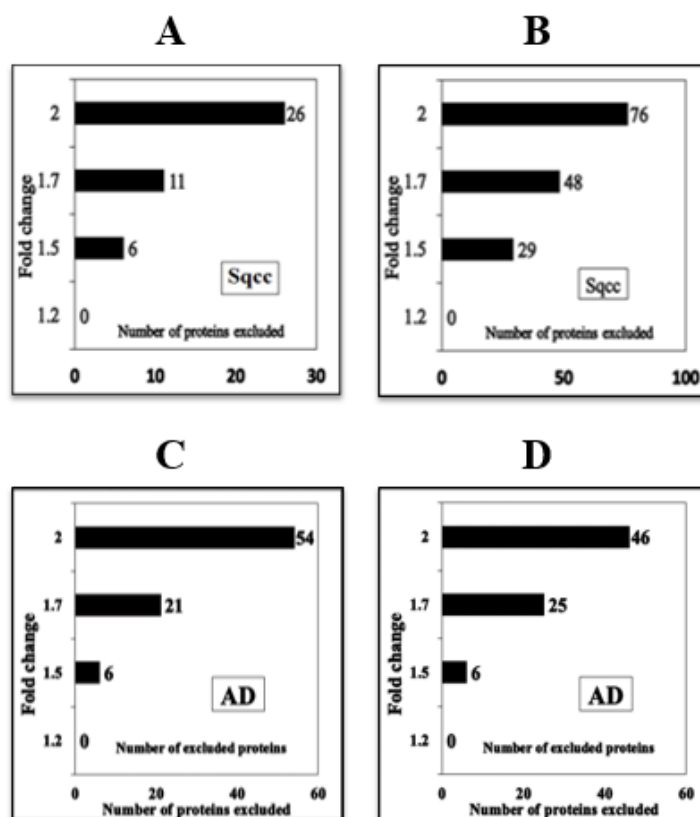


Figure 8: The number of proteins excluded per fold change cut-off value for upregulation (A) or down-regulation (B) in lung squamous cell carcinoma, and upregulation (C) or down-regulation (D) in adenocarcinoma.

3.3.2. Comparison of lung adenocarcinoma lavage proteome to the control lavage

3.3.2.1. Proteins significantly elevated in AD lavage compared to control.

Label-free mass spectrometry comparative analysis of bronchoalveolar lavage from control (healthy individuals and sarcoid) and lung adenocarcinoma (table 5). Using a 1.2-fold change as cut-off, 479 proteins were found significantly elevated in lung adenocarcinoma broncho-alveolar lavage compared to the control samples (Appendix 1); the top 30 are listed in table 20.

Table 20: Top 30 significantly elevated proteins in AD compared to the controls

Accession	P/C	P/C*	Score	p-value	FC (1.2)	Description
P62269	1	1	2	2.E-07	30.1	40S ribosomal protein S18
P07108	6	6	29	6.E-07	4.9	Acyl-CoA-binding protein
P84077	3	3	12	3.E-06	2.8	ADP-ribosylation factor 1
P01009	27	27	206	9.E-07	5.9	Alpha-1-antitrypsin
P35609	9	9	28	3.E-07	3.1	Alpha-actinin-4
P07355	9	9	41	4.E-08	3.4	Annexin A2
P20073	1	1	3	1.E-06	7.7	Annexin A7
P03973	10	10	63	5.E-08	7.6	Antileukoproteinase
P61769	3	3	17	1.E-07	7.2	Beta-2-microglobulin
P31939	1	1	2	5.E-08	241.8	Bifunctional purine biosynthesis protein
P62158	6	6	42	9.E-10	9.6	Calmodulin
P13987	3	3	19	2.E-07	11.3	CD59 glycoprotein
P08962	1	1	2	1.E-08	25.7	CD63 antigen
P21926	1	1	4	8.E-07	12.3	CD9 antigen
Q13387	1	1	5	2.E-10	10.3	C-Jun-amino-terminal kinase-interacting P2
P35606	1	1	3	2.E-08	5.5	Coatomer subunit beta'
P06681	1	1	3	7.E-15	300.3	Complement C2
Q9UGM3	20	20	101	2.E-07	10.9	Deleted in malignant brain tumors 1
P81605	2	2	13	2.E-07	3.6	Dermcidin
P63096	3	3	8	3.E-10	7.3	Guanine NT-binding protein G(i) subunit α 1
Q14103	3	3	12	2.E-06	3.7	Heterogeneous nuclear ribonucleoprotein
P01591	7	7	32	7.E-07	3.9	Immunoglobulin J chain
B9A064	8	8	44	8.E-08	2.5	Ig lambda-like polypeptide 5
P13646	6	6	27	3.E-06	2.8	Keratin, type I cytoskeletal 13
P00338	6	6	24	1.E-07	3.5	L-lactate dehydrogenase A chain
P07195	8	8	28	3.E-07	5	L-lactate dehydrogenase B chain
Q02817	1	1	2	1.E-08	13.4	Mucin-2
P05204	1	1	2	1.E-06	10	Non-histone chromosomal protein HMG17
P15531	3	3	12	3.E-06	4.1	Nucleoside diphosphate kinase A
P62942	1	1	4	2.E-09	192.8	Peptidyl-prolyl cis-trans isomerase FKBP1A

AD: lung adenocarcinoma, P/C: number of peptides, P/C*: number of specific peptides, FC: maximum fold change, control: healthy individuals and sarcoid, 16 Ig removed.

3.3.2.2. Proteins significantly lowered in AD lavage compared to control.

Label-free mass spectrometry comparative analysis of bronchoalveolar lavage from control (healthy individuals and sarcoid) and lung adenocarcinoma (table 5). Using a 1.2-fold change cut-off, 145 proteins were found significantly lowered in lung adenocarcinoma broncho-alveolar lavage compared to the control samples (Appendix 2); the top 30 are listed in table 21.

Table 21: Top 30 significantly lowered proteins in AD compared to the controls

Accession	P/C	P/C*	Score	p-value	FC (1.2)	Description
Q13200	1	1	3	5.E-04	4.2	26S proteasome non-ATPase regulatory sub 2
P46108	1	1	2	3.E-07	9.3	Adapter molecule crk
Q01518	4	4	17	3.E-05	2.6	Adenylyl cyclase-associated protein 1
P08758	9	9	56	2.E-04	3.4	Annexin A5
P07339	8	8	43	3.E-04	2	Cathepsin D
Q8TD46	1	1	3	4.E-05	3.6	Cell surface glycoprotein CD200 receptor 1
P0C0L5	1	1	5	3.E-04	2.3	Complement C4-B
Q9ULV4	1	1	5	5.E-07	4.3	Coronin-1C
P15090	2	2	16	8.E-04	3.7	Fatty acid-binding protein, adipocyte
O75369	3	3	8	1.E-05	2.2	Filamin-B
P09467	2	2	14	4.E-04	6.1	Fructose-1,6-bisphosphatase 1
P13284	2	2	12	6.E-05	4.6	γ-INF-inducible lysosomal thiol reductase
P17900	1	1	4	1.E-05	9.8	Ganglioside GM2 activator
P00390	6	6	31	9.E-04	2.2	Glutathione reductase, mitochondrial
P02042	4	4	33	5.E-04	4.1	Hemoglobin subunit delta
Q16576	1	1	4	9.E-05	38.2	Histone-binding protein RBBP7
Q4G0P3	1	1	3	2.E-04	88.3	Hydrocephalus-inducing protein homolog
O15397	1	1	2	2.E-07	6.9	Importin-8
Q9Y547	1	1	6	8.E-06	3.6	Intraflagellar transport protein 25 homolog
P05787	7	7	31	9.E-07	3	Keratin, type II cytoskeletal 8
P22079	9	9	44	3.E-04	2.1	Lactoperoxidase
Q9UKX2	1	1	2	2.E-09	4.4	Myosin-2
Q9Y3Q0	1	1	3	9.E-06	90.4	N-acetylated-alpha-linked acidic dipeptidase 2
P22894	1	1	5	2.E-11	44.4	Neutrophil collagenase
A8MRT5	1	1	3	7.E-06	20.3	Nuclear pore complex-interacting protein B5**
P13796	16	15	74	7.E-04	2.2	Plastin-2
O60888	1	1	8	6.E-05	3.3	Protein CutA
P06703	3	2	17	5.E-04	2.5	Protein S100-A6
Q96FV2	1	1	3	8.E-04	4.9	Secernin-2

AD: lung adenocarcinoma carcinoma, P/C: number of peptides, P/C: number of specific peptides, FC: maximum fold change, control: healthy individuals and sarcoid, *glutamic acid, ** family member.*

3.3.3. Comparison of lung squamous carcinoma lavage proteome to the control lavage

3.3.3.1. Proteins significantly elevated in SqCC lavage compared to control.

Label-free mass spectrometry comparative analysis of bronchoalveolar lavage from control (healthy individuals and sarcoid) and lung Squamous cell carcinoma (table 5). Using a 1.2-fold change as cut-off, 419 proteins were found significantly elevated in lung squamous cell carcinoma broncho-alveolar lavage compared to the control samples (Appendix 3); the top 30 are listed in table 22.

Table 22: Top 30 significantly elevated proteins in SqCC compared to the controls

Accession	P/C	P/C*	Score	p-value	FC (1.2)	Description
P07108	2	2	7	9.E-06	4.5	Acyl-CoA-binding protein
P19652	4	4	35	2.E-12	8.2	Alpha-1-acid glycoprotein 2
P01009	31	31	273	3.E-08	4	Alpha-1-antitrypsin
P04745	27	27	243	6.E-05	18	Alpha-amylase 1
P08133	1	1	4	9.E-06	3.6	Annexin A6
P01008	8	8	40	2.E-05	2.8	Antithrombin-III
P17213	1	1	3	3.E-08	27	Bactericidal permeability-IP**
P02749	9	9	45	2.E-05	3.4	Beta-2-glycoprotein 1
P27797	6	6	20	4.E-05	3.1	Calreticulin
O43852	1	1	3	4.E-05	238.3	Calumenin
P00450	25	25	169	6.E-05	2.7	Ceruloplasmin
P09871	2	2	7	2.E-06	7.7	Complement C1s subcomponent
P01031	6	6	20	4.E-05	6.9	Complement C5
P08603	12	12	64	1.E-05	4	Complement factor H
P08185	4	4	12	1.E-06	2.9	Corticosteroid-binding globulin
P02671	5	5	21	8.E-07	4.8	Fibrinogen alpha chain
P00738	10	9	62	3.E-05	4.7	Haptoglobin
P00739	8	8	38	3.E-06	8.7	Haptoglobin-related protein
P62805	6	6	17	9.E-06	3.6	Histone H4
P01860	7	7	39	5.E-05	4.1	Ig gamma-3 chain C region
P01765	1	1	8	6.E-05	8.3	Ig heavy chain V-III region TIL
Q8WWA0	1	1	5	2.E-05	23.7	Intelectin-1
P13646	13	13	81	1.E-05	31.2	Keratin, type I cytoskeletal 13
P19013	11	11	59	5.E-05	29.2	Keratin, type II cytoskeletal 4
P13647	8	7	39	2.E-06	4	Keratin, type II cytoskeletal 5
P01042	4	4	15	1.E-06	4.2	Kininogen-1
P02750	4	4	39	5.E-07	4.8	Leucine-rich alpha-2-glycoprotein
P00338	7	7	31	2.E-05	4.3	L-lactate dehydrogenase A chain
E9PGF7	1	1	7	9.E-06	7.6	Mucin-5AC
P35579	12	11	53	3.E-06	5	Myosin-9

SqCC: squamous cell carcinoma, P/C: number of peptides, P/C: number of specific peptides, FC: maximum fold change, control: healthy individuals and sarcoid, ** interacting protein.*

3.3.3.2. Proteins significantly lowered in SqCC lavage compared to the control.

Label-free mass spectrometry comparative analysis of bronchoalveolar lavage from control (healthy individuals and sarcoid) and lung Squamous cell carcinoma (table 5). Using a 1.2-fold change as cut-off, 183 proteins were found significantly lowered in lung squamous cell carcinoma broncho-alveolar lavage compared to the control samples (Appendix 4); the top 30 are listed in table 23.

Table 23: Top 30 significantly lowered proteins in SqCC compared to the controls

Accession	P/C	P/C*	Score	p-value	FC (1.2)	Description
P62195	1	1	2	5.00E-04	24.8	26S protease regulatory subunit 8
P25325	1	1	4	6.00E-04	1.9	3-mercaptopyruvate sulfurtransferase
Q12979	1	1	3	5.00E-06	5.9	Active breakpoint cluster region-RP*
P14550	3	3	15	3.00E-05	2.9	Alcohol dehydrogenase [NADP(+)]
P08758	9	9	55	4.00E-04	3.8	Annexin A5
P63010	1	1	3	4.00E-04	2.7	AP-2 complex subunit beta
P16050	4	4	18	2.00E-04	2.4	Arachidonate 15-lipoxygenase
Q68DU8	1	1	3	8.00E-06	31.1	BTB/POZ domain-O
Q8TD46	1	1	3	2.00E-06	6.1	Cell surface glycoprotein CD200 R1
P50238	1	1	4	2.00E-08	223.9	Cysteine-rich protein 1
Q12926	1	1	3	7.00E-10	12.5	ELAV-like protein 2
Q15056	1	1	4	2.00E-04	51.6	Eukaryotic translation initiation factor 4H
P15090	2	2	15	2.00E-04	6.2	Fatty acid-binding protein, adipocyte
P09467	7	7	29	3.00E-04	5.3	Fructose-1,6-bisphosphatase 1
P48506	1	1	3	4.00E-04	2.9	Glutamate--cysteine ligase CS
P07203	1	1	3	2.00E-04	12.1	Glutathione peroxidase 1
P49773	2	2	15	4.00E-04	2.9	Histidine triad nucleotide-binding P1
P01714	1	1	7	3.00E-06	3.6	Ig lambda chain V-III region SH
O14654	1	1	3	7.00E-10	13.5	Insulin receptor substrate 4
O43240	1	1	3	5.00E-05	4.6	Kallikrein-10
P05787	5	5	21	2.00E-05	2.2	Keratin, type II cytoskeletal 8
O95573	1	1	3	5.00E-04	2.1	Long-chain-fatty-acid--CoA ligase 3
O14745	1	1	4	3.00E-04	2.7	Na(+)/H(+) exchange regulatory cofactor
O96009	1	1	5	5.00E-04	2.4	Napsin-A
P22894	3	3	19	4.00E-05	6.6	Neutrophil collagenase
Q02818	2	2	5	5.00E-06	4.4	Nucleobindin-1
P30041	2	2	9	5.00E-04	1.7	Peroxiredoxin-6
P68402	1	1	2	7.00E-04	7.9	Platelet-AF acetylhydrolase IB subunit-β
P25788	1	1	4	5.00E-04	2.7	Proteasome subunit alpha type-3
P14618	2	2	10	2.00E-04	4.3	Pyruvate kinase PKM

SqCC: squamous cell carcinoma, P/C: number of peptides, P/C*: number of specific peptides, FC: maximum fold change, control: healthy individuals and sarcoid, RP*: regulating protein, P1: prorein 1, CS: catalytic subunit.

3.3.3.3. Proteins were found elevated in AD and SqCC lavage compared to the control.

Label-free mass spectrometry comparative analysis of bronchoalveolar lavage from SqCC and AD using control lavage (healthy individuals and sarcoid) as a reference (table 5). One hundred and ninety-two proteins were found significantly elevated in both adenocarcinoma and squamous cell carcinoma compared to the control lavage; the top 30 are listed in table 24 (full list is in appendix 5).

Table 24: Top 30 significantly elevated proteins in both AD and SqCC compared to controls

Accession	PC	PC*	S	AD ↑	PC	PC*	S	SQ ↑	Description
O15511	2	1	6	3.9	1	1	4	2.7	Actin-related protein 2/3
P61158	3	3	12	3	1	1	5	3.3	Actin-related protein 3
P07108	6	6	29	4.9	2	2	7	4.5	Acyl-CoA-binding protein
P07327	5	5	15	8.2	1	1	4	2.7	Alcohol dehydrogenase 1A
P00326	3	2	13	3.7	2	2	11	11.7	Alcohol dehydrogenase 1C
P02763	6	6	42	2.8	10	10	67	4	Alpha-1-acid glycoprotein 1
P19652	5	5	27	3.1	4	4	35	8.2	Alpha-1-acid glycoprotein 2
P01011	19	19	101	3	13	13	86	3	Alpha-1-antichymotrypsin
P01009	27	27	206	5.9	31	31	273	4	Alpha-1-antitrypsin
P08697	1	1	4	2.6	3	3	13	3.6	Alpha-2-antiplasmin
P02765	5	5	28	2.5	2	2	15	3	Alpha-2-HS-glycoprotein
P04745	30	30	287	4.6	27	27	243	18	Alpha-amylase 1
P07355	9	9	41	3.4	2	2	5	3.2	Annexin A2
P08133	1	1	3	3.9	1	1	4	3.6	Annexin A6
O95994	1	1	2	4.4	3	3	12	2.3	Anterior gradient protein 2 homolog
P03973	10	10	63	7.6	3	3	15	5.6	Antileukoprotease
P01008	9	9	36	2	8	8	40	2.8	Antithrombin-III
Q10567	1	1	4	7.2	1	1	2	4.2	AP-1 complex subunit beta-1
P02652	1	1	4	112.4	1	1	11	7.3	Apolipoprotein A-II
P06727	9	9	44	3.6	3	3	17	5.1	Apolipoprotein A-IV
P00966	1	1	3	1.6	2	2	9	2.6	Argininosuccinate synthase
O00571	1	1	2	3.2	1	1	3	8.3	ATP-dependent RNA helicase
P20160	1	1	4	2.1	5	5	24	2.4	Azurocidin
P02749	11	10	47	2.4	9	9	45	3.4	Beta-2-glycoprotein 1
P61769	3	3	17	7.2	1	1	12	3	Beta-2-microglobulin
Q9NP55	3	2	12	4.7	5	5	27	12	BPI fold-containing family A1
Q96DR5	3	3	10	4.9	2	2	9	11	BPI fold-containing family A2
Q8N4F0	8	8	37	2.1	5	5	42	10.6	BPI fold-containing family B2
P62158	6	6	42	9.6	2	2	8	3.1	Calmodulin
P07384	2	2	6	3.1	1	1	2	10	Calpain-1 catalytic subunit
P15328	2	2	8	3.8	3	3	25	13.9	Folate receptor alpha

PC: peptide count, PC: specific peptide count, AD: adenocarcinoma, SqCC: squamous carcinoma, S: confidence score, control: healthy individuals and sarcoid.*

3.3.3.4. Proteins were found lowered in AD and SqCC lavage compared to the control.

Label-free mass spectrometry comparative analysis of bronchoalveolar lavage from SqCC and AD using control lavage (healthy individuals and sarcoid) as a reference (table 5). Fifty-three proteins were found significantly lowered in adenocarcinoma and squamous cell carcinoma compared to the control lavage (Appendix 6); the top 30 are listed in table 25.

Table 25: Top 30 significantly lowered proteins in both AD and SqCC compared to control

Accession	PC	PC*	S	AD ↓	PC	PC*	S	SqCC ↓	Description
O43598	2	2	8	2	2	2	8	2	2'-DNT-5'-phosphateN-Hase1
P25325	1	1	3	2	1	1	4	1.9	3-mercaptopyruvate sulfurtransferase
P10155	1	1	4	1.6	1	1	4	2.2	60 kDa SS-A/Ro ribonucleoprotein
Q12979	1	1	3	2.1	1	1	3	5.9	Active breakpoint cluster region
P08758	9	9	56	3.4	9	9	55	3.8	Annexin A5
P27824	1	1	3	2.2	1	1	4	2	Calnexin
P07339	8	8	43	2	7	7	28	1.8	Cathepsin D
Q8TD46	1	1	3	3.6	1	1	3	6.1	Cell surface glycoprotein CD200R1
Q9ULV4	1	1	5	4.3	1	1	5	4.9	Coronin-1C
Q13409	1	1	3	1.9	1	1	4	1.4	Cytoplasmic dynein 1 intermediate 2
Q96KP4	9	9	36	1.9	2	2	8	1.6	Cytosolic non-specific dipeptidase
Q16555	1	1	5	1.9	1	1	5	2.9	Dihydropyrimidinase-related P*2
Q9NY33	3	3	13	2.3	2	2	9	1.5	Dipeptidyl peptidase 3
Q12926	1	1	3	2	1	1	3	12.5	ELAV-like protein 2
Q13347	1	1	3	4.5	1	1	3	1.3	Eukaryotic TIF3* subunit I
P15090	2	2	16	3.7	2	2	15	6.2	Fatty acid-binding protein, adipocyte
P02792	4	4	17	5.8	2	2	9	2.8	Ferritin light chain
P09467	2	2	14	6.1	7	7	29	5.3	Fructose-1,6-bisphosphatase 1
P09382	1	1	5	4.7	1	1	5	3.5	Galectin-1
P13284	2	2	12	4.6	1	1	5	2.3	γ-INF -inducible lysosomal reductase
P35754	1	1	3	4.7	2	2	9	2.2	Glutaredoxin-1
P48637	2	2	6	1.5	1	1	5	1.6	Glutathione synthetase
P21695	1	1	3	18.6	1	1	3	9	GAPDH [NAD(+)], cytoplasmic
P61978	2	2	9	1.7	1	1	4	2.1	Heterogeneous NRP K
P49773	2	2	19	2.3	2	2	15	2.9	Histidine triad nucleotide-binding P*1
Q16576	1	1	4	38.2	1	1	4	21.1	Histone-binding protein RBBP7
Q9Y547	1	1	6	3.6	1	1	6	2.1	Intraflagellar transport protein 25
P05787	7	7	31	3	5	5	21	2.2	Keratin, type II cytoskeletal 8
Q14894	1	1	5	2.5	2	2	12	2.8	Ketimine reductase mu-crystallin
P40121	3	3	21	2.7	4	4	24	2.8	Macrophage-capping protein

PC: peptide count, PC*: specific peptide count, AD: adenocarcinoma, SQ: squamous carcinoma, S: confidence score, control: healthy individuals and sarcoid, *: translation initiation factor, DNT: deoxynucleotide, Hase: hydrolase, P*: protein.

3.3.4. Classification of proteins found changed in AD and SqCC compared to control.

Figure 9, Panther biological processes analysis of the proteins that were found elevated or lowered in both AD and SqCC lung lavage by label-free mass spectrometry comparative analysis compared to the control (healthy individuals and sarcoid) lavage.

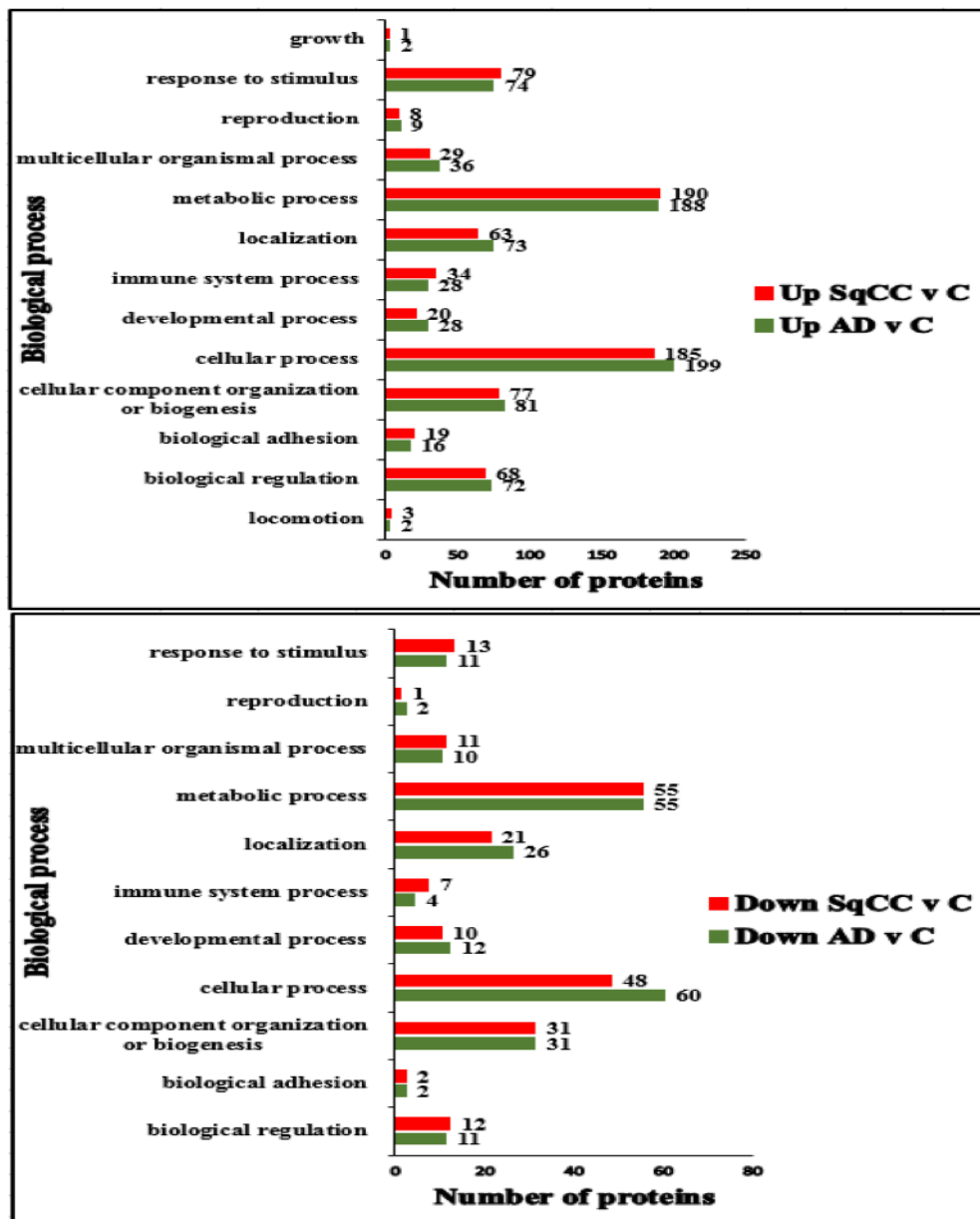


Figure 9: PANTHER GO-Slim Biological Process Analysis of proteins found lowered or elevated in adenocarcinoma (AD) and squamous cell carcinoma (SqCC) lavages compared to the control (C): healthy individuals and sarcoid patients lavages, numbers indicate the number of genes involved per process.

3.3.5. Proteome signature differentiating between lung AD and SqCC.

3.3.5.1. Proteins elevated in SqCC but lowered in AD compared to the control.

Label-free mass spectrometry comparative analysis of bronchoalveolar lavage from SqCC and AD using control lavage (healthy individuals and sarcoid) as a reference (table 5). A total of 23 proteins were found significantly elevated in the lavage collected from squamous cell carcinoma patients compared to the control lavage. In contrast, using the same lavage control samples, these proteins were found lowered in lung adenocarcinoma lavage (Table 26).

Table 26: Proteins significantly elevated in SqCC but lowered in AD compared to the control

Accession	PC	PC*	S	SQ↑	PC	PC*	S	AD↓	Description
P63104	3	3	13	2.5	5	5	32	2.4	14-3-3 protein zeta/delta
P07741	1	1	6	1.2	2	2	6	1.9	Adenine phosphoribosyltransferase
Q01518	5	5	28	1.9	4	4	17	2.6	Adenylyl cyclase-associated protein 1
P04040	3	3	10	1.9	7	7	25	1.6	Catalase
O75369	1	1	3	3	3	3	8	2.2	Filamin-B
P04075	5	5	31	2.3	12	12	64	1.6	Fructose-bisphosphate aldolase A
P06737	1	1	3	24.5	2	2	8	2.4	Glycogen phosphorylase, liver
Q92598	1	1	4	5	3	3	9	2	Heat shock protein 105 kDa
Q14974	1	1	4	10.2	1	1	3	1.6	Importin subunit beta-1
P19823	2	2	5	3.9	6	6	23	2	Inter-alpha-trypsin inhibitor H2
P13645	17	17	111	2.5	26	26	135	1.3	Keratin, type I cytoskeletal 10
Q04695	8	8	39	3.1	5	5	18	2.8	Keratin, type I cytoskeletal 17
P35527	29	29	261	2.1	4	4	25	2.6	Keratin, type I cytoskeletal 9
P35579	12	11	53	5	10	9	37	1.7	Myosin-9
P08246	6	6	41	4.8	3	3	11	15.5	Neutrophil elastase
P40306	2	2	10	3.5	1	1	5	5.7	Proteasome subunit beta type-10
O60888	1	1	7	6.7	1	1	8	3.3	Protein CutA
Q92597	1	1	3	Infinity	3	3	23	1.3	Protein NDRG1
P80511	1	1	5	1.9	1	1	5	1.9	Protein S100-A12
P02753	1	1	3	3.5	3	3	14	1.6	Retinol-binding protein 4
P00441	1	1	12	103.4	2	2	21	1.9	Superoxide dismutase [Cu-Zn]
P29401	8	8	55	2.7	14	14	72	1.7	Transketolase
Q14508	1	1	5	6.2	2	2	17	3	WAP four-disulfide core domain 2

SqCC: squamous cell carcinoma, AD: adenocarcinoma, P/C: number of peptides, P/C*: number of specific peptides, FC: maximum fold change, S: score P1*: protein 1. Numbers in **bold** are fold changes were found elevated in SqCC and lowered in AD compared to control lavages (healthy individuals and sarcoid patients).

3.3.5.2. Proteins elevated in AD but lowered in SqCC compared to the control.

Label-free mass spectrometry comparative analysis of bronchoalveolar lavage from SqCC and AD using control lavage (healthy individuals and sarcoid) as a reference (table 5). There were 58 proteins were found significantly elevated in lung adenocarcinoma lavage (AD) compared to the control lavage (healthy individuals and sarcoid patients) (Table 27). Interestingly, these proteins were significantly lowered in the lavage collected from lung squamous cell carcinoma (SqCC) relative to the same control lavage samples.

Table 27: Proteins significantly elevated in AD but lowered in SqCC compared to the control

Accession	PC	PC*	S	SQ↑	PC	PC*	S	AD↓	Description
P63104	3	3	13	2.5	5	5	32	2.4	14-3-3 protein zeta/delta
P07741	1	1	6	1.2	2	2	6	1.9	Adenine phosphoribosyltransferase
Q01518	5	5	28	1.9	4	4	17	2.6	Adenylyl cyclase-associated protein 1
P04040	3	3	10	1.9	7	7	25	1.6	Catalase
O75369	1	1	3	3	3	3	8	2.2	Filamin-B
P04075	5	5	31	2.3	12	12	64	1.6	Fructose-bisphosphate aldolase A
P06737	1	1	3	24.5	2	2	8	2.4	Glycogen phosphorylase, liver
Q92598	1	1	4	5	3	3	9	2	Heat shock protein 105 kDa
Q14974	1	1	4	10.2	1	1	3	1.6	Importin subunit beta-1
P19823	2	2	5	3.9	6	6	23	2	Inter-alpha-trypsin inhibitor H2
P13645	17	17	111	2.5	26	26	135	1.3	Keratin, type I cytoskeletal 10
Q04695	8	8	39	3.1	5	5	18	2.8	Keratin, type I cytoskeletal 17
P35527	29	29	261	2.1	4	4	25	2.6	Keratin, type I cytoskeletal 9
P35579	12	11	53	5	10	9	37	1.7	Myosin-9
P08246	6	6	41	4.8	3	3	11	15.5	Neutrophil elastase
P40306	2	2	10	3.5	1	1	5	5.7	Proteasome subunit beta type-10
O60888	1	1	7	6.7	1	1	8	3.3	Protein CutA
Q92597	1	1	3	Infinity	3	3	23	1.3	Protein NDRG1
P80511	1	1	5	1.9	1	1	5	1.9	Protein S100-A12
P02753	1	1	3	3.5	3	3	14	1.6	Retinol-binding protein 4
P00441	1	1	12	103.4	2	2	21	1.9	Superoxide dismutase [Cu-Zn]
P29401	8	8	55	2.7	14	14	72	1.7	Transketolase
Q14508	1	1	5	6.2	2	2	17	3	WAP four-disulfide core domain 2

Accession	PC	PC*	S	AD↑	PC	PC*	S	SqCC↓	Description	Table 27 continued
P18065	3	3	13	2.8	2	2	8	1.9	Insulin-like growth factor-binding P*2	
P05362	1	1	3	6.7	1	1	2	18.3	Intercellular adhesion molecule 1	
O43240	2	2	7	1.6	1	1	3	4.6	Kallikrein-10	
Q8WXI7	21	20	74	3.9	1	1	4	1.3	Mucin-16	
P02144	2	2	7	4	1	1	3	2.1	Myoglobin	
O14745	4	4	22	2.3	1	1	4	2.7	Na/H (exchange regulatory cofactor)	
Q02818	5	5	15	3.3	2	2	5	4.4	Nucleobindin-1	
P80303	11	11	50	2.1	2	2	6	2.6	Nucleobindin-2	
P19338	1	1	2	6.1	1	1	4	1.9	Nucleolin	
Q06830	7	7	36	2.3	8	8	47	2.7	Peroxiredoxin-1	
P30041	4	4	11	4.1	2	2	9	1.7	Peroxiredoxin-6	
P30086	5	5	24	2.1	3	3	11	2.2	Phosphatidylethanolamine BP*1	
O43490	9	9	32	2.4	3	3	9	1.3	Prominin-1	
Q14914	1	1	5	6	1	1	5	2.1	Prostaglandin reductase 1	
P14618	9	9	55	1.8	2	2	10	4.3	Pyruvate kinase	
Q5TD94	1	1	3	7.3	1	1	6	1.2	Radial spoke head protein 4A	
P34096	2	2	9	2.7	1	1	3	1.6	Ribonuclease 4	
P07998	2	2	16	4.6	1	1	4	1.4	Ribonuclease pancreatic	
Q9Y265	1	1	3	3	1	1	4	3.2	RuvB-like 1	
Q9NR45	3	3	12	2.4	1	1	5	2.7	Sialic acid synthase	
P49368	1	1	4	2.3	1	1	3	1.1	T-complex protein 1 subunit gamma	
P67936	1	1	4	3.7	1	1	3	1.5	Tropomyosin alpha-4 chain	
Q9H4B7	5	5	18	2.9	4	4	11	2.3	Tubulin beta-1 chain	
Q13509	2	2	7	2.5	1	1	3	1.9	Tubulin beta-3 chain	
Q9BW30	5	5	28	2.1	1	1	5	2.6	Tubulin polymerization-promoting P*3	
O75347	1	1	11	3.9	2	2	8	1.3	Tubulin-specific chaperone A	
P22314	2	2	9	2.1	3	3	16	3.3	Ubiquitin-like modifier-activating E1	
P08670	6	6	21	2.8	1	1	4	1.5	Vimentin	
P12955	1	1	3	1.7	1	1	3	6.2	Xaa-Pro dipeptidase	

AD: lung adenocarcinoma, SqCC: lung squamous cell carcinoma, AC: accession number, PC: peptide count, PC: specific peptide count, S: confidence score, TNS*: tissue non-specific, TIF*: translation initiation factor, CS: catalytic subunit, P*: protein, BP*: binding protein. Numbers in **bold** are fold changes were found elevated in AD and lowered in SqCC lavages compared to the control lavages (healthy individuals and sarcoid patients).*

3.3.6. Classification of proteins that could differentiate between lung AD and lung SqCC

Proteins detected by label-free mass spectrometry and found to differentiate lung adenocarcinoma from lung squamous cell carcinoma in bronchoalveolar lavage were subjected to Panther biological processes analysis (Figure 10). The most prominent types were proteins involved in metabolic and cellular processes.

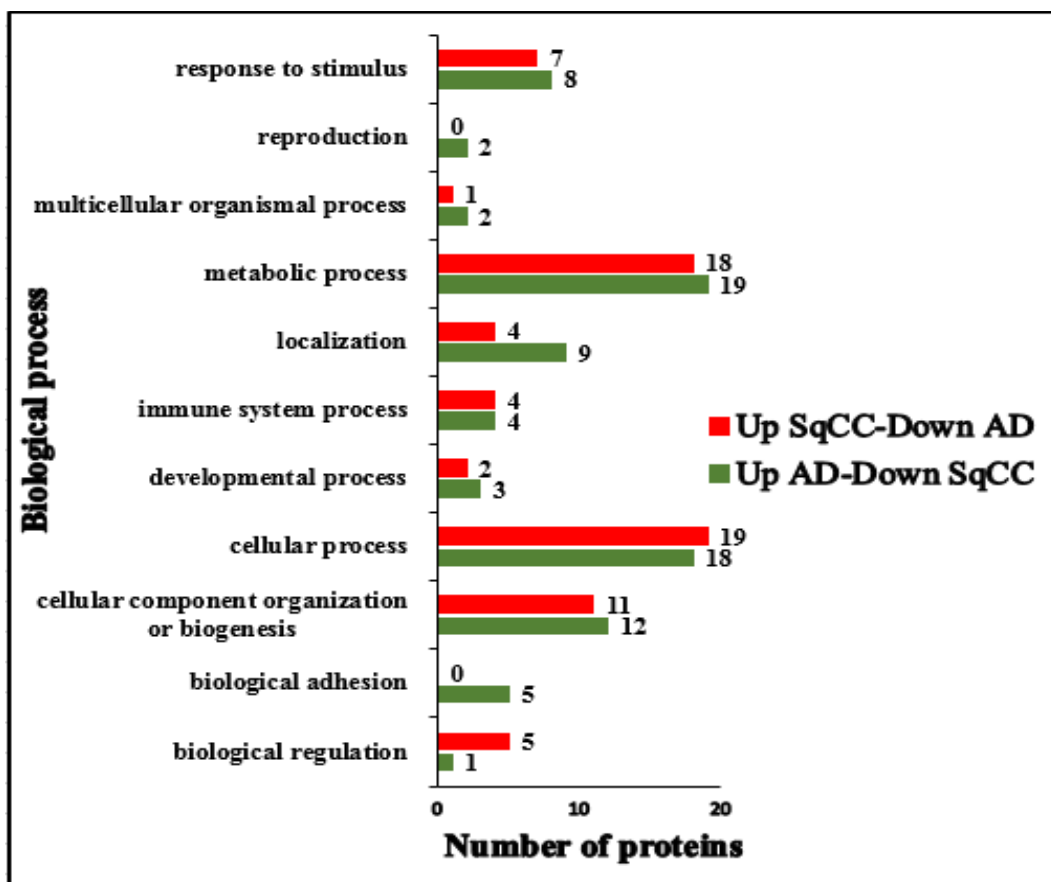


Figure 10: PANTHER GO-Slim Biological Process of unique proteins that were found elevated/lowered in adenocarcinoma (AD) and have opposite profile in squamous cell carcinoma (SqCC) lavages compared to the control: healthy individuals and sarcoid patients lavages, numbers indicate the number of genes involved per process.

3.3.7. ELISA verification

3.3.7.1. Candidate proteins for ELISA validation

Table 28 shows the proteins belong to the families of lipocalins, heat shock proteins and cysteine protease inhibitors identified by label-free mass spectrometry as significantly elevated in NSCLC (AD and SqCC) lavages compared to the control lavage collected from healthy individuals and sarcoid patients (table 5). To validate the label-free mass spectrometry comparative analysis; Cystatin C, HSP 70, TIMP-1 and Lipocalin-2 were selected for the ELISA verification based on their increased abundance in NSCLC lavage compared to the control group lavage used in this study (table 28), and also based on their known role in the pathogenicity of lung cancer.

Table 28: Protein families detected elevated by label-free mass spectrometry in lavage from AD and SqCC patients compared to control (healthy individuals and sarcoid) in this research discovery work and selected for verification by ELISA.

Accession	Fold change (compared to control)		Description
	AD	SqCC	
P01033	2	2.2	TIMP-1
P02763	2.8	4	Alpha-1-acid glycoprotein 1*
P19652	3.1	8.2	Alpha-1-acid glycoprotein 2*
P02647	0	3.9	Apolipoprotein A-I*
P02652	112.4	7.3	Apolipoprotein A-II*
P06727	3.6	5.1	Apolipoprotein A-IV*
P04114	0	25.4	Apolipoprotein B-100*
P02654	0	7.2	Apolipoprotein C-I*
P05090	9.7	0	Apolipoprotein D*
P02649	4.4	0	Apolipoprotein E*
P01040	0	5.9	Cystatin-A
P04080	1.8	0	Cystatin-B
P01034	2	4.5	Cystatin-C
P28325	13.7	4.8	Cystatin-D
P01036	0	3.4	Cystatin-S
P09228	1.6	2.6	Cystatin-SA
P01037	5	3.4	Cystatin-SN
Q01469	2.4	3.7	Fatty acid-binding protein
P11142	1.6	2.2	Heat shock cognate 71 kDa protein
P61604	0	7.2	heat shock protein 10 kDa , mitochondrial
Q92598	0	5	Heat shock protein 105 kDa
P34931	1.9	0	Heat shock protein 70 kDa protein 1-like
P04792	0	7	Heat shock protein beta-1
P54652	2	0	Heat shock-related 70 kDa protein 2
P31025	4.4	9.9	Lipocalin-1*
Q6UWW0	6.4	0	Lipocalin-15*
Q14568	0	2.1	Putative heat shock protein HSP 90- α A2
Q58FF8	3.6	0	Putative heat shock protein HSP 90-beta 2
Q58FF7	2.2	0	Putative heat shock protein HSP 90-beta-3
P27797	3.1	3	Calreticulin, (ER-HSP)

AD: lung adenocarcinoma, SqCC: lung squamous cell carcinoma, *: member of Lipocalins, ER-HSP: endoplasmic reticulum heat shock protein, Cystatin A, B, C, D, S, SA and SN are cystatin isoforms, apolipoproteins A, B, C and D are apolipoprotein isoforms, lipocalin (#s): isoforms.

3.3.7.2. ELISA verification results

Figure 11 shows Box and Whiskers plot representing the levels of four proteins selected for verification of mass spectrometry results in plasma cohort samples (n=72) collected from healthy controls and patients with lung adenocarcinoma and squamous cell carcinomas by ELISA. Heat shock proteins were elevated in squamous cell carcinoma compared to control (healthy individuals) and to patients with lung adenocarcinoma (A). The level of cystatin C was significantly elevated in both adeno and squamous lung carcinomas compared to the control samples (B). The level of lipocalin-1 was elevated in both adeno and squamous lung carcinomas compared to the control samples (C). The level of tissue inhibitor of metalloproteinase (TIMP-1) was also significantly elevated in both types of lung carcinoma (D).

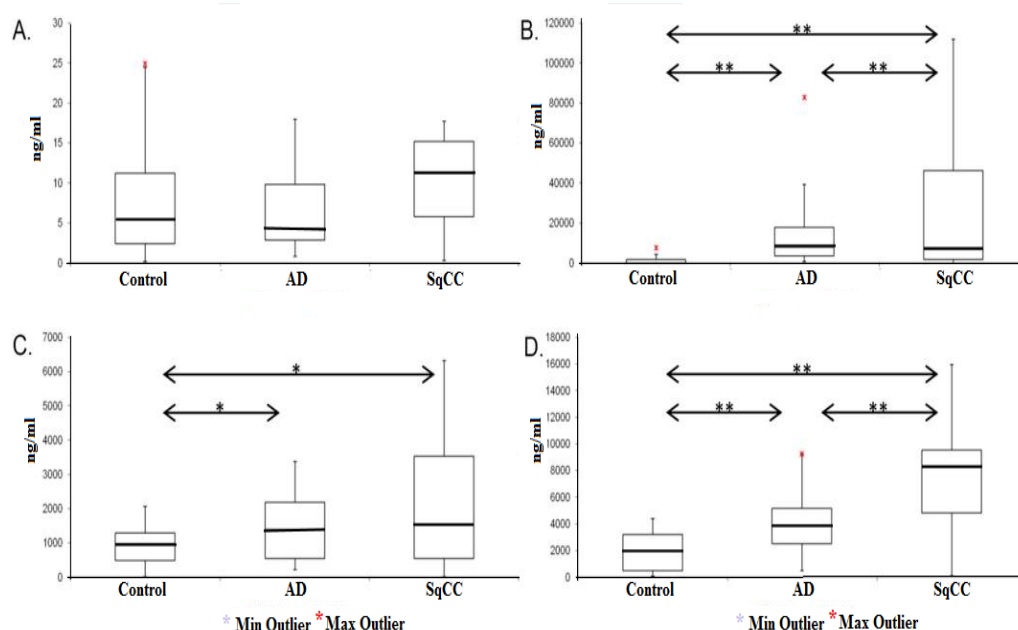


Figure 11: ELISA verification. Box-and-Whisker plots of the levels of (A) HSP70, (B) Cystatin-C, (C) Lipocalin-2, and (D) TIMP-1 in control (healthy and sarcoid) n= 26, AD (n=23) and SqCC (n= 23) plasma samples. Box-and-Whisker plots represent data with boxes ranging from the 25th to the 75th percentile of the observed distribution of values. The **bold** line of the boxes represents the median of plasma levels of HSP70, Cystatin-C, Lipocalin-2 and TIMP-1. Whiskers span the minimum to maximum observed values. Statistical significance was tested by Kruskal-Wallis one-way ANOVA using SPSS 15.0 for Windows. (*p ≤ 0.05: significant; **p ≤ 0.01: very significant).

3.3.8. Metabolism in non-small cell lung cancer

In the Label-free mass spectrometry experiment that comparing bronchoalveolar lavage from SqCC and AD using control lavage (healthy individuals and sarcoid) (table 5). Among the lowered Fifty three proteins in both AD and SqCC, Fifteen out of them were enzymes (Table 29) and also 33 were enzymes out of the 192 proteins that were found significantly elevated in both AD and SqCC were enzymes (Table 30).

Table 29: Enzymes found by LC-MS/MS to be decreased in both lung AD and SqCC

Accession	PC	PC*	S	AD ↓	PC	PC*	S	SqCC ↓	Description
O43598	2	2	8	2	2	2	8	2	2'-DNT- 5'-phosphate N-Hase 1
P25325	1	1	3	2	1	1	4	1.9	3-mercaptopyruvate sulfurtransferase
Q96KP4	9	9	36	1.9	2	2	8	1.6	Cytosolic non-specific dipeptidase
Q16555	1	1	5	1.9	1	1	5	2.9	Dihydropyrimidinase-related P*2
Q9NY33	3	3	13	2.3	2	2	9	1.5	Dipeptidyl peptidase 3
P09467	2	2	14	6.1	7	7	29	5.3	Fructose-1,6-bisphosphatase 1
P13284	2	2	12	4.6	1	1	5	2.3	γ-INF-inducible lysosomal reductase
P48637	2	2	6	1.5	1	1	5	1.6	Glutathione synthetase
P21695	1	1	3	18.6	1	1	3	9	Glycerol-3-PDH [NAD(+)]
Q14894	1	1	5	2.5	2	2	12	2.8	Ketimine reductase mu-crystallin
P22894	1	1	5	44.4	3	3	19	6.6	Neutrophil collagenase
P21980	5	5	27	2	5	5	33	1.9	Protein-glutamine γ-GT** 2
P19971	4	4	20	2.6	4	4	13	2.7	Thymidine phosphorylase
O14773	2	2	9	3	2	2	6	4.1	Tripeptidyl-peptidase 1
P23381	3	3	9	1.8	1	1	5	3	Tryptophan--tRNA ligase, cytoplasmic

PC: peptide count, PC*: specific peptide count, AD: lung adenocarcinoma, SqCC: lung squamous carcinoma, S: confidence score, DNT: deoxynucleotide, Hase: hydrolase, P*: protein.GT**: glutamyltransferase, INF: interferon. *Numbers in bold are fold changes were found downregulated in both AD and SqCC.*

Table 30: Enzymes found by LC-MS/MS to be elevated in both AD and SqCC of lungs

Accession	PC	PC*	S	AD ↑	PC	PC*	S	SqCC ↑	Description
P07327	5	5	15	8.2	1	1	4	2.7	Alcohol dehydrogenase 1A
P00326	3	2	13	3.7	2	2	11	11.7	Alcohol dehydrogenase 1C
P04745	30	30	287	4.6	27	27	243	18	Alpha-amylase 1
P03973	10	10	63	7.6	3	3	15	5.6	Antileukoprotease
P00966	1	1	3	1.6	2	2	9	2.6	Argininosuccinate synthase
O00571	1	1	2	3.2	1	1	3	8.3	ATP-dependent RNA helicase
P00915	4	4	25	4	3	3	25	4.8	Carbonic anhydrase 1
P00918	3	3	10	2	1	1	3	3.8	Carbonic anhydrase 2
P23280	4	4	14	2.1	6	6	31	7.9	Carbonic anhydrase 6
P49327	2	2	8	9.5	3	3	10	3.3	Fatty acid synthase
Q92820	1	1	3	2	1	1	3	3.1	Gamma-glutamyl hydrolase
O60547	2	2	6	7.4	1	1	2	32.3	GDP-mannose 4,6 dehydratase
P06744	14	14	68	1.8	11	11	69	3.7	Glucose-6-phosphate isomerase
P04406	12	12	61	2.1	6	6	43	2.4	GAPDH
P11216	2	2	6	16.3	1	1	4	10	Glycogen phosphorylase, brain
Q6B016	1	1	3	2.3	1	1	3	2.8	Lysine-specific demethylase 4D
P40925	7	7	29	1.6	1	1	3	7.5	Malate dehydrogenase
P14780	9	9	35	2.4	7	7	36	4	Matrix metalloproteinase-9
P01033	6	6	29	2	2	2	11	2.2	Metalloproteinase inhibitor 1
P05164	21	19	76	1.7	21	21	100	2.9	Myeloperoxidase
P80188	15	15	76	1.8	5	5	25	2.2	Lipocalin 2
P43490	2	2	8	3.2	4	4	19	3.2	Nicotinamide P-Rtase
P62937	5	5	31	2.1	2	2	6	2.3	Peptidyl-prolyl cis-trans A
P00558	14	14	63	1.9	2	2	8	2.3	Phosphoglycerate kinase 1
P05155	11	11	55	2.7	2	2	11	2.3	Plasma protease C1 inhibitor
P07237	10	10	35	4	4	4	20	3.6	Protein disulfide-isomerase
Q08188	1	1	3	10	8	8	53	8.4	glutamine γ -glutamyltransferase E
P00491	1	1	2	2.3	3	3	9	3.6	Purine nucleoside phosphorylase
O60361	1	1	3	1.6	2	2	6	4	nucleoside diphosphate kinase
Q9H477	1	1	2	1.8	1	1	2	2.2	Ribokinase
O00584	2	2	6	4.8	1	1	4	4.4	Ribonuclease T2
P27169	1	1	4	6	1	1	3	10.2	Serum paraoxonase/arylesterase 1
Q00796	2	2	6	3.5	1	1	3	1.3	Sorbitol dehydrogenase
P37837	5	5	22	3.1	2	2	6	5.1	Transaldolase
P60174	12	12	60	1.7	5	5	31	2.1	Triosephosphate isomerase
P29144	1	1	2	5.6	1	1	3	3.4	Tripeptidyl-peptidase 2

PC: peptide count, PC*: specific peptide count, AD: lung adenocarcinoma, SqCC: lung squamous carcinoma. Numbers in **bold** are fold changes were found upregulated in both AD and SqCC.

3.4. Discussion

To build up a pool of classifier biomarkers to assist in the diagnosis of lung cancer, and mainly of poorly differentiated lung adenocarcinoma, cut-off values were carefully chosen while avoiding the exclusion of too many proteins (Figure 8). The chosen cut-off value permits validation of candidate biomarkers with the sensitivity of available methodologies. The cancer proteome is very dynamic. The abundance of proteins responsible for the cell cycle, growth, proliferation and survival change upon demand. In general, overexpression of oncogenes and dysregulation of tumour suppressor genes is expected in cancer, as well as changes in the metabolic signature and increased rates of energy substrate utilisation. Also expected is increased abundance of building units, such as histones, DNA, enzymes, and cytoskeletal proteins, and increased mitochondrial activity.

In this part of the study, BALF from normal controls and patients diagnosed with lung AD or SqCC was analysed by LC-MS/MS. The aim was to obtain a proteomic signature that differentiates between the two main types of NSCLC, adenocarcinoma and squamous cell carcinoma, which represent 38.5% and 20% of all lung cancers, respectively (Herbst et al., 2008). The validation of the signature on tissue samples from patients with lung adenocarcinoma is reported in chapter IV.

A 1.2-fold change in protein expression was considered an acceptable threshold for deriving a lung cancer proteome signature (Figure 8). The proteins found to be significantly upregulated in adenocarcinoma compared to the control samples are listed in Appendix 1. After exclusion of all immunoglobulin classes, the top 30 significantly upregulated proteins were listed (Table 20). A list of the top 30 proteins significantly downregulated in adenocarcinoma was derived in the same way (Table 21; full list in Appendix 2). The same approach was taken to identify the top 30

proteins significantly up or down regulated in squamous cell carcinoma (Tables 22 and 23; full list Appendixes 3 and 4). These full lists can serve as reference data for future validation of biomarkers. Proteins that were elevated in both adeno and squamous carcinomas compared to the control samples were also identified (Appendix 5), and from there the top 30 upregulated proteins were identified (Table 24). Proteins down regulated in both carcinomas are listed in appendix 6, and the top significantly down regulated proteins are in table 25.

Interestingly, 58 proteins were found elevated in AD but lowered in SqCC, while 24 proteins were elevated in SqCC but down regulated in AD (Tables 26, 27). The validation of these proteins on formaldehyde-fixed, and -embedded lung adenocarcinoma specimens is described in chapter V. PANTER GO-Slim Biological Process analysis of the proteins found that notable protein categories with increased expression levels in AD and SqCC compared to the controls included proteins involved in the cellular response to stimuli or in cellular biogenesis, biological regulatory proteins, and those involved in metabolic and cellular processes (Figure 9). Figure 10 also represents invaluable data, where the classification of each lung carcinoma (AD/SqCC) is presented. At the cellular metabolism level, 16 enzymes were in low abundance and 36 enzymes were elevated in both AD and SqCC (Tables 29, 30). This provided motivation for undertaking a separate metabolic study focused on the key enzymes controlling the switching between anaerobic and aerobic utilisation of glucose (reported in chapter IV).

The main focus of this research was to identify a panel of protein biomarkers differentially expressed in adenocarcinoma and squamous cell carcinoma and to verify some of them in plasma samples from matched types of lung cancer. Among the elevated proteins differentiating between adenocarcinoma and squamous cell

carcinoma of the lung were folate receptor alpha (FRA), which was increased 13.9-fold in AD compared to SqCC (3.8 fold). Previous work has shown that immunohistochemical analysis of FRA expression can distinguish lung AD from SqCC (O'Shannessy et al., 2012, Nunez et al., 2012).

Folate receptor A (FRA) was proposed as a prognostic marker in lung AD, in which its overexpression was correlated with increased survival (Wood, 2012). Coronin 1A too was elevated in lung AD compared to SqCC. Coronin 1A plays multiple functions: in addition to its actin-related function, it plays a role in the heterotrimeric assembly of proteins and is involved in the calcium-calcineurin signalling axis. Its absence was found to be associated with severe forms of immunodeficiency in humans (Moshous and de Villartay, 2014). On the other hand, it is overexpressed in many cancers, including breast cancer (Kim et al., 2009), renal cell carcinoma (Atrih et al., 2014) and bladder carcinoma (D'Costa et al., 2016).

Another protein that was found elevated in lavage of AD patients and could distinguish AD from SqCC is Cofilin-1, an intracellular actin-modulating protein that binds and depolymerises filamentous F-actin and inhibits the polymerisation of G-actin monomers (Simhadri et al., 2017). Elevation of Cofilin 1 has also been observed in prostate cancer (Lu et al., 2015) and pancreatic ductal adenocarcinoma (PDAC) (Sato et al., 2017), and in NSCLC, in which it has a suppressive effect on growth and invasion (Tsai et al., 2015). Cofilin-1 was also found correlated with cisplatin resistance in lung adenocarcinoma (Becker et al., 2014). Notably, Cofilin-1 was associated with diminished overall survival rates in NSCLC (Castro et al., 2010).

In our study, Calpastatin was found to be overexpressed in lung AD but not in squamous cell carcinoma. Calpastatin is an endogenous cysteine protease inhibitor involved in tumorigenesis, migration and invasion. Targeting Calpastatin was found

to be a promising cancer therapy (Leloup and Wells, 2011). Calpastatin is also downregulated in many cancers, including gastric cancer (Liu et al., 2017) and ovarian cancer (Salehin et al., 2011). In our study, Calcyphosin, a calcium-binding protein belonging to the calmodulin family, was found overexpressed in AD but down regulated in SqCC. Calcyphosin has been reported to be overexpressed in lung cancer (Pastor et al., 2013), ovarian adenocarcinoma (Partheen et al., 2006) and endometrial carcinoma (Li et al., 2010b). Clusterin, also called Apolipoprotein J (ApoJ), is a secreted protein found in most human fluids (Trogakos and Gonos, 2002). In our label-free LC-MS/MS discovery work, Clusterin was elevated in the lavage from lung adenocarcinoma patients compared to normal control lavage, but not in lavage from squamous cell carcinoma patients. Similarly, Clusterin was reported to be upregulated in adenocarcinoma and downregulated in squamous cell carcinoma (Jin et al., 2017a), validating our finding. Clinically, Clusterin overexpression was found to be directly correlated with patient survival in non-small cell lung cancer (Albert et al., 2007) (Panico et al., 2013).

In our study, Cystatin C, MIF, lipocalin-2, TIMP-1, periostin, Cathepsin V, PGRP, VEGF, HSP70 and Clusterin were selected as candidate biomarkers for plasma validation. Only TIMP-1, Cystatin C, HSP70 and lipocalin-2 showed promising results in the initial validation phase and were further validated using a large number of samples (Figure 11).

Cystatins are of three types: type I (also called steffins A and B), type II (Cystatin C, E, M and F) and type III (also called kininogens with multi-functional domains), which play a role in counteracting tumour associated proteases (Henskens et al., 1996). Cystatin overexpression was observed in many malignancies, including lung cancer, and was associated with tumour metastasis and aggressiveness (Ohara et al.,

2012, Werle et al., 2006). Cystatin C is a cysteine protease inhibitor found to be overexpressed at the protein and mRNA levels in oesophageal cancer (Zeng et al., 2011) and in human glioma cell lines (Konduri et al., 2002). On the other hand, Cystatin C was found down regulated in stomach neoplasm (Zeng et al., 2010) and colorectal cancer (Zore et al., 2001).

However, in our study, cystatins C, D, SA and SN were significantly overexpressed in a heterogeneous expression pattern in both adeno and squamous lung carcinomas (table 28). Cystatins D and SN were detected at higher levels in lung lavage of lung adenocarcinoma than in lung squamous carcinoma patients compared to the control lavage from normal individuals; the fold change was 13.7 and 5 in adenocarcinoma compared to 4.8 and 3.4 in squamous cell carcinoma, respectively. In contrast, cystatins C and SA were found more overexpressed in lung squamous cell carcinoma than in lung adenocarcinoma; fold changes were 4.5 and 2.6 compared to 2 and 1.6 respectively. Cystatin C, selected for ELISA validation on plasma samples (Table 28), was significantly elevated ($p \leq 0.01$) in both adeno and squamous cell carcinoma patients' plasma compared to normal individuals (Figure 11-B).

Cystatin A and cystatin S were significantly overexpressed (5.9 and 3.4 fold increases, respectively) only in squamous cell carcinoma, but they were undetectable in adenocarcinoma (Table 28). Cystatin B was significantly overexpressed only in lung adenocarcinoma lavage (1.8 folds) and was not among the differentially expressed proteins in lung squamous cell carcinoma (Table 28). This could have been due to technical issues rather than to the tissue itself.

Tissue inhibitor of metalloproteinase (TIMPs) is a family of four proteins encoded by the TIMP gene, with splice variants designated as TIMP-1, 2, 3 and 4. Only

TIMP-1 and 2 can inhibit all extracellular matrix metalloproteinases (MMPs) (Gomez et al., 1997). TIMPs are known to induce cell proliferation (Ando et al., 2017), interact with Bcl2, and inhibit P53-mediated apoptosis in lung adenocarcinoma (Nalluri et al., 2015). TIMP-1 elevation was found associated with poor prognosis in triple-negative breast cancer (Cheng et al., 2016) and laryngeal squamous cell carcinoma (Ma et al., 2014). TIMP-1 overexpression was found correlated with advanced NSCLC, and so it has a prognostic value (Thomas et al., 2000). Overexpression of TIMP-1 in NSCLC could predict disease recurrence (Gouyer et al., 2005). In this study, TIMP-1 was found elevated in the lavage collected from lung AD and SqCC patients compared to normal control lavage.

The increase was 2- and 2.2-fold in adeno and squamous cell carcinomas, respectively (Table 28). TIMP-1 was selected among the differentially expressed proteins for verification in plasma samples (Table 28) by ELISA: plasma levels of TIMP-1 were significantly elevated ($p \leq 0.01$) in both carcinomas compared to the control group (Figure 11-D).

Lipocalins are a group of small extracellular proteins that perform a wide variety of biological functions (figure 12). All lipocalins can bind hydrophobic molecules, macromolecules, lipids, steroid hormones, and secondary metabolites such as vitamins and co-factors, and they have a cell surface binding receptor (Schiefner and Skerra, 2015). Most lipocalins have in common three highly conserved sequence motifs called kernel, and a few, called outliers lipocalins, share only one conserved sequence motif.

Kernel lipocalins include; Retinol-binding protein (RBP) [RBP 1,2,5,7 are cellular proteins and 4 was detected in plasma], Purpurin (RURP), Cellular retinoic acid-

binding proteins 1&2 (CRABP1&2), α 2u-Globulin (A2U), Major urinary protein (MUP), Bilin-binding protein (BBP), α -Crustacyanin, Pregnancy protein 14 (PP14), β -Lactoglobulin (Blg), α 1-Microglobulin (A1M), Complement component 8 gamma (C8 γ), Apolipoprotein D (ApoD), Apolipoprotein M (ApoM), fatty acid binding proteins, Lazarillo (LAZ), Prostaglandin D synthase (PGDS), Quiescence-specific protein (QSP), neutrophil lipocalin (NGAL, LCN2) and choroid plexus protein (Du et al., 2015). Outlier lipocalins include; Odorant-binding protein 2A and 2B (OBP2A/2B), von Ebner's-gland protein (VEGP), α 1-Acid glycoprotein (AGP), Probasin and Aphrodisin (Flower, 1996).

The role of lipocalins in cancer is modulated through their activation of peroxisome proliferator-activated receptor (PPAR) and retinoic acid receptor (RAR)-retinoid X nuclear receptor (RXR) (figure 12) (Mourey et al., 1994, Poirier et al., 1997). In the current discovery experiment, the mass spectrometry detected a significant increase in some of the above mentioned lipocalins, where the α 1-Acid glycoprotein was elevated by 2.8 fold in the adenocarcinoma lavage and 4.0 fold in the lavage of lung squamous cell carcinoma compared to the normal control lavage (table 28), Apolipoprotein D was also elevated in lung adenocarcinoma lavage with a fold increase of 9.7. Other apolipoproteins were elevated in adenocarcinoma include Apolipoprotein A-II, A-IV and E with fold increase of 112.4, 3.6, 4.4 respectively. Fatty acid-binding protein (FABP) was also found 2.4 and 3.7 fold increased in adenocarcinoma and squamous carcinomas compared to the normal control. The level of apolipoproteins A-IV was also detected elevated in lung SqCC lavage with fold change of 5.1. Apolipoproteins include apolipoprotein A-I, II, B-100 and C-I were also found elevated in SqCC their fold change was 3.9, 7.3, 25.4, 7.2, respectively (table 28). Among Lipocalins, neutrophil lipocalin-2 (NGAL) was

selected for ELISA verification on plasma samples (table 5) and was found to be significantly ($p \leq 0.05$) elevated in both AD and SqCC lavage (figure 11-C).

Shown in figure 12, the downstream signalling of lipocalin receptor [modified from (Bratt, 2000)]. [+] indicates the protein the protein that were found in our study to be significantly elevated in both AD and SqCC.

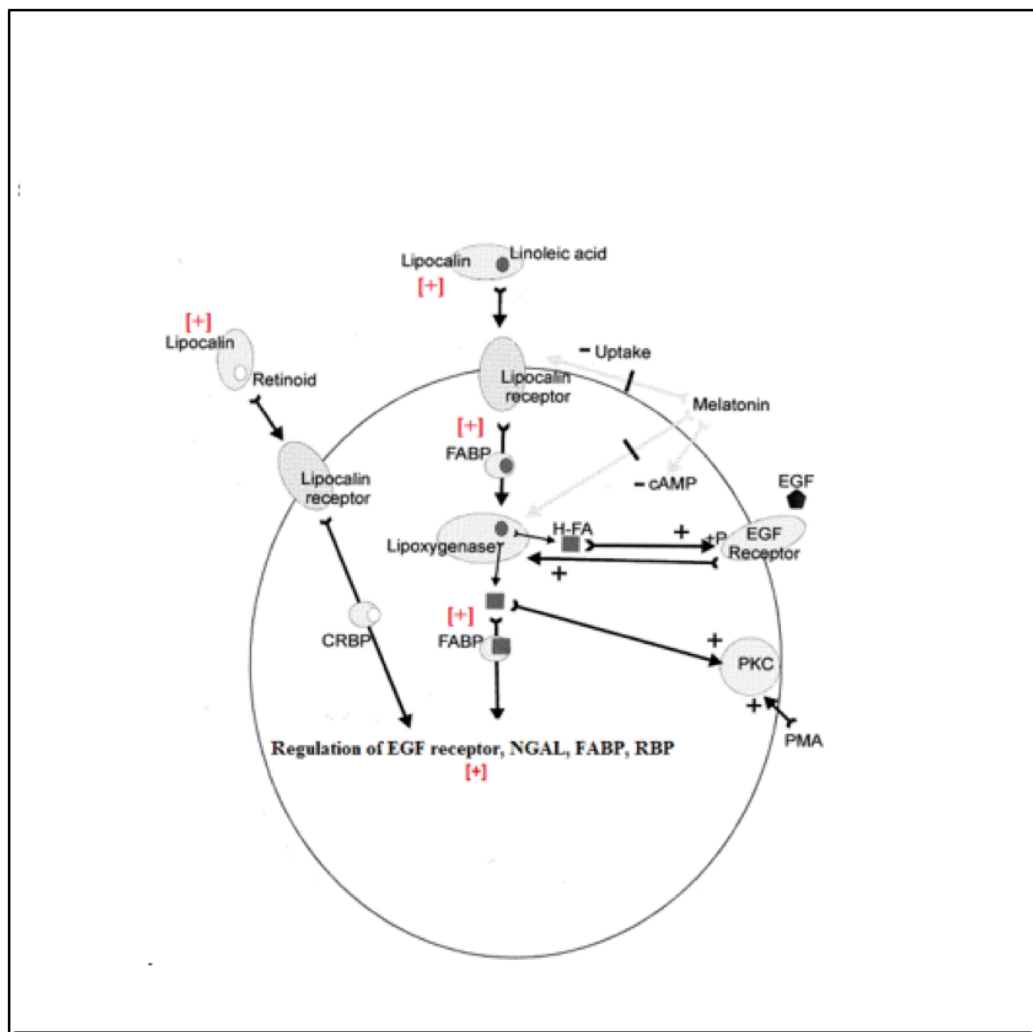


Figure 12: Extracellular lipocalin receptor-mediated intracellular signalling. Faint arrows represent inhibition, EGF: epidermal growth factor, PKC: protein kinase C, PMA: phorbol myristate acetate, NGAL: neurophilin gelatinase-associated lipocalins, FABP: fatty acid binding protein, RBP: retinol binding protein, HFA: hydroxy fatty acids, CREP: c-AMP response element protein, c-AMP: cyclic adenosine triphosphate, arrows through FABP or CRBP indicate carrier protein is involved, (+): activation, (+P): phosphorylate and activate, [+]: was found significantly elevated using mass spectrometry in our study.

Heat shock proteins (HSPs), also called chaperons as they function to protect proteins, during their peptides assembly in the cytoplasm as well as assembly of complex proteins working together, from the physical damage of the stressful cytoplasmic environment such as pH and temperature. Heat shock proteins also play role in cell cycle progression, cell survival and also involved in the proper antigen presentation in antigen presenting cells (macrophages and dendritic cells) (Li and Srivastava, 2004). Heat shock proteins are classified according to their molecular weight and some have specific cell compartment localization such as mitochondrial heat shock proteins including HSP10 which play a role in tolerance of ischemia (Hartman et al., 1992), HSP60 which found overexpressed in sever cell damage and function to induce innate immunity through toll-like receptor activation (Ohashi et al., 2000), mitochondrial HSP70 which play a major role in importing proteins to the mitochondria (Liu et al., 2003). Other HSPs are cytosolic which include HSP27, HSP110, HSP70, HSP90 α/β . The later was found involved in cell cycle control and its inhibition was found to promote cell cycle arrest at G2/M phase (Pastorek et al., 2016). Endoplasmic reticulum heat shock proteins (HSP47) function to maintain proper protein folding and sorting in the cytoplasm (Tasab et al., 2000). Table 28 summarizes heat shock proteins found significantly elevated in the lavage fluid of both lung AD and SqCC by mass spectrometry analysis conducted in this current research work. The endoplasmic reticulum HSP (Calreticulin) was the only significantly overexpressed HSP with a fold change of 3.0 in both carcinomas. HSP70 was known to be overexpressed in most type of cancers (Murphy, 2013), its downregulation was found to induce P53 mediated cell death in several lung cancer cell lines (Frese et al., 2003). Heat shock protein 70 downregulation by Ibuprofen was found to sensitize cisplatin-resistant tumours (Endo et al., 2014). In non-small

cell lung cancer, HSP70 was found significantly elevated in 49 patient serum samples while no significant change was observed on the level of HSP90 compared to normal control samples (Zhong et al., 2003). The verification results conducted in this research work revealed a significant elevation of HSP70 in the plasma from lung squamous cell carcinoma patients while no change among lung adenocarcinoma patients was detected (figure 11-A) despite its significant elevation by the LC-MS/MS.

Finally, the next paragraph was the closing message that translate the philosophy of this sophisticated research work published in BBA clinical. “The utility of mass spectrometry-based quantitative proteomics as an additional piece of information to facilitate clinicians in the classifications of tumours is a significant area in development, as more treatments are specifically aimed at squamous and non-squamous cell carcinoma. Also, a better understanding of the NSCLC histological subtypes may provide valuable insight in support of developing targeted therapeutics that are specific for precisely classified lung tumours. Several new targeted therapies have been recently approved for non-squamous NSCLC that inhibit Vascular Endothelial Growth Factor (VEGF), Epidermal Growth Factor Receptor (EGFR), Anaplastic Lymphoma Kinase (ALK), and Reactive Oxygen Species (ROS-1) (Bansal et al., 2016). As more driver mutations are discovered and therapeutic compounds developed to target these abnormal pathways, precise diagnosis of lung cancer and its subtypes will be crucial (Caparica et al., 2016). Protein expression and signalling in either BALF or plasma may have clinical relevance in the future through its ability to precisely differentiate subtypes and facilitate lung cancer diagnosis”. However, The discussion of this currently presented data will be extended to the next chapter focusing on biomarkers that play a role in cancer metabolism, and also would

be used as a reference for further comparison discovery phase done on formaldehyde-fixed paraffine-embedded (FFPE) lung adenocarcinoma tumour tissue (chapter V).

Chapter 4

Metabolon discovery work

4. Metabolic biomarkers discovery work

4.1 Introduction

To cope with the exceptional increase in energy demand, cancer cells use all the available energy substrates other than the aerobic catabolism of glucose (Devic, 2016, Keibler et al., 2016). Glucose utilisation in cancer is restricted to the lactic acid cycle (Devic, 2016) for two reasons: the increased demand for the production of nitrogen bases *via* the phosphate pentose pathway (Jiang et al., 2014), and the lack of sufficient angiogenesis to supply the tumour environment with enough oxygen required to convert the produced pyruvate to acetyl Co-A, the starting substrate of citric acid cycle (Cairns et al., 2011a, Cairns et al., 2011b). Only two molecules of ATP are produced per glucose molecule, but the rate of ATP production is 100 times higher compared to the full aerobic oxidation of glucose in mitochondria (Devic, 2016). By promoting metabolic adaptation or transformation, Cancer cells can survive in environment that kill normal cells (Cairns et al., 2011a).

Metabolic transformation involves the use of substrates that can be converted into acetyl co-A to compensate for the incomplete utilisation of glucose. Fatty acids, glutamate and urea are the most common energy substrates used by cancer cells (Callejón-Leblic et al., 2016). Interestingly, the incidence of cancer among people with type I diabetes mellitus is very low and *vice versa* in people consuming excessive amounts of carbohydrates (Devic, 2016). Therefore, interesting targets of biomarker discovery and targeted therapy include enzymes controlling the production of acetyl co-A and utilising all possible substrates, as well as those controlling its metabolism, became targets in biomarker discovery and targeted therapy. Sheng, *et al.* have published a good review of inhibitors targeting glucose,

glutamine and free fatty acid metabolism in cancer (Sheng et al., 2009). In the context of the proteome signature that distinguishes lung adenocarcinoma from squamous cell carcinomas and previous work on lung lavage (Callejón-Leblic et al., 2016, Almatroodi et al., 2015), one of the objectives of this study was to carry out biomarkers discovery on metabolomics.

4.2. Experimental design

Serum samples were collected from patients with lung cancer, including both small and non-small lung carcinomas. Control samples were collected from healthy individuals and from patients with non-cancer inflammatory and autoimmune diseases. Samples in quadruplicates were shipped to Metabolon Inc. (N.C., USA) for analysis. Two aliquots were analysed for basic and acidic peptides by UHPLC-MS/MS and one for analysed for relatively small-molecule metabolites GC/MS and the 4th aliquots was kept as a reference. A second set of serum samples was collected and tested for ketone bodies, including acetoacetic acid and 3-hydroxybutyrate ketone bodies. The serum samples were also tested for the levels of pyruvate, acetyl co-A, fatty acids, and glutamate. To avoid misinterpretation of false positive and false negative levels of the candidate biomarkers, non-cancerous common respiratory system inflammatory were included.

4.3. Results

4.3.1. Elevated serum metabolites levels detected by LC/MS and GC/MS analysis in NSCLC compared to control

Seventeen metabolites were significantly elevated in sera of patients with lung squamous and adenocarcinomas compared to the normal control (Table 31).

Table 31: Metabolites significantly up-regulated in sera of lung cancer patients and controls

Compound	Detection method	AD vs C	SqCC vs C
Serine	GC/MS	1.35	1.7
Aspartate		2.42	2.94
Ornithine		4.33	3.29
Glutamate		3.17	3.53
Phenylalanine		1.57	1.64
Tyrosine		1.52	1.53
Kynurenine		1.19	1.44
Tryptophan		1.19	1.04
C-glycosyltryptophan		1.23	1.74
Lsoleucine		LC/MS +	1.69
Leucine	1.6		1.8
Valine	1.18		1.26
Methionine	1.09		1.39
Proline	1.36		1.2
Citrulline	1.82		1.74
5-oxoproline	2.1		1.98
3-methyl-2-oxovalerate	LC/MS –	1.52	1.44

AD: adenocarcinoma, SqCC: squamous cell carcinoma, C: control, +: positive, -: negative

4.3.2. Lowered serum metabolites levels detected by LC/MS and GC/MS analysis in NSCLC compared to control

Table 32 lists the significantly downregulated metabolites in sera compared to normal controls (see also appendix 7).

Table 32: Metabolites found downregulated in sera of lung cancer patients compared to the control normal individuals

Compound		AD vs C	SqCC vs C
Glutaroyl carnitine		0.67	0.82
Tryptophan betaine		0.48	0.53
Serotonin (5HT)	LC/MS +	0.66	0.81
Methylglutaroylcarnitine		0.31	0.74
Indolepropionate		0.58	0.4
3-phenylpropionate (hydrocinnamate)	LC/MS -	0.63	0.48

*Numbers in **bold** indicate $p \leq 0.05$ ϕ : LC/MS positive, θ : GC/MS, Δ : LC/MS negative, D : lowered.*

4.3.3. Serum levels of some acetyl co-A precursors

Serum levels of pyruvate and acetyl Co-A were significantly higher in patients with lung adenocarcinoma or squamous cell carcinoma (n= 96) than in controls (n= 55) (Mann Whitney test, $p < 0.0001$ and 0.01 , respectively). In contrast, the levels of free fatty acids and acetoacetate were significantly lower in the cancer patients ($p = 0.001$ and 0.0004 , respectively). However, there was no significant difference between the two groups in 3-hydroxybutyrate ($p = 0.7$) (figure 13).

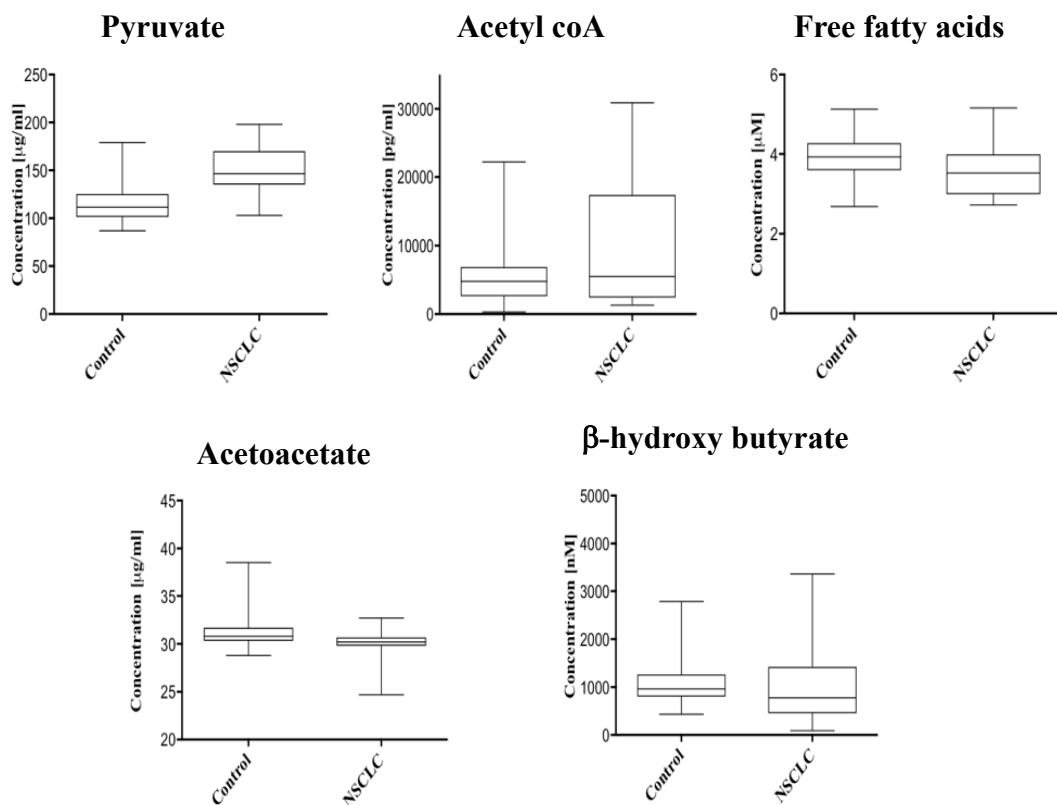


Figure 13: Serum levels of various metabolites in the patients with NSCLC and controls.

4.3.4. Serum glutamate levels

Shown in figure 14, box and whiskers blot analysis of Glutamate levels in lung non-small cell carcinoma: Lung adenocarcinoma serum samples (n=49) [A], Lung squamous cell carcinoma (n=43) [B] compared to the normal control group serum samples (n=79). The result revealed a decreased levels of glutamate in both lung carcinomas compared to normal control with p value of <0.0001 and 0.001 in adenocarcinoma and squamous cell carcinoma, respectively.

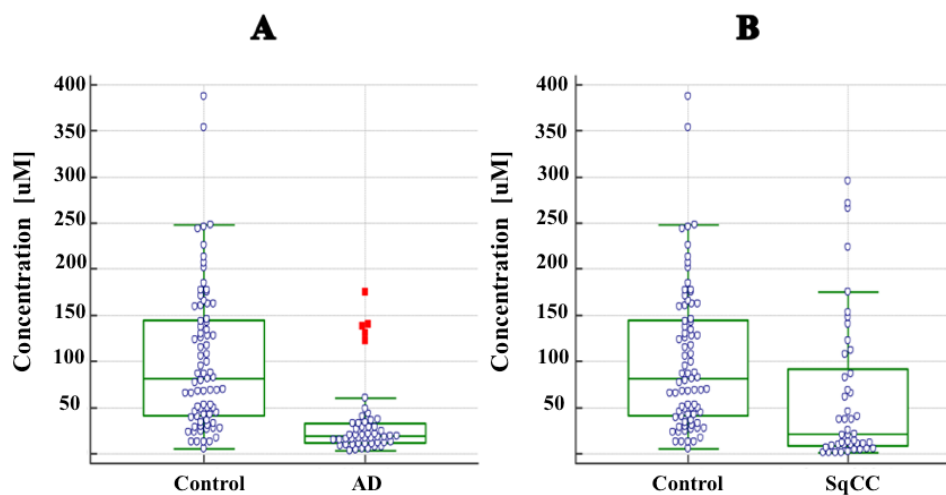


Figure 14: Glutamate levels in non-small cell lung cancer compared to control group, AD: lung adenocarcinoma, SqCC: squamous cell carcinoma, uM: micro molar.

4.4. Discussion

There is insufficient metabolites-based research on cancer, making it difficult to relate any findings to specific types of lung cancer. Therefore, the data obtained in this study will be presented as it is, and the main molecules connecting different processes of energy production will be used as markers to judge the increased utilization of certain energy substrates. Our findings (summarized in figure 15) will be discussed in parallel with the lavage work reported in chapter III.

The increased uptake and utilization of glucose in cancer is accompanied by increased lactate production and activation of gluconeogenesis via the Cori cycle in the liver (Hsu and Sabatini, 2008, Lunt and Vander Heiden, 2011). Lactate was significantly elevated ($p= 0.02$) in lung AD with a 1.45-fold change, but no change was detected in lung SqCC. In this research work, Serum pyruvate found significantly ($p= 3.5E-09$) elevated in NSCLC serum samples compared to the normal controls (figure 13). Pyruvate connects glycolysis, the citric acid cycle, the Cori cycle (gluconeogenesis) and amino acids (as a source of acetyl Co-A). Therefore, this discussion will focus on pyruvate as a central molecule (Figure 15).

Pyruvate kinase M1 and 2 (PKM 1/2) , catalysis the conversion of phosphoenolpyruvate (PEP) to pyruvate in the last step of glycolysis (Mazurek, 2011), and play a crucial role in the tumorigenesis and invasion of cancer via lactate accumulation (Eigenbrodt et al., 1992). PKM2 was detected elevated in the plasma and tumour tissues from NSCLC and colorectal cancer by ELISA and IHC, and such overexpression was found not to correlate with the tumour grade and stage (Kobierzycki et al., 2014, Schneider et al., 2002). Pyruvate kinase M2 was found elevated in many other cancers including stomach, oesophagus and breast cancer

(Kobierzycki et al., 2014). In this research work, PKM was detected significantly elevated in lung AD (4.E-02) and lowered in SqCC ($p= 2.E-04$) patients' lavages compared to the normal control lavage with fold change of 1.8 and 4.2, respectively (appendix 1, 4).

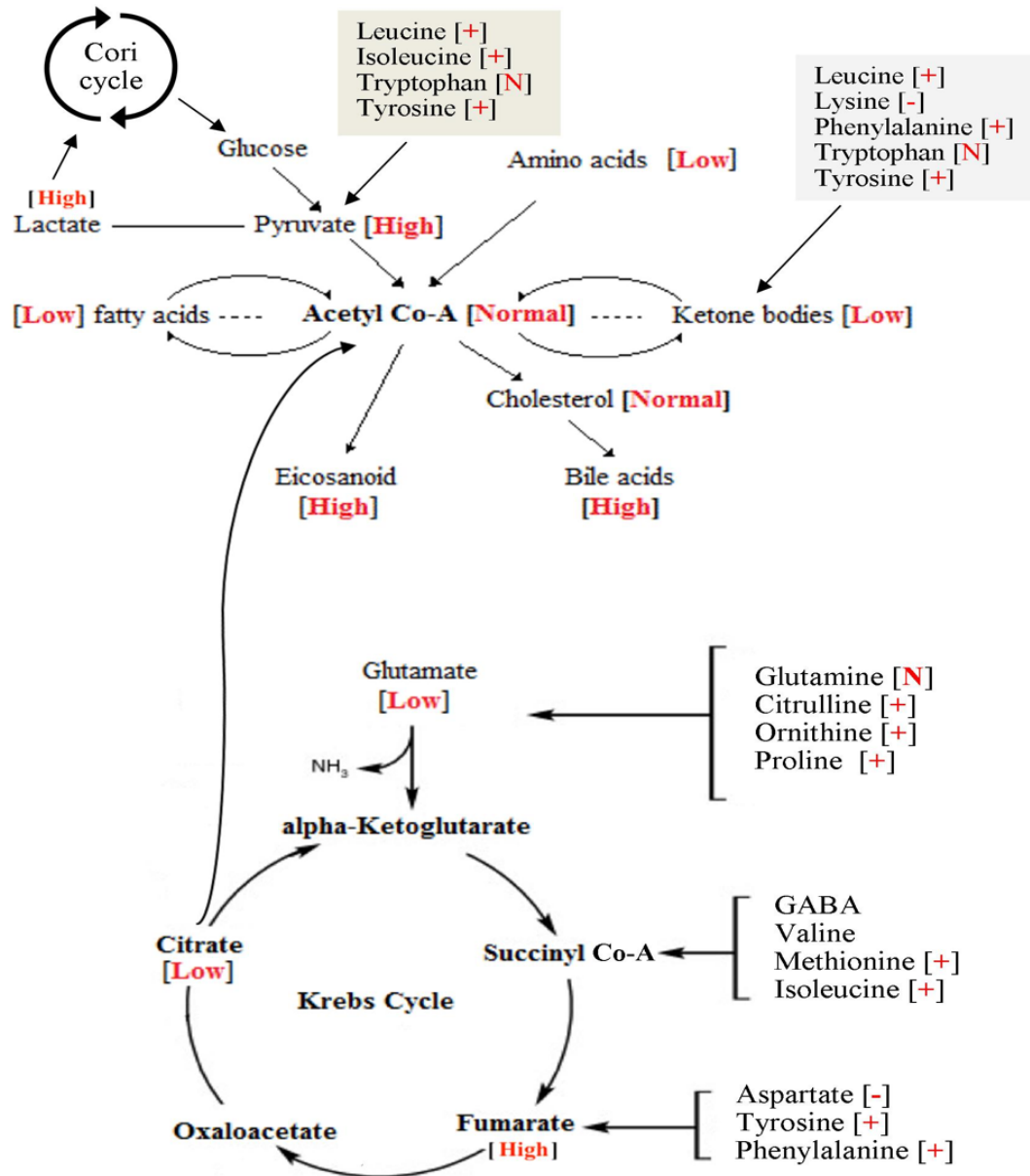


Figure 15: Acetyl Co-A as a central metabolite intermediate for amino acids and fatty acids. Red: significant by colourimetry, ELISA, LC-MS/MS or GC.

In this research work, the levels of pyruvate was also assessed in NSCLC serum samples ($n=92$) compared to normal control samples ($n=79$). The results showed a significant ($p < 0.0001$) increase in the levels of pyruvate in NSCLC in compare to control samples (figure 13). LC-MS/MS analysis of lavage samples revealed a significant increase in the level of lactate dehydrogenase A in lung AD (fold increase of 3.5, $p = 1.E-07$) and SqCC (fold increase 4.3, $p = 2.E-05$) (Tables 20, 22).

It is unlikely that single biomarkers can be found for specific tumour types. The overall metabolic profile would rely on the availability of energy substrates. The overall metabolic signature of NSCLC is that pyruvate production exceeds its conversion to lactate. Lactate dehydrogenase B, which catalyses the conversion of lactate back to pyruvate, was significantly elevated ($p = 3.E-07$) in lung AD lavage (Table 20) but was not detected in SqCC. This might be a regulatory negative feedback mechanism indicating that lactate is produced more in lung AD than in SqCC. The elevations in glucose levels in lung AD and SqCC (1.2 and 1.2 fold changes) were not significant ($p = 0.2$). Cancer cells need an alternative source of energy that can enter the citric acid cycle without harming the cells, which might explain the large loss of fat and muscle mass in cancer patients (cachexia).

Cachexia is the leading cause of death in 20% of cancer deaths worldwide. It results from degradation of body muscles and fat (Tisdale, 2009). Decreased levels of ketone bodies is the main clinical finding of cachexia (Shukla et al., 2014). In the current study, serum levels of free fatty acids and acetoacetic acid were significantly lower in NSCLC patients than in normal controls ($p = 0.002$ and 0.0001 , respectively) (Figures 13). But no significant change was seen in 3-hydroxy butyric acid with overall decreased pattern (Figure 13). Overall, there was greater fat degradation in

lung SqCC than in AD, as indicated by the significant increase in the levels of free, medium and long chain (branched/unbranched) fatty acids.

Muscles contain 98% of total body carnitine, 75% of which comes from dietary intake and 25% is endogenously synthesized from lysine and methionine (Sayed-Ahmed, 2010, Engel and Rebouche, 1984). Carnitine supplementation ameliorates the fatigue induced by cisplatin chemotherapy (Graziano et al., 2002). Here, significant carnitine metabolism was detected in lung SqCC but not in AD (Appendix 8). This finding indicates increased dependence of tumour tissues on fats as an alternative energy source.

Amino acids uptake and utilization with concomitant overexpression of their transporters was demonstrated in many cancers (Bhutia et al., 2015). Cross-talk between ketone bodies and the urea cycle enables provision of another good source of non-essential amino acids in cancer by transamination of acetoacetate into amino acids such as aspartate. GC/MS analysis showed that serum aspartate was significantly elevated in AD and SqCC with fold changes of 2.42 ($p= 0.01$) and 2.9 ($p= 0.05$) compared to control samples (Table 31). Indeed, amino acid deprivation is being adopted in parallel to chemotherapy as a standard cancer treatment (Fung and Chan, 2017). Moreover, elevation of serum histidine, aspartate, phenylalanine, serine and alanine has been observed in NSCLC (Klupczynska et al., 2016). In our study, serine and aspartate were significantly elevated (GC/MS) in AD and SqCC, as well as phenylalanine (LC/MS), with fold changes ranging from 1.35 to 2.9 [Table 31]. Their fold change in respective order were (1.35, 1.7), (2.4, 2.9), (1.57, 1.64) in AD and SqCC compared to control samples. The only difference between the finding of Klupczynska et al. and ours is that citrulline was decreased in

Klupczynska's polish patients but elevated in our Irish patients, with fold changes of 1.8 and 1.7 in AD and SqCC, respectively (Table 31).

In the lavage discovery work, protein-glutamine γ -glutamyltransferase 2 (transglutaminase 2) was significantly elevated in both AD ($p= 5.E-05$) and SqCC ($p= 2.E-05$), with fold changes of 10.0 and 8.4, respectively. Transglutaminase 2 has a role in cancer progression, metastasis and resistance to chemotherapy (Shao et al., 2009, Begg et al., 2006). Glutathione synthetase, the enzyme involved in glutathione synthesis plays a role in detoxification of xenobiotic compounds and in tumour growth and resistance to chemotherapy in many cancers, including breast, colon and lung cancer (Balendiran et al., 2004). In the lavage work, glutathione synthetase was decreased 1.5 fold ($p= 3.0E-02$) in AD and 1.6 fold ($p= 3.0E-02$) in SqCC lavage compared to the normal control (Appendixes 2, 4).

Glutamine synthetase (GS) catalyses the conversion of glutamate to glutamine (Adeva et al., 2012). Increased glutamine and asparagine catabolism mediated by glutamate dehydrogenase is characteristic of the tumour microenvironment (Spinelli et al., 2017). Glutamate dehydrogenase activity is accompanied by accumulation of urea (Adeva et al., 2012), which is recycled in the liver via the urea cycle (Kappler et al., 2017). In our work, no significant change in the level of glutamine was observed by LC-MS/MS, either in lung AD or in SqCC carcinoma (Appendix 7), whereas glutamate was elevated 3.17 fold in AD and 3.53 fold in SqCC compared to control (Appendix 7).

Also serum glutamate was assessed in non-small cell lung cancer (squamous and adenocarcinomas) (Figure 14). Unexpectedly, glutamate was significantly decreased in both AD (n = 49) and SqCC (n = 43) compared to normal control (n = 79). This

reflects increased consumption of glutamate in AD and SqCC. Glutamate is elevated in many cancers, including lung cancer with neurologic symptoms (Michalak et al., 2016), stomach cancer, colon cancer (Okada et al., 1993) and breast cancer with decreased levels of glutamine (Budczies et al., 2015). These reports support our mass spectrometry findings but conflict with the results of our serum colourimetric assay used to validate our discovery work. Factors other than the samples per se might be responsible for this discrepancy. For instance, chemotherapy induces metabolic reprogramming, including diminished glutamate synthesis in tumour tissues, which will directly affect serum or plasma levels. In any case, the increased consumption of ketone bodies, fatty acids, glutamate and aspartate reflects the ability of NSCLC cells to consume substrates other than glucose. Despite the long list of significantly elevated fat metabolites in lung SqCC compared to AD in our study (Appendix 8), it is still too early to speak about metabolic signatures for tumour subtypes. Nevertheless, our findings serve as a reference for future reproducibility of such metabolic signature found to cluster lung squamous cell carcinoma from lung adenocarcinoma.

Chapter 5

Intra-tumour heterogeneity

5. Tumour heterogeneity

5.1. Introduction

Tumour heterogeneity originates from the high mutability of cancer cells and the accumulation of mutations in the tumour cell populations at the very early stages (Andor et al., 2016). This intra-tumour heterogeneity can be due to both genetic factors and diversity of post translational modifications (McGranahan and Swanton, 2017). Dominant sub-clonal cancer cells populations that are resistant to treatment are common in cancer. These cell populations become dominant when the drug sensitive populations are eliminated and became responsible for tumour relapse, drug resistance and the overall treatment outcome (McGranahan and Swanton, 2017, Greaves, 2015). The mosaic nature of cancer makes it very difficult to find stable biomarkers or panels of markers that have good clinical utility in diagnosis and monitoring of patients under treatment. Over the last three decades, no single protein biomarker of lung cancer has been identified and validated sufficiently for clinical use (Hoang, 2017). Due to the lack of standardisation in sample collection and due to sample vulnerability before and during staining, immunohistochemistry-based diagnosis of lung cancer suffers from staining inconsistency and irreproducibility (Zhu et al., 2006). This research work aimed to show the heterogeneity in four adenocarcinoma tumour samples with known TNM staging and to validate the list of proteins found significant in the bronchoalveolar lavage from lung adenocarcinoma patients. The purpose was to cluster a group of proteins specifically related to the tumour but not to background abnormalities in the surrounding tissues.

5.2. Experimental design

The inconsistency of the sensitivity and specificity of biomarkers for samples of different groups is attributed mainly to heterogeneity of tumour tissues. Four tumour specimens were collected from lung adenocarcinoma patients, along with normal lung tissue. Each tumour specimen was randomly divided into four quadrants, three of which were analysed by MS and their protein abundance compared to normal lung tissue from the same patient. Principal component analysis was performed to illustrate the existence of heterogeneity of protein abundance. Heat maps were also used to cluster the protein abundance in different parts of the tumour and to visualise the shared and highly abundant proteins. Venn diagrams were used to identify groups of shared proteins in all parts of the tumour samples and intersect them with the list came off the lavage work in chapter 3.

5.3. Results

5.3.1. Principal component analysis

Principal component analysis (PCA) was done on four lung adenocarcinoma specimens (Figure 16). Based on their proteomic signature [both up and down regulated proteins and how much changed are they (Fold change)?] obtained from the comparative label-free mass spectrometric analysis of the compared biopsies (control vs trisections), PCA clustered normal tissues from malignant ones in the first component of the analysis, while second component examined the difference in abundance in the protein signature among the tumour parts.

Patient #1. The proteomic signature of (Q3) clustered to have some normal tissues' protein abundance profile as it lying to the right of the component 1, at the same time seem different from the other two parts of the tumour (Q1, Q2).

Patient #2. All tumour parts were differentiated from the normal control tissue. The three different parts of the tumour (Q1, Q2 and Q3) showed a wide range of differences in protein abundance. Q3 seems to share some protein signatures with Q1 and Q2, whereas Q1 and Q2 exhibit the highest degree of heterogeneity in their protein signature.

Patient #3. This patient exhibited the same heterogeneity characteristics as patient #2.

Patient #4. The only difference from patient #3 was that Q2 and Q3 were very close to each other, while Q1 showed a very different protein abundance profile.

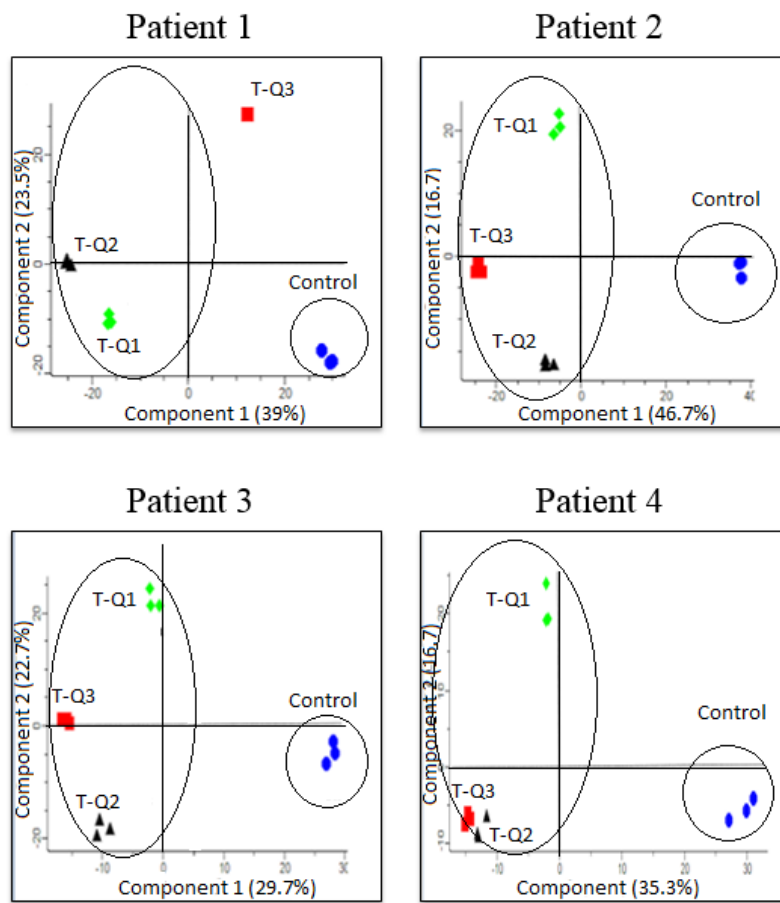


Figure 16: Principal component analysis (PCA) separating tumour from normal control tissue (component 1) and heterogeneity within the tumour quadrants (component 2), the percentages represent the variance between the two compared groups.

5.3.2. Heat map analysis

Figure 17 shows the heat map analysis of the total proteomes signature (up and down regulated proteins detected by mass spectrometry) of three different parts of tumour specimens from four lung adenocarcinoma patients compared to their matched normal lung tissues. The Q1(repeats), Q2(repeats) and Q3(repeats) represent technical repeats of the same sample. The first branch clusters normal from cancerous tissues. The second branch clusters tumour parts based on their abundance.

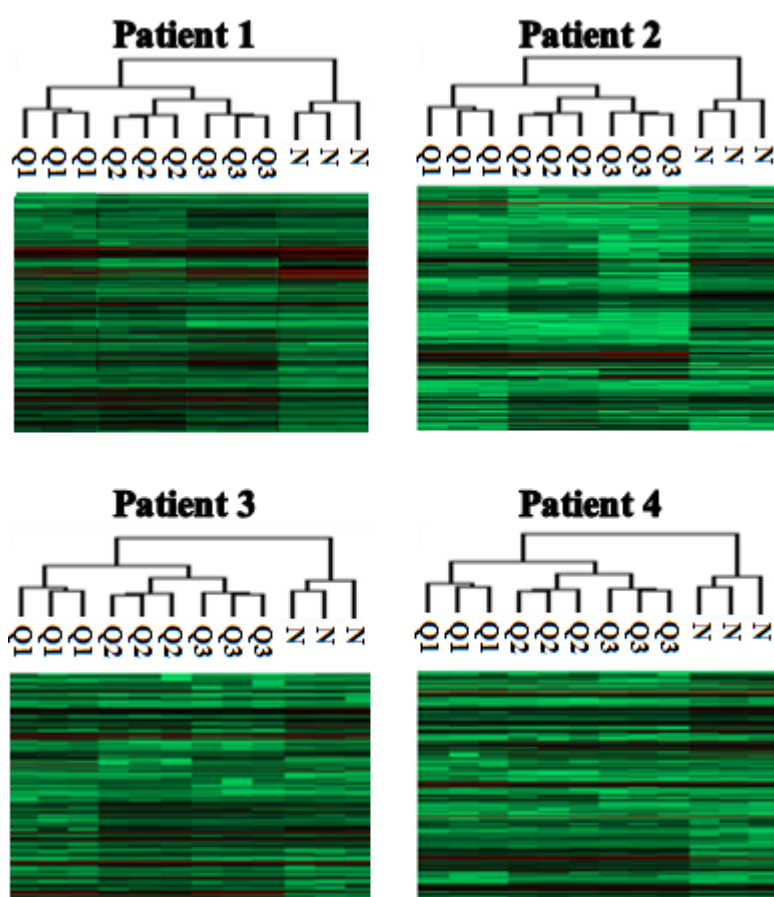


Figure 17: Heat map comparison of total proteomes (up and down regulated proteins) of tumour specimens. N: normal lung tissue, Q: tumour tissue quadrants.

5.3.3. Analysis of shared elevated protein levels in all tumour tissue parts per patient

Figure 18 represents the proteins found significantly elevated by mass spectrometry in different parts of the tumour mass dissected from each patient. In Patient #4; all parts of the tumour share only 5 proteins while tumours from patients; 1,2 and 3 share 56, 52 and 88 proteins in their tumour parts, respectively.

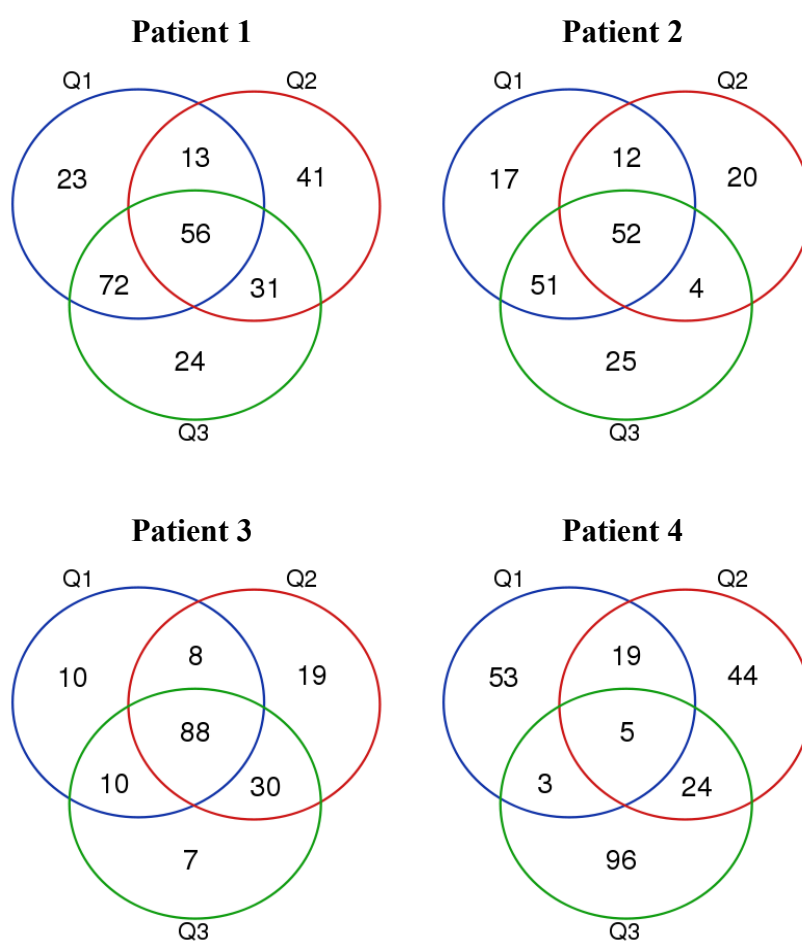


Figure 18: Venn diagrams showing shared up-regulated proteins compared to normal control tissue from the same patient in the three different parts (Q1, Q2, Q3) of the same tumour specimen per patient. The protein abundance fold-change cut-off value was set to ≥ 1.2 .

5.3.3.1. Patient #1 analysis

Table 33 shows the top 30 proteins detected significantly elevated by label-free mass spectrometry in all parts of the tumour specimen (3 quadrants) for patient #1 compared to the matched normal control tissue. The full list is in appendix 12.

Table 33: Top 30 proteins of 488 proteins found significantly elevated in all parts of the tumour tissue of patient #1

Accession	Q1/C	Q2/C	Q3/C	Protein name
B4DT77	1.3	1.4	1.3	Annexin
B9A064	4.1	6.1	5.4	Immunoglobulin lambda-like polypeptide 5
H3BS10	2.7	1.5	5.5	Beta-hexosaminidase
MOR0F0	1.8	2.7	1.7	40S ribosomal protein S5
O75083	1.2	1.8	1.6	WD repeat-containing protein 1
P00338	1.5	1.4	2.6	L-lactate dehydrogenase A chain
P02794	3.2	1.6	3.8	Ferritin heavy chain
P05091	3	1.6	2.4	Aldehyde dehydrogenase, mitochondrial
P05783	4.4	3.4	4.4	Keratin, type I cytoskeletal 18
P06744	1.7	2.5	3.4	Glucose-6-phosphate isomerase
P07099	1.5	2.3	3	Epoxide hydrolase 1
P07195	1.4	1.5	1.9	L-lactate dehydrogenase B chain
P07339	1.4	1.8	2.2	Cathepsin D
P08238	1.9	3.2	1.8	Heat shock protein HSP 90-beta
P0DOY2	1.5	2.3	1.6	Immunoglobulin lambda constant 2
P10599	1.4	1.5	1.4	Thioredoxin
P10809	4.2	1.8	2.3	60 kDa heat shock protein, mitochondrial
P11021	1.8	18.9	1.8	78 kDa glucose-regulated protein
P11142	1.9	2.1	1.7	Heat shock cognate 71 kDa protein
P14618	1.7	2.1	2.1	Pyruvate kinase PKM
P15559	16.5	2	21.8	NAD(P)H dehydrogenase [quinone] 1
P16152	2.9	2.1	5.9	Carbonyl reductase [NADPH] 1
P21397	2.9	2.1	2.5	Amine oxidase [flavin-containing] A
P21796	1.9	1.3	1.2	Voltage-dependent anion-selective channel protein 1
P22314	1.6	10.1	1.8	Ubiquitin-like modifier-activating enzyme 1
P23396	1.9	1.5	1.6	40S ribosomal protein S3
P25788	1.7	1.9	1.6	Proteasome subunit alpha type-3
P27695	1.5	2.3	1.6	DNA-(apurinic or apyrimidinic site) lyase
P28066	2	2.1	1.9	Proteasome subunit alpha type-5
P28838	1.3	4.7	2.4	Cytosol aminopeptidase

Q: tumour tissue quadrant, C: normal lung control tissue.

5.3.3.2. Patient #2 analysis

Table 34 shows the top 30 proteins detected significantly elevated by label-free mass spectrometry in all parts of the tumour tissue specimen (3 quadrants) for patient coded #2 compared to the matched normal control tissue. The full list put in appendix 20.

Table 34: Top 30 proteins of 352 proteins found significantly elevated in all parts of the tumour of patient #2

Accession	Q1/C	Q2/C	Q3/C	Description
E7EMM4	4.8	1.9	1.6	Acid ceramidase
I3L397	1.8	1.3	1.3	Eukaryotic translation initiation factor 5A
O43707	3.5	2.2	3	Alpha-actinin-4
P00352	8	1.5	1.6	Retinal dehydrogenase 1
P02452	8.6	5.2	6.3	Collagen alpha-1
P02545	3.4	2.7	2.6	Prelamin-A/C [Cleaved into: Lamin-A/C
P02743	2.5	1.4	2.3	Serum amyloid P-component
P05387	2.1	1.7	1.4	60S acidic ribosomal protein P2
P07339	2.7	2.2	1.6	Cathepsin D
P07355	2.1	1.7	1.6	Annexin A2
P07384	2.5	1.5	1.5	Calpain-1 catalytic subunit
P08123	4.7	3.8	2.9	Collagen alpha-2
P08758	2.4	2	1.6	Annexin A5
P09211	4.4	1.6	1.7	Glutathione S-transferase P
P12109	2.7	2.6	2.3	Collagen alpha-1
P12110	18.3	15.2	11.9	Collagen alpha-2
P12111	2.6	1.9	1.8	Collagen alpha-3
P12429	4.1	3.6	1.5	Annexin A3
P14550	1.9	1.4	1.6	Alcohol dehydrogenase [NADP
P21291	3.5	1.8	3	Cysteine and glycine-rich protein 1
P21333	5.7	5.1	4.3	Filamin-A
P21810	3.9	1.6	1.8	Biglycan
P21980	1.8	1.5	2.3	Protein-glutamine gamma-glutamyltransferase 2
P23284	1.5	1.3	1.7	Peptidyl-prolyl cis-trans isomerase B
P27348	3.9	1.7	4.1	14-3-3 protein theta
P30044	8.6	1.7	1.6	Peroxiredoxin-5, mitochondrial
P30048	3.2	1.7	1.5	Thioredoxin-dependent peroxide reductase, Mito
P30086	4	1.7	1.5	Phosphatidylethanolamine-binding protein 1
P35579	2.4	3.5	3.2	Myosin-9
P36578	1.7	1.2	1.3	60S ribosomal protein L4

Q: tumour tissue quadrant, C: normal lung control tissue.

5.3.3.3. Patient #3 analysis

Table 35 shows the top 30 proteins detected significantly elevated by mass spectrometry in all parts (3 quadrants) of the tumour specimen from patient #3 compared to the match normal control tissue. The full list is in appendix 28.

Table 35: Top 30 proteins of 396 proteins found significantly elevated in all parts of the tumour specimen from patient #3

Accession	Q1/C	Q2/C	Q3/C	Protein names
E7EN65	2.7	3.6	4.1	Elastin
O14773	3.2	3.7	2.8	Tripeptidyl-peptidase 1
O43399	2.2	2.3	1.9	Tumor protein D54
O43707	1.4	1.3	1.4	Alpha-actinin-4
P00338	1.6	5.3	3.9	L-lactate dehydrogenase A chain
P00352	3.2	1.8	1.7	Retinal dehydrogenase 1
P00558	1.3	1.5	1.7	Phosphoglycerate kinase 1
P00568	2.4	1.7	2	Adenylate kinase isoenzyme 1
P02743	3.2	2.3	3.7	Serum amyloid P-component
P02751	1.3	1.3	1.3	Fibronectin
P02792	3.2	8	4.9	Ferritin light chain
P04004	1.8	1.9	2.3	Vitronectin
P04406	1.6	1.7	1.9	Glyceraldehyde-3-phosphate dehydrogenase
P04899	1.3	1.3	1.3	Guanine nucleotide-binding protein G
P06744	1.2	2.1	2.1	Glucose-6-phosphate isomerase
P06748	1.4	2.3	1.6	Nucleophosmin
P07195	1.6	2.8	2.3	L-lactate dehydrogenase B chain
P07384	2.1	2.3	2.3	Calpain-1 catalytic subunit
P07900	1.4	1.4	1.4	Heat shock protein HSP 90-alpha
P08133	1.7	1.3	1.5	Annexin A6
P08238	1.9	2	2.1	Heat shock protein HSP 90-beta
P08758	2.8	2.7	2.5	Annexin A5
P09211	1.5	2.5	1.8	Glutathione S-transferase P
P09972	1.2	1.4	2	Fructose-bisphosphate aldolase C
P12109	2	1.2	1.2	Collagen alpha-1
P12110	3	1.4	1.7	Collagen alpha-2
P12814	4	3.6	3.6	Alpha-actinin-1
P12956	3	3	3.9	X-ray repair cross-complementing protein 6
P13639	2.2	3.5	3.7	Elongation factor 2
P13797	1.4	1.5	1.6	Plastin-3

Q: tumour tissue quadrant, C: normal lung control tissue.

5.3.3.4. Patient #4 analysis

Table 36 shows the proteins detected significantly elevated by mass spectrometry in all parts of the tumour specimen (3 quadrants) from patient #4 compared to the match normal control tissue. The full list is in appendix 36.

Table 36: Top 5 proteins of 99 proteins found significantly elevated in all parts of the tumour tissue of patient #4.

Accession	Q1/C	Q2/C	Q3/C	Protein name
E7EMM4	1.4	1.8	2.1	Acid ceramidase
F8W7C6	1.3	1.7	1.2	60S ribosomal protein L10
P04229	1.3	1.2	1.5	HLA class II histocompatibility antigen, DRB1-1 beta chain
P21964	1.3	1.4	1.9	Catechol O-methyltransferase
P45880	1.3	1.3	1.3	Voltage-dependent anion-selective channel protein 2

5.3.4. Analysis of proteins diminished in all tumour tissue samples per patient

Figure 19 represents the significantly diminished proteins detected by mass spectrometry in different parts of the dissected tumour for each patient. In patient #4, the three parts of the tumour share only 12 proteins while 60, 38 and 97 proteins were significantly lowered and shared in all parts within same tumour in patient 2,3 and 4 respectively.

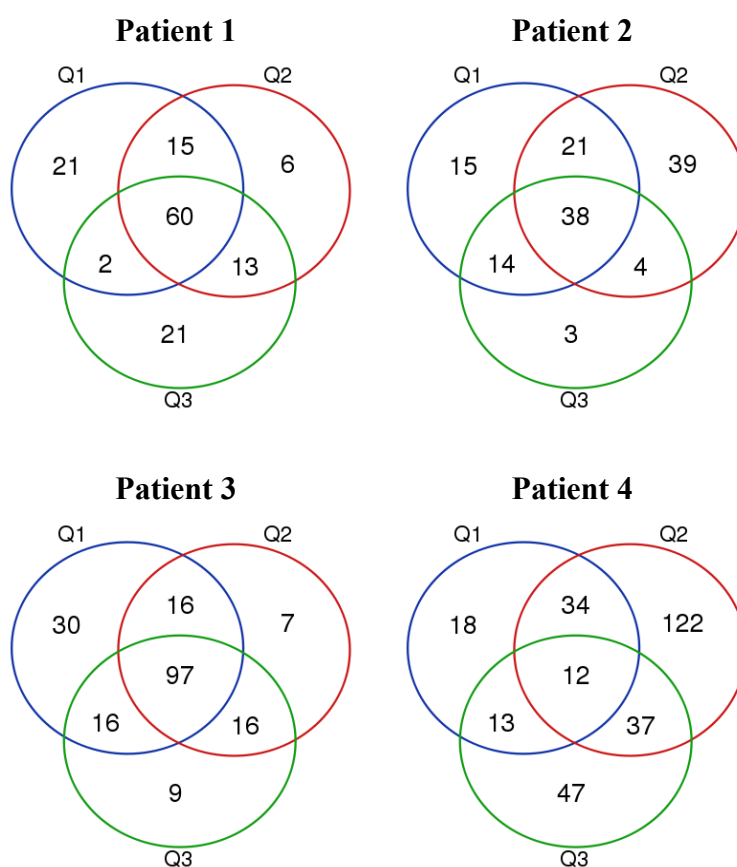


Figure 19: Venn diagrams showing the shared proteins diminished in the three parts (Q1, Q2, Q3) of the same tumour specimen in each patient. The cut-off value for protein abundance fold change was set to ≥ 1.2 .

5.3.4.1. Patient #1 analysis

Table 37 shows the top 30 proteins detected significantly lowered by mass spectrometry in all parts (3 quadrants) of the FFPE specimen for tumour tissue from patient #1 compared to the match normal control tissue. The full list is in appendix 16.

Table 37: Proteins significantly lowered in all parts of the tumour tissue of patient #1

Accession	C/Q1	C/Q2	C/Q3	Protein name
J3QL05	2.6	1.4	1.6	Serine/arginine-rich-splicing factor 2
K7EK07	2	2	1.5	Histone H3
O43707	2.1	2.6	1.3	Alpha-actinin-4
O95865	2.8	4.3	2.4	N(G),N(G)-dimethylarginine dimethylaminohydrolase 2
O95994	2.6	1.4	1.5	Anterior gradient protein 2 homolog
P00915	1.4	3.6	2.1	Carbonic anhydrase 1
P00918	1.4	3.4	2.7	Carbonic anhydrase 2
P01009	3.8	6.3	2.9	Alpha-1-antitrypsin
P01024	1.6	2.1	1.4	Complement C3
P02452	18.8	21.5	4.4	Collagen alpha-1
P02545	1.7	1.7	1.8	Prelamin-A/C [Cleaved into: Lamin-A/C
P02647	2.5	3.1	2.2	Apolipoprotein A-I
P02743	1.5	3.1	2.3	Serum amyloid P-component
P02787	2.5	4	1.4	Serotransferrin
P04004	3.4	3.7	2.4	Vitronectin
P04083	1.2	1.7	2.5	Annexin A1
P05109	3	8.6	2	Protein S100-A8
P05164	4.4	8.2	4.4	Myeloperoxidase
P06702	3.5	7.8	2.9	Protein S100-A9
P07355	1.7	2.9	1.9	Annexin A2
P08123	6.4	10.7	3.5	Collagen alpha-2
P08133	2	2.4	1.8	Annexin A6
P08311	4.1	7.8	4.9	Cathepsin G
P08670	1.3	2.4	1.8	Vimentin
P08758	3.1	3.9	1.5	Annexin A5
P09382	1.6	2	1.4	Galectin-1
P09525	2.1	2	1.8	Annexin A4
P12109	6.6	22.6	5.1	Collagen alpha-1
P12110	11.9	54.1	9.9	Collagen alpha-2
P12277	1.4	4.8	3.4	Creatine kinase B-type

Q: tumour tissue quadrant, C: normal lung control tissue.

5.3.4.2. Patient #2 analysis

Table 38 shows the proteins detected significantly lowered by mass spectrometry in all parts (3 quadrants) of the FFPE specimen for patient #2 compared to the match normal control tissue (Appendix 24).

Table 38: Proteins significantly lower in all parts of the tumour tissue of patient #2

Accession	C/Q1	C/Q2	C/Q3	Description
B9A064	15.5	5	4.3	Immunoglobulin lambda-like polypeptide 5
C9JA05	3	5.3	2.5	Immunoglobulin J chain
P00450	13.6	3.2	2.5	Ceruloplasmin
P00915	1.8	1.7	1.9	Carbonic anhydrase 1
P01008	8.4	3.5	2.6	Antithrombin-III
P01009	12.8	2.8	2.5	Alpha-1-antitrypsin
P01011	5.3	3.2	2.7	Alpha-1-antichymotrypsin
P01023	3.1	1.8	2.8	Alpha-2-macroglobulin
P01024	2.7	1.6	2.1	Complement C3
P01834	7.5	1.5	2.2	Immunoglobulin kappa constant
P01876	9.1	3.8	2.8	Immunoglobulin heavy constant alpha 1
P01903	1.3	2.6	2.4	HLA class II histocompatibility antigen, DR α - chain
P02042	1.6	2.6	1.8	Hemoglobin subunit delta
P02647	4.2	1.6	1.3	Apolipoprotein A-I
P02649	24.6	3.8	1.6	Apolipoprotein E
P02730	3.4	4.8	5.5	Band 3 anion transport protein
P02763	9.6	1.3	2.5	Alpha-1-acid glycoprotein 1
P02766	8	3.1	2.6	Transthyretin
P02774	12.5	1.9	2.8	Vitamin D-binding protein
P02787	8	1.7	2.2	Serotransferrin
P02792	5	3.8	1.2	Ferritin light chain
P04040	1.9	4.2	2.3	Catalase
P04196	8.2	1.6	2.5	Histidine-rich glycoprotein
P04217	14.9	4.2	3.6	Alpha-1B-glycoprotein
P05155	6.6	1.8	2.5	Plasma protease C1 inhibitor
P06727	7.1	5.6	2.1	Apolipoprotein A-IV
P0C0L4	4.3	2.8	1.7	Complement C4-A
P13760	1.2	2	1.4	HLA class II histocompatibility antigen, DRB1-4 β -
P19652	10.3	1.5	2.1	Alpha-1-acid glycoprotein 2
P19827	2.3	3.9	2.8	Inter-alpha-trypsin inhibitor heavy chain H1
P25311	2	3.3	2.3	Zinc-alpha-2-glycoprotein
P32119	1.7	3.2	2	Peroxiredoxin-2
P51884	1.5	2.1	1.2	Lumican
P68871	2.6	2.1	2	Hemoglobin subunit beta
P69905	2.6	2	1.7	Hemoglobin subunit alpha
P98088	3.6	1.7	7.6	Mucin-5AC
Q14624	12.7	4.6	2.9	Inter-alpha-trypsin inhibitor heavy chain H4
Q5T985	2.7	1.5	1.2	Inter-alpha-trypsin inhibitor heavy chain H2

5.3.4.3. Patient #3 analysis

Table 39 shows the top 30 proteins detected significantly low by mass spectrometry in all parts (3 quadrants) of the FFPE specimen for tumour specimen from patient #3 compared to the match normal control tissue (Appendix 32).

Table 39: Proteins significantly low in all parts of the tumour specimen from patient #3

Accession	C/Q1	C/Q2	C/Q3	Protein name
B4E2V5	2	2.4	1.8	cDNA FLJ52062
E7ES10	1.6	1.6	1.2	Calpastatin
E7EVA0	3.3	1.6	1.7	Microtubule-associated protein
F8W1A4	1.4	1.8	1.5	Adenylate kinase 2, mitochondrial
G3V4C1	1.4	1.4	1.2	Heterogeneous nuclear ribonucleoproteins C1/C2
H7BYY1	1.9	1.8	1.3	Tropomyosin 1
J3QS39	2.5	2.4	2.8	Polyubiquitin-B
M0R0F0	1.9	1.8	2.5	40S ribosomal protein S5
O75368	1.8	2.1	2.6	SH3 domain-binding glutamic acid-rich-like protein
O96009	2.2	1.9	2.2	Napsin-A
P00167	3.7	6	3.9	Cytochrome b5
P00367	1.4	1.4	1.3	Glutamate dehydrogenase 1, mitochondrial
P00915	1.9	2.9	2	Carbonic anhydrase 1
P01009	1.5	1.3	2.7	Alpha-1-antitrypsin
P01903	1.3	1.6	1.7	HLA class II histocompatibility antigen, DR alpha chain
P01920	2.2	1.3	1.5	HLA class II histocompatibility antigen, DQ beta 1
P02042	2.1	2.4	1.7	Hemoglobin subunit delta
P02671	1.3	1.4	1.5	Fibrinogen alpha chain
P02675	1.5	2	1.8	Fibrinogen beta chain
P02730	1.9	3.3	2.9	Band 3 anion transport protein
P04040	3.8	4.4	3.6	Catalase
P04632	1.5	1.6	1.5	Calpain small subunit 1
P05091	2.2	3.1	1.8	Aldehyde dehydrogenase, mitochondrial
P05109	2.1	1.7	2.1	Protein S100-A8
P05164	1.3	1.5	1.3	Myeloperoxidase
P07305	2.8	1.9	2.2	Histone H1.0
P08572	1.5	2.3	2	Collagen alpha-2
P09960	1.3	1.4	1.3	Leukotriene A-4 hydrolase
P0DP23	1.8	1.5	1.5	Calmodulin-1
P10301	1.8	2	1.6	Ras-related protein R-Ras

Q: tumour tissue quadrant, C: normal lung control tissue.

5.3.4.4. Patient #4 analysis

Table 40 shows the proteins detected by mass spectrometry to have the lowest abundance in three quadrants of the FFPE specimen for tumour specimen from patient #4 compared to the matched normal control tissue (Appendix 40).

Table 40: proteins significantly low in all parts of the tumour tissue of patient 4

Accession	C/Q1	C/Q2	C/Q3	Protein names
C9JEU5	1.6	3.4	3.5	Fibrinogen gamma chain
P01024	1.4	1.8	1.4	Complement C3
P01871	1.5	2	1.4	Immunoglobulin heavy constant mu
P02671	1.4	3.4	3.2	Fibrinogen alpha chain
P02675	1.5	5	6.5	Fibrinogen beta chain
P05783	1.3	1.3	1.2	Keratin, type I cytoskeletal 18
P06396	1.3	1.7	1.2	Gelsolin
P0C0L4	1.4	2.1	1.5	Complement C4-A
P51659	1.2	1.5	1.4	Peroxisomal multifunctional enzyme type 2
Q01082	1.4	1.2	2.3	Spectrin beta chain, non-erythrocytic 1
Q08380	1.7	1.2	2.1	Galectin-3-binding protein
Q9Y394	1.4	1.3	1.4	Dehydrogenase/reductase SDR member 7

5.3.5. Formaldehyde-fixed paraffin-embedded tumour tissue versus lavage fluid analysis

Table 41: Summary of FFPE specimens heterogeneity and availability in BALF

	Elevated			Shared	BALF [+]	BALF [-]
	Q1	Q2	Q3			
	x/y	x/y	x/y			
Patient 1	164/178	141/171	183/206	56	22	7
Patient 2	136/147	89/97	136/145	52	15	6
Patient 3	118/132	147/163	136/146	88	33	11
Patient 4	80/88	92/100	128/141	5	0	1
	Lowered					
	Q1	Q2	Q3			
	x/y	x/y	x/y			
Patient 1	98/115	98/119	99/110	60	25	3
Patient 2	88/91	104/109	50/63	38	4	22
Patient 3	163/178	139/143	140/157	97	11	17
Patient 4	78/84	208/220	112/116	12	3	4

x/y: Significant/Total detected proteins with fold change cut-off value of 1.2. [-]: low and [+]: high in the lavage from NSCLC compared to the control lavage used.

5.3.5.1. Proteins with opposite patterns in lavage fluid compared to the FFPE biopsies

5.3.5.1.1. Proteins elevated in tumour tissue but in low abundance in lavage

Table 42 lists of proteins detected by mass spectrometry significantly heterogeneously overexpressed in all parts of the tumour in each patient sample compared to the matched control normal lung tissue and were down regulated in the lavage biomarker discovery done on matched tumour types.

Table 42: Proteins elevated in tumour tissues but lowerd in lavage.

Accession	BALF	Q1/C	Q2/C	Q3/C	Protein name	Patient
P31946	1.9	2.9	3.5	1.8	I4-3-3 protein beta/alpha	1
P63104	2.4	1.8	1.6	1.8	I4-3-3 protein zeta/delta	1
P14550	1.2	1.9	1.4	1.6	Alcohol dehydrogenase [NADP]	1
P08758*	3.4	2.4/2.8	2/2.7	1.6	Annexin A5	2, 3
P40199	1.9	6.9	8.9	6.8	Carcinoembryonic Ag-related cell adhesion molecule 6	3
P07339*	2.0	1.4/2.7	1.8/2.2	2.2/1.6	Cathepsin D	1, 2
P13639	1.2	2.2	3.5	3.7	Elongation factor 2	3
P02792	5.8	3.2	8	4.9	Ferritin light chain	3
P08238	1.2	1.9	2	2.1	Heat shock protein HSP 90-beta	3
P61978	1.7	1.5	1.3	1.2	Heterogeneous nuclear ribonucleoprotein K	1
Q00839	1.5	2.3	1.6	2.4	Heterogeneous nuclear ribonucleoprotein U	1
P04229	17	1.3	1.2	1.5	HLA class II histocompatibility antigen, DRB1-1 β chain	4
P05783	2.6	4.4	3.4	4.4	Keratin, type I cytoskeletal 18	1
P35579*	1.7	2.4/2	3.5/1.7	3.2/1.5	Myosin-9	2, 3
Q99497	1.3	3.4	1.3	1.3	Protein DJ-1	2
P21980*	2.0	1.8/1.7	1.5/1.7	2.3/1.9	Protein-glutamine gamma-glutamyltransferase 2	2, 3
P61026	5.3	1.5	1.3	1.9	Ras-related protein Rab-10	3
Q9Y490	3.5	2.3	1.6	2.4	Talin-1	2
P78371	2.0	1.2	4.5	1.5	T-complex protein 1 subunit beta	1
P19971	2.6	1.2	1.8	1.3	Thymidine phosphorylase	3
P37802	3.4	1.5	2.4	2.1	Transgelin-2	1
O14773	3.0	3.2	3.7	2.8	Tripeptidyl-peptidase 1	3
P68363	2.6	2	2	2.6	Tubulin alpha-1B chain	3
O43399	3.6	2.2	2.3	1.9	Tumor protein D54	3

*BALF: bronchoalveolar lavage, Q: tumour tissue quadrant, C: normal lung control tissue. *: found shared in two patients, numbers in **bold** represent the decreased fold change in non-small cell lung cancer lavages compared to normal lavage control. (Q1/C, Q2/C and Q3/C) represent the fold change increase in different parts of adenocarcinoma tissue specimen compared to their matched normal lung tissue.*

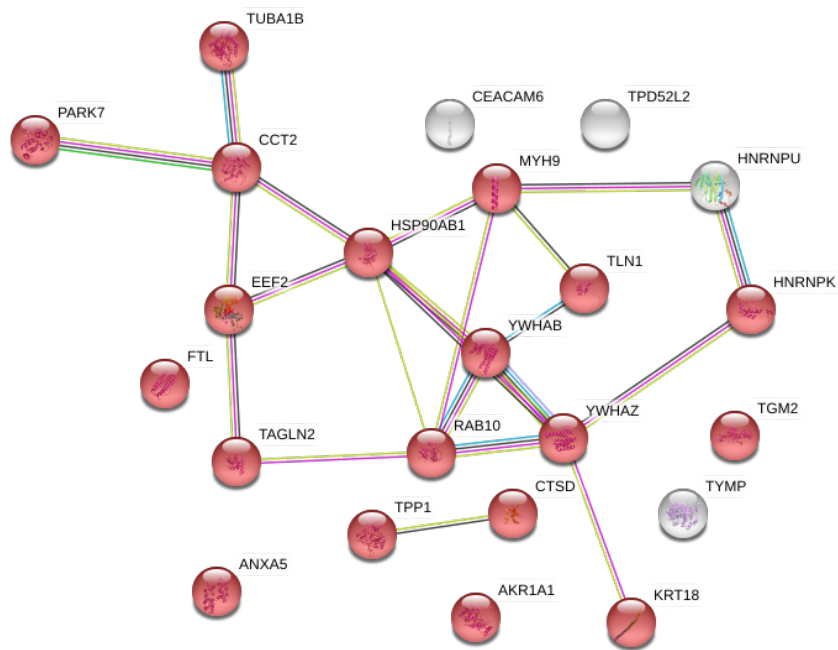


Figure 20: String analysis (GO:0070062 extracellular exosomes) of heterogeneously overexpressed proteins found shared in at least all parts of one FFPE tissue sample and low in the lung lavage from adenocarcinoma. Nodes in red represent the proteins that's excreted via exosomes and can be seen in body fluids.

5.3.5.1.2. Proteins lowered in tumour tissue but at high concentration in lavage

Table 43 shows the significant proteins found heterogeneously downregulated by label-free mass spectrometry in all parts of the tumour in all patient specimens compared to the matched normal lung tissue but were elevated in the lavage discovery done on matched tumour type (appendix 43).

Table 43: down-regulated proteins in tumour tissues found elevated in lavage.

Accession	BALF	C/Q1	C/Q2	C/Q3	Protein name	Patient #
P02671*	5.2	1.4/1.3	3.4/1.4	3.2/1.5	Fibrinogen alpha chain	3,4
P01024*	1.8	2.7/1.4	1.6/1.8	2.1/1.4	Complement C3	2,4
P0C0L4*	4	4.3/1.4	2.8/2.1	1.7/1.5	Complement C4-A	2,4
P01009*	6	12.8/1.5	2.8/1.3	2.5/2.7	Alpha-1-antitrypsin	2,3
P02730*	228	3.4/1.9	4.8/3.3	5.5/2.9	Band 3 anion transport protein	2,3
P00915*	4	1.8/1.9	1.7/2.9	1.9/2	Carbonic anhydrase 1	2,3
Q08380	1.1	1.7	1.2	2.1	Galectin-3-binding protein	4
P01871	4.2	1.5	2	1.4	Immunoglobulin heavy constant mu	4
P27348	4.0	2.2	1.3	1.6	14-3-3 protein theta	3
P61247	4.5	2.3	1.5	1.6	40S ribosomal protein S3a	3
P27797	3.1	2.4	1.5	2.1	Calreticulin	3
P23528	3.2	1.5	1.6	2	Cofilin-1	3
P17661	1.2	1.4	2.4	1.5	Desmin	3
Q01469	2.4	1.7	2.8	3.3	Fatty acid-binding protein, epidermal	3
P02675	1.7	1.5	2	1.8	Fibrinogen beta chain	3
P51858	2.9	2	1.6	2	Hepatoma-derived growth factor	3
P51991	3.6	1.9	1.3	1.4	Heterogeneous nuclear ribonucleoprotein A3	3
P09960	11.5	1.3	1.4	1.3	Leukotriene A-4 hydrolase	3
P05164	1.7	1.3	1.5	1.3	Myeloperoxidase	3
P05109	2.2	2.1	1.7	2.1	Protein S100-A8	3
P02763	2.8	9.6	1.3	2.5	Alpha-1-acid glycoprotein 1	2
P19652	3.1	10.3	1.5	2.1	Alpha-1-acid glycoprotein 2	2
P01011	3	5.3	3.2	2.7	Alpha-1-antichymotrypsin	2
P04217	1.3	14.9	4.2	3.6	Alpha-1B-glycoprotein	2
P01023	1.5	3.1	1.8	2.8	Alpha-2-macroglobulin	2
P01008	2	8.4	3.5	2.6	Antithrombin-III	2
P02647	1.5	4.2	1.6	1.3	Apolipoprotein A-I	2
P06727	3.6	7.1	5.6	2.1	Apolipoprotein A-IV	2
P02649	4.4	24.6	3.8	1.6	Apolipoprotein E	2

**: found shared in two patients, numbers represent the fold change in non-small cell lung cancer compared to normal control.*

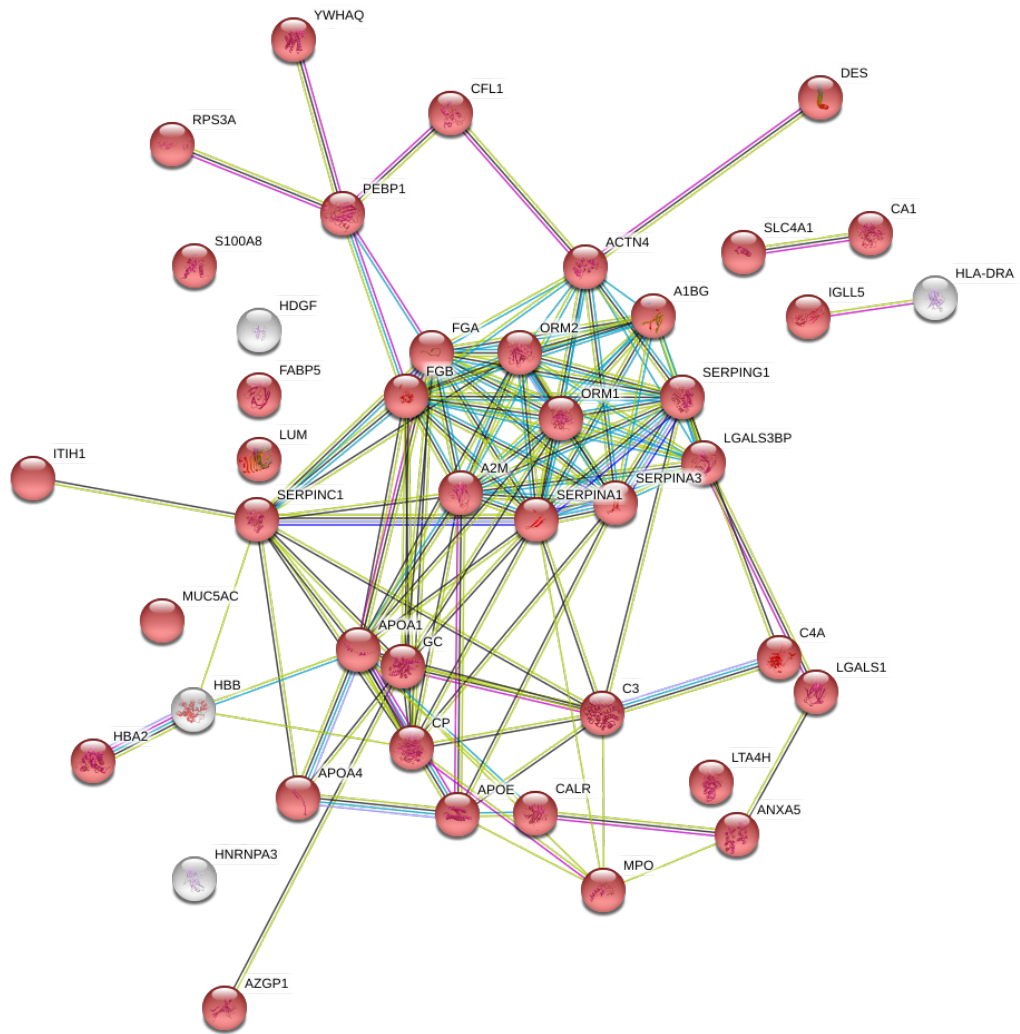


Figure 21: String analysis (GO:0070062 extracellular exosomes) of heterogeneously down regulated proteins found shared in all parts of at least one tissue sample and elevated in the lung lavage from adenocarcinoma. Nodes in red represent proteins that are excreted via exosomes and can be seen in body fluids.

5.3.5.2. Proteins exhibiting the same pattern in lavage and FFPE biopsies

5.3.5.2.1. Proteins overexpressed in tumour tissue and elevated in lavage

Table 44 shows the significant proteins found heterogeneously overexpressed by label-free mass spectrometry in all parts of the tumour in all patient specimens compared to the matched normal lung tissue and also were elevated in the lavage discovery done on matched tumour type (appendix 41).

Table 44: Top 30 proteins found elevated in one or more tumour quadrants and in the lavage

Accession	BALF	Q1/C	Q2/C	Q3/C	Protein name	Patient #
P62277	1.4	1.7/5.3	1.5/4.8	1.5/5.2	40S ribosomal protein S13	2&3
O43707	3.1	3.5/1.4	2.2/1.3	3/1.4	Alpha-actinin-4	2&3
P07384	3.1	2.5/2.1	1.5/2.3	1.5/2.3	Calpain-1 catalytic subunit	2&3
P60842	3.6	1.9/2	1.3/2.5	2.3/2.4	Eukaryotic initiation factor 4A-I	2&3
P23284	3.6	1.5/1.2	1.3/1.8	1.7/1.6	Peptidyl-prolyl cis-trans isomerase B	2&3
Q06323	2.2	1.5/2.2	1.3/2.2	1.2/2.1	Proteasome activator complex subunit 1	2&3
P02743	6.8	2.5/3.2	1.4/2.3	2.3/3.7	Serum amyloid P-component	2&3
P00338	3.5	1.5/1.6	1.4/5.3	2.6/3.9	L-lactate dehydrogenase A chain	1&3
P07195	5	1.4/1.6	1.5/2.8	1.9/2.3	L-lactate dehydrogenase B chain	1&3
P62937	2.1	1.5/1.2	1.9/1.7	1.8/1.5	Peptidyl-prolyl cis-trans isomerase A	1&3
P14618	1.8	1.7/1.9	2.1/3.4	2.1/3.1	Pyruvate kinase PKM	1&3
P37837	3.1	2/1.4	1.8/2.4	4.8/1.9	Transaldolase	1&3
P22314	2.1	1.6/1.3	10.1/1.8	1.8/1.8	Ubiquitin-like modifier-activating enzyme 1	1&3
P62906	6.1	1.5	2.1	1.9	60S ribosomal protein L10a	3
P61158	3	2	2.6	2.4	Actin-related protein 3	3
P00568	4.2	2.4	1.7	2	Adenylate kinase isoenzyme 1	3
P08133	3.9	1.7	1.3	1.5	Annexin A6	3
Q14204	13.3	2.4	1.3	1.5	Cytoplasmic dynein 1 heavy chain 1	3
P49327	9.5	2	2.5	2.5	Fatty acid synthase	3
P04406	2.1	1.6	1.7	1.9	GAPDH	3
P04899	15	1.3	1.3	1.3	Guanine nucleotide-binding protein G	3
Q12905	7	2.9	4.5	5.1	Interleukin enhancer-binding factor 2	3
P14174	2	8.6	10.6	7	Macrophage migration inhibitory factor	3
P35580	4	3.2	1.5	1.3	Myosin-10	3
Q9UJ70	2.5	1.4	1.4	1.5	N-acetyl-D-glucosamine kinase	3
P19338	6.1	1.7	1.3	1.6	Nucleolin	3
Q06830	2.3	1.5	1.8	1.6	Peroxiredoxin-1	3
P00558	1.9	1.3	1.5	1.7	Phosphoglycerate kinase 1	3
P49368	2.3	1.5	1.4	2.6	T-complex protein 1 subunit gamma	3
P04004	2.8	1.8	1.9	2.3	Vitronectin	3

BALF: bronchialveolar lavage fluid, Q/C: value of the protein fold change in the tumour tissue compared to the control. Q1, Q2, Q3: three parts of tumour biopsy.

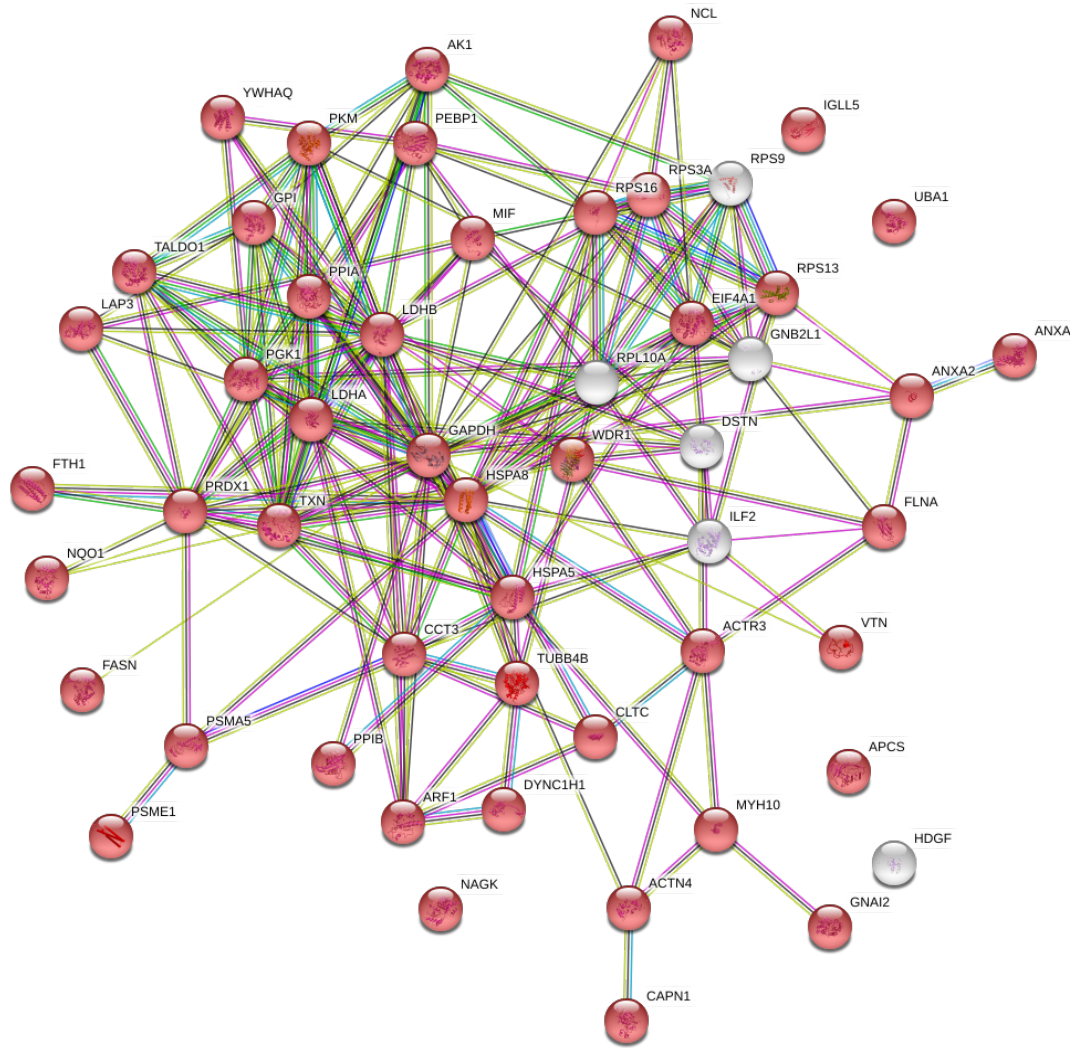


Figure 22: String analysis (GO:0070062 extracellular exosomes) of proteins heterogeneously overexpressed in both FFPE and lung lavage from adenocarcinoma compared to normal controls. Red nodes represent the proteins that are excreted via exosomes and can be seen in body fluids.

5.3.5.2.2. Proteins down regulated in tumour tissue and at low level in lavage

Table 45 shows the significant proteins found heterogeneously down regulated by label-free mass spectrometry in all parts of the tumour in all patient specimens compared to the matched normal lung tissue and also in the lavage discovery done on matched tumour type (appendix 42).

Table 45: Top 30 proteins found down regulated in one or more quadrants and in the lavage

Accession	BALF	C/Q1	C/Q2	C/Q3	Protein name	Patient #
P04040	1.6	1.9/3.8	4.2/4.4	2.3/3.6	Catalase	2, 3
P02042	4.1	1.6/2.1	2.6/2.4	1.8/1.7	Hemoglobin subunit delta	2, 3
P18206	3.6	4.8/1.4	8.4/1.6	3.7/1.5	Vinculin	1, 3
P31946	1.9	3.3	1.7	2.4	14-3-3 protein beta/alpha	3
P62258	1.7	2.4	2.3	2.6	14-3-3 protein epsilon	3
P40121	2.7	2.3	1.7	2.4	Macrophage-capping protein	3
O75368	2.1	1.8	2.1	2.6	SH3 domain-binding glutamic acid-rich protein	3
P37802	3.4	2.4	1.2	1.3	Transgelin-2	3
P67936	2.9	1.7	2	1.5	Tropomyosin alpha-4 chain	3
P23381	1.8	2.2	1.6	1.9	Tryptophan--tRNA ligase, cytoplasmic	3
P02792	5.8	5	3.8	1.2	Ferritin light chain	2
P04196	1.4	8.2	1.6	2.5	Histidine-rich glycoprotein	2
P01009	5.9	3.8	6.3	2.9	Alpha-1-antitrypsin	1
P07355	3.4	1.7	2.9	1.9	Annexin A2	1
P09525	2	2.1	2	1.8	Annexin A4	1
P08133	3.9	2	2.4	1.8	Annexin A6	1
O95994	4.4	2.6	1.4	1.5	Anterior gradient protein 2 homolog	1
Q13938	1.6	4.5	4.2	5.1	Calcyphosin	1
P00915	4	1.4	3.6	2.1	Carbonic anhydrase 1	1
P00918	2	1.4	3.4	2.7	Carbonic anhydrase 2	1
P08311	2.3	4.1	7.8	4.9	Cathepsin G	1
P01024	1.8	1.6	2.1	1.4	Complement C3	1
P21333	4.4	2	3.8	2.3	Filamin-A	1
P68871	7.5	1.4	2.7	1.8	Hemoglobin subunit beta	1
Q6F113	3.5	2.7	2.9	1.8	Histone H2A type 2-A	1
P62805	5	2	1.9	1.6	Histone H4	1
P61626	4.4	2.8	5.5	4.9	Lysozyme C	1
P05164	1.7	4.4	8.2	4.4	Myeloperoxidase	1
P35579	1.7	4.5	4.9	2	Myosin-9	1
P13796	2.2	1.2	2.1	1.2	Plastin-2	1

BALF: bronchoalveolar lavage fluid, Q/C: value of the protein fold change in the tumour tissue compared to the control. Q1, Q2, Q3: three parts of tumour biopsy.

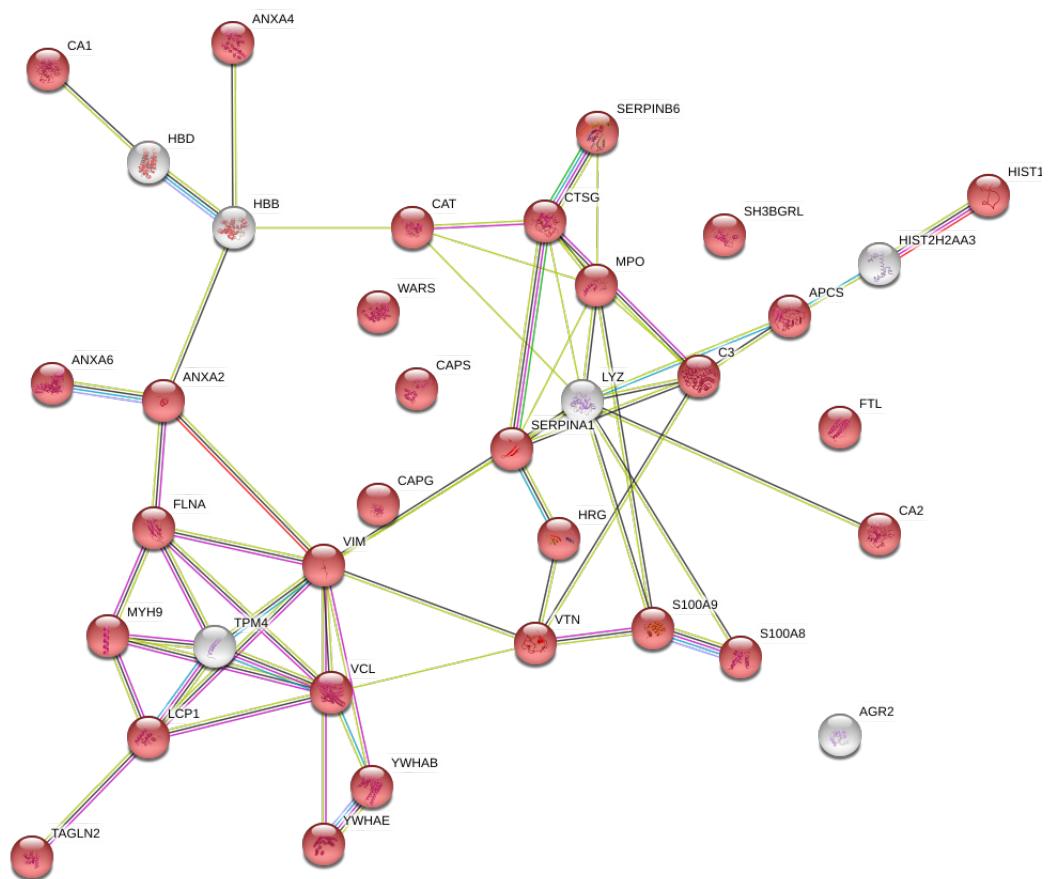


Figure 23: String analysis (GO:0070062 extracellular exosomes) of heterogeneously down regulated proteins that were shared in all parts of at least one tissue sample and in the lung lavage from adenocarcinoma. Nodes in red represent the proteins that are excreted via exosomes and can be seen in body fluids.

5.3.6. Tissue microarray validation

Table 46: Tissue microarray (TMAs) scoring

Tissue type	Score				Biomarker
	0	1	2	3	
Normal LT	8/17(47%)	9/17 (52.9%)	0/17(0%)	0/17(0%)	LDHA
AD	2/28(7.1%)	8/28 (28.5%)	14/28(50%)	4/28(14.2%)	
Sqcc	4/48(8.3%)	10/48(20.8%)	19/48(39.5%)	15/48(31.25)	
Normal LT	None	None	None	None	PDH
AD	4/39(10.2%)	6/39(15.3%)	20/39(51.3%)	9/39(23%)	
Sqcc	2/39(5.1%)	14/39(35.9%)	9/39(23%)	12/39(30.7%)	
Normal LT	No staining in all cores [repeated twice]				FASN
AD					
Sqcc					
Normal LT	5/18 (27.7%)	9/18 (50.0%)	2/18 (11%.0)	2/18 (11.0%)	Talin-1
AD	1/30 (3.30%)	15/30 (50.0%)	12/30 (40.0%)	2/30 (6.60%)	
Sqcc	8/46 (17.0%)	26/46 (56.5%)	11/46 (23.9%)	1/46 (2.0%)	

LT: lung tissue, AD: adenocarcinoma, Sqcc: squamous cell carcinoma, LDHA: lactate dehydrogenase A, PDH: pyruvate dehydrogenase, FASN: fatty acid synthase, x/y: number of positive cores/total cores.

5.3.6.1. Lactate dehydrogenase A

Figure 24 shows immunohistochemistry reactivity of TMA cores from normal lung tissue (A), lung adenocarcinoma (B) and lung squamous cell carcinomas (C) to lactate dehydrogenase A. 0: no staining, 1: weakly stained, 2: good staining, 3: strong staining. The clinical information of the lung adenocarcinoma cores is B0 (IIIA, grade 2, T3N1M0), B1: (IIIA, grade 2-3, T2N1M0), B2 (IIB, grade 2, T3N0M0) and B3:(IIIA, grade 2, T3N1M0). The clinical information of the lung squamous cell carcinoma cores is C0: (IA, T1N0M0), C1: (IIB, grade 2, T2N2M0), C2: (IIIA grade 2, T2N2M0) and C3: (IIIA, grade 2, T2N2M0). The full scoring results are in appendix 44. Normal lung tissue expression of LDHA was very low compared to the malignant tissues; score were restricted to 1 and no cores scored 2 or 3.

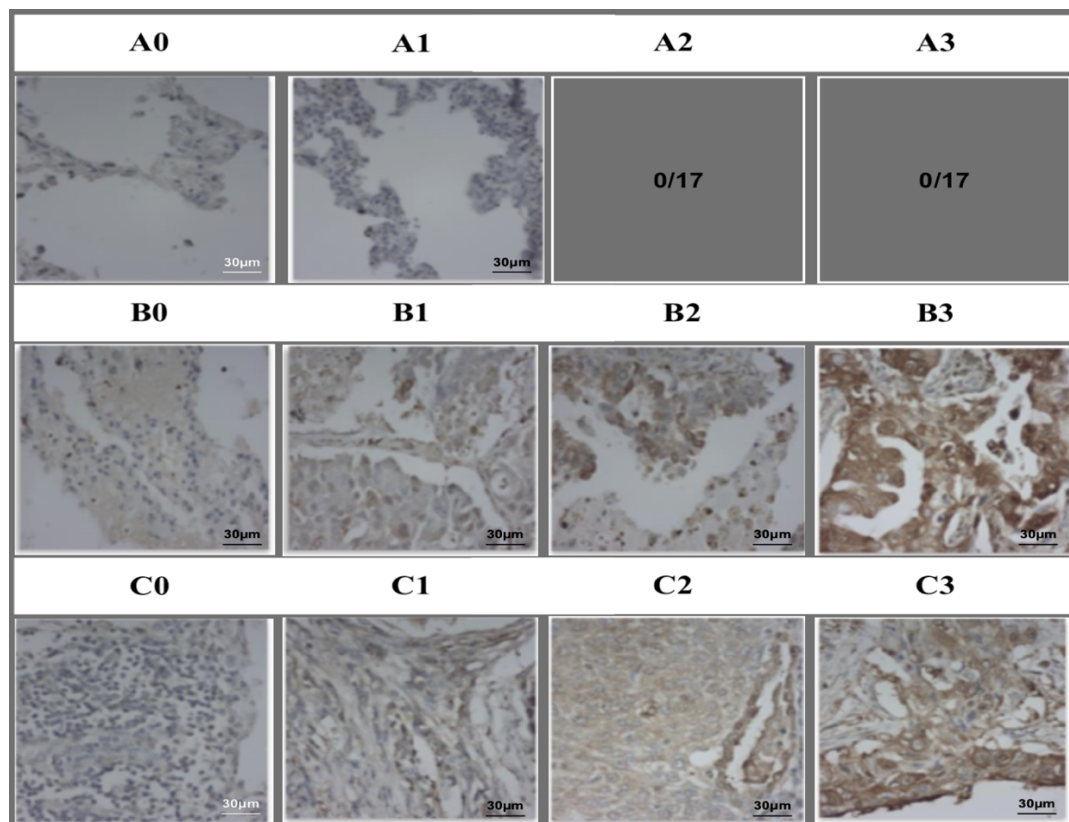


Figure 24: Immunohistochemical staining of FFPE-based TMA for lactate dehydrogenase A (brown) in normal lung tissues (A), lung adenocarcinoma (B) and lung squamous cell carcinoma (C). 0, 1, 2, 3 represent reactivity scoring (colour intensity). Maximum normal lung tissue score was 1. 0/17: none of the normal cores (17 cores) scored as 2 or 3 for their reactivity to LDHA.

5.3.6.2. Pyruvate dehydrogenase

Figure 25 shows immunohistochemical reactivity of TMA cores from lung adenocarcinoma (A) and lung squamous cell carcinoma (B) to pyruvate dehydrogenase. 0: no staining, 1: weakly stained, 2: good staining, 3: strong staining. The clinical information for the lung adenocarcinoma cores is A0 (of stage II, grade 3, T2N1M0), A1: (IIB, grade 3, T2N1M0), A2 (IIB, grade 1, T2N1M0), and A3: (IIIA grade 2, T2N2M0). The clinical information for lung squamous cell carcinoma cores is B0: (IIIA, grade 0, T2N2M0), B1: (IIIA, grade 1, T2N2M0), B2: (IIIA, grade 1, T2N2M0) and B3: (IIIA, grade 3, T2N2M0). The full scoring results are listed in appendix 45.

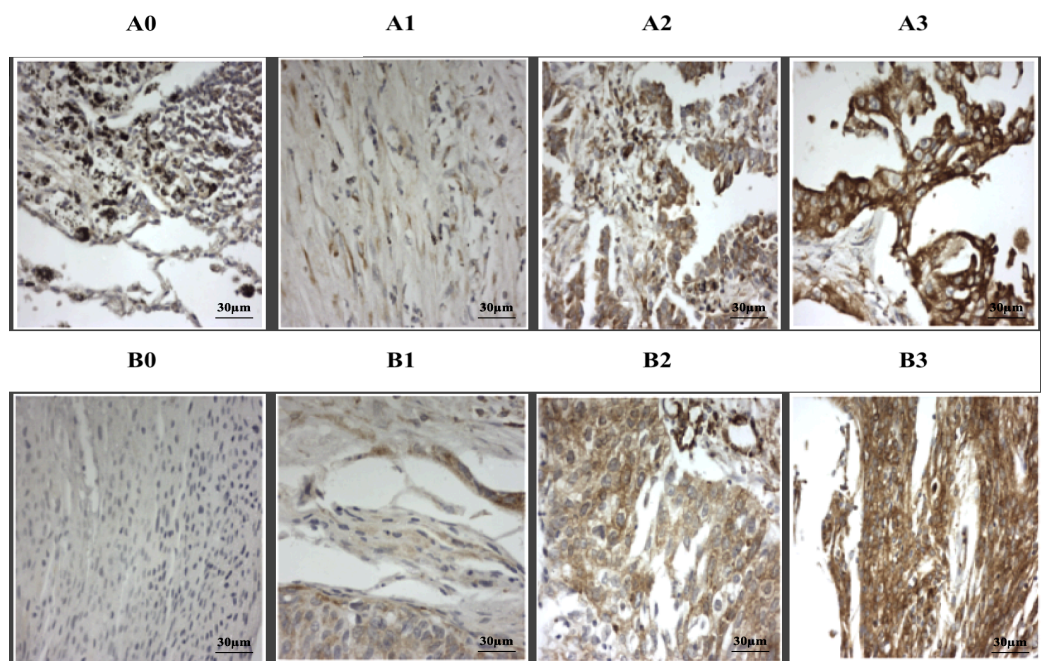


Figure 25: Immunohistochemical staining of FFPE-based TMA for pyruvate dehydrogenase (brown) in lung adenocarcinoma (A) and lung squamous cell carcinoma (B). 0, 1, 2, 3 represent reactivity scoring (colour intensity). FFPE: formaldehyde-fixed and paraffin-embedded.

5.3.6.3. Fatty acid synthase

Fatty acid synthase showed no IHC reactivity in both normal and malignant lung tissue.

5.3.6.4. Talin -1

Figure 26 shows immunohistochemical reactivity of TMA cores from normal lung tissue (A), lung adenocarcinoma (B) and lung squamous cell carcinomas (C) to talin-1. 0: no staining, 1: weakly stained, 2: good staining, 3: strong staining. The clinical information for the lung adenocarcinoma cores is B0: (IIIA, grade 2, T2N2M0), B1: (IIB, grade 2-3, T2N1M0), B2 (IIIA, grade x, T2N2M0), B3:(IIIA, grade 2, T3N1M0). The clinical information for the lung squamous cell carcinoma cores are C0: (IIIA, grade 2, T2N2M0), C1: (IIB, grade 2, T2N1M0), C2: (IIB grade 2, T3N0M0) and C3: (IIIA, grade 2, T2N2M0). The full scoring results are in appendix 46.

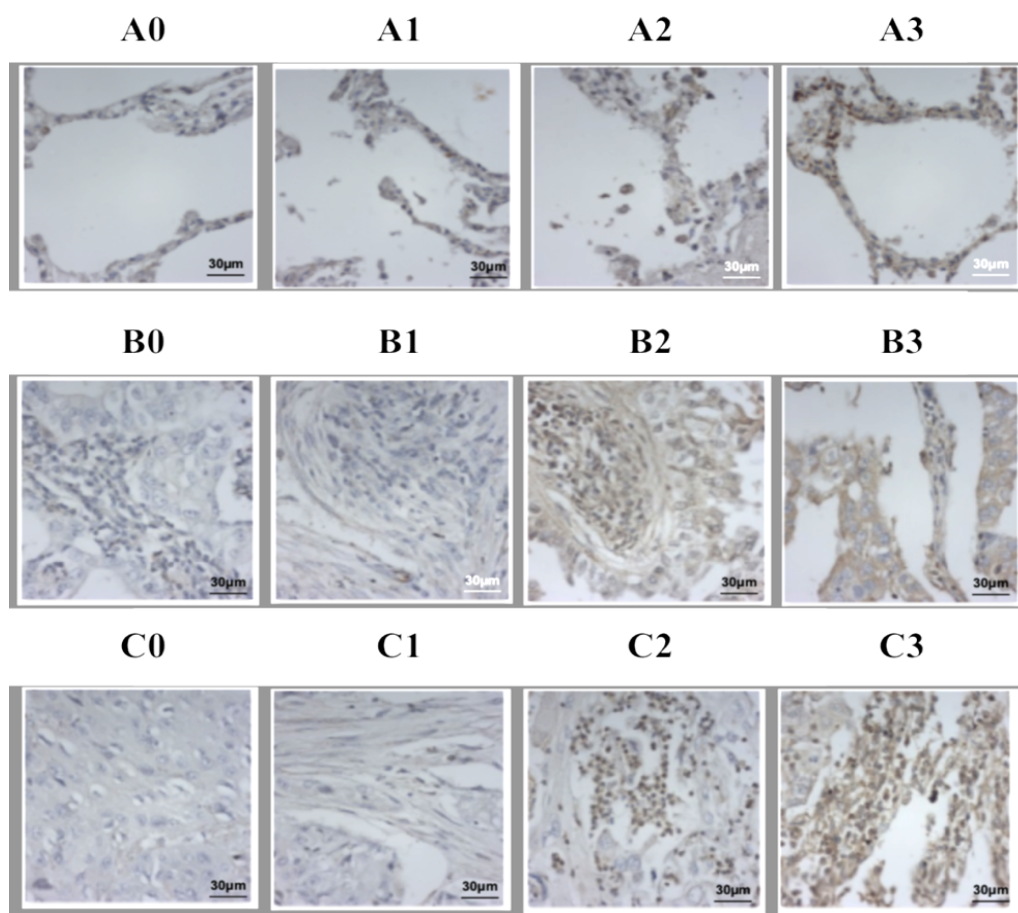


Figure 26: Immunohistochemical staining of FFPE-based TMA for Talin-1 (brown) in normal lung tissues (A), lung adenocarcinoma (B) and lung squamous cell carcinoma (C). 0, 1, 2, 3 represent reactivity scoring (colour intensity). FFPE: formaldehyde-fixed and paraffin-embedded.

5.4. Discussion

In hospital histopathology laboratories, tissue specimens from lung cancer patients are preserved by fixation in formaldehyde, moulded in paraffin (FFPE), and sliced by a microtome for microscopic and immune-histochemical examination to confirm malignancy and determine the correct tumour type. FFPE specimens along with their pathology reports and clinical information are good sources for biomarker discovery (Paulo et al., 2012). The hundreds of thousands of FFPE specimens archived worldwide enable proteomic profiling of enough numbers of each lung cancer subtypes, which is advantageous compared to using fresh or frozen tissues samples collected for specific research (Werner et al., 2000). The use of FFPE specimens allows high through-put validation of biomarkers as in making tissue microarrays (TMAs) for IHC validation of biomarkers (Casadonte and Caprioli, 2011). Despite the excellent preservation obtained by crosslinking proteins *via* methylene bridges formed by interaction of basic protein residues, and DNA with formaldehyde, this crosslinking interferes with trypsin digestion and identification of proteins, leading to loss of experimental reproducibility (Azimzadeh et al., 2010).

Here, FFPE tissue specimens were used to study tumour heterogeneity among four lung AD specimens by LC-MS/MS. The second aim was to compare the proteome signature of the FFPE lung adenocarcinoma tumour specimens with the proteome of the lung lavage of the same lung cancer type in order to focus on proteins that exist in both sample type that represent the tumour rather than the background. So, this discussion will cover only the proteins detected in both discovery experiments.

LC-MS/MS analysis of the first FFPE specimen (patient #1) revealed 56 proteins heterogeneously elevated in all parts of tumour specimen compared to their matched normal lung tissue (Table 33, figure 18). Twenty-two out of these proteins were

found elevated also in the lavage of matched AD compared to lavage from normal individuals. Seven of the 56 proteins listed showed the opposite profile (low) to the lavage (Table 42) and the rest of 27 proteins did not detected by LC-MS/MS in the lavage fluid (Appendix 12).

In contrast, 60 proteins were heterogeneously down regulated in all parts of the tumour tissue of patient #1 compared to the normal tissue from same patient (Table 37, Figure 19), 25 of which were also lowered in the lavages of AD patients compared to the normal. Only three out of the 60 proteins did not match the lavage findings and thirty-three of the 60 proteins were not on the lavage list (Table 43, Appendix 16).

In patient #2, 52 proteins were found heterogeneously overexpressed in lung adenocarcinoma tissues compared to matched normal lung tissues (Table 34, figure 18), Fifteen out of them were matching the lavage work while Six exhibit an opposite profile in the lavage experiment of adenocarcinoma patients (Table 42), the rest were not on the lavage list (Appendix 20).

In patient #2, 34 proteins were heterogeneously down regulated in all parts of the tumour tissue compared to the matched control normal lung tissue (Table 38, Figure 19). Only four of them matched the lavage analysis of the same lung tumour type (AD). Twenty-two proteins exhibited the opposite pattern in the lavage (Table 43) and the other eight were not detected in the lavage by LC-MS/MS (Appendix 24).

In patient #3, analysis of the lung adenocarcinoma specimen revealed that 88 proteins were heterogeneously elevated in the different parts of the tumour tissue (Table 35, Figure 18). Thirty-three of these proteins matched the lavage analysis, 11 of which exhibit showed the opposite pattern (Table 42) and 44 were not detected in the lavage (Appendix 28). On the other hand, 97 proteins were down regulated in all parts the

tumour specimen (Table 39, Figure 19), only 11 were matched the lavage work, 17 exhibited a profile that was opposite to that in the lavage done on the matched tumour type (Table 43), and 69 were not detected in the lavage (Appendix 32).

Comparison of the different parts of the adenocarcinoma specimen from patient #4 showed that only five proteins were elevated in all parts of the analysed tumour tissue, and none of them were detected in the lavage (Table 36, Figure 18), while one protein showed the opposite profile in the lavage (*i.e.*, lowered) (Appendix 36).

In contrast, 12 proteins were down regulated in all tumour tissue parts of patient #4 (Table 40, Figure 19), only 3 of them matched the lavage discovery work of the same lung tumour type, and 4 exhibited the opposite profile from that in the lavage, where it was elevated (Appendix 40).

Principal component analysis (PCA) (Figure 16) and heatmap analysis (Figure 17) of all the differentially expressed proteins were used to show the overall heterogeneity among tumour tissues of the four FFPE lung adenocarcinoma samples used in this study. The greatest variance in proteomic signature between normal and malignant tissues (component 1) was seen in patient #2, where it reached 46%. The variance in the other tumour tissue biopsies compared to the normal tissues was 39% in patient #1, 35% in patient #4 and 29.7% in patient #3. The greatest variance in the proteomic signature among tumour parts tissues (tumour heterogeneity) was seen in patients #1 and #3, where it scored 23.5% and 22.7%, respectively. The variance between the proteomic expression signatures in the tumour tissues of patients 2 and 4 was 16.7%. Heatmap analysis was used to visualise the shared groups of proteins and to cluster biopsies based on the abundance of the proteins. Such mosaic colour intensity would interpret the inconsistency of protein biomarkers between different analysed cohort samples (Figure 17).

Table 41 summarises the total number of significantly changed proteins detected by mass spectrometry per part of the tumour compared to the number of total proteins, using 1.2 fold change as a cut-off value. It also mentions the number of proteins detected in the two discovery experiments (FFPE tissues and BALF), and which of them had same expression profile in the two setups and which had the opposite profile. Tables 42 and 43 list the proteins that had a protein abundance profile in FFPE opposite to that in lavage. Tables 44 and 45 show the proteins that were elevated in FFPE and BALF as well as reduced in both specimens. For biomarker discovery, a better understanding of biomarkers and the factors affecting their levels, it is preferable to compare mass spectrometry data obtained from different types of body fluids and tissues and to cluster those that match and those that do not.

Here, most mass spectrometry results showed fluctuation in the protein levels even among different parts of the same tumour biopsy. To demonstrate this heterogeneity of protein expression, four candidate proteins fulfilling the criteria for a biomarker panel were selected. Lactate dehydrogenase, pyruvate dehydrogenase, fatty acid synthase and talin-1 are excretable (GO: 0070062, Figures 20-23), exist in lung lavage, have a role in lung cancer, and are heterogeneously expressed in the FFPE tumour tissue compared to the matched normal control lung tissues.

In cancer cells, even in the presence of oxygen, pyruvate is converted into lactate (Devic, 2016) by lactate dehydrogenase, which exists as isoforms A and B (Feron, 2009). Isoform A has more affinity for pyruvate than lactate and is involved mainly in the conversion of pyruvate to lactate using NADH as a hydrogen ion donor (enzyme cofactor). This hydrogen is converted back by lactate dehydrogenase isoform B *via* hydrogen ion acceptor NAD (Valvona et al., 2016, Doherty and Cleveland, 2013). Lactate is toxic to the cells, but in cancer the increased production

of lactate is accompanied by increased expression of the facilitated proton-linked monocarboxylate transporters (MCTs) or symporters to shuttle lactate between cancer cells and the circulation, thus maintaining cell acidity (Halestrap, 2012). Targeting both lactate dehydrogenase A and MCTs is among the therapies based on the metabolism of cancer cells and are in clinical trial (Doherty and Cleveland, 2013). Lactate dehydrogenase A is overexpressed in many types of cancer, including gastric cancer (Sun et al., 2014), pancreatic cancer (Rong et al., 2013) and colorectal cancer (Li et al., 2016) and could be useful as a prognostic marker in these cancers.

In this research work, lactate dehydrogenase isoform A (LDHA) was significantly and heterogeneously elevated in two lung adenocarcinoma samples (n:4) analysed three times in different part of the tumour (refer to section 2.3.1) by LC-MS/MS. The fold changes in the two specimens were 1.8 ± 0.6 and 3.6 ± 1.86 (mean \pm SD) (Table 44). LDHA was also detected in one quadrant of sample #4 (fold change 1.4), but it was not detected significantly in the third tumour sample. In contrast, the lavage discovery work showed a significant elevation of LDHA in both adeno and squamous carcinomas, with a fold change of 3.5 and 4.3, respectively (Appendix 1 & 3). In the same FFPE specimens mentioned above, lactate dehydrogenase isoform B (LDHB) showed the same pattern as isoform A, with fold changes of 1.6 ± 0.6 and 2.2 ± 0.6 , respectively (Table 44). LDHB was also found significantly elevated in one part of the third tumour tissue sample, with a fold change of 1.6 but it was not detected in the fourth sample. LDHB was not detected in the lavage from SqCC but was 4.9-fold increased in lung AD lavage compared to normal control (Appendix 1). Therefore, lactate dehydrogenase A was chosen to confirm heterogeneous expression in lung SqCC and AD tissue microarrays (TMAs).

The IHC results obtained from lung FFPE-based tissue microarrays containing normal, AD and SqCC tissue cores revealed the following results (Table 46). In normal lung tissue (n= 47), 47.1% of the tissue cores showed no reactivity to LDHA (score 0) and the other 52.9% only weak reactivity (score 1) (Figure 24). On the other hand, in lung adenocarcinoma tissue cores (n = 28), only 7.1% of the tissue cores exhibited no reactivity (score 0), 28% stained weakly (grade 1), 50% stained well (grade 2) and 14.2% had strong reactivity to LDHA (score 3) (Figure 24). SqCC showed an expression pattern similar to that of AD: 8% of the cores were negative, 20.8% scored 1, 39.5% scored 2, and 31.5% scored 3 (Figure 24). However, these findings indicate that LDHA is overexpressed in both types of non-small cell lung cancer (AD & SqCC) and no correlation was found between the expression of LDHA and the grade or stage of the cancer. Therefore, inhibition of LDHA was thought to have a good therapeutic value in non-small lung cancer (Xie et al., 2014).

Transportation of pyruvate across the inner mitochondrial membrane is facilitated by carriers called mitochondrial pyruvate carriers (MPC) which is controlled by the demand/satiety principle (McCommis and Finck, 2015). For pyruvate to participate in the citric acid cycle, it has to be converted into acetyl Co-A by a reaction involving a decarboxylation reaction catalysed by pyruvate dehydrogenase complex (PDHC) (Holness and Sugden). Pyruvate dehydrogenase (PDH), as the main enzyme of this multi-enzyme complex, is positively regulated by cellular calcium influx, increased cellular ADP concentration, and accumulation of its substrate, pyruvate (Spriet and Heigenhauser, 2002). Pyruvate dehydrogenase is inhibited when it is phosphorylated by pyruvate dehydrogenase kinase (PDK), which is activated by increased ratio of NADH/NAD, and increased levels of acetyl Co-A and reactive oxygen species (ROS) (Hurd et al., 2012). PDK is inhibited by accumulation of pyruvate and

decreased NADH/NAD ratio (Holness and Sugden, 2003). The PDH/PDK pathway was found suppressed in approximately 75% (n = 101) of non-small lung cancer, and only very aggressive tumours were noticed to maintain high levels of PDH (Koukourakis et al., 2005).

It has been shown that the level of PDH in gastric cancer is indirectly correlated to tumour progression. Therefore, its overexpression could be a good prognostic marker in cancer dissected patients (Sun et al., 2015). In prostate cancer, the expression of PDH was positive and heterogeneous by immunohistochemistry in 84% of the samples (n = 88), and the study revealed strong expression of the enzyme in the primary tumour tissue but its expression was weaker in tumours with lymph node metastasis (Zhong et al., 2017). However, PDH was not detected by LC-MS/MS in the four FFPE lung adenocarcinoma specimen examined in our work. The study described in chapter 3 did not reveal any PDH in lavage from both adeno and squamous cell carcinoma. Absence of PDH from the tissue and lavage in addition to the findings of Koukourakis et al. (2005) that correlated the expression of PDH to cancer progression in NSCLC make PDH a candidate for TMA heterogeneity validation (Koukourakis et al., 2005).

Immunohistochemistry examination of PDH expression in FFPE-based tissue microarrays consisting of 39 SqCC and 39 AD tissue cores showed that the expression of pyruvate dehydrogenase was very high (score 3) in both AD (23%) and SqCC (30.7%). While 51% of AD cores exhibited good reactivity (score 2) to PDH antibody, only 23% of SqCC matched this score. More SqCC cores (35.9%) had a weak reactivity compared to only 15.3% in adenocarcinoma. These findings indicate that PDH is more overexpressed in AD (74%) compared to SqCC (53.7%), with a heterogeneous pattern (Table 46, Figure 25).

Increased rate of lipogenesis in cancer is favoured mainly by increased PI3K/AKT pathway signalling. This is well documented and has been reviewed in detail in 2006 (Swinnen et al., 2006). Fatty acid synthase (FASN) is a multifunctional dimer enzyme, and each monomer consists of all the catalytic subunits needed for the synthesis of palmitate from condensation of acetyl co-A and malonyl CoA. These catalytic subunits are thio-esterase, acyl carrier protein, beta-ketoacyl reductase, enoyl reductase, beta-hydroxyacyl dehydratase, acetyl/malonyl transacylase and beta-ketoacyl synthase. Palmitate synthesis and fatty acid synthase overexpression was found correlated with tumour progression, metastasis and resistance to chemotherapy (Ventura et al., 2015). Fatty acid synthase activity was found by immunohistochemistry to be strongly expressed in 42 non-small cell lung cancer patients (Cerne et al., 2010). In the current study, fatty acid synthase was significantly elevated with a heterogenous expression pattern in FFPE tumour tissues, where it was significantly elevated in all parts of one tumour specimen (n = 4) with a fold change of 2.33 ± 0.28 (mean \pm SD) and was increased 9.5-fold in the lavage collected from the same type of tumour compared to the normal individuals (Table 44). Fatty acid synthase was also detected significantly elevated in lung squamous cell carcinoma lavage compared to normal lavage (fold change 3.3). Unfortunately, FASN was not detected in all lung tissue cores (n = 150) in the TMA in this research work, though the antibody stained the positive control cores (repeated twice).

Anoikis is a form of programmed cell death activated by inappropriate cell-matrix interaction. When cancer cells detach from other cells, focal adhesion proteins that mediate interaction of actin with integrins including vimentin, paxillin and talin, are recruited. Talin-1 is the first protein that interacts with the cytoplasmic moiety of

integrin, leading to activation of the integrin signalling pathway; this favours cancer cell survival and proliferation, thus avoiding anoikis (Desiniotis and Kyprianou, 2011). Immunohistochemical analysis revealed that Talin-1 was overexpressed in prostate cancer (n = 199) compared to normal (n = 7) and benign hyperplasia (n = 75), and its overexpression was correlated with lymph node metastasis and advanced stages of the disease (Xu et al., 2016). Talin-1 was also found elevated in hepatocellular carcinoma serum samples and TMAs and was associated with cancer progression and poor prognosis (Chen et al., 2017, Youns et al., 2013).

Here, LC-MS/MS analysis showed that Talin-1 was significantly elevated in one FFPE lung adenocarcinoma specimen (n = 4) with a fold change of 2.1 ± 0.4 (mean \pm SD). Talin-1 was not detected in the other three samples. Interestingly, Talin-1 was significantly low in the lavage from lung adenocarcinoma patients compared to normal controls (fold change 3.5). On the other hand, mass spectrometry did not detect Talin-1 in the lavage from squamous cell carcinomas. Therefore, Talin-1 was selected for tissue microarrays validation, and the results revealed no significant differences between normal and malignant tumour cores. The percentage of lung tissue cores that had negative reactivity (score 0) to Talin-1 was 27.7% (n = 18) in normal tissues, 17% (n = 46) in SqCC, and 3.3% (n = 30) in AD. The percentage of cores exhibiting weak reactivity (score 1) was 50% (n = 18) in normal control, 56.5% (n = 46) in SqCC, and 50% (n = 30) in AD. The percentage of tissue cores exhibiting good reactivity to Talin-1 (score 2) was 11% in normal tissue cores, 23.9% in SqCC cores, and 40% in AD cores. Strong activity (score 3) was seen in 11% of normal tissue cores, 2% in SqCC cores, and 6.6% in AD cores. In summary, both normal and malignant lung tissues exhibited heterogeneous expression of Talin-1, and core reactivity was higher in lung AD than in SqCC and normal tissue cores. The tumour

stage and grade did not correlate with protein expression level (Table 46, Figure 26). These findings support the heterogeneous expression pattern of proteins in tumour tissue.

The disadvantages of using protein biomarkers in clinical diagnosis of cancer have been demonstrated (Hara et al., 2008). The clinical use of protein biomarkers is currently restricted to multiple reaction monitoring (MRM) of treatment in order to minimize patient exposure to the low-dose x-rays in CT-scans or to radionuclides in PET-scans (Table 2, Figure 5) (Crutchfield et al., 2016, Holdenrieder et al., 2016). Our study demonstrates the difficulty of using protein biomarkers in the diagnosis of cancer, at least for lung cancer. Our results also apply a big precaution in using biomarkers for MRM principle because based on the TMA analysis the expression of proteins might not correlate to the stage and grade of the cancer. However, it is very important to study protein biomarker expression patterns for specific tumour types at different stages and grades, and to monitor the expression of proteins correlated with tumour type, as many proteins are affected by the expression of others.

Chapter 6

Cell cycle biomarkers in drug resistance

6. Cell cycle biomarkers in cancer

6.1. Introduction

The high rate of cancer cell proliferation requires increased rates of transcription and translation of the genes responsible for cell survival, growth and proliferation, as well as more rapid production of the building blocks required for making new cells. In the nucleus, about one meter of negatively charged double-stranded DNA is zipped and packaged around positively charged histone proteins in structures called nucleosomes (Mariño-Ramírez et al., 2005). Histone-acetyl transferase family members HATs (PCAF, GCN5L2 and CBP/P300) and their counteracting partner, the histone-deacetylases (HDACs) including HDACs 1, 2, 3, 4, 5 and 13, are the main proteins controlling the dynamicity of histone-DNA zip-unzip states and transcription (Hassig and Schreiber, 1997). Histone acetylation/deacetylation dynamics is tightly connected with cell cycle progression, CREB-binding protein (CBP) is activated by phosphorylation of cyclin E/CDK2 (Ait-Si-Ali et al., 1998). Once transcription factors are activated and localized in the nucleus, they bring with them HAT as part of the transcription complex, acetyl groups (negatively charged) added to the histone lysine residues facilitate release of DNA and facilitate access of the transcription factors to their promoters (Marmorstein and Roth, 2001). The cell cycle is controlled by cyclin-dependent kinases, activation of which involves binding to cell-cycle specific cyclins (As, Bs, Ds, Es, Hs), which unmask the ATP-binding domains, leading to phosphorylation and activation of CDKs by CDK-activating kinase (CAK) (Lolli and Johnson, 2005). In cancer, acceleration of the cell cycle requires availability of excess activated (phosphorylated) CDKs. Increased phosphorylation rates in cancer due to gene amplification or gain of function of protein kinases result in specific and non-specific downstream signalling that

leads to activation of many transcription factors and increased abundance of different proteins (Mariño-Ramírez et al., 2005, Gruber et al., 2017). The NFκB transcription factor plays a role in inflammation, cell survival and proliferation. Phosphorylation of the inhibitory protein (IKK) that binds and sequesters NFκB in the cytoplasm (Whiteside et al., 1997) leads to release of NFκB and its proteasomal degradation, dimerization and translocation of its active forms to the nucleus (Liou and Baltimore, 1993). Increased proteasomal processing and degradation of NFκB in cancer leads to elevation of its active products (P50 and P52) and Rel-A, C-Rel, Rel B proteins, leading to alteration of cell functions. Cancer cells also need to evade apoptosis (programmed cell death) and counteract the effect of tumour suppressor genes. 14-3-3 protein has several tissue-specific isoforms that bind and regulate the proteins involved in cell cycle, apoptosis, and the net function of these adapter proteins is to stop cell proliferation and favour P53-mediated cell death. Release of cytochrome c from mitochondria is needed to activate the caspase cascade, which is crucial to promote apoptosis *via* the main P53 pathway. Abundance and activation of BAX, also called Bcl-2 associated X large protein, favours the release of cytochrome c (Finucane et al., 1999) On the other hand, BCL-XL inhibits the release of cytochrome c and enhances cell proliferation (Janumyan et al., 2003). Cancer results from imbalance between oncogenes and tumour suppressor genes (TSG). The products of these genes and the post-translation modifications that regulate their function are somehow manipulated so that oncogenic genes predominate over TSG. Proteins regulating the cell cycle are valuable in the diagnosis of cancer because they are required to favour the rate of cell division. AKT/PKB is the main operator of the downstream activation of the cell cycle, cell proliferation rate and cell survival in cancer; upstream

inhibition of this AKT/PB decreases the rate of cell proliferation (Wanzel et al., 2005). GDC-0980 is a small molecule that inhibits both phosphatidylinocytol-3-kinase (PI3K) and mammalian target of rapamycin (m-TOR). This inhibitor directly affects the progression of the cell cycle through downstream regulation (Kandel et al., 2002). Many cell cycle controlling proteins, such as P21, are down regulated in non-small cell lung cancer. Downregulation of P21 is indirectly proportional to patient survival in lung cancer (Esposito et al., 2004).

This chapter describes in detail the development of resistance to GDC-0980 in A549 and mainly in H1975 lung adenocarcinoma and how it affects the abundance of cell cycle derived biomarkers. The effect of the inhibitor on the expression of such markers in the resistant cells studied, and extrapolation of biomarkers that can indicate development of tumour resistance to a drug are also stressed.

6.2. Experimental design

Building on the work described in chapters 3-5, biomarker discovery focused on proteins controlling the cell cycle and energy provision. The variability in the abundance of these proteins shown in chapter four is attributable to the complex crosstalk between the signalling pathways controlling the expression of these proteins. The pathways are affected by the use of drugs which directly or indirectly affect their function, so this would have a direct impact on the expression of downstream transcription of such proteins. In this chapter, the cell cycle profile of two lung adenocarcinoma cell lines (H1975 and A549) was read using Cytell® cell imaging system. The development of cellular resistance to GDC-0980 PI3K/AKT dual inhibitor was studied in sensitive and resistant cells. To avoid false negative or false positive findings due to the drug itself, the cell cycle of the resistant cells was studied in (R+) and out (R-) of the drug. This was followed by detailed

western blot scanning of the proteins controlling cell cycle progression, including P53, P21, PCNA, cyclins, HDACs/HATs, NFkB and indirect regulatory adaptor proteins belonging to the 14-3-3 family. KEGG pathway analysis was performed on the mass spectrometry significantly up and down regulated proteins as categorized by KEGG to have a role in cell cycle control.

6.3. Results

6.3.1. H1975 growth curve.

Figure 27 shows the high proliferation rate of the non-treated (R-) GDC-0980 resistant H1975 cells (B) compared with the sensitive cells (A). Shown also is a profound collapse of the proliferation rate when the GDC-0980 resistant H1975 cells were grown in medium containing 1 μ M GDC-0980 (C).

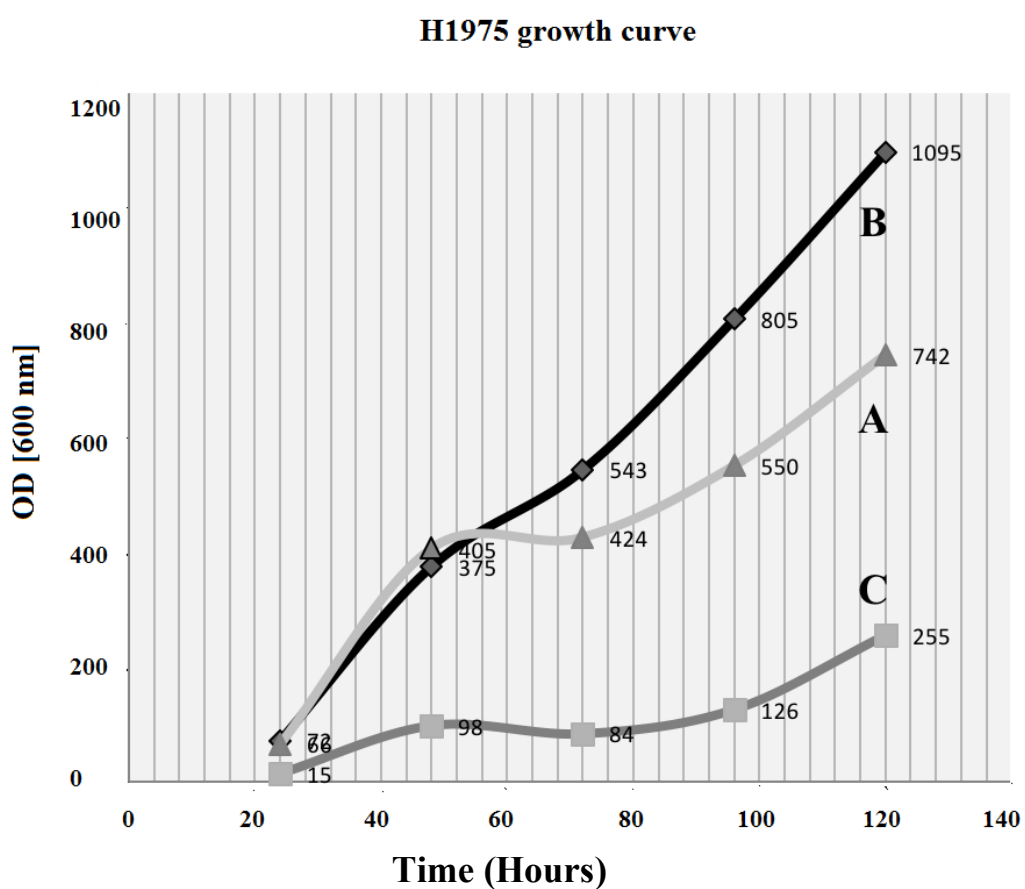


Figure 27: Growth curves of GDC-0980 sensitive P (A), resistant non-treated (B) and resistant treated R+ cells (C). The five OD points (Y-axis) represent consecutive five-day measurements of proliferation rate and the X-axis represents the time interval in hours between measurements.

6.3.2. Mass spectrometry analysis of cell cycle control proteins.

6.3.2.1. List of significantly upregulated proteins in the GDC-0980 resistant H1975 compared to drug sensitive cells.

Tables 47 and 48 list the proteins found significantly elevated by LC-MS/MS in the treated resistant H1975 cells (R+) and non-treated cells (R-) compared to the parent cells (P).

Table 47: Cell cycle regulatory proteins found by mass spectrometry significantly elevated in resistant cells (R+) compared with parent cells

Accession	P/C	P/C*	C/S	p. value	FC	Description
O43684	3	3	22	3.E-04	3	Mitotic checkpoint protein BUB3
O43929	1	1	5	5.E-04	3.2	Origin recognition complex subunit 4
P04637	4	4	32	1.E-07	8.2	Cellular tumor antigen p53
P06493	2	2	14	1.E-08	4.3	Cyclin-dependent kinase 1
P14635	1	1	3	2.E-02	2	G2/mitotic-specific cyclin-B1
P25205	2	2	7	6.E-08	7.2	DNA replication licensing factor MCM3
P33991	11	11	51	1.E-07	4.4	DNA replication licensing factor MCM4
P33992	4	4	12	1.E-09	7.9	DNA replication licensing factor MCM5
P33993	11	11	45	5.E-09	7.2	DNA replication licensing factor MCM7
P49736	6	6	22	9.E-03	1.8	DNA replication licensing factor MCM2
P49841	1	1	4	8.E-06	4.6	Glycogen synthase kinase-3 beta
P61812	1	1	5	4.E-03	15.6	Transforming growth factor β -2
P62258	2	2	6	1.E-06	1.3	14-3-3 protein epsilon
P62877	1	1	5	3.E-03	4.5	E3 ubiquitin-protein ligase RBX1
P78527	50	49	238	8.E-05	3.9	DNA-dependent protein kinase catalytic subunit
Q13257	1	1	4	9.E-03	3.9	Mitotic spindle assembly checkpoint protein MAD2A
Q13315	2	2	9	5.E-06	10.2	Serine-protein kinase ATM
Q13547	3	3	9	2.E-07	10.1	Histone deacetylase 1
Q13616	4	4	14	2.E-05	2.7	Cullin-1
Q14566	6	6	27	6.E-06	3.5	DNA replication licensing factor MCM6
Q8N3U4	6	6	25	7.E-03	1.7	Cohesin subunit SA-2
Q92793	1	1	4	3.E-03	13.4	CREB-binding protein
Q9UQE7	4	4	15	9.E-09	5.1	Structural maintenance of chromosomes Protein 3
Q9Y6D9	1	1	8	3.E-06	10.9	Mitotic spindle assembly checkpoint protein MAD1

P/C: peptide count, P/C: specific peptide count, C/S: confidence score, FC: fold change.*

Table 48: Cell cycle regulating proteins found significantly elevated by mass spectrometry in the resistant cells (R-) compared with parent cells (P).

Accession	P/C	P/C*	C/S	p. value	FC	Description
P11802	1	1	3	3.E-04	2.8	Cyclin-dependent kinase 4
P49841	1	1	4	9.E-06	3.6	Glycogen synthase kinase-3 beta
P61812	1	1	5	2.E-02	4.7	Transforming growth factor beta-2
P62258	2	2	6	3.E-06	1.6	14-3-3 protein epsilon
P62877	1	1	5	1.E-02	2.9	E3 ubiquitin-protein ligase RBX1
P78527	50	49	238	3.E-03	2	DNA-dependent protein kinase catalytic subunit
Q00534	1	1	5	1.E-04	8.1	Cyclin-dependent kinase 6
Q13315	2	2	9	3.E-04	3.2	Serine-protein kinase ATM
Q13547	3	3	9	3.E-04	4.6	Histone deacetylase 1
Q9UQE7	4	4	15	9.E-04	1.8	Structural maintenance of chromosomes protein 3
Q9Y6D9	1	1	8	9.E-03	2.8	Mitotic spindle assembly checkpoint protein MAD1

P/C: peptide count, P/C*: specific peptide count, C/S: confidence score, FC: fold change.

6.3.2.2. Significantly downregulated proteins in the GDC-0980 resistant H1975 compared to drug sensitive cells.

Table 49 and 50 list the proteins that were found significantly downregulated by LC-MS/MS in the treated GDC-0980 resistant H1975 cells (R+) and non-treated cells (R-) compared to the sensitive parent cells, respectively.

Table 49: Cell cycle regulatory proteins found significantly down regulated by mass spectrometry in resistant cells (R+) compared with parent cells (P).

Accession	P/C	P/C*	C/S	p. value	FC	Description
P12004	1	1	4	9.E-03	1.5	Proliferating cell nuclear antigen
P61981	1	1	5	8.E-04	1.8	14-3-3 protein gamma
P63104	4	4	23	2.E-06	1.8	14-3-3 protein zeta/delta

P/C: peptide count, P/C*: specific peptide count, C/S: confidence score, FC: fold change.

Table 50: Cell cycle regulatory proteins found significantly down regulated by mass spectrometry in the resistant cells (R-) compared with parent cells (P).

Accession	P/C	P/C*	C/S	p. value	FC	Description
P31946	2	1	17	8.E-03	1.5	14-3-3 protein beta/alpha
P63104	4	4	23	3.E-05	1.6	14-3-3 protein zeta/delta
Q53H82	3	3	13	4.E-11	19.4	Beta-lactamase-like protein 2
P06493	2	2	14	9.E-03	1.4	Cyclin-dependent kinase 1
P49736	6	6	22	5.E-03	2.8	DNA replication licensing factor MCM2
O60216	2	2	6	3.E-02	1.5	Double-strand-break repair protein rad21 homolog
P14635	1	1	3	2.E-02	1.8	G2/mitotic-specific cyclin-B1
Q13416	1	1	3	3.E-04	3.1	Origin recognition complex subunit 2
O43913	2	2	8	6.E-09	2.2	Origin recognition complex subunit 5
Q14683	3	2	11	2.E-07	2.2	Structural maintenance of chromosomes protein 1A

P/C: peptide count, P/C: specific peptide count, C/S: confidence score, FC: fold change.*

6.3.3. Cell cycle profile

6.3.3.1. H1975 and A549 cell cycle profile of GDC-0980 parent and resistant cells.

Cyell® Cell Imaging System (GE Healthcare Life Sciences) was used to read the cell cycle profile of GDC-0980 sensitive H1975P cells, the cell cycle profile of GDC-0980 resistant H1975 cells incubated with GDC-0980 (H1975GR+), and the effect of GDC-0980 withdrawal (two weeks in drug-free medium) on the cell cycle profile of the GDC-0980 resistant H1975 cells (H1975GR-). The lower three graphs show the cell cycle profile of GDC-0980 sensitive A549P cells, the cell cycle profile of GDC-0980 resistant A549 cells under GDC-0980 incubation A549R+ and the effect of GDC-0980 withdrawal (2 weeks in GDC-0980 free medium) on the cell cycle profile of the GDC-0980 resistant A549R- cells (figure 28).

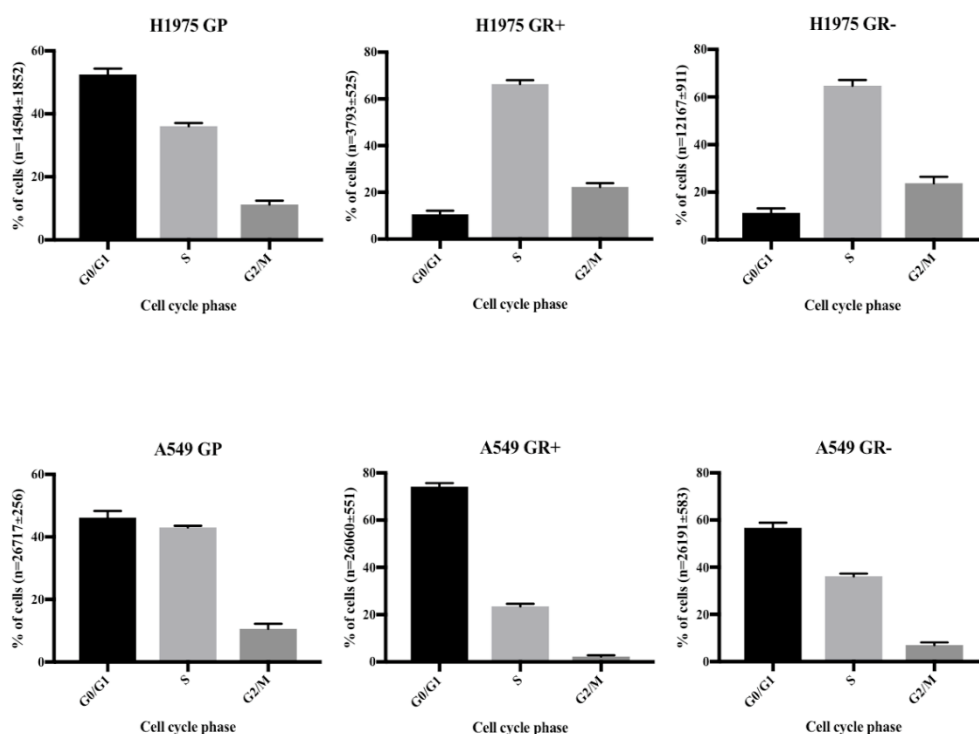


Figure 28: Cell cycle profile of GDC-0980 sensitive parent (P) and resistant (R) H1975 cells and A549 adenocarcinoma cells. [-]: resistant cells cultured without drug and [+]: resistant cells cultured with GDC-0980 (1 μ M for H1975 and 3.34 μ M for A549).

6.3.3.2. Effect of GDC-0980 on the cell cycle phases in A549 and H1975 cells

In the resistant H1975 cells, Cytell® showed a decreased number of cells attending G1 phase by 80% ($p < 0.0001$) leading to accumulation of cells in S ($p < 0.0001$) and G2/M ($p < 0.0001$) phases in both treated (R+) and non-treated (R-) cells (no reversal of GDC-0980 effect up on drug withdrawal for 5 passages, G0/G1 $p = 0.5$, S $p = 0.19$, G2/M $p = 0.27$). In contrast, in A549 cells, GDC-0980 caused accumulation of cells in G1 phase and a profound ($p < 0.0001$) decrease of cells attending S ($p < 0.0001$) and G2/M ($p < 0.0001$) phases. The effect of GDC-0980 on the cell cycle profile of GDC-0980 resistant A549 cells was reversible when the drug was withdrawn from the medium for two weeks ($p < 0.0001$ in all cell phases) (figure 29).

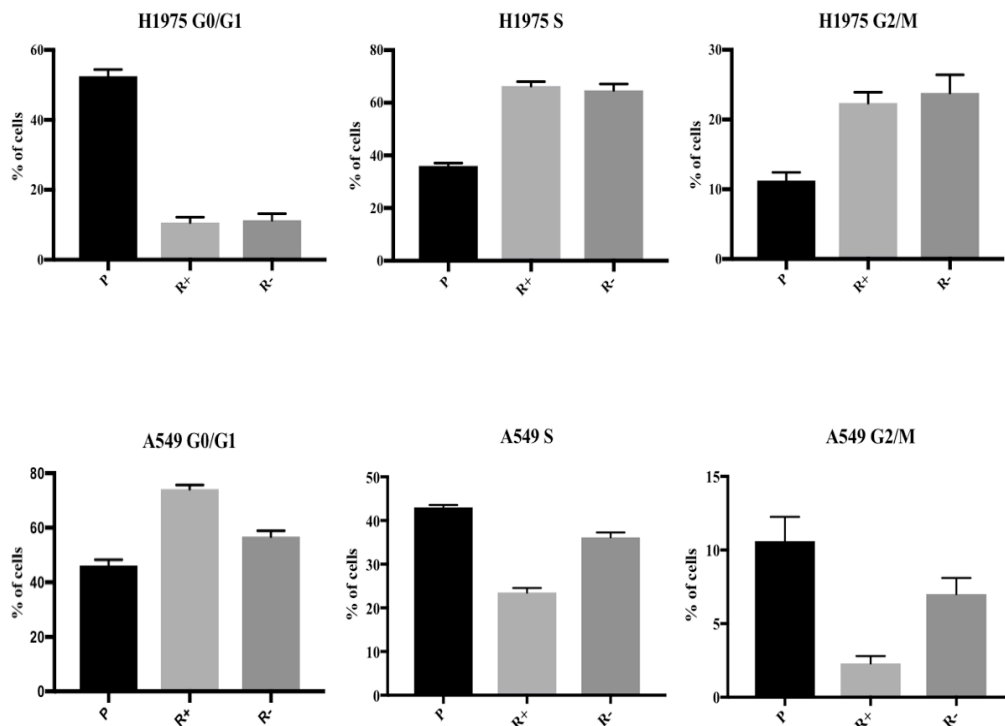


Figure 29: Comparison of cell cycle phases of GDC-0980 sensitive parent (P) and resistant (R) H1975 and A549 adenocarcinoma cells. [-]: resistant cells cultured without drug and [+]: resistant cells cultured with drug (1 μ M and 3.34 μ M final concentration for H1975 and A549 respectively).

6.3.3.3. Histone 3 confirmation of cell cycle arrest at G1 phase in A549 resistant cells

Shown in figure 30 is a western blot comparing histone 3 abundance in GDC-0980 sensitive cells compared to resistant A549 lung adenocarcinoma cells in the presence (R+) and absence (R-) of the drug. H3 was significantly lowered in both treated (B) and non-treated (A) resistant cells compared to the parent cells. The p-values for the differences were 0.01 and 0.003 in R+ and R- cells, respectively.

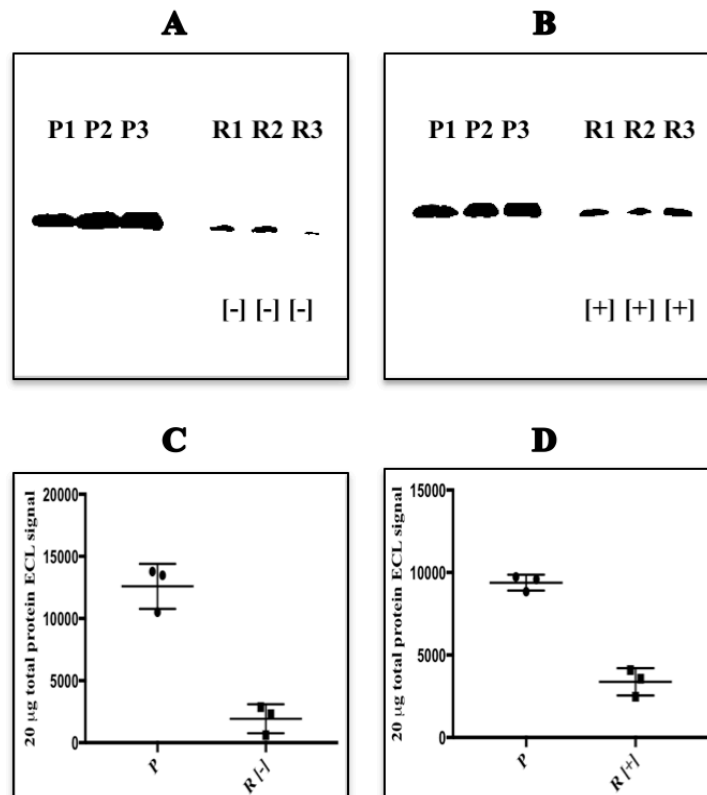


Figure 30: Immunoblotting comparison of histone 3 (H3) levels in GDC-0980 sensitive parent (P) and resistant (R) A549 lung adenocarcinoma cells. P1, P2, P3 and R1, R2, R3 represent triplicates of 20 µg of total cell protein. [-]: resistant cells cultured without drug and [+]: resistant cells cultured in F12 medium containing 3.34 µM GDC-0980. Shown in this figure is a scatter plot representing the 20 µg content of H3 measured by ImageJ and represented as triplicates per phenotype (C and D).

6.3.3.4. Histone 3 levels confirmation of cell cycle arrest at G2/M in H1975 resistant cells

Figure 31 shows a comparative western blot of histone 3 abundance in GDC-0980 sensitive and GDC-0980 resistant H1975 lung adenocarcinoma cells incubated with (R+) or without (R-) the drug. H3 was overexpressed in both treated (B) and non-treated (A) resistant cells compared to the parent cells ($p=0.08$ in both R+ and R- cells, respectively). HDAC I and PCNA proteins were used as a loading control when (R-) and (R+) were compared to the parent cells, respectively (refer to section 2.4.6.6).

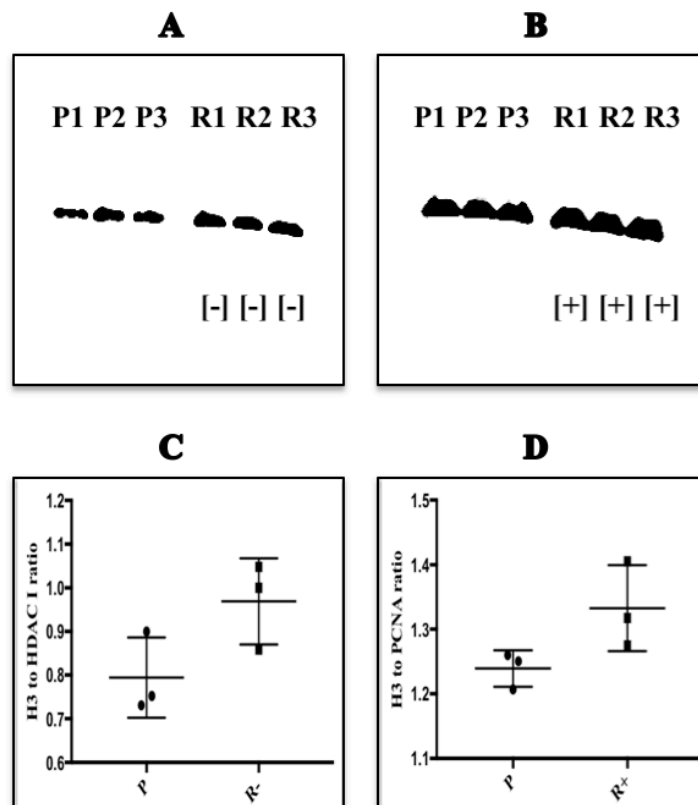


Figure 31: western blot comparison of histone 3 (H3) protein abundance levels in GDC-0980 sensitive parent (P) and resistant (R) H1975 adenocarcinoma cells. P1, P2, P3 and R1, R2, R3 represent triplicates of 20 μ g of cells lysate total protein. [-]: resistant cells cultured without drug and [+]: resistant cells cultured in RPMI medium containing 1 μ M GDC-0980. Shown also is a scatter plot of the ECL-chemiluminescence signal, normalized for the loading control, measured by ImageJ and represented as a H3 to loading control ratio (C and D).

6.3.3.5. Histone 3 co-localization

6.3.3.5.1. H1975 parent cells

Figure 32 shows DAPI staining of DNA of H1975 cells (A), histone 3 (B), and cells visualised by light transmission (C). Histone 3 is localised in the nucleus (D), where the overlap area between DAPI and Alexafluor-488 was 0.89.

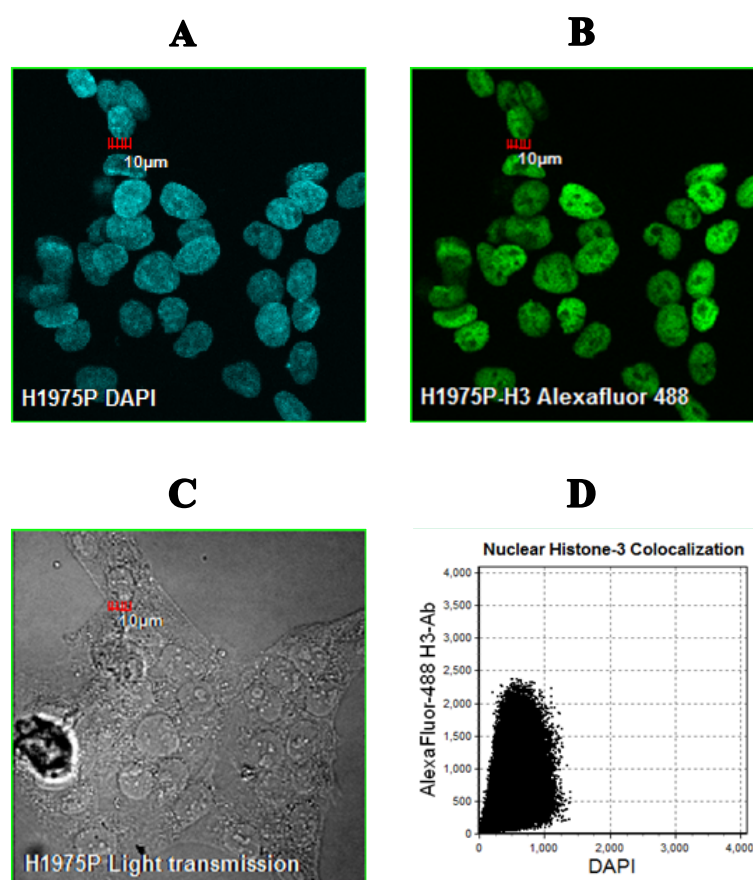


Figure 32: Nuclear histone 3 localisation. (P): GDC-0980 parent sensitive cells. (A) DAPI DNA visualisation, (B) AlexaFluor-488 coupled anti-H3 monoclonal antibody, (C) adherent cells seen under light microscopy, (D) localisation of H3 using DAPI/Alexa-Fluor signals.

6.3.3.5.2. H1975 resistant cells (R-)

Figure 33 shows DAPI staining of H1975 cells' DNA (A), histone 3 (B), and cells visualized using light transmission (C). Histone 3 was localised in the nucleus (D) where the overlap area between DAPI and Alexafluor-488 was 0.92.

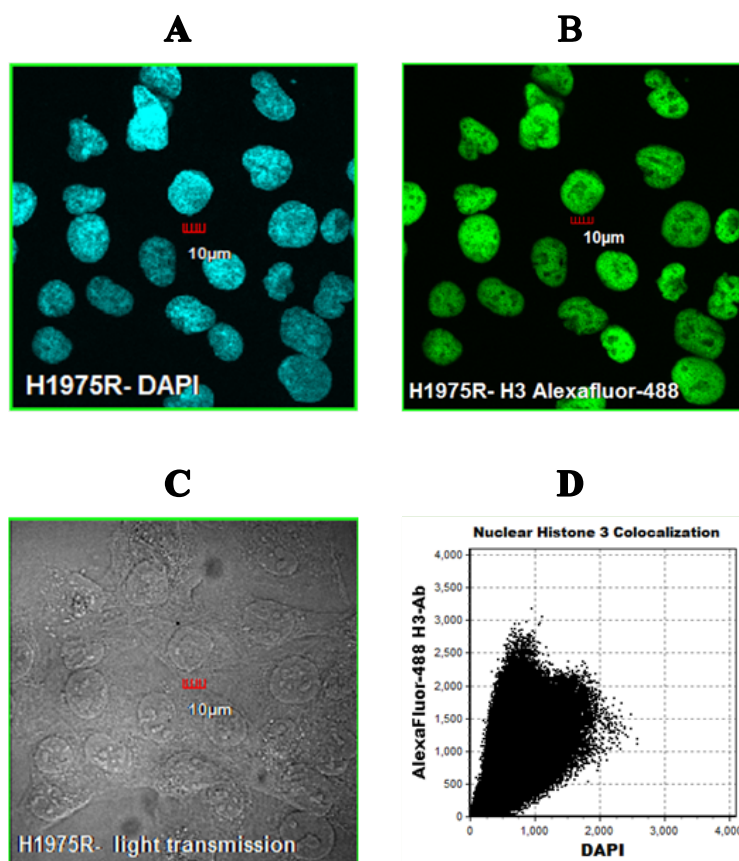


Figure 33: Nuclear histone 3 localisation. (R-): GDC-0980 resistant H1975 cells grown in GDC-0980 free media. (A) DAPI DNA visualisation, (B) AlexaFluor-488 coupled anti-H3 monoclonal antibody, (C) adherent cells seen under light microscopy, (D) localisation of H3 using DAPI/Alexa-Fluor signals.

6.3.3.5.3. H1975 resistant cells (R+)

Figure 34 shows DAPI staining of GDC-0980 resistant H1975 (R+) DNA (A), nuclear histone 3 (B), and cells visualised by light transmission (C). Histone 3 is localised in the nucleus (D), where the overlap area between DAPI and Alexafluor-488 was 0.94.

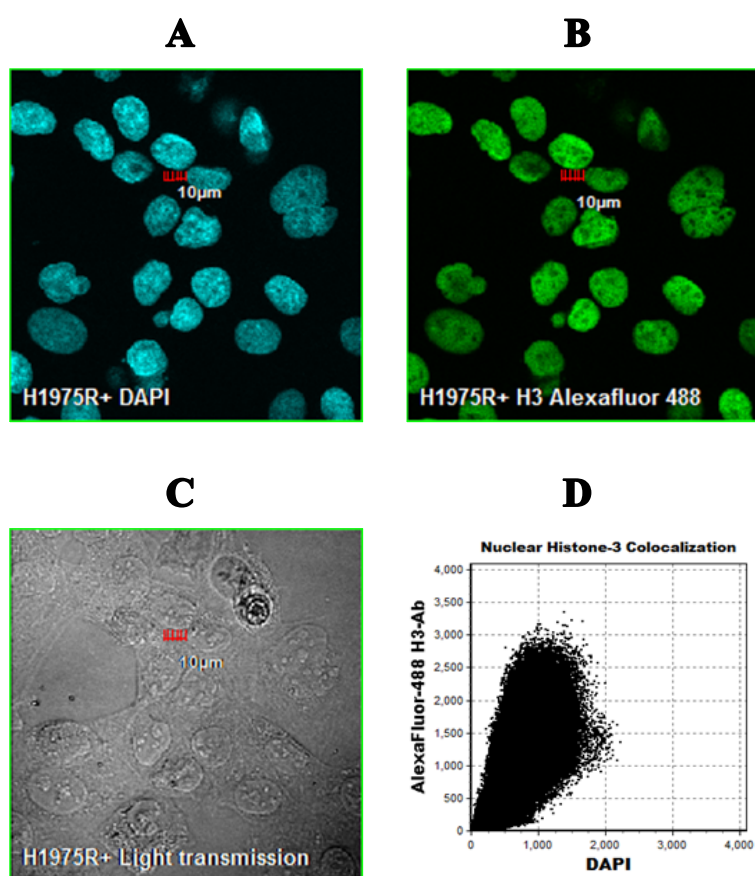


Figure 34: Nuclear histone 3 localisation. (R+): GDC-0980 resistant H1975 cells grown in media containing 1 µM GDC-0980. (A) DAPI DNA visualisation, (B) AlexaFluor-488 coupled anti-H3 monoclonal antibody, (C) adherent cells seen under light microscopy, (D) localisation of H3 using DAPI/Alexa-Fluor signals.

6.3.3.6. H1975 Cyclins profile

6.3.3.6.1. Cyclin D1

Figure 35 shows a western blot comparing cyclin D1 in GDC-0980 sensitive and resistant H1975 lung adenocarcinoma cells with (R+) (B/D) and without (R-) (A/C) drug treatment. The abundance of Cyclin D1 was significantly lowered in both treated and non-treated resistant cells compared to the parent cells. ($p= 0.001$ and 0.0003 in R+ and R- cells, respectively). HDAC I and PCNA proteins were used as a loading control when (R-) and (R+) were compared to the parent cells, respectively (refer to section 2.4.6.6).

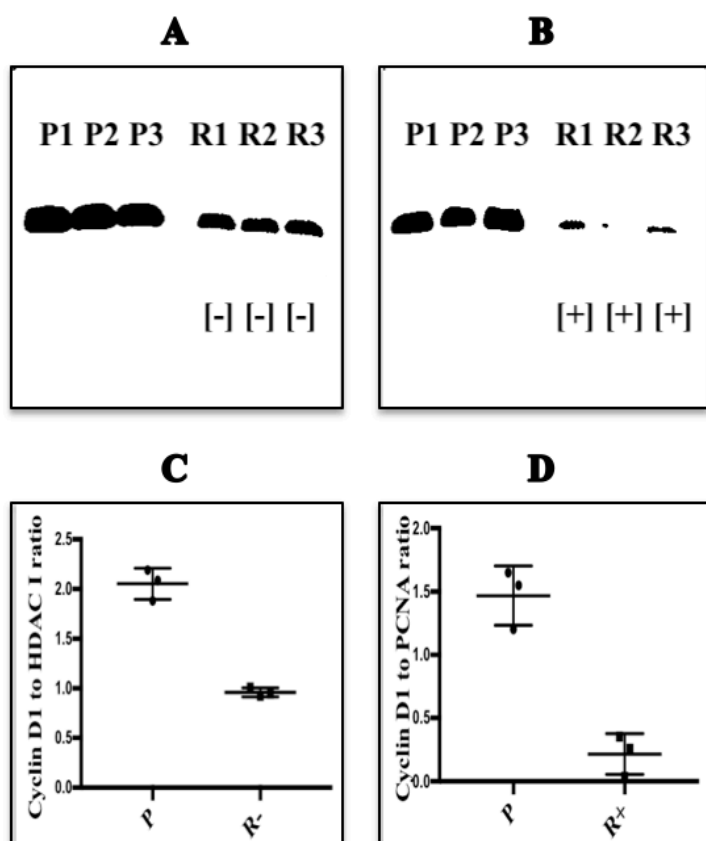


Figure 35: Comparison of cyclin D1 abundance in GDC-0980 sensitive parent (P) cells and resistant (R) H1975 adenocarcinoma cells. P1, P2, P3, and R1, R2, R3 represent triplicates of 20 μ g of total cell protein. [-]: resistant cells cultured without drug and [+]: resistant cells cultured in the presence of 1 μ M GDC-0980. Shown also is a scatter plot of the ECL-chemiluminescence signal, normalized for the loading control, measured by ImageJ and represented as a Cyclin D1 to loading control ratio (C and D).

6.3.3.6.2. Cyclin D3

Figure 36 shows a western blot comparison of Cyclin D3 abundance in GDC-0980 sensitive and resistant H1975 lung adenocarcinoma cells with (R+) and without (R-) drug treatment. The abundance of Cyclin D3 tended to increase in both treated (R+) (B) and non-treated cells (R-) (A) compared to the parent cells, but the changes were not statistically significant ($p=0.26$ and 0.20 in treated and non-treated cells, respectively) (C and D). HDAC I and PCNA proteins were used as a loading control when (R-) and (R+) were compared to the parent cells, respectively (refer to section 2.4.6.6).

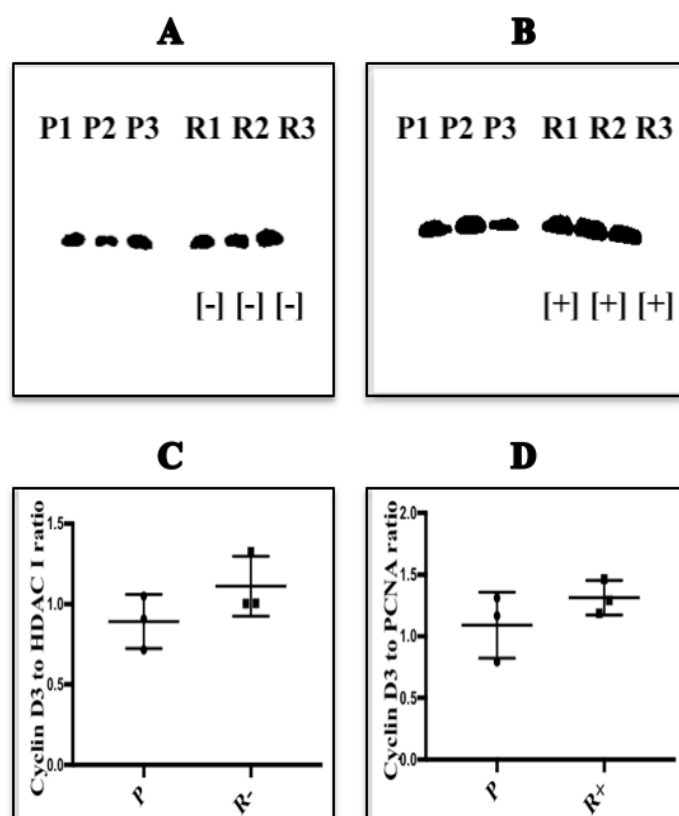


Figure 36: Comparison of cyclin D3 abundance in GDC-0980 sensitive parent (P) and resistant (R) H1975 adenocarcinoma cells. P1, P2, P3 and R1, R2, R3 represent triplicates of 20 μg of total cell protein. [-]: resistant cells cultured without drug and [+]: resistant cells cultured in the presence of 1 μM GDC-0980. Shown also is a scatter plot of the ECL-chemiluminescence signal, normalized for the loading control, measured by ImageJ and represented as a Cyclin D3 to loading control ratio (C and D).

6.3.3.6.3. Cyclin A2

Shown in figure 37 is a western blot comparison of Cyclin A2 expression levels in GDC-0980 sensitive and GDC-0980 resistant H1975 lung adenocarcinoma cells with (R+) and without (R-) the drug treatment. Cyclin A2 was significantly downregulated in both treated cells (R+) (B) and non-treated resistant cells (R-) (A) compared to the parent cells ($p= 0.0007$ and 0.001 in treated and non-treated cells, respectively) (C and D). HDAC I and PCNA proteins were used as a loading control when (R-) and (R+) were compared to the parent cells, respectively (refer to section 2.4.6.6).

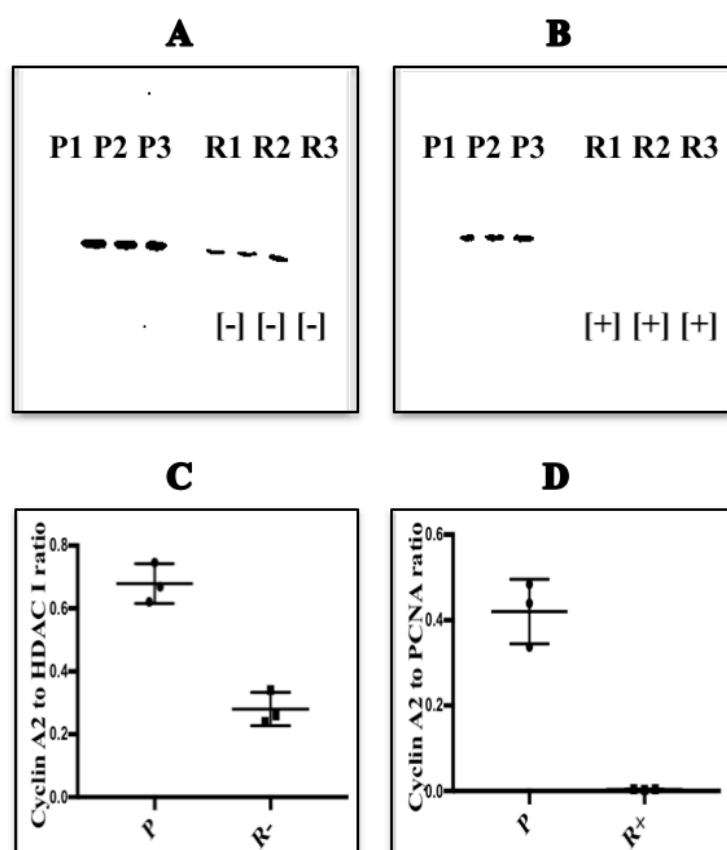


Figure 37: Western blotting comparison of cyclin A2 protein abundance in GDC-0980 sensitive parent (P) and resistant (R) H1975 adenocarcinoma cells. P1, P2, P3 and R1, R2, R3 represent triplicates of 20 μ g of total cell protein. [-]: resistant cells cultured without drug and [+]: resistant cells cultured in the presence of 1 μ M GDC-0980. Shown also is a scatter plot of the ECL-chemiluminescence signal, normalized for the loading control, measured by ImageJ and represented as a Cyclin A2 to loading control ratio (C and D).

6.3.3.6.4. Cyclin B1

Shown in figure 38 is a western blot comparing Cyclin B1 abundance in GDC-0980 sensitive and GDC-0980 resistant H1975 lung adenocarcinoma cells with (R+) and without (R-) drug treatment. Cyclin B1 was significantly downregulated in both treated (R+) (B) and non-treated (R-) resistant cells (A) compared to the parent cells. The p-value of the dysregulation was *0.0009* and *0.002* in treated and non-treated cells, respectively (C and D). HDAC I and PCNA proteins were used as a loading control when (R-) and (R+) were compared to the parent cells, respectively (refer to section 2.4.6.6).

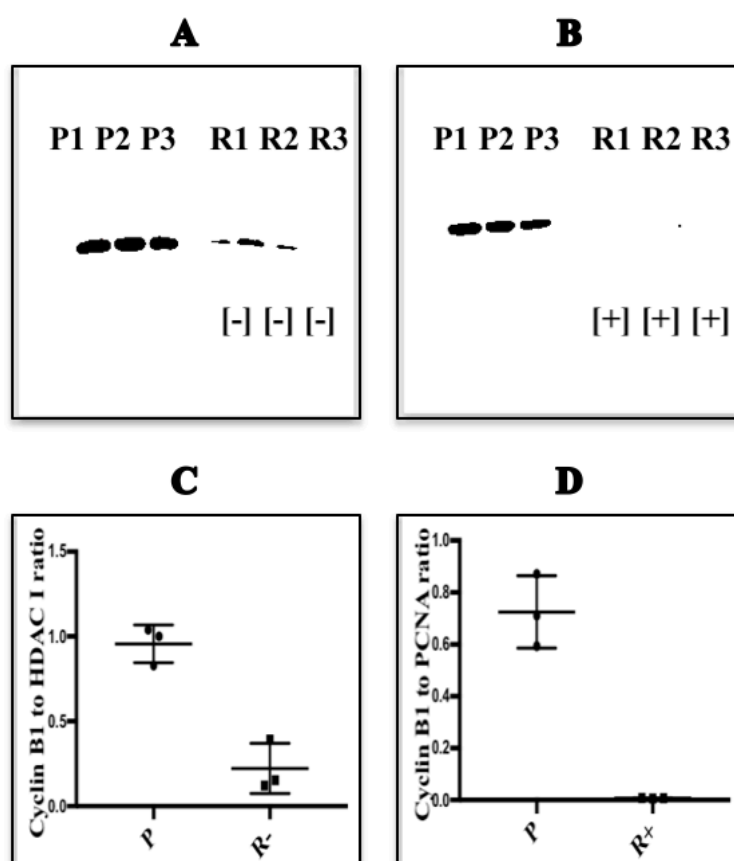


Figure 38: Comparison of cyclin B1 abundance in GDC-0980 sensitive parent (P) and resistant (R) H1975 adenocarcinoma cells. P1, P2, P3 and R1, R2, R3 represent triplicates of 20 μ g of total cell protein. [-]: resistant cells cultured without drug and [+] : resistant cells cultured in the presence of 1 μ M GDC-0980. Shown also is a scatter plot of the ECL-chemiluminescence signal, normalized for the loading control, measured by ImageJ and represented as a Cyclin B1 to loading control ratio (C and D).

6.3.3.6.5. Cyclin H

Shown in figure 39 is a western blot of Cyclin H abundance in GDC-0980 sensitive and GDC-0980 resistant H1975 lung adenocarcinoma cells treated (R+) or not treated (R-) with the drug. Cyclin H was significantly downregulated in both treated (R+) (B) and non-treated (R-) (A) resistant cells compared to the parent cells. P values were; 0.001 and 0.07 when treated and non-treated resistant cells were compared with the parent cells, respectively (C and D). HDAC I and PCNA proteins were used as a loading control when (R-) and (R+) were compared to the parent cells, respectively (refer to section 2.4.6.6).

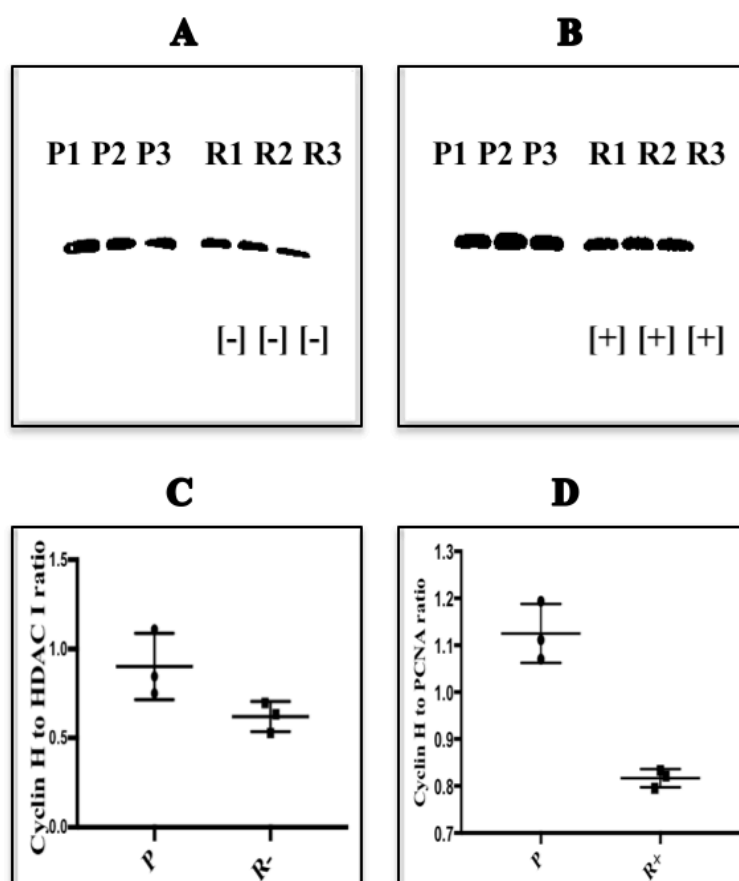


Figure 39: Comparison of cyclin H abundance in GDC-0980 sensitive parent (P) and resistant (R) H1975 adenocarcinoma cells. P1, P2, P3 and R1, R2, R3 represent triplicates of 20 μ g of total cell protein. [-]: resistant cells cultured without drug and [+]: resistant cells cultured in the presence of 1 μ M GDC-0980. Shown also is a scatter plot of the ECL-chemiluminescence signal, normalized for the loading control, measured by ImageJ and represented as a Cyclin H to loading control ratio (C and D).

6.3.3.6.6. Cyclin dependent kinase VI

Shown in figure 40 is a western blot comparing cyclin-dependent kinase 6 (CDK6) abundance in GDC-0980 sensitive and GDC-0980 resistant H1975 lung adenocarcinoma cells with (R+) and without (R-) drug treatment. CDK6 was significantly lowered in both treated and non-treated resistant cells compared to the parent cells. P values were; 0.005 and 0.0007 for treated and non-treated resistant cells, respectively, compared with parent cells (C and D). HDAC I and PCNA proteins were used as a loading control when (R-) and (R+) were compared to the parent cells, respectively (refer to section 2.4.6.6).

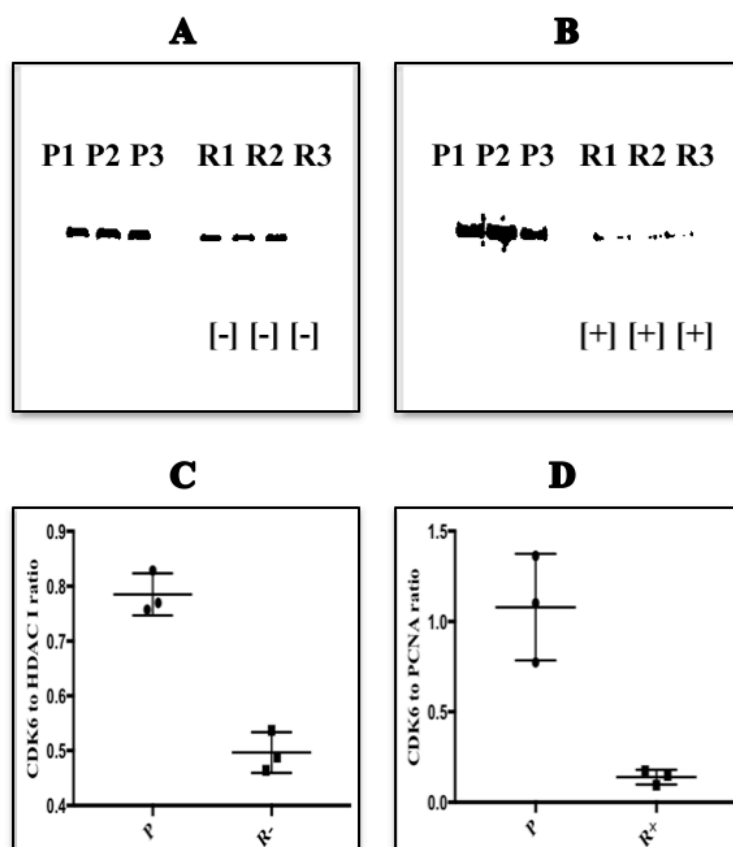


Figure 40: Comparison of cyclin dependent kinase 6 protein (CDK6) abundance in GDC-0980 sensitive parent (P) and resistant (R) H1975 adenocarcinoma cells. P1, P2, P3 and R1, R2, R3 represent triplicates of 20 μg of total cell protein. [-]: resistant cells cultured without drug and [+]: resistant cells cultured in the presence of 1 μM GDC-0980. Shown also is a scatter plot of the ECL-chemiluminescence signal, normalized for the loading control, measured by ImageJ and represented as a CDK6 to loading control ratio (C and D).

6.3.4. Proteins that affecting cell cycle progression

6.3.4.1. P53 tumour suppressant gene

Figure 41 shows a western blot comparison of P53 abundance in GDC-0980 sensitive and GDC-0980 resistant H1975 lung adenocarcinoma cells with (R+) (B) and without (R-) (A) drug treatment. P53 was significantly overexpressed in both treated and non-treated resistant cells compared to the parent cells. $P = 0.0004$ and <0.0001 when treated and non-treated resistant cells were compared with the parent cells, respectively (C and D). HDAC I and PCNA proteins were used as a loading control when (R-) and (R+) were compared to the parent cells, respectively (refer to section 2.4.6.6).

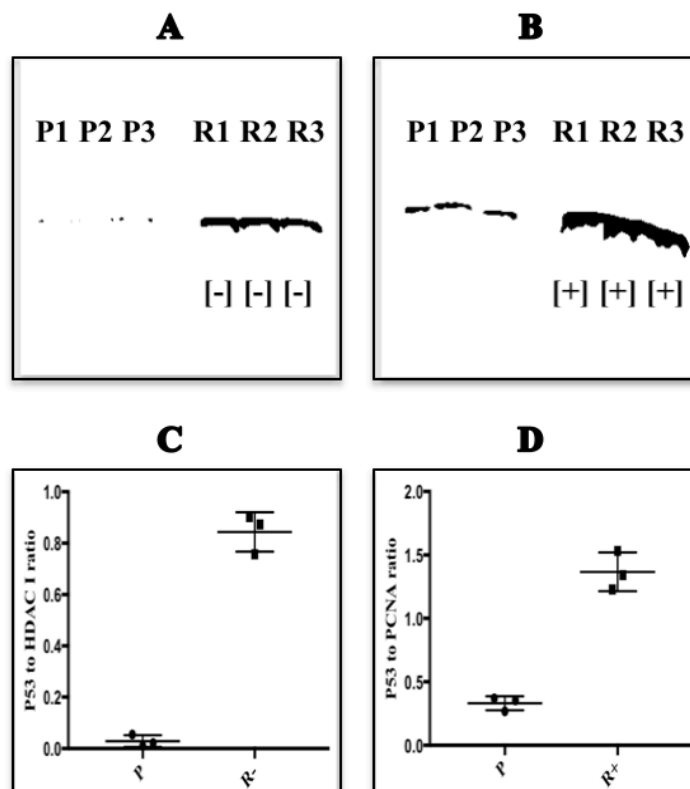


Figure 41: Comparison of P53 levels in GDC-0980 sensitive parent (P) and resistant H1975 lung adenocarcinoma cells. (A): no drug treatment and (R-)(B) when cells were incubated in medium containing $1 \mu\text{M}$ GDC-0980 (R+). P1, P2, P3 and R1, R2, R3 represent triplicates of $20 \mu\text{g}$ of total cell protein. Shown also is a scatter plot of the ECL-chemiluminescence signal, normalized for the loading control, measured by ImageJ and represented as a P53 to loading control ratio (C and D).

6.3.4.2. The adapter proteins (14-3-3)

6.3.4.2.1. Zeta/delta isoform

Figure 42 shows a western blot comparison of 14.3.3 zeta/delta [ζ/δ] abundance in GDC-0980 sensitive compared to GDC-0980 resistant H1975 lung adenocarcinoma cells with (R+) (B) and without (R-) drug treatment (A). 14.3.3 zeta/delta [ζ/δ] was significantly overexpressed in R- and downregulated in R+ compared to the parent cells. *P* values were 0.002 and 0.004, respectively (C and D). HDAC I and PCNA proteins were used as a loading control when (R-) and (R+) were compared to the parent cells, respectively (refer to section 2.4.6.6).

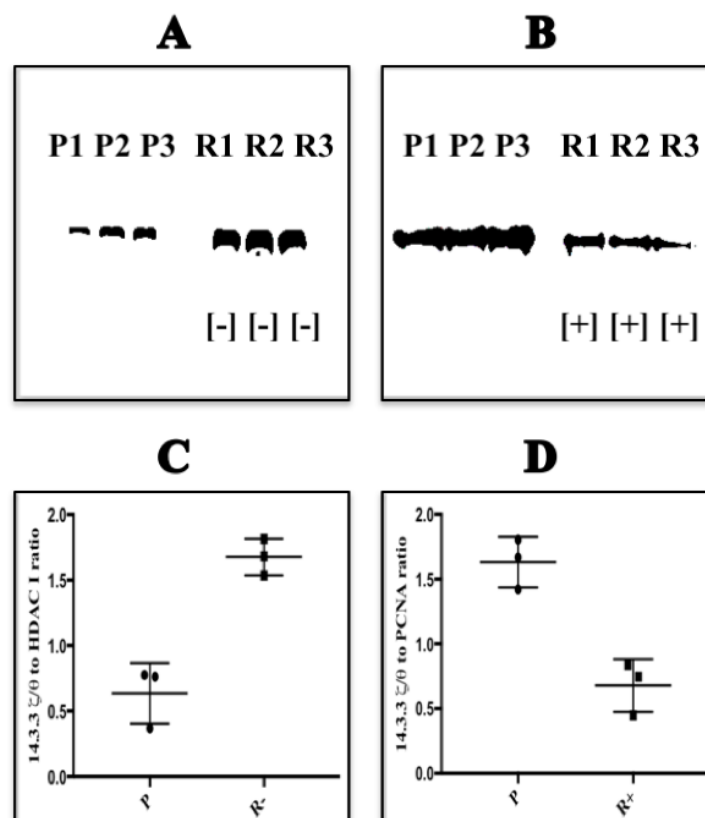


Figure 42: Comparison of 14.3.3 zeta/delta (ζ/δ) protein abundance in GDC-0980 sensitive parent (P) and resistant (R) H1975 adenocarcinoma cells. P1, P2, P3 and R1, R2, R3 represent triplicates of 20 μ g of total cell protein. [-]: resistant cells cultured without drug and [+]: resistant cells cultured in the presence of 1 μ M GDC-0980. Shown also is a scatter plot of the ECL-chemiluminescence signal, normalized for the loading control, measured by ImageJ and represented as a 14.3.3 zeta/delta to loading control ratio (C and D).

6.3.4.2.2. Epsilon isoform

Figure 43 shows a western blot comparison of 14.3.3 epsilon (ϵ) abundance in GDC-0980 sensitive compared to GDC-0980 resistant H1975 lung adenocarcinoma cells with (R+) (B) and without (R-) (A) drug treatment. 14.3.3 ϵ was significantly overexpressed in non-treated (R-) cells ($p= 0.001$) and downregulated in treated (R+) cells ($p= 0.0001$) (C and D). HDAC I and PCNA proteins were used as a loading control when (R-) and (R+) were compared to the parent cells, respectively (refer to section 2.4.6.6).

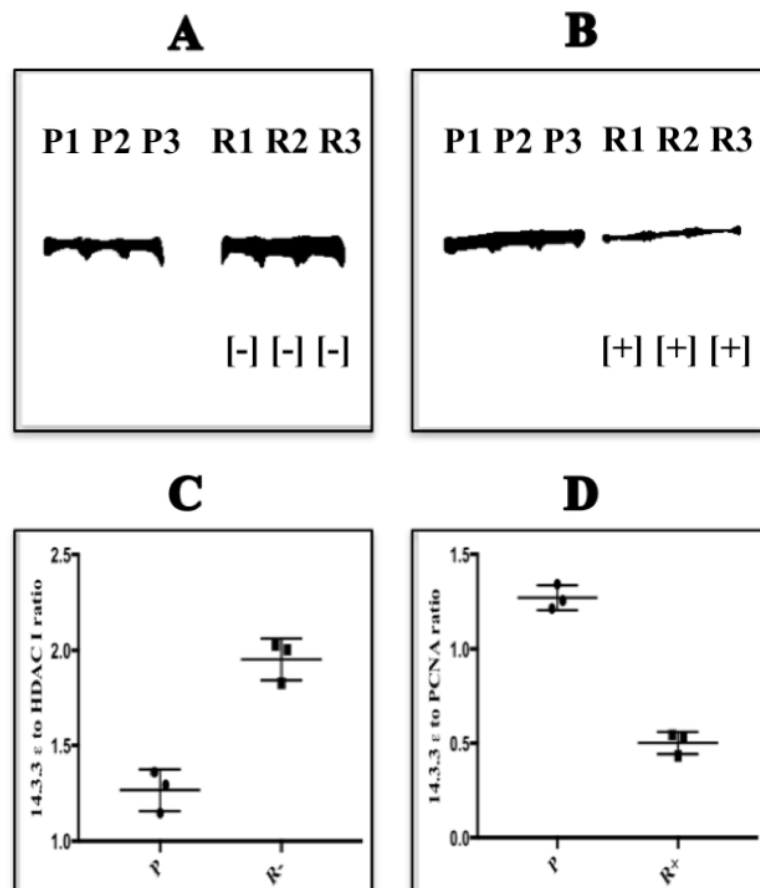


Figure 43: Comparison of 14.3.3 epsilon (ϵ) protein abundance in GDC-0980 sensitive parent (P) and resistant (R) H1975 adenocarcinoma cells. P1, P2, P3 and R1, R2, R3 represent triplicates of 20 μ g of total cell protein. [-]: resistant cells cultured without drug and [+]: resistant cells cultured in the presence of 1 μ M GDC-0980. Shown also is a scatter plot of the ECL-chemiluminescence signal, normalized for the loading control, measured by ImageJ and represented as a 14.3.3 epsilon to loading control ratio (C and D).

6.3.4.2.3. 14.33. gamma isoform (8)

Figure 44 shows a western blot comparison of 14.3.3 gamma (8) abundance in GDC-0980 sensitive compared to GDC-0980 resistant H1975 lung adenocarcinoma cells with (R+) (B) and without (R-) (A) drug treatment. 14.3.3 8 isoform was significantly down regulated in both treated (B) and non-treated (A) resistant cells compared to the parent cells ($p= 0.01$ in both comparison) (C and D). HDAC I and PCNA proteins were used as a loading control when (R-) and (R+) were compared to the parent cells, respectively (refer to section 2.4.6.6).

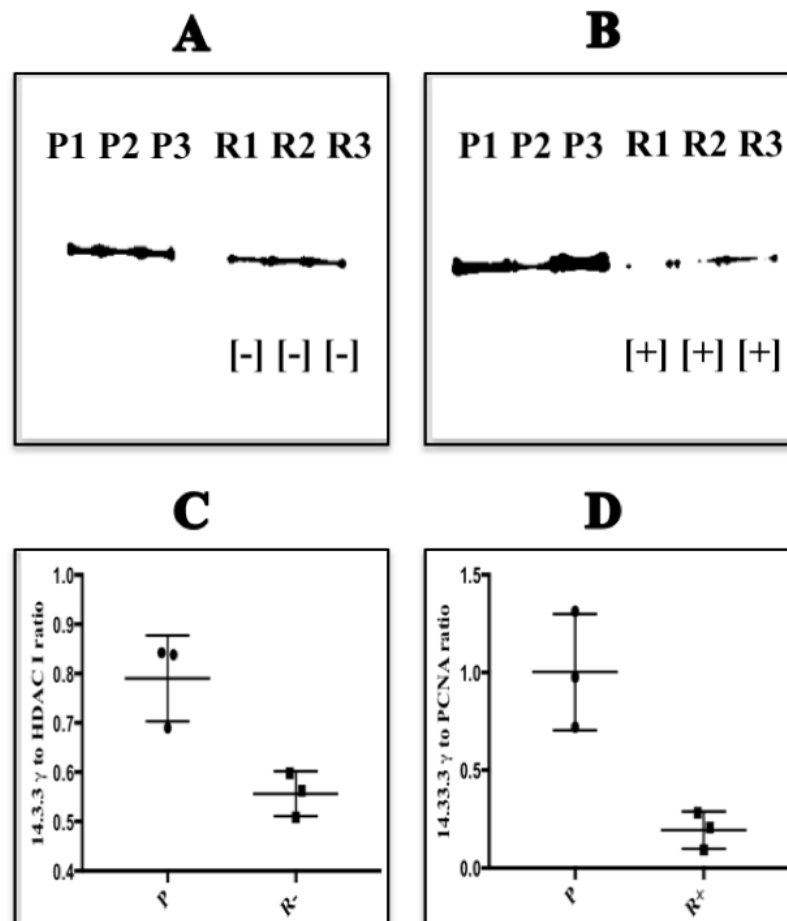


Figure 44: Comparison of 14.3.3 gamma [8] protein abundance in GDC-0980 sensitive parent (P) and resistant (R) H1975 adenocarcinoma cells. P1, P2, P3 and R1, R2, R3 represent triplicates of 20 μ g of total cell protein. [-]: resistant cells cultured without drug and [+]: resistant cells cultured in the presence of 1 μ M GDC-0980. Shown also is a scatter plot of the ECL-chemiluminescence signal, normalized for the loading control, measured by ImageJ and represented as a 14.3.3 gamma to loading control ratio (C and D).

6.3.4.2.4. 14.3.3. alpha/beta isoform (14.3.3 α/β)

Figure 45 shows a western blot comparison of 14.3.3 α/β levels in GDC-0980 sensitive H1975 lung adenocarcinoma cells when compared with the resistant cells with (R+) (B) and without (R-) (A) drug treatment. 14.3.3 α/β isoform was significantly upregulated in (R-) ($p= 0.0006$) and downregulated in (R+) ($p= 0.0003$) compared with the parent cells (C and D). HDAC I and PCNA proteins were used as a loading control when (R-) and (R+) were compared to the parent cells, respectively (refer to section 2.4.6.6).

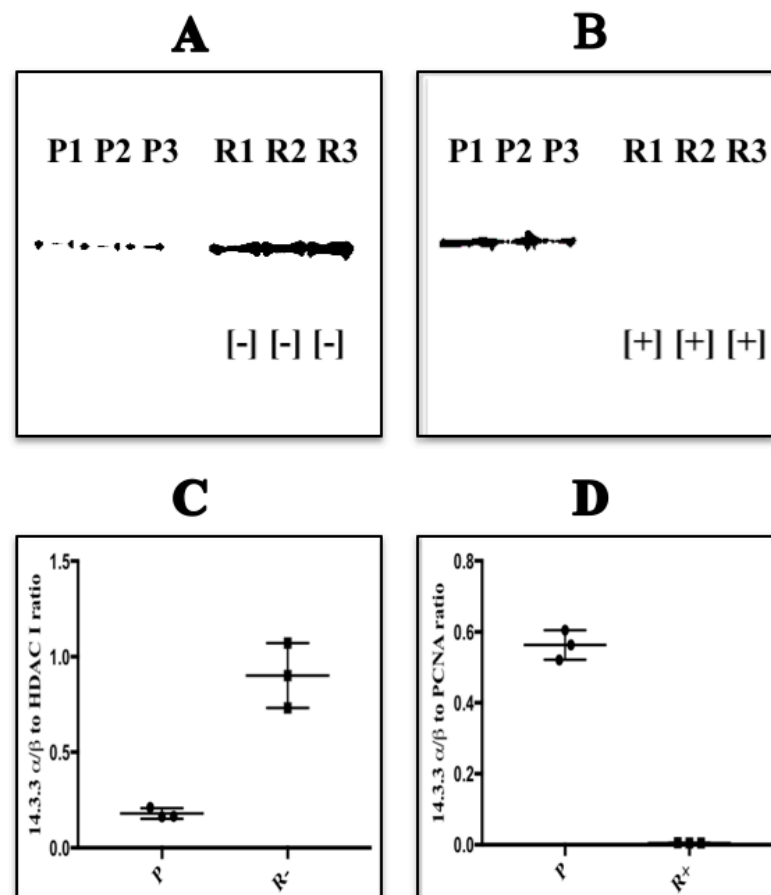


Figure 45: Comparison of 14.3.3 alpha/beta protein abundance levels in GDC-0980 sensitive parent (P) and resistant (R) H1975 adenocarcinoma cells. P1, P2, P3 and R1, R2, R3 represent triplicates of 20 μg of total cell protein. [-]: resistant cells cultured without drug and [+] : resistant cells cultured in the presence of 1 μM GDC-0980. Shown also is a scatter plot of the ECL-chemiluminescence signal, normalized for the loading control, measured by ImageJ and represented as a 14.3.3 α/β to loading control ratio (C and D).

6.3.4.3. P21 regulatory protein

Figure 46 shows a western blot comparison of p21 abundance in GDC-0980 sensitive compared to GDC-0980 resistant H1975 lung adenocarcinoma cells with (R+) and without (R-) drug treatment. p21 was significantly down regulated in both treated (B) and non-treated (A) resistant cells compared to the parent cells. $P < 0.0001$ in both treated (R+) and non-treated (R-) cells, respectively (C and D). HDAC I and PCNA proteins were used as a loading control when (R-) and (R+) were compared to the parent cells, respectively (refer to section 2.4.6.6).

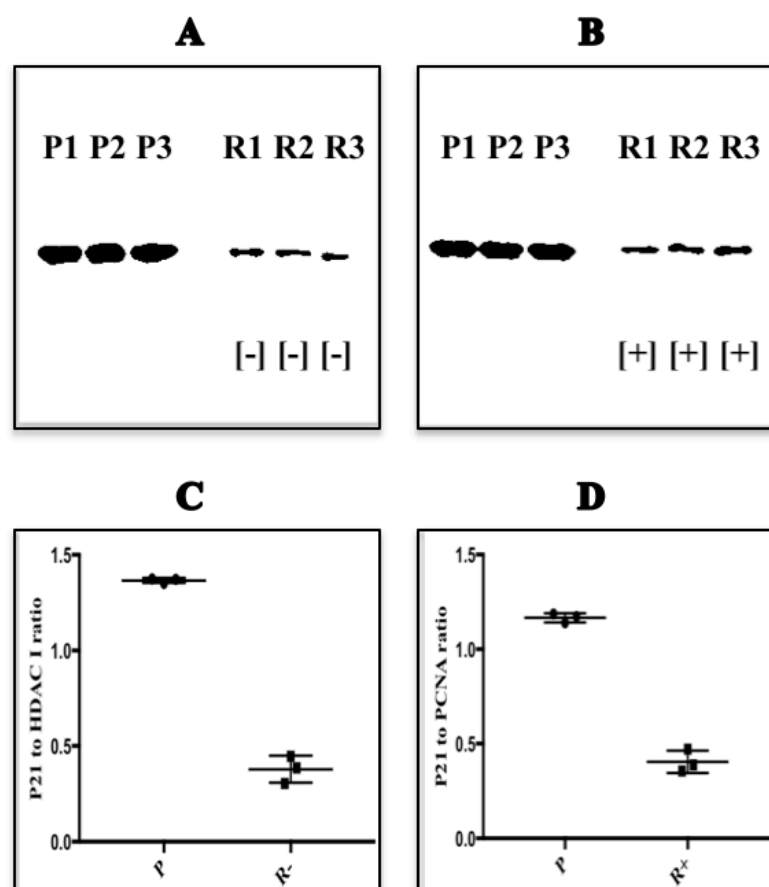


Figure 46: Comparison of p21 protein abundance in GDC-0980 sensitive parent (P) and resistant (R) H1975 adenocarcinoma cells. P1, P2, P3 and R1, R2, R3 represent triplicates of 20 μ g of total cell protein. [-]: resistant cells cultured without drug and [+]: resistant cells cultured in the presence of 1 μ M GDC-0980. Shown also is a scatter plot of the ECL-chemiluminescence signal, normalized for the loading control, measured by ImageJ and represented as a p21 to loading control ratio (C and D).

6.3.4.4. Proliferating cells nuclear antigen [PCNA]

Figure 47 shows a western blot comparison of PCNA abundance in GDC-0980 sensitive compared to GDC-0980 resistant H1975 lung adenocarcinoma cells grown with (R+) or without (R-) the drug. The abundance of PCNA was significantly ($p= 0.01$) downregulated in the non-treated cells (R-) (A) and upregulated ($p=>0.99$) in the treated cells (R+) (B) compared to the parent cells (C and D). HDAC I and PCNA proteins were used as a loading control when (R-) and (R+) were compared to the parent cells, respectively (refer to section 2.4.6.6).

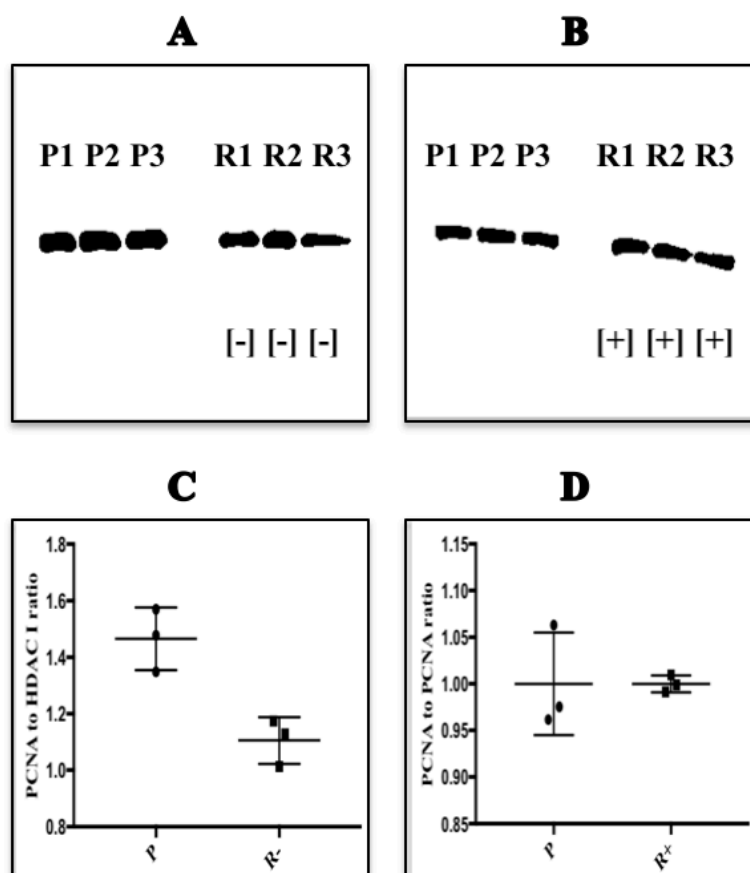


Figure 47: Comparison of Proliferating cells nuclear antigen (PCNA) abundance in GDC-0980 sensitive parent (P) and resistant (R) H1975 adenocarcinoma cells. P1, P2, P3 and R1, R2, R3 represent triplicates of 20 μ g of total cell protein. [-]: resistant cells cultured without drug and [+]: resistant cells cultured in the presence of 1 μ M GDC-0980. Shown also is a scatter plot of the ECL-chemiluminescence signal, normalized for the loading control, measured by ImageJ and represented as a PCNA to loading control ratio (C and D).

6.3.4.5. Ubiquitination levels of PCNA (Ub-PCNA)

Figure 48 shows a western blot comparison of Ub-PCNA levels in GDC-0980 sensitive compared to GDC-0980 resistant H1975 lung adenocarcinoma cells with (R+) (B) or without (R-) (A) the drug. PCNA ubiquitination was significantly downregulated ($p=0.004$) in R+. The decrease in the non-treated cells (R-) was not significant ($p=0.29$) (C and D). HDAC I and PCNA proteins were used as a loading control when (R-) and (R+) were compared to the parent cells, respectively (refer to section 2.4.6.6).

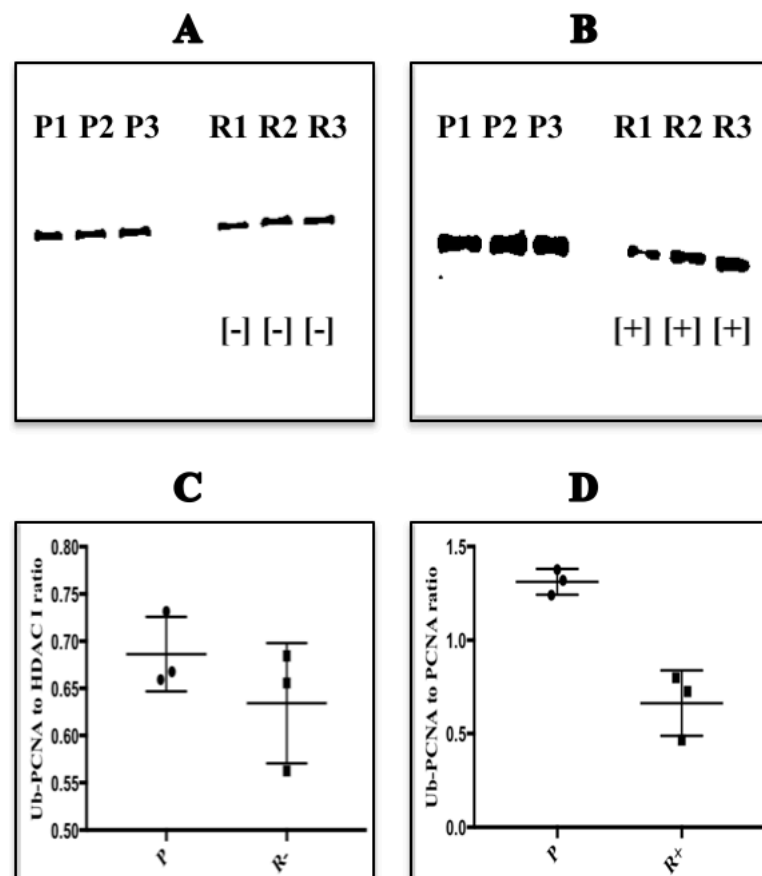


Figure 48: Comparison of the ubiquitination level of PCNA (Ub-PCNA) protein abundance levels in GDC-0980 sensitive parent (P) and resistant (R) H1975 adenocarcinoma cells. P1, P2, P3 and R1, R2, R3 represent triplicates of 20 μ g of total cell protein. [-]: resistant cells cultured without drug and [+] : resistant cells cultured in the presence of 1 μ M GDC-0980. Shown also is a scatter plot of the ECL-chemiluminescence signal, normalized for the loading control, measured by ImageJ and represented as a Ub-PCNA to loading control ratio (C and D).

6.3.4.6. Bcl-associated X protein [BAX]

Figure 49 shows a western blot comparison of BAX abundance in GDC-0980 sensitive and GDC-0980 resistant H1975 lung adenocarcinoma cells with (R+) (B) or without (R-) (A) drug treatment. BAX was significantly down regulated in the non-treated (R-) cells compared with the parent cells ($P= 0.0006$) and its expression was elevated in the treated cells (R+) ($P= 0.5$) (C and D). HDAC I and PCNA proteins were used as a loading control when (R-) and (R+) were compared to the parent cells, respectively (refer to section 2.4.6.6).

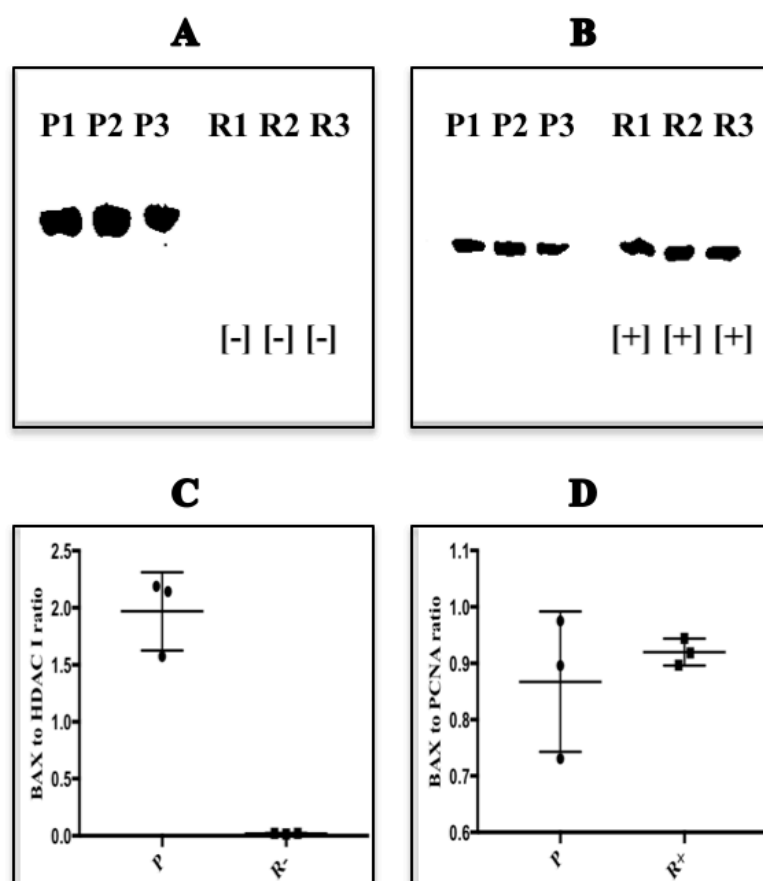


Figure 49: Comparison of Bcl-associated X large protein (BAX) abundance in GDC-0980 sensitive parent (P) and resistant (R) H1975 adenocarcinoma cells. P1, P2, P3 and R1, R2, R3 represent triplicates of 20 μg of total cell protein. [-]: resistant cells cultured without drug and [+]: resistant cells cultured in the presence of 1 μM GDC-0980. Shown also is a scatter plot of the ECL-chemiluminescence signal, normalized for the loading control, measured by ImageJ and represented as a BAX to loading control ratio (C and D).

6.3.4.7. B-cell lymphoma extra-large [BCL-XL]

Shown in figure 50 is a western blot of BCL-XL expression levels in GDC-0980 resistant cells with (R+) or without (R-) drug treatment compared to sensitive cells (P). The levels were significantly upregulated in both treated (B) and non-treated conditions (A) compared to the parent cells. The p-values were 0.01 and 0.0001 in the treated (R+) and non-treated (R-) cells, respectively, compared to the parent cells (C and D). HDAC I and PCNA proteins were used as a loading control when (R-) and (R+) were compared to the parent cells, respectively (refer to section 2.4.6.6).

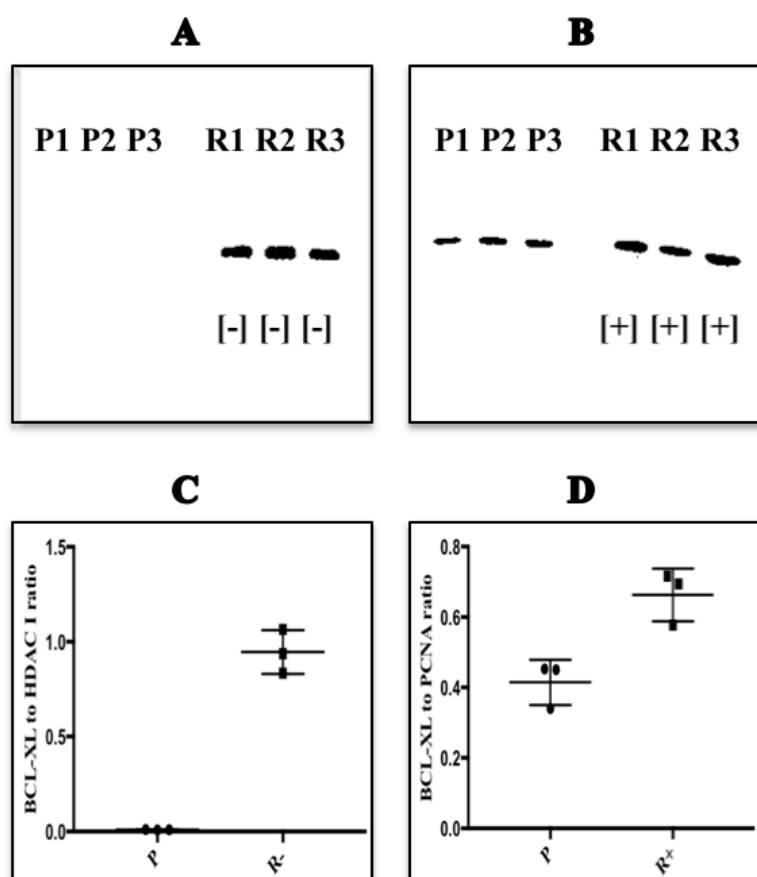


Figure 50: Comparison of the levels of BCL-XL abundance in GDC-0980 sensitive parent (P) and resistant (R) H1975 adenocarcinoma cells. P1, P2, P3 and R1, R2, R3 represent triplicates of 20 μ g of total cell protein. [-]: resistant cells cultured without drug and [+]: resistant cells cultured in the presence of 1 μ M GDC-0980. Shown also is a scatter plot of the ECL-chemiluminescence signal, normalized for the loading control, measured by ImageJ and represented as a BCL-XL to loading control ratio (C and D).

6.3.4.8. Nuclear factor kappa B1 [NFkB1] P105/P50

Shown in figure 51, the resistant cells treated with the drug (R+), native NFkB1 (P105) level was not significantly different ($p= 0.18$) in comparison to parent cells (B). In contrast, non-treated (R-) resistant cells (A) exhibited significant up-regulation of native NFkB1 protein (P105) ($p= 0.001$). On the other hand, P50 in both treatment conditions was significantly up-regulated ($p= 0.01$ and 0.004 , respectively). Shown also is a scatter plot representing the ECL-chemiluminescence correspondent signal measured by ImageJ and plotted in triplicates per phenotype (C and D). HDAC I and PCNA proteins were used as a loading control when (R-) and (R+) were compared to the parent cells, respectively (refer to section 2.4.6.6).

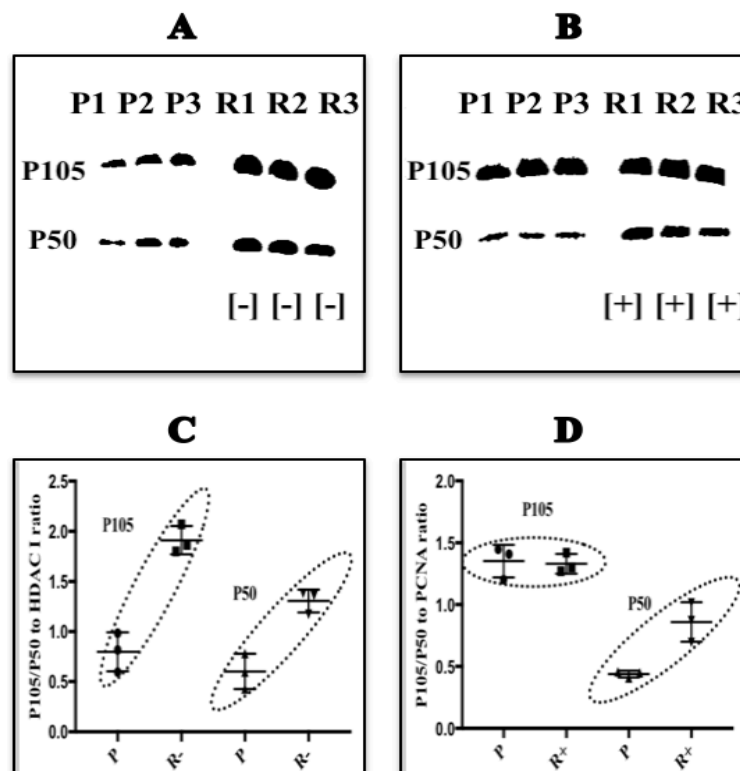


Figure 51: Comparison of the levels of Nuclear factor kappa B1 (P105/P50) abundance and its degradation in GDC-0980 sensitive parent (P) and resistant (R) H1975 adenocarcinoma cells. P1, P2, P3 and R1, P2, R3 represent triplicates of 20 μ g of total cell protein. [-]: resistant cells cultured without drug and [+]: resistant cells cultured in the presence of 1 μ M GDC-0980. Shown also is a scatter plot of the ECL-chemiluminescence signal, normalized for the loading control, measured by ImageJ and represented as a P105/P50 to loading control ratio (C and D).

6.3.4.9. Transcription factor Rel-A (P65)

The level of P65 (Rel-A) showed a non-significant elevation in resistant cells, both treated (R+) (B) and non-treated (R-) (A). The p-value was 0.1 in both treated and non-treated cells, respectively. Shown also is a scatter plot representing the ECL-chemiluminescence correspondent signal measured by ImageJ and plotted as triplicates per phenotype (C and D) (figure 52). HDAC I and PCNA proteins were used as a loading control when (R-) and (R+) were compared to the parent cells, respectively (refer to section 2.4.6.6).

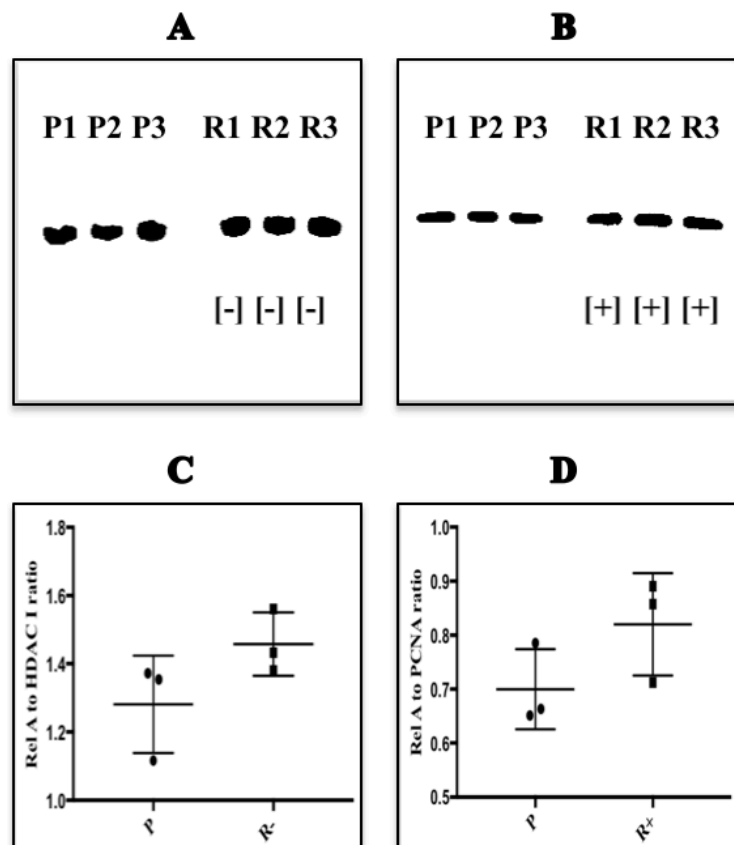


Figure 52: comparison of the Rel- associated protein [Rel-A] abundance levels in GDC-0980 sensitive parent (P) and resistant (R) H1975 adenocarcinoma cells. P1, P2, P3 and R1, R2, R3 represent triplicates of 20 μ g of total cell protein. [-]: resistant cells cultured without drug and [+]: resistant cells cultured in the presence of 1 μ M GDC-0980. Shown also is a scatter plot of the ECL-chemiluminescence signal, normalized for the loading control, measured by ImageJ and represented as a Rel A to loading control ratio (C and D).

6.3.4.10. Transcription factor Rel- B

The level of Rel-B was significantly down-regulated in the both treated (R+) (B) and non-treated (R-) (A) resistant cells compared to their parent cells ($p= 0.0008$ and 0.03 , respectively). Shown also is a scatter plot representing the ECL-chemiluminescence correspondent signal measured by ImageJ and plotted as triplicates per phenotype (C and D) (figure 53). HDAC I and PCNA proteins were used as a loading control when (R-) and (R+) were compared to the parent cells, respectively (refer to section 2.4.6.6).

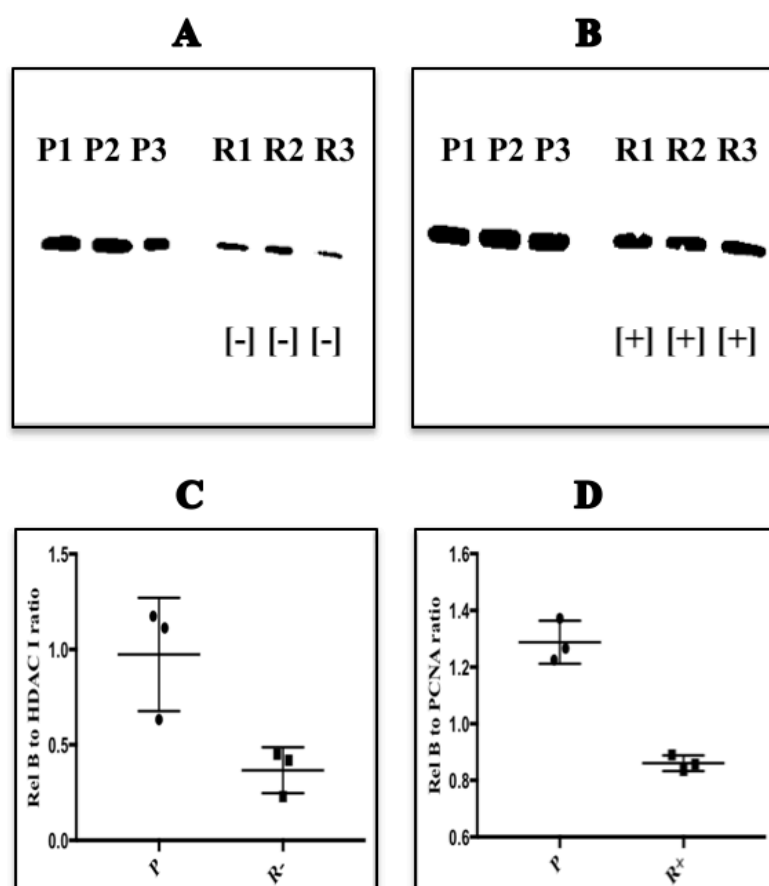


Figure 53: Comparison of Rel-B protein abundance levels in GDC-0980 sensitive parent (P) and resistant (R) H1975 adenocarcinoma cells. P1, P2, P3 and R1, R2, R3 represent triplicates of 20 μ g of total cell protein. (-): resistant cells cultured without drug and (+): resistant cells cultured in the presence of 1 μ M GDC-0980. Shown also is a scatter plot of the ECL-chemiluminescence signal, normalized for the loading control, measured by ImageJ and represented as a Rel B to loading control ratio (C and D).

6.3.4.11. Transcription factor [c-Rel]

c- Rel in treated resistant cells was not significantly different from that in parent cells ($p= 0.1$), while in non-treated cells it was significantly lower ($p= 0.01$). Shown also is a scatter plot representing the ECL-chemiluminescence correspondent signal measured by ImageJ and plotted as triplicates per phenotype (C and D) (figure 54). HDAC I and PCNA proteins were used as a loading control when (R-) and (R+) were compared to the parent cells, respectively (refer to section 2.4.6.6).

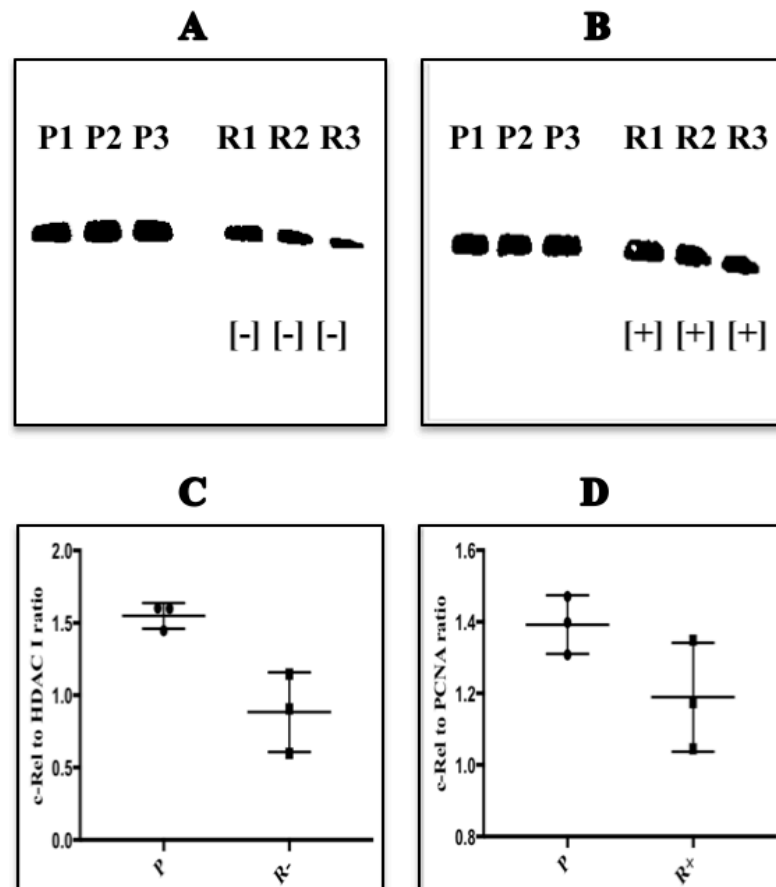


Figure 54: Comparison of c-Rel protein abundance levels in GDC-0980 sensitive parent (P) and resistant (R) H1975 adenocarcinoma cells. P1, P2, P3 and R1, R2, R3 represent triplicates of 20 μg of total cell protein. (-): resistant cells cultured without drug and (+): resistant cells cultured in the presence of 1 μM GDC-0980. Shown also is a scatter plot of the ECL-chemiluminescence signal, normalized for the loading control, measured by ImageJ and represented as a c-Rel to loading control ratio (C and D).

6.3.4.12. Histone acetyltransferase

6.3.4.12.1. General control of amino acid synthesis protein [GCN5L2]

The level of GCN5L2 was significantly down-regulated in treated (R+) cells (B) compared to parent cells and was significantly up-regulated in non-treated resistant cells (R-) (A) ($p= 0.003$ and 0.0004 , respectively). Shown also is a scatter plot representing the ECL-chemiluminescence correspondent signal measured by ImageJ and plotted as triplicates per phenotype (C and D) (figure 55). HDAC I and PCNA proteins were used as a loading control when (R-) and (R+) were compared to the parent cells, respectively (refer to section 2.4.6.6).

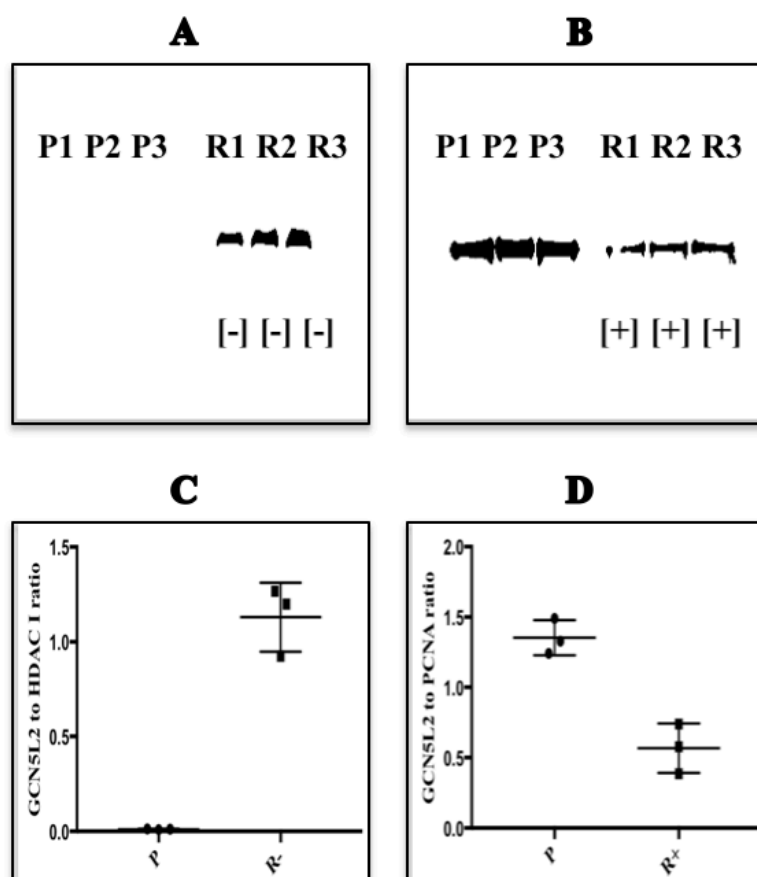


Figure 55: Comparison of general control of amino acid synthesis (GCN5L2) protein abundance levels in GDC-0980 sensitive parent (P) and resistant (R) H1975 adenocarcinoma cells. P1, P2, P3 and R1, R2, R3 represent triplicates of 20 μg of total cell protein. (-): resistant cells cultured without drug and (+): resistant cells cultured in the presence of 1 μM GDC-0980. Shown also is a scatter plot of the ECL-chemiluminescence signal, normalized for the loading control, measured by ImageJ and represented as a GCN5L2 to loading control ratio (C and D).

6.3.4.12.2. p300/CBP-associated protein [PCAF]

The level of PCAF was significantly down-regulated in treated (R+) cells (B) compared to parent cells and was significantly up-regulated in non-treated resistant cells (R-) (A). The p-values were <0.0001 and 0.0007 in treated and non-treated resistant cells, respectively. Shown also is a scatter plot representing the ECL-chemiluminescence correspondent signal measured by ImageJ and plotted as triplicates per phenotype (C and D) (figure 56). HDAC I and PCNA proteins were used as a loading control when (R-) and (R+) were compared to the parent cells, respectively (refer to section 2.4.6.6).

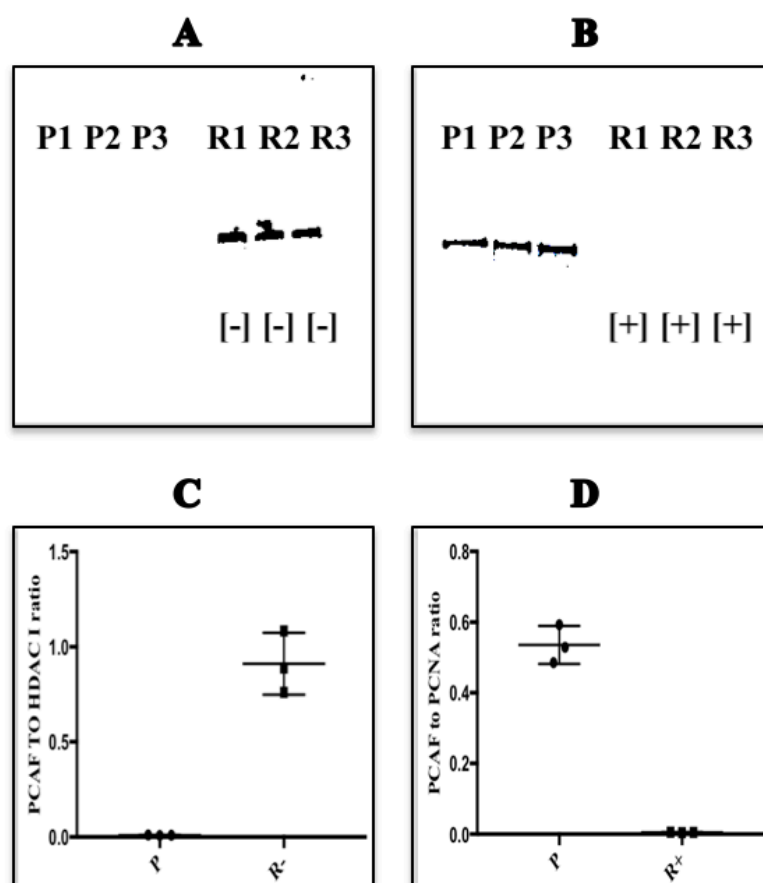


Figure 56: Comparison of p300/CBP-associated protein (PCAF) abundance levels in GDC-0980 sensitive parent (P) and resistant (R) H1975 adenocarcinoma cells. P1, P2, P3 and R1, R2, R3 represent triplicates of 20 μ g of cells lysate total protein. (-): resistant cells cultured without drug and (+): resistant cells cultured in 1 μ M GDC-0980. Shown also is a scatter plot of the ECL-chemiluminescence signal, normalized for the loading control, measured by ImageJ and represented as a PCAF to loading control ratio (C and D).

6.3.4.13. Histone deacetylases

6.3.4.13.1. HDAC I

In the presence of GDC-0980, HDAC I was significantly up-regulated (R+) (B) compared to parent cells ($p= 0.0002$), but it became down-regulated with p value of >0.99 when the drug was cleared from the medium (R-) (A). Shown also is a scatter plot representing the ECL-chemiluminescence correspondent signal measured by ImageJ and plotted as triplicates per phenotype (C and D) (figure 57). HDAC I and PCNA proteins were used as a loading control when (R-) and (R+) were compared to the parent cells, respectively (refer to section 2.4.6.6).

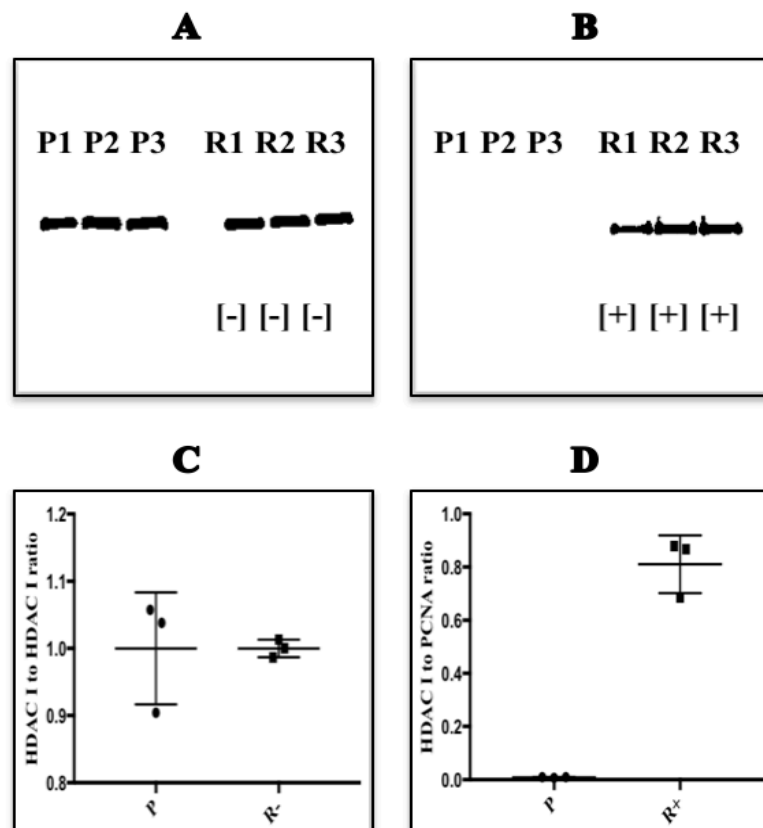


Figure 57: comparison of histone deacetylase I (HDAC I) protein abundance levels in GDC-0980 sensitive parent (P) and resistant (R) H1975 adenocarcinoma cells. P1, P2, P3 and R1, R2, R3 represent triplicates of 20 μ g of cells lysate total protein. (-): resistant cells cultured without drug and (+): resistant cells cultured in 1 μ M GDC-0980. Shown also is a scatter plot of the ECL-chemiluminescence signal, normalized for the loading control, measured by ImageJ and represented as a HDAC I to loading control ratio (C and D).

6.3.4.13.2. HDAC II

HDAC II was significantly upregulated in treated (R+) cells (B) compared to the parent cells ($p= 0.01$), but in non-treated cells (R-) (A) it remained up-regulated ($p= 0.09$). Shown also is a scatter plot representing the ECL-chemiluminescence correspondent signal measured by ImageJ and plotted as triplicates per phenotype (C and D) (figure 58). HDAC I and PCNA proteins were used as a loading control when (R-) and (R+) were compared to the parent cells, respectively (refer to section 2.4.6.6).

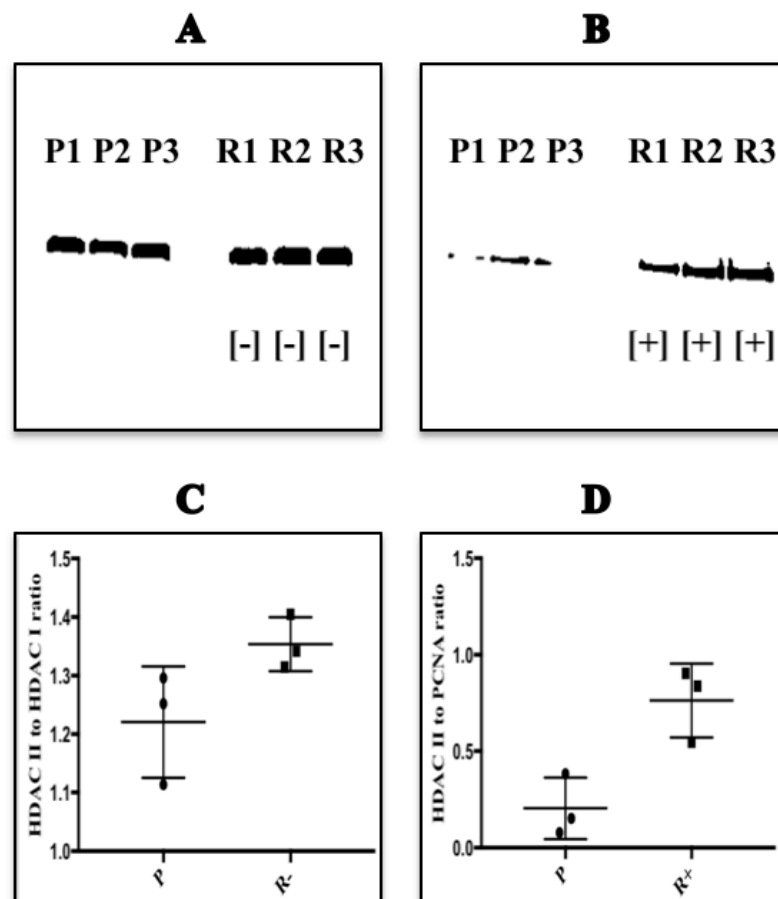


Figure 58: Comparison of histone deacetylase II (HDAC II) protein abundance levels in GDC-0980 sensitive parent (P) and resistant (R) H1975 adenocarcinoma cells. P1, P2, P3 and R1, R2, R3 represent triplicates of 20 μ g of cells lysate total protein. (-): resistant cells cultured without drug and (+): resistant cells cultured in 1 μ M GDC-0980. Shown also is a scatter plot of the ECL-chemiluminescence signal, normalized for the loading control, measured by ImageJ and represented as a HDAC II to loading control ratio (C and D).

6.3.4.13.3. HDAC III

HDAC III was significantly up-regulated in treated (R+) cells (B) compared to parent cells ($p= 0.0003$) while this increase went back to become down-regulated with p value of 0.2 when the inhibitor was cleared from the medium (R-) (A). Shown in this figure also is a numeric representation of the ECL-chemiluminescence signal, measured by ImageJ and represented as triplicates per phenotype (C and D) (figure 59). HDAC I and PCNA proteins were used as a loading control when (R-) and (R+) were compared to the parent cells, respectively (refer to section 2.4.6.6).

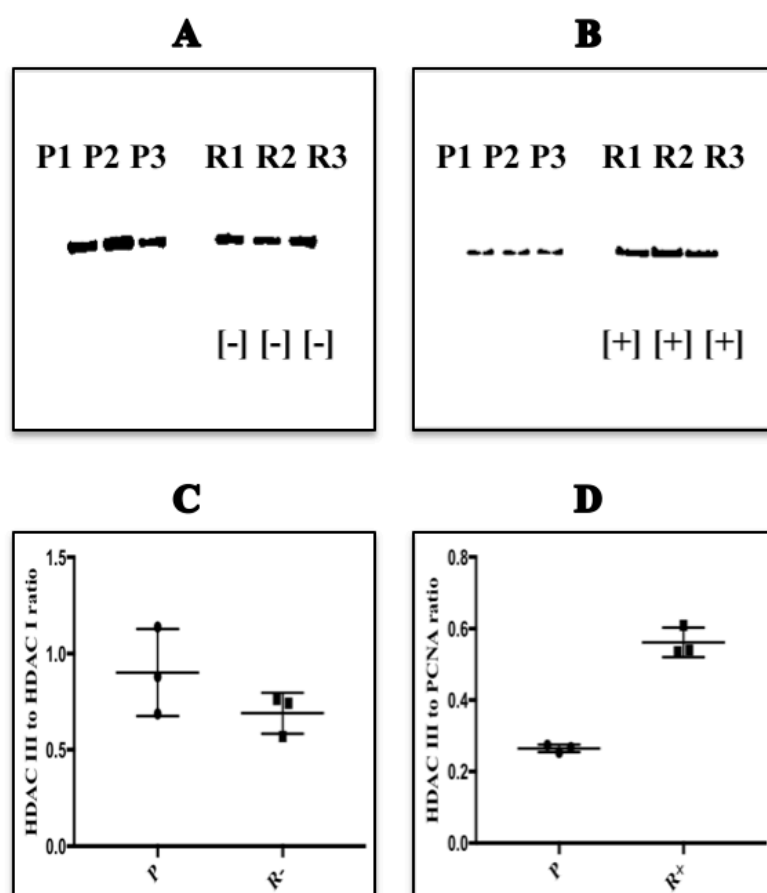


Figure 59: Comparison of histone deacetylase III (HDAC III) protein abundance levels in GDC-0980 sensitive parent (P) and resistant (R) H1975 adenocarcinoma cells. P1, P2, P3 and R1, R2, R3 represent triplicates of 20 μ g of cells lysate total protein. (-): resistant cells cultured without drug and (+): resistant cells cultured in 1 μ M GDC-0980. Shown also is a scatter plot of the ECL-chemiluminescence signal, normalized for the loading control, measured by ImageJ and represented as a HDAC III to loading control ratio (C and D).

6.3.4.13.4. HDAC IV

HDAC IV was significantly up-regulated in treated cells (R+) (B) compared to parent cells ($p= 0.03$) and was significantly decreased ($p= 0.001$) when GDC-0980 was not contained in the medium (R-) (A). Shown also in this figure is a scatter plot representation of the ECL-chemiluminescence signal, measured by ImageJ and represented as triplicates per phenotype (C and D) (figure 60). HDAC I and PCNA proteins were used as a loading control when (R-) and (R+) were compared to the parent cells, respectively (refer to section 2.4.6.6).

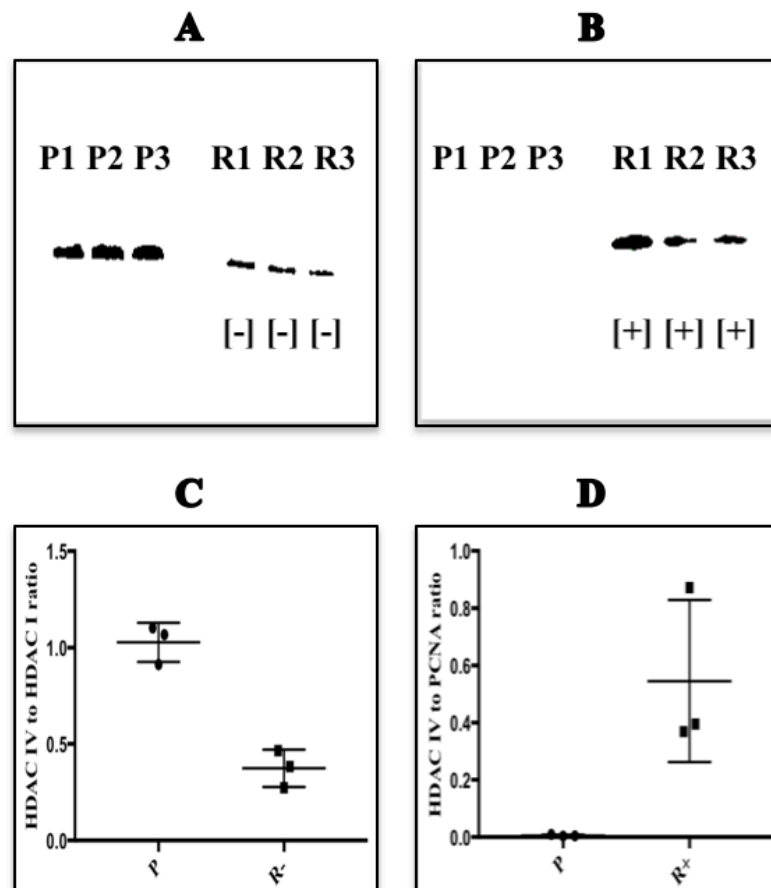


Figure 60: Comparison of histone deacetylase IV (HDAC IV) protein abundance levels in GDC-0980 sensitive parent (P) and resistant (R) H1975 adenocarcinoma cells. P1, P2, P3 and R1, R2, R3 represent triplicates of 20 μ g of cells lysate total protein. (-): resistant cells cultured without drug and (+): resistant cells cultured in 1 μ M GDC-0980. Shown also is a scatter plot of the ECL-chemiluminescence signal, normalized for the loading control, measured by ImageJ and represented as a HDAC IV to loading control ratio (C and D).

6.3.4.13.5. HDAC VI

HDAC VI was significantly up-regulated in the treated cells (R+) (B) compared to the parent cells with, p value of 0.0003, and was significantly decreased ($p=0.001$) when GDC-0980 was not contained in the medium (R-) (A). Shown in this figure also is a numeric representation of the ECL-chemiluminescence signal, measured by ImageJ and represented as triplicates per phenotype (C and D) (figure 61). HDAC I and PCNA proteins were used as a loading control when (R-) and (R+) were compared to the parent cells, respectively (refer to section 2.4.6.6).

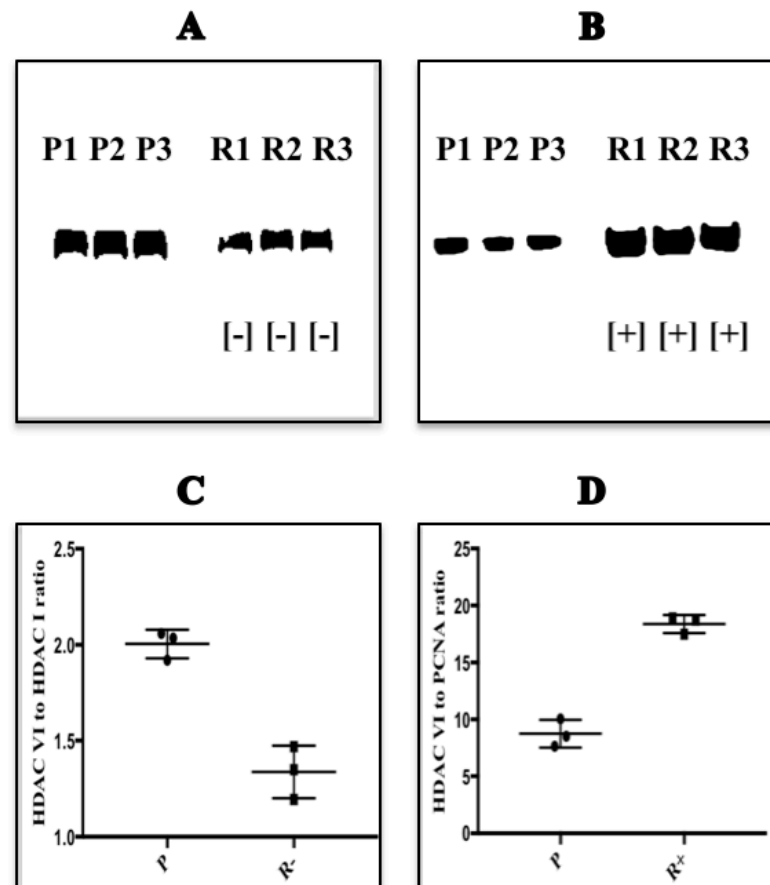


Figure 61: Comparison of histone deacetylase VI (HDAC VI) protein abundance levels in GDC-0980 sensitive parent (P) and resistant (R) H1975 adenocarcinoma cells. P1, P2, P3 and R1, R2, R3 represent triplicates of 20 μ g of cells lysate total protein. (-): resistant cells cultured without drug and (+): resistant cells cultured in 1 μ M GDC-0980. Shown also is a scatter plot of the ECL-chemiluminescence signal, normalized for the loading control, measured by ImageJ and represented as a HDAC VI to loading control ratio (C and D).

6.3.4.13.6. Phospho-HDAC 4,5

Phosphorylated HDAC 4,5 was significantly lowered in both treated cells (R+) (B) and non-treated cells (R-) (A) compared to parent cells. *P-values were < 0.0001* and 0.0003, respectively. Shown also in this figure is a numeric representation of the ECL-chemiluminescence signal, measured by ImageJ and represented as triplicates per phenotype (C and D) (figure 62). HDAC I and PCNA proteins were used as a loading control when (R-) and (R+) were compared to the parent cells, respectively (refer to section 2.4.6.6).

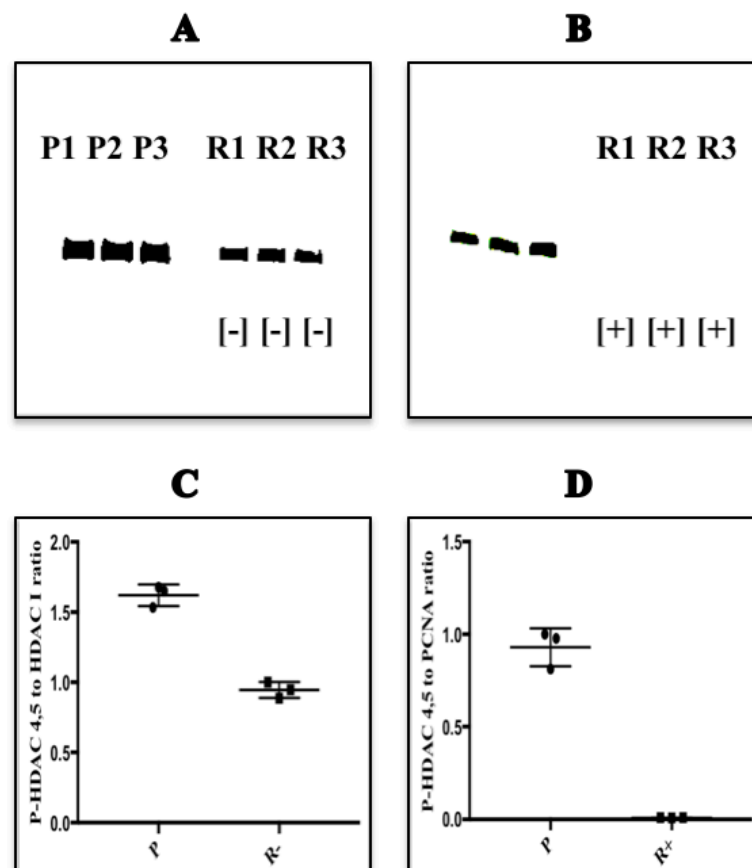


Figure 62: Comparison of phosphorylated HDACs IV and V (P- HDAC IV & V) protein abundance in GDC-0980 sensitive parent (P) and resistant (R) H1975 adenocarcinoma cells. P1, P2, P3 and R1, R2, R3 represent triplicates of 20 μg of cells lysate total protein. (-): resistant cells cultured without drug and (+): resistant cells cultured in 1 μM GDC-0980. Shown also is a scatter plot of the ECL-chemiluminescence signal, normalized for the loading control, measured by ImageJ and represented as a P-HDAC 4,5 to loading control ratio (C and D).

6.3.4.14. Histone acetylation

6.3.4.14.1. H1975 H3K9

The level of acetylated lysine-9 in Histone 3 (H3K9) was increased in the treated cells (R+) ($p = 0.18$) (B). Upon withdrawal of GDC-0980 from the medium (R-) (A), its level went back to below the parent cells, but without significance ($p = 0.3$). Shown in this figure also is a scatter plot representing the ECL-chemiluminescence signal correspondent to acetylation level, measured by ImageJ and represented as triplicates per phenotype (C and D) (figure 63). HDAC I and PCNA proteins were used as a loading control when (R-) and (R+) were compared to the parent cells, respectively (refer to section 2.4.6.6).

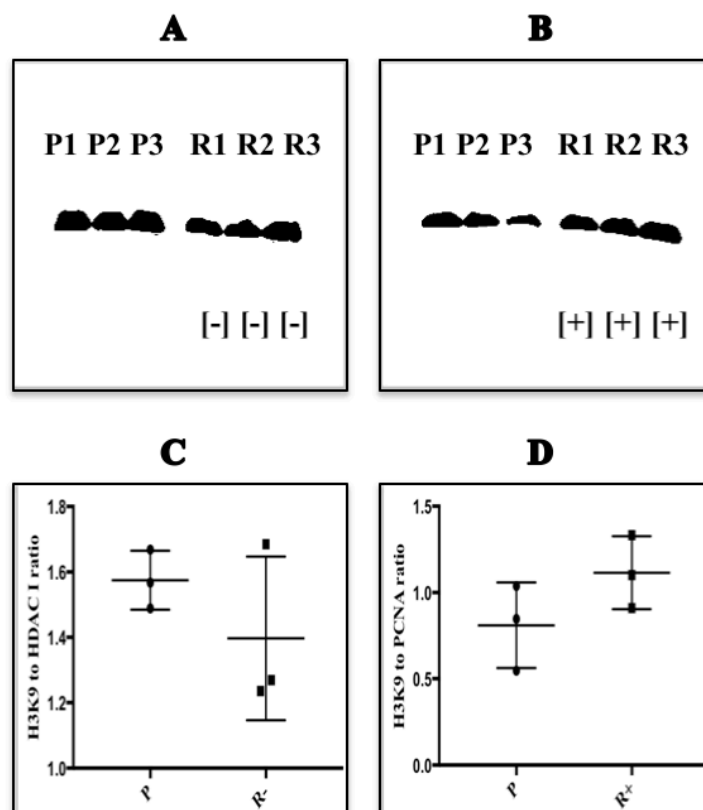


Figure 63: Comparison of acetylated levels of lysine 9 of histone 3 (H3) protein in GDC-0980 sensitive parent (P) and resistant (R) H1975 adenocarcinoma cells. P1, P2, P3 and R1, R2, R3 represent triplicates of 20 μ g of cells lysate total protein. (-): resistant cells cultured without drug and (+): resistant cells cultured in 1 μ M GDC-0980. Shown also is a scatter plot of the ECL-chemiluminescence signal, normalized for the loading control, measured by ImageJ and represented as a H3K9 to loading control ratio (C and D).

6.3.4.14.2. A549 H3K9

Acetylated lysine-9 in Histone 3 (H3K9) was significantly lowered in both treated (R+) (B) and non-treated cells (R-) (A) (both $p < 0.0001$). Shown in this figure also is a scatter plot representation of the ECL-chemiluminescence signal, measured by ImageJ and represented as triplicates per phenotype (C and D) (figure 64).

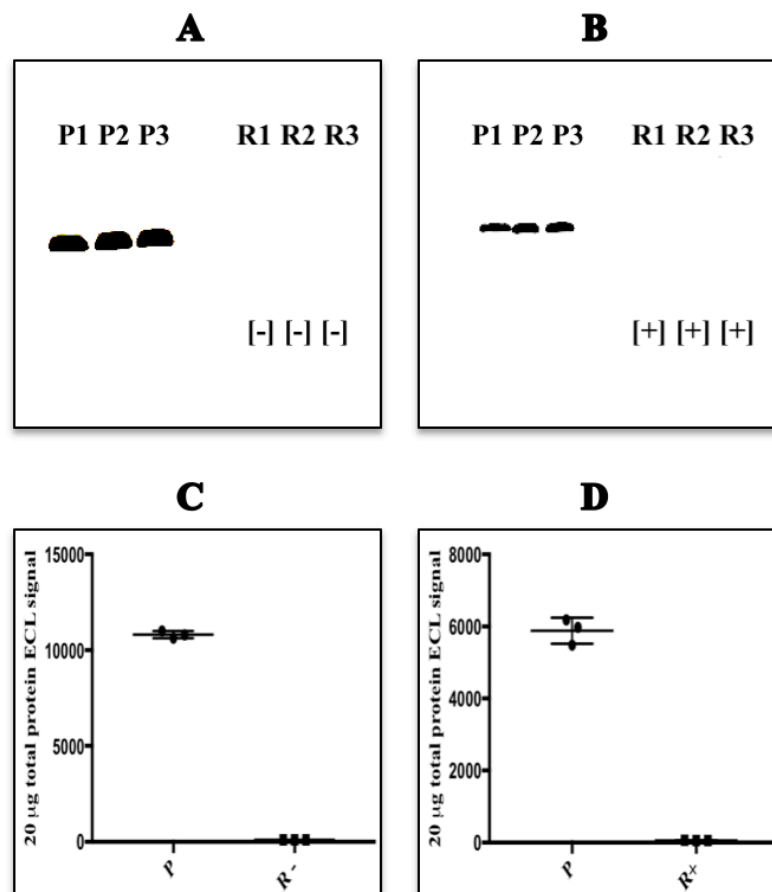


Figure 64: Comparison of acetylated lysine 9 of histone 3 (H3K9) protein abundance levels in GDC-0980 sensitive parent (P) and resistant (R) A549 adenocarcinoma cells. P1, P2, P3 and R1, R2, R3 represent triplicates of 20 μ g of cells lysate total protein. (-): resistant cells cultured without drug and (+): resistant cells cultured in F12 containing 3.34 μ M GDC-0980. Shown in this figure is a scatter plot representing the 20 μ g content of H3K9 measured by ImageJ and represented as triplicates per phenotype (C and D).

6.3.4.14.3. H1975 H3K18

Acetylated lysine-18 in Histone 3 (H3K18) was significantly increased in the treated cells (R+) (B) compared with the parent cells ($p=0.002$). When GDC-0980 was withdrawn from the medium (R-) (A), its level went back to below the parent cells but without significance ($p=0.5$). Shown in this figure also is a scatter plot representation of the ECL-chemiluminescence signal, measured by ImageJ and represented as triplicates per phenotype (C and D) (figure 65). HDAC I and PCNA proteins were used as a loading control when (R-) and (R+) were compared to the parent cells, respectively (refer to section 2.4.6.6).

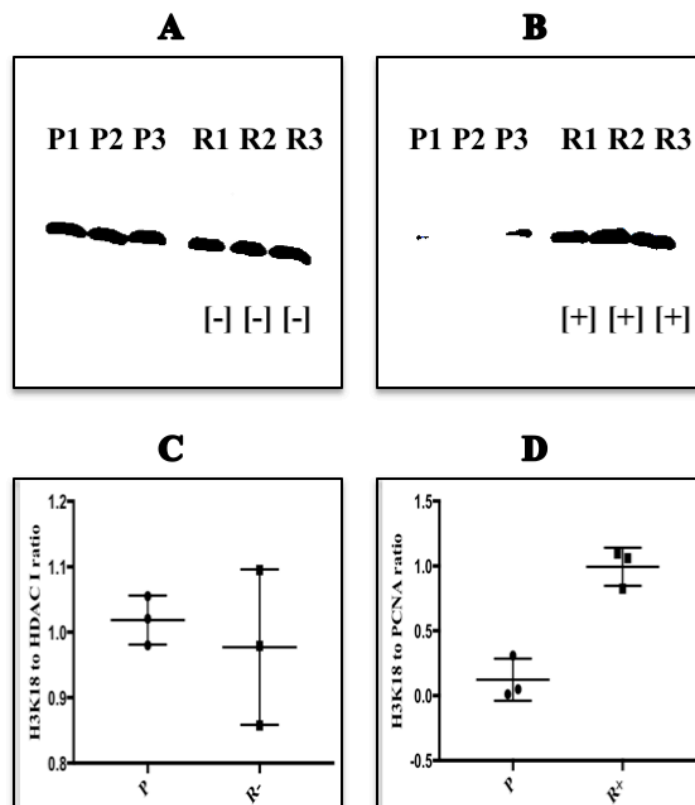


Figure 65: Comparison of acetylated lysine 18 of histone 3 (H3K18) protein abundance levels in GDC-0980 sensitive parent (P) and resistant (R) H1975 adenocarcinoma cells. P1, P2, P3 and R1, R2, R3 represent triplicates of 20 μ g of cells lysate total protein. (-): resistant cells cultured without drug and (+): resistant cells cultured in RPMI containing 1 μ M GDC-0980. Shown also is a scatter plot of the ECL-chemiluminescence signal, normalized for the loading control, measured by ImageJ and represented as a H3K18 to loading control ratio (C and D).

6.3.4.14.4. A549 H3K18

The level of acetylation of H3K18 was significantly lowered in both treated (R+) (B) and non-treated (R-) A549 cells (A) ($p < 0.0001$ in both cases). Shown also is a scatter plot representation of the ECL-chemiluminescence signal, measured by ImageJ and represented as triplicates per phenotype (C and D) (Figure 66).

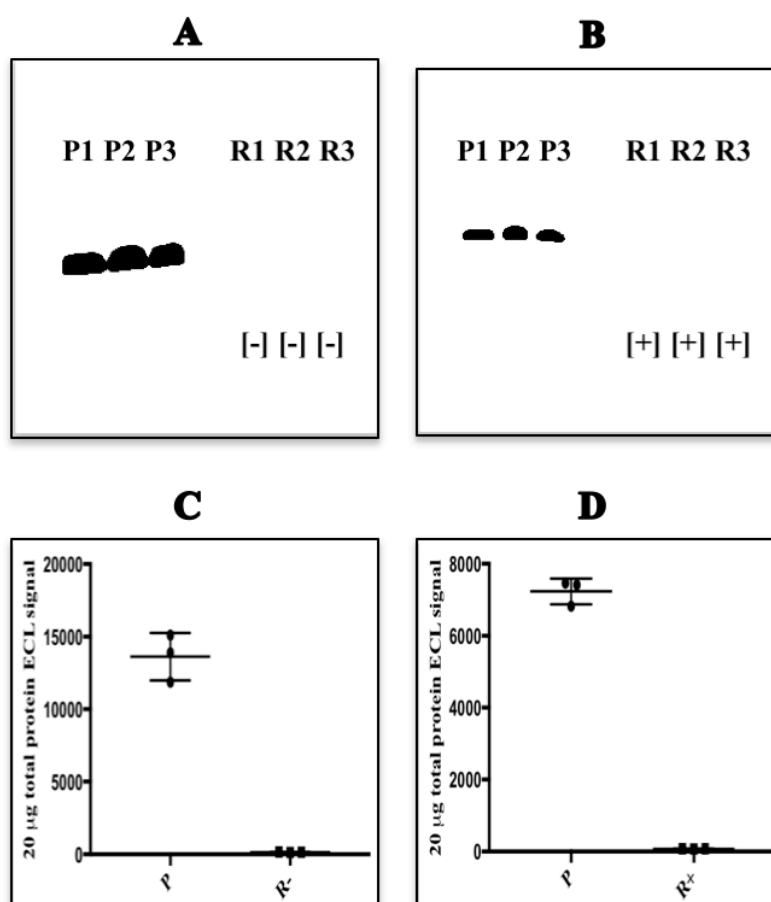


Figure 66: Comparison of acetylated lysine 18 of histone 3 (H3K18) protein abundance levels in GDC-0980 sensitive parent (P) and resistant (R) A549 adenocarcinoma cells. P1, P2, P3 and R1, R2, R3 represent triplicates of 20 μg of cells lysate total protein. (-): resistant cells cultured without drug and (+): resistant cells cultured in F12 containing 3.34 μM GDC-0980. Shown in this figure is a scatter plot representing the 20 μg content of H3K18 measured by ImageJ and represented as triplicates per phenotype (C and D).

6.3.4.14.5. H1975 H3K27

Acetylated lysine-27 in Histone 3 (H3K27) was increased in treated cells (R+) ($p=0.17$) (B). Upon withdrawal of GDC-0980 from the medium (R-) (A), its level went back to below the parent cells but without significance ($p=0.2$). Shown also is a scatter representation of the ECL-chemiluminescence signal, measured by ImageJ and represented as triplicates per phenotype (C and D) (figure 67). HDAC I and PCNA proteins were used as a loading control when (R-) and (R+) were compared to the parent cells, respectively (refer to section 2.4.6.6).

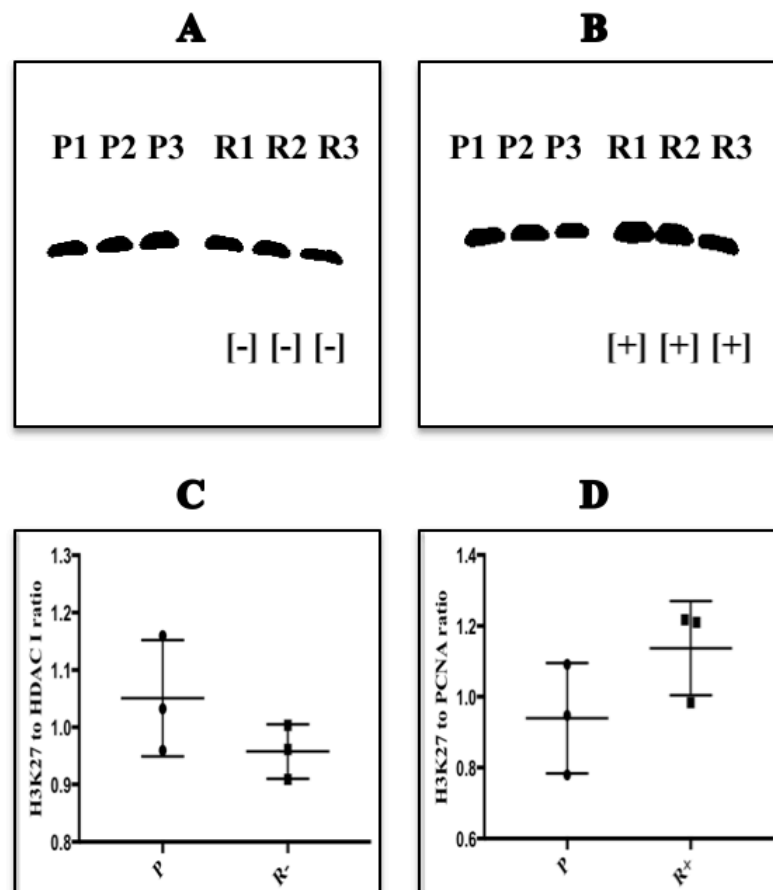


Figure 67: Comparison of acetylated lysine 27 of histone 3 (H3K27) protein abundance levels in GDC-0980 sensitive parent (P) and resistant (R) H1975 adenocarcinoma cells. P1, P2, P3 and R1, R2, R3 represent triplicates of 20 μ g of cells lysate total protein. (-): resistant cells cultured without drug and (+): resistant cells cultured in RPMI containing 1 μ M GDC-0980. Shown also is a scatter plot of the ECL-chemiluminescence signal, normalized for the loading control, measured by ImageJ and represented as a H3K27 to loading control ratio (C and D).

6.3.4.14.6. H1975 histone 4

Histone 4 (H4) was significantly upregulated in GDC-0980 resistant H1975 cells in both treated (R+) (B) and non-treated (R-) cells (A) compared to the parent cells (both $p < 0.0001$). Shown also is a scatter plot representation of the ECL chemiluminescence signal, measured by ImageJ and represented as triplicates per phenotype (C and D) (figure 68). HDAC I and PCNA proteins were used as a loading control when (R-) and (R+) were compared to the parent cells, respectively (refer to section 2.4.6.6).

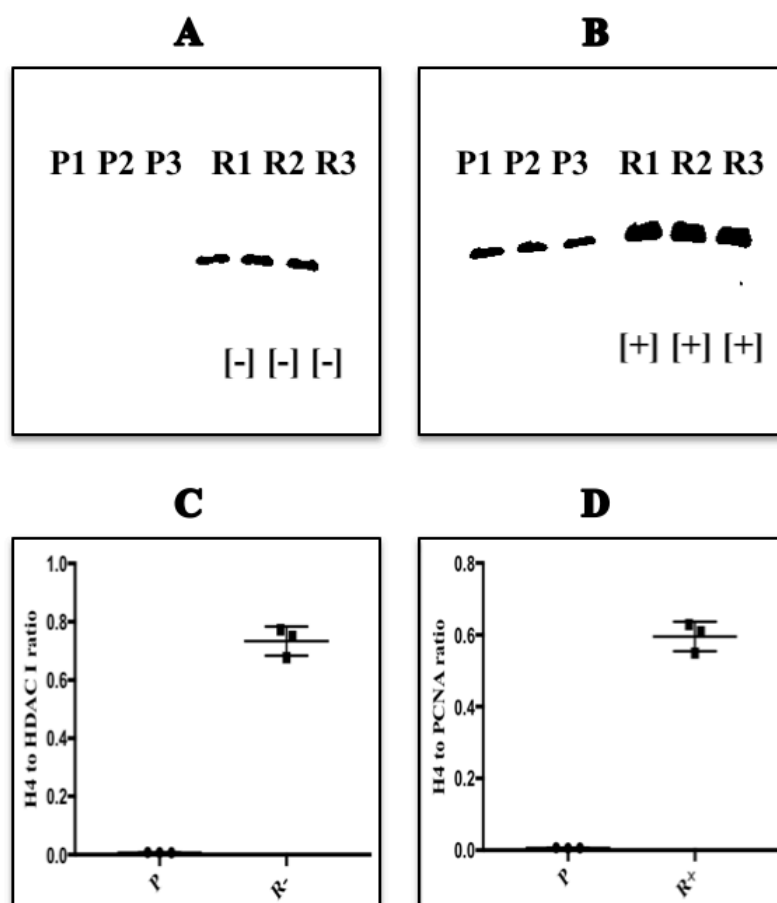


Figure 68: Comparison of histone 4 protein abundance in GDC-0980 sensitive parent (P) and resistant (R) H1975 adenocarcinoma cells. P1, P2, P3 and R1, R2, R3 represent triplicates of 20 μ g of total cell protein. (-): resistant cells cultured without drug and (+): resistant cells cultured in RPMI containing 1 μ M GDC-0980. Shown also is a scatter plot of the ECL-chemiluminescence signal, normalized for the loading control, measured by ImageJ and represented as a H4 to loading control ratio (C and D).

6.3.4.14.7. H1975 H4K5

The level of histone 4 acetylation at lysine 5 (H4K5) was significantly increased in GDC-0980 treated resistant H1975 cells (R+) compared to parent cells (B) ($p=0.0001$). H4K5 levels decreased when the cells passaged in the absence of the drug (R-) (A) ($p=0.42$). Shown in this figure also is a scatter plot representation of the ECL-chemiluminescence signal, measured by ImageJ and represented as triplicates per phenotype (C and D) (figure 69). HDAC I and PCNA proteins were used as a loading control when (R-) and (R+) were compared to the parent cells, respectively (refer to section 2.4.6.6).

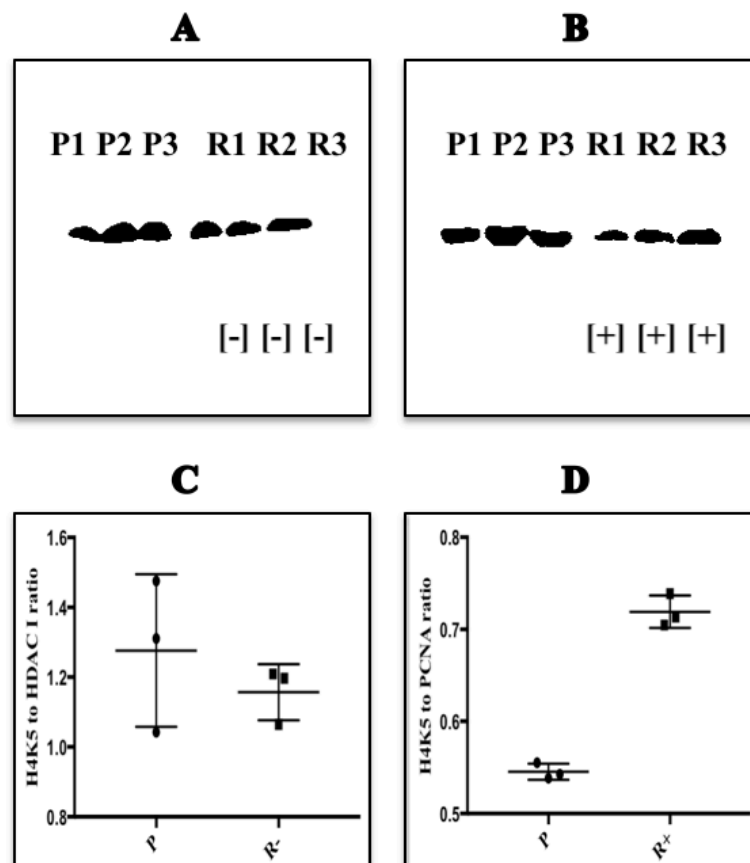


Figure 69: Comparison of acetylated lysine 5 of histone 4 (H4K5) protein abundance levels in GDC-0980 sensitive parent (P) and resistant (R) H1975 adenocarcinoma cells. P1, P2, P3 and R1, R2, R3 represent triplicates of 20 μ g of cells lysate total protein. (-): resistant cells cultured without drug and (+): resistant cells cultured in RPMI containing 1 μ M GDC-0980. Shown also is a scatter plot of the ECL-chemiluminescence signal, normalized for the loading control, measured by ImageJ and represented as a H4K5 to loading control ratio (C and D).

6.3.4.15. GDC-0980 dose-response curve for parent and resistant H1975 cells

Shown in figure 70 are cytotoxicity graph plots shifted to the right in resistant cells compared to sensitive cells. The calculated IC₅₀ values were 1.79 and 16.59 nM for the parent and resistant H1975 cells, respectively.

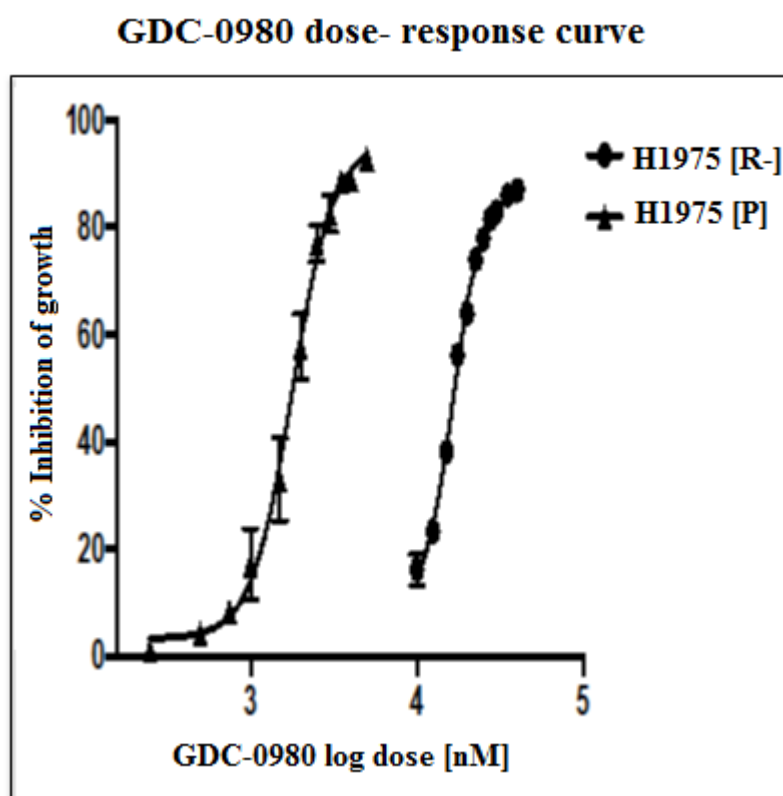


Figure 70: Dose-response curve of GDC-0980 for GDC-0980 resistant [R-] and parent [P] H1975 lung adenocarcinoma cells.

6.3.4.16. SAHA dose-response curve for H1975 parent and resistant cells

Shown in figure 71 is the cytotoxicity dose-response curve of SAHA HDAC inhibitor for the GDC-0980 sensitive parental cells (middle), GDC-0980 resistant cells (R-) (right), and GDC-0980 resistant cells pre-incubated with 1 μ M GDC-0980 (left). The calculated IC₅₀s were 5.2, 8.08 and 4.34 nM in the parent, resistant (R-) and resistant (R+) cells, respectively.

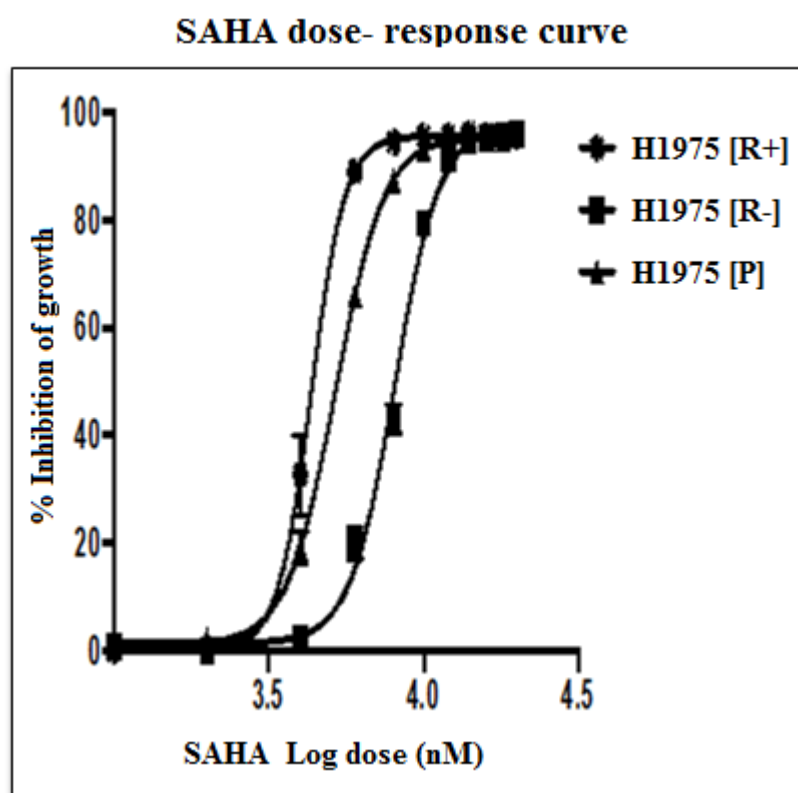


Figure 71: SAHA dose response curve represented as percent inhibition of growth vs the log dose of SAHA. The cells were tested were H1975 GDC-0980 parent, H1975 GDC-0980 resistant cells (R-) and GDC-0980 resistant cells in the presence of 1 μ M GDC-0980 (R+).

Table 51: Western blot assessment of proteins affecting the cell cycle

Protein	P V R-	P-value	P V R+	P-value
Cyclin D1	Down	0.0003	Down	0.001
Cyclin A2	Down	0.001	Down	0.0007
Cyclin B1	Down	0.002	Down	0.0009
Cyclin H	Down	0.07	Down	0.001
CDK6	Down	0.0007	Down	0.005
P21	Down	<0.0001	Down	<0.0001
Rel-B	Down	0.03	Down	0.0008
14.3.3 γ	Down	0.01	Down	0.01
P53	Up	<0.0001	Up	0.0004
BCL-XL	Up	0.0001	Up	0.01
P50	Up	0.004	Up	0.01
Rel-A	S-Up	0.14	S-Up	0.15
Cyclin D3	S-Up	0.2	S-Up	0.26
PCNA	Down	0.01	No change	>0.999
BAX	Down	0.0006	No change	0.51
c-Rel	Down	0.01	S-down	0.1
P105	Up	0.001	No change	0.8
14.3.3 α/β	Up	0.001	Down	<0.0001
14.3.3 ξ/δ	Up	0.002	Down	0.004
14.3.3 ϵ	Up	0.001	Down	0.0001
Ub-PCNA	No change	0.29	Down	0.004

Abundance analysis: S-Up: small increase in the protein abundance, S-down: small decrease in the protein abundance.

Table 52: Western blot analysis of HAT/HDAC and histone acetylation of GDC-0980 resistant H1975 (treated and non-treated) cells compared to the sensitive parent cells.

Protein	P v R-	P-value	P v R+	P-value
A549 H3	Down	0.01	Down	0.003
A549 H3K9	Down	<0.0001	Down	<0.0001
A549 H3K18	Down	0.002	Down	0.5
H1975 P-HDAC 4,5	S-Down	0.0003	Down	<0.0001
HDAC II	Up	0.09	Up	0.01
H1975 H3	S-Up	0.08	S-Up	0.08
H1975 H4	Up	<0.0001	Up	<0.0001
HDACIV	Down	0.001	Up	0.03
HDAC VI	Down	0.001	Up	0.0003
H1975 H3K9	S- Down	0.3	T-Up	0.18
GCN5L2	Up	0.0004	Down	0.003
PCAF	Up	0.0007	Down	<0.0001
H1975 H3K18	Un changed	0.59	Up	0.002
H1975 H3K27	Un changed	0.22	Up	0.17
H1975 H4K5	Un changed	0.42	Up	0.0001
HDAC I	Un changed	>0.999	Up	0.0002
HDAC III	Un changed	0.21	Up	0.0003

Abundance analysis: S-Down: small decrease in the protein abundance, T- Up: tends to rise as it was at low abundance before drug incubation, T-down: tends to decrease as it was higher during drug incubation.

Figure 72 shows the cell cycle KEGG pathway analysis of the proteins detected by LC-MS/MS significantly upregulated in both treated (R+) and non-treated (R-) GDC-0980 resistant H1975 cells compared to parent cells (cut-off value: 1.2-fold increase).

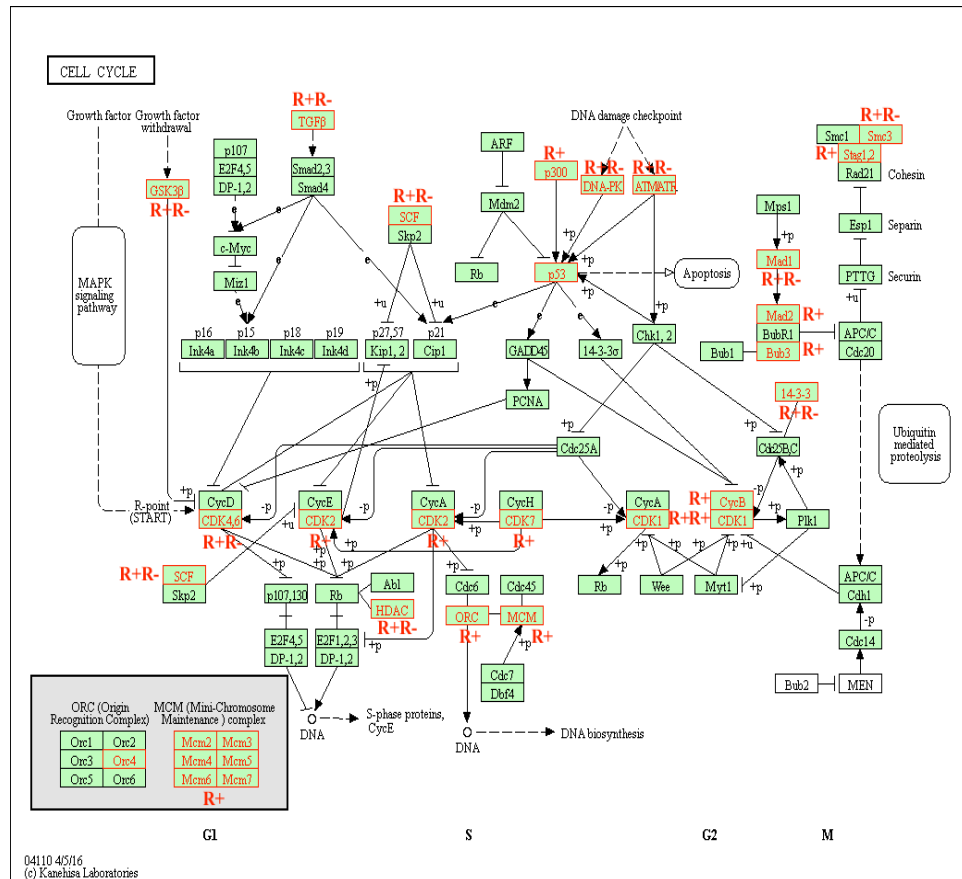


Figure 72: KEGG pathway analysis of the proteins found upregulated in the GDC-0980 resistant cells compared to the parent cells in both treated (R+) and non-treated (R-) cells. Proteins with red letters were significantly upregulated in R+ or/and R-, Smc3: structural maintenance of chromosome 1, Stag 1,2: stromal antigen 1,2, MCM: minichromosome maintenance complex, CDK: cyclin dependent kinase, HDAC: histone deacetylase, ORC: origin recognition complex, Bub3: budding uninhibited by benzimidazoles 3 (mitotic check point, ATM: ataxia telangiectasia mutated (serine/threonine kinase), SCF: stem cell factor, TGFβ: tumour growth factor, GSK: glycogen synthase kinase, ATR: ataxia telangiectasia and Rad3-related protein.

Figure 73 shows the cell cycle KEGG pathway analysis of the proteins detected by LC-MS/MS significantly down regulated in both treated (R+) and non-treated (R-) GDC-0980 resistant H1975 cells compared to parent cells (cut-off value: 1.2-fold decrease).

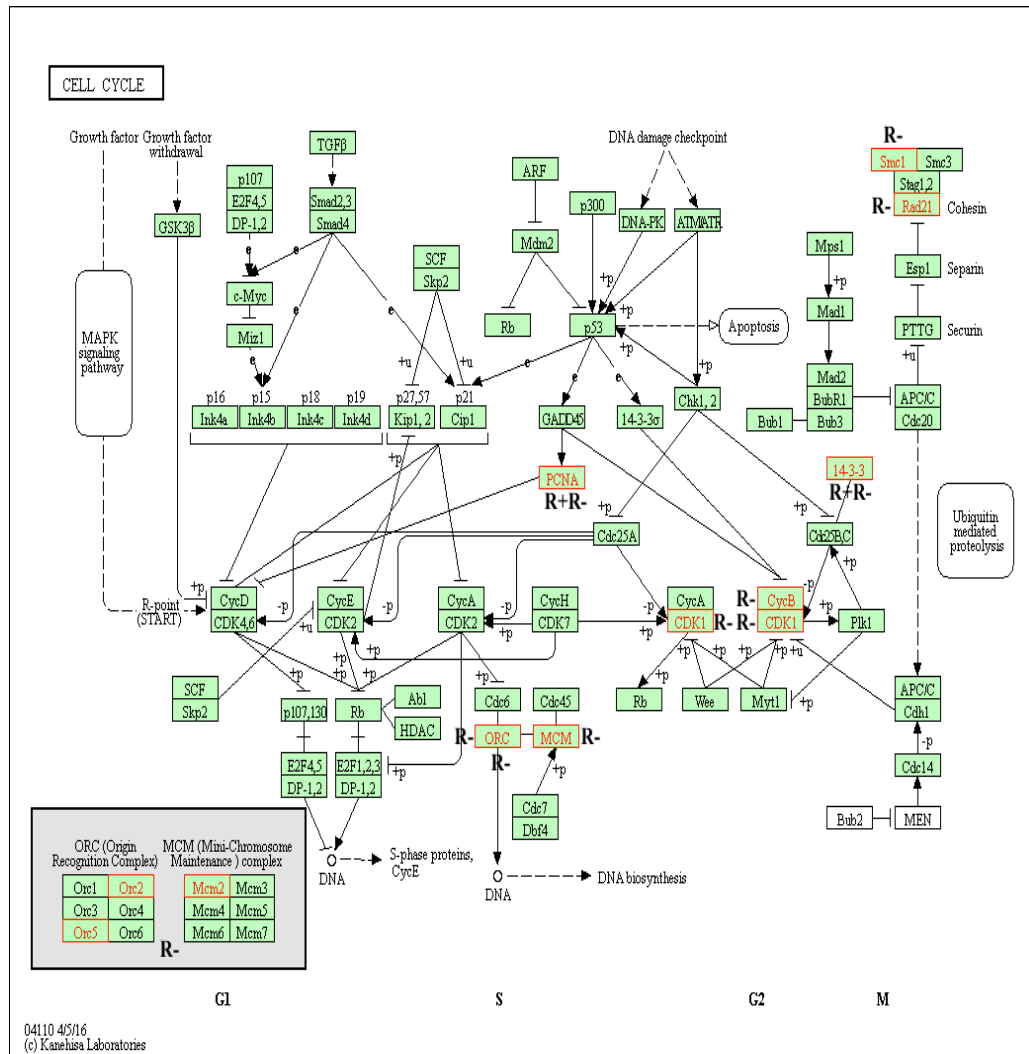


Figure 73: KEGG pathway analysis of cell cycle proteins. Red protein names were found downregulated in the GDC-0980 resistant cells compared to the parent cells in both treated (R+) and non-treated (R-) cells. **Bold** R+/R- denote proteins were found down-regulated in the resistant cells (treated and non-treated). PCNA: proliferating cell nuclear antigen, Smc1: structural maintenance of chromosome 1, CDK: cyclin dependent kinase1, MCM: minichromosome maintenance protein complex, Orc: origin recognition complex, CycB: cyclin B, 14.3.3: protein kinase C inhibitor protein.

6.4. Discussion

The GDC-0980 resistant A549 and H1975 lung adenocarcinoma cells used in this experiment were maintained at all times in F12 medium containing 3.34 μM or RPMI containing 1 μM GDC-0980, respectively, unless stored frozen. The cell cycle profile of GDC-0980-resistant cells in the two cell lines was completely different from their parent sensitive cells (Figure 28). The cell cycle profile of GDC-0980 sensitive A549 was 46.1% in G1, 43.26% in S and 10.6 in G2/M phase (Figure 28: A549P). In contrast, the cell cycle profile of the GDC-0980 resistant A549 cells passaged in F12 medium containing 3.34 μM GDC-0980 (R+) was 74.1% in G1 phase, 23.5% in S phase and 2.3% in G2/M phase (Figure 28: A549R+). After five consecutive passages of 3 days each in GDC-0980 free medium, the cell cycle profile changed and approached that of parent cells, where the percentage of the cells in G1 phase went down to 56.8%, in S-phase increased to 36.2%, and in G2/M phase reached 7% (Figure 28). GDC-0980 was found to cause the cells to accumulate in G1 phase (Figure 29: A549 G1-phase) ($p < 0.0001$), leading to fewer cells entering S ($p < 0.0001$) and G2/M phases ($p < 0.0001$) (Figure 29: A549 S-phase). Upon eliminating the drug effect, the percentage of cells in S ($p < 0.0001$) and G2/M ($p < 0.0001$) phases improved and more cells started to leave G1 phase ($p < 0.0001$) (Figure 29: G2/M phases). These findings indicate that GDC-0980 causes cell cycle arrest in G1 phase in GDC-0980 resistant A549 cells. However, inhibition of the PI3K signalling pathway in tumour cells with the small molecule ZSTK474 caused cell cycle arrest in G0/G1 phase (Dan et al., 2009). GDC-0980, a PI3K-mTOR dual inhibitor, has been reported to cause G1 cell cycle arrest in many cell lines, including A549 lung adenocarcinoma cells (Wallin et al., 2011). Cell cycle arrest was confirmed by comparing the levels

of histone 3 in the parent and resistant cells in (R+) and out (R-) of the drug incubation (Figure 30).

In this research work, mass spectrometry analysis of GDC-0980 resistant H1975 (growing in RPMI medium containing 1 μ M GDC-0980) (R+) compared to the sensitive parent cells (P) showed a significant upregulation (Table 47) and dysregulation (Table 49) of some proteins known to have a role in cell cycle control, such as Cyclin-dependent kinases (CDKs), Histone deacetylases (HDACs), P53, and check point controlling proteins (Figures 72 and 73). When non-treated GDC-0980 resistant cells were compared to the parent cells (P), some proteins were also found differentially expressed (Tables 48, 50). LC-MS/MS detected proteins differentially expressed between the different conditions in addition to other proteins controlling the cell cycle, which were assessed by western blot (Figures 35-69). Some comparisons matched the mass spectrometry findings (table 51).

Using a cell cycle imaging system (Cytell®), GDC-0980 was also found to cause cell cycle arrest in G2/M ($p < 0.0001$) phases and prolongation of the lag time of S phase ($p < 0.0001$) (Figure 29: H1975 S & G2/M phases). The cell cycle profile pattern in GDC-0980 sensitive H1975 cells was 52.5% G1 phase, 36.2% S phase and 11.3 G2/M phase (Figure 28: H1975P). In the presence of 1 μ M GDC-0980, the cell cycle profile of GDC-0980 resistant H1975 cells showed only 10.7% in G1 phase. In contrast, 66.7% and 22.7% of the cells accumulated in phases S ($p < 0.0001$) and G2/M ($p < 0.0001$), respectively (Figure 28: H1975R+). Clearing GDC-0980 from the culture media (15 days) had no significant effect on the cell cycle profile of GDC-0980 resistant cells (Figure 29) [H1975 G0/G1 ($p = 0.5$), S ($p = 0.19$) and G2/M ($p = 0.27$) phases]. The increased accumulation of 4N-containing cells (G2/M) was confirmed by measurement of histone 3 levels in the parent, resistant [R+] and

resistant [R-] cells. The western blot revealed increased levels of histone 3 (Figure 31). This step was followed by histone co-localization using confocal microscopy, which confirmed localization of histone 3 to the nucleus (Figures 32-34).

Moreover, the increased proliferation rate in cancer results from the increased cellular signalling and cross talk caused by gain of function or gene amplification mutations, accompanied by impairment of the balance between oncogenes and tumour suppressant genes. The overall downstream signalling events result in increased phosphorylation rates, which require abundance of adenosine triphosphate (ATP). Therefore, cell cycle controlling pathways have become a hot research area for the development of cancer treatment (Schafer, 1998).

It is well known that the cell cycle is controlled by enzymes called cyclin-dependent kinases (CDKs), activation of which involves their binding to cyclins, whereby the ATP-binding domains become unmasked and are subsequently phosphorylated by CDK-activating kinases (CAK) (Lolli and Johnson, 2005) (figure 74).

Cyclins are cell cycle specific proteins. Cyclins D1, 2, 3 and cyclin E are involved at early stages (G1 and transition from G1/S phase). Cyclins A and B are required at the G2/M transition phase (Viallard et al., 2001). Cyclin- D1 binds and activates CDK4/6, which in turn phosphorylates and inhibits retinoblastoma protein (pRb), which binds and represses E2F transcription factor, needed for transcription of other cyclins and progression of the cell cycle (Ravitz and Wenner, 1997). Inhibition of AKT/PKB phosphorylation by GDC-0980 interferes with CAK activation and progression of the cell cycle.

Cyclin D1 is a proto-oncogene cell cycle protein (Bates and Peters, 1995), and its increased expression has been observed in many cancers (Alao, 2007). Cyclin D1 abundance was found reduced in advanced cancers such as colorectal, breast and

lung squamous cell carcinoma (Li et al., 2010a). Such down regulation was found associated with poor prognosis and increased metastasis and invasion (Lehn et al., 2010). On the other hand, overexpression of cyclin D1 had a proliferation effect and was associated with resistance to chemotherapy (Biliran et al., 2005). Tyrosine kinase inhibitors (TKI) were found to decrease the expression of cyclin D1, D3 and E2 (Petty et al., 2004, Phuchareon et al., 2015). In this study, cyclin D1 was found significantly downregulated in both GDC-0980-treated [R+] H1975 cells ($p= 0.001$) and non-treated [R-] cells ($p= 0.0003$) (Figure 35). Cyclin D3 was found slightly upregulated in both treated [R+] ($p= 0.26$) and non-treated ($p= 0.2$) H1975 cells (Figure 36). Cyclin D3 is also a proto-oncogene, and increases in its levels denote increased tumour aggression and metastasis (Wang et al., 2017a). Overexpression of cyclin D3 was found to indicate erlotinib resistance in aerodigestive tract cancer (Petty et al., 2011).

Cyclin-dependent kinase 6 (CDK6) functions at stage G1 of the cell cycle (Figure 74). Low levels of CDK6 were found to slow the rate of cell proliferation in cancer (Laurenti et al., 2015). In this study, the level of CDK6 was significantly low in the GDC-0980 resistant H1975 cells compared to the sensitive cells in both treated ($p= 0.005$) and non-treated conditions ($p= 0.0007$) (Figure 40). The growth curve showed that GDC-0980 treated cells tended to grow very slowly compared to the parent cells. On the other hand, when the cells were grown in GDC-0980 free medium, they started to proliferate at higher rates and became more aggressive than the parent cells (Figure 27). GDC-0980 inhibits PI3K/mTOR downstream signalling controlling a broad range of transcription factors responsible for cell growth and proliferation. So, diminished phosphorylation by GDC-0980 might be the main reason of slow proliferation in the treated cells rather than the abundance of the

cyclins; cyclin D3 is more important than cyclin D1 for cell progression from G1 to S phase in H1975 lung adenocarcinoma cells (Figure 74).

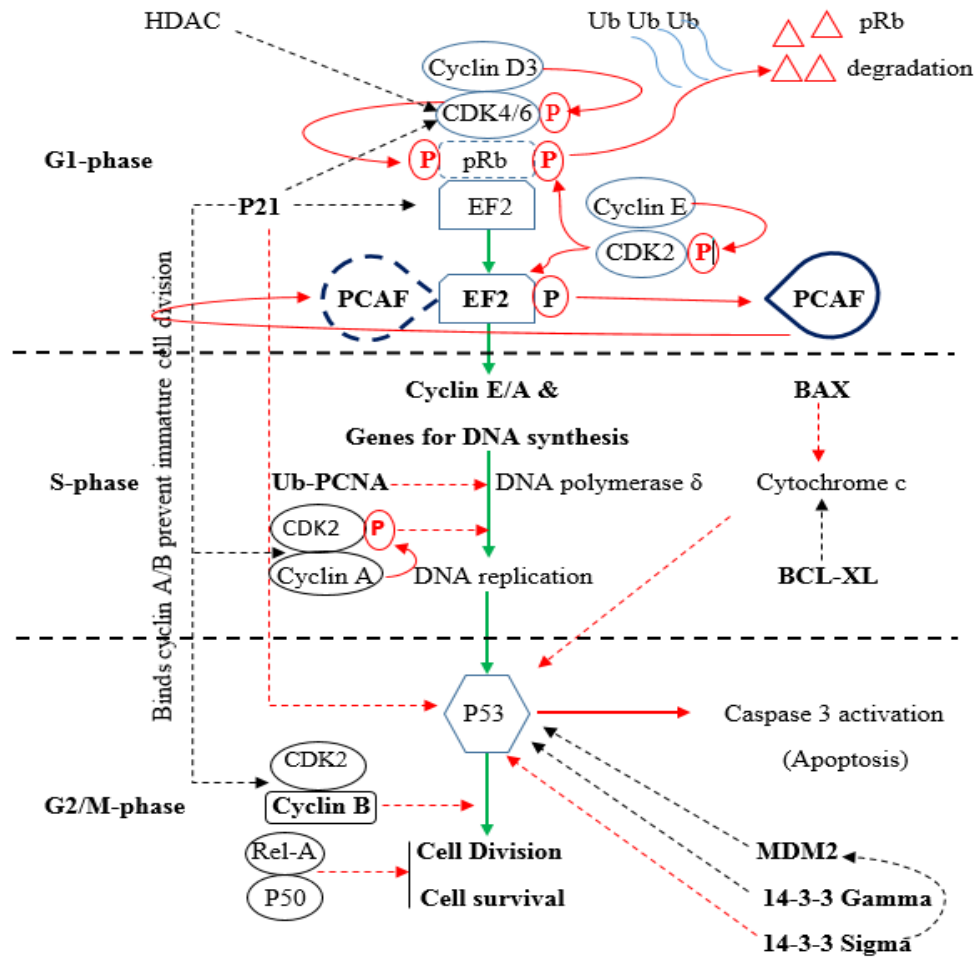


Figure 74: Summary of experimental findings of cell cycle control proteins in H1975 cells. Cell cycle progression (green arrows), proteins favouring the effect of other proteins (red interrupted arrows), proteins interfering with the function of other proteins (black interrupted arrows), consequence of findings (red arrows).

Cyclin E is an oncogenic cell cycle modulating protein required for G1/S transition. Its expression starts to increase at late G1 phase and starts to decline at late S-phase, which explains its role in G1/S-phase (DNA synthesis) transition (Mazumder et al., 2004). Cyclin A is also an oncogenic cell cycle protein functioning to bind, phosphorylate and activate CDK1/2, leading to downstream activation of DNA

synthesis. Cyclin A was found overexpressed in cancer, and such an increase was found associated with increased cancer progression, metastasis and poor prognosis in breast cancer (Baldini et al., 2006, Gray-Bablin et al., 1996) and colorectal cancer (Li et al., 2002). Cyclin A elevation was also used as a marker associated with poor prognosis and low survival rates in non-small cell lung cancer (Mishina et al., 2000). In the GDC-0980 resistant cells, both treated ($p= 0.0007$) and non-treated ($p= 0.001$) resistant cells showed a significant decrease in the level of cyclin A2 (Figure 37). This might explain their prolonged S phase lag time compared to the parent cells. Cyclin B1 and CDK1 together are known as the M phase-promoting factor, which regulates cell entry into M phase (Hunt, 1989). Overexpression of cyclin B1 has been demonstrated in many cancers, including colorectal and non-small cell lung cancer, and they too were found associated with poor prognosis (Wang et al., 1997, Suzuki et al., 2007, Soria et al., 2000). In the current study, cyclin B1 was significantly down-regulated in both treated (R+) and non-treated (R-) GDC-0980 resistant cells compared to the parent cells ($p= 0.009$ and 0.002 , respectively) (Figure 38). Cyclin H is required for cell proliferation, and its overexpression was found elevated in breast cancer (Patel et al., 2016). In this study, Cyclin H was also found decreased in both conditions of the resistant H1975 cells, whether treated ($p= 0.001$) or non-treated ($p= 0.07$) (Figure 39). Cyclins D1, A, B1 and H were all found significantly decreased in the treated and non-treated GDC-0980 resistant H1975 cells. Therefore, these cyclins might be good biomarkers for immunohistochemical monitoring of potential development of tumour resistance to GDC-0980 in lung cancer.

However, after completion of DNA synthesis in S phase, the tumour suppressor gene P53 and its inhibitor the murine double minute 2 (MDM2) play a crucial role in DNA repair and cell cycle progression. MDM2 is negatively regulated by a series of

proteins, such as P21 and 14-3-3 (Reynisdóttir et al., 1995, Viillard et al., 2001, Levkau et al., 1998).

The P53 family, including P53, P63 and P73 isoforms, is composed of pro-apoptotic tumour suppressor transcription factors localised mainly in the cytoplasm and accounting for the main operator responsible for activation of DNA repair and cell cycle arrest (Uramoto et al., 2006). In P53 wild-type cells, any abnormalities (damage) to DNA discovered at the G2/M cell cycle checkpoint leads to cell cycle arrest and activation of the DNA repair machinery by activation of the P53-dependent pathway: failure to do so favours the induction of cell death (Ozaki and Nakagawara, 2011, Sionov and Haupt, 1999). P53 in healthy cells is inactivated by binding to MDM2, an ubiquitin ligase oncogenic enzyme, which keeps its abundance low (Nag et al., 2013). Upon DNA damage, phosphorylation and dissociation of P53 from its partner suppressor (MDM2) leads to increased transcription of cell cycle arrest proteins as well as proteins involved in DNA repair (Piette et al., 1997). The tumour suppressor activity of P53 is favoured when it interacts with some regulatory proteins, such as 14-3-3 sigma, which competes with and inhibits MDM2 binding (Yang et al., 2003). 14-3-3 directly binds and stabilises P53, leading to additive tumour suppressant activities and counteracting the tumorigenic effect of BCL-XL by increasing the P53 mediated increase in BAX expression (Samuels-Lev et al., 2001). P53 activation is inhibited when P53 binds to another regulatory protein called the mediator of DNA damage check point 1 protein (MDC1). When MDC1 binds to P53, it protects it from being phosphorylated by ATM kinase, thus protecting the cell from apoptosis giving DNA repair a chance. Later, when the machinery fails to do so, the complex dissociates, leading to phosphorylation of P53 and induction of apoptosis (Nakanishi et al., 2007). P53 also binds to RUNX3, improving its

transcription performance (Yamada et al., 2010) and increasing P53- mediated P21 transcription (Ozaki and Nakagawara, 2011).

In clinical proteomics, P53 was found overexpressed in cancers of liver (Gillet et al., 2000), head and neck (Watling et al., 1992, Field et al., 1992, Edström et al., 2001), and breast (Davidoff et al., 1991). In lung cancer, P53 abundance was found significantly increased in more than 50% of squamous cell carcinoma and more than 25% in adenocarcinoma (n = 132) (Uramoto et al., 2006). If these findings are normalised for the approximate percentage of mutated P53 in cancer (50%) (Higashitsuji et al., 2007), that would support and confirm P53 loss-of-function as a positive driving force to increase its expression (Blagosklonny, 1997, Higashitsuji et al., 2007). P53 abundance was found significantly overexpressed in both treated (R+) ($p = 0.0004$) and non-treated (R-) ($p < 0.0001$) resistant cells (Figure 41). In H1975 cells used in this study, P53 gene is mutated and its abundance is expected to be elevated. The use of GDC-0980 to interfere with P53 function by upstream inhibition of ATM phosphorylation would lead to induction of P53 expression. The increased level of P53 in GDC-0980 resistant cells in both experimental conditions (R+, R-) might be used as a marker for immunohistochemical detection of tumour resistance to GDC-0980 and to tyrosine kinase inhibitors that target the PI3K/AKT pathway.

The 14-3-3 Protein family consists of phosphoserine/threonine binding proteins that do not possess catalytic subunits that can modify other proteins but can bind and regulate more than 100 phosphorylated proteins (Dougherty and Morrison, 2004) controlling several cellular signalling pathways, including DNA replication, cell cycle, cell growth, apoptosis, proliferation and migration. 14-3-3, sometimes called adaptor proteins, has seven isoforms, including alpha, beta, gamma, sigma, epsilon, zeta and theta. They exist in the cytosol and are exported to play roles in the

extracellular regulation of other proteins involved in several cell communication processes (Kaplan et al., 2017). Theta, sigma and zeta were found to differ in abundance from one tissue to another, meaning that each single isoform has distinct tissue-specific functions (Qi et al., 2005). Studies based on immunohistochemistry and western blot analysis have revealed that all 14-3-3 isoforms, except epsilon and zeta, are found 11 ± 3 times more abundant in lung cancer than in normal lung tissues, and this elevation was confirmed by RT-PCR (Qi et al., 2005).

In all studies, 14-3-3 was claimed to be involved in tumorigenesis and therefore can be used as a marker to diagnose and monitor lung cancer (Marx et al., 2016). 14-3-3 zeta/delta overexpression was found involved in resistance to cisplatin, as its lowered expression was found associated with improved cisplatin-induced inhibition of cell proliferation in A549 lung adenocarcinoma cells (Fan et al., 2007). 14-3-3 zeta/delta was found significantly ($p = 0.004$) down-regulated in GDC-0980 resistant H1975 cells when cultured in the presence of $1\mu\text{M}$ GDC-0980 (R+) and significantly elevated ($p = 0.002$) in the non-treated cells (R-) (Figure 42).

14-3-3 sigma is an epithelial cell-specific isoform found down-regulated in most human carcinomas, including primary bladder, gastric, head and neck tumours (Dellambra et al., 2000, Vellucci et al., 1995, Ostergaard et al., 1997, Suzuki et al., 2000) and was undetectable in most breast, stomach and liver carcinomas (Ferguson et al., 2000, Suzuki et al., 2000, Iwata et al., 2000). 14-3-3 sigma has tumour suppressant activity through its positive regulation of P53-mediated apoptosis (Figure 73) (Yang et al., 2003). It can also bind and inactivate CDK 2 and 4 and compromise the cell cycle (Laronga et al., 2000).

14-3-3 theta exerts oncogenic activity by interfering with binding of P21 to CDKs, preventing cell cycle arrest and enhancing proteasomal degradation of P21 (Wang et

al., 2010). 14-3-3 theta has been found overexpressed in female breast cancer and is responsible for tumour migration and metastasis (Xiao et al., 2014). Overexpression of 14-3-3 theta was also found involved in tamoxifen resistance in breast cancer (Wang et al., 2010). 14-3-3 epsilon has tumour suppressant activity and was found down-regulated in many carcinomas including gastric carcinoma (GC) (Leal et al., 2012) and larynx squamous cell carcinoma (LSCC) (Che et al., 2010). Increased levels of 14-3-3 epsilon was associated with epithelial-mesenchymal transition (EMT) and low survival rates in hepatocellular carcinoma (Liu et al., 2013). In this study, 14.3.3 epsilon was detected significantly overexpressed in the GDC-0980 non-treated resistant cells (R-) ($p= 0.001$) and was significantly ($p= 0.0001$) down regulated in the treated cells (R+) (Figure 43).

Among 14-3-3 isoforms that have oncogenic function is the 14.3.3 gamma. It acts by stabilising DNA and facilitating mitotic check-point bypass at G2/M cell cycle phase. 14.3.3 gamma was found to cause polyploidy in the H322 lung cancer cell line (Qi et al., 2007). Clinically, 14-3-3 gamma was detected overexpressed in lung (Qi et al., 2007) and breast tumours (Song et al., 2012). In this study, the 14-3-3 gamma profile in GDC-0980 resistant H1975 cells was significantly down-regulated compared to sensitive cells in both treated (R+) and non-treated (R-) ($p= 0.01$ both) resistant cells (Figure 44). 14-3-3 beta/alpha was found by western blot to be upregulated in many lung adeno and squamous carcinoma cell lines, but it was undetectable in normal cell lines (Qi et al., 2005). The abundance of this isoform was significantly downregulated ($p < 0.0001$) in treated GDC-0980 resistant H1975 cells and was significantly upregulated ($p= 0.001$) in resistant cells grown without GDC-0980 compared to sensitive cells (Figure 45).

P21, also called p21^{WAF1/Cip1}, which has several anti-tumour activities (Figure 73), functions mainly to bind and inhibit cyclin-dependent kinases (Deng et al., 1995, Abukhdeir and Park, 2008). It also binds and antagonises the proliferating-cell nuclear antigen (PCNA) responsible for activation of DNA synthesis and cell proliferation, as well as DNA repair. P21 positively regulates P53-dependent apoptosis, leading to cell cycle arrest at G1 phase (Luo et al., 1995, Abbas and Dutta, 2009). P21 binds to CDK 1,2, thereby interfering with cell cycle progression at S and G2/M phases (Deng et al., 1995, Abbas and Dutta, 2009). P21 was also found to bind and interfere with E2FI, STAT3 and MYC transcription factors at their promoter sites (Abbas and Dutta, 2009).

Cancer cells counteract the anti-proliferating effect of p21 by two methods. First, it phosphorylates and interferes with its nuclear translocation, which is offered naturally by the higher rates of phosphorylation in cancer (López Villar et al., 2015) via AKT1 (Abbas and Dutta, 2009). The second is to increase p21 degradation by ubiquitin-mediated proteolysis during S-phase upon binding to PCNA (Nishitani et al., 2008). P21 ubiquitination and degradation is also mediated at G2/M cell cycle transition phase by a sensor complex called anaphase-promoting complex-cell division complex 20-E3 ubiquitin ligase complex (APC-CCDC20-E3 ligase complex). This sensor recognises the p21-bound cyclin A or B and prevents immature cell division (Amador et al., 2007). P21 was evaluated as a cancer biomarker in 18 studies reviewed in (Chen et al., 2013). Significant but heterogeneous expression of p21 was observed in nine studies and in the other 9 it was unchanged by immunohistochemistry (IHC). In 2000, a study examined the clinical utility of p21 as a marker of early occupational lung cancer, but it was not detected in any of the serum samples from patients with asbestos-induced lung

cancer (Schneider et al., 2000). However, down-regulation of p21 or loss of its function was found involved in the tumorigenesis of many cancers as well as in development of drug resistance in cancer (Abukhdeir and Park, 2008).

In this study, P21 was down-regulated in GDC-0980 resistant H1975 cells in the presence of the 1 μ M GDC-0980 and in its absence (both $p < 0.0001$) compared to the parent sensitive cells. These findings might be attributed to the elevated P53 levels (Figure 41) (Elbendary et al., 1996). However, GDC-0980 had no effect on the expression of P21. Therefore, dysregulation of P21 can be validated and used to monitor the development of GDC-0980 resistance by immunohistochemistry using normal tissues surrounding the tumour as a control (Figure 46).

Proliferating-cell nuclear antigen (PCNA) is a nuclear proto-oncogene homo-trimer DNA polymerase delta cofactor protein functioning to increase the speed of DNA replication and to prevent the polymerase from falling off the leading strand during DNA replication (Kelman and O'Donnell, 1995). The active form of this protein is the ubiquitylated PCNA (Schurtenberger et al., 1998, Stoimenov and Helleday, 2009). PCNA-mediated activation of DNA polymerase delta is negatively regulated by P21, leading to cell cycle arrest and termination of DNA synthesis (Figure 74) (Waga et al., 1994). Two PCNA isoforms have been detected in breast cancer, PCNA and ca-PCNA (Cancer-associated PCNA). Ca-PCNA overexpression was claimed as a biomarker for detecting breast malignancy by immunohistochemistry (Malkas et al., 2006). Phosphorylation of PCNA at threonine 211 was found crucial for its proliferation promoting activity. Interfering with this phosphorylation site by Y211F (peptide) was found to cause cell cycle arrest at S phase and inhibition of DNA synthesis in prostate cancer cell lines (Zhao et al., 2011).

In breast cancer, Ca-PCNA was found, by IHC, overexpressed six-fold higher than in normal tissues with no differences in post-translation modifications (Naryzhny and Lee, 2007). PCNA is still used as a cell proliferation marker to exclude negative axillary lymph nodes in breast cancer, and its overexpression was found to denote disease relapse and short survival in breast cancer patients (Aaltomaa et al., 1993). Immunohistochemical examination revealed the overexpression of PCNA along with esophagin in 177 pharyngeal neoplasia tumours, including all types of pharyngeal cancers, and was claimed as a promising biomarker in early diagnosis of oesophageal neoplasia (Kimos et al., 2004). PCNA was also found heterogeneously expressed in 94 lung cancer specimens using IHC assays and higher levels of expression were found directly correlated with poor patient outcome (Caputi et al., 1998).

As increased levels of PCNA are indicative of cell proliferation, its decreased levels would be helpful in predicting treatment success and good prognosis. In H1975 resistant cells (R+) treated with GDC-0980, the level of PCNA was elevated ($p > 0.99$) (Figure 47) and the ubiquitylation levels were significantly decreased ($p = 0.01$) (Figure 48). Inhibition of PCNA phosphorylation was found to decrease its proteasome-mediated degradation (Wang et al., 2006). GDC-0980 might interfere with PCNA phosphorylation by inhibiting the upstream phosphorylation of the PI3K/AKT signalling pathway, which might explain the elevated levels of PCNA in GDC-0980 treated cells (R+). The slow rate of proliferation of GDC-0980 resistant H1975 cells might be attributed to dysregulation of the active PCNA form (Ub-PCNA) (Figures 27, 47 and 48) (Wang et al., 2006). In contrast, no change ($p = 0.29$) in the ubiquitination rates of PCNA in the non-treated resistant cells (R-) (which interpret the higher proliferation rates seen in figure 27 with a significant ($p = 0.004$) decreased levels of the native protein due to increase degradation of PCNA by

restoration of PCNA phosphorylation upon withdrawal of the inhibitor (GDC-0980) from the media (Figures 27, 47 and 48).

BAX and BCL-XL control the release of cytochrome c from mitochondria. Bcl2-associated X protein (BAX), a tumour suppressor gene also called apoptosis regulator, releases cytochrome c, leading to initiation of P53-mediated apoptosis *via* activation of the caspase cascade, whereas BCL-XL inhibits its release and so it is categorized as an oncogene (Kimos et al., 2004). BAX expression was found significantly low in many tumours, including 62 breast cancers by flow cytometry and 50 colorectal cancers by IHC (Pluta et al., 2011). BAX was also correlated with advanced stages of cancer; it was found significantly elevated in lymph nodes and in vascular infiltration cells in colorectal cancer (Pryczynicz et al., 2014, Pöhland et al., 2006). However, BAX levels were elevated in breast cancer patients responding to chemotherapy (Gibson et al., 1999). In lung cancer, BAX was found significantly overexpressed in 20% (n = 60) of NSCLC (> 80% of the BAX-positive cancers were adenocarcinoma), but it was overexpressed only in 10% of squamous cell carcinoma (Porebska et al., 2006). In the non-treated GDC-0980 resistant H1975 cells (R-), the levels of BAX were significantly downregulated ($p = 0.0006$), and its abundance tended to exceed the parent levels in the treated cells (R+) ($p = 0.51$) (Figure 49). It can be concluded that downregulation of BAX can be used as a marker for IHC evaluation of tumour resistance to GDC-0980 if a control tissue biopsy is taken as a control before the inhibitor is withdrawn.

B-cell lymphoma extra-large (BCL-XL), a mitochondrial transmembrane anti-apoptosis protein encoded by the BCL2-like 1 gene, functions to prevent BAX-mediated release of cytochrome c from the mitochondria and induction of P53-mediated apoptosis (Korsmeyer, 1995). BCL-XL also plays a role in the endoplasmic

reticulum-induction of cell proliferation by modulating the calcium signalling pathway (Akl et al., 2014). In non-small cell lung cancer, BCL-XL was found overexpressed in 59% of squamous cell carcinoma (n = 27), 28% of adenocarcinoma (n = 25) and 38% of large cell carcinoma (n = 13). In colorectal cancer, BCL-XL was found to function as a driver for tumorigenesis and was found involved in tumour resistance to treatment (Scherr et al., 2016). Therefore, targeting BCL-XL to improve treatment response and avoid the development of resistance has recruited many scientists, as reviewed in (Cory et al., 2016). BXI-72 is a small-molecule inhibitor that binds to BCL-XL and interferes with its inhibition of cytochrome-c release, leading to cytochrome c release and induction of P53-mediated apoptosis *via* activation of caspase-3 (Park et al., 2013).

In this study, significant overexpression of BCL-XL was exhibited by both treated (R+) ($p= 0.01$) and non-treated (R-) ($p= 0.0001$) GDC-0980 resistant H1975 lung adenocarcinoma cells (Figure 50). However, BCL-XL can be used as an IHC marker to detect resistance of tumours to GDC-0980.

Nuclear factor kappa B (NFκB) is a transcription factor belonging to the Rel motif-containing protein family. The five known Rel-containing proteins are Rel-A, Rel-B, c-Rel, P50 and P52. The later two are formed from the proteasomal degradation of their precursors NFκB1 and NFκB 2, respectively. The Rel motif (about 300 amino acids) is located at the amino terminus of members of the NFκB family and is responsible for their dimerisation, nuclear translocation, and binding to their DNA promoters (Hayden and Ghosh, 2004). Rel-A and B have a transactivating domain opposite to the Rel motive, *i.e.*, at the carboxyl terminus. This transactivating domain activates the formation of P50 and P52 heterodimers with other Rels (A, B, C) and acts as a transcription repressor when P50 and P52 form homodimers (Chen, 2005,

Thoms et al., 2010). Two main signalling pathways are involved in the activation of NFκB. The canonical pathway involves hetero-dimerisation of Rel A or c-Rel with P50, and the non-canonical pathway involves dimerisation of P52 with Rel-B. In both cases, the result is nuclear translocation and activation of target genes (Lin et al., 2010). In clinical proteomics, NFκB was found to play a role in many cancers, including lung cancer (Chen et al., 2011, Lin et al., 2010), colorectal cancer (Sakamoto and Maeda, 2010), and breast cancer (Sarkar et al., 2013). Its overexpression was found more correlated with P53-mutated tumours and to play a role in resistance to chemotherapy and radiotherapy (Park et al., 2007, Vaughan et al., 2012). Overexpression of Rel-A and B in NSCLC favours tumour invasion and resistance to chemotherapy and radiotherapy by opposing P53-mediated apoptosis (Tang et al., 2006, Bailey et al., 2014). Therefore, Rel family proteins were scanned by western blot in this research work.

The results revealed a significant increase in the levels of P50 in both the treated (R+) ($p= 0.01$) and non-treated (R-) ($p= 0.004$) GDC-0980 resistant H1975 cells. This was due to activation of proteasomal degradation of the precursor NFκB1 (P105) protein (Figure 51).

Rel A was found elevated in the treated resistant cells (R+) ($p= 0.15$) but no significant change was observed in the non-treated cells (R-) ($p= 0.14$) (Figure 52). Rel-B and Rel-C were both significantly (except C Rel in R+) down regulated in the GDC-0980 resistant cells in both treated (R+) and non-treated (R-) compared to the parent cells (Figures 53, 54). The p values were (0.0008 and 0.03) and (0.1 and 0.01) for Rel B and C-Rel, respectively. In histopathology, P50 and Rel-B might indicate tumour resistance to GDC-0980 as they are not affected by drug.

Histone acetyltransferases (HATs) and histone deacetylase enzymes (HDACs) are among the most important enzymatic machineries regulating the cell cycle and gene expression. Imbalance in regulation of these two enzyme families was found associated with the development of many types of tumours (Timmermann et al., 2001). Histones have lysine residues that can be acetylated by a histone-specific acetyltransferases (HATs), which is mostly part of transcription factors' associated regulatory protein complex (Legube and Trouche, 2003).

In normal cells, HDACs was found to bind and repress retinoblastoma protein (pRB) and to interfere with the transcription of cyclins A and E, which are needed in the cell cycle S-phase. Class I HDACs, including HDAC 1,2 and 3, are recruited to the EF2 responsive elements of DNA by retinoblastoma protein (pRb), leading to repression of transcription of the encoded genes (Lai et al., 2001). In cancer, increased kinases activity interferes with such binding, where phosphorylation of HDACs by these kinases deactivates them and leads to cell cycle progression (Wang et al., 2001). Phosphorylation of pRb by CDK4 leads to its dissociation and proteasomal degradation. The liberated EF2 is then phosphorylated by CDK2/cyclin E. The phosphorylated EF2 then recruits HATs to acetylate histones in order to facilitate its access to its responsive promoters (Chan and La Thangue, 2001).

The levels of HDACs were found downregulated in colorectal and lung cancer, and the dysregulation was associated with poor prognosis (Osada et al., 2004). HDAC inhibitors were also found to induce P21 expression, leading to an additive cell cycle arrest effect at G1 phase (Kim et al., 2000). Drug resistance to tyrosine kinase inhibitors (TKIs) was found accompanied by diminished levels of many histone acetyltransferases (HATs) (Bixby and Talpaz, 2009).

In this study, HATs were significantly down-regulated [PCAF ($p < 0.0001$) and GCN5L2 ($p = 0.0007$)] in the treated GDC-0980 resistant H1975 cells (R+) compared to the parent cells (figures 55, 56). Similar findings have been reported for other tyrosine kinase inhibitors (TKI) in (Bixby and Talpaz, 2009). GDC-0980 was observed to cause H1975 cells to accumulate pyruvate (next chapter), the natural inhibitor of HDACs. GDC-0980 also found to induce HDACs expression [HDAC I ($p = 0.0002$), HDAC II ($p = 0.01$), HDAC III ($p = 0.0003$), HDAC IV ($p = 0.03$), HDAC VI ($p = 0.0003$)] (Figures 57-61) with a significant decrease in their phosphorylation [eg: hypo-phosphorylation of HDAC IV and V ($p < 0.0001$)] (Figure 62). The net result of the inactivated HDACs in H1975 resistant cells was hyper-acetylation of histone 3 [lysine 9 ($p = 0.18$), lysine 18 ($p = 0.002$) and lysine 27 ($p = 0.17$)] (Figures 63, 65 and 67) and histone 4 lysine 5 ($p = 0.0001$) (Figure: 69) when the signal (western blot) was normalized for the abundance of the native histone proteins 3 and 4 (Figures: 30 and 68). A549 was used as a control to support this interpretation (Figures 29, 64, 66).

In non-treated GDC-0980 H1975 (R-), the HATs were significantly overexpressed [PCAF ($p = 0.0007$) and GCN5L2 ($p = 0.0004$)] (Figures 56 and 55). All evaluated HDACs [HDAC I ($p > 0.99$), HDAC III ($p = 0.21$), IV ($p = 0.001$) and VI ($p = 0.001$)] were down-regulated (Figures 57, 59, 60, 61) except HDAC II was overexpressed ($p = 0.09$) when compared with the parent sensitive H1975 cells (Figure 58). The phosphorylation levels and activities of HDAC IV and V ($p = 0.0003$) started to recover, leading to the hypo-acetylation profile of the evaluated histone lysines (Figures 63, 65, 67 and 69). Again, A549 also was used as a control (Figures 29, 64, 66).

The decreased phosphorylation of HDACs and increased acetylation of histones in the treated (R+) GDC-0980 resistant H1975 cells and the hypoacetylation of the histones upon clearing the drug from the media (restoration of HDACs phosphorylation) would suggest GDC-0980 and phosphorylation of HDACs to play a role in acetylation of histones.

Interestingly, GDC-0980 resistant H1975 cells (R-) tolerated higher doses of HDACi (SAHA) than H1975 GDC-0980 sensitive parent cells (Figure 71). This might suggest that HDACs play a role in multiple drug resistance. GDC-0980 at concentrations of 1 μ M (equivalent to about IC₁₀) was found to re-sensitize the GDC-0980/Vorinostat resistant cells to Vorinostat (Figure 71) which support the notion that GDC-0980 mediates deactivation of HDACs by interfering with their phosphorylation and accumulation of pruvate, the endogenous inhibitor of HDACs.

Chapter 7

**GDC-0980 resistant H1975 cells energy
phenotyping**

7. GDC-0980 resistant H1975 lung adenocarcinoma cells energy

7.1. Introduction

Normal proliferating cells obtain their energy from complete oxidation of glucose in the mitochondria. Under anaerobic conditions, cells convert pyruvate to lactate with a net energy production of two ATP molecules per glucose molecule. Cancer cells can convert pyruvate to lactate even in the presence of oxygen, the phenomenon called Warburg effect (Vander Heiden et al., 2009). Due to their increased demand for nucleic acids production, cancer cells utilize glucose-6-phosphate in the pentose phosphate pathway (PPP), the main pathway for purine and pyrimidine production. Fermentation of pyruvate to lactate is inefficient for ATP production, but the rate of ATP production is 100 times faster than in aerobic glycolysis (Devic, 2016). Downstream signalling of the PI3K pathway stimulates the uptake and utilization of glucose by increasing glucose uptake by its transporters (GLUT-transporters), and increases glucose trapping by the enzyme hexokinase (Ben-Haim and Ell, 2009, DeBerardinis et al., 2008, Engelman et al., 2008). PI3K also stimulates through m-TOR signalling pathway the utilization of amino acids for protein synthesis (Vander Heiden et al., 2009). Inhibition of the PI3K signalling pathway was shown by positron emission tomography to decrease the uptake and utilization of glucose (Ben-Haim and Ell, 2009). PI3K inhibitors are in clinical use and cancer cells resistance to this category of treatment is well documented. Here, energy phenotyping of H1975 lung adenocarcinoma cells that are resistant to GDC-0980 (dual inhibitor of PI3K and m-TOR) was compared to their sensitive parent cells, both in the presence (R+) or the absence (R-) of the drug.

7.2. Experimental design

GDC-0980-sensitive parent (P) and resistant H1975 lung adenocarcinoma cells were used. The parent cells were used as control to assess the differences in the metabolic phenotypes of the resistant cells in the presence (R+) and in the absence of the drug (R-). Parent and resistant cells in the presence or absence of the drug were compared by mass-spectrometry, and western blot was used to assess mitochondrial membrane markers involved in oxidative phosphorylation. The mitochondrial membrane voltage potential was assessed by flow-cytometry using TMRE and the extent of active mitochondria in all GDC-0980 phenotypes was performed using MitoTracker® and confocal microscopy. Seahorse (principle see figure 75) energy phenotyping was conducted to validate the interpretation of the findings.

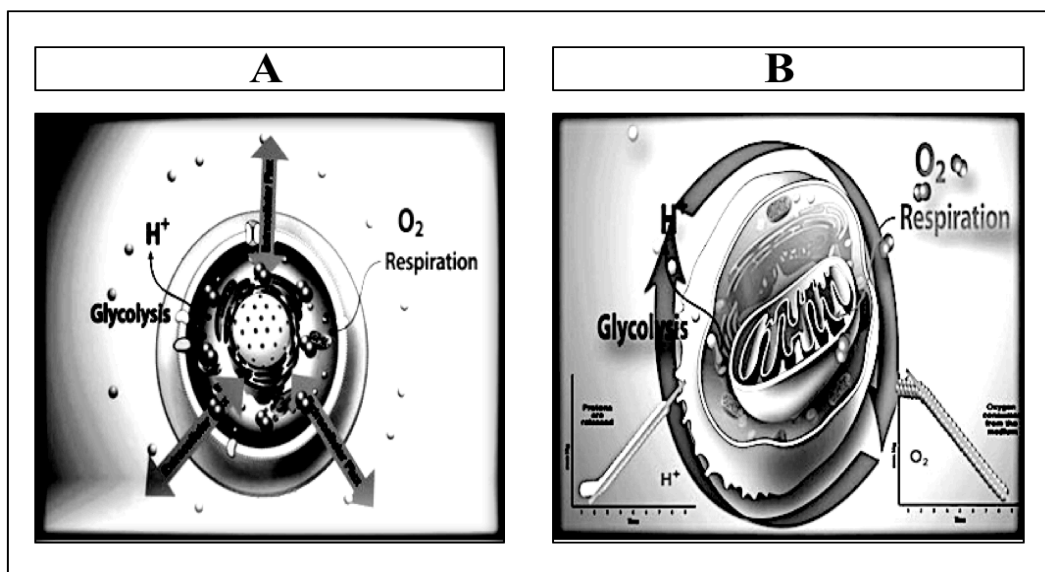


Figure 75: Seahorse basic principle. (a) shows the principle of oxidative phosphorylation consumption of oxygen for production of ATP and the rate of acid production (mainly lactate) through glycolysis, (b) shows how their concentrations utilized by seahorse basic metabolic phenotyping [modified from agilent [www.agilent.com/en/products/cell-analysis-\(seahorse\)/seahorse-analyzers/seahorse-xfp-analyzer](http://www.agilent.com/en/products/cell-analysis-(seahorse)/seahorse-analyzers/seahorse-xfp-analyzer)].

7.3. Results

7.3.1. Glycolysis in the GDC-0980 resistant H1975 cells (GDC-0980 R-).

Figure 76 showed a KEGG pathway analysis of the proteins detected by LC-MS/MS significantly up-regulated in the GDC-0980 resistant H1975 (non-treated) compared to the parent cells focusing on glycolysis/gluconeogenesis pathways, enzymes in red numbers found elevated.

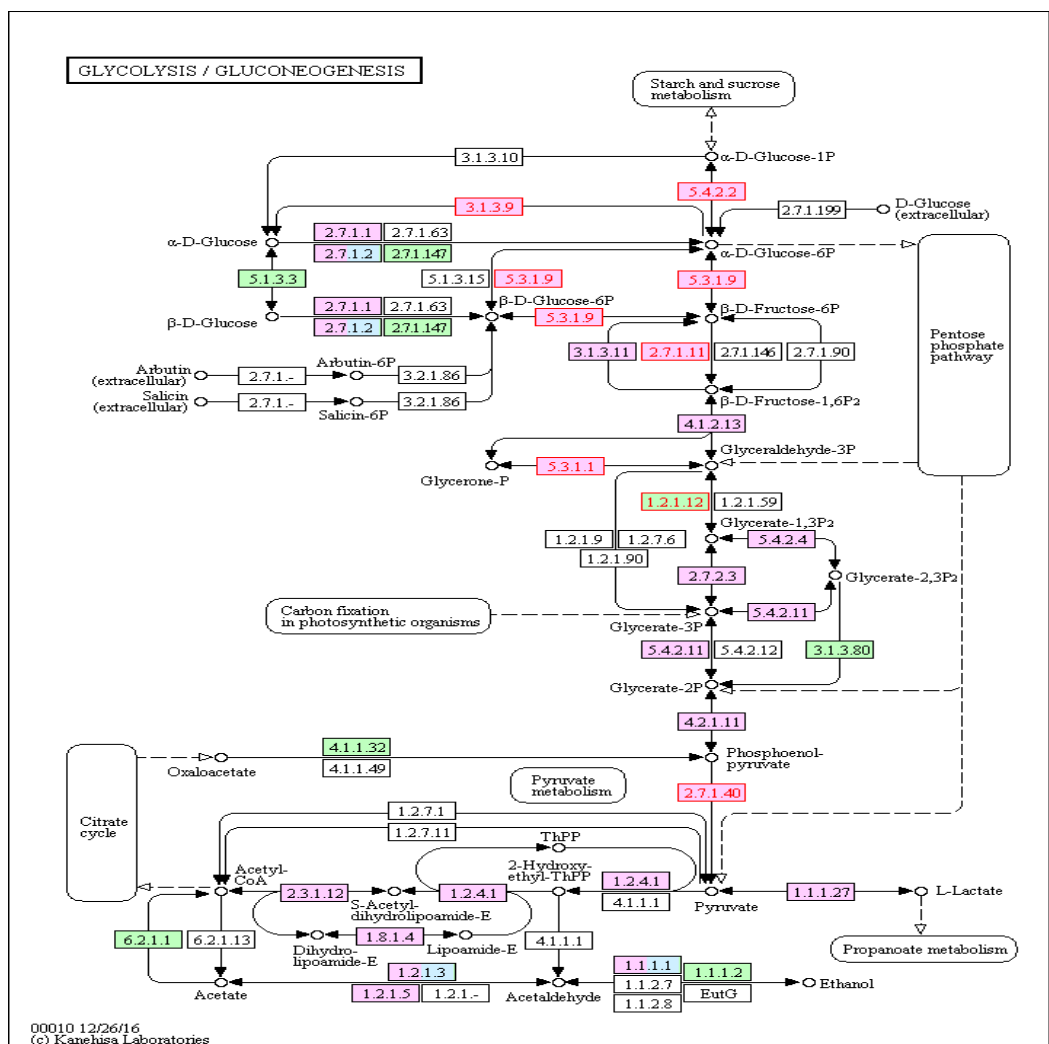


Figure 76: KEGG pathway analysis of up-regulated glycolysis enzymes in GDC-0980 non-treated resistant cells H1975 (R-). Enzyme codes in red numbers were upregulated in the resistant cells (R-) compared to the parent cells (P), [3.1.3.9]: glucose-6-phosphatase, [5.4.2.2]: phosphoglucomutase, [5.3.1.9]: glucose-6-phosphate isomerase, [2.7.1.11]: 6-phosphofructokinase 1, [5.3.1.1]: triosephosphate isomerase, [1.2.1.12]: glyceride 3-phosphate dehydrogenase (GAPDH), [2.7.1.40]: pyruvate kinase.

7.3.2. Glycolysis in the GDC-0980 resistant H1975 cells (GDC-0980 R+).

Figure 77 showed a KEGG pathway analysis of the proteins detected by LC-MS/MS significantly up-regulated in the GDC-0980 resistant H1975 (treated) compared to the parent cells focusing on glycolysis/gluconeogenesis pathways, enzymes in red numbers found elevated.

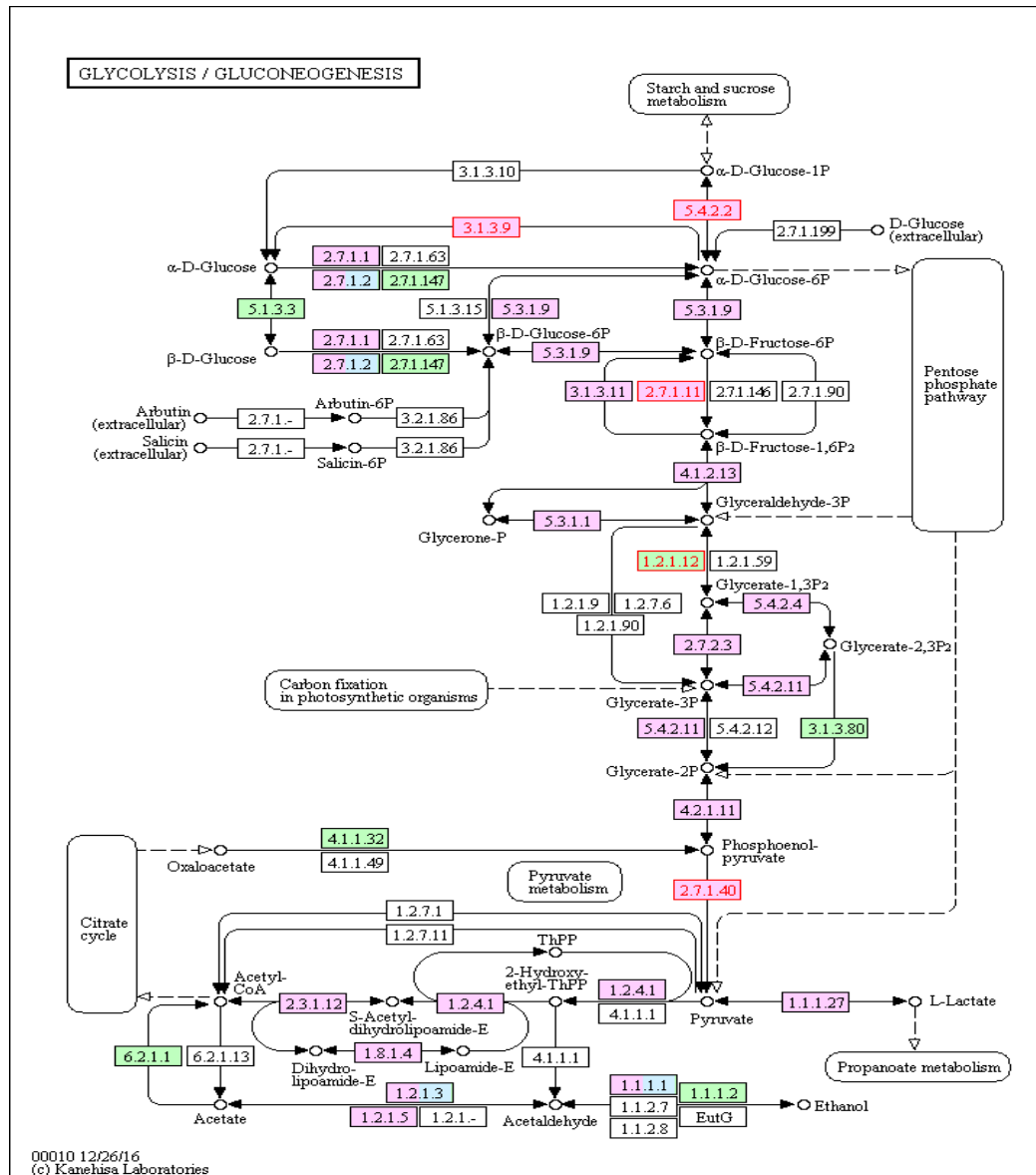


Figure 77: KEGG pathway analysis of up-regulated glycolysis enzymes in GDC-0980 non-treated resistant cells H1975 (R+). Enzyme codes in red numbers were upregulated in the resistant cells (R+) compared to the parent cells (P). [3.1.3.9]: glucose-6-phosphatase, [5.4.2.2]: phosphoglucomutase, [2.7.1.11]: 6-phosphofructokinase 1, [1.2.1.12]: glyceride 3-phosphate dehydrogenase (GAPDH), [2.7.1.40]: pyruvate kinase.

7.3.3. Mitochondrial cytoplasmic distribution

Shown in figure 78, Mito-Tracker®-red mitochondrial labelling-based confocal imaging of GDC-0980 parent (P) and resistant (R) H1975 lung adenocarcinoma cells. Mitochondrial activity has increased in both treated and non-treated GDC-0980 resistant cells compared to the parent cells.

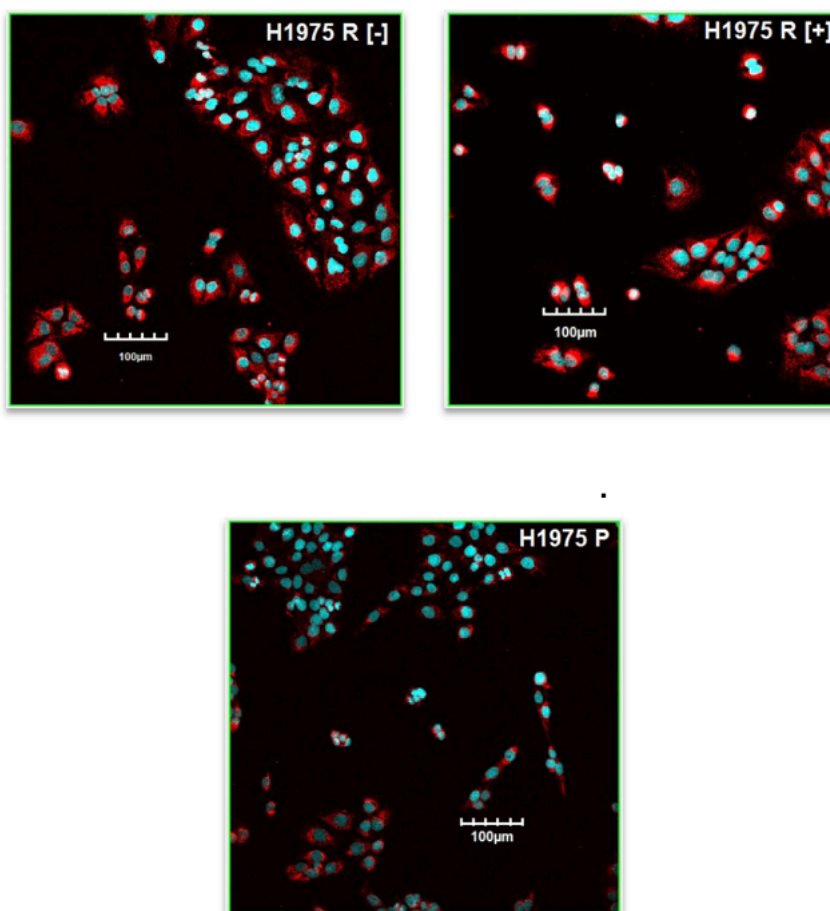


Figure 78: Mito-Tracker®-red mitochondrial labelling-based confocal imaging of GDC-0980 parent (P) and resistant (R) H1975 lung adenocarcinoma cells. [-]: in GDC-0980 free medium and [+]: cells maintained in the presence of 1µM GDC-0980 final concentration. Blue: DAPI staining of nuclei, red: Mito-Tracker staining of mitochondria.

7.3.4. Cell cycle-based mitochondrial activity

Figure 79 shows flow cytometry of GDC-0980 parent and resistant H1975 either treated (R+) or non-treated (R-) using TMRE active mitochondrial staining. TMRE: Tetra-methyl-rhodamine-methyl ester (TMRM) staining was strong in late cell cycle phases (G2/M) or 4N cells in all conditions. Using TMRE, the cells representing G2/M phase cells were shifted from the upper left quadrant to the right upper quadrant, while the G1 remained at the same position (the lower left quadrant). The mitochondrial membrane negative charge of the resistant cells was higher than in parent cells, as indicated by pre-treatment of the cells with FCCP, which abolishes the negativity of the mitochondrial membrane.

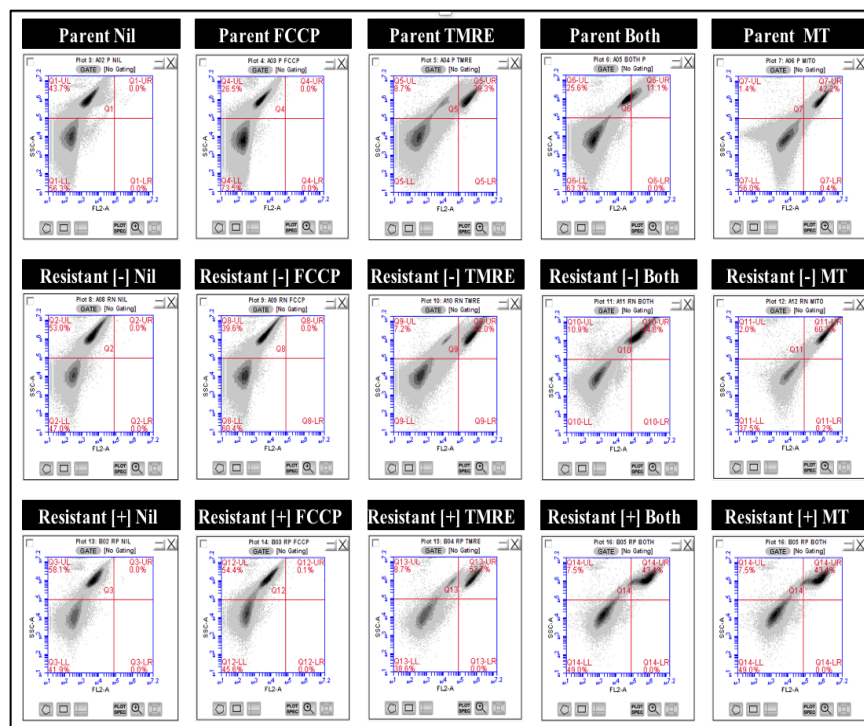


Figure 79: TMRE labelling of mitochondrial activity of GDC-0980 sensitive (P) and resistant (R) H1975 lung adenocarcinoma cells in the presence [+] or absence of the drug incubation [-]. FCCP: carbonyl cyanide-p-trifluoromethoxyphenylhydrazone was used as negative control and mito-Tracker® (MT) was used to label mitochondria of all cells, including G1-attendant cells, nil: only cells, both: cells were pre-treated by FCCP 20 min prior TMRE staining.

7.3.5. Pyruvate dehydrogenase

Figure 80 shows a quantitative western blot comparison of pyruvate dehydrogenase (PDH) abundance between H1975 GDC-0980 sensitive (parent) and resistant cells (R) in the presence [+] or absence [-] of the drug. PDH was significantly down-regulated in the treated (B/D) resistant cells ($p=0.01$) and significantly up-regulated in non-treated (A/C) resistant cells compared to the parent cells ($p=0.002$). HDAC I and PCNA proteins were used as a loading control when (R-) and (R+) were compared to the parent cells (P), respectively (refer to section 2.4.6.6).

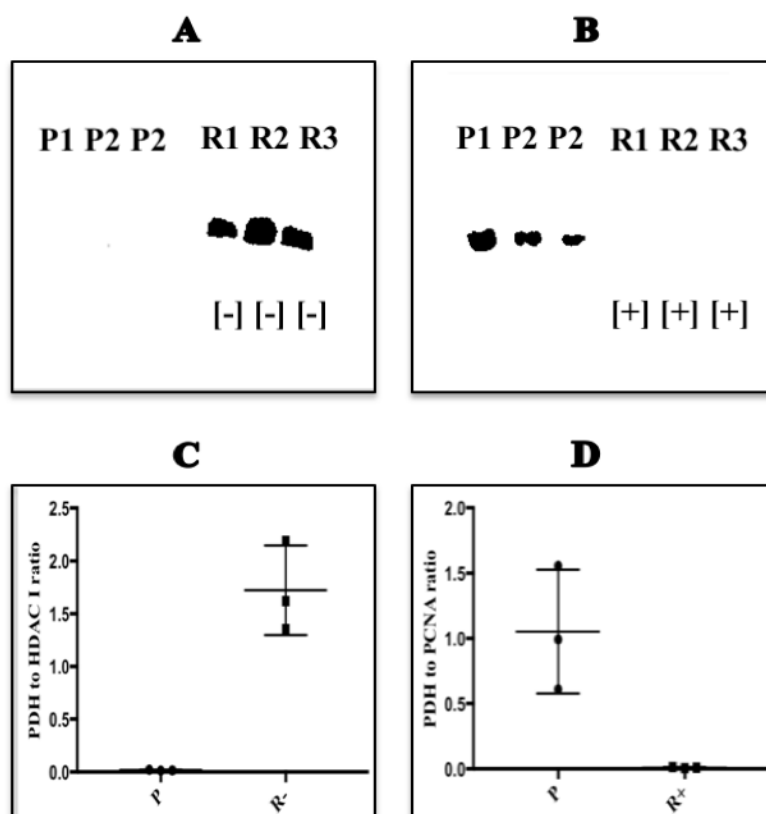


Figure 80: Comparison of pyruvate dehydrogenase abundance in GDC-0980 sensitive parent (P) and resistant (R) H1975 adenocarcinoma cells. P1-3 and R1-3 represents triplicates of 20 μg of total cell protein. [-]: resistant cells cultured in drug-free medium and [+] resistant cells cultured in medium containing 1 μM GDC-0980. C and D are scatter plots representing the ratio of ECL chemiluminescence signal of PDH from 20 μg total protein to the signal of HDAC I or PCNA (loading controls) measured by image J and plotted as triplicates.

7.3.6. Superoxide dismutase

Figure 81 a quantitative western blot comparison between superoxide dismutase abundance in H1975 GDC-0980 sensitive (parent) and resistant cells in the presence or absence of the drug. Protein abundance was significantly up-regulated in the treated (B/D) resistant cells ($p= 0.04$), but significantly down-regulated in non-treated (A/C) resistant cells compared to the parent cells ($p < 0.0001$). HDAC I and PCNA proteins were used as a loading control when (R-) and (R+) were compared to the parent cells (P), respectively (refer to section 2.4.6.6).

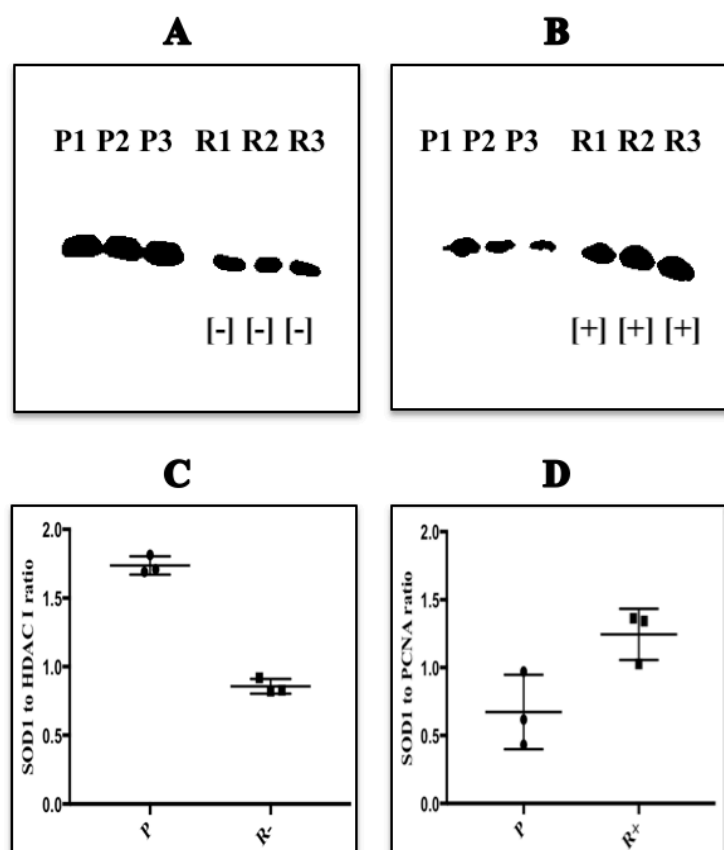


Figure 81: Comparison of superoxide dismutase (SOD1) abundance between GDC-0980 sensitive parent (P) and resistant (R) H1975 adenocarcinoma cells. P1-3 and R1-3 represents triplicates of 20 μg of total cell protein. [-]: resistant cells cultured in drug-free medium and [+] resistant cells cultured in medium containing 1 μM GDC-0980. C and D are scatter plots representing the ratio of ECL chemiluminescence signal of PDH from 20 μg total protein to the signal of HDAC I or PCNA (loading controls) measured by image J and plotted as triplicates.

7.3.7. Succinate dehydrogenase complex flavoprotein subunit A

Figure 82 shows a quantitative western blot comparing the abundance of succinate dehydrogenase complex flavoprotein subunit A between H1975 GDC-0980 sensitive (parent) and resistant cells in the presence or absence of the drug. There was no change in the abundance of the protein in the treated (B/D) resistant cells ($p=0.7$), but it was significantly up-regulated in non-treated (A/C) resistant cells compared to the parent cells ($p < 0.0001$). HDAC I and PCNA proteins were used as a loading control when (R-) and (R+) were compared to the parent cells (P), respectively (refer to section 2.4.6.6).

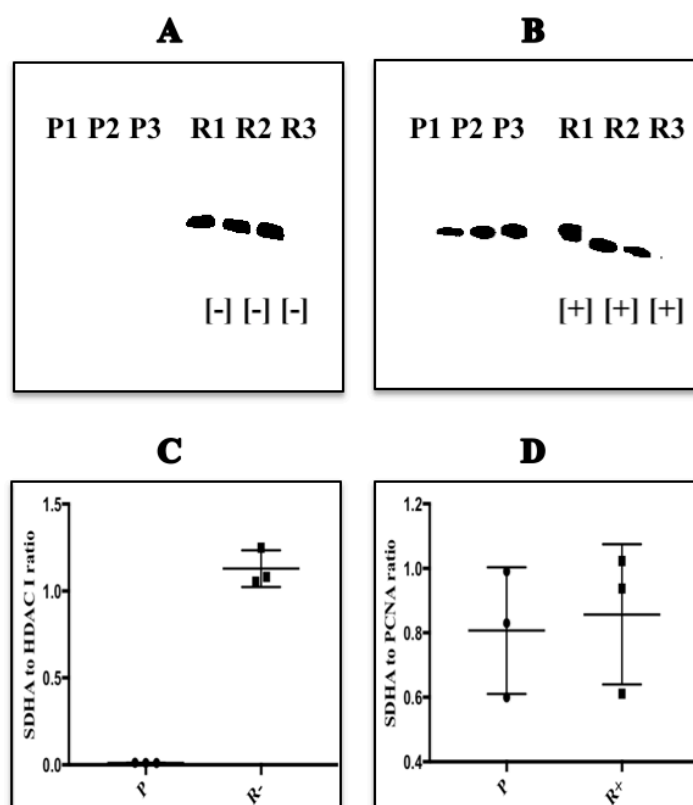


Figure 82: Comparison of succinate dehydrogenase complex flavoprotein subunit A (SDHA) abundance between GDC-0980 sensitive parent (P) and resistant (R) H1975 adenocarcinoma cells. P1-3 and R1-3 represents triplicates of 20 μ g of total cell protein. [-]: resistant cells cultured in drug-free medium and [+] resistant cells cultured in medium containing 1 μ M GDC-0980. C and D are scatter plots representing the ratio of ECL chemiluminescence signal of PDH from 20 μ g total protein to the signal of HDAC I or PCNA (loading controls) measured by image J and plotted as triplicates.

7.3.8. Prohibitin B

Figure 83 is a quantitative western blot comparing prohibitin B (PHB1) abundance between H1975 GDC-0980 sensitive (parent) and resistant cells in the presence or absence of the drug. The protein was significantly up-regulated in both treated (B/D) resistant cells ($p= 0.07$) and non-treated (A/C) resistant cells ($p= 0.0007$) compared to the parent cells. HDAC I and PCNA proteins were used as a loading control when (R-) and (R+) were compared to the parent cells (P), respectively (refer to section 2.4.6.6).

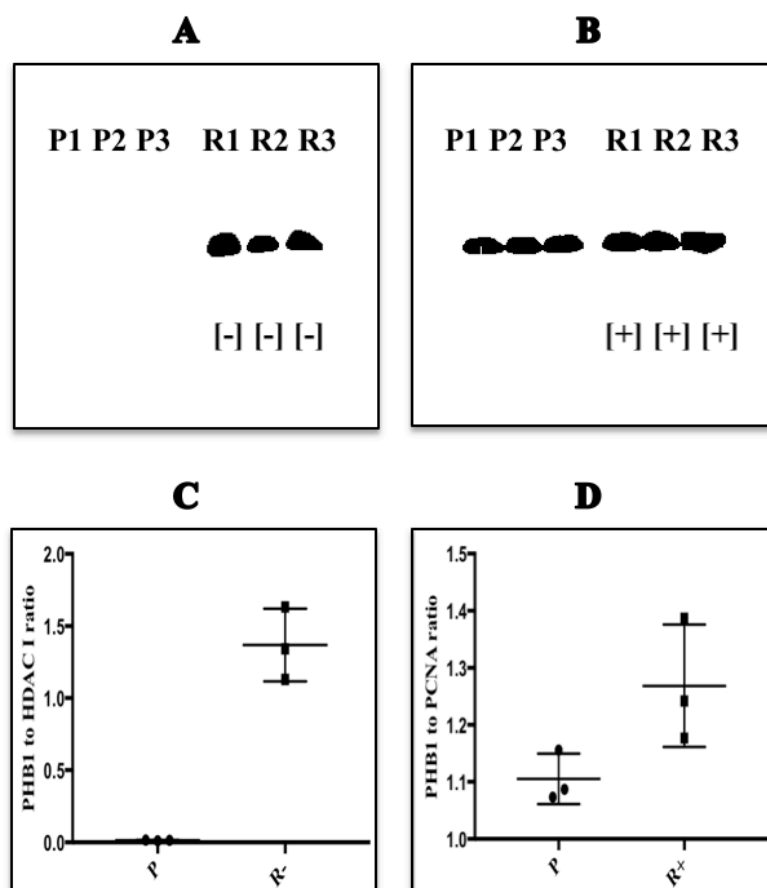


Figure 83: Comparison of prohibitin B abundance between GDC-0980 sensitive parent (P) and resistant (R) H1975 adenocarcinoma cells. P1-3 and R1-3 represents triplicates of 20 μg of cells lysate total protein. [-]: resistant cells cultured in drug-free medium and [+] resistant cells cultured in 1 μM GDC-0980 containing medium. C and D are scatter plots representing the ratio of ECL chemiluminescence signal of PDH from 20 μg total protein to the signal of HDAC I or PCNA (loading controls) measured by image J and plotted as triplicates.

7.3.9. Voltage-dependent anionic channels

Figure 84 shows a quantitative western blot comparison of voltage-dependent anionic channel protein (VDAC) abundance between H1975 GDC-0980 sensitive (parent) and resistant cells in the presence or absence of the drug. There was no change in protein expression levels in the treated (B/D) resistant cells ($p=0.7$), but it was significantly up-regulated in non-treated (A/C) resistant cells compared to the parent cells ($p=0.0006$). HDAC I and PCNA proteins were used as a loading control when (R-) and (R+) were compared to the parent cells (P), respectively (refer to section 2.4.6.6).

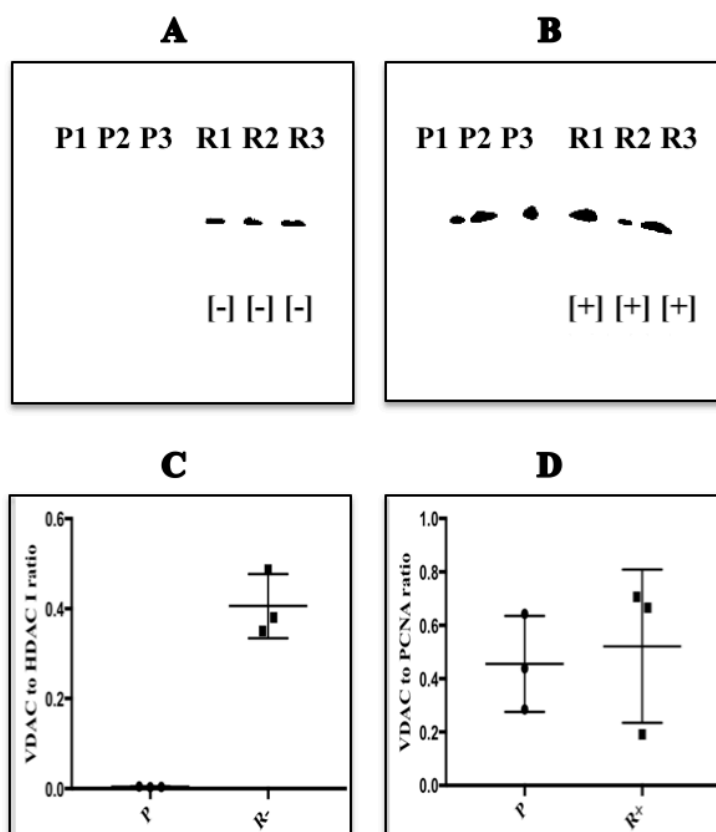


Figure 84: Comparison of the abundance of voltage-dependent anionic channels (VDAC) between GDC-0980 sensitive parent (P) and resistant (R) H1975 adenocarcinoma cells. P1-3 and R1-3 represents triplicates of 20 μ g of total cell proteins. [-]: resistant cells cultured in drug-free medium and [+] resistant cells cultured in medium containing 1 μ M GDC-0980. C and D are scatter plots representing the ratio of ECL chemiluminescence signal of PDH from 20 μ g total protein to the signal of HDAC I or PCNA (loading controls) measured by image J and plotted as triplicates.

7.3.10. Heat shock protein 60

Figure 85 is a quantitative western blot comparison of heat shock protein-60 (HSP60) abundance between H1975 GDC-0980 sensitive (parent) and resistant cells in the presence or absence of the drug. The abundance of HSP60 was significantly down-regulated in the treated (B/D) resistant cells ($p= 0.007$) but significantly up-regulated in the non-treated (A/C) resistant cells compared to the parent cells ($p < 0.0001$). HDAC I and PCNA proteins were used as a loading control when (R-) and (R+) were compared to the parent cells (P), respectively (refer to section 2.4.6.6).

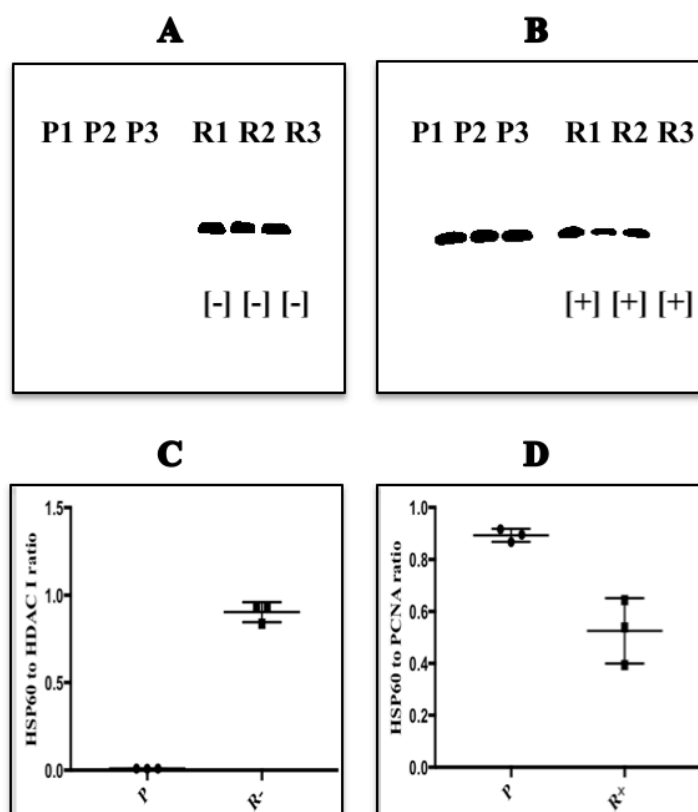


Figure 85: Comparison of heat shock protein 60 (HSP60) abundance between GDC-0980 sensitive parent (P) and resistant (R) H1975 adenocarcinoma cells. P1-3 and R1-3 represent triplicates of 20 μg of total cell protein. [-]: resistant cells cultured in drug-free medium and [+]: resistant cells cultured in medium containing 1 μM GDC-0980. C and D are scatter plots representing the ratio of ECL chemiluminescence signal of PDH from 20 μg total protein to the signal of HDAC I or PCNA (loading controls) measured by image J and plotted as triplicates.

7.3.11. Cytochrome C Oxidase IV

Figure 86 is a quantitative western blot comparison of cytochrome c oxidase (COX IV) abundance between H1975 GDC-0980 sensitive (P) and resistant cells in and out of the drug incubation. Protein abundance was significantly up-regulated in both treated (B/D) and non-treated (A/C) resistant cells compared to the parent cells. The p values were 0.01 and 0.009 in the treated and non-treated conditions, respectively. HDAC I and PCNA proteins were used as a loading control when (R-) and (R+) were compared to the parent cells (P), respectively (refer to section 2.4.6.6).

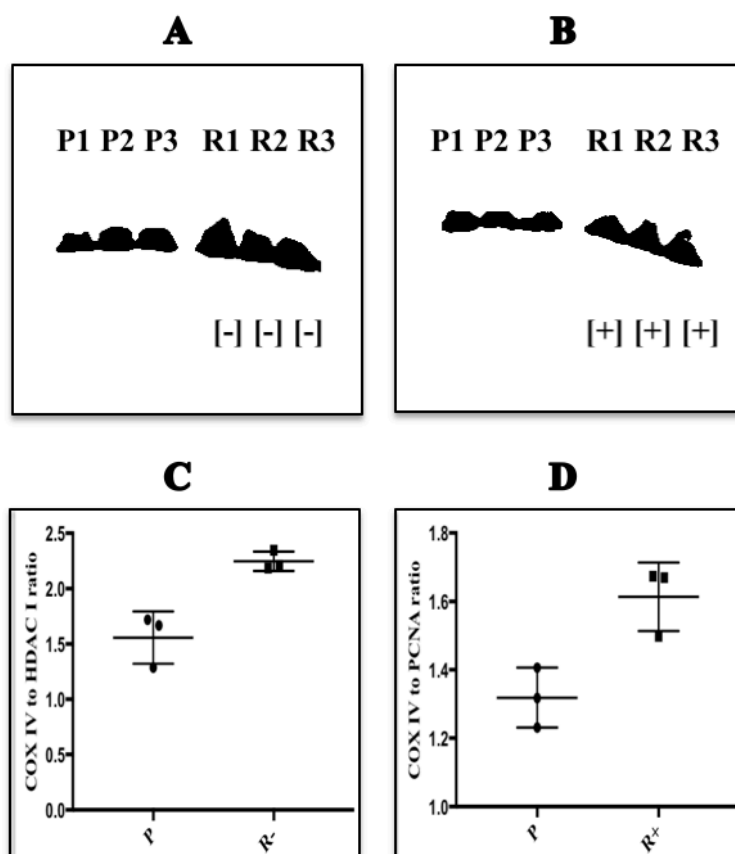


Figure 86: Comparison of cytochrome oxidase (COX IV) protein abundance levels in GDC-0980 sensitive parent (P) and resistant (R) H1975 adenocarcinoma cells. P1-3 and R1-3 represents triplicates of 20 μg of cells lysate total protein. [-]: resistant cells cultured in drug-free medium and [+] resistant cells cultured in 1 μM GDC-0980 containing medium. C and D are scatter plots representing the ratio of ECL chemiluminescence signal of PDH from 20 μg total protein to the signal of HDAC I or PCNA (loading controls) measured by image J and plotted as triplicates.

7.3.12. Cytochrome c

Figure 87 represents a quantitative western blot comparison of cytochrome c (Cyt.c) abundance between H1975 GDC-0980 sensitive (P) and resistant (R) cells in the presence [+] or absence [-] of the drug. Cytochrome c abundance was significantly down-regulated in both treated (B/D) and non-treated (A/C) resistant cells compared to the parent cells. The p-values were 0.01 and 0.006 in the treated and non-treated conditions, respectively. HDAC I and PCNA proteins were used as a loading control when (R-) and (R+) were compared to the parent cells (P), respectively (refer to section 2.4.6.6).

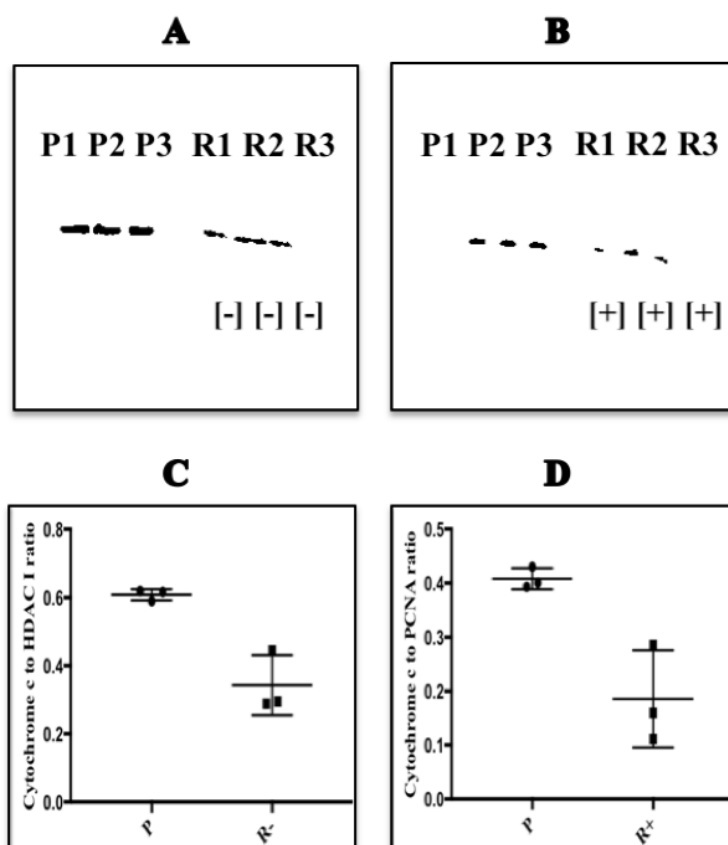


Figure 87: Comparison of cytochrome c protein abundance in GDC-0980 sensitive parent (P) and resistant (R) H1975 adenocarcinoma cells. P1-3 and R1-3 represent triplicates of 20 μg of total cell protein. [-]: resistant cells cultured in drug-free medium and [+] resistant cells cultured in medium containing 1 μM GDC-0980. C and D are scatter plots representing the ratio of ECL chemiluminescence signal of PDH from 20 μg total protein to the signal of HDAC I or PCNA (loading controls) measured by image J and plotted as triplicates.

7.3.13. Acetyl co-A precursors

Figure 88 depicts a colorimetric assay of the levels of the main molecules involved in the synthesis and fate of acetyl Co-A. The level of pyruvate was shown to be significantly up-regulated in the treated (R+) resistant cells ($p= 0.001$) but down-regulated ($p= 0.01$) in the non-treated resistant cells (R-) compared with the parent cells. Free fatty acids were down-regulated in both treated and non-treated resistant cells ($p= 0.16$) but down-regulation was significant only in the treated condition ($p= 0.001$). Acetoacetic acid levels were significantly up-regulated in the treated resistant (R+) cells ($p < 0.0001$) and were little a bit lower than the parent cells in the non-treated (R-) condition ($p= 0.02$). The changes in β -hydroxyl butyrate abundance compared to the parent cells (P) were significant in both conditions. Its abundance was increased in the treated (R+) compared to the parent cells ($p= 0.02$) while it was significantly down-regulated in non-treated resistant cells ($p= 0.002$). Acetyl Co-A was downregulated in the treated resistant cells (R+) compared to the parent cells ($p= 0.07$), but no difference was observed between the non-treated resistant cells (R-) and the parent cells ($p= 0.4$).

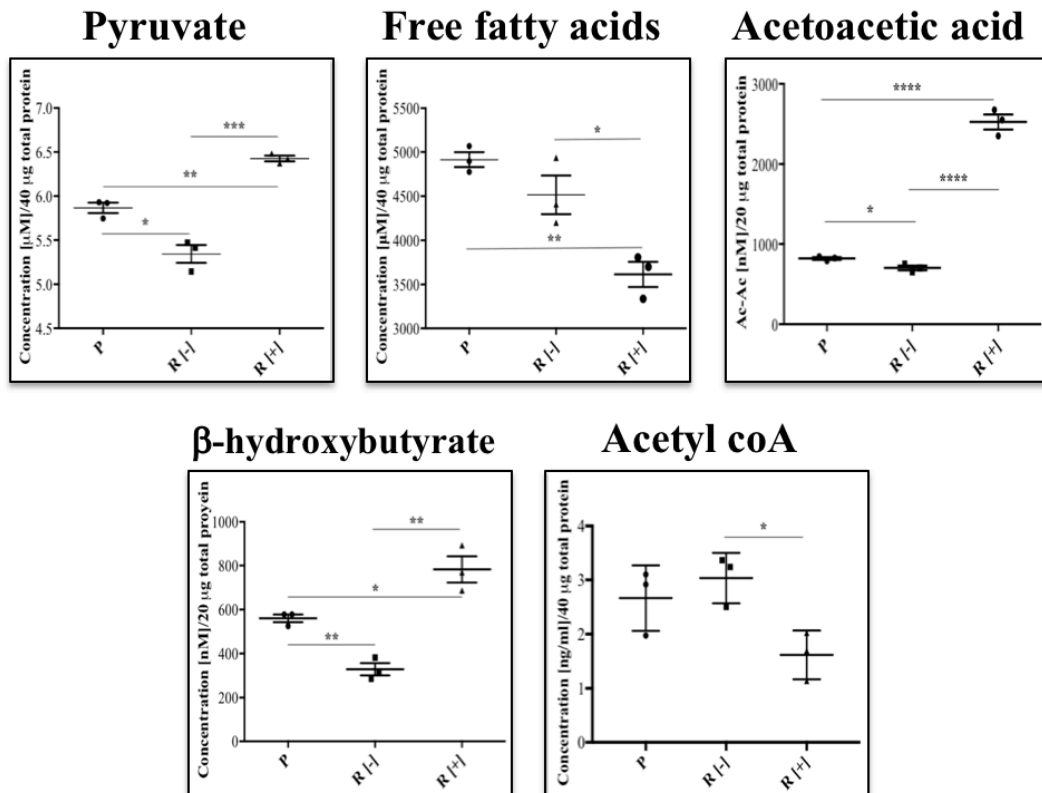


Figure 88: Comparison of acetyl Co-A and its main precursors, pyruvate, free fatty acids, acetoacetic acid and β -hydroxy butyrate, in GDC-0980 sensitive parent (P) and resistant (R) H1975 adenocarcinoma cells. [-]: resistant cells cultured in drug-free medium and [+] resistant cells cultured in medium containing 1 μ M GDC-0980.

7.3.14. Seahorse cell energy phenotyping

Shown in figure 89 is a comparison of oxygen consumption rate (OCR) and extracellular acidification rate (ECAR) between the GDC-0980 resistant H1975 cells (R-) compared to the parent sensitive cells (P). The figure shows the effect of a final concentration of 1 μM GDC-0980 (+) on the energy of the resistant cells. The resistant cells in the absence of drug incubation (R-) were very energetic compared to the parent cells; the former tended to depend on the mitochondria rather than on glycolysis. In the presence of 1 μM GDC-0980, the resistant cells (R+) were quiescent, hypo-energetic, and fully dependent on the aerobic energy production with a profound shut down of glycolysis.

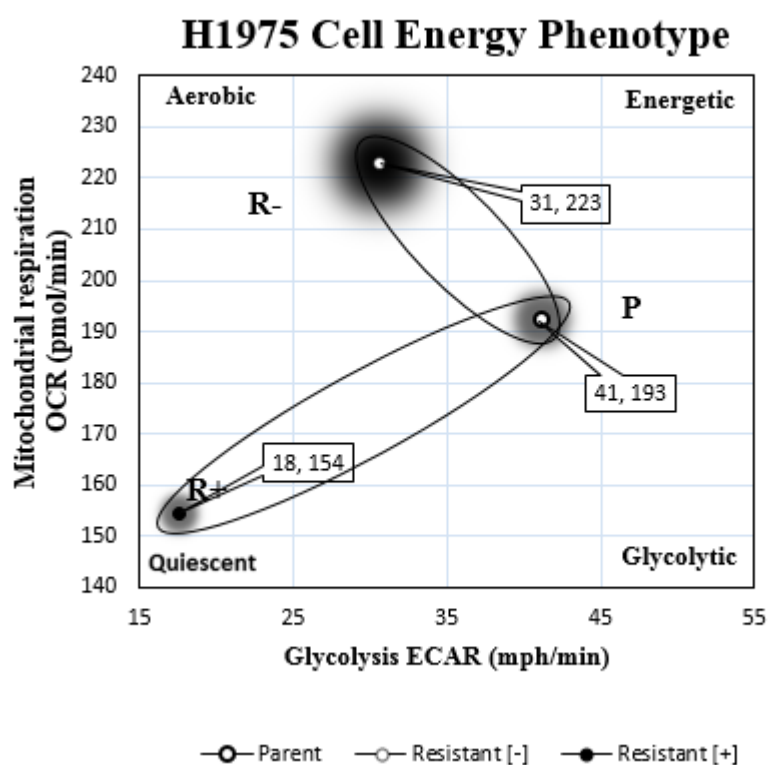


Figure 89: Seahorse energy phenotyping of GDC-0980 resistant H1975 cells in the presence of 1 μM final concentration GDC-0980 or absence of the drug compared to GDC-0980 native H1975 lung adenocarcinoma cells.

7.3.15. Mitochondrial respiration- oxygen consumption rate (OCR).

Shown in figure 90, a comparison of mitochondrial OCR between GDC-0980 parent sensitive (P) and resistant H1975 lung adenocarcinoma cells either GDC-0980 treated (R+) or non-treated (R-) using seahorse XF24 extracellular Flux AnalyZer. The aerobic respiration was significantly increased in the non-treated GDC-0980 cells ($p= 0.02$) as indicated by their increased rate of oxygen consumption. Mitochondrial respiration in the treated resistant cells (R+) was lower than in parent cells, but the difference was not significant ($p= 0.06$). 1 μ M GDC-0980 incubation (R+) reverses the increased mitochondrial respiration in the resistant cells ($p= 0.01$).

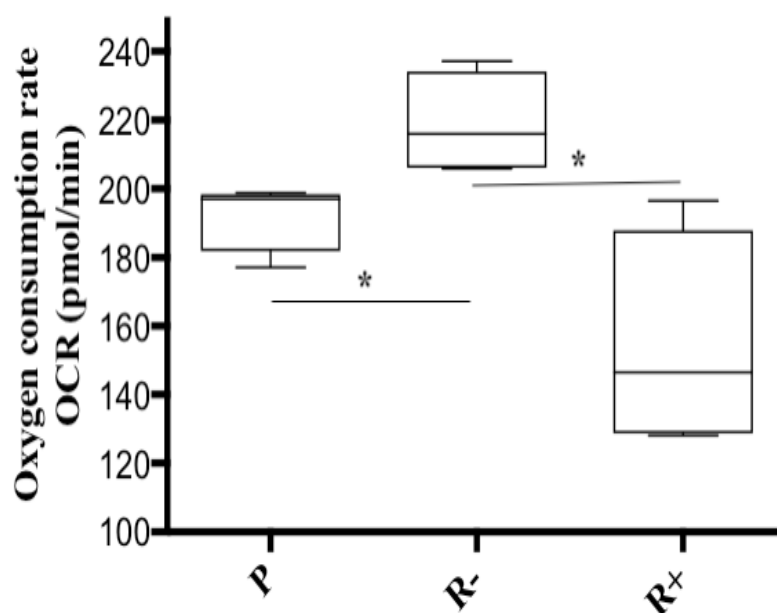


Figure 90: Mitochondrial respiration activity (aerobic respiration) of GDC-0980 resistant H1975 cells compared to GDC-0980 sensitive H1975 lung adenocarcinoma cells (P). R+: effect of 1 μ M GDC-0980 incubation on the drug resistant H1975 cells.

7.3.16. Extracellular acidification rate (ECAR)

Figure 91 shows a comparison of ECAR between GDC-0980 sensitive (P) and resistant H1975 lung adenocarcinoma cells either GDC-0980 treated (R+) or non-treated (R-) using seahorse XF24 extracellular Flux Analyzer . The ECAR was significantly decreased in the non-treated (R-) GDC-0980 resistant cells ($p < 0.0001$). 1 μ M GDC-0980 incubation (R+) had an additive lowering effect on the rate of lactate production compared with the parent cells ($p < 0.0001$).

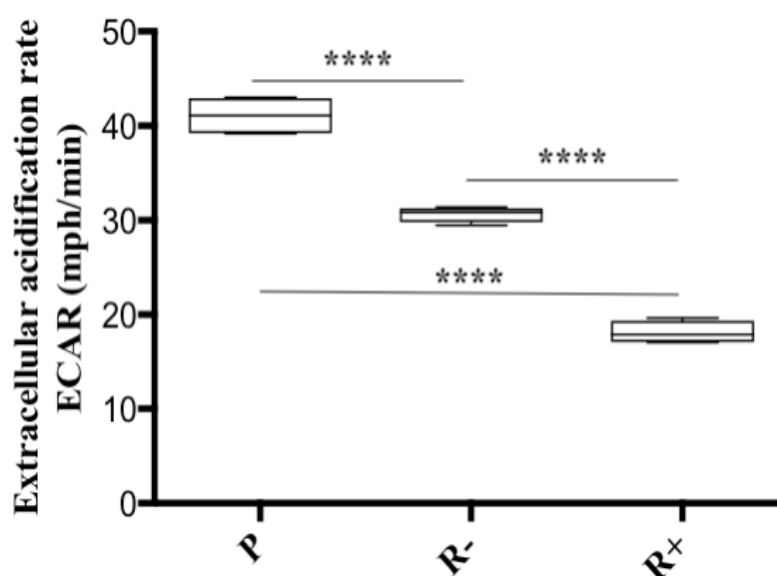


Figure 91: Extracellular acidification rates (Glycolysis) of GDC-0980 resistant H1975 cells compared to GDC-0980 sensitive (P) H1975 lung adenocarcinoma cells. R+: effect of 1 μ M GDC-0980 incubation on the ECAR of the drug resistant H1975 cells.

Table 53: Summary of western blot and biochemical assays findings

Biomarker	PVR-		PVR+	
	Expression	p-value	Expression	p-value
Pyruvate dehydrogenase	Up	0.002	Down	0.019
Superoxide dimutase	Down	< 0.0001	Up	0.04
Succinate dehydrogenase	Up	< 0.0001	Un changed	0.7
Prohibitin	Up	0.0007	Up	0.07
Voltage dependent anionic channel	Up	0.0006	Un changed	0.75
Heat shock protein 60	Up	< 0.0001	Down	0.007
Cytochrome c oxidase IV	Up	0.009	Up	0.01
Cytochrome c	Down	0.006	Down	0.02
Pyruvate	Down	0.01	Up	0.001
Free fatty acids	Un changed	0.16	Down	0.001
Acetoacetic acid	Down	0.02	Up	<0.0001
β -hydroxy butyrate	Down	0.002	Up	0.02
Acetyl CoA	Up	0.4	Down	0.07

7.4. Discussion

Summary of the overall results obtained in this research work with a proposed story approach to connect and interpret these results are summarized in figure 92. Seahorse was used for energy phenotyping of treated (R+) and non-treated (R-) GDC-0980-resistant H1975 lung adenocarcinoma cells and to compare them with the GDC-0980 parent (P) cells (Figure 89). This analysis was very informative when interpreted in parallel with their corresponding rate of proliferation (Figure 27), their mitochondrial membrane potential as measured by TMRE labelling (Figure 79), their mitochondrial mito-Tracker labelling (Figure 78), and their levels of pyruvate and ketone bodies (Figure 88), along with the LC-MS/MS analysis (Appendices: 47-50).

The cytoplasmic conversion of pyruvate into lactate is favoured in cancer cells even in the presence of excess oxygen demand (Vander Heiden et al., 2009). In GDC-0980 resistance, mass spectrometry revealed increased glycolytic activity and increased abundance of pyruvate kinase in both non-treated (R-) and treated (R+) H1975 cells compared to the parent cells (Appendices 87 and 89). The difference in the availability of pyruvate was most likely due to the effect of GDC-0980 (Figure 88).

GDC-0980 was shown to compromise both mitochondrial oxidative phosphorylation and utilization of glucose *via* its conversion into lactate, keeping the resistant cells (R+) at very slow metabolic rates (Figure 88). The rates of lactic acid production (ECAR) (Figure 91) and oxygen consumption (OCR) decreased ($p = 0.06$, $p < 0.0001$, respectively) (Figure 90). In addition, there was a significant decrease in the levels of pyruvate dehydrogenase ($p = 0.01$) (Figure 80). Combined, these results indicate that energy production was at very low levels, and this was reflected on their proliferation rate (Figure 27). The significant decrease in pyruvate dehydrogenase

(PDH) ($p= 0.01$) (Figure 80) and lactate dehydrogenase A ($p= 0.01$) (Appendix 50) might explain the accumulation of pyruvate ($p= 0.001$) and low levels of acetyl Co-A ($p = 0.07$) in the (R+) cells (Figure 88).

Upon withdrawal of GDC-0980, the resistant cells exhibited an aggressive rate of proliferation (Figure 27). Resistant cells (R-) started to utilise oxygen at a higher rate than the parent cells (Figure 90). This indicates that the mitochondria started to utilise glucose and the Warburg effect became less effective. This assumption can be concluded from the increased utilization of pyruvate ($p= 0.01$) and its conversion into acetyl Co-A (Figure 88) by pyruvate dehydrogenase, which was significantly elevated ($p= 0.002$) compared to the parent cells (Figure 80). Their high energetic status (Figure 89) in addition to the significant increase in the oxygen consumption rate ($p= 0.02$) (Figure 90) and their decreased lactic acid production ($p < 0.0001$) compared to the parent cells (P) (Figure 91) is indicative the recovery of mitochondrial utilisation of glucose.

The increased mitochondrial activity is expected to be accompanied by increased levels of reactive oxygen species (ROS), which are cytotoxic (Auten and Davis, 2009). However, cells with normal mitochondrial function would utilise such free radicals through the oxidative phosphorylation (OP) complexes, which are of two categories of ROS consuming complexes: superoxide dismutase (SOD), the main cellular ROS scavenger, and cytochrome c oxidase (COX). The other type of mitochondrial OP complex is the ROS producing succinate dehydrogenase (SDH), which catalyses the transport of electron radicals from succinate to the mitochondrial membrane, thereby connecting OP to the citric acid cycle.

Superoxide dismutase 1 and 2 have been reported as down-regulated in many cell lines representing primary and metastatic colorectal cancer, and their levels were

found directly correlated with the increased ROS concentration (Skrzycki et al., 2015). Tyrosine kinase inhibitors (TKIs) compromises mitochondria and cause increased reactive oxygen species (ROS) (Okon et al., 2015). Therefore the abundance of cytoplasmic superoxide dismutase (SOD1) (Fukai and Ushio-Fukai, 2011) in the treated resistant cells was significantly elevated ($p= 0.02$) (Figure 80). This overexpression might have been due to SOD1 dysfunction (Robbins and Zhao, 2014, Oberley and Buettner, 1979) and increased ROS (Yankovskaya et al., 2003, Horsefield et al., 2004) caused by GDC-0980.

The level of cytochrome c oxidase (COX-IV) (R-) was also upregulated ($p= 0.01$) (Figure 86) compared to the parent cells, and the level of succinate dehydrogenase (SDH) showed no change (Figure 82). These findings support that GDC-0980 compromises the mitochondrial oxidative phosphorylation and increases the levels of ROS scavenger SOD1 protein as a consequence of accumulation of ROS in the absence of mitochondrial membrane function which can be seen clearly in figure 91 (Xu et al., 2014).

The significant accumulation of pyruvate ($p= 0.001$) (Figure 88) and decreased pyruvate dehydrogenase (PDH) ($p= 0.01$) (Figure 80) in the treated resistant cells might serve as a protective mechanism for the cells in order to prevent production of more acetyl co-A (Figure 88), the main source of toxic reactive oxygen species (ROS) which found to induce several cell death mechanisms (Valencia and Morán, 2001).

In contrast, when the resistant cells grow in GDC-0980 free media (R-) they exhibit a low level of superoxide dimutase (SOD) compared to the parent cells ($p<0.0001$) (Figure 81), cytochrome c oxidase was upregulated ($p= 0.009$) (Figure 86) and the level of succinate dehydrogenase was also overexpressed ($p<0.0001$) (Figure 82).

The decreased SOD1 levels can be attributed to the improved levels of phosphorylation and restoration of mitochondrial function as it can be concluded from the increased levels of oxygen consumption (Figure 90). The elevated succinate dehydrogenase enzyme might reflect the increased utilization of amino acids to compensate for the increased energy demand (Figures 27, 82). The lowered pyruvate and ketone bodies (Figure 88) levels also indicate increased mitochondrial function.

Prohibitin B (PHB1) is a mitochondrial inner membrane-bound protein regulating cell morphogenesis and proliferation, and is involved in the integrity of the mitochondrial membrane (Merkwirth and Langer, 2009). PHB1 was evaluated in non-small cell lung cancer by RT-PCR, western blot and IHC and its overexpression was found associated with the clinically aggressive types of the tumours (Jiang et al., 2013). Overexpression of PHB1 was also found associated with poor prognosis and increased tumour invasion in gallbladder cancer (Cao et al., 2016).

PHB1 and Heat shock protein 60 (HSP60), which are known to protect the cells against various types of stress (Pace et al., 2013, Coates et al., 2001) were significantly overexpressed ($p= 0.0007$ and < 0.0001) in the non-treated resistant cells (R-) (Figure 83 and 85, respectively). This might explain the higher proliferation rate of the GDC-0980 resistant cells when grown in drug-free media (Figure 27), while the treated cells (R+) exhibited a slow proliferation factor (Figure 27) despite the elevated PHB1 level ($p= 0.07$) (Figure 82). GDC-0980 interferes with prohibitin phosphorylation, which is required for its function, by upstream blockage of AKT/PB phosphorylation (Jiang et al., 2015), resulting in growth rate depression (Figure 27).

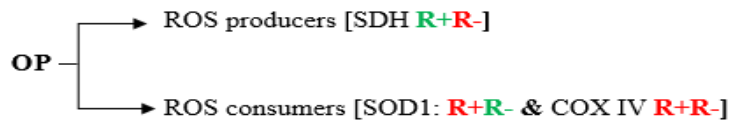
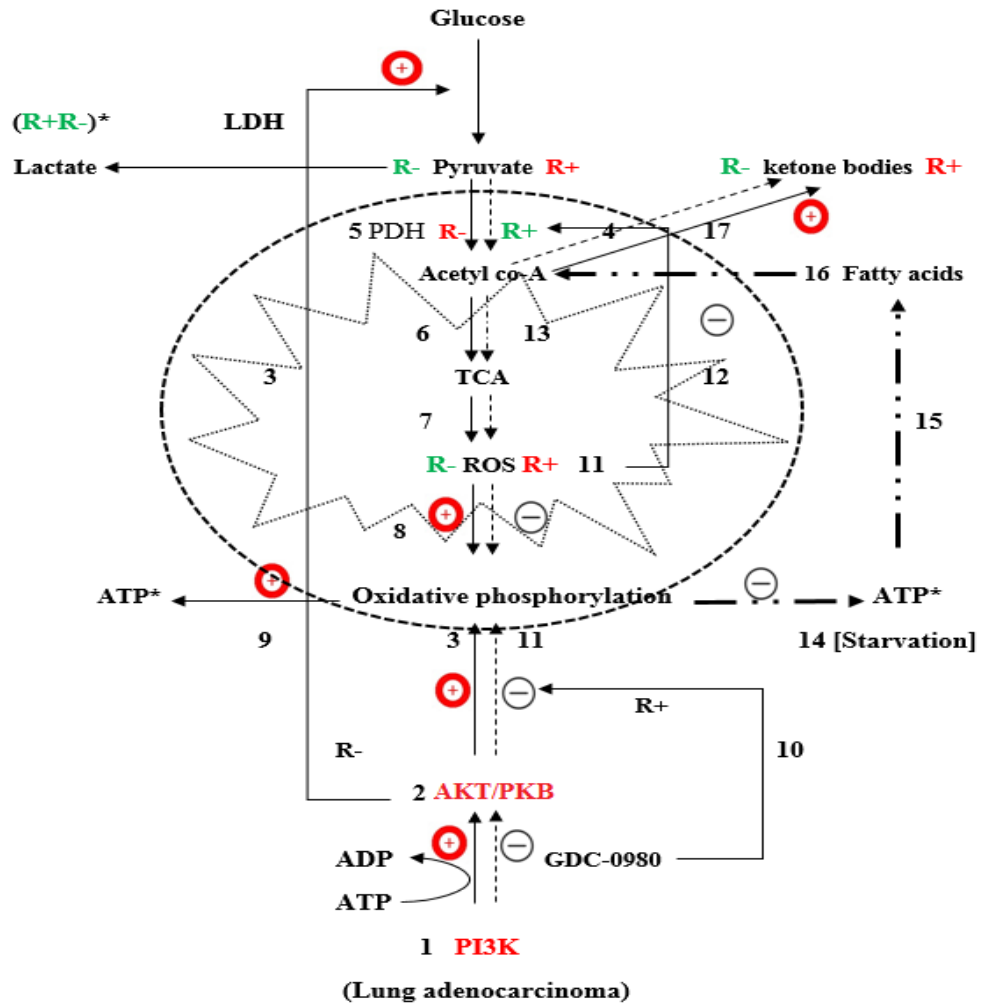


Figure 92: Summary of chapter findings. PI3K: phosphatidyl inositol 3-kinase, AKT/PKB: protein kinase B, ATP: adenosine triphosphate, ADP: adenosine diphosphate, LDH: lactate dehydrogenase, PDH: pyruvate dehydrogenase, ROS: reactive oxygen species, TCA: tricarboxylic acid cycle, OP: oxidative phosphorylation, SDH: succinate dehydrogenase, SOD: superoxide dismutase, COX IV: cytochrome c oxidase 4, ketone bodies: (acetoacetic acid, β -hydroxy butyrate), red R+ or R-: found significantly elevated, green R+ or R-: found significantly lowered, dotted black arrows: status in R+ (inhibited), black arrows: status in R- (activated), numbering (1-9): increased PI3K-AKT/PKB axis activity and increased ATP production from pyruvate, steps (10-17): indicate interrupted ATP production and increased utilization of free fatty acids.

HSP60 is a mitochondrial chaperon that is elevated in early stages of adeno and squamous carcinoma without a significant difference in advanced stages (Ağababaoğlu et al., 2017). HSP60 has two main function, to keep unfolded proteins protected and facilitate their transport through the inner mitochondrial membrane, and to protect the mtDNA during mitochondrial fission (Kaufman et al., 2003). HSP60 is significantly downregulated in the treated cells (R+) compared to the parent cells (P) ($p= 0.007$) (Figure 85). This, along with the decreased levels of Cytochrome c ($p= 0.02$) (Figure 87) and overexpression of BAX ($p = 0.51$) (Figure 49, Chapter 6) when compared to the highly down regulated BAX in (R-), also indicate that apoptosis was increased in (R+). The mitochondrial activity in (R-) (Figures 78 and 79) is also explained by the significant upregulation of the mitochondrial voltage-dependent anionic channel protein (VDAC) ($p= 0.001$) (Figure 84). VDAC is a mitochondrial outer membrane channel protein, when bound to BAX, forms a heterodimer leading to the release of mitochondrial cytochrome c and activation of the caspase cascade and apoptosis; this occurred in (R+). In (R-), the overexpression of VDAC in (R-) was not sufficient to release the folded cytochrome c (Shoshan-Barmatz et al., 2006), as the level of BAX was extremely downregulated ($p= 0.0006$) (Figure 49, Chapter 6). This also demonstrates the increased proliferation rate in (R-) (Figure 27).

In summary, GDC-0980 was shown to cause the resistant cells (R+) to live at very low levels of energy leading to a dramatic decline in their proliferation rate (Figure 27). This might have been due to an increased rate of apoptosis compared to the newly divided cells. GDC-0980 was also found to compromise mitochondrial function and drive the cells to utilise less ROS-producing energy substrates. The overall increased production of ketone bodies and accumulation of pyruvate in (R+)

(Figure 88) supports the mitochondrial dysfunction caused by GDC-0980. Interestingly, the current data showed that mitochondrial activity was restricted to cells that contained 4N ploidy (Figure 79).

Finally, the clinical utility of protein biomarkers found differentially expressed in GDC-0980 resistant H1975 in the presence (R+) or absence (R-) of the drug (Summarized in table 53) should be assessed in experimental animals models of lung cancer (*e.g.*, rodents) (Wang et al., 2012) to monitor their levels before and after starting GDC-0980 treatment, and also before and after development of tumour resistance. Monitoring could be done by IHC staining as an initial validation. This would be the future extension of this piece of research work.

Chapter 8

General discussion, conclusion and future work

8.1. Discussion

Per the most recent estimates held by the International Agency for Research on Cancer, 1.82 million new cases were estimated for lung cancer in 2012 (Ferlay et al., 2015). With an overall ratio of mortality to incidence of 0.87, lung cancer is one of the deadliest cancers worldwide. By region, the highest estimated lung cancer mortality rates (per 100,000) in 2012 were in Northern America (23.5), Northern Europe (19.1), Eastern Asia (16.2), Western Europe (14.8), Oceania (14.1), and Caribbean (12.2).

More-reliable biomarkers are needed to identify the development of lung cancer at the earliest stage and to predict which patients are likely to respond to treatment. Validating a candidate biomarker is a demanding process requiring large numbers of patient samples from multiple sites. Progress has been made over previous years in the early detection and treatment of lung cancer, but more progress is needed so all patients can benefit from new screening approaches and molecularly targeted therapies with associated companion biomarkers.

Blood is the most frequently sampled biofluid, obtaining it is minimally invasive, and it is readily available. Moreover, because blood circulates throughout the body, it contains proteins secreted, shed or released from all cells and tissues. However, using blood as a biofluid in biomarker discovery is especially challenging. The huge dynamic range and the fact that the proteome is represented mainly by a few high abundance proteins (22 most abundant proteins represent approximately 99% of the total protein mass) makes the identification and quantification of lowly abundant proteins extremely difficult. It is very likely that any proteins produced by or associated with the tumour will be of low abundance, so their detection will often be hindered by the masking effect of highly abundant proteins such as albumin, which

can be present at a billion-fold higher level than some of the proteins that are of interest from a biomarker discovery perspective.

Biological material assayed for discovery phase analysis can also originate from proximal fluids, *i.e.*, biofluids in close or direct contact with the site of disease. The protein concentration of potential biomarkers is enriched in these biofluids because masking proteins such as albumin are present at greatly reduced levels, and the proteins secreted or shed by tumours should be present at elevated levels. Therefore, such liquids, which include cerebrospinal fluid, bronchoalveolar lavage fluid, saliva, urine, tears and various gastrointestinal secretions, are valuable resources for initial biomarker discovery.

Lung cancer protein biomarkers currently include carcinoembryonic antigen (CEA), neuron-specific enolase (NSE) and cytokeratin 19 fragment (CYFRA21-1), but more-accurate biomarkers are needed. The number of investigations examining bronchoalveolar lavage fluid (BALF) for protein biomarkers is increasing. BALF samples are used for cytological, hematologic, biochemical, and microbiological examination.

BALF is a mixture of different cell types and a wide variety of soluble components, such as phospholipids, nucleic acids, peptides and proteins. The utility of BALF has been exploited for many years in clinical research, with recent technological advances permitting detailed proteomic profiling of protein/peptide signatures in particular lung diseases. This approach provides a rich source of candidate biomarkers, in addition to providing insight into the complex pathological mediators associated with lung diseases at the molecular level.

The data presented in this study demonstrate that the abundance of proteins involved in cellular and metabolic processes is markedly increased in BALF from patients

with lung cancer compared to controls. Following selection of four candidate proteins for verification in plasma, TIMP-1, Lipocalin-2 and Cystatin-C were all found to be significantly elevated in NSCLC compared to control. This demonstrates that BALF represents a mirror biofluid for blood (serum/plasma), and that many of the signatures discovered in proximal biofluids such as BALF will be identifiable with similar abundance patterns in blood. This opens up the possibility of identifying panels of protein biomarkers in BALF, validating their abundance in blood, and developing unique biomarker panels associated with different types of lung cancer, as well as different stages/grades and signatures associated with response to treatment. A critical finding of this investigation was that the abundance of a substantial number of proteins in BALF was significantly different in lung adenocarcinoma and squamous cell carcinoma of the lung. Some chemotherapeutic regimens are more effective for squamous cell carcinoma, so it is necessary to differentiate the two major types of NSCLCs because treatments options become more extensive and sub-type associated.

Fine needle aspiration (FNA) cytology performed by transthoracic and/or transbronchial procedures are important approaches to obtain tumour tissue for histological diagnosis and molecular characterisation of tumours. In some cases, distinguishing between adenocarcinoma and squamous cell carcinoma by analysis of FNA specimens can be challenging, such as in poorly differentiated NSCLCs and adenosquamous carcinomas. Therefore, an assay of protein abundance in BALF could be useful in cases of poorly differentiated NSCLCs and adenosquamous carcinomas.

Another finding of particular interest is that folate receptor alpha was increased 13.9-fold in adenocarcinoma compared to squamous cell carcinoma (3.8 fold). Previous

work has shown that immunohistochemical analysis of folate receptor alpha expression can effectively discriminate between lung adenocarcinoma and squamous cell carcinoma, a good validation of this current approach.

Drug resistance is a major obstacle facing successful development of anti-cancer therapies. Many cancers initially respond well to therapy but eventually develop drug resistance. Anti-cancer therapies exert an additional selective pressure on cancer cell populations, further affecting the clonal evolution processes resulting in the acquisition of drug resistance (Greaves and Maley, 2012). These processes are extremely difficult to investigate using tumour tissue because the invasive sampling procedures are sometimes impossible to perform. Furthermore, the biopsies might not be representative due to intra-tumour heterogeneity. Therefore, model systems are needed to investigate the mechanisms underlying the acquisition of drug resistance in cancer cells in order to develop hypotheses that can be tested on clinical material and to identify resistance pathways/biomarker signatures that can be associated with specific therapeutics.

The huge wealth of clinical research data clearly shows tumour heterogeneity at both the individual and intratumoural levels. In cancer, nonrecurring mutations and large genomic alterations generate immense heterogeneity, producing tumours populated by cells with particular characteristics. Factors such as clonal evolution and positive selective pressure from anticancer therapies also contribute significantly to tumour heterogeneity. This phenomenon has been a significant obstacle for the development of an accurate biomarker profile and associated targeted anticancer treatments. The literature clearly shows a lack of information on tumour heterogeneity at the protein level, which significantly compromises our knowledge about how protein changes contribute to subpopulation phenotypes. Over the coming years, more-reliable

biomarker signatures of tumour presence and development, together with new therapeutic strategies, will inevitably depend on the ability to further characterise tumour heterogeneity and take it into account. Interrogating proteins in the context of tumour heterogeneity using state-of-the-art omics platforms will unquestionably prove extremely useful in the clinic.

Tumour tissue samples are difficult to analyse cleanly (when compared to cell line models for example) as different cell types are present, including tumour cells, normal epithelial and stromal, and inflammatory cells, as well as vascular cells, which can contribute plasma proteins into the mixture (Schor and Schor, 2001). Many investigations have been done on complete tissue sample homogenates, so the associated proteome reflected a mixture of proteomes from different cell types. Thus, the heterogeneous characteristics of these tissue samples were missed. This is a significant problem with solid tumours, as enrichment techniques employed in studies on blood cancers (plasma cells can be enriched by targeting the marker CD138⁺ that is uniquely expressed on these cells) are difficult to apply to solid tumours.

We contribute to this effort by characterising the proteomic heterogeneity of human lung cancer biopsy samples, by investigating different regions of the tumour and comparing their proteomes to each other and to associated matched control tissue. From the data, many differences in protein abundance exist between matched control and tumour tissue samples. When comparing the quadrants of the tumour, distinct differences are apparent, and while some proteins do show a consistent abundance pattern when comparing the individual quadrant to control and identifying commonality, significant differences exist.

When trying to identify new potential biomarkers or therapeutic targets, these data emphasize the need to include many biopsy samples from the same tumour and matched control tissue in order to identify the most robust protein signatures. In the context of identifying biomarkers associated with subtypes of lung cancer that are common for most or all patients, a comprehensive analysis of many patient samples and many biopsies from these patient is required to identify strong candidate proteins. From an individualised protein signature perspective, multiple tumour biopsies and indeed multiple matched control tissue samples are needed. In tissue proteomics, tissue heterogeneity and inadequate sampling may result in low reproducibility of proteomic data, as the ratio of cells will depend on the tissue area examined.

An example of multiple biopsy testing is HER2 amplification in gastroesophageal adenocarcinoma (GEA). Given the issue of intratumoural heterogeneity in GEA specimens, it is preferable to test multiple biopsy fragments (from a primary or metastatic site) or from the resected primary tumour. The National Comprehensive Cancer Network (NCCN) Guidelines (Jouret-Mourin et al., 2012, Bartley et al., 2016) recommends a minimum of five biopsy specimens, and optimally six to eight, to account for intratumoural heterogeneity and to provide adequate tumour specimens for diagnosis and biomarker testing.

Immunohistochemical analysis of protein expression in a large number of tumour tissue samples is expensive and time consuming. Tissue microarray (TMA) technology can facilitate the sampling of hundreds of tumour and/or control tissue samples on a single slide, which can then be analysed by immunohistochemistry. In this study, TMAs were used to evaluate the abundance of some candidate proteins that were differentially expressed in tumour and control tissues. This approach was

very useful for identifying the strongest candidate biomarkers to include in more intensive investigations, but it also demonstrated the effect of tumour heterogeneity and the difficulty of finding robust biomarkers across multiple patient samples. In the future, when constructing our own TMAs, an important consideration will be to include multiple tissue samples from individual patients, representing heterogeneity at the intratumoural level, and helping refine the process of selecting strong candidate tissue biomarkers.

Laser capture microdissection (LCM), a state-of-the-art technology for isolating pure cell populations from a heterogeneous tissue specimen, may help address some of the limitations of using whole or parts of tissue homogenates. However, LCM is extremely expensive and the quality of microdissected tissues may not meet the standard quality for further analysis due to its exposure to fixatives and staining reagents (Chung and Shen, 2015). This work clearly identifies the need for multiple biopsy samples when performing proteomics analysis and confirms the importance of multiple biopsy sampling for clinical diagnosis and prognosis.

The application of metabolomics to cancer research has led to increasing interest in applying it to the identification and characterisation of metabolites associated with cancer development and progression. Although cancer has factually been regarded as an abnormality associated with uncontrolled proliferation, recent evidence has suggested that it should also be considered a metabolic disease. Growing tumours revamp their metabolic platforms to meet and even exceed the bioenergetic and biosynthetic demands of continuous cell growth and proliferation. The cancer glycolytic phenotype described decades ago by Otto Warburg, commonly known as the Warburg effect, has been found in nearly every type of cancer investigated.

Interest in and publications associated with metabolic abnormalities in cancer dramatically disappeared in the 1960s and 70s as other areas in cancer research came to the fore. Only in the last 10-15 years has interest in metabolomics been revitalised, mostly due to the increased accessibility of metabolomics and the identification of useful cancer metabolite biomarkers or “oncometabolites.” The fact that metabolomics can be performed on a range of different sample types, including tissues, cells, and bio-fluids such as serum, plasma, urine and saliva, makes this platform attractive for mining the oncometabolome.

The most investigated feature of cancer metabolism is central carbon metabolism and the relationship between glycolysis, the tricarboxylic acid (TCA) cycle, and oxidative phosphorylation. Additionally, significant differences exist in the reported levels of amino acids detected in blood samples from cancer patients. Cancer cells require certain amino acids, for example, glutamine (Gln), for DNA synthesis, angiogenesis and ultimately proteins synthesis.

Recently, Kim and co-workers showed that in the early stages of lung cancer (I and II), the relative levels of threonine, citrulline, histidine and tryptophan decrease significantly, whereas proline and isoleucine increase (Kim et al., 2015). However, significant increase in phenylalanine and ornithine during the late stages (III and IV) were discovered. In this study, a significant increase in the serum concentration of many amino acids was observed in advanced lung cancer patients. Determination of the precise mechanism underlying changes in the amino acid profiles has great potential for cancer diagnosis and treatment.

Glutamate, a nonessential amino acid, is a major bioenergetic substrate for proliferating normal and neoplastic cells. Validation studies showed a significant decrease in the level of in serum glutamate in lung cancer patients. However, the

overall profile of this cohort was from more early stage lung cancer. This contrasts with our discovery phase analysis, where a significant increase in serum glutamate was found by mass spectrometry, possibly because these samples were from advanced lung cancer patients.

Research is needed to identify amino acid profiles that discriminate individual cancer types at different stages from healthy controls. Strategies to exploit such ‘metabolic addictions’ in cancer management include depleting amino acids in blood, blocking uptake by transporters, inhibiting biosynthetic and/or catabolic enzymes, and measuring levels of specific amino acids as biomarkers.

Metabolomics and proteomics are promising complementary strategies for the effective understanding the associations between metabolites and proteins on the one hand and disease on the other, and for the development of more accurate diagnostic and monitoring tools and effective therapies. Both omics approaches help researchers to make sense of their research data, with extra layers of information available to understand tumour biology, ultimately leading to the discovery of stronger candidate biomarkers and potential therapeutic targets.

Metabolic reprogramming is a hallmark of cancer (Hanahan and Weinberg, 2011). Increased cells proliferation in cancer is common among tumours. To cope with the increased demand for energy, cancer cells must utilize all possible energy substrates. The candidate energy substrate in cancer cells is very selective. Selection of substrate utilisation is driven by some tumour driving mutations. Most cells with loss of function mutations in the P53 gene are addicted to glutamine as a source of carbon and nitrogen for synthesis of lipids and nucleotides (Xing et al., 2015). Lipid and cholesterol metabolism is also described in tumours with overall increased uptake and synthesis of lipid was observed. The accumulation of lipid droplets in cancer

cells was found associated with the aggressive type of tumours (Bozza and Viola, 2010). Adaptive glucose utilisation was the first known adaptive response of cancer cells to the stresses of nutrient scarcity and poor oxygenation within the tumour.

The mechanistic target of rapamycin (mTOR1), a serine-threonine kinase, plays a master role in regulation of cell growth, proliferation and metabolism. This pathway promotes glycolysis, lipogenesis and nucleotide synthesis and serves as a sensor for amino acids and growth factors (Chantranupong et al., 2015). Signalling of growth factor, also mediated by the PI3K/Akt pathway, promotes glucose uptake and utilisation in lipogenesis as well as regulating the supplement of Krebs's cycle with intermediate metabolites of glucose (Ward and Thompson, 2012).

Interference with tyrosine kinases using GDC-0980, a PI3K/mTOR dual inhibitor, was promising in the treatment of tumours associated with increased expression of growth factor receptors and/or gain of function mutations in the tyrosine kinases (Wallin et al., 2011). Development of tumour cell resistance to tyrosine kinase inhibitors is well documented (Camidge et al., 2014). The GDC-0980 inhibitor, meant to improve the outcome of treatment with tyrosine kinase inhibitors, is still in phase I clinical trial (Dolly et al., 2016). Cell lines provide a good model for studying the mechanisms by which tumours acquire resistance to chemotherapy or targeted therapy, including small-molecule inhibitors.

Drug resistance in cancer can be due to genetic factors and/or acquired through adaptive post-translational modifications to combat the molecular effects of drugs (McGranahan and Swanton, 2017). Dominant sub-clonal cancer cell populations with natural or acquired resistance to treatment are common in cancer. These cell populations become dominant when the drug-sensitive populations are eliminated and became responsible for tumour relapse, drug resistance and the

overall treatment outcome (McGranahan and Swanton, 2017, Greaves, 2015). Tumour resistance to treatment interferes with the clinical utility of markers that can be used for multiple reaction monitoring (MRM) of patients. Therefore, validating a panel of biomarkers for monitoring the development of drug resistance would be of great value.

In the last two chapters, GDC-0980 resistant and GDC-0980 sensitive lung adenocarcinoma H1975 and A549 cell lines (mainly H1975) were used to study and validate biomarkers that could indicate the development of resistance to GDC-0980. In A549 intrinsically resistant cells, GDC-0980 treated cells were arrested at the G1 phase, but this was reversible upon drug withdrawal. This effect was also seen in the parent A549 cells (Wallin et al., 2011). Interestingly, GDC-0980 caused irreversible cell cycle arrest at G2/M with prolonged S- cell cycle phase lag time (Figures 27, 28).

The proteins involved in cell cycle progression, including cyclins D1, D3, A2, B1, H and CDK6, were evaluated in parent H1975 (P) and resistant cells in the presence of GDC-0980 (R+) and in its absence (R-). All tested cyclins and CDK6 were significantly downregulated in resistant H1975 cells in the presence of (R+) and absence of (R-) GDC-0980 compared to the sensitive cells, but the down regulation was stronger in treated resistant cells (Figures 35- 40) (Table 51). Other cell cycle controlling proteins that showed the same expression profile include p53, p21, p50, p65 (Rel-A), Rel-B, Bcl-XL and 14.3.3 gamma. These proteins could serve as biomarkers of tumour resistance to GDC-0980 in matched mutational profile lung adenocarcinoma. Other evaluated cell cycle controlling proteins showed the opposite profiles in (R+) and (R-) cells when compared to the parent cells. These proteins include PCNA (both native and ubiquitinated), 14.3.3 α/β , 14.3.3 ζ/δ , and 14.3.3 ϵ .

Regardless of their expression profiles, these proteins are still valuable for detecting tumour resistance to GDC-0980 of same matching genetic abnormalities.

Acetylation is a post-translational modification controlling the level of gene expression by changing the overall net charge on the histones to relatively negative by adding acetyl groups to the lysine residues on the histones. This modification facilitates accessibility of transcription factors to their promoters, thus favouring gene transcription. The machinery governing the acetylation of histones consists of two set of enzymes, histone acetyl transferases (HATs) (GCN5L2 and PCAF were evaluated) and histone deacetylases (HDAC 1, 2, 3, 4, 6 and phosphorylated HDAC 4, 5 were tested). The levels of histone 3 and 4 acetylation at certain acetylation sites were evaluated in this study as well (Table 52). The results showed decreased HAT levels and elevated HDAC levels in treated H1975 cells compared to the parent cells, despite the overall increased histone acetylation. The phosphorylation of HDACs was found crucial for HDAC activity, and this was validated using SAHA (class I HDACs inhibitor) (Pflum et al., 2001). The GDC-0980 resistant H1975 cells were found to tolerate higher doses of SAHA compared to the parent cells, which indicates that HDACs play a role in the development of multiple drug resistance (Figure 70). When GDC-0980 was included in the culture media, the resistant cells became more sensitive to SAHA than the GDC-0980 parent cells, indicating that GDC-0980 affects the phosphorylation of HDACs required for their activities (Pflum et al., 2001, Steliou et al., 2012). Histone acetylation levels, when normalised for the abundance of the native histone proteins, also indicated decreased acetylation in the non-treated cells due to restoration of HDACs phosphorylation (Figure 62). Therefore, a combination of the two drugs would be better than using them as a monotherapy (Figure 71).

Whether the protein was overexpressed or down regulated (GCN5L2, PCAF, HDAC II, HDAC IV, HDAC VI, H3, H4, H3 and pyruvate levels), these findings might also be applied to immunohistochemically identify resistance to GDC-0980 in solid tumours of the same genetic abnormalities, whenever a control sample was taken before the start of treatment.

Growth curves of GDC-0980 sensitive and GDC-0980 resistant H1975 cells treated (R+) or not treated with GDC-0980 (R-) showed a depressed rate of proliferation in the GDC-0980 treated resistant cells (Figure 27). This indicates that the energy production machinery was affected by GDC-0980 as an adaptive response to maintain cell survival in the stressful environment. Seahorse is an instrument that can assess the overall activity of mitochondrial and non-mitochondrial pathways for production of ATP.

Seahorse energy phenotyping of cells relies on measuring increased acidity of the medium (ECAR), which reflects the rate of lactic acid production and the decline of oxygen concentration in the medium (OCR), which in turn reflects increased mitochondrial activity (Figure 89). Both GDC-0980 treated (R+) and non-treated (R-) GDC-0980 resistant H1975 cells showed a significant decrease in the production of lactic acid production (Figure 91), which was greater in the treated cells. GDC-0980 compromised the mitochondrial oxidative phosphorylation of resistant H1975 cells. Mitochondrial oxidative phosphorylation activity increased in GDC-0980 resistant H1975 cells (R-) compared to parent cells, as indicated by their increased oxygen consumption rate (Figure 90) and decreased production of lactate indicated by their decreased ECAR upon consumption of the glucose in the medium. A concentration of 1 μ M of GDC-0980 compromised mitochondrial oxidative phosphorylation and further depressed ECAR (Figure 91).

In the search for biomarkers to detect tumour resistance to GDC-0980, the mitochondrial membrane oxidative phosphorylation complexes were evaluated by western blot. The results summary is in table 53, and the findings are summarised in figure 92 and discussed in detail in chapter 7. The energy profiling of GDC-0980 sensitive and GDC-0980 resistant H1975 cells revealed several proteins and metabolites that might help in detecting the development of GDC-0980 resistance in solid tumours because their abundance in drug resistant tumour cells differed from that in drug-naive tumour cells. These molecules are pyruvate, acetyl coA, ketone bodies, free fatty acids as well as pyruvate dehydrogenase, lactate dehydrogenase, superoxide dismutase, succinate dehydrogenase, HSP60, Cytochrome c, cytochrome c oxidase, and voltage dependent anionic channel proteins.

8.2. Conclusion

The aims of this research were to identify abnormalities in the abundance of proteins and/or metabolites associated with lung cancer and development of drug resistance. Several strong candidate biomarkers were found in BALF for differentiating between controls and lung cancer as well as for distinguishing adenocarcinoma from squamous cell carcinoma. These potential biomarkers might be used to screen biofluids from high risk individuals (*e.g.*, those with benign lung nodules) and also to examine the BALF proteome when a definitive diagnosis of adenocarcinoma or squamous cell carcinoma is difficult to determine histologically. Many of the proteins the abundance of which was altered in BALF exhibited similar trends in tumour tissue from lung cancer patients compared to matched control. This highlights the strong relationship between tissue protein and biofluid protein levels. However, many proteins did not share such similarity in blood and BALF, results that are confirmed by the obvious tumour heterogeneity discovered by mass spectrometry of different parts of the tumour compared to matched tissue. These results highlight the need for comprehensive experimental designs when screening for new candidate biomarkers or therapeutic targets, as well as the need for multiple biopsies when diagnosing, staging and grading malignancies. The strong metabolic signature found when examining BALF and tissue was also confirmed when applying metabolomics to investigate blood samples from lung cancer patients. Proteomics and metabolomics are complementary techniques and provide additional pieces of information to help unravel the proteome or metabolome respectively. The metabolome is a stable environment, and it is likely that future biomarker panels will contain elements from both the proteome and metabolome.

Biomarker signatures relating to altered cellular pathways were also identified using a cell line model of resistance to Apitolisib (GDC-0980), a dual phosphatidylinositol-3-kinase and mammalian target of rapamycin kinase inhibitor. To that end, A549 and H1975 lung adenocarcinoma cell line models were analysed by mass spectrometry. The analysis of tumour samples from lung cancer patients developing resistance to specific anti-cancer treatments is difficult, mostly due to the difficulty of obtaining clinical material. Cell line models offer an alternative platform to understand changes at the protein level associated with the development of resistance, and to identify biomarker signatures associated with resistance in order to understand the development of resistance pathways and how to avoid or overcome them. The levels of cell cycle specific and mitochondrial associated proteins are perturbed in the resistant phenotype. This valuable information can be used to form the foundation for hypothesis-driven research on clinical material from patients treated with Apitolisib.

8.3. Future Plans

The lists of proteins that were found significantly dysregulated (upregulated and downregulated) in non-small cell lung carcinomas lavages compared to the normal lungs control lavage fluids “especially those distinguishing adenocarcinoma from squamous cell carcinoma and confirmed in the FFPE lung adenocarcinoma tissue specimens” will be studied and validated more. The validation will involve using tissues and bio-fluid samples from patients diagnosed with lung adenocarcinoma, lung squamous cell carcinoma and poorly differentiating non-small cell lung cancer. The future study will also involve training the neural network thinking software to help distinguishing the poorly differentiated and mixed types of lung cancer using the lists of proteins came off this research work in parallel with the currently used tissue- based biomarkers.

My future work would also involve immunohistochemically validation of the proteins that were found significantly changing upon development of tumour resistance to the PI3K-Akt/PKB, m-TOR dual inhibitor (GDC-0980). Some proteins such as HDACs will be tested in other forms of drug resistance in solid tumours to elucidate their possible role in multiple drug resistance. Successful candidate protein(s) that can detect early development of drug resistance in tumour tissue would be utilized to detect the resistance *in vivo* in experimental animal model of drug resistance in tumour using positron emission tomography (PETscan) or single photon emission computed tomography (SPECT).

The future plan would also involve radio-labelling of some metabolites such as glutamine and aspartate and studying their pharmacokinetics in solid tumours after intra-venous administration using PETscan as an approach to increase the clinical utility of such biomarkers and improve diagnosis of lung cancer.

References

- AALTOMAA, S., LIPPONEN, P. & SYRJÄNEN, K. 1993. Proliferating cell nuclear antigen (PCNA) immunolabeling as a prognostic factor in axillary lymph node negative breast cancer. *Anticancer Res*, 13, 533-8.
- ABBAS, T. & DUTTA, A. 2009. p21 in cancer: intricate networks and multiple activities. *Nat Rev Cancer*, 9, 400-14.
- ABRAMYUK, A., APPOLD, S., ZÖPHEL, K., HIETSCHOLD, V., BAUMANN, M. & ABOLMAALI, N. 2012. Quantitative modifications of TNM staging, clinical staging and therapeutic intent by FDG-PET/CT in patients with non small cell lung cancer scheduled for radiotherapy--a retrospective study. *Lung Cancer*, 78, 148-52.
- ABUKHDEIR, A. M. & PARK, B. H. 2008. P21 and p27: roles in carcinogenesis and drug resistance. *Expert Rev Mol Med*, 10, e19.
- ACEVES, S. S. & BROIDE, D. H. 2008. Airway fibrosis and angiogenesis due to eosinophil trafficking in chronic asthma. *Curr Mol Med*, 8, 350-8.
- ADEVA, M. M., SOUTO, G., BLANCO, N. & DONAPETRY, C. 2012. Ammonium metabolism in humans. *Metabolism*, 61, 1495-511.
- AĞABABAOĞLU, İ., ÖNEN, A., DEMİR, A. B., AKTAŞ, S., ALTUN, Z., ERSÖZ, H., ŞANL, A., ÖZDEMİR, N. & AKKOÇLU, A. 2017. Chaperonin (HSP60) and annexin-2 are candidate biomarkers for non-small cell lung carcinoma. *Medicine (Baltimore)*, 96, e5903.
- AGACKIRAN, Y., OZCAN, A., AKYUREK, N., MEMIS, L., FINDIK, G. & KAYA, S. 2012. Desmoglein-3 and Napsin A double stain, a useful immunohistochemical marker for differentiation of lung squamous cell carcinoma and adenocarcinoma from other subtypes. *Appl Immunohistochem Mol Morphol*, 20, 350-5.

AIT-SI-ALI, S., RAMIREZ, S., BARRE, F. X., DKHISSI, F., MAGNAGHI-JAULIN, L., GIRAULT, J. A., ROBIN, P., KNIBIEHLER, M., PRITCHARD, L. L., DUCOMMUN, B., TROUCHE, D. & HAREL-BELLAN, A. 1998. Histone acetyltransferase activity of CBP is controlled by cycle-dependent kinases and oncoprotein E1A. *Nature*, 396, 184-6.

AKL, H., VERVLOESSEM, T., KIVILUOTO, S., BITTREMIEUX, M., PARYS, J. B., DE SMEDT, H. & BULTYNCK, G. 2014. A dual role for the anti-apoptotic Bcl-2 protein in cancer: mitochondria versus endoplasmic reticulum. *Biochim Biophys Acta*, 1843, 2240-52.

ALAO, J. P. 2007. The regulation of cyclin D1 degradation: roles in cancer development and the potential for therapeutic invention. *Mol Cancer*, 6, 24.

ALBERT, J. M., GONZALEZ, A., MASSION, P. P., CHEN, H., OLSON, S. J., SHYR, Y., DIAZ, R., LAMBRIGHT, E. S., SANDLER, A., CARBONE, D. P., PUTNAM, J. B., JOHNSON, D. H. & LU, B. 2007. Cytoplasmic clusterin expression is associated with longer survival in patients with resected non small cell lung cancer. *Cancer Epidemiol Biomarkers Prev*, 16, 1845-51.

ALHDIRI, M. A., SAMAT, N. A. & MOHAMED, Z. 2017. Risk Estimation for Lung Cancer in Libya: Analysis Based on Standardized Morbidity Ratio, Poisson-Gamma Model, BYM Model and Mixture Model. *Asian Pac J Cancer Prev*, 18, 673-679.

ALIJO SERRANO, F., SÁNCHEZ-MORA, N., ANGEL ARRANZ, J., HERNÁNDEZ, C. & ALVAREZ-FERNÁNDEZ, E. 2007. Large cell and small cell neuroendocrine bladder carcinoma: immunohistochemical and outcome study in a single institution. *Am J Clin Pathol*, 128, 733-9.

ALMATROODI, S. A., MCDONALD, C. F., COLLINS, A. L., DARBY, I. A. & POUNIOTIS, D. S. 2015. Quantitative proteomics of bronchoalveolar lavage fluid in lung adenocarcinoma. *Cancer Genomics Proteomics*, 12, 39-48.

AMADOR, V., GE, S., SANTAMARÍA, P. G., GUARDAVACCARO, D. & PAGANO, M. 2007. APC/C(Cdc20) controls the ubiquitin-mediated degradation of p21 in prometaphase. *Mol Cell*, 27, 462-73.

AMMANAGI, A. S., DOMBALE, V. D., MISKIN, A. T., DANDAGI, G. L. & SANGOLLI, S. S. 2012. Sputum cytology in suspected cases of carcinoma of lung (Sputum cytology a poor man's bronchoscopy!). *Lung India*, 29, 19-23.

ANDO, T., CHARINDRA, D., SHRESTHA, M., UMEHARA, H., OGAWA, I., MIYAUCHI, M. & TAKATA, T. 2017. Tissue inhibitor of metalloproteinase-1 promotes cell proliferation through YAP/TAZ activation in cancer. *Oncogene*.

ANDOR, N., GRAHAM, T. A., JANSEN, M., XIA, L. C., AKTIPIS, C. A., PETRITSCH, C., JI, H. P. & MALEY, C. C. 2016. Pan-cancer analysis of the extent and consequences of intratumor heterogeneity. *Nat Med*, 22, 105-13.

ARANDA, N., HERNÁNDEZ-MARTÍNEZ, C., ARIJA, V., RIBOT, B. & CANALS, J. 2017. Haemoconcentration risk at the end of pregnancy: effects on neonatal behaviour. *Public Health Nutr*, 20, 1405-1413.

ATRIH, A., MUDALIAR, M. A., ZAKIKHANI, P., LAMONT, D. J., HUANG, J. T., BRAY, S. E., BARTON, G., FLEMING, S. & NABI, G. 2014. Quantitative proteomics in resected renal cancer tissue for biomarker discovery and profiling. *Br J Cancer*, 110, 1622-33.

AUTEN, R. L. & DAVIS, J. M. 2009. Oxygen toxicity and reactive oxygen species: the devil is in the details. *Pediatr Res*, 66, 121-7.

AZIMZADEH, O., BARJAKTAROVIC, Z., AUBELE, M., CALZADA-WACK, J., SARIOGLU, H., ATKINSON, M. J. & TAPIO, S. 2010. Formalin-fixed paraffin-embedded (FFPE) proteome analysis using gel-free and gel-based proteomics. *J Proteome Res*, 9, 4710-20.

BADIOZAMAN, R., TAHEREH, P., SHIDEH, D., MOHAMMADREZA, B., AHMADREZA, A. & SEYYEDAHMAD, T. 2013. Whole lung lavage of nine children with pulmonary alveolar proteinosis: experience in a tertiary lung center. *Iran J Pediatr*, 23, 95-9.

BAILEY, S. T., MIRON, P. L., CHOI, Y. J., KOCHUPURAKKAL, B., MAULIK, G., RODIG, S. J., TIAN, R., FOLEY, K. M., BOWMAN, T., MIRON, A., BROWN, M., IGLEHART, J. D. & DEBAJIT, K. B. 2014. NF- κ B activation-induced anti-apoptosis renders HER2-positive cells drug resistant and accelerates tumor growth. *Mol Cancer Res*, 12, 408-420.

BALDINI, E., CAMERINI, A., SGAMBATO, A., PROCHILO, T., CAPODANNO, A., PASQUALETTI, F., ORLANDINI, C., RESTA, L., BEVILACQUA, G. & COLLECCHI, P. 2006. Cyclin A and E2F1 overexpression correlate with reduced disease-free survival in node-negative breast cancer patients. *Anticancer Res*, 26, 4415-21.

BALENDIRAN, G. K., DABUR, R. & FRASER, D. 2004. The role of glutathione in cancer. *Cell Biochem Funct*, 22, 343-52.

BANSAL, P., OSMAN, D., GAN, G. N., SIMON, G. R. & BOUMBER, Y. 2016. Recent Advances in Targetable Therapeutics in Metastatic Non-Squamous NSCLC. *Front Oncol*, 6, 112.

BARGAGLI, E., OLIVIERI, C. & ROTTOLI, P. 2011. Cytokine modulators in the treatment of sarcoidosis. *Rheumatol Int*, 31, 1539-44.

BARTLEY, A. N., WASHINGTON, M. K., VENTURA, C. B., ISMAILA, N., COLASACCO, C., BENSON, A. B., CARRATO, A., GULLEY, M. L., JAIN, D., KAKAR, S., MACKAY, H. J., STREUTKER, C., TANG, L., TROXELL, M. & AJANI, J. A. 2016. HER2 Testing and Clinical Decision Making in Gastroesophageal Adenocarcinoma: Guideline From the College of American Pathologists, American Society for Clinical Pathology, and American Society of Clinical Oncology. *Arch Pathol Lab Med*, 140, 1345-1363.

BATES, S. & PETERS, G. 1995. Cyclin D1 as a cellular proto-oncogene. *Semin Cancer Biol*, 6, 73-82.

BATTAFARANO, R. J., FERNANDEZ, F. G., RITTER, J., MEYERS, B. F., GUTHRIE, T. J., COOPER, J. D. & PATTERSON, G. A. 2005. Large cell neuroendocrine carcinoma: an aggressive form of non-small cell lung cancer. *J Thorac Cardiovasc Surg*, 130, 166-72.

BAUGHMAN, R. P., TEIRSTEIN, A. S., JUDSON, M. A., ROSSMAN, M. D., YEAGER, H., BRESNITZ, E. A., DEPALO, L., HUNNINGHAKE, G., IANNUZZI, M. C., JOHNS, C. J., MCLENNAN, G., MOLLER, D. R., NEWMAN, L. S., RABIN, D. L., ROSE, C., RYBICKI, B., WEINBERGER, S. E., TERRIN, M. L., KNATTERUD, G. L., CHERNIAK, R. & GROUP, C. C. E. S. O. S. A. R. 2001. Clinical characteristics of patients in a case control study of sarcoidosis. *Am J Respir Crit Care Med*, 164, 1885-9.

BECKER, M., DE BASTIANI, M. A., MÜLLER, C. B., MARKOSKI, M. M., CASTRO, M. A. & KLAMT, F. 2014. High cofilin-1 levels correlate with cisplatin resistance in lung adenocarcinomas. *Tumour Biol*, 35, 1233-8.

BEGG, G. E., CARRINGTON, L., STOKES, P. H., MATTHEWS, J. M., WOUTERS, M. A., HUSAIN, A., LORAND, L., IISMAA, S. E. & GRAHAM, R.

- M. 2006. Mechanism of allosteric regulation of transglutaminase 2 by GTP. *Proc Natl Acad Sci U S A*, 103, 19683-8.
- BELLO, M. J. & REY, J. A. 1995. [Neurologic diseases due to alterations in oncogenes and tumor suppressing genes]. *Neurologia*, 10 Suppl 1, 20-31.
- BELLOMO, R. & RONCO, C. 2005. New ideas in science and medicine and the renal control of acid-base balance. *Int J Artif Organs*, 28, 957-60.
- BEN-HAIM, S. & ELL, P. 2009. 18F-FDG PET and PET/CT in the evaluation of cancer treatment response. *J Nucl Med*, 50, 88-99.
- BENDEN, C., HARPUR-SINCLAIR, O., RANASINGHE, A. S., HARTLEY, J. C., ELLIOTT, M. J. & AURORA, P. 2007. Surveillance bronchoscopy in children during the first year after lung transplantation: Is it worth it? *Thorax*, 62, 57-61.
- BERENDSEN, H. H., DE LEIJ, L., POPPEMA, S., POSTMUS, P. E., BOES, A., SLUITER, H. J. & THE, H. 1989. Clinical characterization of non-small-cell lung cancer tumors showing neuroendocrine differentiation features. *J Clin Oncol*, 7, 1614-20.
- BHUTIA, Y. D., BABU, E., RAMACHANDRAN, S. & GANAPATHY, V. 2015. Amino Acid transporters in cancer and their relevance to "glutamine addiction": novel targets for the design of a new class of anticancer drugs. *Cancer Res*, 75, 1782-8.
- BILIRAN, H., WANG, Y., BANERJEE, S., XU, H., HENG, H., THAKUR, A., BOLLIG, A., SARKAR, F. H. & LIAO, J. D. 2005. Overexpression of cyclin D1 promotes tumor cell growth and confers resistance to cisplatin-mediated apoptosis in an elastase-myc transgene-expressing pancreatic tumor cell line. *Clin Cancer Res*, 11, 6075-86.

- BINI, A., BRANDOLINI, J., CASSANELLI, N., DAVOLI, F., DOLCI, G., SELLITRI, F. & STELLA, F. 2008. Typical and atypical pulmonary carcinoids: our institutional experience. *Interact Cardiovasc Thorac Surg*, 7, 415-8.
- BIXBY, D. & TALPAZ, M. 2009. Mechanisms of resistance to tyrosine kinase inhibitors in chronic myeloid leukemia and recent therapeutic strategies to overcome resistance. *Hematology Am Soc Hematol Educ Program*, 461-76.
- BLAGOSKLONNY, M. V. 1997. Loss of function and p53 protein stabilization. *Oncogene*, 15, 1889-93.
- BLUM, K. S. & PABST, R. 2006. Keystones in lymph node development. *J Anat*, 209, 585-95.
- BODALAL, Z., AZZUZ, R. & BENDARDAF, R. 2014. Cancers in Eastern Libya: first results from Benghazi Medical Center. *World J Gastroenterol*, 20, 6293-301.
- BORCZUK, A. C. 2008. Benign tumors and tumorlike conditions of the lung. *Arch Pathol Lab Med*, 132, 1133-48.
- BOS, P. D., ZHANG, X. H., NADAL, C., SHU, W., GOMIS, R. R., NGUYEN, D. X., MINN, A. J., VAN DE VIJVER, M. J., GERALD, W. L., FOEKENS, J. A. & MASSAGUÉ, J. 2009. Genes that mediate breast cancer metastasis to the brain. *Nature*, 459, 1005-9.
- BOUCHAL, P., ROUMELIOTIS, T., HRSTKA, R., NENUTIL, R., VOJTESEK, B. & GARBIS, S. D. 2009. Biomarker discovery in low-grade breast cancer using isobaric stable isotope tags and two-dimensional liquid chromatography-tandem mass spectrometry (iTRAQ-2DLC-MS/MS) based quantitative proteomic analysis. *J Proteome Res*, 8, 362-73.

BOUSQUET, J., CLARK, T. J., HURD, S., KHALTAEV, N., LENFANT, C., O'BYRNE, P. & SHEFFER, A. 2007. GINA guidelines on asthma and beyond. *Allergy*, 62, 102-12.

BOZZA, P. T. & VIOLA, J. P. 2010. Lipid droplets in inflammation and cancer. *Prostaglandins Leukot Essent Fatty Acids*, 82, 243-50.

BRADFORD, M. M. 1976. A rapid and sensitive method for the quantitation of microgram quantities of protein utilizing the principle of protein-dye binding. *Anal Biochem*, 72, 248-54.

BRAJER-LUFTMANN, B., NOWICKA, A., KACZMAREK, M., GRABICKI, M., KUŹNAR-KAMIŃSKA, B., BROMIŃSKA, B., SIKORA, J. & BATURA-GABRYEL, H. 2016. Myeloid-derived suppressor cells in bronchoalveolar lavage fluid in patients with chronic obstructive pulmonary disease. *Pol Arch Med Wewn*, 126, 980-988.

BRAMBILLA, C., FIEVET, F., JEANMART, M., DE FRAIPONT, F., LANTUEJOUL, S., FRAPPAT, V., FERRETTI, G., BRICHON, P. Y. & MORO-SIBILOT, D. 2003. Early detection of lung cancer: role of biomarkers. *Eur Respir J Suppl*, 39, 36s-44s.

BRATT, T. 2000. Lipocalins and cancer. *Biochim Biophys Acta*, 1482, 318-26.

BREMNES, R. M., DØNNEM, T., AL-SAAD, S., AL-SHIBLI, K., ANDERSEN, S., SIRERA, R., CAMPS, C., MARINEZ, I. & BUSUND, L. T. 2011. The role of tumor stroma in cancer progression and prognosis: emphasis on carcinoma-associated fibroblasts and non-small cell lung cancer. *J Thorac Oncol*, 6, 209-17.

BREWSTER, C. E., HOWARTH, P. H., DJUKANOVIC, R., WILSON, J., HOLGATE, S. T. & ROCHE, W. R. 1990. Myofibroblasts and subepithelial fibrosis in bronchial asthma. *Am J Respir Cell Mol Biol*, 3, 507-11.

BROCK, M. V., HOOKER, C. M., SYPHARD, J. E., WESTRA, W., XU, L., ALBERG, A. J., MASON, D., BAYLIN, S. B., HERMAN, J. G., YUNG, R. C., BRAHMER, J., RUDIN, C. M., ETTINGER, D. S. & YANG, S. C. 2005. Surgical resection of limited disease small cell lung cancer in the new era of platinum chemotherapy: Its time has come. *J Thorac Cardiovasc Surg*, 129, 64-72.

BROWNBACK, K. R. & SIMPSON, S. Q. 2013. Association of bronchoalveolar lavage yield with chest computed tomography findings and symptoms in immunocompromised patients. *Ann Thorac Med*, 8, 153-9.

BUDCZIES, J., PFITZNER, B. M., GYÖRFFY, B., WINZER, K. J., RADKE, C., DIETEL, M., FIEHN, O. & DENKERT, C. 2015. Glutamate enrichment as new diagnostic opportunity in breast cancer. *Int J Cancer*, 136, 1619-28.

BURKE, L. M., RUSH, W. I., KHOOR, A., MACKAY, B., OLIVEIRA, P., WHITSETT, J. A., SINGH, G., TURNICKY, R., FLEMING, M. V., KOSS, M. N. & TRAVIS, W. D. 1999. Alveolar adenoma: a histochemical, immunohistochemical, and ultrastructural analysis of 17 cases. *Hum Pathol*, 30, 158-67.

BYERS, L. A. & RUDIN, C. M. 2015. Small cell lung cancer: where do we go from here? *Cancer*, 121, 664-72.

CAIRNS, R. A., HARRIS, I., MCCRACKEN, S. & MAK, T. W. 2011a. Cancer cell metabolism. *Cold Spring Harb Symp Quant Biol*, 76, 299-311.

CAIRNS, R. A., HARRIS, I. S. & MAK, T. W. 2011b. Regulation of cancer cell metabolism. *Nat Rev Cancer*, 11, 85-95.

CALLEJÓN-LEBLIC, B., GARCÍA-BARRERA, T., GRÁVALOS-GUZMÁN, J., PEREIRA-VEGA, A. & GÓMEZ-ARIZA, J. L. 2016. Metabolic profiling of potential lung cancer biomarkers using bronchoalveolar lavage fluid and the

integrated direct infusion/ gas chromatography mass spectrometry platform. *J Proteomics*, 145, 197-206.

CAMIDGE, D. R., PAO, W. & SEQUIST, L. V. 2014. Acquired resistance to TKIs in solid tumours: learning from lung cancer. *Nat Rev Clin Oncol*, 11, 473-81.

CAMPBELL, I. A. & BAH-SOW, O. 2006. Pulmonary tuberculosis: diagnosis and treatment. *BMJ*, 332, 1194-7.

CAO, Y., LIANG, H., ZHANG, F., LUAN, Z., ZHAO, S., WANG, X. A., LIU, S., BAO, R., SHU, Y., MA, Q., ZHU, J. & LIU, Y. 2016. Prohibitin overexpression predicts poor prognosis and promotes cell proliferation and invasion through ERK pathway activation in gallbladder cancer. *J Exp Clin Cancer Res*, 35, 68.

CAPARICA, R., DE CASTRO, G., JR., GIL-BAZO, I., CAGLEVIC, C., CALOGERO, R., GIALLOMBARDO, M., SANTOS, E. S., RAEZ, L. E. & ROLFO, C. 2016. BRAF mutations in non-small cell lung cancer: has finally Janus opened the door? *Crit Rev Oncol Hematol*, 101, 32-9.

CAPUTI, M., ESPOSITO, V., GROGER, A. M., PACILIO, C., MURABITO, M., DEKAN, G., BALDI, F., WOLNER, E. & GIORDANO, A. 1998. Prognostic role of proliferating cell nuclear antigen in lung cancer: an immunohistochemical analysis. *In Vivo*, 12, 85-8.

CARDARELLA, S. & JOHNSON, B. E. 2013. The impact of genomic changes on treatment of lung cancer. *Am J Respir Crit Care Med*, 188, 770-5.

CARPAGNANO, G. E., FOSCHINO-BARBARO, M. P., RESTA, O., GRAMICCIONI, E. & CARPAGNANO, F. 2004. Endothelin-1 is increased in the breath condensate of patients with non-small-cell lung cancer. *Oncology*, 66, 180-4.

CARPAGNANO, G. E., SPANEVELLO, A., PALLADINO, G. P., GRAMICCIONI, C., RUGGIERI, C., CARPAGNANO, F. & FOSCHINO

- BARBARO, M. P. 2010. Cigarette smoke and increased COX-2 and survivin levels in exhaled breath condensate of lung cancer patients: how hot is the link? *Lung Cancer*, 67, 108-13.
- CARRIAGA, M. T. & HENSON, D. E. 1995. The histologic grading of cancer. *Cancer*, 75, 406-21.
- CASADONTE, R. & CAPRIOLI, R. M. 2011. Proteomic analysis of formalin-fixed paraffin-embedded tissue by MALDI imaging mass spectrometry. *Nat Protoc*, 6, 1695-709.
- CASTAÑÓN, E., SOLTERMANN, A., LÓPEZ, I., ROMÁN, M., ECAY, M., COLLANTES, M., REDRADO, M., BARAIBAR, I., LÓPEZ-PICAZO, J. M., ROLFO, C., VIDAL-VANACLOCHA, F., RAEZ, L., WEDER, W., CALVO, A. & GIL-BAZO, I. 2017. The inhibitor of differentiation-1 (Id1) enables lung cancer liver colonization through activation of an EMT program in tumor cells and establishment of the pre-metastatic niche. *Cancer Lett*, 402, 43-51.
- CASTRANOVA, V. & VALLYATHAN, V. 2000. Silicosis and coal workers' pneumoconiosis. *Environ Health Perspect*, 108 Suppl 4, 675-84.
- CASTRO, M. A., DAL-PIZZOL, F., ZDANOV, S., SOARES, M., MÜLLER, C. B., LOPES, F. M., ZANOTTO-FILHO, A., DA CRUZ FERNANDES, M., MOREIRA, J. C., SHACTER, E. & KLAMT, F. 2010. CFL1 expression levels as a prognostic and drug resistance marker in nonsmall cell lung cancer. *Cancer*, 116, 3645-55.
- CERILLI, L. A., RITTER, J. H., MILLS, S. E. & WICK, M. R. 2001. Neuroendocrine neoplasms of the lung. *Am J Clin Pathol*, 116 Suppl, S65-96.
- CERNE, D., ZITNIK, I. P. & SOK, M. 2010. Increased fatty acid synthase activity in non-small cell lung cancer tissue is a weaker predictor of shorter patient survival than increased lipoprotein lipase activity. *Arch Med Res*, 41, 405-9.

- CHADHA, M., KULSHRESTHA, M. & BIYANI, A. 2015. Anaesthesia for bronchoscopy. *Indian J Anaesth*, 59, 565-73.
- CHAFT, J. E., REKHTMAN, N., LADANYI, M. & RIELY, G. J. 2012. ALK-rearranged lung cancer: adenosquamous lung cancer masquerading as pure squamous carcinoma. *J Thorac Oncol*, 7, 768-9.
- CHAN, H. M. & LA THANGUE, N. B. 2001. p300/CBP proteins: HATs for transcriptional bridges and scaffolds. *J Cell Sci*, 114, 2363-73.
- CHANTRANUPONG, L., WOLFSON, R. L. & SABATINI, D. M. 2015. Nutrient-sensing mechanisms across evolution. *Cell*, 161, 67-83.
- CHARIOT, P., RATINEY, R., AMMI-SAID, M., HÉRIGAULT, R., ADNOT, S. & GHERARDI, R. 1994. Optimal handling of blood samples for routine measurement of lactate and pyruvate. *Arch Pathol Lab Med*, 118, 695-7.
- CHASSAGNON, G., BENNANI, S. & REVEL, M. P. 2017. [New TNM classification of non-small cell lung cancer]. *Rev Pneumol Clin*, 73, 34-39.
- CHE, X. H., CHEN, H., XU, Z. M., SHANG, C., SUN, K. L. & FU, W. N. 2010. 14-3-3epsilon contributes to tumour suppression in laryngeal carcinoma by affecting apoptosis and invasion. *BMC Cancer*, 10, 306.
- CHEN, K. N. 2016. [Small Cell Lung Cancer and TNM Staging]. *Zhongguo Fei Ai Za Zhi*, 19, 409-12.
- CHEN, M., HUANG, J., ZHU, Z., ZHANG, J. & LI, K. 2013. Systematic review and meta-analysis of tumor biomarkers in predicting prognosis in esophageal cancer. *BMC Cancer*, 13, 539.
- CHEN, P., ZHENG, X., ZHOU, Y., XU, Y., ZHU, L. & QIAN, Y. 2017. Talin-1 interaction network promotes hepatocellular carcinoma progression. *Oncotarget*, 8, 13003-13014.

- CHEN, W., LI, Z., BAI, L. & LIN, Y. 2011. NF-kappaB in lung cancer, a carcinogenesis mediator and a prevention and therapy target. *Front Biosci (Landmark Ed)*, 16, 1172-85.
- CHEN, W., ZHENG, R., BAADE, P. D., ZHANG, S., ZENG, H., BRAY, F., JEMAL, A., YU, X. Q. & HE, J. 2016. Cancer statistics in China, 2015. *CA Cancer J Clin*, 66, 115-32.
- CHEN, Z. J. 2005. Ubiquitin signalling in the NF-kappaB pathway. *Nat Cell Biol*, 7, 758-65.
- CHENG, G., FAN, X., HAO, M., WANG, J., ZHOU, X. & SUN, X. 2016. Higher levels of TIMP-1 expression are associated with a poor prognosis in triple-negative breast cancer. *Mol Cancer*, 15, 30.
- CHHAJED, P. N., ABOYOUN, C., MALOUF, M. A., HOPKINS, P. M., PLIT, M. L. & GLANVILLE, A. R. 2003. Risk factors and management of bleeding associated with transbronchial lung biopsy in lung transplant recipients. *J Heart Lung Transplant*, 22, 195-7.
- CHILES, C. 2014. Lung cancer screening with low-dose computed tomography. *Radiol Clin North Am*, 52, 27-46.
- CHUANG, M. T., MARCHEVSKY, A., TEIRSTEIN, A. S., KIRSCHNER, P. A. & KLEINERMAN, J. 1984. Diagnosis of lung cancer by fiberoptic bronchoscopy: problems in the histological classification of non-small cell carcinomas. *Thorax*, 39, 175-8.
- CHUNG, S. H. & SHEN, W. 2015. Laser capture microdissection: from its principle to applications in research on neurodegeneration. *Neural Regen Res*, 10, 897-8.
- CICENAS, S., ZALIENE, A. & ATKOCIUS, V. 2009. [Treatment outcome of locally advanced stage IIIA/B lung cancer]. *Medicina (Kaunas)*, 45, 452-9.

CINETTO, F., COMPAGNO, N., SCARPA, R., MALIPIERO, G. & AGOSTINI, C. 2015. Rituximab in refractory sarcoidosis: a single centre experience. *Clin Mol Allergy*, 13, 19.

CIOPPA, A. B. G. D. 2017. *Fundamentals of Clinical Research*.

COATES, P. J., NENUTIL, R., MCGREGOR, A., PICKSLEY, S. M., CROUCH, D. H., HALL, P. A. & WRIGHT, E. G. 2001. Mammalian prohibitin proteins respond to mitochondrial stress and decrease during cellular senescence. *Exp Cell Res*, 265, 262-73.

CONCANNON, J. P., DALBOW, M. H. & FRICH, J. C. 1973. Carcinoembryonic antigen (CEA) plasma levels in untreated cancer patients and patients with metastatic disease. *Radiology*, 108, 191-3.

CONCANNON, J. P., DALBOW, M. H., LIEBLER, G. A., BLAKE, K. E., WEIL, C. S. & COOPER, J. W. 1974. The carcinoembryonic antigen assay in bronchogenic carcinoma. *Cancer*, 34, 184-92.

CORTI, L., TONIOLO, L., BOSO, C., COLAUT, F., FIORE, D., MUZZIO, P. C., KOUKOURAKIS, M. I., MAZZAROTTO, R., PIGNATARO, M., LOREGGIAN, L. & SOTTI, G. 2007. Long-term survival of patients treated with photodynamic therapy for carcinoma in situ and early non-small-cell lung carcinoma. *Lasers Surg Med*, 39, 394-402.

CORY, S., ROBERTS, A. W., COLMAN, P. M. & ADAMS, J. M. 2016. Targeting BCL-2-like Proteins to Kill Cancer Cells. *Trends Cancer*, 2, 443-460.

CRUTCHFIELD, C. A., THOMAS, S. N., SOKOLL, L. J. & CHAN, D. W. 2016. Advances in mass spectrometry-based clinical biomarker discovery. *Clin Proteomics*, 13, 1.

- CRYSTAL, R. G., REYNOLDS, H. Y. & KALICA, A. R. 1986. Bronchoalveolar lavage. The report of an international conference. *Chest*, 90, 122-31.
- CUADRAS, A., ROVIRA, E., MARCÉ, R. M. & BORRULL, F. 2016. Lung cancer risk by polycyclic aromatic hydrocarbons in a Mediterranean industrialized area. *Environ Sci Pollut Res Int*, 23, 23215-23227.
- CULLINAN, P. & REID, P. 2013. Pneumoconiosis. *Prim Care Respir J*, 22, 249-52.
- CUTTING, G. R. 2015. Cystic fibrosis genetics: from molecular understanding to clinical application. *Nat Rev Genet*, 16, 45-56.
- D'COSTA, J. J., GOLDSMITH, J. C., WILSON, J. S., BRYAN, R. T. & WARD, D. G. 2016. A Systematic Review of the Diagnostic and Prognostic Value of Urinary Protein Biomarkers in Urothelial Bladder Cancer. *Bladder Cancer*, 2, 301-317.
- DALLINGA, J. W., SMOLINSKA, A. & VAN SCHOOTEN, F. J. 2014. Analysis of volatile organic compounds in exhaled breath by gas chromatography-mass spectrometry combined with chemometric analysis. *Methods Mol Biol*, 1198, 251-63.
- DAN, S., YOSHIMI, H., OKAMURA, M., MUKAI, Y. & YAMORI, T. 2009. Inhibition of PI3K by ZSTK474 suppressed tumor growth not via apoptosis but G0/G1 arrest. *Biochem Biophys Res Commun*, 379, 104-9.
- DANCEWICZ, M., SZYMANKIEWICZ, M., BELLA, M., SWINIARSKA, J. & KOWALEWSKI, J. 2009. [Bronchial bacterial colonization in patients with lung cancer]. *Pneumonol Alergol Pol*, 77, 242-7.
- DAVIDOFF, A. M., KERNS, B. J., PENCE, J. C., MARKS, J. R. & IGLEHART, J. D. 1991. p53 alterations in all stages of breast cancer. *J Surg Oncol*, 48, 260-7.
- DAVIES, A. M., LARA, P. N., LAU, D. H. & GANDARA, D. R. 2004. Treatment of extensive small cell lung cancer. *Hematol Oncol Clin North Am*, 18, 373-85.

- DE WEERDT, A., DENDOOVEN, A., SNOECKX, A., PEN, J., LAMMENS, M. & JORENS, P. G. 2017. Prognosis and treatment of FOLFOX therapy related interstitial pneumonia: a plea for multimodal immune modulating therapy in the respiratory insufficient patient. *BMC Cancer*, 17, 586.
- DEBERARDINIS, R. J., LUM, J. J., HATZIVASSILIOU, G. & THOMPSON, C. B. 2008. The biology of cancer: metabolic reprogramming fuels cell growth and proliferation. *Cell Metab*, 7, 11-20.
- DEIDDA M, P. C., BASSAREO P, DESSALVI C, MERCURO G. 2015. Metabolomics, a promising approach to translational research in cardiology. *IJC Metabolic & Endocrine*.
- DELLAMBRA, E., GOLISANO, O., BONDANZA, S., SIVIERO, E., LACAL, P., MOLINARI, M., D'ATRI, S. & DE LUCA, M. 2000. Downregulation of 14-3-3sigma prevents clonal evolution and leads to immortalization of primary human keratinocytes. *J Cell Biol*, 149, 1117-30.
- DENG, C., ZHANG, P., HARPER, J. W., ELLEDGE, S. J. & LEDER, P. 1995. Mice lacking p21CIP1/WAF1 undergo normal development, but are defective in G1 checkpoint control. *Cell*, 82, 675-84.
- DESINIOTIS, A. & KYPRIANOU, N. 2011. Significance of talin in cancer progression and metastasis. *Int Rev Cell Mol Biol*, 289, 117-47.
- DEVIC, S. 2016. Warburg Effect - a Consequence or the Cause of Carcinogenesis? *J Cancer*, 7, 817-22.
- DEVOUASSOUX-SHISHEBORAN, M., HAYASHI, T., LINNOILA, R. I., KOSS, M. N. & TRAVIS, W. D. 2000. A clinicopathologic study of 100 cases of pulmonary sclerosing hemangioma with immunohistochemical studies: TTF-1 is expressed in

both round and surface cells, suggesting an origin from primitive respiratory epithelium. *Am J Surg Pathol*, 24, 906-16.

DOHERTY, J. R. & CLEVELAND, J. L. 2013. Targeting lactate metabolism for cancer therapeutics. *J Clin Invest*, 123, 3685-92.

DOLLY, S. O., WAGNER, A. J., BENDELL, J. C., KINDLER, H. L., KRUG, L. M., SEIWERT, T. Y., ZAUDERER, M. G., LOLKEMA, M. P., APT, D., YEH, R. F., FREDRICKSON, J. O., SPOERKE, J. M., KOEPPEN, H., WARE, J. A., LAUCHLE, J. O., BURRIS, H. A. & DE BONO, J. S. 2016. Phase I Study of Apitolisib (GDC-0980), Dual Phosphatidylinositol-3-Kinase and Mammalian Target of Rapamycin Kinase Inhibitor, in Patients with Advanced Solid Tumors. *Clin Cancer Res*, 22, 2874-84.

DONNEM, T., HALD, S. M., PAULSEN, E. E., RICHARDSEN, E., AL-SAAD, S., KILVAER, T. K., BRUSTUGUN, O. T., HELLAND, A., LUND-IVERSEN, M., POEHL, M., OLSEN, K. E., DITZEL, H. J., HANSEN, O., AL-SHIBLI, K., KISELEV, Y., SANDANGER, T. M., ANDERSEN, S., PEZZELLA, F., BREMNES, R. M. & BUSUND, L. T. 2015. Stromal CD8+ T-cell Density—A Promising Supplement to TNM Staging in Non-Small Cell Lung Cancer. *Clin Cancer Res*, 21, 2635-43.

DOUGHERTY, M. K. & MORRISON, D. K. 2004. Unlocking the code of 14-3-3. *J Cell Sci*, 117, 1875-84.

DOWLING, P. 2018. DIGE Saturation Labeling for Scarce Amounts of Protein from Formalin-Fixed Paraffin-Embedded (FFPE) Tissue. *Methods Mol Biol*, 1664, 87-91.

DOWLING, P., HAYES, C., TING, K. R., HAMEED, A., MEILLER, J., MITSIADES, C., ANDERSON, K. C., CLYNES, M., CLARKE, C., RICHARDSON, P. & O'GORMAN, P. 2014. Identification of proteins found to be

significantly altered when comparing the serum proteome from Multiple Myeloma patients with varying degrees of bone disease. *BMC Genomics*, 15, 904.

DU, Z. P., WU, B. L., WU, X., LIN, X. H., QIU, X. Y., ZHAN, X. F., WANG, S. H., SHEN, J. H., ZHENG, C. P., WU, Z. Y., XU, L. Y., WANG, D. & LI, E. M. 2015. A systematic analysis of human lipocalin family and its expression in esophageal carcinoma. *Sci Rep*, 5, 12010.

DUBREY, S., SHARMA, R., UNDERWOOD, R., MITTAL, T. & WELLS, A. 2016. Sarcoidosis of the cardio-pulmonary systems. *Clin Med (Lond)*, 16, 34-41.

EDGE, S. B. & COMPTON, C. C. 2010. The American Joint Committee on Cancer: the 7th edition of the AJCC cancer staging manual and the future of TNM. *Ann Surg Oncol*, 17, 1471-4.

EDSTRÖM, S., CVETKOVSKA, E., WESTIN, T. & YOUNG, C. 2001. Overexpression of p53-related proteins predicts rapid growth rate of head and neck cancer. *Laryngoscope*, 111, 124-30.

EDWARDS, S. L., ROBERTS, C., MCKEAN, M. E., COCKBURN, J. S., JEFFREY, R. R. & KERR, K. M. 2000. Preoperative histological classification of primary lung cancer: accuracy of diagnosis and use of the non-small cell category. *J Clin Pathol*, 53, 537-40.

EHRHART, N. 1998. Principles of tumor biopsy. *Clin Tech Small Anim Pract*, 13, 10-6.

EIGENBRODT, E., REINACHER, M., SCHEEFERS-BORCHEL, U., SCHEEFERS, H. & FRIIS, R. 1992. Double role for pyruvate kinase type M2 in the expansion of phosphometabolite pools found in tumor cells. *Crit Rev Oncog*, 3, 91-115.

EL MISTIRI, M., SALATI, M., MARCHESELLI, L., ATTIA, A., HABIL, S., ALHOMRI, F., SPIKA, D., ALLEMANI, C. & FEDERICO, M. 2015. Cancer incidence, mortality, and survival in Eastern Libya: updated report from the Benghazi Cancer Registry. *Ann Epidemiol*, 25, 564-8.

EL MISTIRI, M., VERDECCHIA, A., RASHID, I., EL SAHLI, N., EL MANGUSH, M. & FEDERICO, M. 2007. Cancer incidence in eastern Libya: the first report from the Benghazi Cancer Registry, 2003. *Int J Cancer*, 120, 392-7.

ELBENDARY, A. A., CIRISANO, F. D., EVANS, A. C., DAVIS, P. L., IGLEHART, J. D., MARKS, J. R. & BERCHUCK, A. 1996. Relationship between p21 expression and mutation of the p53 tumor suppressor gene in normal and malignant ovarian epithelial cells. *Clin Cancer Res*, 2, 1571-5.

ENDO, H., YANO, M., OKUMURA, Y. & KIDO, H. 2014. Ibuprofen enhances the anticancer activity of cisplatin in lung cancer cells by inhibiting the heat shock protein 70. *Cell Death Dis*, 5, e1027.

ENGEL, A. G. & REBOUCHE, C. J. 1984. Carnitine metabolism and inborn errors. *J Inherit Metab Dis*, 7 Suppl 1, 38-43.

ENGELMAN, J. A., CHEN, L., TAN, X., CROSBY, K., GUIMARAES, A. R., UPADHYAY, R., MAIRA, M., MCNAMARA, K., PERERA, S. A., SONG, Y., CHIRIEAC, L. R., KAUR, R., LIGHTBOWN, A., SIMENDINGER, J., LI, T., PADERA, R. F., GARCÍA-ECHEVERRÍA, C., WEISSLEDER, R., MAHMOOD, U., CANTLEY, L. C. & WONG, K. K. 2008. Effective use of PI3K and MEK inhibitors to treat mutant Kras G12D and PIK3CA H1047R murine lung cancers. *Nat Med*, 14, 1351-6.

ESPOSITO, V., BALDI, A., TONINI, G., VINCENZI, B., SANTINI, M., AMBROGI, V., MINEO, T. C., PERSICHETTI, P., LIUZZI, G.,

MONTESARCHIO, V., WOLNER, E., BALDI, F. & GROEGER, A. M. 2004. Analysis of cell cycle regulator proteins in non-small cell lung cancer. *J Clin Pathol*, 57, 58-63.

FALA, L. 2016. Portrazza (Necitumumab), an IgG1 Monoclonal Antibody, FDA Approved for Advanced Squamous Non-Small-Cell Lung Cancer. *Am Health Drug Benefits*, 9, 119-22.

FAN, T., LI, R., TODD, N. W., QIU, Q., FANG, H. B., WANG, H., SHEN, J., ZHAO, R. Y., CARAWAY, N. P., KATZ, R. L., STASS, S. A. & JIANG, F. 2007. Up-regulation of 14-3-3zeta in lung cancer and its implication as prognostic and therapeutic target. *Cancer Res*, 67, 7901-6.

FENG, J., SHENG, H., ZHU, C., QIAN, X., WAN, D., SU, D., CHEN, X. & ZHU, L. 2016. Correlation of neuroendocrine features with prognosis of non-small cell lung cancer. *Oncotarget*, 7, 71727-71736.

FERGUSON, A. T., EVRON, E., UMBRICH, C. B., PANDITA, T. K., CHAN, T. A., HERMEKING, H., MARKS, J. R., LAMBERS, A. R., FUTREAL, P. A., STAMPFER, M. R. & SUKUMAR, S. 2000. High frequency of hypermethylation at the 14-3-3 sigma locus leads to gene silencing in breast cancer. *Proc Natl Acad Sci U S A*, 97, 6049-54.

FERLAY, J., SOERJOMATARAM, I., DIKSHIT, R., ESER, S., MATHERS, C., REBELO, M., PARKIN, D. M., FORMAN, D. & BRAY, F. 2015. Cancer incidence and mortality worldwide: sources, methods and major patterns in GLOBOCAN 2012. *Int J Cancer*, 136, E359-86.

FERON, O. 2009. Pyruvate into lactate and back: from the Warburg effect to symbiotic energy fuel exchange in cancer cells. *Radiother Oncol*, 92, 329-33.

- FESTIC, E. & SCANLON, P. D. 2015. Incident pneumonia and mortality in patients with chronic obstructive pulmonary disease. A double effect of inhaled corticosteroids? *Am J Respir Crit Care Med*, 191, 141-8.
- FIELD, J. K., SPANDIDOS, D. A. & STELL, P. M. 1992. Overexpression of p53 gene in head-and-neck cancer, linked with heavy smoking and drinking. *Lancet*, 339, 502-3.
- FILOSSO, P. L., GUERRERA, F., EVANGELISTA, A., GALASSI, C., WELTER, S., RENDINA, E. A., TRAVIS, W., LIM, E., SARKARIA, I., THOMAS, P. A. & CONTRIBUTORS, E. L. N. W. G. 2017. Adjuvant chemotherapy for large-cell neuroendocrine lung carcinoma: results from the European Society for Thoracic Surgeons Lung Neuroendocrine Tumours Retrospective Database. *Eur J Cardiothorac Surg*.
- FINUCANE, D. M., BOSSY-WETZEL, E., WATERHOUSE, N. J., COTTER, T. G. & GREEN, D. R. 1999. Bax-induced caspase activation and apoptosis via cytochrome c release from mitochondria is inhibitable by Bcl-xL. *J Biol Chem*, 274, 2225-33.
- FLOWER, D. R. 1996. The lipocalin protein family: structure and function. *Biochem J*, 318 (Pt 1), 1-14.
- FORMAN, D. T. & YOUNG, D. S. 1976. Drug interference in laboratory testing. *Ann Clin Lab Sci*, 6, 263-71.
- FRESE, S., SCHAPER, M., KUSTER, J. R., MIESCHER, D., JÄÄTTELÄ, M., BUEHLER, T. & SCHMID, R. A. 2003. Cell death induced by down-regulation of heat shock protein 70 in lung cancer cell lines is p53-independent and does not require DNA cleavage. *J Thorac Cardiovasc Surg*, 126, 748-54.

- FUERTES, M. A., CASTILLA, J., ALONSO, C. & PÉREZ, J. M. 2003. Cisplatin biochemical mechanism of action: from cytotoxicity to induction of cell death through interconnections between apoptotic and necrotic pathways. *Curr Med Chem*, 10, 257-66.
- FUJIWARA, N., INOUE, J., KAWANO, T., TANIMOTO, K., KOZAKI, K. & INAZAWA, J. 2015. miR-634 Activates the Mitochondrial Apoptosis Pathway and Enhances Chemotherapy-Induced Cytotoxicity. *Cancer Res*, 75, 3890-901.
- FUKAI, T. & USHIO-FUKAI, M. 2011. Superoxide dismutases: role in redox signaling, vascular function, and diseases. *Antioxid Redox Signal*, 15, 1583-606.
- FUNG, M. K. L. & CHAN, G. C. 2017. Drug-induced amino acid deprivation as strategy for cancer therapy. *J Hematol Oncol*, 10, 144.
- GAZDAR, A. F., GAO, B. & MINNA, J. D. 2010a. Lung cancer cell lines: Useless artifacts or invaluable tools for medical science? *Lung Cancer*, 68, 309-18.
- GAZDAR, A. F., GIRARD, L., LOCKWOOD, W. W., LAM, W. L. & MINNA, J. D. 2010b. Lung cancer cell lines as tools for biomedical discovery and research. *J Natl Cancer Inst*, 102, 1310-21.
- GEE, J. B. & FICK, R. B. 1980. Bronchoalveolar lavage. *Thorax*, 35, 1-8.
- GIBBS, A. R. & THUNNISSEN, F. B. 2001. Histological typing of lung and pleural tumours: third edition. *J Clin Pathol*, 54, 498-9.
- GIBSON, L. F., FORTNEY, J., MAGRO, G., ERICSON, S. G., LYNCH, J. P. & LANDRETH, K. S. 1999. Regulation of BAX and BCL-2 expression in breast cancer cells by chemotherapy. *Breast Cancer Res Treat*, 55, 107-17.
- GILLET, R., GRIMBER, G., BENNOUN, M., CARON DE FROMENTEL, C., BRIAND, P. & JOULIN, V. 2000. The consequence of p53 overexpression for liver

tumor development and the response of transformed murine hepatocytes to genotoxic agents. *Oncogene*, 19, 3498-507.

GJEVRE, J. A., MYERS, J. L. & PRAKASH, U. B. 1996. Pulmonary hamartomas. *Mayo Clin Proc*, 71, 14-20.

GOLD, P. & FREEDMAN, S. O. 1965. DEMONSTRATION OF TUMOR-SPECIFIC ANTIGENS IN HUMAN COLONIC CARCINOMATA BY IMMUNOLOGICAL TOLERANCE AND ABSORPTION TECHNIQUES. *J Exp Med*, 121, 439-62.

GOMEZ, D. E., ALONSO, D. F., YOSHIJI, H. & THORGEIRSSON, U. P. 1997. Tissue inhibitors of metalloproteinases: structure, regulation and biological functions. *Eur J Cell Biol*, 74, 111-22.

GONZÁLEZ-ARAGONESES, F., MORENO-MATA, N., CEBOLLERO-PRESMANES, M., GARCÍA-YUSTE, M., CAÑIZARES-CARRETERO, M. A., MOLINS-LÓPEZ-RODÓ, L., QUEVEDO-LOSADA, S., TORRES-LANZAS, J., ALVAREZ-FERNÁNDEZ, E. & SPANISH MULTICENTER STUDY OF NEUROENDOCRINE TUMOURS OF THE LUNG OF THE SPANISH SOCIETY OF PNEUMONOLOGY, T. O. E.-S. 2007. Prognostic significance of synaptophysin in stage I of squamous carcinoma and adenocarcinoma of the lung. *Cancer*, 110, 1776-81.

GOUYER, V., CONTI, M., DEVOS, P., ZERIMECH, F., COPIN, M. C., CRÉME, E., WURTZ, A., PORTE, H. & HUET, G. 2005. Tissue inhibitor of metalloproteinase 1 is an independent predictor of prognosis in patients with nonsmall cell lung carcinoma who undergo resection with curative intent. *Cancer*, 103, 1676-84.

- GRAY-BABLIN, J., ZALVIDE, J., FOX, M. P., KNICKERBOCKER, C. J., DECAPRIO, J. A. & KEYOMARSI, K. 1996. Cyclin E, a redundant cyclin in breast cancer. *Proc Natl Acad Sci U S A*, 93, 15215-20.
- GRAZIANO, F., BISONNI, R., CATALANO, V., SILVA, R., ROVIDATI, S., MENCARINI, E., FERRARO, B., CANESTRARI, F., BALDELLI, A. M., DE GAETANO, A., GIORDANI, P., TESTA, E. & LAI, V. 2002. Potential role of levocarnitine supplementation for the treatment of chemotherapy-induced fatigue in non-anaemic cancer patients. *Br J Cancer*, 86, 1854-7.
- GREAVES, M. 2015. Evolutionary determinants of cancer. *Cancer Discov*, 5, 806-20.
- GREAVES, M. & MALEY, C. C. 2012. Clonal evolution in cancer. *Nature*, 481, 306-13.
- GRIFFIN, J. P., EASTRIDGE, C. E., TOLLEY, E. A. & PATE, J. W. 2006. Wedge resection for non-small cell lung cancer in patients with pulmonary insufficiency: prospective ten-year survival. *J Thorac Oncol*, 1, 960-4.
- GRUBER, W., SCHEIDT, T., ABERGER, F. & HUBER, C. G. 2017. Understanding cell signaling in cancer stem cells for targeted therapy - can phosphoproteomics help to reveal the secrets? *Cell Commun Signal*, 15, 12.
- GUJAM, F. J., GOING, J. J., EDWARDS, J., MOHAMMED, Z. M. & MCMILLAN, D. C. 2014. The role of lymphatic and blood vessel invasion in predicting survival and methods of detection in patients with primary operable breast cancer. *Crit Rev Oncol Hematol*, 89, 231-41.
- GUNTUPALLI, K. K. 1984. Acute pulmonary edema. *Cardiol Clin*, 2, 183-200.
- GUO, T., WANG, W., RUDNICK, P. A., SONG, T., LI, J., ZHUANG, Z., WEIL, R. J., DEVOE, D. L., LEE, C. S. & BALGLEY, B. M. 2007. Proteome analysis of

microdissected formalin-fixed and paraffin-embedded tissue specimens. *J Histochem Cytochem*, 55, 763-72.

GUO, Y., WANG, X., QIU, L., QIN, X., LIU, H., WANG, Y., LI, F., CHEN, G., SONG, G., GUO, S. & LI, Z. 2012. Probing gender-specific lipid metabolites and diagnostic biomarkers for lung cancer using Fourier transform ion cyclotron resonance mass spectrometry. *Clin Chim Acta*, 414, 135-41.

HALESTRAP, A. P. 2012. The monocarboxylate transporter family--Structure and functional characterization. *IUBMB Life*, 64, 1-9.

HANAHAN, D. & WEINBERG, R. A. 2011. Hallmarks of cancer: the next generation. *Cell*, 144, 646-74.

HANSEN, C. P., HOLTVEG, H., FRANCIS, D., RASCH, L. & BERTELSEN, S. 1992. Pulmonary hamartoma. *J Thorac Cardiovasc Surg*, 104, 674-8.

HANSEN JL & EF, F. 1978. direct assays of lactate, pyruvate, /3-hydroxybutyrate, and acetoacetate in plasma with the GEMSAEC centrifugal analyzer. *CLINICAL CHEMISTRY*, 24, 5.

HANSEN, J. L. & FREIER, E. F. 1978. Direct assays of lactate, pyruvate, beta-hydroxybutyrate, and acetoacetate with a centrifugal analyzer. *Clin Chem*, 24, 475-9.

HARA, M., KANEMITSU, Y., HIRAI, T., KOMORI, K. & KATO, T. 2008. Negative serum carcinoembryonic antigen has insufficient accuracy for excluding recurrence from patients with Dukes C colorectal cancer: analysis with likelihood ratio and posttest probability in a follow-up study. *Dis Colon Rectum*, 51, 1675-80.

HARRIES, A. D. & DYE, C. 2006. Tuberculosis. *Ann Trop Med Parasitol*, 100, 415-31.

- HARTMAN, D. J., HOOGENRAAD, N. J., CONDRON, R. & HØJ, P. B. 1992. Identification of a mammalian 10-kDa heat shock protein, a mitochondrial chaperonin 10 homologue essential for assisted folding of trimeric ornithine transcarbamoylase in vitro. *Proc Natl Acad Sci U S A*, 89, 3394-8.
- HASSIG, C. A. & SCHREIBER, S. L. 1997. Nuclear histone acetylases and deacetylases and transcriptional regulation: HATs off to HDACs. *Curr Opin Chem Biol*, 1, 300-8.
- HAYDEN, M. S. & GHOSH, S. 2004. Signaling to NF-kappaB. *Genes Dev*, 18, 2195-224.
- HAYES, S. A., HAEFLIGER, S., HARRIS, B., PAVLAKIS, N., CLARKE, S. J., MOLLOY, M. P. & HOWELL, V. M. 2016. Exhaled breath condensate for lung cancer protein analysis: a review of methods and biomarkers. *J Breath Res*, 10, 034001.
- HEAVEY, S., CUFFE, S., FINN, S., YOUNG, V., RYAN, R., NICHOLSON, S., LEONARD, N., MCVEIGH, N., BARR, M., O'BYRNE, K. & GATELY, K. 2016. In pursuit of synergy: An investigation of the PI3K/mTOR/MEK co-targeted inhibition strategy in NSCLC. *Oncotarget*, 7, 79526-79543.
- HEELAN, R. 2004. Staging and response to therapy of malignant pleural mesothelioma. *Lung Cancer*, 45 Suppl 1, S59-61.
- HELLAND, A. & BRUSTUGUN, O. T. 2009. [Lung cancer in smokers and never-smokers]. *Tidsskr Nor Laegeforen*, 129, 1859-62.
- HELLMANN, M. D., CHAFT, J. E., RUSCH, V., GINSBERG, M. S., FINLEY, D. J., KRIS, M. G., PRICE, K. A., AZZOLI, C. G., FURY, M. G., RIELY, G. J., KRUG, L. M., DOWNEY, R. J., BAINS, M. S., SIMA, C. S., RIZK, N., TRAVIS, W. D., RIZVI, N. A. & PAIK, P. K. 2013. Risk of hemoptysis in patients with resected

squamous cell and other high-risk lung cancers treated with adjuvant bevacizumab. *Cancer Chemother Pharmacol*, 72, 453-61.

HENKE, R. T., EUN KIM, S., MAITRA, A., PAIK, S. & WELLSTEIN, A. 2006. Expression analysis of mRNA in formalin-fixed, paraffin-embedded archival tissues by mRNA in situ hybridization. *Methods*, 38, 253-62.

HENSKENS, Y. M., VEERMAN, E. C. & NIEUW AMERONGEN, A. V. 1996. Cystatins in health and disease. *Biol Chem Hoppe Seyler*, 377, 71-86.

HERBST, R. S., HEYMACH, J. V. & LIPPMAN, S. M. 2008. Lung cancer. *N Engl J Med*, 359, 1367-80.

HIGASHITSUJI, H., MASUDA, T., LIU, Y., ITOH, K. & FUJITA, J. 2007. Enhanced deacetylation of p53 by the anti-apoptotic protein HSCO in association with histone deacetylase 1. *J Biol Chem*, 282, 13716-25.

HIKITA, H., KODAMA, T., TANAKA, S., SAITO, Y., NOZAKI, Y., NAKABORI, T., SHIMIZU, S., HAYASHI, Y., LI, W., SHIGEKAWA, M., SAKAMORI, R., MIYAGI, T., HIRAMATSU, N., TATSUMI, T. & TAKEHARA, T. 2015. Activation of the Mitochondrial Apoptotic Pathway Produces Reactive Oxygen Species and Oxidative Damage in Hepatocytes That Contribute to Liver Tumorigenesis. *Cancer Prev Res (Phila)*, 8, 693-701.

HILAL, T. 2017. Current understanding and approach to well differentiated lung neuroendocrine tumors: an update on classification and management. *Ther Adv Med Oncol*, 9, 189-199.

HIROSHIMA, K., IYODA, A., SHIDA, T., SHIBUYA, K., IIZASA, T., KISHI, H., TANIZAWA, T., FUJISAWA, T. & NAKATANI, Y. 2006. Distinction of pulmonary large cell neuroendocrine carcinoma from small cell lung carcinoma: a

morphological, immunohistochemical, and molecular analysis. *Mod Pathol*, 19, 1358-68.

HIRSCH, F. R., MERRICK, D. T. & FRANKLIN, W. A. 2002. Role of biomarkers for early detection of lung cancer and chemoprevention. *Eur Respir J*, 19, 1151-8.

HOANG, C. D. 2017. Protein-based prognostic biomarkers in lung cancer: Promise or pitfall? *J Thorac Cardiovasc Surg*.

HOARE, Z. & LIM, W. S. 2006. Pneumonia: update on diagnosis and management. *BMJ*, 332, 1077-9.

HOLDENRIEDER, S., PAGLIARO, L., MORGENSTERN, D. & DAYYANI, F. 2016. Clinically Meaningful Use of Blood Tumor Markers in Oncology. *Biomed Res Int*, 2016, 9795269.

HOLGATE, S. T. 2008. Pathogenesis of asthma. *Clin Exp Allergy*, 38, 872-97.

HOLGATE, S. T., DAVIES, D. E., LACKIE, P. M., WILSON, S. J., PUDDICOMBE, S. M. & LORDAN, J. L. 2000. Epithelial-mesenchymal interactions in the pathogenesis of asthma. *J Allergy Clin Immunol*, 105, 193-204.

HOLNESS, M. J. & SUGDEN, M. C. 2003. Regulation of pyruvate dehydrogenase complex activity by reversible phosphorylation. *Biochem Soc Trans*, 31, 1143-51.

HOOD, B. L., CONRADS, T. P. & VEENSTRA, T. D. 2006. Unravelling the proteome of formalin-fixed paraffin-embedded tissue. *Brief Funct Genomic Proteomic*, 5, 169-75.

HOOD, B. L., DARFLER, M. M., GUIEL, T. G., FURUSATO, B., LUCAS, D. A., RINGEISEN, B. R., SESTERHENN, I. A., CONRADS, T. P., VEENSTRA, T. D. & KRIZMAN, D. B. 2005. Proteomic analysis of formalin-fixed prostate cancer tissue. *Mol Cell Proteomics*, 4, 1741-53.

- HORSEFIELD, R., IWATA, S. & BYRNE, B. 2004. Complex II from a structural perspective. *Curr Protein Pept Sci*, 5, 107-18.
- HORVÁTH, I., HUNT, J., BARNES, P. J., ALVING, K., ANTCZAK, A., BARALDI, E., BECHER, G., VAN BEURDEN, W. J., CORRADI, M., DEKHUIJZEN, R., DWEIK, R. A., DWYER, T., EFFROS, R., ERZURUM, S., GASTON, B., GESSNER, C., GREENING, A., HO, L. P., HOHLFELD, J., JÖBSIS, Q., LASKOWSKI, D., LOUKIDES, S., MARLIN, D., MONTUSCHI, P., OLIN, A. C., REDINGTON, A. E., REINHOLD, P., VAN RENSEN, E. L., RUBINSTEIN, I., SILKOFF, P., TOREN, K., VASS, G., VOGELBERG, C., WIRTZ, H. & CONDENSATE, A. E. T. F. O. E. B. 2005. Exhaled breath condensate: methodological recommendations and unresolved questions. *Eur Respir J*, 26, 523-48.
- HSU, P. P. & SABATINI, D. M. 2008. Cancer cell metabolism: Warburg and beyond. *Cell*, 134, 703-7.
- HUNT, T. 1989. Maturation promoting factor, cyclin and the control of M-phase. *Curr Opin Cell Biol*, 1, 268-74.
- HURD, T. R., COLLINS, Y., ABAKUMOVA, I., CHOUCANI, E. T., BARANOWSKI, B., FEARNLEY, I. M., PRIME, T. A., MURPHY, M. P. & JAMES, A. M. 2012. Inactivation of pyruvate dehydrogenase kinase 2 by mitochondrial reactive oxygen species. *J Biol Chem*, 287, 35153-60.
- IRWIN, M. R. & MILLER, A. H. 2007. Depressive disorders and immunity: 20 years of progress and discovery. *Brain Behav Immun*, 21, 374-83.
- IWATA, N., YAMAMOTO, H., SASAKI, S., ITOH, F., SUZUKI, H., KIKUCHI, T., KANETO, H., IKU, S., OZEKI, I., KARINO, Y., SATOH, T., TOYOTA, J., SATOH, M., ENDO, T. & IMAI, K. 2000. Frequent hypermethylation of CpG

islands and loss of expression of the 14-3-3 sigma gene in human hepatocellular carcinoma. *Oncogene*, 19, 5298-302.

IYODA, A., HIROSHIMA, K., NAKATANI, Y. & FUJISAWA, T. 2007. Pulmonary large cell neuroendocrine carcinoma: its place in the spectrum of pulmonary carcinoma. *Ann Thorac Surg*, 84, 702-7.

IYODA, A., HIROSHIMA, K., TOYOZAKI, T., HAGA, Y., FUJISAWA, T. & OHWADA, H. 2001. Clinical characterization of pulmonary large cell neuroendocrine carcinoma and large cell carcinoma with neuroendocrine morphology. *Cancer*, 91, 1992-2000.

JANUMYAN, Y. M., SANSAM, C. G., CHATTOPADHYAY, A., CHENG, N., SOUCIE, E. L., PENN, L. Z., ANDREWS, D., KNUDSON, C. M. & YANG, E. 2003. Bcl-xL/Bcl-2 coordinately regulates apoptosis, cell cycle arrest and cell cycle entry. *EMBO J*, 22, 5459-70.

JEREMIC, B., GOMEZ-CAAMANO, A., DUBINSKY, P., CIHORIC, N., CASAS, F. & FILIPOVIC, N. 2017. Radiation Therapy in Extensive Stage Small Cell Lung Cancer. *Front Oncol*, 7, 169.

JEWELL, E. L., HUANG, J. J., ABU-RUSTUM, N. R., GARDNER, G. J., BROWN, C. L., SONODA, Y., BARAKAT, R. R., LEVINE, D. A. & LEITAO, M. M. 2014. Detection of sentinel lymph nodes in minimally invasive surgery using indocyanine green and near-infrared fluorescence imaging for uterine and cervical malignancies. *Gynecol Oncol*, 133, 274-7.

JIA, Y., LI, F., LIU, Y. F., ZHAO, J. P., LENG, M. M. & CHEN, L. 2017. Depression and cancer risk: a systematic review and meta-analysis. *Public Health*, 149, 138-148.

JIANG, L., DONG, P., ZHANG, Z., LI, C., LI, Y., LIAO, Y., LI, X., WU, Z., GUO, S., MAI, S., XIE, D., LIU, Z. & ZHOU, F. 2015. Akt phosphorylates Prohibitin 1 to

mediate its mitochondrial localization and promote proliferation of bladder cancer cells. *Cell Death Dis*, 6, e1660.

JIANG, P., DU, W. & WU, M. 2014. Regulation of the pentose phosphate pathway in cancer. *Protein Cell*, 5, 592-602.

JIANG, P., XIANG, Y., WANG, Y. J., LI, S. M., WANG, Y., HUA, H. R., YU, G. Y., ZHANG, Y. & LEE, W. H. 2013. Differential expression and subcellular localization of Prohibitin 1 are related to tumorigenesis and progression of non-small cell lung cancer. *Int J Clin Exp Pathol*, 6, 2092-101.

JIANG, S. X., KAMEYA, T., SHOJI, M., DOBASHI, Y., SHINADA, J. & YOSHIMURA, H. 1998. Large cell neuroendocrine carcinoma of the lung: a histologic and immunohistochemical study of 22 cases. *Am J Surg Pathol*, 22, 526-37.

JIN, R., CHEN, X., HAN, D., LUO, X. & LI, H. 2017a. Clusterin modulates transdifferentiation of non-small-cell lung cancer. *BMC Cancer*, 17, 661.

JIN, X., XU, X., XU, H., LV, L. & LU, H. 2017b. The Diagnostic Value of Carcinoembryonic Antigen and Squamous Cell Carcinoma Antigen in Lung Adenosquamous Carcinoma. *Clin Lab*, 63, 801-808.

JOURET-MOURIN, A., HOORENS, A., DE HERTOOGH, G., VANDERVEKEN, J., DEMETTER, P. & VAN CUTSEM, E. 2012. Analysis of HER2 expression and gene amplification in adenocarcinoma of the stomach and the gastro-oesophageal junction: rationale for the Belgian way of working. *Acta Gastroenterol Belg*, 75, 9-13.

JUDSON, M. A., BAUGHMAN, R. P., COSTABEL, U., DRENT, M., GIBSON, K. F., RAGHU, G., SHIGEMITSU, H., BARNEY, J. B., CULVER, D. A., HAMZEH, N. Y., WIJSENBEK, M. S., ALBERA, C., HUIZAR, I., AGARWAL, P.,

- BRODMERKEL, C., WATT, R. & BARNATHAN, E. S. 2014. Safety and efficacy of ustekinumab or golimumab in patients with chronic sarcoidosis. *Eur Respir J*, 44, 1296-307.
- JUNKER, K., WIETHEGE, TH., MULLER, K.M. 2000. pathology of small-cell lung cancer. *journal of cancer research and clinical oncology*, 126, 8.
- KAISER, L. R. & BAVARIA, J. E. 1993. Complications of thoracoscopy. *Ann Thorac Surg*, 56, 796-8.
- KANDEL, E. S., SKEEN, J., MAJEWSKI, N., DI CRISTOFANO, A., PANDOLFI, P. P., FELICIANO, C. S., GARTEL, A. & HAY, N. 2002. Activation of Akt/protein kinase B overcomes a G(2)/m cell cycle checkpoint induced by DNA damage. *Mol Cell Biol*, 22, 7831-41.
- KAPLAN, A., BUENO, M. & FOURNIER, A. E. 2017. Extracellular functions of 14-3-3 adaptor proteins. *Cell Signal*, 31, 26-30.
- KAPPLER, M., PABST, U., ROT, S., TAUBERT, H., WICHMANN, H., SCHUBERT, J., BACHE, M., WEINHOLDT, C., IMMEL, U. D., GROSSE, I., VORDERMARK, D. & ECKERT, A. W. 2017. Normoxic accumulation of HIF1 α is associated with glutaminolysis. *Clin Oral Investig*, 21, 211-224.
- KAPUSCINSKI, J. 1995. DAPI: a DNA-specific fluorescent probe. *Biotech Histochem*, 70, 220-33.
- KARAMAN, S. & DETMAR, M. 2014. Mechanisms of lymphatic metastasis. *J Clin Invest*, 124, 922-8.
- KARIM, Z., ATTMANE-ELAKEB, A. & BICHARA, M. 2002. Renal handling of NH₄⁺ in relation to the control of acid-base balance by the kidney. *J Nephrol*, 15 Suppl 5, S128-34.

KARIYAWASAM, H. H. & ROBINSON, D. S. 2007. The role of eosinophils in airway tissue remodelling in asthma. *Curr Opin Immunol*, 19, 681-6.

KARTNER, N., HANRAHAN, J. W., JENSEN, T. J., NAISMITH, A. L., SUN, S. Z., ACKERLEY, C. A., REYES, E. F., TSUI, L. C., ROMMENS, J. M. & BEAR, C. E. 1991. Expression of the cystic fibrosis gene in non-epithelial invertebrate cells produces a regulated anion conductance. *Cell*, 64, 681-91.

KASHYAP, S. & SARKAR, M. 2010. Mycoplasma pneumonia: Clinical features and management. *Lung India*, 27, 75-85.

KATURI, K. K., DASARI, A. B., KURAPATI, S., VINNAKOTA, N. R., BOLLEPALLI, A. C. & DHULIPALLA, R. 2016. Association of yoga practice and serum cortisol levels in chronic periodontitis patients with stress-related anxiety and depression. *J Int Soc Prev Community Dent*, 6, 7-14.

KAUFMAN, B. A., KOLESAR, J. E., PERLMAN, P. S. & BUTOW, R. A. 2003. A function for the mitochondrial chaperonin Hsp60 in the structure and transmission of mitochondrial DNA nucleoids in *Saccharomyces cerevisiae*. *J Cell Biol*, 163, 457-61.

KEIBLER, M. A., WASYLENKO, T. M., KELLEHER, J. K., ILIOPOULOS, O., VANDER HEIDEN, M. G. & STEPHANOPOULOS, G. 2016. Metabolic requirements for cancer cell proliferation. *Cancer Metab*, 4, 16.

KELMAN, Z. & O'DONNELL, M. 1995. Structural and functional similarities of prokaryotic and eukaryotic DNA polymerase sliding clamps. *Nucleic Acids Res*, 23, 3613-20.

KENFIELD, S. A., WEI, E. K., STAMPFER, M. J., ROSNER, B. A. & COLDITZ, G. A. 2008. Comparison of aspects of smoking among the four histological types of lung cancer. *Tob Control*, 17, 198-204.

- KERR, K. M., BUBENDORF, L., EDELMAN, M. J., MARCHETTI, A., MOK, T., NOVELLO, S., O'BYRNE, K., STAHEL, R., PETERS, S., FELIP, E. & MEMBERS, P. 2014. Second ESMO consensus conference on lung cancer: pathology and molecular biomarkers for non-small-cell lung cancer. *Ann Oncol*, 25, 1681-90.
- KHAN, M. M., SANSONI, P., ENGLEMAN, E. G. & MELMON, K. L. 1985. Pharmacologic effects of autacoids on subsets of T cells. Regulation of expression/function of histamine-2 receptors by a subset of suppressor cells. *J Clin Invest*, 75, 1578-83.
- KIM, D. H., BAE, J., LEE, J. W., KIM, S. Y., KIM, Y. H., BAE, J. Y., YI, J. K., YU, M. H., NOH, D. Y. & LEE, C. 2009. Proteomic analysis of breast cancer tissue reveals upregulation of actin-remodeling proteins and its relevance to cancer invasiveness. *Proteomics Clin Appl*, 3, 30-40.
- KIM, H. J., JANG, S. H., RYU, J. S., LEE, J. E., KIM, Y. C., LEE, M. K., JANG, T. W., LEE, S. Y., NAKAMURA, H., NISHIKATA, N., MORI, M., NOGUCHI, Y., MIYANO, H. & LEE, K. Y. 2015. The performance of a novel amino acid multivariate index for detecting lung cancer: A case control study in Korea. *Lung Cancer*, 90, 522-7.
- KIM, V. & CRINER, G. J. 2013. Chronic bronchitis and chronic obstructive pulmonary disease. *Am J Respir Crit Care Med*, 187, 228-37.
- KIM, Y. B., KI, S. W., YOSHIDA, M. & HORINOUCHE, S. 2000. Mechanism of cell cycle arrest caused by histone deacetylase inhibitors in human carcinoma cells. *J Antibiot (Tokyo)*, 53, 1191-200.
- KIMOS, M. C., WANG, S., BORKOWSKI, A., YANG, G. Y., YANG, C. S., PERRY, K., OLARU, A., DEACU, E., STERIAN, A., COTTRELL, J.,

PAPADIMITRIOU, J., SISODIA, L., SELARU, F. M., MORI, Y., XU, Y., YIN, J., ABRAHAM, J. M. & MELTZER, S. J. 2004. Esophagin and proliferating cell nuclear antigen (PCNA) are biomarkers of human esophageal neoplastic progression. *Int J Cancer*, 111, 415-7.

KINKADE, S. & LONG, N. A. 2016. Acute Bronchitis. *Am Fam Physician*, 94, 560-565.

KITTERINGHAM, N. R., JENKINS, R. E., LANE, C. S., ELLIOTT, V. L. & PARK, B. K. 2009. Multiple reaction monitoring for quantitative biomarker analysis in proteomics and metabolomics. *J Chromatogr B Analyt Technol Biomed Life Sci*, 877, 1229-39.

KLABUNDE, R. E. 2012. *Cardiovascular Physiology Concepts*, Lippincott Williams & Wilkins.

KLUPCZYNSKA, A., DEREZIŃSKI, P., DYSZKIEWICZ, W., PAWLAK, K., KASPRZYK, M. & KOKOT, Z. J. 2016. Evaluation of serum amino acid profiles' utility in non-small cell lung cancer detection in Polish population. *Lung Cancer*, 100, 71-76.

KNUTSON, D. & BRAUN, C. 2002. Diagnosis and management of acute bronchitis. *Am Fam Physician*, 65, 2039-44.

KOBIERZYCKI, C., PULA, B., WERYNSKA, B., PIOTROWSKA, A., MUSZCZYNSKA-BERNHARD, B., DZIEGIEL, P. & RAKUS, D. 2014. The lack of evidence for correlation of pyruvate kinase M2 expression with tumor grade in non-small cell lung cancer. *Anticancer Res*, 34, 3811-7.

KOÇDOR, H., KOÇDOR, M. A., ASTARCIOĞLU, H. & FADILOĞLU, M. 2003. Serum tumor necrosis factor-alpha, glutamate and lactate changes in two different stages of mechanical intestinal obstruction. *Turk J Gastroenterol*, 14, 115-20.

- KOCIJANCIC, M., CARGONJA, J. & DELIC-KNEZEVIC, A. 2014. Evaluation of the BD Vacutainer(®) RST blood collection tube for routine chemistry analytes: clinical significance of differences and stability study. *Biochem Med (Zagreb)*, 24, 368-75.
- KODAMA, T. 1997. [Principles of histological diagnosis and clinical staging evaluation for lung cancer]. *Gan To Kagaku Ryoho*, 24 Suppl 3, 359-65.
- KOKKAT, T. J., PATEL, M. S., MCGARVEY, D., LIVOLSI, V. A. & BALOCH, Z. W. 2013. Archived formalin-fixed paraffin-embedded (FFPE) blocks: A valuable underexploited resource for extraction of DNA, RNA, and protein. *Biopreserv Biobank*, 11, 101-6.
- KONDURI, S. D., YANAMANDRA, N., SIDDIQUE, K., JOSEPH, A., DINH, D. H., OLIVERO, W. C., GUJRATI, M., KOURAKLIS, G., SWAROOP, A., KYRITSIS, A. P. & RAO, J. S. 2002. Modulation of cystatin C expression impairs the invasive and tumorigenic potential of human glioblastoma cells. *Oncogene*, 21, 8705-12.
- KONSTANTINIDI, E. M., LAPPAS, A. S., TZORTZI, A. S. & BEHRAKIS, P. K. 2015. Exhaled Breath Condensate: Technical and Diagnostic Aspects. *ScientificWorldJournal*, 2015, 435160.
- KOPITAR-JERALA, N. 2006. The role of cystatins in cells of the immune system. *FEBS Lett*, 580, 6295-301.
- KORNUM, J. B., THOMSEN, R. W., RIIS, A., LERVANG, H. H., SCHØNHEYDER, H. C. & SØRENSEN, H. T. 2007. Type 2 diabetes and pneumonia outcomes: a population-based cohort study. *Diabetes Care*, 30, 2251-7.
- KORSE, C. M., HOLDENRIEDER, S., ZHI, X. Y., ZHANG, X., QIU, L., GEISTANGER, A., LISY, M. R., WEHNL, B., VAN DEN BROEK, D.,

- ESCUADERO, J. M., STANDOP, J., HU, M. & MOLINA, R. 2015. Multicenter evaluation of a new progastrin-releasing peptide (ProGRP) immunoassay across Europe and China. *Clin Chim Acta*, 438, 388-95.
- KORSMEYER, S. J. 1995. Regulators of cell death. *Trends Genet*, 11, 101-5.
- KOUKOURAKIS, M. I., GIATROMANOLAKI, A., SIVRIDIS, E., GATTER, K. C., HARRIS, A. L. & GROUP, T. A. A. R. 2005. Pyruvate dehydrogenase and pyruvate dehydrogenase kinase expression in non small cell lung cancer and tumor-associated stroma. *Neoplasia*, 7, 1-6.
- LACKNER, L. L. 2013. Determining the shape and cellular distribution of mitochondria: the integration of multiple activities. *Curr Opin Cell Biol*, 25, 471-6.
- LAI, A., KENNEDY, B. K., BARBIE, D. A., BERTOS, N. R., YANG, X. J., THEBERGE, M. C., TSAI, S. C., SETO, E., ZHANG, Y., KUZMICHEV, A., LANE, W. S., REINBERG, D., HARLOW, E. & BRANTON, P. E. 2001. RBP1 recruits the mSIN3-histone deacetylase complex to the pocket of retinoblastoma tumor suppressor family proteins found in limited discrete regions of the nucleus at growth arrest. *Mol Cell Biol*, 21, 2918-32.
- LANA, A., ALVAREZ-GUERRERO, S., HERRERO-PUENTE, P., FOLGUERAS, M. V. & LÓPEZ, M. L. 2014. [Suspected diagnosis of cancer in hospital emergency services]. *An Sist Sanit Navar*, 37, 59-67.
- LARONGA, C., YANG, H. Y., NEAL, C. & LEE, M. H. 2000. Association of the cyclin-dependent kinases and 14-3-3 sigma negatively regulates cell cycle progression. *J Biol Chem*, 275, 23106-12.
- LAURENTI, E., FRELIN, C., XIE, S., FERRARI, R., DUNANT, C. F., ZANDI, S., NEUMANN, A., PLUMB, I., DOULATOV, S., CHEN, J., APRIL, C., FAN, J. B.,

- ISCOVE, N. & DICK, J. E. 2015. CDK6 levels regulate quiescence exit in human hematopoietic stem cells. *Cell Stem Cell*, 16, 302-13.
- LAVENDER, C. F. 1946. Mechanisms of control of acid-base balance. *Arch Pediatr*, 63, 509-27.
- LEAL, M. F., CALCAGNO, D. Q., DEMACHKI, S., ASSUMPCÃO, P. P., CHAMMAS, R., BURBANO, R. R. & SMITH, M. E. A. 2012. Clinical implication of 14-3-3 epsilon expression in gastric cancer. *World J Gastroenterol*, 18, 1531-7.
- LEE, J., CHOI, K. J., MOON, S. U. & KIM, S. 2016. Theragnosis-based combined cancer therapy using doxorubicin-conjugated microRNA-221 molecular beacon. *Biomaterials*, 74, 109-18.
- LEGUBE, G. & TROUCHE, D. 2003. Regulating histone acetyltransferases and deacetylases. *EMBO Rep*, 4, 944-7.
- LEHN, S., TOBIN, N. P., BERGLUND, P., NILSSON, K., SIMS, A. H., JIRSTRÖM, K., HÄRKÖNEN, P., LAMB, R. & LANDBERG, G. 2010. Down-regulation of the oncogene cyclin D1 increases migratory capacity in breast cancer and is linked to unfavorable prognostic features. *Am J Pathol*, 177, 2886-97.
- LELOUP, L. & WELLS, A. 2011. Calpains as potential anti-cancer targets. *Expert Opin Ther Targets*, 15, 309-23.
- LEQUAGLIE, C., MARINO, P., MAIOLI, C., PREDA, F. & RAVASI, G. 1995. Cyfra 21-1 - a new tumor-marker for lung-cancer. *Oncol Rep*, 2, 119-22.
- LEVKAU, B., KOYAMA, H., RAINES, E. W., CLURMAN, B. E., HERREN, B., ORTH, K., ROBERTS, J. M. & ROSS, R. 1998. Cleavage of p21Cip1/Waf1 and p27Kip1 mediates apoptosis in endothelial cells through activation of Cdk2: role of a caspase cascade. *Mol Cell*, 1, 553-63.

- LI, G., WANG, Z., XU, J., WU, H., CAI, S. & HE, Y. 2016. The prognostic value of lactate dehydrogenase levels in colorectal cancer: a meta-analysis. *BMC Cancer*, 16, 249.
- LI, J. Q., MIKI, H., WU, F., SAOO, K., NISHIOKA, M., OHMORI, M. & IMAIDA, K. 2002. Cyclin A correlates with carcinogenesis and metastasis, and p27(kip1) correlates with lymphatic invasion, in colorectal neoplasms. *Hum Pathol*, 33, 1006-15.
- LI, L., LI, X., YIN, J., SONG, X., CHEN, X., FENG, J., GAO, H., LIU, L. & WEI, S. 2014. The high diagnostic accuracy of combined test of thyroid transcription factor 1 and Napsin A to distinguish between lung adenocarcinoma and squamous cell carcinoma: a meta-analysis. *PLoS One*, 9, e100837.
- LI, L., TIAN, T. & ZHANG, X. 2017. The Impact of Radiation on the Development of Lung Cancer. *J Theor Biol*.
- LI, Z., JIAO, X., WANG, C., SHIRLEY, L. A., ELSALEH, H., DAHL, O., WANG, M., SOUTOGLU, E., KNUDSEN, E. S. & PESTELL, R. G. 2010a. Alternative cyclin D1 splice forms differentially regulate the DNA damage response. *Cancer Res*, 70, 8802-11.
- LI, Z., MIN, W., HUANG, C., BAI, S., TANG, M. & ZHAO, X. 2010b. Proteomics-based approach identified differentially expressed proteins with potential roles in endometrial carcinoma. *Int J Gynecol Cancer*, 20, 9-15.
- LI, Z. & SRIVASTAVA, P. 2004. Heat-shock proteins. *Curr Protoc Immunol*, Appendix 1, Appendix 1T.
- LIAO, S. & VON DER WEID, P. Y. 2015. Lymphatic system: an active pathway for immune protection. *Semin Cell Dev Biol*, 38, 83-9.

- LIN, Y., BAI, L., CHEN, W. & XU, S. 2010. The NF-kappaB activation pathways, emerging molecular targets for cancer prevention and therapy. *Expert Opin Ther Targets*, 14, 45-55.
- LIOU, H. C. & BALTIMORE, D. 1993. Regulation of the NF-kappa B/rel transcription factor and I kappa B inhibitor system. *Curr Opin Cell Biol*, 5, 477-87.
- LIU, B., ZHOU, Y., LU, D., LIU, Y., ZHANG, S. Q., XU, Y., LI, W. & GU, X. 2017. Comparison of the protein expression of calpain-1, calpain-2, calpastatin and calmodulin between gastric cancer and normal gastric mucosa. *Oncol Lett*, 14, 3705-3710.
- LIU, Q., D'SILVA, P., WALTER, W., MARSZALEK, J. & CRAIG, E. A. 2003. Regulated cycling of mitochondrial Hsp70 at the protein import channel. *Science*, 300, 139-41.
- LIU, T. A., JAN, Y. J., KO, B. S., LIANG, S. M., CHEN, S. C., WANG, J., HSU, C., WU, Y. M. & LIOU, J. Y. 2013. 14-3-3 ϵ overexpression contributes to epithelial-mesenchymal transition of hepatocellular carcinoma. *PLoS One*, 8, e57968.
- LOBUE, P. A., ENARSON, D. A. & THOEN, T. C. 2010. Tuberculosis in humans and its epidemiology, diagnosis and treatment in the United States. *Int J Tuberc Lung Dis*, 14, 1226-32.
- LOGAN, D. M., LOCHRIN, C. A., DARLING, G., EADY, A., NEWMAN, T. E. & EVANS, W. K. 1997. Adjuvant radiotherapy and chemotherapy for stage II or IIIA non-small-cell lung cancer after complete resection. Provincial Lung Cancer Disease Site Group. *Cancer Prev Control*, 1, 366-78.
- LOLLI, G. & JOHNSON, L. N. 2005. CAK-Cyclin-dependent Activating Kinase: a key kinase in cell cycle control and a target for drugs? *Cell Cycle*, 4, 572-7.

- LÓPEZ VILLAR, E., MADERO, L., A LÓPEZ-PASCUAL, J. & C CHO, W. 2015. Study of phosphorylation events for cancer diagnoses and treatment. *Clin Transl Med*, 4, 59.
- LOW, J. S. H., KOH, W. Y., YAP, S. P. & FONG, K. W. 2007. Radical radiotherapy in stage I non-small cell lung cancer (NSCLC)--Singapore National Cancer Centre experience. *Ann Acad Med Singapore*, 36, 778-83.
- LU, L. I., FU, N. I., LUO, X. U., LI, X. Y. & LI, X. P. 2015. Overexpression of cofilin 1 in prostate cancer and the corresponding clinical implications. *Oncol Lett*, 9, 2757-2761.
- LU, Z., ZHANG, X., LI, Y., JIN, J. & HUANG, Y. 2013. TLR4 antagonist reduces early-stage atherosclerosis in diabetic apolipoprotein E-deficient mice. *J Endocrinol*, 216, 61-71.
- LUDBROOK J., D. H. 1998. Why permutation tests are superior to *t* and *F* tests in biomedical research, *Am Stat.* .
- LUNT, S. Y. & VANDER HEIDEN, M. G. 2011. Aerobic glycolysis: meeting the metabolic requirements of cell proliferation. *Annu Rev Cell Dev Biol*, 27, 441-64.
- LUO, Y., HURWITZ, J. & MASSAGUÉ, J. 1995. Cell-cycle inhibition by independent CDK and PCNA binding domains in p21Cip1. *Nature*, 375, 159-61.
- MA, J., WANG, J., FAN, W., PU, X., ZHANG, D., FAN, C., XIONG, L., ZHU, H., XU, N., CHEN, R. & LIU, S. 2014. Upregulated TIMP-1 correlates with poor prognosis of laryngeal squamous cell carcinoma. *Int J Clin Exp Pathol*, 7, 246-54.
- MAGISTER, S. & KOS, J. 2013. Cystatins in immune system. *J Cancer*, 4, 45-56.
- MALKAS, L. H., HERBERT, B. S., ABDEL-AZIZ, W., DOBROLECKI, L. E., LIU, Y., AGARWAL, B., HOELZ, D., BADVE, S., SCHNAPER, L., ARNOLD, R. J., MECHREF, Y., NOVOTNY, M. V., LOEHRER, P., GOULET, R. J. & HICKEY,

- R. J. 2006. A cancer-associated PCNA expressed in breast cancer has implications as a potential biomarker. *Proc Natl Acad Sci U S A*, 103, 19472-7.
- MANZANARES-MIRALLES, L., SARIKAYA-BAYRAM, Ö., SMITH, E. B., DOLAN, S. K., BAYRAM, Ö., JONES, G. W. & DOYLE, S. 2016. Quantitative proteomics reveals the mechanism and consequence of gliotoxin-mediated dysregulation of the methionine cycle in *Aspergillus niger*. *J Proteomics*, 131, 149-62.
- MARCHETTI, A., ARDIZZONI, A., PAPOTTI, M., CRINÒ, L., ROSSI, G., GRIDELLI, C., BARBERIS, M., MAIORANO, E., NORMANNO, N., TADDEI, G. L., SCAGLIOTTI, G., CLEMENTE, C. & PINTO, C. 2013. Recommendations for the analysis of ALK gene rearrangements in non-small-cell lung cancer: a consensus of the Italian Association of Medical Oncology and the Italian Society of Pathology and Cytopathology. *J Thorac Oncol*, 8, 352-8.
- MARCHEVSKY, A. M. & WICK, M. R. 2015. Diagnostic difficulties with the diagnosis of small cell carcinoma of the lung. *Semin Diagn Pathol*, 32, 480-8.
- MARIÑO-RAMÍREZ, L., KANN, M. G., SHOEMAKER, B. A. & LANDSMAN, D. 2005. Histone structure and nucleosome stability. *Expert Rev Proteomics*, 2, 719-29.
- MARMORSTEIN, R. & ROTH, S. Y. 2001. Histone acetyltransferases: function, structure, and catalysis. *Curr Opin Genet Dev*, 11, 155-61.
- MARR, A. S. & GANTI, A. K. 2016. Resected small cell lung cancer-what do we do next? *Ann Transl Med*, 4, 288.
- MARSHALL, H. M., BOWMAN, R. V., YANG, I. A., FONG, K. M. & BERG, C. D. 2013. Screening for lung cancer with low-dose computed tomography: a review of current status. *J Thorac Dis*, 5 Suppl 5, S524-39.

- MARX, A., BACKES, C., MEESE, E., LENHOF, H. P. & KELLER, A. 2016. EDISON-WMW: Exact Dynamic Programming Solution of the Wilcoxon-Mann-Whitney Test. *Genomics Proteomics Bioinformatics*, 14, 55-61.
- MATTHAY, M. A., WARE, L. B. & ZIMMERMAN, G. A. 2012. The acute respiratory distress syndrome. *J Clin Invest*, 122, 2731-40.
- MATTHAY, M. A. & ZEMANS, R. L. 2011. The acute respiratory distress syndrome: pathogenesis and treatment. *Annu Rev Pathol*, 6, 147-63.
- MATTSON, M. E., POLLACK, E. S. & CULLEN, J. W. 1987. What are the odds that smoking will kill you? *Am J Public Health*, 77, 425-31.
- MAZUMDER, S., DUPREE, E. L. & ALMASAN, A. 2004. A dual role of cyclin E in cell proliferation and apoptosis may provide a target for cancer therapy. *Curr Cancer Drug Targets*, 4, 65-75.
- MAZUREK, S. 2011. Pyruvate kinase type M2: a key regulator of the metabolic budget system in tumor cells. *Int J Biochem Cell Biol*, 43, 969-80.
- MCCOMMIS, K. S. & FINCK, B. N. 2015. Mitochondrial pyruvate transport: a historical perspective and future research directions. *Biochem J*, 466, 443-54.
- MCDERMOTT, M., EUSTACE, A. J., BUSSCHOTS, S., BREEN, L., CROWN, J., CLYNES, M., O'DONOVAN, N. & STORDAL, B. 2014. In vitro Development of Chemotherapy and Targeted Therapy Drug-Resistant Cancer Cell Lines: A Practical Guide with Case Studies. *Front Oncol*, 4, 40.
- MCFADDEN, E. R. 1970. Respiratory control of acid base balance and respiratory causes of imbalance. *Southwest Med*, 51, 37-9.
- MCGRANAHAN, N. & SWANTON, C. 2017. Clonal Heterogeneity and Tumor Evolution: Past, Present, and the Future. *Cell*, 168, 613-628.

- MD, J. H. 2017. Exhaled breath condensate: An evolving tool for noninvasive evaluation of lung disease - ScienceDirect. *Journal of Allergy and Clinical Immunology* [Online], 110. Available: <http://www.sciencedirect.com/science/article/pii/S0091674902000362>.
- MEEKER, W. R., KASHMIRI, R., HUNTER, L., CLAPP, W. & GRIFFEN, W. O. 1973. Clinical evaluation of carcinoembryonic antigen test. *Arch Surg*, 107, 266-74.
- MERKWIRTH, C. & LANGER, T. 2009. Prohibitin function within mitochondria: essential roles for cell proliferation and cristae morphogenesis. *Biochim Biophys Acta*, 1793, 27-32.
- MEYER, K. C. 2007. Bronchoalveolar lavage as a diagnostic tool. *Semin Respir Crit Care Med*, 28, 546-60.
- MEYER, K. C., RAGHU, G., BAUGHMAN, R. P., BROWN, K. K., COSTABEL, U., DU BOIS, R. M., DRENT, M., HASLAM, P. L., KIM, D. S., NAGAI, S., ROTTOLI, P., SALTINI, C., SELMAN, M., STRANGE, C., WOOD, B. & DISEASE, A. T. S. C. O. B. I. I. L. 2012. An official American Thoracic Society clinical practice guideline: the clinical utility of bronchoalveolar lavage cellular analysis in interstitial lung disease. *Am J Respir Crit Care Med*, 185, 1004-14.
- MICHALAK, S., RYBACKA-MOSSAKOWSKA, J., AMBROSIUS, W., GAZDULSKA, J., GOŁDA-GOCKA, I., KOZUBSKI, W. & RAMLAU, R. 2016. The Markers of Glutamate Metabolism in Peripheral Blood Mononuclear Cells and Neurological Complications in Lung Cancer Patients. *Dis Markers*, 2016, 2895972.
- MILNE, M. D. 1955. Renal control of acid-base balance. *Lect Sci Basis Med*, 5, 404-20.
- MISHINA, T., DOSAKA-AKITA, H., HOMMURA, F., NISHI, M., KOJIMA, T., OGURA, S., SHIMIZU, M., KATOH, H. & KAWAKAMI, Y. 2000. Cyclin E

expression, a potential prognostic marker for non-small cell lung cancers. *Clin Cancer Res*, 6, 11-6.

MOLINA, R., MARRADES, R. M., AUGÉ, J. M., ESCUDERO, J. M., VIÑOLAS, N., REGUART, N., RAMIREZ, J., FILELLA, X., MOLINS, L. & AGUSTÍ, A. 2016. Assessment of a Combined Panel of Six Serum Tumor Markers for Lung Cancer. *Am J Respir Crit Care Med*, 193, 427-37.

MONTUSCHI, P. 2007. Analysis of exhaled breath condensate in respiratory medicine: methodological aspects and potential clinical applications. *Ther Adv Respir Dis*, 1, 5-23.

MONTUSCHI, P. & BARNES, P. J. 2002. Analysis of exhaled breath condensate for monitoring airway inflammation. *Trends Pharmacol Sci*, 23, 232-7.

MOORE, G., , S. H., , K. O. B., , S. F., , S. C., , M. O. N. & , K. G. 2017. Resistance Mechanisms to PI3K-mTOR Inhibition in NSCLC. *Journal of thoracic oncology*.

MORAN, C. A., SUSTER, S., ASKIN, F. B. & KOSS, M. N. 1994. Benign and malignant salivary gland-type mixed tumors of the lung. Clinicopathologic and immunohistochemical study of eight cases. *Cancer*, 73, 2481-90.

MORRISSEY, B., O'SHEA, C., ARMSTRONG, J., ROONEY, C., STAUNTON, L., SHEEHAN, M., SHANNON, A. M. & PENNINGTON, S. R. 2013. Development of a label-free LC-MS/MS strategy to approach the identification of candidate protein biomarkers of disease recurrence in prostate cancer patients in a clinical trial of combined hormone and radiation therapy. *Proteomics Clin Appl*, 7, 316-26.

MOSHOUS, D. & DE VILLARTAY, J. P. 2014. The expanding spectrum of human coronin 1A deficiency. *Curr Allergy Asthma Rep*, 14, 481.

MOSKOWITZ, S. M., CHMIEL, J. F., STERNEN, D. L., CHENG, E., GIBSON, R. L., MARSHALL, S. G. & CUTTING, G. R. 2008. Clinical practice and genetic counseling for cystic fibrosis and CFTR-related disorders. *Genet Med*, 10, 851-68.

MOUREY, M. S., QUADRO, L., PANARIELLO, L. & COLANTUONI, V. 1994. Retinoids regulate expression of the retinol-binding protein gene in hepatoma cells in culture. *J Cell Physiol*, 160, 596-602.

MUCCILLI, V., SALETTI, R., CUNSOLO, V., HO, J., GILI, E., CONTE, E., SICHILI, S., VANCHERI, C. & FOTI, S. 2015. Protein profile of exhaled breath condensate determined by high resolution mass spectrometry. *J Pharm Biomed Anal*, 105, 134-49.

MUNNIA, A., GIESE, R. W., POLVANI, S., GALLI, A., CELLAI, F. & PELUSO, M. E. M. 2017. Bulky DNA Adducts, Tobacco Smoking, Genetic Susceptibility, and Lung Cancer Risk. *Adv Clin Chem*, 81, 231-277.

MURPHY, M. E. 2013. The HSP70 family and cancer. *Carcinogenesis*, 34, 1181-8.

MURPHY, S., ZWEYER, M., HENRY, M., MELEADY, P., MUNDEGAR, R. R., SWANDULLA, D. & OHLENDIECK, K. 2015. Label-free mass spectrometric analysis reveals complex changes in the brain proteome from the mdx-4cv mouse model of Duchenne muscular dystrophy. *Clin Proteomics*, 12, 27.

MURRAY, J. F. 2011. Pulmonary edema: pathophysiology and diagnosis. *Int J Tuberc Lung Dis*, 15, 155-60, i.

NAG, S., QIN, J., SRIVENUGOPAL, K. S., WANG, M. & ZHANG, R. 2013. The MDM2-p53 pathway revisited. *J Biomed Res*, 27, 254-71.

NAKANISHI, M., OZAKI, T., YAMAMOTO, H., HANAMOTO, T., KIKUCHI, H., FURUYA, K., ASAKA, M., DELIA, D. & NAKAGAWARA, A. 2007. NFBD1/MDC1 associates with p53 and regulates its function at the crossroad

between cell survival and death in response to DNA damage. *J Biol Chem*, 282, 22993-3004.

NALLURI, S., GHOSHAL-GUPTA, S., KUTIYANAWALLA, A., GAYATRI, S., LEE, B. R., JIWANI, S., ROJANI, A. M. & ROJANI, M. V. 2015. TIMP-1 Inhibits Apoptosis in Lung Adenocarcinoma Cells via Interaction with Bcl-2. *PLoS One*, 10, e0137673.

NARYZHNY, S. N. & LEE, H. 2007. Characterization of proliferating cell nuclear antigen (PCNA) isoforms in normal and cancer cells: there is no cancer-associated form of PCNA. *FEBS Lett*, 581, 4917-20.

NATTIE, E. E. 1990. The alaphastat hypothesis in respiratory control and acid-base balance. *J Appl Physiol* (1985), 69, 1201-7.

NEAL, R. D., HAMILTON, W. & ROGERS, T. K. 2014. Lung cancer. *BMJ*, 349, g6560.

NIMDET, K. & TECHAKEHAKIJ, W. 2017. Congestive heart failure in children with pneumonia and respiratory failure. *Pediatr Int*, 59, 258-264.

NISHITANI, H., SHIOMI, Y., IIDA, H., MICHISHITA, M., TAKAMI, T. & TSURIMOTO, T. 2008. CDK inhibitor p21 is degraded by a proliferating cell nuclear antigen-coupled Cul4-DDB1Cdt2 pathway during S phase and after UV irradiation. *J Biol Chem*, 283, 29045-52.

NOGUCHI, M., KODAMA, T., SHIMOSATO, Y., KOIDE, T., NARUKE, T., SINGH, G. & KATYAL, S. L. 1986. Papillary adenoma of type 2 pneumocytes. *Am J Surg Pathol*, 10, 134-9.

NOMURA, F., KOYAMA, A., ISHIJIMA, M., TAKANO, S., NARITA, M. & NAKAI, T. 1998. Serum levels of five tumor markers for lung cancer in patients with chronic renal failure. *Oncol Rep*, 5, 389-92.

NUNEZ, M. I., BEHRENS, C., WOODS, D. M., LIN, H., SURAOOKAR, M., KADARA, H., HOFSTETTER, W., KALHOR, N., LEE, J. J., FRANKLIN, W., STEWART, D. J. & WISTUBA, I. I. 2012. High expression of folate receptor alpha in lung cancer correlates with adenocarcinoma histology and EGFR [corrected] mutation. *J Thorac Oncol*, 7, 833-40.

O'SHANNESY, D. J., YU, G., SMALE, R., FU, Y. S., SINGHAL, S., THIEL, R. P., SOMERS, E. B. & VACHANI, A. 2012. Folate receptor alpha expression in lung cancer: diagnostic and prognostic significance. *Oncotarget*, 3, 414-25.

OBERLEY, L. W. & BUETTNER, G. R. 1979. Role of superoxide dismutase in cancer: a review. *Cancer Res*, 39, 1141-9.

OBERTACKE, U., JOKA, T., PISON, U., RIEWENDT, H. D. & STIMMING, W. 1987. [Normal values of cell distribution and function in the human alveolus. Bronchoalveolar lavage as a diagnostic tool in intensive care medicine]. *Anasth Intensivther Notfallmed*, 22, 224-8.

ODDONE, E., FERRANTE, D., CENA, T., TUNESI, S., AMENDOLA, P. & MAGNANI, C. 2014. [Asbestos cement factory in Broni (Pavia, Italy): a mortality study]. *Med Lav*, 105, 15-29.

OHARA, G., MIYAZAKI, K., KURISHIMA, K., KAGOHASHI, K., ISHIKAWA, H., SATOH, H. & HIZAWA, N. 2012. Serum levels of cystatin C in elderly lung cancer patients. *Oncol Lett*, 3, 303-306.

OHASHI, K., BURKART, V., FLOHÉ, S. & KOLB, H. 2000. Cutting edge: heat shock protein 60 is a putative endogenous ligand of the toll-like receptor-4 complex. *J Immunol*, 164, 558-61.

OKADA, A., TAKEHARA, H., YOSHIDA, K., NISHI, M., MIYAKE, H., KITA, Y. & KOMI, N. 1993. Increased aspartate and glutamate levels in both gastric and colon cancer tissues. *Tokushima J Exp Med*, 40, 19-25.

OKAMOTO, T., SUZUKI, Y., FUJISHITA, T., KITAHARA, H., SHIMAMATSU, S., KOHNO, M., MORODOMI, Y., KAWANO, D. & MAEHARA, Y. 2014. The prognostic impact of the amount of tobacco smoking in non-small cell lung cancer--differences between adenocarcinoma and squamous cell carcinoma. *Lung Cancer*, 85, 125-30.

OKON, I. S., COUGHLAN, K. A., ZHANG, M., WANG, Q. & ZOU, M. H. 2015. Gefitinib-mediated reactive oxygen specie (ROS) instigates mitochondrial dysfunction and drug resistance in lung cancer cells. *J Biol Chem*, 290, 9101-10.

ONAITIS, M. W., PETERSEN, R. P., BALDERSON, S. S., TOLOZA, E., BURFEIND, W. R., HARPOLE, D. H. & D'AMICO, T. A. 2006. Thoracoscopic lobectomy is a safe and versatile procedure: experience with 500 consecutive patients. *Ann Surg*, 244, 420-5.

ORDÓÑEZ, N. G. 2000. Value of thyroid transcription factor-1 immunostaining in distinguishing small cell lung carcinomas from other small cell carcinomas. *Am J Surg Pathol*, 24, 1217-23.

OSADA, H., TATEMATSU, Y., SAITO, H., YATABE, Y., MITSUDOMI, T. & TAKAHASHI, T. 2004. Reduced expression of class II histone deacetylase genes is associated with poor prognosis in lung cancer patients. *Int J Cancer*, 112, 26-32.

OSTASIEWICZ, P., ZIELINSKA, D. F., MANN, M. & WIŚNIEWSKI, J. R. 2010. Proteome, phosphoproteome, and N-glycoproteome are quantitatively preserved in formalin-fixed paraffin-embedded tissue and analyzable by high-resolution mass spectrometry. *J Proteome Res*, 9, 3688-700.

OSTERGAARD, M., RASMUSSEN, H. H., NIELSEN, H. V., VORUM, H., ORNTOFT, T. F., WOLF, H. & CELIS, J. E. 1997. Proteome profiling of bladder squamous cell carcinomas: identification of markers that define their degree of differentiation. *Cancer Res*, 57, 4111-7.

OZAKI, T. & NAKAGAWARA, A. 2011. Role of p53 in Cell Death and Human Cancers. *Cancers (Basel)*, 3, 994-1013.

PACE, A., BARONE, G., LAURIA, A., MARTORANA, A., PICCIONELLO, A. P., PIERRO, P., TERENCE, A., ALMERICO, A. M., BUSCEMI, S., CAMPANELLA, C., ANGILERI, F., CARINI, F., ZUMMO, G., DE MACARIO, E. C., CAPPELLO, F. & MACARIO, A. J. 2013. Hsp60, a novel target for antitumor therapy: structure-function features and prospective drugs design. *Curr Pharm Des*, 19, 2757-64.

PAI, M. 2013. Diagnosis of pulmonary tuberculosis: recent advances. *J Indian Med Assoc*, 111, 332-6.

PANICO, F., CASALI, C., ROSSI, G., RIZZI, F., MORANDI, U., BETTUZZI, S., DAVALLI, P., CORBETTA, L., STORELLI, E. S., CORTI, A., FABBRI, L. M., ASTANCOLLE, S. & LUPPI, F. 2013. Prognostic role of clusterin in resected adenocarcinomas of the lung. *Lung Cancer*, 79, 294-9.

PARK, B. K., ZHANG, H., ZENG, Q., DAI, J., KELLER, E. T., GIORDANO, T., GU, K., SHAH, V., PEI, L., ZARBO, R. J., MCCAULEY, L., SHI, S., CHEN, S. & WANG, C. Y. 2007. NF-kappaB in breast cancer cells promotes osteolytic bone metastasis by inducing osteoclastogenesis via GM-CSF. *Nat Med*, 13, 62-9.

PARK, D., MAGIS, A. T., LI, R., OWONIKOKO, T. K., SICA, G. L., SUN, S. Y., RAMALINGAM, S. S., KHURI, F. R., CURRAN, W. J. & DENG, X. 2013. Novel small-molecule inhibitors of Bcl-XL to treat lung cancer. *Cancer Res*, 73, 5485-96.

- PARTHEEN, K., LEVAN, K., OSTERBERG, L. & HORVATH, G. 2006. Expression analysis of stage III serous ovarian adenocarcinoma distinguishes a subgroup of survivors. *Eur J Cancer*, 42, 2846-54.
- PASTOR, M. D., NOGAL, A., MOLINA-PINELO, S., MELÉNDEZ, R., SALINAS, A., GONZÁLEZ DE LA PEÑA, M., MARTÍN-JUAN, J., CORRAL, J., GARCÍA-CARBONERO, R., CARNERO, A. & PAZ-ARES, L. 2013. Identification of proteomic signatures associated with lung cancer and COPD. *J Proteomics*, 89, 227-37.
- PASTOREK, M., MÜLLER, P. & VOJTĚŠEK, B. 2016. [Impact of HSP90 Inhibition on Viability and Cell Cycle in Relation to p53 Status]. *Klin Onkol*, 29 Suppl 4, 40-45.
- PATEL, H., ABDULJABBAR, R., LAI, C. F., PERIYASAMY, M., HARROD, A., GEMMA, C., STEEL, J. H., PATEL, N., BUSONERO, C., JERJEES, D., REMENYI, J., SMITH, S., GOMM, J. J., MAGNANI, L., GYÖRFFY, B., JONES, L. J., FULLER-PACE, F., SHOUSHA, S., BULUWELA, L., RAKHA, E. A., ELLIS, I. O., COOMBES, R. C. & ALI, S. 2016. Expression of CDK7, Cyclin H, and MAT1 Is Elevated in Breast Cancer and Is Prognostic in Estrogen Receptor-Positive Breast Cancer. *Clin Cancer Res*, 22, 5929-5938.
- PATNAIK, S., MALLICK, R., KANNISTO, E., SHARMA, R., BSHARA, W., YENDAMURI, S. & DHILLON, S. S. 2015. MiR-205 and MiR-375 microRNA assays to distinguish squamous cell carcinoma from adenocarcinoma in lung cancer biopsies. *J Thorac Oncol*, 10, 446-53.
- PAULO, J. A., LEE, L. S., BANKS, P. A., STEEN, H. & CONWELL, D. L. 2012. Proteomic analysis of formalin-fixed paraffin-embedded pancreatic tissue using liquid chromatography tandem mass spectrometry. *Pancreas*, 41, 175-85.

- PAUWELS, R. & VAN DER STRAETEN, M. 1975. Plasma levels of carcinoembryonic antigen in bronchial carcinoma and chronic bronchitis. *Thorax*, 30, 560-2.
- PETERSEN, R. H., HANSEN, H. J., DIRKSEN, A. & PEDERSEN, J. H. 2012. Lung cancer screening and video-assisted thoracic surgery. *J Thorac Oncol*, 7, 1026-31.
- PETTY, W. J., DRAGNEV, K. H., MEMOLI, V. A., MA, Y., DESAI, N. B., BIDDLE, A., DAVIS, T. H., NUGENT, W. C., MEMOLI, N., HAMILTON, M., IWATA, K. K., RIGAS, J. R. & DMITROVSKY, E. 2004. Epidermal growth factor receptor tyrosine kinase inhibition represses cyclin D1 in aerodigestive tract cancers. *Clin Cancer Res*, 10, 7547-54.
- PETTY, W. J., VOELZKE, W. R., URBANIC, J. J., VARELA, V. A., WALLER, L. L., SWIFT, C. B., GRAHAM, R. M., MEMOLI, V. A. & DRAGNEV, K. H. 2011. High cyclin D3 expression confers erlotinib resistance in aerodigestive tract cancer. *Lung Cancer*, 74, 384-91.
- PFLUM, M. K., TONG, J. K., LANE, W. S. & SCHREIBER, S. L. 2001. Histone deacetylase 1 phosphorylation promotes enzymatic activity and complex formation. *J Biol Chem*, 276, 47733-41.
- PHUCHAREON, J., MCCORMICK, F., EISELE, D. W. & TETSU, O. 2015. EGFR inhibition evokes innate drug resistance in lung cancer cells by preventing Akt activity and thus inactivating Ets-1 function. *Proc Natl Acad Sci U S A*, 112, E3855-63.
- PIETTE, J., NEEL, H. & MARÉCHAL, V. 1997. Mdm2: keeping p53 under control. *Oncogene*, 15, 1001-10.
- PLUTA, P., SMOLEWSKI, P., PLUTA, A., CEBULA-OBZUT, B., WIERZBOWSKA, A., NEJC, D., ROBAK, T., KORDEK, R., GOTTWALD, L.,

- PIEKARSKI, J. & JEZIORSKI, A. 2011. Significance of Bax expression in breast cancer patients. *Pol Przegl Chir*, 83, 549-53.
- PLYMOTH, A., LÖFDAHL, C. G., EKBERG-JANSSON, A., DAHLBÄCK, M., LINDBERG, H., FEHNIGER, T. E. & MARKO-VARGA, G. 2003. Human bronchoalveolar lavage: biofluid analysis with special emphasis on sample preparation. *Proteomics*, 3, 962-72.
- PÖHLAND, T., WAGNER, S., MAHYAR-ROEMER, M. & ROEMER, K. 2006. Bax and Bak are the critical complementary effectors of colorectal cancer cell apoptosis by chemopreventive resveratrol. *Anticancer Drugs*, 17, 471-8.
- POIRIER, H., BRAISSANT, O., NIOT, I., WAHLI, W. & BESNARD, P. 1997. 9-cis-retinoic acid enhances fatty acid-induced expression of the liver fatty acid-binding protein gene. *FEBS Lett*, 412, 480-4.
- POPPER, H. H., WIRNSBERGER, G., JÜTTNER-SMOLLE, F. M., PONGRATZ, M. G. & SOMMERSGUTTER, M. 1992. The predictive value of human papilloma virus (HPV) typing in the prognosis of bronchial squamous cell papillomas. *Histopathology*, 21, 323-30.
- POREBSKA, I., WYRODEK, E., KOSACKA, M., ADAMIAK, J., JANKOWSKA, R. & HARŁOZIŃSKA-SZMYRKA, A. 2006. Apoptotic markers p53, Bcl-2 and Bax in primary lung cancer. *In Vivo*, 20, 599-604.
- POWELL, J. M. 1988. Metastatic carcinoid of bone. Report of two cases and review of the literature. *Clin Orthop Relat Res*, 266-72.
- POWERS, B. E., HOOPEES, P. J. & EHRHART, E. J. 1995. Tumor diagnosis, grading, and staging. *Semin Vet Med Surg (Small Anim)*, 10, 158-67.
- PRELAJ, A., REBUZZI, S. E., DEL BENE, G., GIRÒN BERRIÒS, J. R., EMILIANI, A., DE FILIPPIS, L., PRETE, A. A., PECORARI, S., MANNA, G.,

- FERRARA, C., ROSSINI, D. & LONGO, F. 2017. Evaluation of the efficacy of cisplatin-etoposide and the role of thoracic radiotherapy and prophylactic cranial irradiation in LCNEC. *ERJ Open Res*, 3.
- PRYCZYNICZ, A., GRYKO, M., NIEWIAROWSKA, K., CEPOWICZ, D., USTYMOWICZ, M., KEMONA, A. & GUZIŃSKA-USTYMOWICZ, K. 2014. Bax protein may influence the invasion of colorectal cancer. *World J Gastroenterol*, 20, 1305-10.
- PUDDICOMBE, S. M., POLOSA, R., RICHTER, A., KRISHNA, M. T., HOWARTH, P. H., HOLGATE, S. T. & DAVIES, D. E. 2000. Involvement of the epidermal growth factor receptor in epithelial repair in asthma. *FASEB J*, 14, 1362-74.
- QI, W., LIU, X., CHEN, W., LI, Q. & MARTINEZ, J. D. 2007. Overexpression of 14-3-3gamma causes polyploidization in H322 lung cancer cells. *Mol Carcinog*, 46, 847-56.
- QI, W., LIU, X., QIAO, D. & MARTINEZ, J. D. 2005. Isoform-specific expression of 14-3-3 proteins in human lung cancer tissues. *Int J Cancer*, 113, 359-63.
- RAMSEY, K. A., FOONG, R. E., GRDOSIC, J., HARPER, A., SKORIC, B., CLEM, C., DAVIS, M., TURKOVIC, L., STICK, S. M., DAVIS, S. D., RANGANATHAN, S. C., HALL, G. L. & CF, A. 2017. Multiple Breath Washout Outcomes Are Sensitive to Inflammation and Infection in Children with Cystic Fibrosis. *Ann Am Thorac Soc*.
- RANDOLPH, G. J., ANGELI, V. & SWARTZ, M. A. 2005. Dendritic-cell trafficking to lymph nodes through lymphatic vessels. *Nat Rev Immunol*, 5, 617-28.
- RAVITZ, M. J. & WENNER, C. E. 1997. Cyclin-dependent kinase regulation during G1 phase and cell cycle regulation by TGF-beta. *Adv Cancer Res*, 71, 165-207.

RECK, M., VON PAWEL, J., ZATLOUKAL, P., RAMLAU, R., GORBOUNOVA, V., HIRSH, V., LEIGHL, N., MEZGER, J., ARCHER, V., MOORE, N. & MANEGOLD, C. 2009. Phase III trial of cisplatin plus gemcitabine with either placebo or bevacizumab as first-line therapy for nonsquamous non-small-cell lung cancer: AVAIL. *J Clin Oncol*, 27, 1227-34.

REKHTMAN, N. 2010. Neuroendocrine tumors of the lung: an update. *Arch Pathol Lab Med*, 134, 1628-38.

REKHTMAN, N., ANG, D. C., SIMA, C. S., TRAVIS, W. D. & MOREIRA, A. L. 2011. Immunohistochemical algorithm for differentiation of lung adenocarcinoma and squamous cell carcinoma based on large series of whole-tissue sections with validation in small specimens. *Mod Pathol*, 24, 1348-59.

REUNGWETWATTANA, T. & DY, G. K. 2013. Targeted therapies in development for non-small cell lung cancer. *J Carcinog*, 12, 22.

REYNISDÓTTIR, I., POLYAK, K., IAVARONE, A. & MASSAGUÉ, J. 1995. Kip/Cip and Ink4 Cdk inhibitors cooperate to induce cell cycle arrest in response to TGF-beta. *Genes Dev*, 9, 1831-45.

REYNOLDS, H. Y. & NEWBALL, H. H. 1974. Analysis of proteins and respiratory cells obtained from human lungs by bronchial lavage. *J Lab Clin Med*, 84, 559-73.

REYNOSO G, C. T., HOLYOKE D, COHEN E, NEMOTO T, WANG J, CHUANG J, GUINAN P, MURPHY GP. 1972. Carcinoembryonic Antigen in Patients With Different Cancers. *JAMA [Online]*, 220.

RIFAI, N., GILLETTE, M. A. & CARR, S. A. 2006. Protein biomarker discovery and validation: the long and uncertain path to clinical utility. *Nat Biotechnol*, 24, 971-83.

- ROBBINS, D. & ZHAO, Y. 2014. Manganese superoxide dismutase in cancer prevention. *Antioxid Redox Signal*, 20, 1628-45.
- ROBEY, R. W., CHAKRABORTY, A. R., BASSEVILLE, A., LUCHENKO, V., BAHR, J., ZHAN, Z. & BATES, S. E. 2011. Histone deacetylase inhibitors: emerging mechanisms of resistance. *Mol Pharm*, 8, 2021-31.
- ROBINS, A. G. 1983. Pathophysiology of emphysema. *Clin Chest Med*, 4, 413-20.
- ROBINSON, D. S., HAMID, Q., YING, S., TSICOPOULOS, A., BARKANS, J., BENTLEY, A. M., CORRIGAN, C., DURHAM, S. R. & KAY, A. B. 1992. Predominant TH2-like bronchoalveolar T-lymphocyte population in atopic asthma. *N Engl J Med*, 326, 298-304.
- ROMMENS, J. M., IANNUZZI, M. C., KEREM, B., DRUMM, M. L., MELMER, G., DEAN, M., ROZMAHEL, R., COLE, J. L., KENNEDY, D. & HIDAKA, N. 1989. Identification of the cystic fibrosis gene: chromosome walking and jumping. *Science*, 245, 1059-65.
- RONG, Y., WU, W., NI, X., KUANG, T., JIN, D., WANG, D. & LOU, W. 2013. Lactate dehydrogenase A is overexpressed in pancreatic cancer and promotes the growth of pancreatic cancer cells. *Tumour Biol*, 34, 1523-30.
- ROSENMAN, K. D. & ZHU, Z. 1995. Pneumoconiosis and associated medical conditions. *Am J Ind Med*, 27, 107-13.
- ROSSI, G., MURER, B., CAVAZZA, A., LOSI, L., NATALI, P., MARCHIONI, A., MIGALDI, M., CAPITANIO, G. & BRAMBILLA, E. 2004. Primary mucinous (so-called colloid) carcinomas of the lung: a clinicopathologic and immunohistochemical study with special reference to CDX-2 homeobox gene and MUC2 expression. *Am J Surg Pathol*, 28, 442-52.

- SAIKA, K. & SOBUE, T. 2013. [Cancer statistics in the world]. *Gan To Kagaku Ryoho*, 40, 2475-80.
- SAKAMOTO, K. & MAEDA, S. 2010. Targeting NF-kappaB for colorectal cancer. *Expert Opin Ther Targets*, 14, 593-601.
- SALEHIN, D., FROMBERG, I., HAUGK, C., DOHMEN, B., GEORG, T., BOHLE, R. M., BAUERSCHLAG, D., THILL, M. & FRIEDRICH, M. 2011. Immunohistochemical analysis for expression of calpain 1, calpain 2 and calpastatin in ovarian cancer. *Eur J Gynaecol Oncol*, 32, 628-35.
- SAMSON, D. J., SEIDENFELD, J., SIMON, G. R., TURRISI, A. T., BONNELL, C., ZIEGLER, K. M., ARONSON, N. & PHYSICIANS, A. C. O. C. 2007. Evidence for management of small cell lung cancer: ACCP evidence-based clinical practice guidelines (2nd edition). *Chest*, 132, 314S-323S.
- SAMUELS-LEV, Y., O'CONNOR, D. J., BERGAMASCHI, D., TRIGIANTE, G., HSIEH, J. K., ZHONG, S., CAMPARGUE, I., NAUMOVSKI, L., CROOK, T. & LU, X. 2001. ASPP proteins specifically stimulate the apoptotic function of p53. *Mol Cell*, 8, 781-94.
- SANDERS, K. M., MARRAS, T. K. & CHAN, C. K. 2006. Pneumonia severity index in the immunocompromised. *Can Respir J*, 13, 89-93.
- SANDLER, A., GRAY, R., PERRY, M. C., BRAHMER, J., SCHILLER, J. H., DOWLATI, A., LILENBAUM, R. & JOHNSON, D. H. 2006. Paclitaxel-carboplatin alone or with bevacizumab for non-small-cell lung cancer. *N Engl J Med*, 355, 2542-50.
- SANTRA, M., SHAUGHNESSY, J. D. & BELLAMY, W. T. 2011. Expression of multiple myeloma associated markers in bone marrow spicules using a novel immunohistochemical technique. *Biotech Histochem*, 86, 119-23.

SARKAR, D. K., JANA, D., PATIL, P. S., CHAUDHARI, K. S., CHATTOPADHYAY, B. K., CHIKKALA, B. R., MANDAL, S. & CHOWDHARY, P. 2013. Role of NF- κ B as a Prognostic Marker in Breast Cancer : A Pilot Study in Indian Patients. *Indian J Surg Oncol*, 4, 242-7.

SATOH, M., TAKANO, S., SOGAWA, K., NODA, K., YOSHITOMI, H., ISHIBASHI, M., MOGUSHI, K., TAKIZAWA, H., OTSUKA, M., SHIMIZU, H., MIYAZAKI, M. & NOMURA, F. 2017. Immune-complex level of cofilin-1 in sera is associated with cancer progression and poor prognosis in pancreatic cancer. *Cancer Sci*, 108, 795-803.

SAYED-AHMED, M. M. 2010. Role of carnitine in cancer chemotherapy-induced multiple organ toxicity. *Saudi Pharm J*, 18, 195-206.

SCAGLIOTTI, G., HANNA, N., FOSSELLA, F., SUGARMAN, K., BLATTER, J., PETERSON, P., SIMMS, L. & SHEPHERD, F. A. 2009. The differential efficacy of pemetrexed according to NSCLC histology: a review of two Phase III studies. *Oncologist*, 14, 253-63.

SCHAFFER, K. A. 1998. The cell cycle: a review. *Vet Pathol*, 35, 461-78.

SCHERR, A. L., GDYNIA, G., SALOU, M., RADHAKRISHNAN, P., DUGLOVA, K., HELLER, A., KEIM, S., KAUTZ, N., JASSOWICZ, A., ELSSNER, C., HE, Y. W., JAEGER, D., HEIKENWALDER, M., SCHNEIDER, M., WEBER, A., ROTH, W., SCHULZE-BERGGKAMEN, H. & KOEHLER, B. C. 2016. Bcl-xL is an oncogenic driver in colorectal cancer. *Cell Death Dis*, 7, e2342.

SCHIEFNER, A. & SKERRA, A. 2015. The menagerie of human lipocalins: a natural protein scaffold for molecular recognition of physiological compounds. *Acc Chem Res*, 48, 976-85.

- SCHNEIDER, J., NEU, K., GRIMM, H., VELCOVSKY, H. G., WEISSE, G. & EIGENBRODT, E. 2002. Tumor M2-pyruvate kinase in lung cancer patients: immunohistochemical detection and disease monitoring. *Anticancer Res*, 22, 311-8.
- SCHNEIDER, J., PRESEK, P., BRAUN, A., LÖFFLER, S. & WOITOWITZ, H. J. 2000. Serum ras (p21) as a marker for occupationally derived lung cancer? *Clin Chem Lab Med*, 38, 301-5.
- SCHOR, S. L. & SCHOR, A. M. 2001. Phenotypic and genetic alterations in mammary stroma: implications for tumour progression. *Breast Cancer Res*, 3, 373-9.
- SCHURTENBERGER, P., EGELHAAF, S. U., HINDGES, R., MAGA, G., JÓNSSON, Z. O., MAY, R. P., GLATTER, O. & HÜBSCHER, U. 1998. The solution structure of functionally active human proliferating cell nuclear antigen determined by small-angle neutron scattering. *J Mol Biol*, 275, 123-32.
- SCHUTT, A. C., BULLINGTON, W. M. & JUDSON, M. A. 2010. Pharmacotherapy for pulmonary sarcoidosis: a Delphi consensus study. *Respir Med*, 104, 717-23.
- SCICCHITANO, M. S., DALMAS, D. A., BOYCE, R. W., THOMAS, H. C. & FRAZIER, K. S. 2009. Protein extraction of formalin-fixed, paraffin-embedded tissue enables robust proteomic profiles by mass spectrometry. *J Histochem Cytochem*, 57, 849-60.
- SCULIER, J. P. 2013. Nonsmall cell lung cancer. *Eur Respir Rev*, 22, 33-6.
- SEO, C. W., UM, I. C., RICO, C. W. & KANG, M. Y. 2011. Antihyperlipidemic and body fat-lowering effects of silk proteins with different fibroin/sericin compositions in mice fed with high fat diet. *J Agric Food Chem*, 59, 4192-7.
- SHAO, M., CAO, L., SHEN, C., SATPATHY, M., CHELLADURAI, B., BIGSBY, R. M., NAKSHATRI, H. & MATEI, D. 2009. Epithelial-to-mesenchymal transition

and ovarian tumor progression induced by tissue transglutaminase. *Cancer Res*, 69, 9192-201.

SHENG, H., NIU, B. & SUN, H. 2009. Metabolic targeting of cancers: from molecular mechanisms to therapeutic strategies. *Curr Med Chem*, 16, 1561-87.

SHIMOSATO, Y. 2002. [Histological Typing of Lung and Pleural Tumors (3rd edition, 1999): Malignant epithelial tumors]. *Nihon Rinsho*, 60 Suppl 5, 123-31.

SHOSHAN-BARMATZ, V., ISRAELSON, A., BRDICZKA, D. & SHEU, S. S. 2006. The voltage-dependent anion channel (VDAC): function in intracellular signalling, cell life and cell death. *Curr Pharm Des*, 12, 2249-70.

SHUKLA, S. K., GEBREGIWORGIS, T., PUROHIT, V., CHAIKA, N. V., GUNDA, V., RADHAKRISHNAN, P., MEHLA, K., PIPINOS, I. I., POWERS, R., YU, F. & SINGH, P. K. 2014. Metabolic reprogramming induced by ketone bodies diminishes pancreatic cancer cachexia. *Cancer Metab*, 2, 18.

SIEGEL, R. L., MILLER, K. D. & JEMAL, A. 2017. Cancer Statistics, 2017. *CA Cancer J Clin*, 67, 7-30.

SIMHADRI, P. K., MALWADE, R., VANKA, R., NAKKA, V. P., KUPPUSAMY, G. & BABU, P. P. 2017. Dysregulation of LIMK-1/cofilin-1 pathway: A possible basis for alteration of neuronal morphology in experimental cerebral malaria. *Ann Neurol*, 82, 429-443.

SINGLETARY, M. L., PHILLIPPI-FALKENSTEIN, K. M., SCANLON, E., BOHM, R. P., VEAZEY, R. S. & GILL, A. F. 2008. Modification of a common BAL technique to enhance sample diagnostic value. *J Am Assoc Lab Anim Sci*, 47, 47-51.

SIONOV, R. V. & HAUPT, Y. 1999. The cellular response to p53: the decision between life and death. *Oncogene*, 18, 6145-57.

- SKRZYCKI, M., CZECZOT, H., CHRZANOWSKA, A. & OTTO-ŚLUSARCZYK, D. 2015. [The level of superoxide dismutase expression in primary and metastatic colorectal cancer cells in hypoxia and tissue normoxia]. *Pol Merkur Lekarski*, 39, 281-6.
- SOLDATSKI, I. L., ONUFRIEVA, E. K., STEKLOV, A. M. & SCHEPIN, N. V. 2005. Tracheal, bronchial, and pulmonary papillomatosis in children. *Laryngoscope*, 115, 1848-54.
- SONG, Y., YANG, Z., KE, Z., YAO, Y., HU, X., SUN, Y., LI, H., YIN, J. & ZENG, C. 2012. Expression of 14-3-3 γ in patients with breast cancer: correlation with clinicopathological features and prognosis. *Cancer Epidemiol*, 36, 533-6.
- SORIA, J. C., JANG, S. J., KHURI, F. R., HASSAN, K., LIU, D., HONG, W. K. & MAO, L. 2000. Overexpression of cyclin B1 in early-stage non-small cell lung cancer and its clinical implication. *Cancer Res*, 60, 4000-4.
- SPINELLI, J. B., YOON, H., RINGEL, A. E., JEANFAVRE, S., CLISH, C. B. & HAIGIS, M. C. 2017. Metabolic recycling of ammonia via glutamate dehydrogenase supports breast cancer biomass. *Science*, 358, 941-946.
- SPITZ, M. R., WEI, Q., DONG, Q., AMOS, C. I. & WU, X. 2003. Genetic susceptibility to lung cancer: the role of DNA damage and repair. *Cancer Epidemiol Biomarkers Prev*, 12, 689-98.
- SPRIET, L. L. & HEIGENHAUSER, G. J. 2002. Regulation of pyruvate dehydrogenase (PDH) activity in human skeletal muscle during exercise. *Exerc Sport Sci Rev*, 30, 91-5.
- STAHL, D. L., RICHARD, K. M. & PAPADIMOS, T. J. 2015. Complications of bronchoscopy: A concise synopsis. *Int J Crit Illn Inj Sci*, 5, 189-95.
- STAUB, N. C. 1974. Pulmonary edema. *Physiol Rev*, 54, 678-811.

STEINBERG, W. 1990. The clinical utility of the CA 19-9 tumor-associated antigen. *Am J Gastroenterol*, 85, 350-5.

STELIOU, K., BOOSALIS, M. S., PERRINE, S. P., SANGERMAN, J. & FALLER, D. V. 2012. Butyrate histone deacetylase inhibitors. *Biores Open Access*, 1, 192-8.

STOIMENOV, I. & HELLEDAY, T. 2009. PCNA on the crossroad of cancer. *Biochem Soc Trans*, 37, 605-13.

SU, J., ANJUMAN, N., GUARNERA, M. A., ZHANG, H., STASS, S. A. & JIANG, F. 2015. Analysis of Lung Flute-collected Sputum for Lung Cancer Diagnosis. *Biomark Insights*, 10, 55-61.

SU LIM, C., SUN KIM, E., YEON KIM, J., TAEK HONG, S., JAI CHUN, H., EUN KANG, D. & RAE CHO, B. 2015. Measurement of the Nucleus Area and Nucleus/Cytoplasm and Mitochondria/Nucleus Ratios in Human Colon Tissues by Dual-Colour Two-Photon Microscopy Imaging. *Sci Rep*, 5, 18521.

SUMMERFIELD, A. & MCCULLOUGH, K. C. 2009. Dendritic Cells in Innate and Adaptive Immune Responses against Influenza Virus. *Viruses*, 1, 1022-34.

SUN, X., SUN, Z., ZHU, Z., GUAN, H., ZHANG, J., ZHANG, Y., XU, H. & SUN, M. 2014. Clinicopathological significance and prognostic value of lactate dehydrogenase A expression in gastric cancer patients. *PLoS One*, 9, e91068.

SUN, X. R., SUN, Z., ZHU, Z., GUAN, H. X., LI, C. Y., ZHANG, J. Y., ZHANG, Y. N., ZHOU, H., ZHANG, H. J., XU, H. M. & SUN, M. J. 2015. Expression of pyruvate dehydrogenase is an independent prognostic marker in gastric cancer. *World J Gastroenterol*, 21, 5336-44.

SUN, Y., MI, W., CAI, J., YING, W., LIU, F., LU, H., QIAO, Y., JIA, W., BI, X., LU, N., LIU, S., QIAN, X. & ZHAO, X. 2008. Quantitative proteomic signature of

liver cancer cells: tissue transglutaminase 2 could be a novel protein candidate of human hepatocellular carcinoma. *J Proteome Res*, 7, 3847-59.

SUZUKI, H., ITOH, F., TOYOTA, M., KIKUCHI, T., KAKIUCHI, H. & IMAI, K. 2000. Inactivation of the 14-3-3 sigma gene is associated with 5' CpG island hypermethylation in human cancers. *Cancer Res*, 60, 4353-7.

SUZUKI, T., URANO, T., MIKI, Y., MORIYA, T., AKAHIRA, J., ISHIDA, T., HORIE, K., INOUE, S. & SASANO, H. 2007. Nuclear cyclin B1 in human breast carcinoma as a potent prognostic factor. *Cancer Sci*, 98, 644-51.

SWEISS, N. J., LOWER, E. E., MIRSAEIDI, M., DUDEK, S., GARCIA, J. G., PERKINS, D., FINN, P. W. & BAUGHMAN, R. P. 2014. Rituximab in the treatment of refractory pulmonary sarcoidosis. *Eur Respir J*, 43, 1525-8.

SWINNEN, J. V., BRUSSELMANS, K. & VERHOEVEN, G. 2006. Increased lipogenesis in cancer cells: new players, novel targets. *Curr Opin Clin Nutr Metab Care*, 9, 358-65.

TAHA BEYASED, F. A. 2017. Cancer Incidence in Western Libya: First Results from Tripoli. Medical Center. In: NABIL ENATTAH, F. E., NUREDDIN ASHAMMAKHI, ADAM ELZAGHEID. (ed.). *Ibnosina J Med BS*, 9, 37-45.

TAKENAKA, T., TAKENOYAMA, M., INAMASU, E., YOSHIDA, T., TOYOKAWA, G., NOSAKI, K., HIRAI, F., YAMAGUCHI, M., SHIMOKAWA, M., SETO, T. & ICHINOSE, Y. 2015. Role of surgical resection for patients with limited disease-small cell lung cancer. *Lung Cancer*, 88, 52-6.

TANG, X., LIU, D., SHISHODIA, S., OZBURN, N., BEHRENS, C., LEE, J. J., HONG, W. K., AGGARWAL, B. B. & WISTUBA, I. I. 2006. Nuclear factor-kappaB (NF-kappaB) is frequently expressed in lung cancer and preneoplastic lesions. *Cancer*, 107, 2637-46.

- TANOUE, L. T. & DETTERBECK, F. C. 2009. New TNM classification for non-small-cell lung cancer. *Expert Rev Anticancer Ther*, 9, 413-23.
- TASAB, M., BATTEN, M. R. & BULLEID, N. J. 2000. Hsp47: a molecular chaperone that interacts with and stabilizes correctly-folded procollagen. *EMBO J*, 19, 2204-11.
- TELLONI, S. M. 2017. Tumor Staging and Grading: A Primer. *Methods Mol Biol*, 1606, 1-17.
- TENG, X. D. 2005. [World Health Organization classification of tumours, pathology and genetics of tumours of the lung]. *Zhonghua Bing Li Xue Za Zhi*, 34, 544-6.
- THOMAS, J. S., LAMB, D., ASHCROFT, T., CORRIN, B., EDWARDS, C. W., GIBBS, A. R., KENYON, W. E., STEPHENS, R. J. & WHIMSTER, W. F. 1993. How reliable is the diagnosis of lung cancer using small biopsy specimens? Report of a UKCCCR Lung Cancer Working Party. *Thorax*, 48, 1135-9.
- THOMAS, P., KHOKHA, R., SHEPHERD, F. A., FELD, R. & TSAO, M. S. 2000. Differential expression of matrix metalloproteinases and their inhibitors in non-small cell lung cancer. *J Pathol*, 190, 150-6.
- THOMS, H. C., LOVERIDGE, C. J., SIMPSON, J., CLIPSON, A., REINHARDT, K., DUNLOP, M. G. & STARK, L. A. 2010. Nucleolar targeting of RelA(p65) is regulated by COMMD1-dependent ubiquitination. *Cancer Res*, 70, 139-49.
- THOMSON, D. M., KRUPPEY, J., FREEDMAN, S. O. & GOLD, P. 1969. The radioimmunoassay of circulating carcinoembryonic antigen of the human digestive system. *Proc Natl Acad Sci U S A*, 64, 161-7.
- THUNNISSEN, F. B. 2003. Sputum examination for early detection of lung cancer. *J Clin Pathol*, 56, 805-10.

TIMMERMANN, S., LEHRMANN, H., POLESSKAYA, A. & HAREL-BELLAN, A. 2001. Histone acetylation and disease. *Cell Mol Life Sci*, 58, 728-36.

TISDALE, M. J. 2009. Mechanisms of cancer cachexia. *Physiol Rev*, 89, 381-410.

TRAVIS, W. D., BRAMBILLA, E., BURKE, A. P., MARX, A. & NICHOLSON, A. G. 2015a. Introduction to The 2015 World Health Organization Classification of Tumors of the Lung, Pleura, Thymus, and Heart. *J Thorac Oncol*, 10, 1240-1242.

TRAVIS, W. D., BRAMBILLA, E., NICHOLSON, A. G., YATABE, Y., AUSTIN, J. H., BEASLEY, M. B., CHIRIEAC, L. R., DACIC, S., DUHIG, E., FLIEDER, D. B., GEISINGER, K., HIRSCH, F. R., ISHIKAWA, Y., KERR, K. M., NOGUCHI, M., PELOSI, G., POWELL, C. A., TSAO, M. S., WISTUBA, I. & PANEL, W. 2015b. The 2015 World Health Organization Classification of Lung Tumors: Impact of Genetic, Clinical and Radiologic Advances Since the 2004 Classification. *J Thorac Oncol*, 10, 1243-60.

TRAVIS, W. D., GIROUX, D. J., CHANSKY, K., CROWLEY, J., ASAMURA, H., BRAMBILLA, E., JETT, J., KENNEDY, C., RAMI-PORTA, R., RUSCH, V. W., GOLDSTRAW, P. & INSTITUTIONS, I. S. C. A. P. 2008. The IASLC Lung Cancer Staging Project: proposals for the inclusion of broncho-pulmonary carcinoid tumors in the forthcoming (seventh) edition of the TNM Classification for Lung Cancer. *J Thorac Oncol*, 3, 1213-23.

TRAVIS, W. D., REKHTMAN, N., RILEY, G. J., GEISINGER, K. R., ASAMURA, H., BRAMBILLA, E., GARG, K., HIRSCH, F. R., NOGUCHI, M., POWELL, C. A., RUSCH, V. W., SCAGLIOTTI, G. & YATABE, Y. 2010. Pathologic diagnosis of advanced lung cancer based on small biopsies and cytology: a paradigm shift. *J Thorac Oncol*. United States.

- TROJAN, B., TANG, A., CHANDRAPAL, J., FILLEUR, S. & NELIUS, T. 2013. The clinical usefulness of nuclear matrix protein-22 in patients with end-stage renal disease and microscopic hematuria. *Ren Fail*, 35, 72-6.
- TROUGAKOS, I. P. & GONOS, E. S. 2002. Clusterin/apolipoprotein J in human aging and cancer. *Int J Biochem Cell Biol*, 34, 1430-48.
- TSAI, C. H., LIN, L. T., WANG, C. Y., CHIU, Y. W., CHOU, Y. T., CHIU, S. J., WANG, H. E., LIU, R. S., WU, C. Y., CHAN, P. C., YANG, M. H., CHIOU, S. H., LIAO, M. J. & LEE, Y. J. 2015. Over-expression of cofilin-1 suppressed growth and invasion of cancer cells is associated with up-regulation of let-7 microRNA. *Biochim Biophys Acta*, 1852, 851-61.
- TSUJI, B., HAYASHI, K., KONDO, N. & NISHIYASU, T. 2016. Characteristics of hyperthermia-induced hyperventilation in humans. *Temperature (Austin)*, 3, 146-60.
- URAMOTO, H., SUGIO, K., OYAMA, T., NAKATA, S., ONO, K., NOZOE, T. & YASUMOTO, K. 2006. Expression of the p53 family in lung cancer. *Anticancer Res*, 26, 1785-90.
- VALDIGLESIAS, V., PÁSARO, E., MÉNDEZ, J. & LAFFON, B. 2011. Assays to determine DNA repair ability. *J Toxicol Environ Health A*, 74, 1094-109.
- VALENCIA, A. & MORÁN, J. 2001. Role of oxidative stress in the apoptotic cell death of cultured cerebellar granule neurons. *J Neurosci Res*, 64, 284-97.
- VALVONA, C. J., FILLMORE, H. L., NUNN, P. B. & PILKINGTON, G. J. 2016. The Regulation and Function of Lactate Dehydrogenase A: Therapeutic Potential in Brain Tumor. *Brain Pathol*, 26, 3-17.
- VAN BEEK, E. J., MIRSADRAEE, S. & MURCHISON, J. T. 2015. Lung cancer screening: Computed tomography or chest radiographs? *World J Radiol*, 7, 189-93.

- VAN'T WESTEINDE, S. C. & VAN KLAVEREN, R. J. 2011. Screening and early detection of lung cancer. *Cancer J*, 17, 3-10.
- VANDER HEIDEN, M. G., CANTLEY, L. C. & THOMPSON, C. B. 2009. Understanding the Warburg effect: the metabolic requirements of cell proliferation. *Science*, 324, 1029-33.
- VAUGHAN, C. A., SINGH, S., WINDLE, B., SANKALA, H. M., GRAVES, P. R., ANDREW YEUDALL, W., DEB, S. P. & DEB, S. 2012. p53 mutants induce transcription of NF- κ B2 in H1299 cells through CBP and STAT binding on the NF- κ B2 promoter and gain of function activity. *Arch Biochem Biophys*, 518, 79-88.
- VELLUCCI, V. F., GERMINO, F. J. & REISS, M. 1995. Cloning of putative growth regulatory genes from primary human keratinocytes by subtractive hybridization. *Gene*, 166, 213-20.
- VENTURA, R., MORDEC, K., WASZCZUK, J., WANG, Z., LAI, J., FRIDLIB, M., BUCKLEY, D., KEMBLE, G. & HEUER, T. S. 2015. Inhibition of de novo Palmitate Synthesis by Fatty Acid Synthase Induces Apoptosis in Tumor Cells by Remodeling Cell Membranes, Inhibiting Signaling Pathways, and Reprogramming Gene Expression. *EBioMedicine*, 2, 808-24.
- VIALARD, J. F., LACOMBE, F., BELLOC, F., PELLEGRIN, J. L. & REIFFERS, J. 2001. [Molecular mechanisms controlling the cell cycle: fundamental aspects and implications for oncology]. *Cancer Radiother*, 5, 109-29.
- VINCENT, R. G. & CHU, T. M. 1973. Carcinoembryonic antigen in patients with carcinoma of the lung. *J Thorac Cardiovasc Surg*, 66, 320-8.
- VOLLMER, R. T., BIRCH, R., OGDEN, L. & CRISSMAN, J. D. 1985. Subclassification of small cell cancer of the lung: the Southeastern Cancer Study Group experience. *Hum Pathol*, 16, 247-52.

WAGA, S., HANNON, G. J., BEACH, D. & STILLMAN, B. 1994. The p21 inhibitor of cyclin-dependent kinases controls DNA replication by interaction with PCNA. *Nature*, 369, 574-8.

WAITHMAN, J. & MINTER, J. D. 2012. Dendritic cells and influenza A virus infection. *Virulence*, 3, 603-8.

WAKABAYASHI, H., WAKISAKA, S., HIRAGA, T., HATA, K., NISHIMURA, R., TOMINAGA, M. & YONEDA, T. 2017. Decreased sensory nerve excitation and bone pain associated with mouse Lewis lung cancer in TRPV1-deficient mice. *J Bone Miner Metab*.

WALLIN, J. J., EDGAR, K. A., GUAN, J., BERRY, M., PRIOR, W. W., LEE, L., LESNICK, J. D., LEWIS, C., NONOMIYA, J., PANG, J., SALPHATI, L., OLIVERO, A. G., SUTHERLIN, D. P., O'BRIEN, C., SPOERKE, J. M., PATEL, S., LENSUN, L., KASSEES, R., ROSS, L., LACKNER, M. R., SAMPATH, D., BELVIN, M. & FRIEDMAN, L. S. 2011. GDC-0980 is a novel class I PI3K/mTOR kinase inhibitor with robust activity in cancer models driven by the PI3K pathway. *Mol Cancer Ther*, 10, 2426-36.

WANG, A., KUBO, J., LUO, J., DESAI, M., HEDLIN, H., HENDERSON, M., CHLEBOWSKI, R., TINDLE, H., CHEN, C., GOMEZ, S., MANSON, J. E., SCHWARTZ, A. G., WACTAWSKI-WENDE, J., COTE, M., PATEL, M. I., STEFANICK, M. L. & WAKELEE, H. A. 2015. Active and passive smoking in relation to lung cancer incidence in the Women's Health Initiative Observational Study prospective cohort. *Ann Oncol*, 26, 221-30.

WANG, A., YOSHIMI, N., INO, N., TANAKA, T. & MORI, H. 1997. Overexpression of cyclin B1 in human colorectal cancers. *J Cancer Res Clin Oncol*, 123, 124-7.

WANG, B., LIU, K., LIN, H. Y., BELLAM, N., LING, S. & LIN, W. C. 2010. 14-3-3Tau regulates ubiquitin-independent proteasomal degradation of p21, a novel mechanism of p21 downregulation in breast cancer. *Mol Cell Biol*, 30, 1508-27.

WANG, C., FU, M., MANI, S., WADLER, S., SENDEROWICZ, A. M. & PESTELL, R. G. 2001. Histone acetylation and the cell-cycle in cancer. *Front Biosci*, 6, D610-29.

WANG, H., NICOLAY, B. N., CHICK, J. M., GAO, X., GENG, Y., REN, H., GAO, H., YANG, G., WILLIAMS, J. A., SUSKI, J. M., KEIBLER, M. A., SICINSKA, E., GERDEMANN, U., HAINING, W. N., ROBERTS, T. M., POLYAK, K., GYGI, S. P., DYSON, N. J. & SICINSKI, P. 2017a. The metabolic function of cyclin D3-CDK6 kinase in cancer cell survival. *Nature*, 546, 426-430.

WANG, S. C., NAKAJIMA, Y., YU, Y. L., XIA, W., CHEN, C. T., YANG, C. C., MCINTUSH, E. W., LI, L. Y., HAWKE, D. H., KOBAYASHI, R. & HUNG, M. C. 2006. Tyrosine phosphorylation controls PCNA function through protein stability. *Nat Cell Biol*, 8, 1359-68.

WANG, Y., DUAN, J., CHEN, H., BAI, H., AN, T., ZHAO, J., WANG, Z., ZHUO, M., WANG, S. & WANG, J. 2017b. Analysis of EGFR mutation status in tissue and plasma for predicting response to EGFR-TKIs in advanced non-small-cell lung cancer. *Oncol Lett*, 13, 2425-2431.

WANG, Y., ROUGGLY, L., YOU, M. & LUBET, R. 2012. Animal models of lung cancer characterization and use for chemoprevention research. *Prog Mol Biol Transl Sci*, 105, 211-26.

WANZEL, M., KLEINE-KOHLBRECHER, D., HEROLD, S., HOCK, A., BERNS, K., PARK, J., HEMMING, B. & EILERS, M. 2005. Akt and 14-3-3eta regulate Miz1 to control cell-cycle arrest after DNA damage. *Nat Cell Biol*, 7, 30-41.

- WARD, P. S. & THOMPSON, C. B. 2012. Signaling in control of cell growth and metabolism. *Cold Spring Harb Perspect Biol*, 4, a006783.
- WARK, P. 2015. Bronchitis (acute). *BMJ Clin Evid*, 2015.
- WATLING, D. L., GOWN, A. M. & COLTRERA, M. D. 1992. Overexpression of p53 in head and neck cancer. *Head Neck*, 14, 437-44.
- WAWRUCH, M., KRČMERY, S., BOZEKOVA, L., WSOLOVA, L., LASSAN, S., SLOBODOVA, Z. & KRISKA, M. 2004. Factors influencing prognosis of pneumonia in elderly patients. *Aging Clin Exp Res*, 16, 467-71.
- WEIGEL, T. L. & MARTINI, N. 2000. Occult lung cancer treatment. *Chest Surg Clin N Am*, 10, 751-62, vii.
- WERLE, B., SCHANZENBÄCHER, U., LAH, T. T., EBERT, E., JÜLKE, B., EBERT, W., FIEHN, W., KAYSER, K., SPIESS, E., ABRAHAMSON, M. & KOS, J. 2006. Cystatins in non-small cell lung cancer: tissue levels, localization and relation to prognosis. *Oncol Rep*, 16, 647-55.
- WERNER, M., CHOTT, A., FABIANO, A. & BATTIFORA, H. 2000. Effect of formalin tissue fixation and processing on immunohistochemistry. *Am J Surg Pathol*, 24, 1016-9.
- WHITESIDE, S. T., EPINAT, J. C., RICE, N. R. & ISRAËL, A. 1997. I kappa B epsilon, a novel member of the I kappa B family, controls RelA and cRel NF-kappa B activity. *EMBO J*, 16, 1413-26.
- WIATROWSKA, B. A., KROL, J. & ZAKOWSKI, M. F. 2001. Large-cell neuroendocrine carcinoma of the lung: proposed criteria for cytologic diagnosis. *Diagn Cytopathol*, 24, 58-64.
- WILSON, M. S. & WYNN, T. A. 2009. Pulmonary fibrosis: pathogenesis, etiology and regulation. *Mucosal Immunol*, 2, 103-21.

- WIŚNIEWSKI, J. R., ZOUGMAN, A., NAGARAJ, N. & MANN, M. 2009. Universal sample preparation method for proteome analysis. *Nat Methods*, 6, 359-62.
- WONG, J. Y., WESTALL, G. P. & SNELL, G. I. 2015. Bronchoscopic procedures and lung biopsies in pediatric lung transplant recipients. *Pediatr Pulmonol*, 50, 1406-19.
- WOOD, L. D. 2012. Folate receptor alpha: a new tool in the diagnosis and treatment of lung cancer. *Oncotarget*, 3, 668-9.
- WYKES, M. & MACPHERSON, G. 2000. Dendritic cell-B-cell interaction: dendritic cells provide B cells with CD40-independent proliferation signals and CD40-dependent survival signals. *Immunology*, 100, 1-3.
- XIAO, Y., LIN, V. Y., KE, S., LIN, G. E., LIN, F. T. & LIN, W. C. 2014. 14-3-3 τ promotes breast cancer invasion and metastasis by inhibiting RhoGDI α . *Mol Cell Biol*, 34, 2635-49.
- XIE, H., HANAI, J., REN, J. G., KATS, L., BURGESS, K., BHARGAVA, P., SIGNORETTI, S., BILLIARD, J., DUFFY, K. J., GRANT, A., WANG, X., LORKIEWICZ, P. K., SCHATZMAN, S., BOUSAMRA, M., LANE, A. N., HIGASHI, R. M., FAN, T. W., PANDOLFI, P. P., SUKHATME, V. P. & SETH, P. 2014. Targeting lactate dehydrogenase--a inhibits tumorigenesis and tumor progression in mouse models of lung cancer and impacts tumor-initiating cells. *Cell Metab*, 19, 795-809.
- XIE, H. & HE, S. H. 2005. Roles of histamine and its receptors in allergic and inflammatory bowel diseases. *World J Gastroenterol*, 11, 2851-7.
- XING, Y., ZHAO, S., ZHOU, B. P. & MI, J. 2015. Metabolic reprogramming of the tumour microenvironment. *FEBS J*, 282, 3892-8.

XU, N., CHEN, H. J., CHEN, S. H., XUE, X. Y., CHEN, H., ZHENG, Q. S., WEI, Y., LI, X. D., HUANG, J. B., CAI, H. & SUN, X. L. 2016. Upregulation of Talin-1 expression associates with advanced pathological features and predicts lymph node metastases and biochemical recurrence of prostate cancer. *Medicine (Baltimore)*, 95, e4326.

XU, X., LU, Z., QIANG, W., VIDIMAR, V., KONG, B., KIM, J. J. & WEI, J. J. 2014. Inactivation of AKT induces cellular senescence in uterine leiomyoma. *Endocrinology*, 155, 1510-9.

YAMADA, C., OZAKI, T., ANDO, K., SUENAGA, Y., INOUE, K., ITO, Y., OKOSHI, R., KAGEYAMA, H., KIMURA, H., MIYAZAKI, M. & NAKAGAWARA, A. 2010. RUNX3 modulates DNA damage-mediated phosphorylation of tumor suppressor p53 at Ser-15 and acts as a co-activator for p53. *J Biol Chem*, 285, 16693-703.

YANG, D. W., ZHANG, Y., HONG, Q. Y., HU, J., LI, C., PAN, B. S., WANG, Q., DING, F. H., OU, J. X., LIU, F. L., ZHANG, D., ZHOU, J. B., SONG, Y. L. & BAI, C. X. 2015. Role of a serum-based biomarker panel in the early diagnosis of lung cancer for a cohort of high-risk patients. *Cancer*, 121 Suppl 17, 3113-21.

YANG, H. Y., WEN, Y. Y., CHEN, C. H., LOZANO, G. & LEE, M. H. 2003. 14-3-3 sigma positively regulates p53 and suppresses tumor growth. *Mol Cell Biol*, 23, 7096-107.

YANKOVSKAYA, V., HORSEFIELD, R., TÖRNROTH, S., LUNA-CHAVEZ, C., MIYOSHI, H., LÉGER, C., BYRNE, B., CECCHINI, G. & IWATA, S. 2003. Architecture of succinate dehydrogenase and reactive oxygen species generation. *Science*, 299, 700-4.

- YOKOMIZO, A., TAKAKURA, M., KANAI, Y., SAKUMA, T., MATSUBARA, J., HONDA, K., NAITO, S., YAMADA, T. & ONO, M. 2011. Use of quantitative shotgun proteomics to identify fibronectin 1 as a potential plasma biomarker for clear cell carcinoma of the kidney. *Cancer Biomark*, 10, 175-83.
- YOUNS, M. M., ABDEL WAHAB, A. H., HASSAN, Z. A. & ATTIA, M. S. 2013. Serum talin-1 is a potential novel biomarker for diagnosis of hepatocellular carcinoma in Egyptian patients. *Asian Pac J Cancer Prev*, 14, 3819-23.
- YU, D., ZHANG, X., LIU, J., YUAN, P., TAN, W., GUO, Y., SUN, T., ZHAO, D., YANG, M., XU, B. & LIN, D. 2008. Characterization of functional excision repair cross-complementation group 1 variants and their association with lung cancer risk and prognosis. *Clin Cancer Res*, 14, 2878-86.
- ZAPPA, C. & MOUSA, S. A. 2016. Non-small cell lung cancer: current treatment and future advances. *Transl Lung Cancer Res*, 5, 288-300.
- ZARIC, B., STOJSIC, V., TEPAVAC, A., SARCEV, T., ZAROGOULIDIS, P., DARWICHE, K., TSAKIRIDIS, K., KARAPANTZOS, I., KESISIS, G., KOUGIOUMTZI, I., KATSIKOIANNIS, N., MACHAIRIOTIS, N., STYLIANAKI, A., FOROULIS, C. N., ZAROGOULIDIS, K. & PERIN, B. 2013. Adjuvant chemotherapy and radiotherapy in the treatment of non-small cell lung cancer (NSCLC). *J Thorac Dis*, 5 Suppl 4, S371-7.
- ZENG, Q., ZHAO, Y., YANG, Y., CHEN, X. X., WANG, G., ZHANG, P., CUI, Y., SU, S. & LI, K. 2010. Expression of Cystatin C in human stomach neoplasms. *Mol Med Rep*, 3, 607-11.
- ZENG, Q., ZHAO, Y., YANG, Y., ZHENG, G., WANG, G., ZHANG, P., CUI, Y., SU, S. & LI, K. 2011. Expression of cystatin C in human esophageal cancer. *Tumori*, 97, 203-10.

ZHAN, C., YAN, L., WANG, L., SUN, Y., WANG, X., LIN, Z., ZHANG, Y., SHI, Y., JIANG, W. & WANG, Q. 2015. Identification of immunohistochemical markers for distinguishing lung adenocarcinoma from squamous cell carcinoma. *J Thorac Dis*, 7, 1398-405.

ZHAO, H., LO, Y. H., MA, L., WALTZ, S. E., GRAY, J. K., HUNG, M. C. & WANG, S. C. 2011. Targeting tyrosine phosphorylation of PCNA inhibits prostate cancer growth. *Mol Cancer Ther*, 10, 29-36.

ZHONG, L., PENG, X., HIDALGO, G. E., DOHERTY, D. E., STROMBERG, A. J. & HIRSCHOWITZ, E. A. 2003. Antibodies to HSP70 and HSP90 in serum in non-small cell lung cancer patients. *Cancer Detect Prev*, 27, 285-90.

ZHONG, Y., LI, X., JI, Y., LI, Y., YU, D., YUAN, Y., LIU, J., LI, H., ZHANG, M., JI, Z., FAN, D., WEN, J., GOSCINSKI, M. A., YUAN, L., HAO, B., NESLAND, J. M. & SUO, Z. 2017. Pyruvate dehydrogenase expression is negatively associated with cell stemness and worse clinical outcome in prostate cancers. *Oncotarget*, 8, 13344-13356.

ZHU, C. Q., SHIH, W., LING, C. H. & TSAO, M. S. 2006. Immunohistochemical markers of prognosis in non-small cell lung cancer: a review and proposal for a multiphase approach to marker evaluation. *J Clin Pathol*, 59, 790-800.

ZHU, C. Q. & TSAO, M. S. 2014. Prognostic markers in lung cancer: is it ready for prime time? *Transl Lung Cancer Res*, 3, 149-58.

ZINGONE, A., WANG, W., CORRIGAN-CUMMINS, M., WU, S. P., PLYLER, R., KORDE, N., KWOK, M., MANASANCH, E. E., TAGEJA, N., BHUTANI, M., MULQUIN, M., ZUCHLINSKI, D., YANCEY, M. A., ROSCHEWSKI, M., ZHANG, Y., ROCCARO, A. M., GHOBRIAL, I. M., CALVO, K. R. &

LANDGREN, O. 2014. Altered cytokine and chemokine profiles in multiple myeloma and its precursor disease. *Cytokine*, 69, 294-7.

ZORDAN, A. 2011. Fluorescence in situ hybridization on formalin-fixed, paraffin-embedded tissue sections. *Methods Mol Biol*, 730, 189-202.

ZORE, I., KRASOVEC, M., CIMERMAN, N., KUHELJ, R., WERLE, B., NIELSEN, H. J., BRÜNNER, N. & KOS, J. 2001. Cathepsin B/cystatin C complex levels in sera from patients with lung and colorectal cancer. *Biol Chem*, 382, 805-10.

Appendicies

<https://drive.google.com/file/d/1g5LCS7wjGbqfyH9CArC99Y7kIasscNUA/view?usp=sharing>